Behaviour of Polymeric Materials in Machining

by

Yong - Hwan, KIM
(B.S.c, M.S.c)

This Thesis has been submitted for the degree of
Doctor of Philosophy

Dept. of Engineering
University of Warwick

May 1989

(Vol. I)

Dedicated to my parents and

my wife H.J. KIM

Acknowledgements

The author wishes to express his sincere gratitude to Project Supervisor, Ian Pashby of the University of Warwick for his supervision, specialised advice and encouragement during the course of this research.

Thanks are also extended to Dr. J. Wallbank for his technical guidance in the final stage of this research.

Thanks are also due to Mr. M. Robinson and Mr. K. Cooper of the University of Warwick for their tremendous help in carrying out the practical experiments. Without their assistance this project would not have been completed.

Thanks are also extended to Mrs. V. Taylor for assistance in SEM work, Mr. G.C. Canham for processing the films and Mrs. L. Miller for typing the manuscript.

The author wishes to express his appreciation to the Ministry of Science and Technology in South Korea for providing the opportunity to carry out this research. Finally, the author is most sincerely grateful to his parent's and wife's supportive role throughout the course.

<Abstract>

The machining characteristics of a glassy thermoplastic (Polyvinyl Chloride) and a semi-crystalline thermoplastic (High Density Polyethylene) have been studied. Chip formation mechanisms, cutting forces and surface integrity were found to be dependent on the cutting conditions and tool geometry. Results were explained by considering the different nature of the microstructure. Segmented and discontinuous chips were produced with PVC, and continuous and segmented chips were produced with HDPE. It was observed that surface damage was closely related to the nature of chip formation in these plastics.

Chip formation, surface damage and tool wear mechanisms when machining Glass-Fibre-Reinforced-Plastic (GFRP) were also studied. Cutting tools used were High-Speed-Steel (HSS), cemented carbide (P type and K type) and coated carbide (titanium carbide - and triple-coated). Discontinuous chips were always produced when machining GFRP. Sliding contact is present at the tool/chip and tool/work interface. The principal aspects of surface damage include fibre breakage, resin cracking, resin decomposition and fibre/resin interface debonding. Cutting temperature is not high, but excessive heat generates when the flank wear land develops. Coated carbide tools showed the best performance and HSS tools the poorest. The main wear mechanisms are abrasive wear with HSS tools, attrition wear with cemented carbides, and discrete plastic deformation followed by attrition wear with coated carbides.

TABLE OF CONTENTS

LIST OF TABLES

LIST OF FIGURES

LIST OF ABBREVIATIONS

AFRP : Aramid Fibre Reinforced Plastic

BUE : Built-up-edge

CFRP : Carbon Fibre Reinforced Plastic

CVD : Chemical Vapor Deposition

FRP : Fibre Reinforced Plastic

GFRP : Glass Fibre Reinforced Plastic

HDPE : High Density Polyethylene

HSS : High Speed Steel

LDPE : Low Density Polyethylene

LHW : Left-hand Wound

PCD : Poly-crystalline Diamond

PMMA : Polymethyl methacrylate

PTFE : Polytetrafluoroethylene

PVC : Polyvinyl Chloride

Ra : Average Surface Roughness

RHW : Right-hand Wound

SEM : Scanning Electron Microscope

CHAPTER 1.

Introduction

In all aspects of light construction and energy saving, it is expected that, in the near future, plastic materials will be used in technical ranges which are nowadays a domain of metals. However, it was not until the 19th century that the first synthetic polymer material, cellulose, was discovered [1]. The modern plastics industry started with the development of Phenol-Formaldehyde (Bakelite) in 1909. About the time of World War II materials such as nylon, polyethylene, and acrylic appeared. The future of plastics is bright because of their advantages such as lightness, resilience, resistance to corrosion, colour fastness, transparency and ease of processing.

Composite materials have recently undergone significant development because of their unique properties and characteristics. The steady increase in the consumption of reinforced plastics indicates that the high strength, light weight combinations of resins and reinforcing fibres are proving their value as competitive engineering materials. These materials have been highly successful in such areas as aerospace, transportation, recreational equipment, military, agricultural and various industrial applications.

It is known that ancient Egyptians recognised the concept of composites as early as 1500 B.C. Ancient crafts utilised

this principle of fibre reinforcements in such applications as brick making, long bows, armour plates and swords. The use of glass dates back as far as 2,500 B.C. However, it was not until the late 1930's that a successful commercial operation for making glass fibres became a reality. Pioneer work was done in the United States and Britain, and under the pressure of the technological demand of the second World War, rapid progress was made and the first practical uses of Glass-Reinforced-Plastic (GRP) emerged in the form of aircraft components [2]. With the development of filled polymers, there are increasing needs in the areas of transportation, marine, construction, electronics appliance and business equipment, consumer and recreation, aircraft and aerospace components, and in a number of miscellaneous applications. New types of synthetic fibres such as carbon, aramid, boron, etc were recently developed. However, the future of GRP is bright, because of their high performance, ease of handling and processing into composites, their availability and low cost.

Polymers are large, high-molecular weight macromolecules constructed from a repeating series of smaller structural units [3]. Polymers may be natural in origin and derived from plants, animal, or mineral substances, or may be synthetically created from petrochemicals or silicones. Polymers can be classified into two groups : thermoplastics and thermosets. Thermoplastic polymers are characterised by softening upon heating, and hardening on cooling. Thermosetting polymers possess quite different characteristics. Because of the

irreversible reaction by which they polymerise, they form a rigid, hard and often brittle material. If excessive heat is applied to these materials, they will char and degrade. Polymers can also be classified into two groups (amorphous and crystalline). In amorphous polymers, the molecules are intertwined in no apparent order. In crystalline polymers, the long chain molecules are folded into regular arrays in small thin crystallites gathered into bundles in larger aggregates called spherulites. These compose the gross internal structure like the grains in metals [4]. The wide variety of organic polymers which exist can be attributed to the ability of the carbon atoms to form macromolecules by covalent bonding with other carbon atoms as well as oxygen, sulphur and nitrogen. The mechanical and physical properties of polymers are influenced by the degree of crystallinity and molecular weight.

Glass-Fibre-Reinforced-Plastics (GFRP) are composites made by reinforcing a resin with glass fibre. They can be fabricated into several commercial forms: continuous, chopped fibres and woven or non-woven mats. Glass fibres provide stiffness and strength, while the resin provides a matrix to transfer the load to the fibres, giving them stability. Composites materials are usually classified into fibrous, laminar, and particulate types. GFRP has the advantage in formulating and designing to provide a wide range of properties. Mechanical properties will be influenced by the percentage of glass fibre, composition of glass fibre, fibre orientation, fibre surface treatment, processing technique, and

the type of matrix used.

There are three general processing steps for plastic products; (1) softening, (2) moulding, (3) hardening. The most important processes are probably injection moulding for thermoplastics and compression and transfer moulding for thermosets. The original injection moulding machines were based on the pressure die casting techniques used for metals. The next major development was the introduction of hydraulically operated machines which didn't occur until the late 1930's. The major advantages are its versatility in moulding a wide range of products, the ease with which automation can be introduced, the possibility of high production rates, and the manufacture of articles with close tolerances. Compression moulding is usually used with thermoplastics if the part required is too large to be produced by injection moulding [5]. Extrusion is similar to injection moulding, but the difference is that it is continuous rather than a batch process. Casting involves pouring molten polymer or resins into a mould without the use of pressure.

Many processes are available to produce the desired combination of design performance and economics of glass fibre composites. Glass fibres are made by thermally softening glass and pulling. The basic processes can be classified into two groups; open and closed mould processes. Open mould processes include hand lay-up, spray-up, filament-winding, casting and pultrusion; whereas closed mould processes include injection moulding, continuous laminating and matched-die moulding.

Filament winding is used in parts whose large circular cross sections will experience internal pressure. Laminating is the building-up of sheet structures which may be flat, tubular, or rod-like, depending on the final shape of the products. Many of the techniques for filled polymer are similar to those for unfilled polymer, but require some modifications because of the higher viscosity which needs higher moulding pressures to give the same output [6].

Plastic products can be easily made by moulding and forming, but they require costly moulds and forms. Conventionally, machining processes have been used to remove excess materials in flash, runners etc, or to trim the sheet to the required size. However, machining processes have many advantages compared to the conventional manufacturing processes for plastic products. Hard to mould forms, such as threads and dimensions with small tolerances can be made successfully by machining process. Machining becomes an economic process in small or medium-scale production. Machining is also needed for FRPs because dimensional accuracy and surface quality may not be achieved successfully in the curing processes. The advantages of machining for FRPs are smaller to those for unfilled plastics. The conventional machining processes used on cured composites are principally drilling and cutting off (trimming). Grinding has been applied successfully to the end-finishing of GFRP.

Very little research has been done in the area of the machining of plastics and reinforced plastics, probably because

researchers do not have clear knowledge about the properties of both materials. The knowledge and information obtained from the previous research on metal cutting cannot be applied successfully to the machining of plastics and reinforced plastics. The rheological, physical and thermal properties of plastics should be understood when machining plastics, and the properties and deformation behaviour of anisotropic material should be understood when machining reinforced plastics.

The chisel may be the first cutting tool used by man and the first lathe was probably developed in the Bronze Age for cutting wood. The invention of the steam engine presented the impetus for the development of the metal cutting industry [7]. A lathe is a machine tool by which a piece of material is held and rotated while being shaped by a tool. The development of carbon steel was the first major development in cutting tool materials. The first High-Speed-Steel (HSS) tools were introduced at an exposition in Paris in 1900. The alloying materials consist chiefly of tungsten (about 18%) and chromium (4%) and may contain cobalt, vanadium or molybdenium. Cemented carbides were first produced for use as cutting tools in the 1920's. Varying the amount of tungsten carbide and cobalt made it practically suitable for machining cast iron. New grades of cemented carbides containing titanium and tantalum carbides, were developed to machine steel. These tool materials are usually formed by the powder-metallurgy process.

Ceramic tools were put to use during World War II when tungsten was in short supply at a time when demand was high.

The earliest ceramics were alumina. Whilst these materials demonstrated extremely high resistance to wear and deformation at high temperature, they lacked toughness. The first generation of coated carbides was introduced in 1969. Polycrystalline diamond (PCD) tools were developed in search for a harder ceramic tool, but their high cost can be a disadvantage.

Although remarkable progress has been made in the development of tool materials, there is no cutting tool material which can be applied successfully to all available work material. No matter how strong, fast, rigid or accurate the machine tool may be, it is still limited by the qualities of the cutting tools. The abrasive nature of composites requires careful selection of tool material.

There are difficulties in the machining of high performance plastics when using conventional methods. On the other hand, water jet and laser cutting are able to cut at conditions under which mechanical tools fail. With increasing fibre volume, the difficulties of mechanical machining will increase. The quality of cut-faces has a great influence on the mechanical properties of the part. In the cutting of contours, the water jet can successfully replace mechanical tools in a number of applications. Although there are many advantages in using water jet and laser cutting for their high performance, there are still some drawbacks such as high capital cost, safety problems and severe heat affection. Therefore, further research on the conventional machining of

high-performance plastics will be required.

This project is aimed at investigating the machining characteristics of engineering plastics and glass-fibre reinforced plastics. Poly-Vinyl-Chloride (PVC) and High-Density-Polyethylene (HDPE) were chosen as work materials. PVC is a glassy polymer, and HDPE is a semi-crystalline polymer. The different nature of the structure between these materials influences characteristics such as chip formation, cutting forces, surface roughness and surface damage. Investigations were carried out to find the effects of cutting conditions and tool geometry on these machining characteristics, and the results of each work material were compared. Results were explained by considering the different nature of the microstructures, elastic-plastic deformation of the work material, stress, strain, strain-rate, and temperature.

In the second part of the project, surface characteristics and tool wear in GFRP machining were studied. The change in the nature of the surface according to cutting conditions and tool geometry was investigated. Wear mechanisms of various cutting tools (HSS, cemented carbides, coated carbides) were also investigated. The performance of each cutting tool material in GFRP machining was compared and explained by considering the properties of tool material and work material under various cutting conditions.

CHAPTER 2. LITERATURE SURVEY

2.1. Metal Cutting

2.1.1. Terms and definitions

The following are the most commonly used terms in metal cutting. For simplicity, only single point cutting operations are taken into consideration. Fig 1 shows aspects of a single point tool used in a turning operation.

'Single point tools' are tools with one cutting part and one shank, whereas multipoint tools are tools with two or more cutting parts such as milling cutters or drills.

'Cutting Speed' is the surface speed at which the work passes the cutter.

'Feed' is the rate at which the cutter moves along or into the surface of the workpiece.

'Depth of Cut' is the thickness of material removed and measured in a radial direction from the bar.

'Orthogonal cutting' takes place when the cutting edge is straight, normal to the direction of relative work-tool motion and only the primary cutting edge is used for the cutting operation.

'Semi-orthogonal cutting' is when the primary cutting edge,nose radius and the secondary cutting edge are used to generate the chip.

'Non-orthogonal cutting' is when an approach angle on the primary cutting edge is used, so that the cutting edge is not normal to the direction of relative work-tool motion.

'Flank face' is the surface over which the freshly machined surface passes.

'Rake face' is the surface over which chip flows during machining.

'Primary cutting edge' is the intersection between the rake face and flank.

'Secondary cutting edge' is the remainder of the cutting edge,and the intersection of rake face and minor flank face

'Nose' is the junction of the primary and secondary cutting edges and usually rounded to strengthen the cutting edge.

2.1.2. Metal Cutting Operation

Turning is a process using a single point tool that removes unwanted material to provide a surface of revolution. The chip, or swarf, is a thin layer which is removed from the surface of the work material, and passes over the rake face while moving in a direction away from the motion of the workpiece. During continuous chip formation without built-up-edge (BUE), the work is sheared in a zone close to the shear plane (OD in Fig 2). The shear plane is the plane within the work material where plastic deformation occurs. This zone where chip formation takes place is known as the 'primary deformation zone'. The forces which are transmitted to the chip across the interface between the chip and the tool are sufficient to deform the lower layer of the chip as it slides along the tool face [8]. This interface region is known as the 'Secondary deformation zone'. When a continuous chip is

formed, the actual operation of cutting involves three main processes; plastic deformation, movement of the chip over the tool, and formation of the new surface. Most of the work energy in cutting is spent in deforming the material plastically during chip formation and to overcome the resistance between chip and tool. The inclination of shear plane (shear plane angle) is influenced by the rake angle. The shear strain becomes less with an increase in rake angle. Chip formation usually involves severe plastic deformation, resulting in considerable work-hardening and structural change [9]. Metals and alloys which lack ductility are periodically fractured on the shear plane.

The machinability of a material can be regarded as a measure of (a) ease with which it can be cut by the tool (b) the quality of surface finish obtained (c) the tool life (d) the power consumed.

2.1.3 Forces and Stresses in Metal Cutting.

When a metal is cut, the cutting forces act mainly through a small area of the tool face which is in contact with the chip. A knowledge of cutting forces is required to estimate the power requirements.

Cutting forces can be analysed into a compression force normal to the rake face, and a shearing force parallel to the rake face, in the direction of the chip flow. As shown in Fig 2, cutting force (Fc) acts in the direction of the cutting velocity, feed force (F_f) acts in the direction of the tool

feed, and radial force (Fr) acts perpendicular to the machined surface.

The force required to form the chip is dependent on the shear yield strength of the work material and on the area of the shear plane. It has been observed by many researchers that the cutting forces are directly proportional to the contact length between the tool and the chip.

High strength materials require large forces due to high stress on the shear plane. They also cause greater tool and work deflection, increase heat generation and require bigger work input. In metal cutting, an increase in cutting speed usually causes a corresponding increase in shear plane angle, resulting in thinner chips and reduction in cutting forces. Rake angle can also influence cutting forces. An increase in rake angle lowers cutting forces, However, high rake angles reduce the strength of the cutting edge which may lead to a premature failure of the edge. An increase of feed usually results in an increase of contact length, which also results in an increase of cutting forces although the relationship is not proportional.

There have been many researchers [10,11,12,13] who have investigated the stress distribution on the rake face using photoelastic techniques and split tools equipped with strain gauges. Distribution of compressive stress is influenced by the work material. In general, compressive stress is maximum at the cutting edge, and falls to zero with distance from the cutting edge to the end of contact zone. The shear stress is

more uniform near the cutting edge, but decreases gradually at some distance from the edge until it becomes zero at the end of the contact zone (Fig 3). Trent [9] verified experimentally, by using a tool with restricted contact, that contact length could be the important factor in determining the size of the cutting forces. The maximum stress near the cutting edge is strongly related to the yield stress of the work material. The very high normal stress near the cutting edge will facilitate the seizure condition on the rake face.

2.1.4. Heat and Temperature in Metal Cutting.

Knowledge about the factors which influence the heat generation, the flow of heat and the temperature distribution in the tool and work material near the tool edge is a pre-requisite for reliable prediction of tool life.

There are three main sources of heat during machining; these are the plastic deformation zone (shear zone), secondary deformation zone (tool-chip contact zone) and flank of the tool. With an increase of cutting speed, the temperature aspects of cutting become increasingly important. The upper limit of cutting speed is usually determined by the ability of the tool to withstand the compressive stress near the edge at the elevated temperature. Temperature distribution in tools is influenced by aspects of tool geometry such as rake angle, and nose radius. About 97% of the work is dissipated as heat in metal cutting [8].

At high cutting speed, more work is done in a unit of time in shearing the chip and moving it over the tool face, resulting in more heat and higher temperatures. With an increase in feed rate, there is an increase in tool pressure against the material and an increase in contact area which results in an extension of the heated area further from the edge, and deeper below the rake face. However, an increase of feed causes a smaller rise in temperature than does a corresponding increase in cutting speed. (Fig 4)

Low cutting speeds, low rake angles and other factors which give a small shear plane angle, tend to increase the heat flow into the workpiece [9].

Several researchers [14,15,16] investigated the temperature distribution within the tool using the thermocouple technique or by measurement of structural and hardness changes in HSS tools in the near surface region which had been heated above the tempering temperature.

When machining steel, there was a maximum temperature on the rake face at a distance of about 1.5mm from the edge [17]. The maximum temperature zone when cutting titanium alloys is much closer to the edge.

Temperature is greatest in the spots of greatest heat concentration such as the area of maximum chip deformation and the friction surface of chip and tool face. The maximum temperature in the chip occurs when the material leaves the secondary deformation zone, which limits the rate of metal removal when cutting the higher melting point materials. The

mean shear zone temperature increases slightly with increasing cutting speed and then tends to become constant, whereas the maximum tool-face temperature increases rapidly with increasing cutting speed [8].

2.1.5. Tool/Chip Interface

The frictional state at the tool/chip interface can be classified into two situations; sticking friction and sliding friction.

Trent [9,17] reported that seizure (sticking) is the normal condition over most of the interface, in which movement can continue only by shear through the weaker of the two bodies close to, but not at the interface. Metallic-bonding or mechanically interlocking of the interface is a normal feature. The above observations are consistent with those of Zorev [10] and Takeyama and Usui [11].

The sliding zone is situated outside the seizure zone, where the compressive stress is relatively small and atmospheric oxygen or lubricant can penetrate. A sliding condition is promoted by low cutting speed and the presence of an effective lubricant.

In the seizure zone, the movement of the chip over the tool face takes place by intense shear in a thin layer, namely the flow zone or secondary deformation zone, of the work material. The material in the secondary shear zone is deformed to extremely high strains without fracture because of the increased ductility at elevated temperatures. The temperature rise in this zone can be attributed to the energy required to

shear the material at the high amount and rate of strain. The degree of secondary shear zone is influenced by the character of bonding and the mechanism by which these can be broken to cause localised sliding [18].

The conditions prevailing at the chip/tool interface influence tool wear. A seizure zone contributes to adhesion, diffusion wear and plastic deformation of the tool asperities; whereas in the sliding zone, abrasive wear can operate in which hard particles on the chip underside erode the tool's bonding material and undermine the harder phase.

2.1.6. Classification of Chip Type.

Metal cutting is primarily a process of plastic deformation involving intense shear of small region of the workpiece near the tool point. Chip fracture occurs when the material cannot withstand the intense plastic shear in the primary deformation zone, resulting in shear fracture on the shear plane producing a segmented or completely discontinuous chip.

Ernst [19] described three fundamental types of chip in orthogonal cutting, as follows: discontinuous, continuous (ribbon-like) and continuous with built-up edge.

Iwata [20] classified the chip type into four groups based on the mechanism of crack formation and its propagation.

i) 'Continuous chips' contain no obvious cracks, and are produced mainly by a catastrophic shear slip mechanism based on dislocation activity.

ii) 'Quasi-discontinuous chips' are produced by large strain deformation accompanied by partial fracturing.

iii)'Discontinuous chips' are produced when the crack nucleated below the flank face of the tool propagates right through the shear band.

iv) 'Chips with BUE' appears when machining materials which can adhere to the tool face, or when the cutting conditions are such that the tendency to adhesion is strong.

Three kinds of chip types (continuous, segmented, discontinuous) will be discussed in this chapter.

2.1.7. Continuous Chip Formation

Continuous chips are produced when the ductility of the workpiece is not exhausted by the chip forming process. The deformation may be considered in a steady state. The material in the plastic flow zone in front of the tool is subjected to compression and shear. When the elastic limit is reached, plastic deformation begins and the flowing material is constrained to move in a direction away from the workpiece by the rake face of the tool.

Dislocation activities on a large scale occur in the workpiece material prior to its entrance into the shear front region [21]. The shear front originates very close to the tool tip on a very narrow set of planes.

Material deformed in the primary deformation zone will either pass into the bulk of the chip or it is reworked in the secondary shear zone. The high strains in the primary zone

sometimes generate enough heat to cause hot-working along the zone.

Some researchers [22] reported that even the continuous ribbon chip formation involved fracture to generate the new surface. The micro-cracks responsible for the surface generation will form at the microvoids present in the material. Later on, many researchers [23,24,25] also reported that even the continuous chip formation was heterogeneous in nature because of plastic instabilities. Adiabatic shear enhances plastic instability by the reduction of the capacity to resist the applied shear stress when the rate of strain-softening (by thermal recovery) exceeds the rate of strain-hardening. Micro-crack formation along the shear plane also contributes to the plastic instability because the variation in density of micro-cracks causes fluctuations in the flow stress of the workpiece material.

In this sense, several researchers [26] stressed the importance of micro-cracks during deformation. The existence of micro-cracks in the deformation zone decreases the shear stress of work material, and hence cutting forces, due to the reduction of deformation zone area and the activation of dislocations by the local stress concentration near the void tip.

The ductility of material can be increased under the influence of compressive stress, which may contribute to delaying the formation of microcracks at low strains and restricting the growth and coalescence of micro-cracks at high

strains [27]. The number of micro-cracks in the deformation zone gradually decreases with increasing cutting speed and rake angle or with decreasing undeformed chip thickness, resulting in tendency for continuous chip formation.

2.1.8. Segmented Chip Formation

A segmented chip is a continuous chip with a periodic variation in chip thickness. The cutting process can be characterised by large shear strains, low oscillating shear angle, large cycle variations in cutting forces, and stick-slip movement on the rake face [28].

The difference between the segmented and discontinuous chip is that, in segmented chip formation, fracture is not complete and the individual serrations are separated by shear bands.

Rice [25] explained the process of segmented chip formation;

i) Compression of work material with bulging upward until fracture.

ii) Displacement of segment along the fracture surface.

iii) Formation of next segment.

iv) Sliding of previous formed segment along the tool face.

There are many reasons for chip segmentation.

i) Plastic instabilities due to material properties [29,30]

ii) Adiabatic shear or microcrack formation [23,31]

iii) Stick-slip friction [32]

Sullivan et al [30] reported that, when machining

austenitic stainless steel, the segmented chip was not caused by tool vibration but the inherent metallurgical features of the material at the given cutting conditions. The shear bands on the chip indicate a large strain deformation separated by less heavily deformed regions when machining titanium which has poor thermal conductivity and high strength at elevated temperature.

Material with a low thermal diffusivity like titanium or stainless steel is more likely to produce catastrophic shear chips than that with a high thermal diffusivity, probably because temperature rise is more localised and much higher [33]. Catastrophic shear occurs when local temperature gradients offset the strengthening effects of strain-hardening. In this type of chip formation, a very small portion of the material will support the plastic strain.

Segmented chips are more likely to be produced when the work material is embrittled by stain-hardening during the previous cut, heat treatment or cutting fluid.

Turkovich [23] attributed the cyclic pattern of these chips to adiabatic shear. Localised heating in the shear zone can be reached easily because of the thin deformation zone.

The inclusions in two-phase alloys also contribute to plastic instability because of the strain incompatibility of the particle-matrix interface during chip formation [34]. In segmented chip formation, the number of microcracks is not sufficient to fracture the chip, but sufficient to cause periodic fluctuation in material flow stress and hence an

oscillation of shear angle.

One of the possible causes of chip segmentation is stick-slip friction on the rake face leading to relaxation oscillations [32]. Segmentation is found to decelerate during the sticking process and accelerate during the sliding process.

D. Lee [35] investigated the effect of cutting speed on chip formation with aluminium, 4340 steel and titanium. The titanium chips were segmented at all speeds, but became more continuous with increasing speed. As for aluminium and steel, the shear deformation becomes more uniform as speed increases.

2.1.9. Discontinuous Chip Formation

Discontinuous chips are produced when cutting inherently brittle materials like grey cast iron, or due to substantial friction between tool and chip when machining ductile materials at low cutting speed without coolant. Discontinuous chips with ductile materials occur as a result of periodic rupture due to brittle fracture [20].

Field and Merchant [36] and Palmer [37] investigated discontinuous chip formation by taking motion pictures. The chip formation begins with the partially formed chips welded on to the rake face. Compressive stress on the shear plane prevents rupture during the early stage. With the build-up of compressive stress, there is a pre-pile up of the uncut material. With the progress of the tool, the shear plane angle falls until the compressive stress becomes sufficiently low to permit fracture along a plane of weakness which runs from the

cutting edge to the free surface. It can be concluded that discontinuous chip formation is one of compression producing bulging at the surface, followed by intense shear, and finally fracture, on the shear plane. As is the case with segmented chip formation, the thermally-aided or adiabatic instabilities from the interaction of strain-rate, flow stress and temperature can be the reasons for the discontinuous chip formation [38].

Grey cast iron produces a brittle discontinuous chip, with cracks eminated from the flakes of graphite due to stress concentration. Tensile fracture may be observed when large inhomogeneities are present, the cutting temperature is low or a large depth of cut is used.

Doyle [39] reported that, when machining leaded brass, the fracture of the chip at the shear plane occurred by a ductile rupture process evidenced by elongated voids. The role of the lead particle was to reduce the area of work material capable of withstanding the applied shear stress, resulting in failure at a high shear plane angle.

Several researchers [20,37] mentioned the importance of cracks in discontinuous chip formation. The cracks were found near the cutting edge and primary shear zone. The cracks in the primary deformation zone are due to void formation near the inclusions, or brittle fracture of inclusions. The cracks near the cutting edge occur when inclusions pass near to the cutting edge, tensile stresses are present below the flank face, or severe secondary shearing takes place near tool/chip

contact zone. After the growth of these cracks, the tool's further motion will force the chip to rupture by shear and to slide off along the rake face.

Work-hardening of material at the tool/chip interface contributes to discontinuous chip formation. A high degree of seizure promotes a low shear plane angle which gives a high shear strain. With the initiation of plastic instability, shear fracture occurs when primary shear strain is larger than the fracture strain of the material.

2.1.10. Transition of Chip Type

The response of different materials to the change in strain, strain-rate, and temperature accounts for the many types of chip. The transition of chip type depends on changes in cutting conditions such as the rake angle, cutting temperature, and microscopic parameters such as inclusion morphology. Sharma et.al. [40] reported that the transition from ribbon-like to segmented chips occurred when a critical value of the normal shearing strain was exceeded. The critical value depends on the normal stress on the shear plane and it is a property of the work material.

Shoukry [41] investigated the change of the chip type under different cutting conditions with aluminium, mild steel and brass. It was found that the combined effects of feed, speed and rake angle are the main parameters affecting the chip type. In discontinuous chip formation, the mean coefficient of friction between chip and tool was found constant for a given

cutting condition. But in continuous chip formation, the mean coefficient of friction became variable and larger than in discontinuous chip formation.

Discontinuous chips are usually observed at a low cutting speed when machining mild steel and brass, probably because the effect of heat is not significant.

However, with an increase in speed, the heat generated reduces the shear strength and allows the chip to move rapidly up to the tool face, so increasing the shear plane angle. Therefore, shear fracture becomes limited and the chip becomes continuous. However, at very high speed, segmented chips are produced because the effect of strain rate in the secondary shear zone becomes important and can introduce a stick-slip mechanism on the rake face [42].

With an increase in rake angle, there may be a transition from a discontinuous (segmented) chip to a continuous chip. Rice [25] attributed it to the fact that the available frictional force at the large rake angle was less than that at the small rake angle. At high rake angles, the imposed geometric strain becomes less than the shear fracture strain of the material. The tendency for discontinuous chip formation increases with increasing depth of cut.

Discontinuous chips tend to occur when machining brass with lead additions because lead is effective in reducing ductility and frictional stress on the rake face of the tool [37]. The presence of lead leads to the lowering of compressive stress, and ductile failure reduces the strain on

the shear plane. When a ductile metal that is free of gross inhomogeneity is machined, the micro-cracks responsible for the new surface will form at the microvoids present in all materials owing to the concentration of stress. The fracture that occurs in metal cutting is either of the ductile shear type or the brittle tensile type. The majority of chip fracture observed in cutting is of the shear type, where most cracks are in the direction of maximum shear stress.

2.1.11 Surface Integrity

2.1.11.1. Introduction

Recently, the quality of surface produced by machining operations has become more important due to the increasing need for fine tolerances and high reliability. Moreover, the development of new material with increased strength has made it possible to be operated in more severe conditions in terms of stress, temperature and environment. Surface damage produced by machining may decrease the mechanical and physical properties such as fatigue strength, stress corrosion resistance, crack propagation rate and also affect residual stress [43]. Surface integrity is defined as the inherent or enhanced condition of a surface produced in a machining or other surface generating operations. It includes not only the characteristics of the surface and the layers beneath the machined surface, but also the mechanical, metallurgical and technological properties.

The condition of the surface and layers underneath it

depends on cutting conditions, and is also process dependent through factors which influence the temperature, plastic deformation, wear, fatigue, diffusion and corrosion [44]. The types of surface alterations in conventional and non-conventional machining include plastic deformation, fracture, cracking, phase transformation and chemical changes.

2.1.11.2 Nature of Machined Surface

(1) Surface Roughness

The surface roughness is caused by the fact that the tool generates its shape into the surface. In theory ridges which are left behind on the finished surface should correspond to the geometry of the tool and have a pitch equal to the axial feed. The theoretical surface roughness can be defined as the surface roughness caused by the macrogeometrical tool properties and by the feed.

However, there are many factors which contribute to the dimensional accuracy, such as tool geometry and material, cutting condition, vibration etc. The difference between the theoretical and measured surface roughness is caused by factors such as sharpness of the cutting edge, the nature of chip formation, BUE formation, vibration, and thermal effects [45]. Nakayama et.al. [46] stated this difference was caused by the escape of plastic material around the cutting tool.

Shouckry [47] identified three forms of the macrogeometrical deviations.

i) Shape deviation due to geometrical errors of the machine and elastic deformation

ii) Surface waviness due to relative motion between tool and workpiece

iii) Tool track which is strongly dependent on the geometrical form of the cutting.

Other researchers [48] also identified three primary deviations from a geometrical perfect surface finish; roughness, waviness, and flaws. Roughness is dependent on the machining variables such as feed, depth of cut, and cutting speed. Waviness is controlled by the deflection, vibration and chatter in the machine tool system.

In orthogonal cutting, ideal surface roughness is zero and independent of the macroscopic tool geometry. The measured surface roughness arises from microscopic variations in tool geometry at the cutting edge, and instabilities within the cutting system [49].

(2) Surface Damage

The principal factors controlling surface condition are the type of chip produced, and the interaction between the tool nose and freshly machined material. Sub-surface damage is often neglected in the investigation of surface integrity. It includes plastic deformation, hardness change, residual stress, heat-affected zone, microcracking and phase transitions.

The residual stress left beneath the machined surface deteriorates the surface finish because tensile stress on the surface ruptures the outer elements and a portion of the surface is pulled apart and raised above the general level [50]. With an increase in tool wear at high speed, the residual stress increases and can be found deep into the layers underneath the surface, leading to microcracks.

Increase up to 60% in micro-hardness just beneath the generated surface was observed when turning steel [44].

Micro and macro-cracking are often caused by thermal stresses. Plastic deformation can be detected in the form of elongated grains and sometimes torn work surfaces [43]. Large grains can be developed by re-crystallisation of surfaces which have been cold-worked during machining, and then stress relieved in further processing work.

Long straight grooves (grinding marks) are series of ridges on the new workpiece surface and arise from irregularities or asperities along the tool cutting edge which penetrate into the work surface because of high temperature and high normal stress. Wallbank [51] reported that the contact between the flank face and the new workpiece surface was responsible for the surface roughness which could occur even with polished tools. Damage of the tool results in a replication on the newly formed surface. In two-phase alloys containing a hard secondary phase, plastic deformation can lead to microvoid formation because of decohesion at the particle-matrix interface. This decohesion and subsequent void

formation may lead to micro-crack formation behind the tool tip [52].

Squeezing effects can be observed by the displacement of surface metal in a direction opposite to the feed direction and burr formation on the feed mark ridges. The portion of the workpiece below the flank face is squeezed to the side which causes side flow to occur because of the increased stress and high temperatures [53]. During this squeezing, metal in front of the tool rake face is pushed by the approaching tool and, as the primary shear zone is under compression, it flows towards the sides. Squeezing effects are not observed at low cutting speed because of the low cutting temperature.

The mechanism of micro-chip formation was proposed by Nakayama, et.al. [46], as shown in Fig 5. Large microchips can induce a failure produced by fatigue, stress, creep or stress corrosion cracking, because surface damage from the micro-chips can produce severe stress concentration. Micro-chip formation occurs through a process of shear with the development of a primary deformation zone as in the case of chip removal.

2.1.11.3 Measurement of Surface Roughness

Machined surfaces can be classified into two types [54].

i) Surfaces produced by a tool nose as in turning, boring and planing

ii) Surfaces produced by the primary cutting edge as in reaming and broaching.

In tool edge cutting, surface finish does not include the

feed mark, and can be measured in the direction of cutting velocity.

In tool nose cutting, surface finish is produced by the secondary cutting edge, and can be measured in a direction perpendicular to the cutting velocity. Surface finish is complicated by feed marks, plastic side flow and the formation of grooves at the edge of the chip.

The surface roughness in tool nose cutting generally consists of four terms; the ideal geometrical term, a swelling term, a vibration term and a tool-shape term [55]. The surface roughness in tool edge cutting is mainly controlled by the edge roughness of the tool.

Swelling of material can occur when the cutting force pushes aside the work material near the tool nose causing it to flow to the free surface. The extent of swelling decreases with brittle work material.

The predominant method of measuring surface roughness is one using an instrument which amplifies the motion of a stylus perpendicular to the surface over which the stylus is traversed.

Arithmetic roughness average (Ra) is the most commonly used parameter and can be defined as the arithmetic average value of the departure of the profile above and below the mean line throughout the sampling length.

Maximum height (Rmax) is the distance between the reference lines passing through the highest and the lowest point of the profile on the sample length.

Mean total height (Rtm) is the mean distance between the five highest and five lowest points of the profile on the sample length in relation to the reference line [54].

2.1.11.4. Influence of Technological Variables on Surface Finish

(1) Cutting Condition

Generally, surface finish improves with high speed, large rake angle and large nose radius, and deteriorates with an increase of feed rate. Feed is the most important factor influencing the surface finish.

Petropolous [56] reported that the difference between the theoretical and measured surface roughness decreased as feed rate is increased. This may be attributed to side flow of material due to the size effect. Size effect can be defined as a rise in the specific cutting pressure, or in energy per unit volume, with a decrease in the undeformed chip thickness [54]. Surface finish generally improves with increasing cutting speed. At low speed, surface damage arises because of partially discontinuous chip formation and the relative motion between tool nose and workpiece [57]. At high speed, surface damage is in the form of metallurgical changes associated with the sub-surface region due to the high temperatures and seizure conditions.

The seizure condition at high speed contributes to the increase in the number and size of cavities left by microchip generation [49]. At high speed, micro-chip grooves are large

because of the increased ductility of material, whereas at low speed, microchips will easily fracture along the primary shear zone, or separate at the interface, because of rapid work-hardening and limited adhesion or pressure welding. When the temperature is sufficiently high, plastic deformation will occur without fracture.

(2) Tool Geometry

An increase in nose radius causes a decrease in the surface roughness, but has an unfavourable effect on the stability of the tool system.

Continuous chip formation and good surface finish can be obtained when large rake angles are used, and built-up-edge and poor surface finish are associated with small rake angles.

However, a high rake angle may weaken the tool and cause the formation of long chips which might damage the surface but improve the stability. Negative rake angles cause an increase of cutting force and decrease of stability. There is a harmful effect of high negative rake angles on the surface finish because increased cutting force can produce plastic deformations and fracture in surface region [54].

(3) Other Variables

In addition to the cutting conditions and tool geometry, other variables such as type of work material, tool material and coolant also contribute to the surface finish.

The depth of the work hardened layer with ceramic tools was found to be thinner than that with carbide tools when machining steel [58]. The extent of plastic deformation depends on the stress state at the tool nose and the deformation characteristics of the work material [59]. Ductile material shows severe surface deformation, probably because work-hardening can produce an increase in surface hardness and dislocation intensity. In brittle materials, the fracture strain of the material may be exceeded leading to the generation of macro and microcracks in the surface and sub-surface.

Lubricant generally contributes to reducing the extent of plastic deformation and residual stress, and improves surface finish by reducing the temperature and friction at the tool-chip, and tool-workpiece interfaces through boundary lubrication [48]. However, it seems that lubricant is not effective at the chip-tool interface where extreme pressure condition exists as no lubrication film can exist and metallic contact prevails.

2.1.11.5 Surface Finish in Discontinuous Chip Formation

A discontinuous chip is usually obtained when cutting brittle metals like brass and grey cast iron. Fracture of the metal occurs across a shear plane and the chips are produced as a series of broken or segmented pieces. The surface finish is good when the pitch of segments is small.

The segmented or discontinuous chips produce a bad surface

finish because of cracks formed in the region of the cutting edge. With the progress of cutting, the flow of material further away from the tool occurs by shearing, probably because of the strain-hardening which results in the increase of shear plane length [60]. A larger shear plane contributes to tensile stress near the tool tip and high shear strain, resulting in the formation of cracks near the tool tip.

A machined surface with discontinuous chip formation shows relatively smooth areas when cutting has occurred, and rough, irregular areas where fracture has occurred. The removal of large fragments of workpiece below the general level of surface form cavities as shown in Fig 6. During crack formation, additional plastic deformation at the cavity surface occurs with the formation of microcracks and voids [61].

Shaw et.al. [62] investigated the surface finish produced by discontinuous chip formation when machining resulfurised steel. It was found that cutting speed and sulphur content contributed to the quality of the machined surface. With the increase of sulphur content, the period of the uncut/cut pattern was found to be decreased due to the closer spacing of points of stress concentration, as shown in Fig 7. With an increase in cutting speed, more cracks were found in the form of islands on the machined surface.

2.1.12. Tool Requirement

The choice of tool material for specific applications is dependent on the work material to be cut and the nature of the

machining operation.

Ideally, the tool must maintain the original shape of the cutting edge through the machining operation. The tool edge must not be plastically deformed or fractured, and change of edge shape by wear must be as slow as possible.

The tool performance is strongly dependent on the material's intrinsic properties such as high temperature stability, oxidation resistance, chemical reactivity, elastic modulus, thermal expansion coefficient, ambient and elevated temperature strength, and wear resistance [63]. Hot hardness is one of the most important factors, influencing the mechanism of adhesion, abrasion and plastic deformation of the cutting edge. (Fig 8)

A lot of research has been done to develop tool materials that have wear and abrasion resistance during the machining operation. According to Trent [9], a cutting tool material should have the following properties.

i) High hardness and strength at elevated temperature
ii) Sufficient toughness to resist deformation and avoid fracture
iii) High compressive strength
iv) High chemical stability to resist crater wear
v) High abrasion resistance
vi) Good frictional behaviour
vii) High insusceptibility to temperature changes

The cutting tool must satisfy three basic requirements;

wear resistance, fracture resistance and plastic deformation resistance.

2.1.13. Tool Life and Tool Wear Mechanism

Tool life is defined as the cutting time required to reach a tool-life criterion, which is dependent on the tool material and work material used. The end of tool life is usually determined by flank wear at moderate speed, and by crater wear at high speed when turning steel.

As shown in Fig 9, the flank wear is in the form of an even band, and the crater wear is in the form of a groove which locates some distance from the cutting edge. Crater wear becomes deeper with time and may terminate tool life by weakening the cutting edge.

Tool wear can be classified into two groups; gradual reduction in tool dimensions resulting from frictional and abrasive wear, and catastrophic failure resulting from local fracture such as chipping or spalling.

It is very difficult to identify tool wear mechanisms because more than one wear mechanism may be operating during machining, as shown in Fig 10 [64].

(1) Adhesive (Attrition) Wear

Adhesive wear is the change of tool shape by the periodic removal of distinct small fragments of the tool material. Carbide and ceramic tools are more easily damaged by this wear than HSS tools. It usually occurs at a lower speed with BUE

formation, but it can also occur at high speed when the chip cleans the rake face and cutting edge region, so that intimate contact is made. Vibration and lack of rigidity in tool system result in attrition wear by promoting an uneven flow of work material over the surface. This wear is more likely if the tool has a non-uniform strength. In adhesive wear incomplete bonding between contacting surfaces results in frequent removal of small fragments from the tool surface as the work material bonded to it is pulled away or flows unevenly across the tool. Adhesion wear usually involves seizure conditions in which chip movement over the tool takes place by a process of bulk shear, rather than by sliding at the interface [65]. Fig 11 shows schematically the contribution of various processes to tool wear as a function of cutting temperature [66].

(2) Diffusion Wear

Diffusion wear is the mechanism in which tool shape is changed by the transfer of atomic particles from the tool into the work or the work into tool. There are three basic requirements for diffusion wear [17]; i) metallurgical bonding ii) high cutting temperature iii) good solubility of tool material into the work material. It is chemical wear, and dependent on the relative solubility, rather than the hardness of the tool. The wear rate is dependent on the rate of diffusion, the change in structure of work material near the tool surface, and the formation of intermediate layer at the interface [67]. Diffusion rate is controlled by the rate of

mutual dissolution and the degree of surface layer softening. Cutting speed increases the rate of diffusion wear, because it increases both the temperature and the rate of flow in the work material.

(3) Abrasive Wear

Abrasion is a process by which material is removed from a softer surface by harder particles which remove small amounts of material by mechanical action. Abrasive wear is pronounced when the hardness of the tool is not high and the work material contains hard inclusions. The hardness of a tool is a good measure of its resistance to abrasive wear. Abrasive wear is dependent on the cutting distance as well as the shape, hardness and distribution density of the abrasive particles. Sharper inclusions may produce micro-cutting and hence high rates of abrasion wear [68]. With the progress of the wear land, the abrasive particles are more likely to be embedded in the tool and hence remove less material. Most of the external work by the abrasive particles is dissipated through plastic deformation of the newly created surface.

(4) Plastic Deformation

Plastic deformation is the displacement of portions of the cutting edge due to plastic flow of the edge at high temperature and high pressure. The plastically deformed

cutting edge causes an additional heat source as it rubs on the newly generated surface, further weakening the material and leading to plastic collapse. Plastic deformation causes a bulging of the clearance face as well as a displacement of cutting edge, accelerating abrasive wear in addition to generating heat. The critical cutting speed for the plastic deformation is a function of the type of tool and work material as well as the feed, depth of cut, and machining environment. Plastic deformation has been observed when machining materials of very high yield strength like nickel-base alloys, even at low speed, because the stress generated is high enough to cause deformation even at relatively low temperatures [9].

(5) Chipping and Breakage

Chipping is a microscopic form of breakage involving the loss of many small particles from the edge, due to high shear stress at the cutting edge [69].

Breakage is a catastrophic failure and is the loss of one large particle or a few smaller particles from the edge. It is a brittle fracture originating from the rake face at a local maximum of tensile strength. Breakage is the result of mechanical shock, thermal shock, thermal cracks or excessive wear [70]. Tool fracture usually occurs with the tool which has high hardness and low ductility like ceramic tools, or wedge shape with relatively sharp edges. It is also a severe problem in interrupted cutting or when the work material is unusually hard and strong.

(6) Notch Wear

Notch wear usually occurs when machining high temperature alloys, very soft steel or other material with a strong tendency to strain-hardening [54]. In semi-orthogonal cutting, deep grooves can be found at the extremity of the depth of cut, and immediately behind the nose radius where oxygen cannot penetrate to the rear of the chip-tool contact area [68]. The presence of notch wear on the end cutting edge is a source of surface roughness and additional grooves on the end cutting edge. Wallbank [51] and Hogland [71] summarized the possible reasons for the notch wear as follows.

i) Strain-hardening of previous cut surface.

ii) Oxidation due to high temperature and free oxygen supply.

iii) Squeezing effect leading to the increase in the height of feed marks and in hardness.

iv) Break-through of crater wear through the end clearance edge.

v) Microcrack formation due to extreme temperature gradient.

vi) Possible abrasion wear due to no-BUE protection.

vii) High specific cutting force due to minimal chip thickness.

2.1.14. High Speed Steel (HSS) Tools

2.1.14.1. Introduction

Following the discovery of the benefits of adding tungsten, manganese and chromium to high carbon steels to resist softening under the influence of frictional heat, HSS was developed with the introduction of 18% tungsten allied with

a high temperature hardening treatment to develop optimum red-hardness [72].

HSS tools are available in three different forms; cast, wrought and sintered using powder metallurgy. Improper processing can lead to undesirable micro-structural features including carbide segregation, formation of large carbide particles and significant variation of carbide size. The powder metallurgy HSS tools are costly but offer a more uniform product. They have increased the availability of more highly alloyed grades with greater cutting potential. They are also tougher and easier to grind than conventionally processed steels without sacrificing wear resistance and generally give better tool performance.

There are several advantages in using HSS tools [73].

i) Good hardenability.

ii) Higher hardness than carbon steel.

iii) Higher toughness than other tool material.

iv) Easy heat treatment.

v) Reasonable cost and easy availability.

There are also some disadvantages such as

i) Low hot hardness.

ii) Limited wear resistance and chemical stability.

iii) Greater tendency for adhesion of chips to tool.

Recently, composite materials or coated HSS by CVD have been developed.

2.1.14.2 Compositions and Properties

The hardness and wear resistance of HSS depend on the composition, size and distribution of carbides in the steel, and upon the stability of the matrix at elevated temperature. There are many alloying elements used in HSS to improve the mechanical and thermal properties [73].

i) Carbon forms wear resistant carbides and helps promote secondary hardening during tempering.

ii) Molybdenium can be substituted for tungsten and increases hardness and hot hardness of the matrix.

iii) Vanadium significantly increases the wear resistance and helps maintain a very fine grain size.

iv) Cobalt increases hot hardness by retarding the breakdown of martensite at high temperature, without forming carbides itself.

Generally, the properties improve with small carbide size and uniformity.

HSS tools are hardened from the austenizing temperature to obtain high room-temperature and hot hardness and good cutting properties. Low austenizing temperatures lead to a higher toughness and to a finer grain size. The tempering heat treatment results in stress relief, the transformation of retained austenite and the precipitation of secondary carbides which are responsible for the secondary hardening.

2.1.14.3 Wear Mechanism of HSS Tools

(1) Superficial plastic deformation by shear

This is a rapid acting wear mechanism, forming deep craters which weaken the cutting edge so that the tool may be fractured. The following are the major requirements for this kind of wear mechanism [74].

i) The cutting speed must be high.

ii) Flow zone should exist at the tool/chip interface.

iii) Work material should have a high melting temperature, so that stress and temperature in the flow zone are high enough to shear the tool steel.

iv) Tool material must be softened enough to be sheared by the work material.

The chip, which was deformed at a high shear strain rate, should be able to exert sufficient shear stress on the thermally softened tool surface to induce local plastic flow at a low strain rate [9]. This wear mechanism occurs at much lower cutting speeds with high strength alloys rather than with pure metals, because the shear stress developed is higher and the tool is sheared at lower interface temperature.

(2) Plastic deformation under compressive stress

This is not a wear process because there is no removal of tool material, but a change of tool shape. Other wear processes can follow because of the local increase in forces and temperature, and the modification of chip flow pattern. The chip flow pattern influences plastic deformation of the cutting edge, because of the change in the distribution of stress near the cutting edge. The high compressive stress at

the cutting edge is the main reason for this deformation. Work material of high hardness induces plastic deformation at low cutting speed, mainly by excessive stress rather than by temperature.

(3) Diffusion Wear

Diffusion wear with HSS is small when machining mild steel but it may cause depletion of carbon and chromium from the tool surface, thus making it more prone to wear by abrasion and plastic deformation [75]. At moderate speed, the crater is caused mainly by diffusion, but as temperatures are relatively low the crater develops slowly. As cutting speed is increased plastic deformation becomes dominant rather than diffusion. Diffusion wear depends both on high temperatures and a rapid flow rate in the work material very close to the seized surface to carry away the tool material atoms. The rate of diffusion wear may be determined by a balance between [76];

i) The heat generated in the adherent layer.

ii) The temperature and strain-rate dependence of the flow stress of work material.

iii) The temperature dependence of the flow stress of the tool steel.

(4) Adhesive Wear (Attrition Wear)

Adhesive wear occurs because of strong bonding between the interlocking surfaces which results in a pulling away of

fragments of tool material subjected to localised tensile stresses [77]. It is usually observed when the BUE is formed. High cutting speed sometimes results in adhesive wear, because the rubbing action of the chip cleans the tool surface and promotes strong bonds. Attrition wear is a slow form of wear in continuous cutting operations using HSS tools. It can be reduced by applying an inert coating to the tool materials, or increasing the cutting speed to produce a laminar chip flow. HSS tools show better resistance to adhesive wear than cemented carbide tools because they have a much higher transverse rupture strength.

(5) Abrasion Wear

Abrasion wear occurs when there are particles in the work material harder than the martensitic matrix. It can be observed on the flank face as well as the rake face. Very localised plastic deformation of the surface layers occurs when the tool material is pushed ahead of the advancing abrasive particles [77]. Abrasion may play a more significant role under sliding or intermittent contact conditions rather than under seizure conditions. A layer of TiC or TiN on HSS tools may reduce the abrasion wear. Coatings reduce the contact length and temperature, so that the tool material is less thermally weakened and hence more resistant to abrasive attack.

2.1.14.4. The Effect of Cutting Variables on Tool Wear

Cutting conditions such as speed and feed as well as tool

geometry can significantly influence the cutting performance of HSS tools. High speed and high feed rate require tools with good hot hardness, while low speed and low feed rate need tools with good wear resistance.

Cutting speed has the greatest influence on tool wear. The effect of cutting speed is to change the cutting temperature at the flank and rake faces of the cutting tool. At low speed, mechanical abrasion, shearing and breaking off of welded junctions between work material and the tool can be a major cause of wear [78]. High cutting speed usually results in a steep increase of flank and crater wear because of the great loss of strength of HSS tools at high temperatures.

Under BUE conditions, flank wear increases because of a continuous sliding-off of BUE particles; whereas crater wear decreases because the stable part of the BUE protects the rake face. With increase of cutting speed, BUE disappears because the temperature of the chip bottom lies above the blue-brittleness range [54].

Feed rate is also effective in increasing the flank wear, because a higher temperature is generated due to an increased contact area. Wear is diminished with an increase in rake angle because smaller cutting forces and lower cutting temperatures are generated. However, the cutting edge becomes more sensitive to spalling and breaking.

Tool failures usually occur at slightly higher cutting speed when using cutting fluid, probably due to heat transfer through the cutting fluid. Moreover, with coolants, the hot

hardness of HSS tool is not lost as quickly as in dry cutting. Some researchers [79] have reported that, in wet cutting of steel, less adhesion between the chip and tool prevented cracked and torn surfaces resulting in smooth wear surfaces, but there was more wear than in dry cutting because a stationary layer was not formed. The crater formed on HSS tool is a closed one, and does not break into the cutting edge. Possible reasons for crater wear are plastic deformation, abrasion and adhesion [80].

2.1.15. Cemented Carbide Tools

2.1.15.1.Introduction

Cemented carbides are generally found in three major compositions; tungsten carbide (WC), titanium carbide (TiC) and tantalum carbide (TaC). They contain a large volume fraction (>80%) of fine grain, hard refractory carbides in a metal binder produced by cold pressing.

Cemented carbides differ from HSS in many respects [9,72,73].

i) Much harder but less tough.

ii) Superior hot hardness and chemical stability with steel.

iii) Stiffer with high Young's modulus.

iv) Less tendency for adhesion.

v) Expensive to fabricate and shape.

The high hardness and high temperature strength of cemented carbides arise not from the metastable structures of martensite and precipitation hardening, but from the very hard,

elements achieved by a combination of metallic and covalent bonding of metal and carbon atoms [54]. The metallic phase acts as a crack arrester by undergoing plastic deformation when the crack tip reaches the binder phase.

There are many different grades of cemented carbides according to the cobalt content, size, type and volume of carbides. The higher cobalt grades or coarser carbide size grades are tougher and less hard. More complex carbides are harder, weaker and chemically more stable with respect to steel than WC-Co alloys.

Cemented carbide tools are usually rounded off by honing or given a chamfer or negative rake angle to strengthen the edge.

2.1.15.2. Compositions and Properties

(1) Straight grade (WC-Co)

Straight grade carbides are made from tungsten carbide and cobalt, and mainly used for machining cast iron and titanium alloys. Tungsten carbide has a low coefficient of thermal expansion and a high thermal conductivity. This combination gives the straight grades excellent shock resistance and an ability to conduct away heat.

Cobalt is used as a binder phase which influences the resistance to mechanical fracture, the compressive strength at high temperature. Increasing cobalt reduces the compressive strength at high temperature, and lowers the maximum metal removal rate when cutting steel or high melting point alloys.

(2) Mixed Carbide Grades (Steel Cutting Grades)

Since high temperatures are generated by the chip when machining steel, carbides such as TiC, TaC, and NbC are added to the straight grade carbides to improve resistance to diffusion wear [73]. TiC base tools have excellent crater wear resistance and high heat resistance when machining steel.

TiC is added to increase hot hardness and crater resistance. The low thermal conductivity of TiC can reduce the temperature at the cutting edge, thus increasing tool life. However, TiC reduces abrasive wear resistance and toughness [81].

TaC provides crater resistance with less loss of impact strength compared with TiC, since it restricts the grain growth during sintering. TaC also reduces the tendency of welding and BUE formation.

The major reason for using mixed carbide grades in steel machining is not because of the greater hardness of TiC or TaC, but because of the resistance of TiC or TaC to diffusion wear when in contact with steel at high temperature.

(3) Cemented TiC Tools

TiC has the highest hardness of any of the readily available carbides. It also has an adequately high melting point. Cemented TiC has markedly increased oxidation

resistance, hot hardness and strength. These tools are more wear-resistant than straight WC, but have the disadvantage of lower strength. The advantages of using these tools in machining steel are as follows [82].

- Unusually high resistance to Built-up-edge and cratering
- Finest surface finish attainable
- Longer tool life, wider variation of cutting speed

2.1.15.3. Wear Mechanism of Cemented Carbide Tools

(1) Introduction

Cemented carbide has a tensile strength of the same order as hardened steel, and hardness is maintained up to high temperatures. Compared to other ultra hard materials, they are relatively tough, but still brittle compared to HSS tools. Fracture can start due to tensile stresses developed during bending or contact loading. They have exceptionally good rigidity with a Young's modulus about three times that of steel.

Examination of wear in cemented carbide tools suggests many wear mechanisms such as abrasion, attrition, thermal shock, oxidation, adhesion, welding fusion, chemical interactions, brittle fracture and plastic deformation. The following wear mechanisms were reported for these tools [83].

i) Mechanical wear with the possibility of local crushing.

ii) Plastic deformation by the effect of high temperature.

iii) Oxidation by atmospheric oxygen.

iv) Welding of chip to the tool, resulting in spalling of the

tool.

v) Diffusion between the tool and chip.

vi) Fracture by high mechanical stress.

(2) Abrasive Wear

Because of the high hardness of tungsten carbide, abrasive wear is much less likely to be a significant wear process with cemented carbides than with high speed steel [9]. Abrasive wear is promoted by the influence of high normal, tangential and shearing stresses as well as temperature. The carbide grains at the cutting edge have only little protection against crumbling since there is only small support provided by the surrounding matrix [84]. BUE also increases abrasion wear because of its high hardness which causes carbide grains to crumble away from the cutting edge.

Where sliding contacts exist at the interface, there is a greater probability of significant abrasive wear. The flank wear of carbide tools is a kind of 'self-wear', because the hard particles causing abrasive wear are carbides themselves [85]. The abrasion of the cutting tool is promoted by an increase of speed because of the decrease in hardness and elastic limit with increasing heat.

During abrasive wear, tool material at the rake face is prone to plastic deformation by small abrasive particles, whereas the flank face material behaves in a brittle manner because of relatively low temperature at the flank [86].

(3) Adhesive (Attrition) Wear

Adhesive wear is dominant at lower cutting speeds. Uneven flow of work material around the cutting edge promotes the break away of carbide grains from the tool surface. Depending on the location of the lowest adhesive strength, a separation at the location of pressure welding occurs within the work material or the tool material, forcing carbide grains to crumble out of the cutting edge.

Low cutting speed, feed rate, uneven depth of cut, vibration, uneven chip flow and interruption of cut promote this kind of wear. For attrition wear, grain size is more important than hardness and cobalt content. Fine grained carbides are more resistant than coarse grained carbides. Straight grade carbides are more resistant than mixed carbides, because of the higher strength of WC grains or the strength of their bonding to cobalt, resulting in higher tensile strength and more plastic deformation before fracture [74].

The tendency to adhere to steel increases with increased cobalt content. The adhesion temperature between steel and carbide tools is greater than that between steel and HSS tools [70].

(4) Diffusion Wear

Some researchers [67] verified that the crater wear when cutting steel with carbide tools was the result of atomic diffusion into the work material flowing over the tool, rather than the mechanical detachment of fragments of tool material.

They proposed crater wear mechanisms as follows;

i) Diffusion of cobalt and iron across the interface.

ii) Decarburization of WC and formation of diffusion layers containing complex carbides.

iii) Bonding of these carbides to the chip bottom.

iv) Detachment of these carbides from the tool face.

However, Dixon et.al. [87], reported that the most likely mechanism of crater wear was the adhesion and the related micro-mechanical fracture of the WC particles.

Diffusion rate increases exponentially with temperature. TiC-based carbides are more resistant than WC-based tools because of the low solubility of TiC in steel. WC grains are lost by diffusion, but TiC grains are undermined and eventually carried bodily away [65]. Large TiC grains are less readily undermined than small ones. Diffusion may be greatly reduced when oxygen can penetrate at the periphery of the contact area. The rate of diffusion is dependent on the pattern of flow as well as temperature.

(5) Plastic Deformation

During the plastic deformation process, overstressing of a tool material starts in small local areas within the wear land, then progresses until the complete deformation and displacement of the cutting edge.

Appreciable plastic deformation has been observed in carbide tools [65]. It occurs primarily at the tool nose, so that nose radius can be the important factor affecting the tool

deformation. It causes increased flank wear due to the increased rate of metal removal. The deformation of carbide tools ends in fracture because carbides can deform only up to a limited amount before cracks appear, even at high temperature.

Resistance to plastic deformation increases with an increase in TiC content and a decrease in grain size.

(6) Chipping and Tool Breakage

The inherent brittleness of cemented carbide tools renders them susceptible to severe damage by cracking. Chipping is the result of using carbide edges unhoned, or excessive chatter vibration [70]. Breakage by mechanical shock occurs at the start of the cut, or after the edge has been in a cut for a short time. The breakage by thermal shock usually involves sudden cooling of a very hot cutting edge. Breakage by thermal cracks involves a severe thermal gradient on the tool surface. Breakage after excessive wear involves the dull cutting edges, high cutting forces and pressures, and high temperature.

During chipping, fracture occurs in the middle of the cobalt layer which may have flowed before final fracture, while breakage occurs at the interfaces or even across the carbide grains [69].

2.1.15.4. The Effect of Cutting Variables on Tool Wear

At low speeds, carbide tool wear is mainly by abrasion which is promoted by the periodic formation and disappearance of BUE. With an increase in speed, abrasion, in combination

with plastic deformation, becomes dominant. At a much higher speed tool failure occurs because of oxidation wear [84].

Large rake angles reduce the cutting forces so that plucking out the carbide grains can be minimised but, it will weaken the cutting edge. Small rake angles result in large tool forces, high temperature and shorter tool life. A large approach angle is desirable to reduce notching of the cutting edge at the depth of cut. A short contact length on the rake face reduces cutting forces at impact during milling and prevents chipping.

2.1.16. Coated Carbide Tools

2.1.16.1. Introduction

With the advent of many difficult-to-machine materials possessing high strength, abrasive constituents, chemical reaction, poor thermal conductivity and high temperature deformation resistance, the development of coated carbides in the 1960's and coated HSS in the late 1970's was necessary to achieve economic cutting speeds [73]. Several refractory coatings have been developed, including single coating of TiC, TiN, Al_2O_3, HfN or HfC, and multiple coatings of Al_2O_3 or TiN on top of TiC.

There are many advantages in using coated carbide tools.

i) Longer tool life and increased productivity.

ii) Improved workpiece quality.

iii) Additional cost savings.

For coated tools to be successful, the coatings must have

properties such as high room temperature and hot hardness, good chemical stability, freedom from porosity, low coefficient of friction, good adherence to the tool and low cost. The substrate must have good toughness, chemical compatibility with coating material and good thermal conductivity.

The improved cutting performance of coated tools results from several properties of the coating material [88,89].

i) High inertness resulting in reduced dissolution, diffusion and oxidation wear.

ii) High hardness resulting in a reduction in abrasive wear.

iii) Low affinity with steel reducing the tendency to form BUE, reducing cutting forces and toughness demand on the cutting edge.

iv) Reduction in frictional heat.

v) Prevention of galling at low cutting speed.

There are also disadvantages in using coated carbide tools [90].

i) The thin coating cannot be formed along the sharp cutting edge in CVD coating process.

ii) The coating is very thin and does not have the abrasion resistance of cemented tungsten carbide.

iii) The hard coating decreases the transverse rupture strength and the fracture strength.

iv) The decarburization (eta phase) zone results in a lower transverse rupture strength.

The coating thickness is in the range of 2 to 9 μm. The increase of coating thickness improves the wear resistance, but reduces the toughness. Steel cutting grade carbides are

usually used as a substrate to prevent catastrophic failure. Lighter cobalt content of substrate which increases the thermal expansion coefficient of carbide tool is recommended to alleviate differential thermal expansion.

2.1.16.2. Types and Properties of Coating

(1) TiC Coating

TiC coating was first introduced, and has been used primarily for metal forming tools, where abrasive wear is the predominant mode of failure [91].

TiC provides excellent resistance to wear because of its high hardness and abrasion resistance, as well as the chemical stability. The coating also has a low coefficient of friction and resists cold welding. The low thermal conductivity of TiC enables the tool to be used at higher cutting speed.

TiC coating reduces the cutting forces and temperature significantly because of lower friction. However, micro-chipping of the coating limits their application to light or finishing operation on materials which tend to adhere to the tool.

The presence of TiC in the substrate improves the resistance to plastic deformation. The presence of cobalt in the coated layer or in the interface layer is very harmful, because cobalt causes easy breaking or peeling off of the coating with the progress of flank wear [92]. TiC coating is less chemically stable than other coatings at elevated temperatures.

The main problem with TiC coating is the formation of a hard, brittle eta phase at the interface during the deposition of TiC. This layer is developed because the coating is carbon deficient and some of the carbon diffuses from the substrate into the coating.

(2) TiN Coating

TiN coating is used for HSS tools and for carbide tools requiring sharp edges. TiN is a refractory material which enables it to withstand extreme heat. TiN is gold in colour, and has a hardness in the range of 2500-3000 Hv. TiN resists abrasion, adhesion, galling, welding, cratering, and the formation of BUE at low speeds and feeds. The chemical stability of TiN resists chip welding and BUE. TiN possesses a lower coefficient of friction than TiC, resulting in lower frictional heat. However, it was found that TiN coated tools were not suitable for turning titanium alloys because of the increased affinity of chips to the tool.

TiN coating was found to have greater crater wear resistance than TiC or Al_2O_3 coating when cutting steel [93].

(3) Al_2O_3 Coating

Alumina (Al_2O_3) coating is usually used on a TiC or TiC-Ti (C,N) interlayer and also with TiN on top. Al_2O_3 coated tools are chemically inert, but their melting point is low, being 2045°C [94]. Al_2O_3 is harder than TiN, but not as hard as TiC at low temperatures. However, Al_2O_3 is the hardest material at

elevated temperatures. The low thermal conductivity of Al_2O_3 at high temperatures tends to concentrate the heat in the chip rather than the tool. Breakage and chipping resistance are better than ceramic tools and nearly equal to that of cemented carbide tools. The success of Al_2O_3 coated tools in machining steel is a result of extremely high chemical inertness of alumina to steels.

(4) Multi-layer Coating

Single TiN coating on normal substrates may not be good because of the large difference in the coefficient of thermal expansion. Therefore an intermediate layers of TiC is deposited first on the substrate, followed by TiN coating to relieve the residual stress. Similarly alumina coating uses a TiC layer as an intermediate layer. The metallurgical and mechanical interaction between different layers can minimise the cracking and flaking of the coating.

A TiC layer adjacent to the substrate can provide a stable diffusion barrier to prevent carbon from leaving the substrate and iron from entering the cobalt phase. Intermediate layers in multi-layer coating can function as follows [94].

i) Isolate the base alloy from the outer layer.

ii) Improve the adhesion properties of the alloy.

iii) Provide a gradual transition in the coefficient of thermal expansion from the alloy to coating.

iv) Promote the formation of a more uniform and fine grained outer layer.

2.1.16.3 Wear Mechanism of Coated Carbide Tools

(1) Introduction

The dominant mode of coated carbide tool failure may be associated with thermal cracking due to difference in thermal expansion coefficients between the coating and substrate, and the microcracking of the cutting edge [95].

Microcracking (flaking) of the coating layer is a rupture which can be caused by plastic deformation of the substrate. TiC coated tools show superior performance compared to sintered carbides in many respects [96].

i) Higher abrasion resistance because of the higher interatomic bonding force.

ii) Higher adhesion resistance because of the lower temperature generated at the tool/chip interface.

iii) Higher oxidation wear resistance because of the presence of a protective titanium oxide layer at the cutting edge.

iv) Higher diffusion wear resistance because of slower diffusion rate.

(2) Flank Wear

There are many mechanisms for flank wear when machining steel with coated carbides, such as abrasion wear, plastic deformation, and diffusion wear. Venkatesh [97], reported that flank wear was partly attributed to the plastic deformation of the rake face which resulted in bulging of the flank face. Bulging of the flank face can crack the coating layer making it easier to remove, and the WC substrate is exposed and worn by

an abrasion mechanism. Chubb and Billingham [98], also suggested abrasion wear as the main mechanism. The rubbing of the flank on the workpiece results in coating breakthrough by a combined diffusion and abrasion mechanism in the iron-rich layer adhering to the flank surface.

Heydari et.al. [99], also reported that abrasion wear at high speeds resulted from the chipping of the coating material at the cutting edge.

Dearnley and Trent [100,101] stated that a possible flank wear mechanism was diffusion rather than abrasion when machining steel. This process involves the dissociation of the TiC, TiN or Al_2O_3 coatings into their atomic components, and the diffusion of the metal and non-metal atoms across the tool/work interface into the workpiece, to be carried away by it. TiC coating showed the lowest flank wear rate, probably because of the TiC's lower rate of solution into the workpiece. Compared to those on the rake face, the temperature on the flank face is low, but the shear stress is probably equally high. At lower temperatures, flank wear may be the result of abrasion in which case the hardest material would be the most wear resistant.

Hale and Graham [102] reported that flank wear didn't increase even though the coating was penetrated. The bottom of the flank wear scar was found to be the critical contact zone between the flank side of the cutting edge and the workpiece. Coating thus improves flank wear resistance by providing a

contact bearing surface which wears slowly by a combination of mechanical abrasion and chemical reaction.

(3) Crater Wear

Crater wear is a result of a combination of attrition, abrasion, diffusion, thermal cracking, oxidation and fracture, depending on the cutting condition, tool/work material and coating thickness.

Venkatesh [97] reported that crater wear took place by plastic deformation, rather than diffusion, when machining mild steel with TiC coated tools. Plastic deformation becomes easier at high temperatures (above 1000^{o}C), because TiC has poor mechanical properties, particularly hardness and compressive strength at elevated temperatures. The TiC layer acts as a diffusion barrier preventing diffusion of cobalt to the chip/tool interface [103].

Other researchers [100,104] also suggested the possibility of plastic deformation as a crater wear mechanism rather than the chemical interaction.

On the other hand, Heydari et.al. [99], reported that the crater wear was formed predominantly by diffusion, but with the evidence of abrasion caused by hard particles of coating. The formation of ridges on rake face was thought to be caused by abrasive wear and oxidation, rather than plastic deformation. However, the cracks near the cutting edge may be formed by plastic deformation of the substrate at high cutting temperatures and high stress. Chubb and Billingham [98] stated

that the crater wear process began with adhesion/attrition wear followed by thermal cracking which facilitated diffusion wear.

Dearnley and Trent [100,101] reported that the crater wear mechanism was dependent on the coating material. TiN coating is worn by atomic diffusion, TiC by plastic deformation and atomic diffusion and Al_2O_3 by plastic deformation. The discrete plastic deformation of TiC and Al_2O_3 coatings probably culminates in ductile fracture and the physical removal of fractured fragments of coating by the chip.

TiN coated tools show better resistance to crater wear than TiC coated tools [105]. TiN coated tools result in higher contact stress but lower contact area. Moreover, the absence of hard and brittle eta phase in TiN coated tools improves tool performance.

The presence of coating material in the crater zone after the coating has apparently worn through has been verified by many researchers [92,102,103,104]. It may be due firstly to the flow of TiC into the base of the crater from the sides at high temperature, and secondly to the crater sides which were still coated, supporting much of the stress produced by the chip as it moved over the rake face. Moreover, the crater zone may be filled up with stagnant workpiece material which isolates the cemented carbide from direct contact with the chip, and consequently reduces the wear of the substrate. After the coating material is removed, coating at the end of the crater retards crater growth at a rate which is dependent on the chip thickness.

2.2. Plastics

2.2.1. Introduction

Plastics can be defined as 'materials that contain as an essential ingredient, organic substances of high molecular weight which are solid in the finished state, but are shaped by flow at some stage of their manufacture or during processing into the finished articles' [106].

Plastics can be divided into two distinct groups; thermoplastics and thermosets. Thermoplastics can be separated into two groups; crystalline and non-crystalline (amorphous).

The giant molecules have no strong bonds between individual molecules in thermoplastics, so that they can be repeatedly hardened and re-softened by removing and applying heat and pressure.

Crosslinking molecular structures with strong chemical bonds between polymer chains cause thermosets to be rigid and hard as no slippage can occur between the polymer chains [107]. With excessive heat, the material will char, burn, sublime and decompose because no chain flow or softening can occur due to the strong bonds.

A plastic molecule can have two shapes, either 'linear' or 'branched'. Linear molecules can pack very close together and produce crystalline areas in the polymer. Branched molecules with short carbon chains protruding from the main chain prevent the molecules from packing close together, resulting in an amorphous region. [1]

2.2.2. Bonding and Structure of Plastics

Strong covalent bonding exists between the carbon atoms within a polymer chain and between the carbon and hydrogen atoms. The individual molecules interact by intermolecular forces such as a Van-der-Waals force. When stressed, the chains tend to slide over another and failure is by interchain separation, rather than by breaking the intrachain bonds. The presence of side chains or cross-linking usually increases strength by making interchain sliding more difficult [108].

In a glassy polymer, the long-chain molecules show the same amorphous or completely disordered type of arrangement as the molecules of rubber. The forces which maintain the structure are the weaker secondary forces between the molecules, resulting in lower values of elastic modulus. The presence of long chains and the corresponding high internal viscosity is a factor leading to glassy state rather than the regular crystalline state.

In crystalline polymers, the individual crystallites, which are comparatively hard and undeformable, are embedded in an amorphous or rubber-like medium. Crystalline regions may be formed when the chains can approach significantly close to each other for strong inter-chain forces to operate. The crystalline regions consist of aligned and folded chains, and the amorphous regions consist of crystal defects and randomly entangled chains [109]. Polymer crystals are extremely anisotropic because of the covalent bonding in the chain direction.

2.2.3. Processing of Plastics

The raw material commonly used for the manufacture of polymers are coal, water, wood, air, petroleum, limestone and salt, which contain two or more of the six chemical elements such as carbon, oxygen, hydrogen, nitrogen, chlorine and flourine.

A polymer is formed by the union of two or more structural units of simple compounds through a special type of chemical reaction, namely polymerization. There are two major polymerization processes; addition and condensation polymerization. Polymers contain additives such as stabilisers, lubricants, fillers, pigments etc, to enhance the properties of the material. These additions can be classified into four groups; [110]

i) Lubricants and heat stabilisers which assist processing.

ii) Fillers, impact modifiers, plasticizers and reinforcements which modify mechanical properties.

iii) Flame retardants which modify the combustion properties.

iv) Stabilizers which increase the degradation resistance.

Plasticizers are usually low molecular weight polymers which separate the polymer chains and reduce crystallinity. This makes the polymer more flexible and less brittle, and can be used in glassy polymer to increase ductility and toughness below the glass-transition temperature (Tg) of the unplasticized material. The addition of fillers such as carbon black, silica or asbestos, reduces the mobility of polymer chains. Sufficient filler is usually added to increase

crystallization and strengthen the polymer. However, too much filler may restrict cold drawing and molecular orientation, and increase the risk of brittle fracture.

2.2.4. Properties of Plastics

The strength properties of polymers are directly related to molecular weight as well as to degree of crystallinity (Fig 12). The lower the molecular weight and crystallinity, the softer and weaker is the polymer. The presence of impurities or low molecular weight additives will produce softening, as well as weakening effects. The network structure of thermosets results in high yield strength because a network structure prevents uncoiling of the molecules, resulting in little elongation at all temperatures.

When a polymer is cooled from the melt through Tg, there is an abrupt change in viscosity, Young's modulus, heat capacity and thermal expansion coefficient (Fig 13 and Fig 14). Tg will increase as the molar mass is increased, and the amount of branching is reduced, because the free volume allows molecular motion to take place more easily [111]. Polymers are viscoelastic because they display both elastic and viscous nature. At low temperatures and high rates of strain, they display elastic behaviour, whereas at high temperatures and low rates of strain, they behave in a viscous manner, flowing like a liquid.

The reduction in stiffness of crystalline polymers with increasing temperature is less pronounced than that of

amorphous polymers and the transition temperature associated with Tg is generally widened [112].

Both amorphous and crystalline polymers are characterised by a marked anisotropy of binding forces. The intrachain forces are usually much higher than the interchain forces (Van-der-Waals forces). Many physical properties of polymers such as melting or softening point, depend on the cohesive energy and hence on the interchain forces.

2.2.5. Deformation Behaviour of Polymers

2.2.5.1. Glassy Polymers

An inorganic glass is quite brittle because of the absence of any mechanism to relieve applied tensile stress. Glassy polymers are less brittle than inorganic glasses because local molecular movement or re-arrangement is possible under high stresses.

Glassy polymers are not perfectly elastic, but show a limited amount of deformation of a plastic or viscous type which is irreversible. Fracture of brittle polymers is accompanied by a local deformation process involving plastic flow and molecular orientation [113].

Glassy polymers show an inhomogeneous nature of deformation because of strain softening which may occur after the yield [111]. Strain softening is an intrinsic property of the material which results in easier local deformation because the resistance to further plastic deformation falls locally with shear strain (Fig 15).

Glassy polymers have a high Young's modulus and are generally hard and have high tensile strength.

2.2.5.2. Crystalline Polymers

Most crystalline polymers are two phase materials consisting of a non-crystalline amorphous region and crystals. With the exception of HDPE, most polymers contain a considerable fraction of non-crystalline material, ranging from 25 to 50%. The crystallization of polymers requires that polymer molecules have a regular structure, and that there are strong attractive forces.

Crystalline polymers are not normally ductile, and their deformation is non-linear because of the large-scale yielding in the vicinity of the crack tip. They are elastically stiff and have high fracture strengths because of the high degree of molecular alignment in the polymer crystals.

When semi-crystalline polymers are stressed, the non-crystalline regions undergo shear yielding, whereas the crystalline regions deform through processes such as slip, twinning, and martensitic transformation [111,113]. Polymer crystals tend to be mechanically anisotropic because of the relatively strong covalent bonding in the chain direction and weak secondary bonding between the chains. The amorphous constituent of semi-crystalline polymers gives some degree of rubber-like deformity (flexibility), whereas the crystalline component makes the material harder and stiffer than a rubber.

Elastic or plastic deformation increases the crystallinity

and enables the preferred alignment of a polymer to be obtained. Polymer crystallisation can be increased by thermal processes such as annealing at elevated temperature or slow cooling from the melting temperature. Fig 16 shows the typical stress/strain curves for a series of crystalline polymers of different morphological forms. The material becomes brittle and strong with increasing crystallinity.

2.2.6. Typical Thermoplastics

2.2.6.1. Polyethylene (PE)

Polyethylene, commonly called polythene, is a high molecular weight crystalline, linear polymer. The structure is quite simple, and material properties depend upon the chain length. Its strength is low, especially in the branch or low-density form. High-density polyethylene (HDPE) is more linear and highly crystalline, with improved strength and stiffness and good chemical inertness. Polyethylene is tough and flexible, and has a low softening temperature which enables easy moulding and shaping. It is also cheap and has a low Tg so that it can be used over a wide range of temperatures.

Low-density polyethylene (LDPE) has a high volume, and thus a low density, because of the many branches present on the polymer backbone. The degree of crystallinity is 60-70 % [106]. According to the ASTM standards, HDPE has a density of 0.941 - 0.965 g/cm^3. LDPE has a density of less than 0.920 g/cm^3. The degree of crystallinity is more than 85% for the

HDPE. Compared to LDPE, HDPE is slightly more expensive, but stronger and stiffer.

2.2.6.2. Poly-Vinyl-Chloride (PVC)

Poly-Vinyl-Chloride (PVC) is the most widely used of the amorphous plastics. It has a good strength in the unplasticized (rigid) form. It is available in two forms; plasticized or unplasticized. Plasticized PVC has a plasticizer added that produces a soft, flexible and rubbery material. Unplasticized PVC is a hard, strong material but shows a brittle nature and deteriorates at temperatures above 100°C.

PVC has been widely used because of its good physical properties, its compounding versatility for a wide range of applications, low cost and ease of processing. Its beneficial properties include self-extinguishing characteristics, water, chemical and abrasion resistance, good strength and availability in a wide range of colours.

The quantity of plasticizer used in PVC varies from 5 to 10% by weight. The principal plasticizer is dioctyl phthalate (DOP). Additives such as stabiliser, lubricants, pigments and fillers are incorporated in plasticized PVC [110].

The mechanical properties of PVC make it appropriate for bottles and containers, and when plasticized, in sheets and fibre forms for clothing and covers.

2.2.7. Frictional Behaviour of Plastics

The classical Amonton's law which states that friction is proportional to the load and independent of the area of contact, holds only approximately for metals and frequently does not hold for plastics [112].

Polymer sliding friction consists of an adhesion component and a deformation component. The frictional behaviour of polymers is due to tangential resistance produced by deformation of the surface adjacent to the contact region, rather than the shearing of the junctions formed at the contact points. The polymer at the sliding interface is subjected to enormous shear strains, so that the frictional process involves the shear strength of the polymer rather than some small-strain viscoelastic property. Over the contact region, intimate atomic contact exists between the two surfaces and adhesion occurs with the Van-der-Waals forces or stronger chemical forces acting across the surface [113,114,115]. Therefore, sliding requires either breaking the adhesional bonds or shearing of one of contacting materials.

In polymers, frictional behaviour depends on speed and temperature in a way that reflects the strain-rate and temperature dependence of the strength properties.

2.3. Machining of Plastics

2.3.1. Introduction

The recent development of plastics has been remarkable and plastics are widely used as engineering material due to their

variety and unique characteristics. Most plastic parts are produced by moulding processes, and machining operations have been used only to supplement these moulding processes. For this reason, little research work has been carried out on the machining of plastics. Knowledge about the rheological, physical and thermal properties of each plastic is required for successful results.

There are many advantages in using machining processes for plastic products [116].

i) Good dimensional accuracy can be achieved.

ii) Expensive dies can be eliminated in small-scale production.

iii) Machining is the best way to produce flat surfaces,very small parts, thin sections, shapes difficult to mould and parts which need several design changes.

Conventionally, machining has been used to remove flash along the mould parting lines of moulded parts, or to cut out and trim sheet.

2.3.2. Peculiarities in the machining of Plastics

There are many differences between metals and plastics in their mechanical and thermal properties which result in their different machining characteristics.

The rheological properties of plastics mean chip formation is strongly dependent on strain-rate and temperature. Since plastics are thermal insulators and do not conduct heat away from the machining area, they will expand, thus increasing tool

friction which increases the rate of heat generation. Moreover, the deformation, softening, and degradation temperature of plastics are relatively low. Therefore, if frictional heat is allowed to build up, burning or discoloration in thermosets and gumming or discoloration in thermoplastics can occur [117].

Due to low thermal conductivity, most of the cutting heat will be conducted to the cutting tool. The heat conducted into the plastic stays close to the surface and raises the temperature significantly [118].

Plastics are resilient in nature, and thermal expansion coefficient can be about 10 times that for steel [119]. Cutting tools must be provided with enough clearance to compensate for these effects.

The compressive strength of most plastics is several times larger than their tensile strength, hence plastics are more resistant to compressive failure than to tensile fracture.

2.3.3. Chip formation

2.3.3.1. Type of Chips

Chip formation is dependent on the cutting conditions and the kind of plastics. Kobayashi [118] classified chips into six types and Kazanski [120] identified five types when machining plastics. The characteristics of each chip type were explained as follows. (the classification by Kazanski is in brackets)

i) Continuous Flow Chip (free swarf)

A chip is produced by high elastic deformation, not by plastic fracture, resulting in a chip thickness the same as the undeformed chip thickness. It is not observed in metal cutting. There are no shear planes and variation of cutting force is insignificant.

ii) Continuous Shear Chip (shearing swarf)

This kind of chip is often observed in metal cutting. The chip is continuous because of the small shear intervals between the successive shear planes, and is produced by shearing action along the shear plane.

iii) Discontinuous Simple-Shear Chip (Homogeneous Swarf)

The chip is formed by a shearing action along a shear plane but shear intervals are rather large, resulting in discontinuous chips. There are variations in the cutting force and surface quality is poor.

iv) Discontinuous Complex Chip (Fracture Swarf)

The chip is formed by high compressive stress with shear stress when cutting with negative raked tools. Surface quality is poor because of the large stresses acting during cutting.

v) Discontinuous Crack Chip (Inhomogeneous Swarf)

The chip is formed by elastic fracture, not by plastic deformation. A crack occurs around the point of the tool, and propagates at an oblique downward direction until the bending movement is sufficient to produce discontinuous chips. This chip is usually observed in brittle thermosets or some thermoplastics like polystyrene or PMMA when cutting with

large rake angles, large depths of cut, and high cutting speeds. The surface quality is poor with many cracks remaining along the cut surface. This chip is rarely observed in metal cutting, only with some cast irons.

vi) Discontinuous Complex Crack-Type Chip

A crack occurs at a downward angle from the cutting point in addition to the separation along the shear plane. A new shear plane forms from the crack tip upward to the free surface after the growth of the crack. The plastic deformation zone is then enlarged and the apparent shear plane angle increases. Surface quality is very poor because of the cracks remaining on the cut surface.

2.3.3.2. Chip Formation and Cutting Condition

Chip formation when machining plastics is dependent on the cutting condition, especially cutting speed. With an increase in cutting speed and hence strain rate, the strength of the material increases and elastic deformation may occur instead of plastic shear or brittle fracture [120]. However, strength reduces and elongation at fracture increases with a lowering of cutting speed (strain rate). The cutting speed also influences the cutting zone temperature and the interface conditions on the rake face.

Since cutting temperature has an effect on the stress-strain relationship of work material, fracture becomes ductile as the temperature rises and brittle as it falls.

Rubenstein and Storie [121] reported that not only in the

case of discontinuous chip formation did chip material move up the rake face by successive 'stick' and 'slip', but that the same movement occurred when segmented or continuous chips were formed. This stick and slip movement can explain the rough side of the chip underside observed when machining acrylic polymers.

However, a smooth top surface and rough under-surface of chip were observed when machining polypropylene [122]. The rugged under-surface was explained as the result of gumming, namely instability at the chip/tool interface. The reason for the segmentation of the chip and the corrugated form of the chip under-surface was explained as the result of repetition of cyclic pile-up and gumming. High speed may promote instability at the chip/tool interface owing to the higher interface temperature, thus causing a sticky situation at the interface.

When machining PVC, cutting does not occur if the depth of cut is smaller than the roundness of tool edge [118]. Work material under the tool is simply compressed without chip forming. Scrutton [123] investigated the ductile-brittle transition when machining PERSPEX. He found a dependence of transition on the feed rate and cutting speed, and expressed this relationship by the following equation.

$$Vc = Af^m \qquad (1)$$

Where Vc=critical speed relating to ductile/brittle transition

f = feed rate

A.m = Constants

He concluded that even the most brittle substances such as

glass can be machined in a ductile manner, by decreasing the feed rate and cutting speed significantly.

Rake angle has a big influence on the deformation mode during cutting. At positive rake angles, the work material near the tool point undergoes tensile strain perpendicular to the cutting direction and compressive strain along it [118]. At 0^{o} rake angle, the compressive strain is generated perpendicular to the cutting direction and extends to the material. At negative rake angles, compressive strains of a relatively large size exist both perpendicular to, and along the cutting direction. It can be concluded that the direction and magnitude of strain vary with the rake angle.

2.3.4. Cutting Mechanism

2.3.4.1. Stress, Strain and Shear Plane Angle

Owing to the much higher yield strain of thermoplastics compared to metal, it is essential that the shear strain in the yield plane (shear plane) be as large as possible.

In metal cutting, metals are assumed to be an ideal plastic material which yield at a constant maximum shearing stress. However, this assumption cannot be applied to plastics, because of the rheological behaviour of these materials [117]. The chip type is dependent on the strain during machining, which can be in the elastic or plastic region. When the strain is in the elastic region, the mean shear stress along the shear plane is smaller than the yield stress, resulting in continuous flow chip formation, and chip

thickness is the same as the un-deformed chip thickness [118]. Since the frictional angle is almost zero in continuous flow chip formation,the shear plane angle can be derived from the equation;

$$\phi = \frac{\pi}{4} + \frac{a}{2} \qquad (2)$$

(Where ϕ is the shear plane angle, a is the rake angle)

When the strain during machining is in the plastic region, shear occurs along the shear plane. The continuous shear type of chip is produced when the shear on the shear plane is smaller than the limiting rupture strain. In discontinuous shear chip formation, the intervals of shear are large and rupture occurs intermittently along the shear plane. Discontinuous complex shear chips are produced by a complex shear stress combined with compressive or tensile stresses. Discontinuous crack chips are generated by brittle fracture that occurs in the elastic range of stored strain energy.

Due to compressibility effects, the shear plane angle for thermoplastics is expected to be somewhat lower than for metals, producing a larger value of shear strain [124].

A shear plane type of analysis and the minimum energy principles at low tool/chip contact friction were found to be successfully applied to nylon resins [125]. The discontinuous chips of acetal resins at negative rake angles were explained by excessive shear strain at the shear plane, and the cracks at

large rake angle were caused by tensile loading in the region ahead of the tool.

2.3.4.2. Cutting Forces

Cutting forces in the machining of plastics are small compared to those in metal cutting. Cutting condition and tool geometry have some influence on the cutting forces.

Rake angle is one of the most important factors which influence the direction and magnitude of cutting forces, as follows [117].

i) Cutting forces become smaller with an increase of rake angle.

ii) The direction of thrust force changes from downward to upward as the rake angle increases from negative to positive.

Cutting speed has a small influence on the cutting forces, compared to the rake angle. There are opposing effects of increased strain rate and temperature when the cutting speed increases. The increase of cutting force with speed in a low speed range (up to 1^m/min) for PTFE and PMMA, may be due to the increase in the number of molecular bands which resist deformation because stress relaxation velocity is unable to follow the deforming velocity [116]. However, the cutting force shows a decreasing trend with further increases in cutting speed, because the work material acts as a brittle material. Several researchers reported that thrust force had a

big influence on the surface finish, and defined 'critical rake angle' which gave best surface finish.

2.3.4.3. Critical Rake Angle

Kobayashi [118] defined the critical rake angle as the rake angle at which the thrust force equalled zero. At this rake angle, the direction of the resultant force exactly coincides with the direction of cutting, and the work material doesn't deform upwards or downwards during machining. The critical rake angle varies with work material as well as with the cutting condition used.

Kazanski [120] supported the idea of critical rake angle on the surface finish. The tensile or compressive stress under the action of the thrust force on the work surface, reduces the accuracy and increases the friction with cutting tool because of subsequent relaxation process.

The thrust force is zero at the critical rake angle, so the critical rake angle is equal to the frictional angle [126]. Therefore, the value of the critical rake angle is influenced by the frictional behaviour of chips on the rake face of the tool.

The critical rake angle for ductile metals is of the order of 40 to 50 degrees, and appears to be much larger than for plastics, probably because of the greater resistance occurring with metals [125].

Several researchers [127,128] verified, using photoelastic methods and physical measurements, that the stress in the

workpiece and dimensional error are both minimised by using the critical rake angle. The critical rake angle was shown to be influenced by several parameters such as undeformed chip thickness, the mechanical properties of material, and, to a lesser extent, cutting speed. The critical rake angle was found reduced with an increase in the undeformed chip thickness [127].

2.3.5. Surface Finish

2.3.5.1. Surface Roughness

Optimum surface finish can be obtained by machining at the critical rake angle. However, there are many parameters which should be taken into account, such as work and tool properties, tool geometry and other cutting conditions.

Surface roughness tends to decrease with an increase in cutting speed. However, surface finish was found not to be affected by cutting speed, when using a diamond tool for PVC, PMMA and nylon [118]. Other researchers [122] reported that surface roughness increased with cutting speed when machining Polypropylene. They explained that an increase in tool tip temperature at the high cutting speed resulted in instability. Application of liquid nitrogen improved the surface finish, probably because of the reduction in instability. They also reported that the surface finish was primarily influenced by the depth of cut, and to a lesser extent by the tool geometry and cutting speed.

O'Brien et.al. [129] developed a statistical model to

predict surface texture using a factorial design method where four major variables (speed, feed,depth of cut, and rake angle) were considered. Velocity, feed and rake angle were found to be significant in determining surface texture, among those velocity having the greatest effect.

2.3.5.2. Surface Damage

The machined surface of plastics shows many cracks and chatter marks resulting in rough and inaccurate surfaces. Burnt surfaces in thermosetting plastics and gummed surfaces in thermoplastics are caused by the heat generated in cutting.

The quality of the surface finish is dependent on the recovery of plastic deformation due to a temperature rise in the cutting zone. Large recovery increases the friction and fracture strain resulting in 'stick-slip-tear' effects on the surface of the plastic material with the subsequent formation of localised asperities and roughness [124].

Surface cracks can be observed during discontinuous chip formation in brittle materials such as polystyrene or acetal resin. Too large a depth of cut often results in cracks along the machined surface, but too small a depth of cut leads to burning or gumming [118]. Similar results were found with increasing feed rate. When cutting nylon with feed rates of more than 0.41 ^{mm}/rev, pitting of the surface was observed and surface finish deteriorated sharply [117].

2.3.6. Tool Wear

Heat may be the most important factor controlling the tool wear. Plastics have low thermal conductivity, large elastic deformation and high thermal expansion coefficients, so that the cutting point tends to become over heated. If the temperature is allowed to build up, plastics will expand resulting in increased tool/work material contact and the generation of more heat.

Masuko et.al. [130] investigated tool wear when cutting phenolic resin, hard PVC resin and nylon. High speed steel tools show larger flank wear than carbide tools. P type carbide tools are suitable for machining nylon, which has high ductility, whereas K type is better for hard PVC resin and particularly for phenolic resin which are hard and brittle.Cutting speed had a strong influence on the extent of flank wear but the effect of rake angle was found insignificant.

Bogdanov [131] investigated the effects of cutting conditions on tool wear when turning rigid PVC and nylon. Rigid PVC can be turned at high cutting speeds without a significant increase in tool wear. However, nylon was found difficult to machine, because of intensive wear and low allowable cutting speeds. Slight notch wear was observed at the end of the depth of cut when machining nylon with single crystal diamond tools, but fracture was not observed [132].

More intensive wear was observed when machining un-reinforced and reinforced plastics with HSS and carbide tools

at high cutting speed and small depth of cut. HSS tools are acceptable for short runs providing cutting edges are kept sharp, but for certain compounds and for long production runs, cemented carbide tools are preferred [133].

2.4. Composite Material

2.4.1. Introduction

The demands of special applications such as aerospace, automobile, aircraft, etc, are so diverse and severe that they cannot be met by one material. Composites are materials made up of various parts, in which a matrix material is reinforced with particles, filaments, fibres or fibrous materials, giving the resulting material enhanced mechanical properties over those of either the matrix or the reinforcement when used alone. At the present time, polymer-based composites are the most practical type for engineering use because of their fabrication simplicity. Advanced composites typically utilise boron, graphite or aramid fibres in either a polymer or metal matrix. Composites with a metal matrix such as aluminium, titanium or nickel, which are strengthened by graphite, boron or silica carbide are used when higher temperatures are encountered [134].

In comparison with metals, polymer-matrix composite materials have high specific modulus and specific strength, so that weight can be reduced. They can be easily moulded and cured to a required shape, eliminating operations required in conventional metallic products.

The anisotropic nature of composites can be disadvantageous but cost or weight saving can be achieved through orienting the reinforced fibres in the plane where they will be most effective. Polymer-matrix composite materials will be mainly discussed in this chapter.

2.4.2. Classification of Composites

Composite materials can be classified into three categories [135].

- Dispersion strengthened composites
- Particle reinforced composites
- Fibre reinforced composites

In dispersion strengthened composites, the strengthened matrix is the major load bearing constituent. The objective of this strengthening is to have the particles small enough and spaced closely enough so that dislocations cannot easily move between them. These composites have a metallic matrix instead of a polymer matrix. In particle strengthened composites, the load is shared by matrix and particles.

In fibre reinforced composites, the fibre is the major load bearing component. These can also be divided into two groups; composites with continuous fibres and those with discontinuous fibres. Discontinuous fibres can be mixed with the matrix material to produce either a random or preferred orientation. Continuous fibres are normally unidirectionally aligned as tapes, woven into a fabric in an orthogonal

arrangement, or wound around a mandrel. Fig 17 shows the typical fibre arrangements used for composite material.

2.4.3. Mechanical Properties

There are various factors which contribute to the mechanical behaviour of composites as a whole [6].

- Chemical nature of the filler and the matrix
- Shape and length of fibres
- Nature of adhesion between polymer and fibre
- Sensitivity to environmental factors and temperature

In general, fibres contribute high modulus, high strength, and brittleness, whereas resins contribute toughness, low density, low strength, low stiffness, high thermal expansion and low thermal stability.

Fig 18 and Table 1 show the enhanced properties of various Fibre Reinforced Plastic (FRP) materials compared to metals [136]. Most FRP materials, except glass composites, break when they have been stretched by ½ % of their length. Glass composites are almost as stiff as aluminium, but considerably stronger. Carbon composites are somewhat stiffer than titanium, but titanium is stronger.

Because of their anisotropic nature, the mechanical properties of aligned FRPs transverse to the fibres are much lower than those parallel to the fibres (Fig 19). Therefore, crack propagation in a direction parallel to the fibre will be restricted.

Because of a relatively high strength, and low modulus of

FRPs, a large amount of energy can be absorbed before failure occurs, and therefore high impact strengths are achieved.

Composites exhibit a variety of failure modes including matrix crazing or microcracking, fibre fractures, debonding, delamination and void growth [137].

2.4.4. Thermal Properties

Polymers have low thermal conductivity compared to metals and many inorganic materials, although a substantial increase in thermal conductivity can be achieved by incorporating metal and carbon filaments.

Because of the differential thermal properties of resin and fibre, thermal stress can occur which leads to microcracks near the surface.

The strength of FRP is strongly temperature dependent because most of the resins are either softened or degraded at temperatures in excess of $100^{o}C$.

2.4.5. Glass Fibre Reinforced Plastics (GFRP)

2.4.5.1. Introduction

It was not until the late 1930's that a successful commercial operation for making glass fibres became a reality. Glass can be defined as an inorganic product of fusion which when cooled, becomes rigid without crystallising [138]. Glass is a non-crystalline or amorphous solid, and characterised by short-range atomic order rather than the long-range order of most crystalline solids.

Glass fibres are relatively inexpensive and give outstanding strength to weight characteristics, high tensile strength, excellent moisture resistance, outstanding dimensional stability and excellent electrical characteristics. They are used with thermoplastic or thermoset resins for such products as aircraft and missile parts, ducts, electrical components, transportation parts, construction uses, sporting goods, protective covers and housing.

2.4.5.2. The Production of GFRP

Glass fibres are produced by extruding molten glass through a small orifice, then drawing the resulting form to a very fine diameter ranging from 3 to 20 μm. The glass fibres are then sized and impregnated with an appropriate matrix material during production.

Commercial glass fibres are mainly based on silica (SiO_2) with addition of oxides of calcium, boron, sodium, iron and aluminium, as shown in Table 2 [134]. The glass fibres can be designated according to their applications; A glass (soda glass), E (electrical grade), C (chemical grade) and S (high strength). E glass is most commonly used because it draws well and has good strength, stiffness, electrical and weathering properties.

The basic forms of glass fibres are continuous strand, fabric, woven roving, chopped strand, reinforcing mats and surface matrix [139].

- Continuous strand or roving gives reinforcements in the

direction of lay of the strand or roving

- Fabric reinforces in two directions
- Woven roving gives high strength and low cost
- Reinforcing mat gives a random reinforcement and low cost
- Surface mat gives no reinforcement, but gives a smooth decorative surface finish

2.4.5.3. Resins

Both thermoplastic and thermoset resins can be used for the matrix of GFRP. Resins protect the reinforcing phase from structural damage, corrosive attack and reactions that degrade their reinforcement properties. Polyester resins are widely used for GFRP because of their low cost.

A. Thermosetting Resins

Unlike thermoplastics, thermosets do not melt on heating, but lose their stiffness at the heat distortion temperature. The mechanical properties depend on the molecular units making up the network and on the length and density of the cross-links. Shrinkage during curing and thermal contraction on cooling after cure can lead to built-in stresses in composite materials.

Thermosetting resins include polyester, epoxy, phenolic, melamine, vinyl ester and silicone. Epoxy resins are more expensive than polyester resins, but give better strength, dimensional stability and chemical resistance. The strength of the interfacial bond between fibre and resin is higher for epoxy resins. Epoxy-glass is a major material for filament

wound structures and can be used for aircraft, ducting and rocket parts.

B. Thermoplastic Resins

Polyolefins are the most widely used thermoplastic resins, followed by others such as nylon, styrene based materials, acetal and polycarbonate.

There are several disadvantages in using thermoplastic resins [138].

i) The lack of an efficient method of combining the thermoplastic resin with the glass reinforcement

ii) Lower strength and stiffness compared to thermoset resins

iii) The lack of heat resistance of the resins

Thermoplastics are not cross-linked, so that they derive their strength and stiffness from the inherent properties of the monomer units and their very high molecular weight.

2.4.5.4. Properties of Glass Fibre

Mechanical properties of GFRP depend upon the combined effects of the amount of fibre reinforcement used and its arrangement in the finished product.

Because of the size effect, very small diameter fibres can display much greater strength values than that of larger sections, even though their composition is identical [139]. The surface condition of the fibre has a significant influence on the strength and behaviour of a glass fibre because of the larger surface area to volume ratio.

Generally, the strength increases directly in relation to the amount of glass. For a given fibre volume fraction in unidirectional arrangements, maximum strength and modulus are obtained in the filament direction, but in bi-directional arrangements, strength is equal in both directions, but lower than with a unidirectional arrangement. A random arrangement results in equal but lower strength in all directions.

Bulk glass has a softening temperature of about 850°C but the strength and modulus of E glass fibres decrease rapidly above 250°C. The properties of glass are influenced strongly by the temperature.

The observed strength value depends upon the rate of loading, ie. the more rapid the loading, the higher the strength. The specific modulus of fibre glass is almost the same as that of aluminium and steel.

The viscosity of fibre glass becomes low enough to yield plastically at sufficiently elevated temperatures [139]. Elastic modulus is determined by the matrix as well as by the fibre. The yield strain is determined by the relative modulus of fibre and matrix.

Table 3 shows the mechanical and thermal properties of glass fibre compared to boron and carbon fibres.

2.4.5.5. Fibre/Resin Interface

In composite materials, at least two component phases are separated by an interface which has a big influence on the character of the final composite.

The Van-der-Waals interactions of the glass surface and the resin is sufficient to form a strong bond so long as resin and glass make intimate contact with every 'hill and valley' and all the air is displaced in these conditions. The strength of the bond between glass and resin will exceed the tensile strength of the resin [140]. If the fibre surface is rough, containing many minute irregularities, the matrix material may not penetrate the depressions and a poor interfacial bond will result. Good matrix wetting over the fibre surface is therefore necessary to obtain good molecular or atomic interaction between the constituents.

High interface bonding results in brittle fracture characteristics in which the cracks propagate through the matrix and across the neighbouring fibres leading to composite failure. If the interface is weak, then fibre-matrix debonding will occur extensively and crack tips will be re-directed along the interface [6].

2.4.5.6. Deformation and Failure of GFRP

The deformation process of continuous fibre reinforced plastics can be summarized as follows [137]

i) Both the fibre and resin deform elastically.

ii) The fibres continue to deform elastically, but the matrix deforms plastically.

iii) The fibre and resin deform plastically.

iv) The fibres fracture followed by composite fracture.

At room temperature and low strain, glass fibre and resin

obey Hooke's law. With increasing temperature, the proportion of non-Hookean deformation increases and reduces the Young's modulus because the deformation is opposed by a force originating from increasingly random thermal motion in the polymer [134]. At lower temperatures, resins are brittle materials and the failure mechanism of resins is similar to glass. With an increase in temperature, the strength decreases progressively because of reduced intermolecular forces.

Reinforced plastics usually have low shear strength compared to their tensile strength because of weak zones (the interface between strong fibres and weak matrix, and the thin zone of pure matrix between fibres). The limiting shear strength of a FRP is usually close to that of the matrix polymer [135].

Fibre debonding usually occurs because of the concentration of both shear and tensile stresses in the vicinity of crack tips during the propagation of cracks normal to the direction of reinforcement [140,141]. The shear strength is dependent upon the strength of the interfacial bond, and is found to be reduced by the presence of voids in the matrix.

Shearing forces at the interface can cause debonded regions to spread even further along the fibres [136].

2.4.5.7. GFRP Laminates

Glass laminated products are sheets of glass fibres which are impregnated with a thermosetting resin material. The

process used can be a high pressure technique with the heating of several layers, or a low-pressure technique involving curing of the built-up product.

The glass component is mainly in the form of woven fabrics, where yarn and rovings are arranged in the directions of warp and weft [138].

i) 'Yarns' are woven into cloth, and can give certain differential strength characteristics.

ii) 'Rovings' are packages of glass fibre strands, wound up without twist.

iii) 'Chopped strand mat' is an uneven fabric consisting of 2-5 cm lengths of chopped glass fibre strands which consist of 50 - 200 individual glass fibres.

iv) 'Fabrics' are sheets of fibres or yarns that are woven, knitted, or otherwise physically bonded together.

Because of their high Young's modulus, the fibres are more highly stressed than the matrix, resulting in transfer of the stresses from the matrix to the reinforcing phase. The resultant stresses in the laminar are proportional to their respective elastic moduli and shear moduli [140]. Interlaminar shearing is the typical mode of failure for laminated composites.

Three main failure mechanisms have been identified around a fibre fracture. (1) brittle crack in fibre and matrix (2) shear yield of matrix, which was followed by spread of yield zone along the fibre (3) interface crack, allowing unloaded fibres to shrink back into matrix (Fig 20). For a laminate

with different orientations, failure occurs when both sets of laminate have fractured, provided the applied load is sufficient to overcome the interlaminar bonding forces.

High strength laminate requires an effective transfer of stress in all parts of the laminate from fibre to fibre across the resin/fibre interface.

2.4.6. Carbon Fibre Reinforced Plastics (CFRP)

Since the 1950's, carbon fibres have been used for high strength, light-weight reinforcements in such applications as aerospace components.

The basic units of graphite are quite anisotropic. They consist of parallel layers of carbon atoms strongly bonded within the layers and weakly bonded between layers [138]. To obtain high modulus and strength, the layer planes of the graphite have to be aligned parallel to the axis of the fibre. Whiskers and filaments are unique forms of graphite because they exhibit extremely high preferred orientations of graphite layers parallel with the filament axis.

The Young's modulus of carbon fibres depends on the degree of perfection of alignment which varies considerably with the manufacturing route and conditions.

Carbon fibres are used with resins such as nylon, polyester, poly-propylene and polycarbonate. Although CFRP is expensive, it has a promising future because of its high specific strength and stiffness and low expansion coefficient.

2.4.7. Aramid Fibre Reinforced Plastics (AFRP)

Aramid fibres were introduced in 1972, and are available as woven and non-woven fabrics, fibres and rovings, but not in the form of chopped fibres because of the difficulty in cutting them . These fibres do not melt. The higher elongation to fracture and its tendency to yield in compression without fracture result in a fibre that is tougher and less brittle than other commonly available reinforcing fibres [139]. These fibres suffer irreversible deterioration due to changes in internal structures with high temperature.

2.4.8. Boron Fibre Composites

Boron was the first available continuous reinforcement for light weight, high performance composites. The conventional manufacturing method is by deposition of boron on tungsten wire. These multi-phase filaments are placed on a tape impregnated with resin. The tape is then layed up in the correct orientation and cured in an autoclave.

The ratio of modulus to density is about 5 times that of glass filaments. Boron fibre was found to be much less sensitive to temperature than glass fibres [139].

2.5. Machining of Composites

2.5.1. The Need for Machining Operations

Composite materials are advantageous with their abilities to be moulded and cured to various shapes required in engineering applications, thus minimising material waste and

eliminating many of the costly machining operations.

However, machining of cured FRP is sometimes required, because dimensional accuracy and surface quality may not be achieved in the moulding and curing processes. Moreover, machining operations can avoid the high production expenditure involved with plastic moulding, and reduces the throughput times when processing small runs [142]. However, there has been little research in this area because researchers do not have clear knowledge about the properties and deformation behaviours of these anisotropic materials. Fig 21 shows various composite components produced by machining operations.

2.5.2. Characteristics and Problems in Machining

The physical and mechanical properties of fibres and matrix, and fibre orientation are the main factors which determine machining characteristics.

Glass and carbon fibres fracture in a brittle manner but aramid fibres fracture in a ductile manner. Glass fibres are anisotropic due to their amorphous structure, and carbon fibres consist of several entwisted graphite bands [143]. These structures result in brittle fracture without plastic deformation at low loads.

Glass fibre which is a poor heat conductor, melts at 1300^{o}C, whereas another poorly conducting aramid fibre decomposes at about 550^{o}C. Carbon fibre, which shows good thermal conductivity, decomposes at 3600^{o}C in the absence of air [134].

Glass fibre has a positive coefficient of thermal expansion in longitudinal and transverse direction, whereas carbon and aramid fibres expand in the transverse direction and shrink in the longitudinal direction.

The major problems in machining composites can be summarised as follows [144].

- The influence of mechanical and thermal stress on the properties of the moulding.
- The formation of highly abrasive discontinuous chips and fibre fragments,and the increased tool wear.
- Health risks among workers due to fibre fragments.
- Decomposition of products in the matrix.
- Frequent necessity to dispense with cutting fluids during machining.
- Electrical conductivity of carbon fibre particles.

The cutting temperature should be limited to below the melting or decomposition temperature of the matrix. Burning can be accelerated by heat choking due to poor thermal conductivity of matrix and fibre [143]. Moreover, the difference in coefficients of thermal expansion between matrix and fibre can result in thermally generated residual stress leading to dimensional inaccuracy.

The following are typical machining characteristics of commonly used polymer-matrix composite materials.

(1) Glass Fibre Reinforced Plastic (GFRP)

Tool wear is severe because of the abrasive action of hard

glass fibres and the low thermal conductivity of the material which results in increased cutting temperatures. The highly abrasive nature of glass fibres causes premature rounding of cutting edges. The distinct difference in hardness between fibres results in edge chipping.

Delamination may occur if machining forces are high in the transverse direction, because of low transverse tensile strength. Thermal delamination can occur due to different coefficients of expansion between fibres and resin.

The use of coolants is not usually permitted with polymer materials because of their contamination of the surface. Air cooling by a jet aimed at the tool is recommended [143].

Thermosetting resins permit higher cutting speed than thermoplastic resins due to their higher heat resistance. Because of their resistance, glass laminates require greater clearance and less rake angle on cutting tools than do metals. Honed single-point cutting tools are always advisable.

(2) Carbon Fibre Reinforced Plastic (CFRP)

The main problems when drilling CFRP are the delamination of the material and short tool lives. The cutting process consists of a series of fractures without plastic deformation. A similar type of tool wear can be observed as with GFRP machining. The flank wear of carbide tools when drilling CFRP is nearly four times than in drilling GFRP. It was observed that during the drilling operation, the top layers of CFRPs

tend to spall single fibres due to the low flexural strength of the fibres [143].

(3) Aramid Fibre Reinforced Plastic (AFRP)

The machining characteristics of AFRP are similar to those of wood, both of which are characterised by the presence of highly oriented fibrous material, embedded or bound together in a matrix of different properties [145]. It is advisable in machining operations to preload the fibre component and then cut with a shearing action. Otherwise, due to the relatively low compressive strength, the aramid fibre will tend to recede within the matrix, instead of being sheared-off [146]. The following criteria were suggested for AFRP drilled holes, to assess the quality.

i) Delamination at tool entry and exit.

ii) Fuzzing at the outside diameter and burrs.

iii) Roughness of the drilled hole wall.

Typical fuzzing, consisting of pulled-out and crushed fibres, may result because aramid fibres fail only by tensile stress and dislocate under bending load. Delamination of the composite is usually made on tool exit because a high feed force is required to penetrate the laminate [147].

Unlike glass and carbon fibres, aramid fibres tend to cling to the tool and curl around when they are pulled out and stretched. If the matrix is molten due to excessive friction, it sticks to the tool and tends to clog.

(4) Boron Composites

The extreme hardness of boron fibres produces excessive tool wear and fibre break-out when conventional tools are used. Doran and Hanley [148] reported that there was little relationship between tool life and cutting speed.

Most of the machining problems arise from the high hardness of the boron fibres, although the low heat conductivity of the matrix helps to increase the cutting temperature. The relatively weak matrix doesn't prevent fibre break-out, which can be severe in the case of drill exit [149].

Conventional drills, whose hardness is less than that of boron, cannot cut the boron material. Instead, the tool fractures into small pieces, which later act as agents that abrade the cutting edge. Boron-epoxy composites are relatively easier to machine than boron-metal matrix composites because the boron filaments and resin are relatively brittle [150]. The major problem encountered is the cutting heat which damages the resin system if proper tools and cooling systems are not used. Quickly worn-out tools which generate high thrust forces have the effect of splitting the composite along the direction of the filament [151]. Interlamellar shear of the composite can also be a possible source of failure.

2.5.3. Performance of Tool Material

When machining FRPs, tool wear is severe on account of the abrasive nature of hard fibres and the increased cutting temperature. Tool materials require high strengths and hot

hardness. Abrasion resistant cutting tool materials having high hardness properties include cemented carbide, cubic boron nitride and polycrystalline diamond (PCD).

(1) Conventional Tool Materials

HSS tools are not suitable because of the rapid deterioration of the cutting edges. They are used only in exceptional cases. Ceramic tools are not recommended due to their lack of toughness resulting in severe chipping.

Carbide and single crystal diamond tools were used before the advent of PCD tools. The abrasive effect of the fibres on cemented carbides results in rapid edge dulling and the subsequent danger of thermal damage to the resin-based workpiece. Carbide tools can be used only at low cutting speeds or when severe interrupted cutting condition exists. Carbide and diamond tools were found successful when machining silica-reinforced plastics [152]. Carbide tools are suitable for rough cutting because of their high toughness, whereas diamond tools are better for finish machining because of their exceptional hardness. Because of the deterioration of surface finish with progress of tool wear, carbide tools should be replaced and the workpiece surface has to be sanded with coarse and then fine grinding paper in order to produce an acceptable surface finish [153]. Tool life can be increased by coating the tool with TiC or TiN.

(2) Advanced Tool Materials

The diamond tools used for FRP machining, range from single point drills through various types of hollow drills, solid drills, counter sinks, milling cutters and circular saws [154].

Single crystal diamonds have excellent wear resistance, but are not capable of withstanding high shock loading. However, PCD tools have a higher toughness because of the completely random orientation of the crystal structure which prevents cracks from propagating through the structure and provides uniform wear [155]. Because of their free cutting action, diamond tools have no tendency to produce delamination when cutting laminated pieces and, if correctly used, will not overheat and burn the product [156].

Smooth edges without chipping can be produced on sawn cuts or drilled holes by using diamond tools. The same holds true for milled, reamed and ground faces. However, there is a problem of detachment with cutting inserts from their base during turning operations, due to the heat generated at the cutting point [157]. Moreover, diamond tools are not suitable for intricate parts, because of the difficulty in fabrication of anything more sophisticated than simple cutting tools.

Diamond tools don't damage the internal structure of the reinforced plastics by exerting a heavy shearing force on the fibres. They actually cut through the fibres instead of breaking them [158]. It is recommended to use low feed rates to reduce the breakage and chipping of diamond tool. Diamond

tools are suitable for lighter finishing cuts at high speeds because most commonly available cutting tools tipped with PCD have a maximum usable cutting edge length of about 4mm.

2.5.4. Chip Formation

There has been little research on chip formation in FRPs. GFRP and CFRP usually produce a fine powder-like chip, whereas AFRP exhibits a fibrous chip. The fragmentary chips when machining GFRP indicate that the proportion of the energy consumed by the shearing and separating actions is relatively small. With an increase in cutting speed, excessive heat will cause the resin to become sticky and produce a lumpy type of chip [159]. The GFRP chip becomes rather flaky as the tool dulls. When machining CFRP, the chips are small fragments, illustrating that the cutting process consists of a series of fractures without the large plastic deformation.

Koplev [160] investigated chip formation using quick-stop and macro-chip methods when cutting unidirectional CFRP perpendicular and parallel to the fibre direction. When cutting in a parallel direction, the chip forming process includes crack initiation ahead of the tool tip, bending of the fibres ahead of the tool, followed by fracture perpendicular to the fibre direction which releases the chip from the workpiece. Chip formation in a direction perpendicular to the fibres includes crack initiation below the tool and a chip releasing mechanism.

As in the case of metal cutting, heat build-up can take

place at the chip/tool and tool/workpiece interface. During the machining of glass/epoxy composites, 90% of the heat was reported to be conducted into the tool because of the low thermal conductivity of the work material [161].

2.5.5. Cutting Forces and Surface Finish

2.5.5.1. Introduction

In the machining of FRPs, cutting forces and surface finish are dependent on the cutting speed, the type of work and tool material, tool geometry, tool wear and fibre orientation.

Resulting surface quality of FRPs is important when the machined surface has to transmit loads. However, the measurement of surface roughness is difficult because protruding fibres may lead to incorrect results.

The abrasive fibres severely wear the cutting edge resulting in a deterioration of surface quality due to an increase in the amount of friction which can cause thermal damage to the resin with melting and smearing of the surface layers [162].

Cutting forces when machining GFRP are much lower than those when machining steel [163]. In machining steel, its main cutting force is about 300N, while in machining GFRP, it is about 30N. It was found that tool wear is relatively large in machining GFRP although cutting forces are remarkably low.

2.5.5.2. The Effects of Cutting Conditions

The cutting forces in machining GFRP and CFRP were found

to rise significantly with increase in feed rate, but cutting speed has only a little influence [143].

When cutting speed is increased to a higher level, there is a risk of thermal damage primarily in the work material, whilst too low a cutting speed may cause receding of the individual fibres in front of the penetrating cutting edge, particularly during the turning of AFRP [146]. Too high a feed rate generates excessive cutting forces, resulting in delamination at the tool entry and exit during drilling AFRP. However, with too low a feed rate the individual filaments are not cut and heat intensive crushing occurs. There is a problem of melting and burning the matrix at high cutting speed and low feed rates. Low feed rates generally produce less thrust forces and torque as well as less delamination.

Koplev [161] states that cutting forces are strongly dependent on the depth of cut when orthogonal cutting CFRP because a larger horizontal force is required to detach the chips from the work material. An increase in cutting speed results in rapidly decreasing cutting forces which then remain constant above a certain limit.

Several researchers [142,144] reported that the surface finish was not influenced by cutting speeds, but deteriorated with increasing feed rate when turning GFRP. It was also found that cutting speed had a larger influence on cutting tool temperature than feed rate. Therefore, high feed rates are preferred over high cutting speeds when high material removal rates are required.

When drilling graphite-epoxy/titanium composites, both cutting speed and feed rate were found to have a large influence on hole quality [164]. Increased cutting speeds induce vibrations which deteriorate the surface finish. With an increase of feed rates, there is a tendency for extrusion to occur during the period of breakdown, resulting in longer length burrs.

2.5.5.3. The Effect of Tool Geometry

As in the case of metal cutting, the cutting force decreases with increasing rake angle when shaping CFRP [161]. The vertical force drops rapidly as the relief angle increases, but there is no change in horizontal force. It was explained that decreased relief angle resulted in a larger contact area, and thus in an increasing vertical force. The same author states that the chip-forming force is independent of tool wear, because the tool tip doesn't cut into the specimen, but applies pressure on it, resulting in a series of fractures.

Dull tools reduce surface quality, because the increased friction leads to greater frictional heat in the cutting area which causes thermal damage to the resin by melting and smearing of the surface layers [165,166,167].

It is generally recommended for successful drilling of FRPs to use a positive rake angle because the fibres are pulled from the workpiece and sheared or broken between the cutting edge and the uncut work material [154, 159]. A thin chisel edge is better because thrust force is reduced and therefore

there is a reduction in the deflection of the workpiece. However, a positive rake angle and thin chisel edge may weaken the cutting edge.

2.5.5.4. The Effect of Fibre Orientation

The inhomogeneity of FRPs contributes to the different machining characteristics from those of more homogeneous materials such as steel and cast iron.

Spur and Wunsch [142,144] reported that, owing to the laminated structure of GFRP, surface finish was not constant around the circumference of the material, but depended on the angular orientation of the layers in relation to the cutting edge. They defined 'Normal circumference angle' as the angle between fibre orientation and the direction of cut. Fig 22 shows the surface roughness variation according to the change of angular position and feed. The best surface finish was obtained at angles of 135^{o} and 315^{o}.

Sakuma [163] states that the surface roughness with multi-layer composites is coarse compared to that with the homogeneous material, probably because of the fact that glass fibres are in different directions on each other and thus the surface forming mechanism is different on each layer. The same author also compared the surface finish in cutting left-hand-wound (LHW) material and right-hand-wound (RHW) material. In LHW material, fibres are broken by tension, whereas in RHW material fibres are broken by shearing. The cutting resistance of LHW material was found to be larger than that of RHW.

material, because of GFRP's relatively small shear strength compared to its tensile strength. Moreover, the surface roughness of RHW material is considerable higher than that of LHW material because of the difference in fibre breaking mechanism.

Similar work has been done by Koplev [160,161] who compared the surface finish when shaping CFRP parallel and perpendicular to the fibres. It was found that the surface finish when cutting in a parallel direction is significantly worse than that in perpendicular direction.

2.5.6. Tool Wear

2.5.6.1. Tool Wear Pattern

Crater wear has not been reported when machining most abrasive FRPs. Tool wear was concentrated on the tool nose and flank face. Therefore, the crater wear resistance of tool material is not an important factor. Instead, the deformation speed of the work, the contact area between the work and tool, the flexural rigidity of the fibres and visco-elasticity of resins have an influence on the tool wear [168].

When turning GFRP with carbide tools, a remarkable nose wear appears in the shape of a triangle at the low speed, probably due to the heat concentration and ploughing action of the glass fibre [169]. With increasing speed, flank wear becomes uniform along the cutting edge, roundish in its cross section and small in size [170,171]. The spreading of the contact area causes an accumulation of heat at the cutting

edge and promotes nose wear.

Sakuma [166] reported the difference in tool wear pattern when turning GFRP and CFRP with carbide, ceramic and cermet tools, as follows.

i) When machining GFRP, chipping and cracks took place in the wear zone, whereas when machining CFRP, no chipping and cracks were observed with all kinds of tool material.

ii) When machining GFRP, triangular abnormal nose wear was observed in all kinds of tool materials at high speeds. However, when machining CFRP, it was observed at low speeds with Al_2O_3 ceramics, TiC, TiN and TaN tools.

iii) Wear on the rake face was observed only near the cutting edge and no crater wear could be seen in both GFRP and CFRP.

2.5.6.2. The Effect of Cutting Conditions

When turning GFRP, cutting conditions such as cutting speed and feed rate have big influence on tool wear. Increasing flank wear with increasing cutting speed and feed rate was observed with most of the tool materials [172]. The viscosity of cutting fluid was also found to be of importance with regard to tool wear [173]. Low viscosity fluid decreases tool wear, whereas the high viscosity fluid increases tool wear. Sakuma [166] investigated the effect of cutting speed on the wear rate when face turning CFRP. Several different tendencies in wear rate were observed depending on the tool material. With cermet tools, the wear rate increases almost linearly with increase in speed. When sintered carbides and

Al_2O_3.TiC ceramics are used, tool wear rate is almost constant.

2.5.6.3. The Effect of Tool Material

When machining GFRP, the transfer of heat from the cutting zone to the workpiece is very small because of the low thermal conductivity of GFRP [163]. Therefore, the accumulation of heat on the cutting edge results in higher tool temperatures. For this reason, it was recommended to use a tool material of high thermal conductivity. Ceramic tools are not suitable for GFRP machining because of the immediate appearance of cutting edge spalling, but cemented carbides and diamond tools can give a good result [142].

Sakuma et.al. [166,170] reported that, when turning CFRP, the wear rate of carbide tools was small and depended on the compressive strength and thermal conductivity of the tool, whereas the wear rate of ceramic tools was high and depended mainly on the thermal conductivity and transverse rupture strength. Thermal cracks were not observed when machining CFRP, and cutting speed had less effect on tool wear than when machining GFRP. Compressive strength and thermal expansion coefficient rather than thermal conductivity are the factors which give an improvement in wear resistance. A tool with a large thermal expansion coefficient results in an increase in tool wear, because of the increase in the contact pressure caused by the thermal expansion of the tool.

2.5.6.4. The Effect of Fibre Orientation

The anisotropic nature of FRPs results in the difference

in wear rate according to the fibre orientation.

Tsueda, et.al. [172] compared the tool wear when milling GFRP in parallel with, and perpendicular to the laminate. Rapid wear occurs when cutting parallel to the laminate because the contact pressure between the corner of the cutting edge and glass fibre becomes higher than that of other portions, resulting in larger wear on the corner of the cutting edge. However, the wear land of the tool becomes nearly parallel to the cutting edge when cutting perpendicular to the laminate.

Sakuma [163] investigated the tool wear when cutting left-hand-wound (LHW) material and right-hand-wound (RHW) material. Tool wear with LHW material was found to be larger than that with RHW material for the following reasons.

i) LHW material offers a higher cutting resistance than RHW material, because of the difference in cutting mechanism.
ii) The contact area when cutting LHW material is larger than that when cutting RHW material, so that the cutting heat is released more slowly, hence accelerating tool wear.
iii) LHW material generates more heat at the cutting edge because of the larger cutting resistance and larger contact area.

2.5.6.5. The Effect of Work Material

Tool wear is influenced by the types of fibres and resins in FRPs. The highly abrasive glass and carbon fibres cause premature rounding and chipping of the cutting edge, whereas

aramid fibres tend to cling to the tool and curl around when they are pulled out and stretched [143]. The different wear rate when machining GFRP and CFRP may result from a difference in strength. Tool wear with CFRP is higher than that with GFRP, because carbon fibres are hard to break and fibres left unbroken are subject to elastic deformation and rub the relief surface of the tool, thus accelerating tool wear [166]. When machining GFRP with carbide tools, the bonding phase shows plastic flow and is removed selectively under the influence of cutting heat, whereas when machining CFRP the hard particles are worn away mechanically.

CHAPTER 3. Experimental Techniques

3.1. Introduction

The project aims to determine the machining characteristics of thermoplastics and glass-fibre-reinforced-plastics (GFRP). Major areas of investigation include chip formation, cutting forces, surface integrity and tool wear.

Most of the experimental techniques used in this project are similar to those employed in metal cutting. Particular caution was needed during quick-stop tests and sample preparation due to the low strength of work material. Gold coating of specimens was needed to prevent charging in the SEM (Scanning Electron Microscope). Measurement of surface roughness was not carried out with GFRP, because protruding fibres on the machined surface give inaccurate results. No attempt has been made to find the tool life and optimum cutting conditions of each tool material when machining GFRP. Quick-stop technique was frequently used to investigate the chip formation and surface generation of thermoplastics and GFRP.

3.2. Work Material

Two of the most widely used thermoplastics were selected for machining; PVC as a glassy polymer, and HDPE as a semi-crystalline polymer. The properties of these two thermoplastics are compared in Table 4. The PVC work material used was unplasticized in which colour agents (pigments) were added. It is widely used because of its good physical

properties and ease of processing. The HDPE work material used is almost pure with few additives. It is a tough and flexible material which does not show brittleness. The degree of crystallinity for HDPE is generally known to be more than 85%.

Both PVC and HDPE work materials were in the form of cylindrical bars, 150mm diameter manufactured by a casting process.

GFRP work material was supplied by Tufnol Ltd., and designated RL G/1 (woven glass-epoxide grade) by them. It was in the form of a tube whose inside diameter was 160mm, wall thickness 25mm and length is 1200mm. This was halved prior to machining in order to maximise rigidity. The work material consists of two-directional reinforcements and resins. Fibre bundles were interwoven at right direction. The following information was obtained from the manufacturer.

Relative Density = 1.8

Cohesion between layers = 450 MPa

Water absorption = 0.15 mg/cm^2

The other mechanical, physical and thermal properties of GFRP material can be found in Tables 1 and 3. The tube is a rolled laminate type which was manufactured by wrap-winding sheets of glass fibres impregnated with expoxy resin on to a steel mandrel using heated pressure rollers. The tightly wound tubes are placed in heated ovens where the resin flows, on curing this forms rigid, light-weight tubes of a tough hard-wearing material.

A steel plate was fitted into the outer edge of the work

material and held by the tail stock of lathe, so that vibration was minimised.

3.3. Machining Operations

Machining was carried out using a Boehringer DM 640 lathe. The lathe has a speed selection ranging from 9 to 1800 rpm and a feed selection ranging from 0.05 to 1.8 mm/rev. Continuously variable motor current allows any surface speed to be set within the range of the machine. For speed setting, a tachometer was employed. The feed rate was intermittently checked to avoid any variation during the machining. Cutting fluid was not used in any of the trials to avoid possible damage of the plastic materials. All the experimental results were obtained using non-orthogonal turning conditions. The surface layer was removed prior to experimentation. A chamfer was cut on the outer edge of the work material, so that the entire length of the cutting edge could be engaged instantaneously at the beginning of the cut.

3.4. Tool Material

Indexable square inserts (thickness 5mm) of HSS were used throughout the machining of thermoplastics. These wrought HSS tools were M2 grade with the following composition; 0.85% C, 4% Cr, 5% Mo, 6.5% W, 2% V. Hardness of the HSS tools were measured using a Vickers hardness testing machine. The average value of three hardness measurements was 920 Hv. These tools had sharp edges without chamfers. The inserts were clamped

mechanically in rigid tool holders which were themselves held in rigid tool posts. The clamping action of the tool didn't act as a chip breaker.

Five different tool materials were used in the machining of GFRP; M2 HSS, P10 Carbide, K20 Carbide, TiC-Coated-Carbide and Triple-Coated Carbide. High-speed tools were supplied in the form of a bar, which was cut to the required size by a cutter grinder. Other tools were used in the 'as supplied' condition throughout the tests. All the carbide tools were supplied from Sandvik Ltd, and their designation are as follows.

TOOL TYPE	SANDVIK GRADE	ISO GEOMETRY DESIGNATION
P10 Carbide	S1P	SNGN 120412
K20 Carbide	H13A	SNMG 120412
Triple-Coated-Carbide	GC 435	SNMM 120412
TiC-Coated Carbide	GC 315	SNMM 120412

Composition and properties of carbide tools were obtained from the manufacturer [174].

	P-10 Carbide	K-20 Carbide
Composition (%)	55.5 WC+19 TiC+16Ta (Nb)C+9.5Co	94WC + 6Co
Hardness (Hv)	1550	1600
Grain Size (um)	2-3	1-2
Transverse Rupture Strength (N/mm^2)	1700	2200
Thermal Conductivity(W/mk)	25	100
Coefficient of thermal expansion (/K)		
20^o - 400^o	6.5×10^{-6}	4.9×10^{-6}
20^o - 800^o	7.2×10^{-6}	5.4×10^{-6}

The thickness of all the carbide inserts is 4.76 mm. Nose radius is 1.2 mm, and clearance angle is 0^{o}.

The properties of coated carbide tools were not available from the manufacturer. TiC coated carbide has only a single coating of TiC whose thickness is 5 um. Triple-coated carbide has TiN as an outer coating, Al_2O_3 as an intermediate coating, and TiC as an inner coating. The total thickness of the triple-coating is 8 um

3.5. Tool Holder

When machining plastics, the inserts were clamped in a CSDPN 2525 M12 tool holder to provide the following geometry.

Approach angle = 45^{o}

Side Rake angle = 6^{o}

Back rake angle = 0^{o}

Clearance angle = 11^{o}

Because of the elastic recovery of plastics, a high value of clearance angle was chosen to prevent rubbing between the clearance face of the tool and the machined surface.

During the machining tests with GFRP, a MSSNR/L 2525 M12 tool holder was used. The main differences from the previous tool holder are that the rake angle is -8^{o} and clearance angle is 0^{o}.

3.6. Modification of Tool Geometry

Various rake angles and nose radii were ground onto the HSS inserts to investigate their effects on chip formation,

cutting forces, surface integrity and tool wear.

A specially designed grinding fixture which could be rotated 360^{o} and be tilted in any direction was used to produce the desired geometry on the inserts.

A cutter grinder was used to remove the unnecessary part of tool material. The effective rake angle and clearance were calculated taking into account the geometry of the tool holder. Wide areas of tool rake face should be ground to prevent its role as a chip breaker. The following geometries were produced by grinding the tool face.

- Effective rake angle = -20^{o}, -10^{o}, 0^{o}, 10^{o}, 20^{o}, 30^{o}
- Nose radius (mm) = 0.25, 0.5, 1.0, 1.5
- Effective clearance angle = 10^{o}

3.7. Measurement of Cutting Forces

Cutting forces were measured using a KISTLER piezo electric dynamometer, which can record three component forces in the X, Y, and Z directions. The tool was clamped to a dynamometer to measure the cutting force in the direction of cutting, and the feed force normal to the direction of cutting. These outputs from the dynamometer were magnified by an amplifier and recorded on a chart recorder. The dynamometer was calibrated with the help of static loads before use, and frequently checked. Force measurements were made after about 5 sec of cutting and repeated to get the average value.

3.8. Measurement of Surface Roughness

A portable Surtronic 3 was used to measure the average surface roughness (Ra) The moving stylus was positioned on the surface to be measured. The direction of stylus movement was perpendicular to the feed marks. Before using the Surtronic 3, it was calibrated using a standard, known surface to achieve maximum accuracy. This device is advantageous in that it can eliminate the need to remove the work material from the lathe for each measurement. Three measurements were taken and an average value was calculated for each cutting condition.

3.9. Quick-Stop Tests

A quick-stop technique is useful in order to study chip formation and surface generation. The device used consists of a humane killer gun positioned above the tool holder which was supported by a notched shear pin (Fig 23). When the gun is fired, a solid captive bolt is projected at high speed, and drives away a pivoted tool holder from the cutting zone. The rapid removal of the tool leaves the chip attached to the work material. Sufficient clearance of the tool holder is needed to avoid interference between the tool and the workpiece when the tool moves downward very quickly.

A low cutting speed (less than 50 ^{m}/min) is required for a successful quick-stop test with the brittle PVC material. However, chip roots were successfully obtained with HDPE even at a cutting speed of 150 ^{m}/min. Three different feed rates (0.08, 0.16, 0.25 ^{mm}/rev) were used during quick-stop testing.

The depth of cut was set to 1.5 mm throughout the test. The cut was allowed to continue long enough to ensure steady conditions, after which the quick-stop test was carried out.

Quick-stop tests with GFRP are extremely difficult because of the powder-like chip form. In order to overcome this, super-glue was put on the transient machined surface to hold the powder chips together. This was successful at very low cutting speeds (15 ^{m}/min). The top surface of the GFRP chip obtained is covered by the super-glue. However, the chip under-surface and newly-machined surface are clean of adhering super-glue, enabling further investigation using a SEM.

3.10. Tool Wear Measurement

Inserts were pre-examined before the machining under the microscope to discover any faults or defects which had occurred during manufacture. Flank wear was measured after set cutting times (usually 30 sec or 1 min), using a travelling microscope. The average flank wear was measured by locating the intersection of the rake face and flank face, and measuring the flank wear from that intersection using the rake face as a reference. However, because of the high wear rates of HSS, tool measurement of progressive wear was difficult. No attempt was made to find the tool life of each tool material relative to the generally accepted criteria, because of shortage of work material.

3.11 Preparation of Specimens

Three kinds of specimens were obtained during the investigation; quick-stop specimen, work-surface specimen and tool specimen. Quick-stop specimens and surface specimens were removed with a hacksaw and mounted in a fast hardening resin in order to minimise thermal damage to the specimen. Once the resin was set, the specimens were ground on Silicon Carbide paper of 200, 320, 400 and 600 grit sizes respectively. Water was used as a lubricant. Specimens were then polished to 6 and 1 micron finishes using a nylon pad impregnated with diamond pastes. A dialap fluid was used as the lubricant during polishing.

After machining, the adhering work material on the tool was removed by immersing in hydrochloric acid (50%) for 3 minutes. Inserts were then washed ultrasonically in acetone.

Prior to SEM examination, inserts were mounted on aluminium stubs using an araldite glue. Because of the non-conductivity of the work material, a thin layer of gold was vacuum deposited to prevent charging in the SEM. The same method was used when quick-stop and surface specimens were examined using SEM.

An optical microscope was used to investigate the tool microstructure and evaluate wear mechanisms. Examination of chip root specimens using the optical microscope was also found to be useful in understanding chip formation.

Specimens of the tool were prepared by slitting the inserts using a cutter grinder (for HSS tools) and a diamond

slitting wheel (for carbide tool). These specimens were mounted in a bakelite mould with the help of a Buehler Simplimet hand mounting press. Grinding of the carbide specimens was done using diamond-impregnated plates. However, HSS specimens were found to be damaged by the hard diamond grits. SiC paper was found successful in grinding the HSS tool without damaging the structure. The grinding and polishing method for tool specimen are the same as those for quick-stop and surface specimens. The polished HSS specimens were etched with 2% Nital solution (Nitric acid in ethylene) for 1 minute, whereas the polished carbide specimens were etched with Murakami's solution (KOH and $K_3 F_e (CN)_6$) for 3 minutes.

After grinding and polishing operations, the etched specimen reveals a cross section of the cutting edge at one half of the depth of cut. The specimens were then observed using an optical microscope and photographs were taken at different magnifications.

3.12. SEM Examination

A stereoscan 90 SEM produced by Cambridge Instruments Ltd was used (Fig 24). The SEM is basically used for the production of an image of three dimensional appearance through the addition of an electron beam scanning across the surface of the specimen. The SEM was found to be very useful in this project in understanding chip formation, surface damage and

tool wear mechanisms. Studies of plastic samples were carried out at a voltage of 15KV. Some damages of the surface topography were observed at high magnification during SEM examination.

CHAPTER 4 Experimental Results

4.1 Machining of Plastics

4.1.1 Chip Formation

4.1.1.1 Poly-Vinyl-Chloride (PVC)

Investigations into the transition of PVC chip type were carried out by changing the speed, feed rate and rake angle. Fig 25 shows the transition of PVC chip type at different rake angles and cutting speeds. Continuous chips are produced at zero rake angle irrespective of the cutting speeds used. Chips tend to become discontinuous with increasing cutting speed when -20^{o} and 30^{o} rake angles are used. At a rake angle of 30^{o}, chips become completely discontinuous when the speed exceeds 75m/min, whereas at a rake angle of -20^{o}, discontinuous chips are observed only at a speed of 250m/min. Fig 26 shows the types of PVC chips at different rake angles and feed rates. The effect of rake angle is similar to that shown in Fig 25. Chips tend to become discontinuous with increasing feed rates irrespective of the rake angles used. Discontinuous chips can be found when the feed rate exceeds 0.15 mm/rev at -20^{o} and $+30^{o}$ rake angles, and 0.20 mm/rev at zero rake angle. Continuous chips are produced at the lower feed rate (0.05 mm/rev) irrespective of the rake angle used.

Figs 27 and 28 show the transition of PVC chip type at various cutting conditions. The principal types of chip have been classified into continuous, semi-discontinuous, and discontinuous chips. Continuous chips were found in a serrated

form and discontinuous chips were semi-discontinuous or fully-discontinuous, according to the cutting condition and tool geometry used. Large feed rates and large positive or negative rake angles tend to produce discontinuous chips (Fig 27). The general trend is similar at cutting speeds of 30 and 150 m/min. Continuous chips can be mostly found near the rake angle of 10^{o}. As speed increases the range over which discontinuous chips occur becomes larger, and the region of continuous chips becomes smaller.

Fig 28 shows the effect of rake angle and speed on chip types at different feed rates. Chips become more continuous when rake angles of 0^{o} and 10^{o} are used. The effect of rake angle is similar to one shown in Fig 27. Increasing feed rates results in an increased area of discontinuous chips and a decreased area of continuous chips. Continuous chips are not produced at any of the cutting speeds used when high negative rake angle (-20^{o}) and high feed rate (0.25 mm/rev) are used. Although it is not shown in Fig 28, continuous chips are always produced at a feed rate of 0.05 mm/rev, irrespective of cutting speeds and rake angles used in this investigation.

Fig 29 shows a typical continuous chip with a lamellar structure. Each lamellar has a nearly constant width of 0.1 mm. The bonding between lamellae is not complete. Tool marks can be seen running across the lamellar structure. A semi-discontinuous PVC chip can be seen in Fig 30. This chip was obtained at high cutting speed (250 m/min) and high negative rake angle (-20^{o}). The top surface of the chip is

discontinuous with intermittent gaps, whereas the bottom surface is continuous. Each lamellar has the same width as in the case of Fig 30. A segmented chip is shown in Fig 31, which was obtained at a high positive rake angle (30^{o}) and low cutting speed (25 m/min). The surface consists of intermittent smooth and rough regions due to the segmented chip formation. Large fractured areas at the bottom of the chip surface were probably produced during chip movement on the tool surface. Fig 32 shows typical discontinuous chips, which were produced at the high cutting speed (250 m/min) and high rake angle (30^{o}). The top and bottom surfaces of each chip show a different nature. The length of each chip is not uniform. The fractured surfaces have numerous cavities and voids.

A quick stop technique has been used to investigate the chip formation of PVC at the following cutting conditions.

Cutting Speed (m/min) : 30, 50

Feed Rate (mm/rev) : 0.08, 0.16, 0.25

Rake Angle (degree) : -20, 0, 20, 30

Depth of cut was set to 1.5 mm.

Figs 33-35 show the chip roots of PVC at different rake angles. The actual rake angle and the apparent rake angle were found to be different, probably because of the recovery of material after the removal of the tool. Work movement is from left to right.

Segmented chips are produced with an undulating chip thickness when -20^{o} rake angle is used (Fig 33). After quick stop testing the flow of work material was observed at the area

previously occupied by the tool nose. The undersurface of chip shows a rough surface, suggesting intermittent contact with the tool face. When zero rake angle is used, less segmented chips are produced compared to the previous conditions (Fig 34). The bonding areas between chip segments seem to have a uniform size. The surface layer visible on the machined work surface and top surface of the chip is thought to be produced during the previous machining pass. The undersurface of the chip does not follow a straight line. The discontinuity of the top surface outline of the chip was produced during preparation of the sample. When -20^{o} rake angle is used, the chip appears to be continuous but the chip root shown is the remains of the discontinuous chip (Fig 35). Unlike the previous ones, chip segmentation is not severe, resulting in a more uniform chip thickness. Fig 36 shows the magnified view of the segmented chip in Fig 33. The contact areas between segments are not uniform in size, some having small contact areas and others having large contact areas. Both top and bottom surfaces of the chip have a saw-toothed shape. Fig 37 is a magnified view of the segmented chip shown in Fig 34. The chip is reasonably continuous with a saw-toothed shape at the top and bottom surface. The white bands between the segments suggest concentration of shear in these regions.

A scanning electron microscope (S.E.M.) was found useful in investigating chip formation. Figs 38-40 show the chip roots at different rake angles. When zero rake angle was used the formation of a lamellar structure can be clearly observed

(Fig 38). Bulging of new lamellar occurred near the boundary between the previously machined surface and the top surface of the chip. When a -20^{o} rake angle was used, a segmented chip with fibrous structure was produced (Fig 39). The chip material at the tool/chip interface has oriented fibrillars along the chip movement direction. When a 30^{o} rake angle was used, discontinuous chips were produced, whose undersurface consisted of fractured and cut areas (Fig 40). The machined work surface shows large cavities produced during discontinuous chip formation.

Figs 41-43 show the chip undersurfaces at different cutting conditions. When a segmented chip is produced, the undersurface of the chip shows the step-like shape (Figs 41 and 42). Fig 42 is the chip undersurface in severe segmented chip formation. Fibrillar structures were stretched in the direction of chip movement (Fig 41). The step-like structure suggests non-uniform chip movement on the tool face, ie. stick-slip movement. In semi-discontinuous chip formation, fractured areas are intermittently spaced on the undersurface of the chip (Fig 43). The fractured areas consist of numerous voids and microcracks. A smooth surface can be seen at the area where the cutting has occurred. Deep cracks were observed across the chip width at the bottom of the fractured areas.

Fig 44 shows the lamellar structure on the top surface of a chip which was obtained at a high negative rake angle (-20^{o}), and high feed rate (0.25 mm/rev). Initiation of lamellae can be observed near the bottom of the chip. Newly generated

lamellae are short compared to the chip width. With the progress of chip movement on the tool face, these separate lamellae are joined together to form long lamellae across the chip width. Magnified views of semi-discontinuous chips show the shear front in each chip segment (Fig 45). Numerous voids can also be observed on the chip surface.

4.1.1.2 High-Density-Polyethylene (HDPE)

Continuous chips were usually produced during the machining of HDPE under the cutting conditions used. However, a segmented chip was sometimes produced at a high negative rake angle (-20^{o}) and low speed (30m/min), as shown in Fig 46. Chip thickness is not uniform, and its variation is found to be cyclic. The smooth undersurface of the chip can also be observed, with little evidence of segmentation in this region. Fig 47 shows a typical continuous chip which was produced at a rake angle of zero degree. The undersurface of the chip is quite smooth. There are no visible differences in the structure between the bulk work material and chip material. Fig 48 shows the side view of a chip root during segmented chip formation. The initiation of new lamella can be observed near the top surface of the chip. The free surface of the chip is corrugated. A magnified view of the segmented chip shown in Fig 46 can be seen in Fig 49. Compared to the free surface, the undersurface of the chip has a smooth outline. A S.E.M. photograph of the top and side surfaces of this segmented chip is shown in Fig 50. In the middle of the top surface,

regularly spaced lamellar structures can be observed. However, lamellar structures become distorted at the outer edge of the chip. Fig 51 shows the top surface of a continuous chip having a lamellar structure,which was produced at a rake angle of 0^{o} and a cutting speed of 150 m/min. Narrow gaps between the lamellae can be observed. Tool marks are shown along the direction of chip movement, which break the continuity of the lamellar structure. A HDPE chip root obtained at a high negative rake angle (-20^{o}) and low feed rate (0.08 mm/rev) is shown in Fig 52. The top surface of the chip is corrugated, whereas the bottom surface doesn't show the lamellar structure. Tool marks can be observed on the newly machined surface. Fig 53 shows the undersurface of the chip which illustrates contact conditions of different nature . The grinding marks of the tool are not observed at the bottom of undersurface, suggesting seizure conditions. Grinding marks can be seen at some distance (about 80 μm) from the cutting edge, which suggest sliding contact. The formation of shear fronts can be observed near the boundary between the previously machined surface and top surface of the chip (Fig 54). New shear fronts developed homogeneously across the chip width. The shear fronts shown are not continuous but discrete across the chip width. The number and intensity of shear fronts diminish with the distance from the cutting edge. Fig 55 shows a magnified view of the top surface of the chip produced during continuous chip formation. The surface consists of thin shear fronts which are discontinuous across the chip width, arising from the

inhomogeneous nature of chip formation. Long, straight grooves are elongated in the direction of chip movement.

4.1.2 Cutting Force and Surface Roughness

Investigations were carried out to find the effect of various cutting variables (speed, feed, and rake angle) on the cutting forces and surface roughness. Measurement of surface roughness with these plastics does not give accurate results because of the relatively soft work material compared to the stylus. Measured surface roughness sometimes gives a smaller value than the ideal surface roughness. Even though there are problems in measuring surface roughness, surface finish measurements were found useful in giving some idea about the effect of cutting variables on surface roughness. Cutting conditions used were as follows.

Test 1. : The effect of cutting speed (5-250 m/min)
Rake angle = -20^{o}, 0^{o}, 30^{o}
Feed = 0.16 mm/rev, DOC = 1.5 mm

Test 2. : The effect of feed rate (0.05-0.315 mm/rev)
Rake angle = -20^{o}, 0^{o}, 30^{o}
Cutting speed = 150m/min, DOC = 1.5 mm

Test 3. : The effect of rake angle (-20^{o} - 30^{o})
Cutting speed = 30, 100, 200 m/min
Feed = 0.10 mm/rev, DOC = 1 mm

With PVC, the variation of cutting forces with speed is dependent on the rake angles used (Fig 56). When the rake angle is 30^{o}, a big drop in cutting forces is seen at low

speeds (less than 75 m/min), whereas cutting forces do not change significantly with speed at rake angles of -20^{o} and 0^{o}. Surface roughness also does not change significantly with speed irrespective of the rake angles used. Fig 57 shows the variation of cutting force and surface roughness against feed rates when various rake angles are used. Both cutting force and surface roughness increase almost linearly with increasing feed rate, irrespective of the rake angles used. Fig 58 shows the effect of rake angle on cutting force and surface roughness at various cutting speeds. Cutting forces decrease consistently with an increase in the rake angle, irrespective of cutting speeds used. However, surface roughness doesn't show a linear relationship with rake angle. Lower surface roughness is obtained near the rake angle of 0^{o}. With a change of rake angle, positively or negatively, the surface roughness tends to increase. The result shows that the surface roughness does not have a direct relationship with cutting force.

With HDPE, a drop of cutting forces with speed was observed at low speeds (less than 25 m/min), as shown in Fig 59. With an increase of speed, cutting forces become almost constant irrespective of the rake angles used. The surface roughness also shows a big drop at low cutting speeds (less than 50 m/min). However, with increasing speed, the surface finish becomes slightly rougher. Variation of cutting force and surface roughness against feed rate is shown in Fig 60. As in the case of PVC, cutting force and surface roughness increase almost linearly with feed rate, irrespective of rake

angles used. Fig 61 shows the effect of the rake angle on the cutting force and surface roughness at various cutting speeds. The results shown are similar to those of PVC.

Fig 62 shows the variation of the cutting force and the feed force with rake angle when machining PVC and HDPE. The feed (tangential) force becomes zero when the rake angles are between 10 and 20 degrees. The critical rake angle of these plastics does not vary greatly as cutting conditions are changed.

Investigations were also carried out on the cutting mechanism by measuring the cutting forces and chip thickness. Measurement of chip thickness was found to be difficult with these plastics because of the brittleness and segmentation of PVC chips, and the softness of HDPE chips. Due to these difficulties only limited measurements of chip thickness were made. However, some estimation of shear plane angle and stresses on the shear plane can be attempted. Table 5 shows the result of the investigation. Shear plane angle, strain, and stresses on the shear plane were calculated using the equations which are usually used in orthogonal cutting conditions [8,9]. Contact length was assumed to be 3 times the undeformed chip thickness to calculate the normal stress on the tool face. Depth of cut was set to 1.5 mm during the investigation.

Average shear strains are 2.1 for PVC, and 2.7 for HDPE. Normal and shear stresses on the shear plane with PVC are larger than those with HDPE. Average normal stresses on tool face are 65 (MN/m^2) for PVC and 51 (MN/m^2) for HDPE.

4.1.3 Surface Damage

4.1.3.1 Poly-Vinyl-Chloride (PVC)

Figs 63-65 show the machined surfaces obtained from quick-stop tests. In continuous chip formation, the surface shows no sign of fracture (Fig 63). Only long straight grooves were observed along the direction of work movement. In segmented chip formation the newly machined surface shows a groove running across the chip width (Fig 64). These grooves are intermittently spaced along the work movement, suggesting intermittent fracture during chip formation. However, in discontinuous chip formation large cavities do not completely run across the chip width (Fig 65). This machined surface was obtained at a high positive rake angle (30^{o}). Tool marks were found only on the cut surfaces and they were not observed in fractured areas.

Figs 66-68 show the surfaces cut by primary and secondary cutting edges. In continuous chip formation, the machined surface shows a ductile nature without evidence of tensile fracture (Fig 66). This surface was obtained at very low cutting speeds (20m/min). Fig 67 shows the surface produced by semi-discontinuous chip formation. This was obtained at a relatively high rake angle (20^{o}) and cutting speed (100m/min). The surface consists of two distinct areas; smooth surface areas where the cutting was done, and rough surface areas where fracture occurred. The fractured areas are scattered randomly along the feed marks. In discontinuous chip formation involving tensile fracture, the surface mostly consists of

fractured areas, resulting in a very rough surface finish (Fig 68). This surface was obtained with a high positive rake angle (30^{o}).

Figs 69-71 show the surfaces obtained from quick-stop test with different rake angled tools. When -20^{o} rake angle is used, the surface shows a ductile nature having a fibrillar structure which extends along the direction of work movement (Fig 69). When a zero rake angle tool is used, the surface has a brittle nature without evidence of a fibrillar structure (Fig 70). Long, straight grooves can be clearly observed along the work movement. When a 30^{o} rake angle tool is used, the surface shows intermittent fractured areas because of partially discontinuous chip formation. Long, straight grooves are also observed (Fig 71).

Figs 72 and 73 show the effect of cutting speed during continuous chip formation. These surfaces were obtained by a zero raked tool at a low feed rate (0.05 mm/rev). No significant differences in surface nature can be observed. Both surfaces show a ductile nature with fibrous structures. Voids were observed on the surface, suggesting ductile fracture. Figs 74 and 75 show the surfaces produced by the large raked tool (30^{o}) at different cutting speeds. A significant change in the nature of the surface can be observed at the high speed because of changes in chip formation. At low speed ductile shear type chip formation results in smooth surface without areas of brittle fracture (Fig 74). With an increase in speed, discontinuous chip

formation involving tensile fracture results in a rough surface finish because of numerous fractured areas (Fig 75). Some of the discontinous chips adhere near the fractured areas and others are removed.

Feed is an important factor influencing the amount of surface damage. Figs 76 and 77 show surfaces obtained at a high cutting speed (250 m/min) and zero rake angle. Significant changes in the nature of the surface were not observed with increasing feed rate, probably because of little change in chip formation at this cutting condition. Both surfaces show numerous voids again suggesting ductile shear fracture during chip formation.

Figs 78-80 show the effect of rake angle at a cutting speed of 150 m/min. When the rake angle is -20^{o}, a fibrous structure can be observed as shown in Fig 69. Discontinuous chips were produced by shear fracture at this cutting condition, but no fractured areas were observed on the surface. At the zero rake angle, very smooth surfaces were produced with fibrous structures near the feed marks. At a rake angle of 30^{o}, large cavities were produced along the feed marks owing to discontinuous chips produced by tensile fracture. Large fragments of work material have been removed from below the generated level of the surface. Feed marks are ill-defined because of the extensive fractured areas.

Fig 81 shows a magnified view of the surface produced during continuous chip formation. This surface was obtained at a rake angle of 10^{o}, and cutting speed of 150 m/min. The

surface consists of many isolated and elongated voids, showing the ductile nature of fracture. Fig 82 shows the magnified view of a surface produced by discontinuous chip formation involving tensile fracture. This surface was obtained at a high rake angle (30^{o}) and cutting speed (150 m/min). Within the cavity, numerous voids and microcracks can be observed.

4.1.3.2 High-Density-Polyethylene (HDPE)

Figs 83-85 show the surfaces obtained from quick-stop tests using different raked tools. The surfaces were therefore cut by the primary cutting edge only. When the rake angle is -20^{o}, the surface shows intermittent cavities across the chip width around which microchips adhere (Fig 83). The size and shape of these cavities are not uniform. With an increase of rake angle, microchips disappear (Figs 84 and 85). Only long, straight grooves can be observed running in the direction of work movement.

Figs 86 and 87 show the surfaces at different cutting speeds, which were obtained at a rake angle of -20^{o}. At low speed (25m/min), the surface shows ridges perpendicular to the cutting direction. With an increase in cutting speed, these ridges disappear, and a smooth cut surface is produced.

Figs 88-90 show the surfaces machined by tools with different rake angles. They were produced by both primary and secondary cutting edges. These surfaces were obtained at low cutting speed (25 m/min). When the rake angle is -20^{o}, intermittent ridges appear on the surface cut by the primary cutting edge (Fig 88). Work movement is from the top to the

bottom. A more detailed view is shown in Fig 86. When the zero raked tool is used, a smooth surface is produced with some evidence of ridges (Fig 89). Well defined feed marks can be observed. When the rake angle is 30^{o}, ridges have almost completely disappeared (Fig 90). Work movement is from the bottom to the top. Long, straight grooves are present in the direction of work movement.

Figs 91-93 show the machined surfaces produced by tools with different rake angles. High cutting speed (250 m/min) was used in this investigation. No significant difference can be found between these surfaces because there is no change in the chip formation mechanism at these cutting conditions. A relatively rough cut surface is produced when the rake angle was -20^{o} (Fig 91). Work movement is from the bottom to the top. When the zero raked tool is used a good surface finish can be seen (Fig 92). Long, straight grooves are present in the direction of work movement. When the rake angle is 30^{o}, relatively smooth surfaces are produced with some evidence of side flow (Fig 93). The direction of work movement is from the top to the bottom.

Figs 94 and 95 show the machined surfaces produced at different feed rates. These surfaces were obtained at a rake angle of 10^{o}, and cutting speed of 250 m/min. The direction of work movement is from the top to the bottom. At a low feed rate (0.05 mm/rev), the surface shows plentiful evidence of ductile fracture (Fig 94). However, at a high feed rate (0.315 mm/rev), fracture appears to become less ductile with little

evidence of work material flow (Fig 95). Interruption of feed marks and long, straight grooves can be observed. Side flow of work material in the opposite direction to the feed is also present.

Fig 96 shows a magnified view of the surface cut at a rake angle of -10^{o} and cutting speed of 30 m/min. Elongated cavities can be seen, which differ in size and shape. Fig 97 shows the surface produced at low speed (25 m/min) and high negative rake angle (-20^{o}). Ductile work material has flown over the feed marks. Ridges were also produced on the cut surface by the primary cutting edge. Fig 98 shows the surface generated at high speed (250 m/min) with a high negative rake angle (-20^{o}). Side flow of work material resulted in intermittent bulges near the feed marks.

4.2 Machining of GFRP

4.2.1 Chip Formation and Surface Generation

The work material used has two directional reinforcement fibres which are interwoven with each other as shown in Fig 99. Numerous glass fibres are present in each yarn, and the white area near the fibres is epoxy resin which links the fibres. Fig 100 shows a cross section of the workpiece surface, in which two directional fibre bundles and resins are clearly observed. The white dots in the yarn are fibre ends.

The chip root of GFRP was obtained by the macro-chip technique using super-glue. An investigation was carried out at following cutting conditions using the quick-stop technique (Cutting speed = 15 m/min, Feed = 0.25 mm/rev, DOC = 1.5 mm, Rake angle = -5^{o}). The top surface of the chip was covered by the glue, so that only the undersurface of the chip and the newly machined surface produced by primary cutting edge could be investigated (Fig 101). Quite a rough chip undersurface can be seen in Fig 102, in which numerous fractured areas are present. No boundary between seizure and the sliding zone can be found. There is no evidence of melting on the chip undersurface or machined surface. Fig 103 shows a highly magnified view of the chip undersurface, on which fractured short fibres and cracked resins are present. Unlike metal cutting, a nearly flattened chip undersurface was not produced. Fig 104 shows the machined surface where intermittently fractured fibres and cracked resins are present. Fibres are

not pulled out and remain embedded in the surface. Contrary to Fig 104, the ductile nature of the resin can be seen in Fig 105, Debonding of resin from the fibre/resin interface and fibre breakages can also be observed. Ductile resin was stretched along the direction of tool/work movement. It seems that debonding and separation of resin were followed by fibre breakage.

The generated surface has an inhomogeneous nature because of the effect of fibre orientation (Fig 106). The fibres normal to the surface protrude, whereas those parallel with the surface are relatively undamaged and remain embedded on the surface.

4.2.2 Cutting Forces

An investigation was carried out to find the effect of cutting variables on tool forces. Cutting variables include speed, feed and rake angle. The following cutting conditions were used.

Test 1. : The effect of cutting speed

Cutting speed = 15 - 350 m/min

Feed rate = 0.05, 0.125, 0.20 mm/rev

Tool = TiC-coated carbide

Test 2. : The effect of feed rate

Cutting speed = 30, 100, 250 m/min

Feed rate = 0.05 - 0.315 mm/rev

Tool = TiC-coated carbide

Test 3. : The effect of rake angle

Cutting speed = 30 m/min

Feed rate = 0.125, 0.25 mm/rev

Rake angle = -30^{o} - $+30^{o}$

Tool = HSS

Depth of cut was set to 1.5 mm throughout the tests. Relatively small cutting forces were obtained when machining GFRP. Cutting forces decrease slightly with an increase in cutting speed, irrespective of the feed rates used (Fig 107). Cutting forces show a decreasing tendency with increasing speed at low cutting speeds (less than 50m/min). With further increase in cutting speed, cutting forces become constant.

Cutting forces increase almost linearly with increasing feed rate as shown in Fig 108. Feed forces increase less steeply compared to the cutting forces. Feed forces are larger than cutting forces at low feed rates (less than 0.10 mm/rev). Cutting forces tend to decrease with an increase in rake angle (Fig 109). Feed forces are larger than cutting forces at a feed rate of 0.125 mm/rev, irrespective of rake angle. At the given cutting condition, feed forces do not become zero as rake angle increases.

4.2.3 The Machined Surface

Investigations were carried out to find the effect of cutting variables on the surface finish of GFRP. Cutting variables include speed, feed, rake angle and sharpness of tool. Cutting conditions used are as follows.

Test 1. : The effect of feed rate (0.05 and 0.20 mm/rev)

(TiC coated carbide, speed = 150 m/min)

Test 2. : The effect of cutting speed (30 and 200 m/min)
(TiC coated carbide, feed = 0.125 mm/rev)

Test 3. : The effect of tool sharpness (sharp tool, worn tool)
(HSS tool, speed = 100 m/min, feed = 0.125 mm/rev)

Test 4. : The effect of rake angle (-20^{o}, 0^{o}, 30^{o})
(HSS tool, speed = 30m/min, feed = 0.125 mm/rev)

Depth of cut was set to 1.5 mm.

Feed rate was found to have a big influence on the incidence of fibre breakage. At low feed rate (0.05 mm/rev), the fibres were not broken and remained embedded on the surface with slight evidence of debonding (Fig 110). The resin was cracked into small pieces, but most of it remained on the surface. At high feed rate (0.20 mm/rev), severe fibre breakage can be seen (Fig 111). Most of the resin was cracked and removed from the surface. Fig 112 shows a low magnification view of the surface produced with a high feed rate. The inhomogeneous nature of the surface occurs because of the effect of fibre orientation. Work movement is from right to left. Fibres aligned along the cutting direction were not damaged much, whereas protruding and fractured fibres were produced when the fibres were normal to the cutting edge. As a result, intermittent smooth and rough areas were produced on the surface.

Glass fibres are fractured in a brittle manner as shown in

Fig 113. The fractured surface is quite smooth without showing any voids or cracks. The machined surface shown in Fig 114 suggests a combination of various fracture mechanisms, such as fibre breakage, debonding and resin cracking. Relatively clean fibre surface with little adhering resin can be seen.

Cutting speed also has some influence on the surface finish. At low cutting speed (30 m/min) relatively smooth surface can be seen with little fibre pull-out and breakage (Fig 115). At high cutting speed (200m/min), the surface becomes rougher with fractured bundles of fibres, resulting in a discontinuity of yarns (Fig 116).

Figs 117 and 118 show the effect of tool sharpness on the surface finish. When a sharp tool is used, the surface shows relatively clean debonding and broken fibres (Fig 117). Most of the resin is cracked and removed from the surface. However, when a worn tool is used severe heat generation results in decomposition of the resin (Fig 118). The ductile epoxy resin adheres to the fibres due to the high cutting temperature. Debonding and fibre breakage are not severe. Fig 119 shows the surface when using high speed (200 m/min) and a small nose radiused (0.25 mm) tool. Adhering resin on the fibre surface suggests that debonding hasn't occurred at the fibre/resin interface.

Rake angle is also an important factor in controlling surface finish. The best surface finish was obtained when using zero rake angle (Fig 120). With an increase or a

decrease in rake angle, surface finish deteriorates because of severe fibre fracture (Figs 121 and 122).

4.2.4 Tool Wear

4.2.4.1 Microstructure of Tool Material

The microstructure of HSS tool shows a number of carbides embedded in a supporting matrix (Fig 123). The carbides and martensitic matrix vary in size according to their location within the tool. The distribution of carbides is quite random. Fig 124 shows the microstructure of P10 carbide, which is a steel grade having mixed carbides. The grey coloured rounded shape is the triple carbides which have different sizes according to the location. Dark-coloured small grains are tungsten carbides. Fig 125 shows the structure of K20 carbide, which is a cast iron grade consisting of tungsten carbide and cobalt. WC grains have non-uniform sizes and shapes. Only a small portion of cobalt is present. The microstructure of the substrate of the TiC coated carbide is shown in Fig 158. This is similar to that of the K20 carbide. The microstructure of the substrate of triple-coated carbide also shows a similar structure as that of the K20 carbide (Fig 168). The exact composition of the substrate in TiC or Triple coated carbide is not available, but a high proportion of tungsten carbides can be observed.

4.2.4.2 HSS Tool

Fig 126 shows the microstructure of a worn HSS tool which

has a heat affected zone on the flank. The white band on the flank face suggests that the temperature in this region has exceeded 900°C. The darkened area below this region also results from exposure to relatively high temperatures, but the temperature in this region is lower than that experienced by material in the white band. The highly heat-affected area is not observed on the flank wear land, suggesting lower temperatures have been experienced in this region. The flank wear land shows little evidence of partial fracture or plucking. Depression of the rake face was not observed near the tool nose, suggesting the absence of plastic deformation. Moreover, deformed grains were not observed below the flank wear land.

A typically worn HSS tool is shown in Fig 127. Extensive flank wear has occurred even after a cutting time of ½ minute.Long, straight grooves are observed stretched running along the cutting direction. A close view of the flank wear land can be seen in Fig 128. A relatively smooth surface can be observed near the cutting edge. Ridges were formed on the flank wear land, below which smooth areas were produced. Adhering work material can be observed near these ridges. Fig 129 shows nose chipping when using a large raked tool (30°). Cracks can be observed in this region. Both smooth and rough surfaces were present on the tool nose. The rake face near the cutting edge shows a series of grooves parallel to the chip movement direction (Fig 130). The spacing of these grooves is not uniform, and the depth of the grooves diminishes with

distance from the cutting edge. Fig 131 shows cracks on the flank wear land which have propagated in directions both parallel and perpendicular to the cutting direction. This crack formation is localised and other areas do not exhibit cracking. Fig 132 shows the rake face, where no crater was formed. The smooth rake face shows only slight evidence of abrasive wear. Severe abrasive wear occurs even at low cutting speed (50 m/min) after a cutting time of 1 min (Fig 133). Long, straight abrasive marks can be seen on the flank face running along the direction of work movement. When a high cutting speed (200 m/min) was used, abrasive wear becomes more severe as shown in Fig 134. Adhering work material can be observed near the grooves on the flank face.

Tool nose chipping was observed at a low feed rate (0.10 mm/rev) (Fig 135). However, at a high feed rate (0.25 mm/rev), the cutting edge at the tool nose was relatively undamaged by fracture (Fig 136). Abrasive wear was found to be more severe at the high feed rate.

When the rake angle is highly negative (-20^{o}), the top of the flank wear land has a smooth surface, and grooves and ridges can be seen below this region (Fig 137). However, at a high positive rake angle (30^{o}), the smooth area at the top of the flank is smaller (Fig 138).Instead, the wear land consists of a series of ridge structures on a large scale whose spacing is between 130 and 170 um. Abrasive marks are aligned in the cutting direction between these ridges. Fig 139 shows the worn flank when a tool with a large nose radius (1mm) was used.

Little chipping was observed and the cutting edge in this region remains relatively unfractured.

4.2.4.3 P10 Carbide Tool

A typically worn P10 carbide tool shows two distinct flank wear lands (Fig 140). Removal of tool material is more severe near the cutting edge, resulting in a deeply-worn wear land. Below this region, tool wear is less severe, giving a relatively smooth wear land. Flank wear was found to be more severe near the tool nose region. No notch wear was observed at the depth of cut region. A magnified view of the flank wear land near the cutting edge can be seen in Fig 141. A small number of pulled-out carbide grains are present in this region. A highly magnified view of the flank wear land near the cutting edge (Fig 142) shows protruding carbide grains, which suggests the preferential removal of carbides. Fig 143 shows the microstructure of the flank wear land. The pull-out of aggregates of carbide grains suggests attrition type tool wear. The intensity of segregation of carbides differs according to the location.

4.2.4.4 K20 Carbide Tool

A typically worn K20 carbide shows smoothly worn flank and rake face wear lands with no evidence of catastrophic fracture (Fig 144). Plastic deformation was not observed near the tool nose. Unlike the case of P10 carbide, the intensity of flank and rake face wear is relatively uniform. A magnified view of

this wear land is shown in Fig 145. When high cutting speed (300m/min) and high feed rate (0.25 mm/rev) were used, numerous pits were observed near the tool nose and cutting edge, probably because of large scale attrition wear (Fig 146). Figs 147 and 148 show the magnified wear lands on rake and flank faces, which were obtained at high cutting speed (200m/min) and high feed rate (0.20 mm/rev). Abrasive marks are not observed on either surface. Instead, roughly worn surfaces with some protruding carbides suggest attrition wear. The intensity of attrition wear is more severe on the flank face than on the rake face. In some areas, large scale pull-out (pluckings) of carbides can be seen. The microstructure of the flank wear land is shown in Fig 149. Pull-out of carbide grains can be observed on the outer surface. However, the intensity of attrition wear is not as severe as in the case of the P10 carbide tool.

4.2.4.5 TiC-coated Carbide Tool

A typically worn TiC-coated carbide tool shows a flank wear land of uniform length, which is much shorter than that of uncoated carbides (Fig 150). Figs 151 and 152 show the wear lands at different cutting speeds. Plastic deformation of the coating can be seen even at low cutting speed (50 m/min). With an increase in cutting speed to 250m/min, the discrete plastic deformation becomes more severe. Flank wear lands show rough surfaces with some evidence of attrition wear, and the rake faces show little evidence of tool material removal.

There was no evidence of bulk plastic deformation or catastrophic failure near the cutting edge. Fig 153 shows the flank wear land produced at high cutting speed (300 m/min) and high feed rate (0.20 mm/rev). The removal of the coating is not uniform on the flank face, resulting in black and white-coloured bands.

On the rake face discrete plastic deformation in the direction of chip movement can be observed near the cutting edge (Fig 154). The length of this region is about half of the undeformed chip thickness. Beyond this region the rake surface is relatively undamaged. Fig 155 shows cracks on the rake face near the secondary cutting edge. These cracks propagate in random directions. Flaking of the coating was observed near the tool nose (Figs 156-157). A rough surface was produced on the fractured area. The non-uniform depth of the flaked area suggests that the flaking action involves fracture of the substrate as well as the coating layer. Fig 158 shows the microstructure of the flank wear land which illustrates the non-uniform removal of the coating layer, and the plucking of carbides from the substrate after the removal of the coatings.

4.2.4.6. Triple-coated Carbide Tool

A typically worn triple coated carbide shows uniformly worn flank and rake wear lands, with occasional flaking of the coating near the tool nose (Fig 159). The severity of tool wear near the nose area can be seen in Fig 160. The coating was

almost completely removed in this region, and severe wear occurs on the substrate resulting in a loss of the original tool nose shape. The fractured area near the secondary cutting edge has a brittle appearance in which both coating and substrate have been chipped off (Fig 161). Fig 162 shows the flank wear near the tool nose which is more than three times greater than the average flank wear. However, large scale fracture was not observed in this region. Fig 163 shows a magnified view of the wear lands at the middle of the depth of cut. Attrition wear on the substrate results in rough surfaces on the wear lands.

Cutting edge chipping was sometimes observed as shown in Fig 164. The depth of the fractured area (about 12 um) suggests that fracture occurred in both the coating and the substrate (coating thickness=8 um). Fig 165 shows an enlarged view of the rake face with roughly worn surfaces. The length of the rake face wear land is almost the same as the undeformed chip thickness (200 um). Discrete plastic deformation of the coating layer can be seen on the rake face wear land (Fig 166). The removal of the coating and subsequent wear concentration on the substrate can be observed near the cutting edge. Outside this region the coating layer remained on the rake face but with some evidence of plastic deformation in the direction of chip movement. The region in which plastic deformation of the coating layer occurred is within the tool/chip contact zone (undeformed chip thickness 250 um). Flaking of the coating was also observed on the rake face near the nose region, as in

the case of TiC-coated carbide (Fig 167). Moreover, discrete plastic deformation of the coating layer can be clearly observed in the tool/chip contact zone. Flaking involves the fracture of both coating and substrate. The microstructure of the flank wear land is shown in Fig 168. The coating was almost completely removed and pull-out of individual grains occurred. This proves attrition wear has occurred on the substrate.

4.2.4.7 The Effects of Cutting Conditions on Tool Wear

(1) HSS tools

The HSS tools gave the poorest performance of the tools used. Measurement of flank wear with HSS tools is difficult, because of the rapid increase in wear land length. Moreover, a clear boundary of the flank wear land is difficult to distinguish as wear progresses. Flank wear was hence measured after ½ min machining time. The effect of cutting speed and feed rate on flank wear was investigated at the following cutting conditions. Depth of cut was set to 1.5 mm.

Test 1 : The effect of speed (50, 100, 150, 200 m/min)
Feed rate = 0.20 mm/rev

Test 2 : The effect of feed rate (0.10, 0.16, 0.25, 0.32 mm/rev)
Cutting speed = 150 m/min

A significant increase in flank wear was observed when the cutting speed exceeded 100 m/min (Fig 169). The flank wear at all the cutting conditions used was far above the generally accepted wear criteria for tool rejection. An almost linear

increase in flank wear with feed rate can be observed in Fig 170. HSS tool could not withstand even ½ min cutting at any of the feed rates used.

(2) Cemented Carbide Tools

Average flank wear was measured at predetermined intervals of cutting time. The cutting conditions used were as follows.

Test 1 : P10 Carbide : The effect of speed (100, 150, 200 250 m/min)
Feed rate = 0.20 mm/rev)

Test 2 : K20 Carbide : The effect of speed (200, 250, 300 350 m/min)
Feed rate = 0.20 mm/rev

Test 3 : K20 Carbide : The effect of feed rate (0.10, 0.20, 0.25 mm/rev)
Cutting speed = 300 m/min

Flank wear increases almost linearly with increasing cutting speeds when using uncoated carbides (Figs 171 and 172). Moreover, P10 carbides gave a poor performance compapared to K20 carbides under all cutting conditions. Similar results were produced with increasing feed rates (Fig 173). The cutting time was relatively short (2 min), but flank wear at the end of the cutting time exceeded the commonly accepted wear criteria. The difference in flank wear between P10 and K20 carbides became larger as the cutting time increased.

(3) Coated Carbide Tool

The cutting conditions used were as follows.

Test 1 : TiC-coated carbide : The effect of speed (50, 150, 250, 350 m/min)
Feed rate = 0.20 mm/rev

Test 2 : Triple-coated carbide : The effect of speed (100, 150,250, 400 m/min)
Feed rate = 0.20 mm/rev

Test 3 : TiC-coated carbide : The effect of feed rate (0.10,0.20 mm/rev)
Cutting speed = 250 m/min

The effect of cutting speed on flank wear with TiC-coated carbide is shown in Fig 174. At low speeds (50 and 150 m/min), flank wear shows a rapid increase, followed by constant value, and then gradual increase with the progress of time. At high speeds (250 and 350 m/min), the acceleration of flank wear is rather steeper than at low speeds. Similar results were observed with triple-coated carbide (Fig 175). A steep increase in flank wear was obtained at a cutting speed of 400 m/min. As in the case of HSS and uncoated carbides, increasing the feed rate results in an increase in flank wear with TiC-coated carbide (Fig 176).

4.2.4.8 Comparison of Tool Performance

An investigation was carried out to compare the performance of uncoated and coated carbides at various cutting conditions. Average flank wear was compared according to the

cutting time and cutting speed with each tool material. The following cutting conditions were used.

Test 1 : Cutting Speed=250 m/min Feed rate = 0.20 mm/rev
Cutting time=5 min (with intervals of ½ or 1 min)

Test 2 : Cutting Speed=50, 100, 150, 200, 250, 300, 350, 400 m/min
Feed rate = 0.20 mm/rev, Cutting time = 1 min

The results show that coated carbides out-perform the uncoated carbides (Figs 177 and 178). Moreover, P10 carbides (steel grade) perform worse at all cutting conditions used, when compared to K20 carbides (cast iron grade). However, significant differences in tool performance were not observed with these coated carbides. Triple coated carbides showed slightly better performance than TiC-coated carbides at low cutting speeds, and the opposite result was obtained at high cutting speeds.

CHAPTER 5. DISCUSSION

5.1 Machining of Plastics

5.1.1 Critical Rake Angle

When machining PVC and HDPE, the direction of feed force (Ft) changes with an increase of the rake angle (Fig 62). The work material tends to be pulled up with a high positive raked tool, and pushed down with a high negative raked tool. Kobayashi [118] defined a critical rake angle at which feed force became zero. Several researchers [122, 127, 128] verified that the critical rake angle gave the highest dimensional accuracy, because the direction of the resultant cutting force coincided with the direction of cutting. Therefore, the work material is neither deformed into the worksurface or away from it during cutting.

From geometrical considerations (Fig 179), the critical rake angle should be related to the 'frictional' angle on the rake face. Therefore, the critical rake angle (Ac) can be expressed as follows;

$$Ac = f\,[\tan^{-1}(F/N)]$$

(where N is the normal, F is the shear force on the rake face.

Table 6 shows a comparison of the ratio of shear to normal force on the rake face when machining plastics and metals. To ensure compatability of results, all materials are compared at a rake angle of 6^{o}.

The results show that ratio of forces for plastics is

lower than that of metals, and hence the magnitude of critical rake angle is lower. Fig 180 shows the simplified force diagram on the rake face at zero rake angle, where the direction and magnitude of normal and shear forces are the same as those of cutting and feed forces. Because of the lower ratio of forces, these plastics (PVC and HDPE) will have a resultant force which is directed closer to the direction of the normal force. With an increase of rake angle, the direction of the resultant force rotates clockwise in relation to the external measured force system, but gives an approximate constant angle with the rake face. At some rake angle, the resultant force will be in the direction of cutting. With metals, a large rake angle will be required for this condition, thus a large critical rake angle occurs.

Different ratios of forces may occur as the rake angle varies. Since the above discussion ignores the effect of contact lengths and other possible variations, the actual ratio of forces will probably be larger at negative rake angles and smaller at positive rake angles.

Even free cutting steel, in which the shear force on the rake face is minimised by inclusions, was found to have a larger ratio of forces (hence critical rake angle) than these plastics. It is known that, when machining free machining steel, a shorter contact length also results in low feed forces [9]. Moreover, cast iron, which has lower shear forces than the free cutting steel, could be expected to have low forces on the rake face, but the ratio of forces is larger. This

suggests that the magnitude of shear force on the rake face does not have controlling influence on the critical rake angle. In the above examples, the addition of weak second phases affects not only the rake face forces but also the primary shear plane forces and hence both the normal and feed forces measured externally are affected. The small ratio of shear to normal force for plastics can be attributed mainly to the low shear force on the rake face, probably because of weak bonding which allows easy chip movement on the tool face.

5.1.2. Chip Formation

5.1.2.1 PVC

(1) Segmented Chip Formation

A segmented chip is a continuous chip with a periodic but asymmetric variation in chip thickness as shown in Figs 36 and 37. This kind of chip is usually observed with stainless steel, titanium alloys, high strength steels, and nickel base superalloys [54].

PVC segmented chips consist of a series of lamellar structures as shown in Figs 38 and 44. These structures may have resulted from the inherent properties of PVC such as strain-softening or poor thermal conductivity. Fig 181 shows the strain-softening of glassy polymers. As the stress increases after yield, the flow stress decreases slightly (strain-softening) and then increases again (orientation-hardening) [175]. This strain softening is an intrinsic property of glassy polymers, and may result from structural

changes which allow the deformation to continue at a lower stress before the molecular chains are aligned. Strain-softening can also be observed with titanium. In this case it is due to micro-cracking at large strains with a consequent decrease in the effective area of the stressed material [28,31]. The average shear strain of 2.1 for PVC in the primary deformation zone is much bigger than the shear strain (0.8-1.0) at which strain-softening occurs.

On initial deformation, the strain in some regions will be larger than elsewhere. Because of the effect of strain-softening, the material at this point becomes softer locally (Fig 44). The low thermal conductivity and low specific heat of PVC will encourage a localised softening because of the heat arising from plastic strain on the shear plane. This causes more strain to occur locally on the shear plane and more deformation energy will be spent in this region. Shear continues in this region with the shear plane rotating because of material flow. However, when the shear plane angle increases to a certain value (more than 45^{o} for 0^{o} rake angle), the shear strain required increases (Fig 182). This being energetically unfavourable, a new part of the structure will begin to shear, resulting in a rotation of shear plane in the opposite direction. Therefore, the shear plane will oscillate. The shear plane thus jumps to the next weak region leaving the material between the two positions relatively unstrained.

It may be reasonable to suggest that plastic shear occurs intermittently during segmented chip formation. At the initial

stage, compressive stress is built up until it becomes large enough to initiate the shear on the shear plane. Unlike discontinuous chip formation, complete fracture will not occur because cracks will be arrested as a result of a decrease in the shear strain as the plastic zone rotates towards the tool [176].

The highly deformed area (shear bands) can be observed between the segments (Fig 37). It suggests that shear deformation is concentrated in these bands. Compared to the case of titanium, the undersurface of a PVC segmented chips is not flattened (Figs 36 and 37). The almost planar chip undersurfaces of titanium result from high normal stress and seizure conditions at the tool/chip interface. The chip movement over the tool face is accompanied by considerable plastic deformation of the chip undersurface. It seems that relatively low normal stress and weak bonding result in a rough undersurface of the chip when machining PVC. Relatively low shear force probably results from the small contact area, because the contact area is only at the apex of each segment. However, the bottom of chip segments becomes nearly flattened near the tool nose (Figs 33 and 34) probably because of higher normal stress in this region. More segmented chips can be found with the distance from the cutting edge due to the decrease of normal stress, which allows the relative movement of chips on the tool face.

The lamellar structure on the top surface of the chip in Figs 38 and 44 is due to discontinuous shear, in which the

lamellae themselves are not sheared. New lamella is formed intermittently across the chip width, because of inhomogeneous strain softening on the work material. However, with the progress of cutting, the intermittently generated lamellae are combined to form continuous lamellae across the chip width.

No evidence of melting in the bulk of the chip suggests that the cutting temperature is below the melting point of PVC. Segmented or discontinuous chips do not produce much heat in the primary deformation zone, because there is little plastic deformation. Moreover, the weak bonding and rolling movement of chip segments over the rake face will not produce much heat at the tool/chip interface. However, a fibrous structure on the chip undersurface was sometimes observed at high negative rake angles as shown in Figs 39 and 41. This may be partially due to the effect of the quick stop technique. Fibrous structures suggests that the effect of temperature is such as to cause considerable ductility, outweighing the embrittling nature of strain rate on the tool/chip interface. No evidence of viscous (fibrous) structure is seen in the primary deformation zone which suggests that the effect of strain rate may be more significant in this region than that of temperature. Therefore, the yield strength at the tool/chip interface is lower than that along the primary deformation zone, and this facilitates the formation of fibrous structures.

(2) Discontinuous Chip Formation

As in the case of metal cutting, both ductile shear and

brittle tensile fracture were observed during discontinuous chip formation according to the cutting variables used.

Discontinuous chips formed by ductile shear are produced on the shear plane where the shear stress is maximum as in the case of continuous chip formation. This type of chip formation is usually observed at high negative rake angles, high cutting speeds and high feed rates (Figs 25-28). As in the case of segmented chips, thermal softening and low thermal conductivity of the work material enhance discontinuous chip formation by a reduction in strength of the material in the primary shear zone. The main difference from segmented chips is that the ductility of the work material is completely exhausted in discontinuous chip formation, resulting in complete fracture across the shear plane. The machined surface is not involved in the fracture in this type of discontinuous chip formation. There is thus an absence of cavities on the surface (Figs 77 and 78).

Discontinuous chips formed by tensile fracture are produced near the tool point due to the cracks which result from tensile stress concentration. Then the ductility of work material will be exceeded, resulting in rapid propagation of cracks at a downward angle from the cutting point leading to rupture along the plane of maximum shear stress [20,37]. This type of chip formation occurs at high positive rake angles, high cutting speeds and high feed rates (Figs 25-28). It does not involve fracture on the shear plane. Large cavities were produced on the machined surface because of tensile fracture

near the tool nose as shown in Figs 68 and 80. Figs 40 and 43 show the discontinuous chips formed by tensile fracture, in which the intermittent cutting and fracture regions are present. It may result from the build-up of tensile stress to initiate a crack near the tool point.

5.1.2.2 HDPE

Continuous chips are always produced when machining HDPE. Again this is probably structure dependent, HDPE being a semi-crystalline polymer. The rubbery state of the amorphous regions helps the crystals deform plastically without catastrophic fracture [111]. Therefore, most of the energy will be spent in plastic deformation before fracture. Contrary to atomic solids like metals, in which all the individual crystals are close in contact with other crystals along the boundaries, polymer crystals are embedded in amorphous, rubber-like medium and deformation can only involve sliding of molecules relative to one another, which breaks only secondary Van-der-Waals or hydrogen bonds [114]. Fracture of polymer chains requires much higher stresses.

At room temperature, tensile elongation of HDPE is about 15-200%. The calculated shear strain on the primary shear zone of HDPE is about 2 to 3 (table 5). Therefore, shear strain is larger than the fracture strain. In metal cutting, continuous chip formation occurs, because of the effects of increased temperature and compressive stress on the shear plane, and seizure conditions at the tool/chip interface. High

temperature and compressive stress on the shear plane enable the work material to withstand more strain before fracture. Seizure conditions suppress fracture in the primary deformation zone by increasing the compressive stress which makes the material more ductile. However, unlike metals and glassy polymers, seizure contact does not appear to be necessary for continuous chip formation with HDPE. This is because polyethylene becomes more brittle when the pressure is increased, resulting in fracture at lower strains (Fig 183). Therefore, with HDPE, seizure contact has an opposing influence on the continuous chip formation. The reason for continuous chip formation is hence the unique deformational behaviour of HDPE, rather than seizure contact. Compressive stress on the primary shear zone was approximately 40 MN/m^2 when machining HDPE. This compressive stress is small and thus its influence on fracture strain is very small. Even though there is a change in compressive stress when the rake angle is changed, the change of fracture strain can be neglected. Therefore, there is no abrupt change of chip type when the rake angle is changed. It is reasonable to state that continuous chips are more apt to occur when the compressive stress on the shear plane decreases, which is contrary to the case of metals and glassy polymers.

Close examination of the top surface of the HDPE chip in Figs 50, 51, 54 and 55 illustrates that the chip formation is not homogeneous, probably because of plastic instabilities. In glassy polymers, strain-softening is responsible for plastic

instabilities, but, in semi-crystalline polymers, rapid strain hardening masks any possible strain-softening [113,175]. It seems that these plastic instabilities are due to the unique nature of the microstructure, resulting in different deformational behaviour of amorphous and crystalline regions. The amorphous region is rubbery enough to undergo plastic deformation, whereas the crystalline region is more resistant to deformation. Moreover, the presence of impurities or low molecular weight additives such as moisture or organic liquids may produce a softening as well as a weakening effect [112]. Therefore, plastic strain in some local regions may increase more rapidly than in others, However, the degree of regional softening is not as significant as with PVC, resulting in nearly uniform chip thickness but with some evidence of a lamellar structure.

A distorted lamellar structure at the free surface of the chip may result from side flow of work material (Fig 50). As the free edge of the chip is in plane stress instead of plane strain conditions, side flow of material brings about larger plastic deformation when compared to the central portion of the chip [177]. Moreover, the ductile nature of HDPE chips promotes side flow to the chip edge.

The segmented chip with a lamellar structure was observed only at high negative rake angles, as shown in Figs 49 and 50. During segmented chip formation, the deformation may be more concentrated in thin shear bands between the segments. The crystallinity of HDPE is known to be more than 85% [106].

Relatively small volumes of amorphous region (less than 15%) seem to influence the degree of segmented chip formation. It is not clear why the plastic instability observed in continuous chip formation is enhanced by the high negative rake angle, but increased strain and the increased compressive stress on the shear plane may play a part. Increase in strain-rate and temperature are discounted as these are associated also with an increase in cutting speed, and this does not accentuate the lamellar chip structure.

Many researchers [23,32,35,54] attributed titanium segmented chips to the plastic instabilities caused by low thermal conductivity. The thermal conductivity of plastics is much lower than that of titanium. However, HDPE rarely exhibits segmented chips and usually produces continuous chips with a uniform thickness. As discussed earlier, the low thermal conductivity of work material like titanium results in segmented chips by forming a locally softened area which allows for the oscillation of shear plane angle during chip formation. However, this phenomenon is not significant with HDPE. Therefore, it can be said that the main reason for the segmented chip with titanium or PVC is not the low thermal conductivity. Instead, the detailed deformational behaviour of work material during cutting seems to control the segmented chip formation and with PVC this appears to involve strain softening.

5.1.2.3 The effects of Cutting Variables

(1) Cutting Speed

Cutting speed was found to be an important factor influencing the chip type when machining PVC, as shown in Figs 25 and 28. Both tensile and shear fracture are encouraged with increasing speed. Increase of cutting speed results in two opposing effects; an increase in strain rate which increases the yield strength and reduces the ductility, and an increase in cutting temperature which results in decrease of yield strength and increase of ductility. Both types of fracture will be facilitated when the work material exhausts the ductility, which suggests that the dominant effect when increasing cutting speed is strain-rate.

In shear type chip formation, increased cutting speeds result in a decrease in the strain to fracture on the shear plane due to the effect of strain rate, leading to discontinuous chip formation. However, at low cutting speeds, the material properties even at low temperatures are such that the material can undergo greater strain before fracture, resulting in a tendency for continuous chip formation. When machining steel, discontinuous chips are usually produced at low cutting speeds because of the presence of an oxide layer which suppresses seizure conditions at the tool/chip interface [178]. Continuous chips in steel are usually produced at high cutting speeds because the uniform chip flow on the tool face removes the oxide layerat the interface, hence promoting seizure contact[9]. The opposing transition of chip type with

PVC compared to that with steel can be attributed to the viscoelastic nature of PVC. It comes from the inherent flexibility and relaxation behaviour of the molecule chains of polymers [111, 113]. The strong effect of strain rate at high cutting speeds is due to the increase in the number of molecular bonds which resist deformation, because the stress relaxation velocity is unable to follow the deforming velocity [118]. Moreover, at low strain rate, the molecular chains in polymers have time to align themselves under the influence of the applied stress, resulting in viscous deformation. The opposite will happen at high strain-rate.

Cutting forces decrease with an increase of speed at low cutting speeds when machining PVC and HDPE, but they become almost constant with further increase of cutting speed (Figs 56 and 59). An increase in cutting speed results in an increase in temperature at the primary and secondary deformation zone, leading to a decrease in the flow stress of the work material. This may produce an increase in shear plane angle and hence a decrease in cutting forces. It seems that, at high cutting speeds, the effect of temperature on the flow stress of the work material is balanced by that of strain-rate, resulting in constant cutting forces.

(2) Feed Rate

Discontinuous chips formed by shear or tensile fracture are prevalent at high feed rates when machining PVC (Figs 26 and 27). An increase in cutting forces with feed is similar to

that observed in metal cutting (Figs 57 and 60).

An increase in feed rate can result in two opposing effects; increased cutting temperature which decreases the compressive stress on the primary shear zone and increased contact length which increases the compressive stress in that region.

In the case of tensile fracture, the total compressive stress should be a minimum to allow a build-up of the tensile stress state near the tool point. Thus increases in the temperature which decreases the materials properties may aid fracture.

In the case of shear fracture, compressive stress on the shear plane should also be the minimum amount required to initiate the fracture because compressive stress increases the ductility of the work material (Fig 184). The negligible effect of contact length may result from segmented type chip formation where the contact area is smaller than that in continuous chip formation. Decreased compressive stress on the shear plane will decrease the fracture strain on the shear plane, leading to the tendency for discontinuous chip formation. An increase of cutting temperature with increasing feed rate arises from an increase in contact length (contact time) in the secondary deformation zone. High cutting forces at high feed rates can mainly be attributed to the increased amount of work material being sheared (Figs 57 and 60).

(3) Rake Angle

Rake angle is an important factor influencing PVC chip type. Discontinuous chips were observed when increasing the rake angle positively or negatively (Figs 25-28).

Tensile fracture at high positive rake angles can be attributed to the decrease in compressive (shear) stress near the tool point, which promotes a tensile stress state in this region. PVC's relatively low tensile strength compared to the compressive strength may accentuate the discontinuous chip formation. However, in metal cutting, continuous chips are more apt to occur with an increase of rake angle, probably because of their relatively high tensile strength.

Shear fracture at high negative rake angles when machining PVC is similar to that in metal cutting. Shear strain on the shear plane increases with a decrease of rake angle due to the geometrical constraint (Fig 182). Excessive shear strain on the shear plane will exhaust the ability of work material to strain in a ductile manner. When the shear strain is larger than the fracture strain of the material, discontinuous chips are produced. Tensile fracture was not observed at high negative rake angle, because the high compressive state near the tool point suppresses crack formation. The cracks are preceded by a large amount of plastic flow near the crack tip. However, there is an opposing effect of increased compressive stress on the shear plane, which makes the material ductile. There is no information available about the deformational behaviour of PVC under compressive pressures at this time. However, when applying the data in Fig 184, the change of

fracture strain with change of rake angle from 0^{o} to -20^{o}, is less that 0.02, which is negligible when compared to the total shear strain (2-3). Therefore, it can be said that the change of compressive stress on shear plane with rake angle is too small to influence the chip type.

Continuous chips observed near zero rake angle can be attributed to the fact that the ductility of work material is not exhausted by the chip forming process. The absence of excessive shear strain on the shear plane and tensile stress state near the tool point suppresses discontinuous chip formation.

A decrease in cutting forces with increase in rake angle (Figs 58 and 61) can be attributed to the decrease in contact length and shear strain on the shear plane. This may result in an increase of shear plane angle.

5.1.2.4 Tool/Chip Interface

The undersurface of a PVC chip in Fig 41 shows that seizure contacts are intermittent at the tool/chip interface. In metal cutting, bonding is strong enough to cause seizure contact, in which the chip shears rather than the interface moving [9]. During segmented chip formation with PVC, the stick-slip movement of the chip is reasonable. This movement was also observed by Komanduri [28] when machining titanium. As cutting progresses, work material bulges, and sticks to the tool face as shown in Fig 38. When the shear stress is sufficient, shear occurs intermittently along the shear plane.

Similar results were observed in metal cutting by Cook et al. [22] and Sullivan [176]. Weak atomic bonding at the junctions between the PVC chip and the tool face may suppress the seizure contact. Moreover, the estimated normal stress on the tool face is quite low with PVC ($65MN/m^2$) and HDPE ($51MN/m^2$), compared to that with medium carbon steel ($770\ MN/m^2$) [9]. When compared to the tensile strength of these materials, the ratios of the normal stress to the tensile strength of these plastics are higher (PVC - 1.6, HDPE - 1.8) than that of steel (1.1). This result will be favourable for the seizure contact with these plastics.

Seizure contact was also observed with HDPE (Fig 53). Stick-slip chip movement was not observed with HDPE, because of the continuous-shear type chip formation encouraged by the absence of strain-softening behaviour. Longitudinal scratches (tool marks) on the chip undersurface start at some distance behind the cutting edge, suggesting both seizure and sliding contact. Despite weak atomic bonding at the interface, seizure contact may occur because of the relative softness of HDPE, which facilitates one-to-one contact by the interpenetration of hard asperities on the tool face. During chip movement, the harder asperities remove the soft ones by the combined effects of micro-ploughing, micro-cutting and micro-cracking [179,180]. Sliding movement at some distance behind the cutting edge can be attributed to the decrease of normal stress on the tool face.

Built-up-edge (BUE) was not produced when machining PVC

and HDPE. It is generally acknowledged that single phase materials cannot produce BUE because they cannot produce high yield stress by strain-hardening at the tool/chip interface and yield strain cannot be maintained at high temperature [181]. For this reason, single phase material like PVC cannot produce BUE. Wallbank [178] states that BUE is produced due to the strain incompatibility between phases which leads to microcracking. It seems that the absence of BUE with HDPE is due to the rubbery state of the amorphous region which absorbs most of the plastic deformation and suppresses microcrack formation. Moreover, weak atomic bonding at the tool/chip interface may suppress BUE formation.

5.1.3 Surface Integrity

5.1.3.1 Surface Damage

Many kinds of surface damage were observed when machining PVC and HDPE; these are grooves (tool marks), cavities, fibrous structures, feed marks, voids, cracks, microchips, work debris, ridges, and side flow. Some of them are similar to those observed in metal cutting, whereas others are unique, and can be observed only when machining plastics.

The structure and properties of the work material influence the surface damage. Several researchers [182,183,184] investigated the surface characteristics of polymers after sliding. With long chain polymers like polyethylene, the surface layers may consist of molecules drawn out in the direction of motion, so that sliding actually occurs

over very highly orientated material. Therefore, evidence of catastrophic fracture areas or cavities may not be observed. Moreover, the crystals in HDPE may act as anchorage points for the molecules preventing molecular pull-out [111]. However, with brittle and entangled-chain polymers like PVC, the material will be torn, sheared, and heavily distorted and chain rupture may occur. The presence of chain entanglement and side groups usually increase the strength by making interchain sliding more difficult. Therefore, there will be more fracture of molecular chains with PVC than with HDPE, resulting in surface defects.

The type of chip formation has a significant influence on the surface finish when machining PVC. During continuous chip formation, shear fracture occurs in a ductile manner with the formation of microcracks and voids on the machined surface. (Figs 72,76 and 81) These voids may have originated from defects in the work material such as flaws, air bubbles or molecular inhomogeneity which act as stress concentrators [113]. The ductile nature of the surface suggests that the cutting temperature is above T_g.

During segmented chip formation the surface shows long, straight grooves parallel to the cutting edge (Fig 64). These grooves may result from cracks associated with plastic instabilities which influence the chip thickness. A surface of a similar nature was obtained by Turley and Doyle [45] when machining titanium.

During discontinuous chip formation, the nature of the

machined surface is dependent on the type of fracture. Shear fracture does not involve fracture on the surface as in the case of continuous chip formation (Fig 77). However, tensile fracture produces numerous fractured areas (cavities) on the surface, the number of which is dependent on the severity of fracture (Figs 65,67,68,75 and 80). A magnified view of these cavities in Fig 82 suggests that they originated from the voids which were formed during deformation which then grew and coalesced to form large cavities. During the deformation, void formation may be easier than rupture on a large scale, because the rupture stress is much larger than the stress required to nucleate the voids [111,175]. The fracture process may be highly localised near the voids resulting in brittle fracture.

Tool marks (grooves) were frequently observed with PVC and HDPE. They are produced by the ploughing action of hard asperities on the tool during relative movement. It is an abrasive type of surface damage. These grooves were only observed in non-fracture areas as shown in Fig 65, probably because tensile fracture masks the groove formation.

Feed marks were clearly observed with both materials. They are in the form of ridges which correspond to the tool geometry at its nose, and their separation is equal to the feed rate. Tensile fracture of the feed marks were observed during discontinuous chip formation (Figs 67 and 68).

Side flow of work material was observed on the HDPE surface (Figs 93,95 and 98). Since the material near the trailing edge of the tool is subjected to high compressive

stress, it will flow to the side to relieve the stress [53]. The displacement of surface material is in the direction of the surface already generated in previous revolutions.

Fibrous structures were often observed with PVC and HDPE as shown in Figs 69,78,94 and 97. They indicate the high cutting temperature and sliding contact without catastrophic fracture. They may be formed from the asperities of soft work material which was torn out and drawn along in the direction of work movement. During plastic deformation of HDPE, the stacked crystals are cracked and chains are pulled out, so that molecules and crystal blocks align themselves along the force direction resulting in fibrillar structures [113]. Therefore, these fibrous structures are obtained when the applied stress is large enough to break the original lamellar structure.

Microchips were observed on the surface of HDPE (Fig 83). Asperities of ductile HDPE are easily deformable, so that they can be drawn in the direction of stress. With the progress of cutting, they ultimately break off and roll between the sliding component. Cocks [185] and Nakayama [46] investigated microchip formation in metal cutting. Microchip formation occurs through the process of shear with the development of a deformation zone similar to that normally associated with the production of chips. Fewer microchips are observed with these plastics and this can be attributed to the softness of work material, which facilitates the easy penetration without shearing at the tool/work interface. It is known that rigid work material prevents the asperity from raising far above the

general level of the machined surface, resulting in little microchip formation [186]. Because of the big difference in hardness between these plastics and the tool, the hard asperities on the tool face usually make deep grooves instead of producing microchips (Figs 70,84, and 85).

Elongated cavities were observed on the HDPE surface during continuous chip formation (Fig 96), which suggests that there has been ductile fracture with large amounts of plastic deformation. These cavities may occur when the microvoids formed during plastic deformation, grow and coalesce.

5.1.3.2 The Effects of Cutting Variables

(1) Cutting Speed

With PVC, surface characteristics are closely related to the type of chip formation. At zero rake angle, the effect of cutting speed on surface damage is not significant because continuous chips form at both cutting speeds (Figs 72 and 73). However, different surface characteristics can be observed with increasing speed at a rake angle of 30^{o} (Figs 74 and 75) As discussed before, discontinuous chip formation by tensile fracture is apt to occur at high positive rake angles and high cutting speeds, resulting in cavities on the machined surface.

With HDPE, the effect of speed on surface finish is not significant (Figs 86 and 87) because of little change in the mechanism of chip formation. It may be because ductile HDPE requires large amounts of plastic deformational energy to uncoil and displace the molecules. Relatively rough cut

surface at high speed may result from the effect of increased temperature, which promotes pressure bonding. Small voids may be produced during separation at the tool/work interface. Nakayama [46] reported that fewer microchips could be produced at high cutting speeds, because thermal softening of the work material resulted in recession of asperities downward into the surface of work material.

Almost constant surface roughness was produced with PVC when increasing cutting speed (Fig 56). At rake angles of -20^{o} and 0^{o}, discontinuous chips by shear fracture tend to be produced at high cutting speed, which do not lead to a big increase in surface roughness. The constant surface roughness with speed at 30^{o} rake angle is contary to expectation, because discontinuous chips produced by tensile fracture are generated at high speed as shown in Fig 80. Although not observed, the movement of the stylus may be confined to the smooth cut surface or the boundary of the cavities. Moreover, big differences in hardness between the diamond stylus and PVC may result in penetration of the stylus into the work surface leading to a false measurement. With HDPE, the results show a high surface roughness at low cutting speeds and constant values at high cutting speeds (Fig 59). This decreasing tendency can be attributed to the dominant effect of temperature with increasing speed, which leads to homogeneous surface generation.

(2) Feed Rate

With PVC, the effect of feed rate on surface finish is significant, because of its influence on chip formation. Ductile fibrous structure at low feed rate (Fig 76) results from continuous chip formation. Significant differences were not observed at high feed rate (Fig 77), probably because of the discontinuous chip formation by ductile shear fracture. Numerous voids on the surface suggest the ductile nature of fracture. Similar results were observed with HDPE as shown in Figs 94 and 95.

A linear increase in surface roughness with feed rate was observed with both PVC (Fig 57) and HDPE (Fig 60). This results from an increase in the ideal surface roughness with feed rate.

(3) Rake Angle

Rake angle has a big influence on surface finish when machining PVC because it controls the type of fracture during chip formation. Figs 78-80 compare the machined surface produced at different rake angles. The smooth surface with high negative rake angle is due to discontinuous chip formation by shear fracture. The absence of cavities at this condition may be due to the large hydrostatic compressive stresses and high temperature at the interface which prevent the propogation of the cracks formed around the cutting edge. As discussed earlier, high positive rake angles induce discontinuous chip formation by tensile fracture resulting in cavities on the

machined surface (Fig 80). These results coincide with the results of measurements of surface roughness (Fig 58).

With HDPE, microchips are produced at high negative rake angles, probably because of the strong bond at the tool/work interface which arises from the high temperature and high normal stress at the junctions (Fig 83). Microchips disappeared as rake angle was increased as shown in Figs 84 and 85. Instead, long, straight grooves were produced probably because of low normal stress on the work surface which facilitates a ploughing action by the hard asperities on the tool face, on the soft work surface.

Rake angle has a greater effect on the surface of HDPE at low rather than high cutting speeds (Figs 88-93). Intermittent ridges on the cut surface at low cutting speed and high negative rake angle may be related to segmented chip formation, as discussed earlier (Figs 49 and 88). These ridges may result from the variation of chip thickness during segmented chip formation, and an increase in contact bond with the flank face. The disappearance of ridges with an increase of rake angle and feed rate can be attributed to homogeneous continuous chip formation (Figs 65-69).

5.2 Machining of GFRP

5.2.1 Chip Formation

During machining of GFRP, the chips produced are in the form of fine powder, suggesting little plastic deformation during the cutting process. The proportion of cutting energy

consumed by shearing in the primary shear zone is believed to be relatively small. The fine powder chips result from the brittleness of both glass fibres and epoxy resins. The fracture strains of glass fibres and epoxy resins are only 3-5%. The brittleness of glass fibres results from the amorphous structure [140]. Epoxy resin is also a non-crystalline, hard brittle solid due to chemical cross-linking which leads to the formation of a tightly bound three-dimensional network of polymer chains [134]. Therefore, GFRP chips cannot withstand a large amount of plastic deformation as is generally the case with metal cutting. Lumpy types of chips were sometimes observed at high cutting speeds probably because cutting temperature exceeds the glass-transition temperature (Tg) of epoxy resin (150^{o}C). Above Tg, epoxy resin has a ductile nature promoting sticking of the powder-like chips.

Investigation of chip formation was carried out using a macro-chip technique, as shown in Fig 101 and Fig 102. The absence of cavities on the newly machined surface suggests that discontinuous chips were produced by shear fracture near the shear zone, rather than tensile fracture near the cutting edge. For this reason, cracks didn't propagate down into the workpiece. Fracture in the shear zone may arise from the excessive shear strain compared to the relatively small amounts of fracture strain of GFRP. The cutting process consists of a series of fractures in the shear zone. Moreover, the large difference of thermal expansion between the fibres and resins may accentuate the fracture process. Completely discontinuous

chips do not generate much heat in the primary shear zone, so that significant thermal softening of work material in this region will be absent, promoting discontinuous chip formation.

The underside of the chip shows a combination of broken fibres and cracked resin (Figs 102 and 103). There is no evidence of seizure contact at the tool/chip interface, probably because protruding fibres prohibit intimate contact between the chip and the tool face. The exposed fibres on the chip undersurface will support most of the applied normal stress, and hence reduce the penetration of the asperities on the tool face into the chip surface. Therefore, the real contact area becomes smaller than the apparent contact area, promoting sliding contact at the tool/chip interface. Relatively small forces will be required to move the chip on the tool face because of weak atomic bonding and sliding contact conditions. In sliding conditions, chip movement is by the shearing of junctions formed at the region of real contact between chip and tool face. Since there is no constraint on the rake face, chips can move easily with no further deformation. The absence of seizure contact could be another factor promoting discontinuous chip formation. Contact pressure on the chip/tool interface when machining GFRP is less than 200 MN/m^2, which is much less than that when machining steel (770 MN/m^2) [9]. When contact pressure is compared to the compressive strength of the work material, the ratio of contact pressure to compressive strength with GFRP is still lower (less than 60%) than that with steel. Relatively low

normal stress compared to the compressive strength of the material can facilitate sliding contact, so that broken fibres can move along the interface. The strength of the resin can also be an important factor which influences the contact condition. Weak resins may increase the contact area because they facilitate pull-out of fibres from the chip undersurface, and the penetration of hard asperities of tool into the weak resins. Pulled-out fibres may break other fibres during sliding under the influence of the normal stress, resulting in fibres of very short length as shown in Fig 103.

5.2.2 Heat Generation

Investigation of heat generation when machining GFRP was carried out by observing the microstructural change of HSS tool, as shown in Fig 126.

There are three heat zones during the machining, namely primary and secondary deformation zones, and the tool flank [8]. Heat generation at the primary deformation zone when machining GFRP is very small, because there is little deformation in discontinuous chip formation. Most of the heat is generated by the material rubbing the tool flank as evidenced by the light etching band in this area. The cutting temperature in this region is believed to be more than 900^{o}C.

Having a relatively low temperature on the rake face is quite different from when machining steels, where the maximum temperature occurs about half way along the contact length on the rake face, as a result of extremely high shear stress

present in the flow zone under seizure condition [9]. The sliding contact at the tool/chip interface when machining GFRP results in a lower interface temperature because a smaller amount of work is required to shear the isolated junctions. Therefore more heat will be generated at the tool/chip interface with GFRP. With steel, heat is generated near the interface due to the development of a secondary shear zone as strong bonding occurs across the interface.

Rapid flank wear may result in excessive heat generation at the flank face. Large flank wear results in a loss of the tool clearance, promoting further heat generation. The low thermal conductivity of GFRP also leads to the accumulation of heat at the cutting face. Some researchers [163] reported that 90% of the heat was conducted to the tool when machining epoxy/glass material. The cutting edge encounters the glass fibres almost constantly, some of these are discharged as chips and other are pushed under the clearance face of the tool. Therefore, the cutting edge is constantly heated.

Hard glass fibres can quickly wear away the flank face. Therefore, this region is still at a low temperature and stronger, compared to the bottom of the flank face which rubs with the work material continuously. The depth of the heat-affected zone at the flank wear land increases with the distance from the cutting edge.

5.2.3 Surface Integrity

5.2.3.1 Surface Characteristics

During the investigation, many kinds of surface damage modes were observed; these are fibre breakage (fracture), resin cracking, and fibre/resin interface debonding.

Breakage of fibres occurs when enough fibre surface is in contact with hard asperities of the tool surface, so that the friction force on the fibre exceeds the fibre-resin bond strength and the transverse strength of the fibre [187]. Fibre breakage can be seen in Figs 111 and 117. The fibre-resin debonding occurs because of the concentration of both shear and tensile stresses in the vicinity of crack tips during propagation of cracks normal to the direction of reinforcement [140]. However, if the maximum shear stress exceeds the shear strength of the interface, fracture will occur at the interface. Debonding can be seen in Figs 105 and 114.

During the fracture process, cracks are initiated in the weaker resin and then propagated to the interface or to the fibres. According to the strength of the interface, interface debonding or fibre breakage occurs. If the interface is strong, the cracks will propagate through the resin across the neighbouring fibres leading to fibre breakage without involving debonding (Fig 104). However, if the interface is weak, the cracks will propagate along the interface before fibre breakage occurs (Fig 105). After debonding, the fibres are unsupported resulting in easier breakage by shear stress operating (Fig 114). Resin removed from the interface after debonding will make more direct contact with the tool surface, resulting in excessive frictional heat. Both brittle (Figs 104

and 114) and ductile (Fig 105) resin behaviours were observed according to the amount of heat generated on the surface. As discussed earlier, the temperature at the tool/work interface is higher than the Tg (150^{o}C) of epoxy resin, suggesting that the rubbery resin requires a very high temperature to decompose the material. When there is fibre breakage without debonding (Fig 104), only a little frictional heat was generated because the resin was still supported by the interface.

The different modes of fracture according to the location of the surface may result from the inhomogeneous nature of GFRP, characterised by the presence of inherent flaws such as voids in the resin, resin or fibre-rich regions, and misalignment of fibres. These structural variations may influence the temperature and stress state near the cutting edge, which will influence the magnitude and direction of crack propagation. Unlike metals which show plastic deformation near the crack tips, cracks in GFRP can propagate easily through both fibres and resins, and the fracture energy is only a little higher than that of resin [188].

5.2.3.2 The Effect of Fibre Orientation

The differences in surface nature according to fibre orientation is caused by the anisotropic nature of GFRP, which contributes to the different surface forming mechanisms.

Figs 106 and 112 show the different nature of fibre fracture between warp yarns and fill yarns. During the machining, warp yarns are in the feed direction and

perpendicular to the cutting edge, whereas fill yarns are in the cutting direction. In the case of warp yarns, the work movement is transverse to the cutting edge, and fibres may be bent before breaking by a shearing mechanism [189]. Moreover, tools may indent the exposed fibres directly and cracking and fracture of the fibres will be facilitated. Because of the bending before the breakage, fibres are easily separated from the interface and less energy will be required.

In the case of fill yarns, debonding will be difficult because of the absence of bending. Since the movement of fill yarns is normal to the cutting edge, some of the fill yarns will be removed from the surface as chips, and others will be left on the surface. In addition, relatively undamaged fill yarn on the surface (Fig 112) may result from the low interlamellar strength, which makes the separation of each lamella easier.

5.2.3.3 The Effect of Cutting Variables

(1) Cutting Conditions

Cutting forces decrease slightly with increase in cutting speed as shown in Fig 107. This may result from the effect of increased strain-rate, which makes the work material more brittle. Thus less cutting energy will be required and the cutting force will decrease. In metal cutting, the decrease of cutting forces with increasing speed is mainly due to the reduction of the chip/tool contact length and a drop in the shear strength in the flow zone as temperature rises [181].

However, these effects may not be applied to GFRP, probably because of (a) relatively short contact length (b) absence of seizure contact and (c) the discontinuous chip formation mechanism. It is known that the strength and modulus of glass fibres decrease above 250°C, whereas epoxy resin becomes more ductile above Tg (150°C) [6]. As discussed earlier, a sharp cutting tool does not generate high temperatures when machining GFRP, and the contact time between the fibre and tool is extremely short. Therefore, it is unlikely that there is sufficient heat at the interface to reduce the yield strength of work material. Evidence of little thermal softening of glass fibres on the surface supports this idea. An increase of cutting speed results in more severe pull-out and breakage of fibres as shown in Figs 115 and 116. At the high cutting speed, the large thermal expansion of epoxy resin compared to that of glass fibres may increase localised stresses, encouraging the pull-out of fibres. Moreover, the increased cutting temperature may result in increased real contact area between tool and workpiece, leading to an increased fractured area as cutting progresses.

The almost linear increase in cutting forces with feed rate can be observed in Fig 108. This may result from the increased fracture path on the shear zone, which requires larger cutting energy. As in the case of speed, increasing feed rate results in higher temperature generation because of increased contact time and increased material removal rate.

The reason for more fibre pull-out and breakage at high feed rate will be the same as that at high cutting speed.

(2) Tool Geometry

The decrease in cutting forces with increasing rake angle (Fig 109) can be attributed to the lower compressive stress on the shear zone and shorter fracture path at high rake angles. Moreover, easier chip movement on the tool face with an increase of rake angle can also accentuate this result. The opposite will happen at low rake angles. Relatively high feed forces were produced because the work material has two-directional reinforcements (one in the cutting direction and one in the feed direction). Most of the feed forces are generated during the fracture of warp yarns. As discussed earlier, warp yarns are fractured by a shearing mechanism, which requires less energy. But, with increasing the rake angle negatively, high forces are required because of the geometric constraint.

Best surface finish was obtained when using zero rake angle (Figs 120-122). Unlike the unreinforced plastics, the critical rake angle doesn't correspond with the best surface finish when machining GFRP. Fig 109 shows that the critical rake angle is much larger than 30^{o} when machining GFRP, and this is similar to the case of metals. The ratio of feed force to cutting force at zero rake angle is about 0.98, which is much higher than those of PVC and HDPE. The high ratio of forces contributes to the high critical rake angle when

machining GFRP.

Figs 117 and 118 compare the machined surface using sharp and worn cutting tool. When a sharp cutting tool was used, flow of degraded resin was not observed because of the low cutting temperature. However, when a worn tool was used, the very ductile nature of the resin was observed because of the increased cutting temperature. With increases in flank wear land, the tool/work contact area will be increased, resulting in higher cutting temperature. Epoxy resin doesn't melt at high temperatures, but thermal degradation occurs through a depolymerisation or 'unzipping' mechanism, leading to a virtual or complete breakdown of the polymer chains [134].

Little debonding was observed when machining with worn cutting tools. This may be because of the ductile nature of the resin suppressing the crack propagation at the interface by absorbing more deformation energy. Severe debonding with sharp cutting tools results from the fact that low cutting temperatures encourage brittle cracking of the resin. Therefore, little energy will be expended in brittle fracture and cracks will propagate easily at the interface, leading to debonding and fibre breakage.

5.2.4 Tool Wear

5.2.4.1 High-Speed-Steel (HSS) Tools

HSS tools show the poorest performance of all the tools used because of severe abrasive wear (Fig 127). The severe abrasive wear during initial cutting eliminates the clearance

angle and increases the contact area between the flank face and the work material, resulting in increase in cutting temperature and decrease in yield stress of the tool material. This leads to an acceleration of the abrasive wear (Fig 126).

The evidence of abrasive wear can be clearly seen in Figs 133 and 134. Abrasive wear is the displacement of tool material due to hard particles of work material. Glass fibres are fractured into small particles during cutting, and some of these particles can be trapped at the tool/work contact zone and abrade the tool material. Sliding contact in this region may facilitate the abrasive action. It doesn't seem that broken tool material abrades the flank face, because HSS tools have few hard particles (carbides) which could cause self-wear of the cutting tool [85].

A deep crater was not observed on the rake face, probably because of the absence of chemical inter-diffusion (Figs 130 and 132). The sliding movement of the chip on the tool face may also accentuate this phenomenon by suppressing the formation of a flow zone at the interface. Instead, deep grooves were observed near the cutting edge. The diminishing of the deep grooves with distance from the cutting edge may have some relationship with the distribution of normal stress on the rake face. It is generally known than the normal stress is highest near the cutting edge and diminishes across the rake face to zero where the chip breaks contact with the tool [10]. Moreover, protruded glass fibres on the chip underside probably become flattened with the progress of chip movement. Less

evidence of abrasive wear on the rake face than on the flank face may be the result of lower contact pressure at the tool/chip interface.

Severe chipping was observed on the tool nose, where the tool was in direct contact with the workpiece (Fig 129). Similar result was obtained by Tsueda [172] who attributed the high rate of nose wear when machining GFRP to the flexural rigidity of glass fibres. Since the stress state near the tool nose has a highly compressive component, there will be an increase in real contact area, resulting in severe tool wear. Nose chipping occurs when the applied stress exceeds the ability of the tool material to resist fracture. When the tool nose loses its ability to cut, great sliding forces arise between tool and work material, leading to a rapid heating of tool material and a loss of hot hardness [190]. Temperature may have some influence on nose chipping, when a high temperature is produced after wear occurs in this area.

Cracks were sometimes observed on the flank wear land (Fig 131) and nose area (Fig 129). These cracks are thought to be produced by tensile stresses arising from cyclic heating and cooling at the tool/work interface. This cracking may be accentuated by structural features in the workpiece because the intermittent contact of fibres with tool may produce the cyclic thermal stresses that lead to crack formation.

Plastic deformation was not observed with HSS tools (Fig 126). In metal cutting, plastic deformation usually require high cutting temperatures and high normal stress on the tool

faces [9,54]. As discussed earlier, relatively low normal stress and low temperature on the rake face result in an absence of plastic deformation when machining GFRP. For these reasons, catastrophic tool failure was not observed.

Less severe nose chipping was observed at the high feed rate, probably because of less heat concentration (Figs 135 and 136). Increasing feed rate results in an increase of cutting forces and cutting temperatures. However, since the contact area at the tool/chip interface becomes small at low feed rate, the heat build-up and normal stress will be concentrated in this region. At high feed rates, the temperature will be more uniformly distributed, resulting in a smaller reduction in tool strength. Similar results were obtained by increasing the nose radius of the tool (Fig 139). A large nose radius increases the cutting forces, but reduces the heat build-up at the tool nose. Improvement of tool point strength with increase of nose radius may also contribute to the reduction in nose chipping. The distinct difference in hardness between fibres and resin combined with the high cutting resistance of fibres can also contribute to edge chipping by mechanical fatigue.

Figs 137 and 138 show the wear lands when machining at different rake angles. The flattened surface at the top of the flank wear land (Fig 137) is thought to be the result of crumbling which can be attributed to the increased contact pressure at the high negative rake angle. It was found that contact pressure increased about four times when the rake angle was changed from 30^{o} to -20^{o}. The loss of clearance angle with

an increase of flank wear land results in this crumbling action. The intermittent ridges on the flank face (Figs 128 and 138) were usually obtained when zero or positive rake angles were used. This may result from the decreased contact pressure which enables relative movement at the tool/work interface.The ridge formation may have some relationship with the two-directional fibre reinforcements. Warp yarns are easily broken by a shearing mechanism, resulting in little abrasion by these. Long, straight grooves between ridges are thought to be caused by the fibres in the fill yarns.

5.2.4.2 Cemented Carbide Tools

Figs 177 and 178 show that K20 carbides outperform the P10 carbides when machining GFRP. It is generally known that the toughest carbides are those containing only WC and cobalt,while the addition of other carbides such as TiC or TaC reduces the toughness [73,81]. The better performance of K20 carbides results from their higher tensile strength and toughness.

The main wear mechanism of cemented carbide tools when machining GFRP is attrition wear. Attrition wear can clearly be observed in Figs 143 and 149. Because of the high hardness of WC and mixed carbides, abrasive wear is much less likely to be a significant wear process. The reason for attrition wear can be mechanical or thermal fatigue instead of the breakage of adhesive junctions. It may result from the fact that there was little adhesion at the interface due to the brittle nature of the fracture. Moreover, uneven GFRP surface with protruding

fibres results in the fluctuating flow of work material on the tool flank and rake face.

Mechanical or thermal fatigue can be attributed mainly to the intermittent contact between warp yarns and flank face. In each revolution, the fill yarns are in contact with the flank face continuously, whereas warp yarns are contacted intermittently. The space between warp yarns is about 0.6 mm. When the work material was cut at a cutting speed of 100m/min and feed rate of 0.10 mm/rev for 2 minutes, warp yarns were cut intermittently 3.3×10^5 times, whereas fill yarns were cut much less frequently. Different cutting mechanisms between warp yarns and fill yarns may result in fluctuating mechanical and/or thermal stress on the tool face. Moreover, in the case of fill yarns, the fibre diameter (0.01 mm) is much less than the undeformed chip thickness used (0.10 - 0.25 mm), and each fibre is closely spaced to others. Therefore, more than 10 fibres could be present in the contact area at the tool/chip interface, resulting in extremely intermittent contact between fibres and tool face. Localised high temperatures may be generated when in contact with fibres and much lower temperatures when in contact with the resin.

During the investigation with uncoated carbide tools, only attrition wear was observed with little evidence of other wear mechanisms. Self-wear may be masked by the high rate of attrition wear.

Plucking can be observed near the tool nose and cutting edge when high cutting speed and feed rate are used (Fig 146).

This suggests that large scale attrition wear occurs when the strength of the tool is not sufficient to withstand the forces on the tool surface. Relative movement between plucked particles and the tool surface can cause grains of tool material to be further dislodged and carried away by this process [9]. Moreover, the varying coefficients of thermal expansion between the carbides and binder may assist the break out of carbides at high temperature [85]. Concentration of plucking (attrition wear) near the tool nose results from the high compressive stress in this region (Fig 140). Little evidence of attrition wear was observed with HSS tools.This may result from their inherent toughness. Instead, mechanical or thermal fatigue results in the microcracks which propagate into cracks as observed in Figs 129 and 131.

5.2.4.3 Coated Carbide Tools

When machining GFRP, coated carbides outperformed the uncoated carbides (Figs 177 and 178). Slightly better results were obtained with triple coated carbides at low speeds and with TiC coated carbides at high speeds. Better performance of coated carbides can be attributed to the high hardness and abrasion resistance of the coating material. The presence of hard, brittle eta phase in TiC coated carbides may accentuate poor performance due to a drop in strength and embrittlement of the cutting edge [95]. It may also encourage attrition wear by mechanical or thermal fatigue. In metal cutting, the high thermal expansion of the TiC coating results in a thermal

stress which influences the tool performance at high speeds [96]. However, the relatively good performance of TiC coated toolsat high speeds when machining GFRP may be due to the fact that the cutting temperature is not high enough to reduce the strength of the coating.

Abrasion by the work material doesn't seem to be a likely wear mechanism because GFRP used doesn't contain particulate inclusions of sufficient hardness to abrade the coating layer. As in the case of HSS and uncoated carbides, bulk plastic deformation of coated carbide tools was not observed due to the low temperatures and low normal stress on the tool face.

Figs 152 and 166 show the plastically deformed coating on the rake face. Similar results were obtained by Dearnley [100] when machining steel. He attributed it to the excessive shear stress followed by ductile failure. During this discrete plastic deformation, coated layers are flattened and somewhat extended in the chip flow direction. When machining GFRP, the average shear stress on the rake face is quite low (less than 170 MN/m^2) compared to that with steel (200 - 500 MN/m^2) [191]. However, the shear stress on the real contact area will be considerably higher, because most of the load is borne by the fibres due to the softness of the resin. In addition, flattened fibres may exert less shear stress than the protruding fibres. Therefore, the shear stress on the protruding fibres may be high enough to induce discrete plastic deformation by repeated contacts with the coated layer.

The discrete plastic deformation may also be the reason

for the removal of the coating from the flank face. It is generally known that the shear stress on the flank face is several times higher than that on the rake face because compressive stress above the cutting edge will be experienced as a shear stress on the flank face [101]. Moreover, the fluctuating flow of work material at the tool/work interface may accentuate discrete plastic deformation by allowing high shear concentration on the protruding fibres. Because of the uneven flow of work material, the exposure of the substrate will be localised after the preferential removal of the coating. Attrition wear may be difficult on the coating because of its extremely small grain size and high strength. However, the exposed substrate becomes prone to the attrition wear as observed with uncoated carbides (Figs 158,165 and 168). The surface worn by attrition wear was found to be rougher than that which suffered discrete plastic deformation, because discrete plastic deformation only involves the deformation of the thin surface layer without removing or wearing the tool surface by hard asperities of fibres. (Figs 166 and 167)

Discrete plastic deformation was observed on the rake face even at low cutting speeds (50m/min) (Figs 151 and 154). Moreover, considering the low temperature on the rake face when machining GFRP, it can be said that discrete plastic deformation doesn't require a high cutting temperature, which is a pre-requisite for bulk plastic deformation. Flaking of the coating on the rake face was sometimes observed as shown in Figs 156, 157 and 167. The thermal cracking shown in Fig 155

may be one of the reasons for the flaking of the coating. It may occur due to the different coefficients of thermal expansion between coating and substrate. TiC coated carbide may experience more thermal stress than triple-coated carbide due to TiC's high thermal expansion coefficient. These cracks are also thought to be formed during cooling after high temperature deposition of the coating layer. Dearnley [191] attributed the cracking of the coating to plastic deformation of the substrate which caused distortion of the tool edge, resulting in cracking in a tensile mode around the edge radius, but in a shear mode on the flank face. It seems that the propagation of these cracks leads to the flaking of the coating catastrophically.

As in the case of HSS and cemented carbide tools, the flank wear and flaking of the coating were severe near the tool nose (Figs 156,160,162 and 167), probably because of the high compressive stress in this region. The fractured area on the end clearance face (Fig 161) can be attributed to the repeated contact between tool face and protruding fibres on the newly machined surface resulting in large scale discrete plastic deformation followed by severe attrition wear.

5.2.4.4 The effects of cutting conditions

Cutting speed was found to have a strong influence on the flank wear of all the tools used (Figs 169,171,172,174 and 175). Flank wear is the dominant failure mode when machining GFRP. Increased flank wear at high cutting speeds can be

attributed to the increased cutting temperature and increased work material removal. It is unlikely that the tool/chip interface contributes much to the increase in cutting temperature at high cutting speeds, because of the absence of seizure conditions. With HSS tools, abrasive wear will occur easily when the tools are thermally softened at high speeds. With carbide tools, cutting temperatures will not be sufficient to soften the tool materials, but may reduce the fatigue life. In metal cutting, attrition wear decreases with increasing cutting speed, because of the uniform flow of chip and work on the tool faces [9]. However, when machining GFRP, the protruding fibres on the chip and work surface suppress the intimate contact at all cutting speeds due to the brittle fracture process. Therefore, attrition wear will not decrease with increasing cutting speed. Shortening of the fatigue life at high cutting speeds can be one of the important factors in the increase of attrition wear for both uncoated and coated carbide tools.

Similar results were obtained with increasing feed rates, as shown in Figs 170, 173 and 176. Machining at high feed rates leads to an increase in both the contact time and compressive stress on the tool face. The compressive stress was found to increase three fold when the feed rate was increased from 0.05 to 0.315 mm/rev. In metal cutting, abrasive wear is dominant at low feed rates because the heat is concentrated near the cutting edge [91]. The increase of feed rate moves the maximum heat zone away from the cutting zone,

resulting in large areas of wear land. Thus, large flank wear can be produced at high feed rates because of an increased heat affected zone. Moreover, attrition wear in carbide tools will not decrease with feed rate probably because there is little change in the flow patterns of work material on the tool faces.

CHAPTER 6. CONCLUSIONS

6.1 Machining of Plastics

1. Segmented or discontinuous chips were produced when machining PVC. With HDPE, continuous chips were more common and segmented chips were rarely produced.

2. PVC chips tend to become discontinuous as speed, feed and rake angle (positive or negative) increase.

3. With PVC, discontinuous chips involving shear fracture tend to be produced with increasing speed and feed rate, and decreasing the rake angle. Discontinuous chips formed by tensile fracture were produced at high cutting speeds, high feed rates, and high positive rake angles.

4. Both seizure and sliding contact are observed at the tool/chip interface when machining PVC and HDPE. Segmented PVC chips move on the tool face by the stick-slip mechanism.

5. Surface integrity of PVC has a close relationship with the type of chip formation, which depends on the cutting conditions, and tool geometry. With PVC and HDPE, surface roughness increases with feed rate and rake angle (positive or negative).

6. Cutting forces increase consistently with increasing feed rate or decreasing rake angle when machining PVC and HDPE.

6.2 Machining of GFRP

1. Discontinuous chips are always produced by fracture near the shear zone. There is only sliding contact at the tool/chip and tool/work interface.

2. Cutting temperature is not high when machining GFRP. However, when the flank wear land develops, there can be excessive heat generation at the tool/work interface. Unlike in metal cutting, the temperature on the rake face is relatively low due to the absence of seizure contact.

3. Cutting forces are generally lower than those when machining steel. Cutting forces decrease slightly with cutting speed, increase with feed rate, and decrease consistently with an increase in rake angle.

4. Surface damage such as fibre breakages, resin cracking, fibre/resin interface debonding, and resin decomposition are produced. Fibre orientation as well as cutting conditions have some influence on fibre breakage. Worn cutting tools result in the thermal decomposition of the resin.

5. HSS tools show the poorest performance due to the excessive abrasive wear. Nose chipping becomes less severe with an increase in feed rate and nose radius. Cyclic heating and cooling result in cracking on the flank wear land and nose area.

6. Cemented carbide tools outperform HSS tools. K20 carbides show better performance than P10 carbides. Attrition wear is the main wear mechanism resulting from mechanical or thermal fatigue by intermittent contacts between fibres and tool faces.

7. Coated carbide tools have the best performance among the tools used. Discrete plastic deformation followed by attrition wear is the main wear mechanism on the flank and rake faces. Discrete plastic deformation occurs by the concentration of shear stress between the tool faces and the protruding fibres. Flaking of the coating occurs catastrophically, initiated by thermal cracks.

8. Diffusion wear and bulk plastic deformation of cutting tools were not observed in any of the tools used.

9. Increasing cutting speed and feed rate results in an increase in flank wear with all the tools used.

REFERENCES

1. R.J. Crawford, Plastics Engineering, Pergamon Press, 1985
2. A. Leggart, GRP and buildings, Butterworths, 1984
3. P.A. Thornton, Fundamentals of Engineering Materials, Prentice Hall, 1985
4. Van Vlack, Elements of Materials Science and Engineering, Addison-Wesley Pub., 1985
5. M.S. Ray, The technology and applications of engineering materials, Prentice Hall, 1987
6. R.P. Sheldon, Composite Polymeric Materials, Applied Science Pub. Ltd, 1982
7. L.T.C. Rolt, Tools for the job, Batsford, 1965
8. G. Boothloyd, Fundamentals of Metal Cutting and Machine Tools, McGraw Hill, 1981
9. E.M. Trent, Metal Cutting, Butterworth, 1979
10. N.N. Zorev, Int. Res. in Prod. Eng. Proc, 1963, p.42
11. H. Takeyama and E. Usui, ASME, J. of Eng. for Ind., 82, 4, 1960, p.303
12. S. Kato et al, ASME. J. of Eng. for Ind., Vol. 82, 1960, p.303
13. G. Barrow et al, J. Mach. Tool Des. Res, 22,1, 1982, p.75
14. T. Kurimoto and G. Barrow, Annals of CIRP, 31,1, 1982, p.19
15. P.K. Wright and E.M. Trent, J.I.S.I., May 1973, p.364
16. P.A. Dearnley et al, Wear, 54, 1979, p.371
17. E.M. Trent, Treatise on Material Science and Technology, vol. 13, p.443
18. P.K. Wright et al, Wear, 54, 1979, p.371
19. H. Ernst, Physics of Metal Cutting, ASM, 1938
20. K. Iwata, Annals of CIRP, vol. 25, no.1, 1976, p.65
21. J.T. Black, ASME, J. of Eng. for Ind., 93, 1971, p.507
22. N.H. Cook. et al, ASME, ser. B, 76, 1954, p.153
23. B.F. Von Turkovich, Proc. Int. Conf. on Prod. Eng., Tokyo, 1974
24. H.S. Luong, Australian conf. on Manu. Eng., Aug. 1977, p.122
25. W.B. Rice, The Engineering Journal, vol. 44,pt.2, 1961, p.41
26. T.J. Walker and M.C.Shaw, Proc. Int. Conf. M.T.D.R., Manchester, 1969. p.241
27. H.S. Luong and R.H. Brown, ASME, J. of Eng. for Ind., vol. 103, 1981, p. 431
28. R. Komanduri, et al, ASME, J. of Eng. for Ind., vol. 104, 1982, p.121
29. R.F.Recht, ASME, J. of Appl. Mech., 1964, p.189
30. K.F. Sullivan, et al, ASME, ser.B, 76, 1954, p.153
31. R. Komanduri and R.H. Brown, Metals and Materials, vol. 6, 1972, p.531
32. R. Komanduri and R.H. Brown, ASME, J. of Eng. for Ind., vol. 103, p.33
33. E.D. Doyle, et al, Proc. Fourth Tewksbury Symposium, Melbourne, 1979
34. J. Hazra, Proc. Int. Conf. on Prod. Eng., Tokyo, 1974

35. D. Lee, ASME, J. Eng. for Ind., 1985, vol. 107, p.55
36. M. Field and M.E. Merchant, ASME, 71, 1949, p.421
37. W.B. Palmer, J. Mech. Eng. Sci., 1967, 9,1
38. D. Lee, ASME. J. of Eng. Mat. Sci., vol. 196, 1984, p.9
39. E.D. Doyle, Proc. Int. Conf. on Prod. Eng., Tokyo, 1974
40. C.S. Sharma et al, Annals of CIRP, 1971, p.545
41. A.S. Shouckry, Wear, 69, 1981, p.345
42. P.K. Wright and K.C. Maine, Proc. Fourth Tewksbury Symposium, Melbourne, 1979
43. J.F.Kahles and M. Field, Proc. Instn. Mech. Engrs, 1967-68, vol. 182, pt. 3k, 1979
44. P. Leskovar and J. Peklenik, CIRP Annals, vol. 31, no.1, 1982, p.447
45. D.M. Turley and E.D.Doyle, Wear, 57, 1979, p.237
46. K. Nakayama et al, CIRP Annals, vol. 14, p.211
47. A.S. Shouckry, Wear, 80, 1982, p.197
48. L.G. Jamar and R.A. Dudek. Inst. J. Prod. Res., Vol. 5, No. 4, 1967, p.307
49. J.A. Bailey and S.E. Becker, ASME, 96, 1974, p.163
50. H.J. Lambert, CIRP Annals, vol. 10, 1961/62. p.246
51. J. Wallbank, Wear, 56, 1979, p.391
52. J.T.Black and S. Ramalingam, Int.J. Mach. Tool. Des. Res., vol. 10, 1970, p.439
53. M.C. Selvam and V. Radhakrishman, Wear, 26, 1973, p.393
54. M.C. Shaw, Metal Cutting Principles, Clarendon Press,1984
55. T. Sate, CIRP Annals, 12, 4, 1963, p. 190
56. P.G. Petropolous, Wear, 23, 1973, p.299
57. J.A. Bailey, et al, ASME, J. of Eng. for Ind., 98, 1976 p.999
58. K. Okushima and Y Fugii, Bull. of JSME, vol. 4, no. 4, 1961, p.365.
59. J.A. Bailey and G.A. Azargoon, SME Tech Paper, IQ 75-126
60. K.L. Chandriramani and N.H. Cook, ASME ser. B,1964, p.134
61. J.A. Bailey, Wear, 42, 1977 p.277
62. M.C. Shaw et al, ASME, Ser.B, 83,1961, p.181
63. N.P. Suh, Wear, 62, 1980, p.1
64. V.C. Venkatesh, Annals of CIRP. Vol. 29, no. 1, 1980, p.19
65. E.M. Trent, SME Tech Paper, MR71-913, 1971
66. A.E. Focks, et al, Int. Conf. on the wear of materials, St.Louis, Apr. 1977, P.228.
67. Y. Naerheim and E.M. Trent, Metals Technology, Dec. 1977, p.548
68. P.K. Wright et. al, Proc. Int. conf. on Cutting Tool Materials, Kentucky, 1980
69. J. Tlustry and Z. Masood, ASME, J. of Eng. for Ind., Vol. 100, 1978, p.403
70. J.M. Galimberti, ASME Tech Paper, MR68-173
71. V. Höglund, Annals of CIRP, Vol. 25, No. 1, 1976, p.99
72. R.W. Bratt, Proc. Int. Conf. on Cutting Tool Materials, Kentucky, 1980.
73. R. Komanduri and J.D. Desai, G.E. Tech. Paper, Aug. 1982
74. P.K. Wright and E.M. Trent, Metals Technology, 1974,p.13
75. V.C. Ventatesh, ASME, vol. 100, 1978, p.436
76. R. Brownsword, et al, ibid, 38

77. P.K. Wright, Proc. Fagersta HSS Symposium, 1981, p.13
78. W. König, Annals of CIRP, vol. 24, No.1, 1975, p.1
79. T.H.C. Childs and A.B. Smith, Metals Technology, vol. 9 1982, p.292
80. V.C. Venkatesh, Proc. Int. Conf. on Hard Mat. Tech., 1976, p.144
81. M.M. Prokosch, Modern Machine Shop, June 1983, p. 76
82. H.S. Kalish, SME Tech. Paper, MR71-914, 1971
83. H. Jonsson, Planseeverichte fur pulvermetallurgie, bd.20 1972, p.39
84. B. Blankenstein, SME Tech. Paper, MR71-914, 1971
85. W. König, SME Tech. Paper, MR71-214, 1971
86. S. Ramalingam and P.K. Wright, ASME. J. of Eng. Mat. and Tech., vol. 103, 1981, p.151
87. G. Dixon et al, Wear of Materials, ASME, 1983, p.218
88. M.E. Sjöstrand and A.G. Thelin, Metal Powder Report, Dec. 1986, p.905
89. W. Schintlmeister, et al, Wear, 100, 1984, p.153
90. H.S. Kalish, Proc. Int. Conf. on Hard Mat. Tech., 1976
91. C. Wick. Manufacturing Engineering, Dec. 1986, p.26
92. M. Lee and M.H. Richman, Metals Technology, Dec. 1974, p.538
93. P. Walsh, Cutting Tool Materials, Feb. 1987, p.26
94. N.P. Suh, Proc. Int. Conf. on Hard Mat. Tech., Pittsburgh, 1976
95. C.R. Cline, Proc. 3rd NAMRC, May 1975, Pittsburgh, p.555
96. J.I. Elgomayel, et.al, Int. J. Mach. Tool. Des.Res., vol.19, p.205
97. V.C. Venkatesch, Annals of CIRP, vol. 25, No. 1. 1977, p.5
98. J.P. Chubb and J. Billingham, Wear, 61, 1980 ,p.283
99. F. Heydari, J. Wallbank and I.R. Pashby, Int. Conf. on Wearof Materials, Apr. 1987, Houston, P.313
100. P.A. Dearnley and E.M. Trent, Metals Technology, Feb. 1982, vol. 9, p.60
101. P.A. Dearnley, Surface Engineering, Vol. 1, No. 1, 1985, p.43
102. T.E. Hale and D.E. Graham, Proc. Int. Conf on Cutting Tool Materials, Kentucky, Sep. 1980
103. P.O. Snell, Jernkont Ann, 154, 1980, p.413
104. K. Stjernberg and A. Thelin, Proc. Int. Conf. on High Productivity Machining, Kentucky, Sep. 1980
105. A.S. Raju, et al, Proc. Int. Conf. on Hard Mat. Tech., 1976 p.144
106. R.B. Seymour, Modern Plastics Technology, Reston Pub. Co., 1975
107. R.J. Beird, Industrial Plastics, The Goodheart-Willcox. Co., 1971
108. R.M. Brick et al. Structure and Properties of Engineering Materials, McGraw-Hill Book Co, 1985
109. W.R. Moore, An Introduction to Polymer chemistry, Univ. of London Press Ltd., 1963
110. R.W. Hertzberg, Deformation and Fracture Mechanics of Engineering Materials, John Wiley and Sons, 1976

111. A.J. Kinloch and R.J. Young, Fracture Behaviour of Polymers, Elsevier Applied Science Pub., 1985
112. C. Hall, Polymer Materials, McMillan Press Ltd, 1981
113. R.J.Young, Introduction to Polymers, Chapman & Hall, 1981
114. L.R.G. Treloar, Introduction to Polymer Chemistry, The Wykeham Science Series, 1970
115. D. Tabor, Advances in Polymer Friction and Wear (Ed. L.H. Lee), Plenum Press, New York & London, 1972
116. A. Kobayashi and K. Sato, Bull. of Electro-Tech Lab. 27, 4, 1963, p.291
117. A. Kobayashi, Modern Plastics, Part I, July 1963, Part II, Aug. 1963, Part III, Sep. 1963, Part IV, Oct. 1963, Part V, Nov. 1963, Part VI, Dec. 1963, Part VII, Jan. 1964
118. A. Kobayshi, Machining of Plastics, New York, McGraw Hill, 1967
119. A. Astrop, Machining and Production Engineering, June 1981, p.35
120. Y.B. Kazanski, Sov. Plastics, n5, 1971, p.78
121. C. Rubenstein and R.M. Storie, Int. J. Mach. Tool & Res., vol. 9, 1969, p.117
122. E.A. Peirce and A.E. Young, Plastics and rubber: Processing, Sep. 1977, p.92
123. R.F. Scrutton, Int. J. of Prod. Res., v.4, No.1, 1965
124. L. Marsia, Thermoplastics : Materials Engineering, Applied Science Pub., 1982
125. U.M. Rao, J.D. Cumming and E.G. Thomson, ASME, J. of Eng. for Ind., p.117, 1964
126. A. Kobayashi, J. of Polymer Science, 58, 1962, p.1377
127. A.E. Young and J.H. Wilson, Plastics and rubber: processing, Sep. 1978. p.77
128. A.E. Young, 'Critical Rake Angle when Machining Plastics' Ph.D Thesis, Queens Univ., Belfast, 1978
129. P.D. Brien, W. Thompson and J.K. Russel, CIRP, 1977, Vol. 25, No. 1, p.339
130. M. Masuko, J. Kumabe and S. Ammi, Bull. of JSME, 7,25, 1964, p.209
131. V.M. Bogdanov, Machines and Tooling, vol. XLI. No.3, p.40
132. R. Wada, et al., CIRP Annals, 29, 1, 1980, p.47
133. J.A. Kozacki, Westtec/North Engineering Conf. and Exposition, 1968
134. Derok Hull, An Introduction to Composite Materials, Cambridge Univ Press, 1981
135. M.O.W. Richardson, Polymer Engineering Composites, Applied Science Pub. Ltd., 1977
136. R.L. McCullough, Concepts of Fibre Reinforced Composites, Marcel Dekker Inc., 1971
137. Holliday (Editor), Composite Materials, Elsevier Pub. Co., Amsterdam, 1966
138. G. Lubin, Handbook of Fibre-glass and Advanced Plastics, Composites, Van Nostrand Reinhold Co., 1969
139. L.J. Broutman and R.H. Krock, Modern Composite Materials, Addison-Wesley Pub., 1967
140. N.G. McCrum, Review of the Science of FRP, London H.M. Stationery Office, 1971

141. John Hubber, SME Tech. Paper, MR 71-820, 1971
142. G. Spur and U.E. Wunsch, Kunststoffe German Plastics, 76, 1986, 3, p.8
143. W. König, et al, Annals of CIRP, vol. 34, No.2, 1985, p.537
144. G. Spur and U.E. Wunsch, Ind. Dia.Rev., Apr. 1985, p.195
145. L.M. Miner and F.J. Penoza, SAMPE Quarterly, July 1976
146. W. König, et al, Tech Sym. V, Design and use of Kevlar Aramid Fibre in Composite Structures, 1984, p.95
147. E.G. Semler (ed.), Engineering Materials and Methods, IME, 1971
148. J.H. Doran and F. Hanley, Metals Engineering Quarterly, Aug. 1972, p.38
149. C.T. Yang, Western Machinery and Steel World, Vol. 62, Pt. 7, 1971, p.10
150. J.H. Doran and C.R. Maikish, Composite Materials in Engineering Design, Proc. 6th Sym., St. Louis, May 1972, p.242
151. M.D. Weisinger, ASM Paper, W70-5.2, 1970
152. R.P. Bergstorm, Manufacturing Engineering, Nov. 1983, p.61
153. W. Köglmeier, et al, Ind. Dia. Rev., Feb. 1979, p.52
154. W. König, et al, The Production Engineer, Sep. 1984, p.56
155. S. Kalpakjian, Manufacturing Process for Engineering Materials, Addison-Wesley, Pub. Co., 1984
156. W. Schröder and W. Gaspel, Ind. Dia. Rev., June 1976, p.200
157. W. Schneider, Ind. Dia. Rev., Oct. 1973, p.389
158. D.A. Saville, Ind. Dia. Rev., Feb. 1964, vol.24, p.26
159. Bruce Mackey, 35th Annual Tech. Conf., 1980
160. A. Koplev, Proc. 3rd, Int. Conf. on Composite Material, Paris, Aug. 1980
161. A. Koplev, Composites, vol. 14, No.4, Oct. 1983, p.371
162. I.J. Toth et.al, J. of Metals, vol. 24, Oct. 1972, p.37
163. K. Sakuma and M. Seto, Bull. of JSME, vol.26, No. 218, 1983, p.1420
164. S. Rujikietgumjorn, 'Development of Predictive Modelling for drilling Composite Materials', Ph.D Thesis, Texas Tech Univ., 1978
165. A.T. Notter and P.A. Bex, Ind. Dia. Rev., Oct. 1977, p.336
166. K. Sakuma, et al, Bull. of JSME, vol. 28, No. 245, Nov.1985, p.2781
167. M.M. Schwartz, American Machinist, Mar. 1983, p.103
168. Y. Hasegawa and S.Hanasaki, Bull. of JSME, vol. 12, No. 51, 1969, p.610
169. K. Sakuma, Y. Yokoo and M. Seto, Bull. of JSME, vol. 27, No.228, 1984, p.1237
170. K. Sakuma and M. Seto, Bull. of JSME, vol. 22, No.163, 1979, p.107
171. K. Sakuma and M. Seto, Bull. of JSME, vol. 24, No. 190 1981, p.748
172. M. Tsueda, et al, Bull. of JSME, vol. 12, No.51, 1969, p.601
173. Y. Hasegawa, et al, Bull. of JSME, vol. 12, No.51, 1969, p616

174. K.J.A. Brookes (Ed.), World Directory and Handbook of Hard Metals, Int. Carbide. Data, 1987
175. P.B. Bowden, In: The Physics of glassy polymers, Ed. by R.N. Haward, Applied Science Publishers, Ltd, London, 1973, p.279
176. K.F. Sullivan et. al. Metals Technology, June 1978, p.181
177. K. Nakayama, Proc. Int. Conf. on Prod. Eng., Tokyo, 1974 p.572
178. Private Communication with J. Wallbank in Engineering Dept. of Univ. of Warwick, 1989
179. D. Tabor, Polymer Science and Technology, vol. 5A, Plenum Press, 1974
180. B.J. Briscoe, (ed. Klaus Friedrich) Friction and Wear of Polymer Composites, Elsevier, 1986
181. E.M. Trent, Wear, 128, 1988, p.29-45, p.47-64, p.65-81
182. J.K. Lancaster, Plastics and Polymers, Dec. 1973, p.297
183. V.K. Jain and S. Bahadur, Wear of Materials, 1979, p.581
184. M.K. Kar and S. Bahadur, Wear, 46, 1978, p.189
185. M. Cocks, Wear, 8, 1965, p.85
186. J.A. Bailey and S.E. Becker, ASME, J. of Eng. Mat. Tech. July, 1974, p.163
187. A.C. McGree, et. al, Wear, 114, 1987, p.97
188. T. Tsukizoe and N. Ohmae, Friction and Wear of Polymer Composites, Elsevier, 1986
189. N.P. Suh, Wear, 53, 1979, p.129
190. H. Opitz and W. König, ibid, p.6
191. P.A. Dearnley, Wear, 101, 1985, p.33

Behaviour of Polymeric Materials in Machining

by

Yong - Hwan, KIM
(B.S.c, M.S.C)

This Thesis has been submitted for the degree of

Doctor of Philosophy

Dept. of Engineering
University of Warwick

May 1989

(Vol. II)

Material	Density ($Mg\ m^{-3}$)	Young's modulus ($GN\ m^{-2}$)	Tensile strength ($MN\ m^{-2}$)	Elongation to fracture (%)	Coefficient of thermal expansion ($10^{-6}\ °C^{-1}$)	Specific Young's modulus, Y. modulus / density ($GN\ m^{-2}$)	Specific tensile strength, T. strength / density ($MN\ m^{-2}$)	Heat resistance (°C)
High strength Al–Zn–Mg alloy	2.80	72	503	11	24	25.7	180	350
Quenched and tempered low alloy steel	7.85	207	2050–600	12–28	11	26.4	261–76	800
Nimonic 90 (nickel-based alloy)	8.18	204	1200	26	16	24.9	147	1100
Nylon 6.6	1.14	2	70	60	90	1.8	61	150
Glass-filled nylon ($V_f = 0.25$)	1.47	14	207	2.2	25	9.5	141	170
Carbon fibre–epoxy resin unidirectional laminae ($V_f = 0.60$)								
(i) parallel to fibres	1.62	220	1400	0.8	−0.2	135	865	260
(ii) perpendicular to fibres	1.62	7	38	0.6	30			
Glass fibre–polyester resin unidirectional laminae ($V_f = 0.50$)								
(i) parallel to fibres	1.93	38	750	1.8	11	19.7	390	250
(ii) perpendicular to fibres	1.93	10	22	0.2				
Glass fibre–polyester resin planar random fibres ($V_f = 0.20$)	1.55	8.5	110	2	25	5.5	71	230

Note: V_f is the volume fraction of fibres.

Table 1. Comparison of the physical and mechanical properties of some polymers, composites and metals (134)

	E glass	C glass	S glass
SiO_2	52.4	64.4	64.4
Al_2O_3, Fe_2O_3	14.4	4.1	25.0
CaO	17.2	13.4	—
MgO	4.6	3.3	10.3
Na_2O, K_2O	0.8	9.6	0.3
Ba_2O_3	10.6	4.7	—
BaO	—	0.9	—

Note: Data from Fibreglass Ltd.

Table 2. Main components of common glass fibres (by weight (%)) (134)

Properties	Fiber			Matrix
	Glass	Boron	Carbon	Epoxy
Mechanical				
Modul: , 10^6 lbs/in^2				
Longitudinal	11	60	50	0.5
Transverse	11	60	1.5	0.5
Shear	4	25	4	0.2
Poisson's Ratio	0.2	0.2	0.2	0.4
Strength, 10^3 lbs/in^2	500	445	300	5
Critical Strain, %	4.5	0.7	0.6	10
Density, lbs/in^3	.083	.098	.060	.04
Thermal				
Coefficient of expansion, 10^{-6} in/in°F	2.8	2.8	1.5	32
Thermal conductivity, BTU / hr-ft.^{2}-°F/in.	7.5	70	60	1.7
Cost, $/lb	$1	$300	$350	$1
Shape			(PAN) (RAYON)	
Diameter, in	0.0004	0.005	0.0003	

Table 3. Typical properties of materials used in composites (136)

	T_m (°C)	Tg (°C)	Density	T.S. (MPA)	Elongation (%)	Thermal Conductivity (W / m.k.)	Coeff. of Thermal Expansion (µm / m.k.)
HDPE	135	-20	0.96	20 - 35	10 - 200	0.48	60 - 110
PVC	-	75 - 105	1.4	35 - 65	40 - 80	0.12 - 0.2	50 - 100

(from Modern Plastics Encyclopedia, McGraw-Hill, N.Y. 1985)

Table 4. Typical properties of PVC and HDPE

WORK	V	a	f	t_2	Fc	Ft	Ø	r	x	y	z
PVC	200	0	0.16	0.22	49	21	36	2.1	65.9	111.7	68.1
PVC	10	0	0.16	0.17	44	18	44	2.0	54.3	124.6	61.1
HDPE	10	-20	0.16	0.21	31	17	33	2.9	38.0	70.9	43.1
HDPE	50	-20	0.05	0.07	15	10	28	3.0	16.7	31.0	65.2
HDPE	50	0	0.05	0.06	10	6	29	2.1	11.8	20.4	43.5

Table 5. Comparison of forces, stresses, shear plane angle and strain when machining PVC and HDPE

(V is the cutting speed (m/min), a is the rake angle (degree), f is the feed rate (mm/rev), t_2 is the chip thickness (mm), Fc is the cutting force (Newton), Ft is the feed force (Newton), Ø is the shear plane angle (degree), r is the shear strain, x is the shear stress (MN/m^2) on the shear plane, y is the normal stress (MN/m^2) on the shear plane, and z is the normal stress (MN/m^2) on the tool face).

WORK	V	a	f	Fc	Ft	N	F	F/N
PVC	200	-20	0.16	52	26	59.6	7.1	0.12
PVC	200	0	0.16	49	21	49	2.1	0.43
PVC	200	30	0.16	36	5	33.1	25.8	0.78
HDPE	200	-20	0.16	37	15	42.5	1.5	0.04
HDPE	200	0	0.16	21	4	21	4	0.19
HDPE	200	30	0.16	14	2	12.8	10.1	0.79
Copper	150	6	0.16	500	250	474	303	0.64
Mild Steel	150	6	0.16	417	271	389	315	0.81
Free Cutting Steel	150	6	0.16	396	292	365	334	0.92
Austenitic Stainless Steel	150	6	0.16	479	417	435	467	1.07
Cast Iron	122	6	0.16	267	338	231	267	1.16

(The data for metals were obtained from Ref.9)

Table 6. Comparison of the ratio of shear to normal force on the rake face when machining plastics and metals

(V is the cutting speed (m/min), a is the rake angle (degree), f is the feed rate (mm/rev), Fc is the cutting force (Newton), Ft is the feed force (Newton), N is the normal and F is the shear force (Newton) on the rake face)

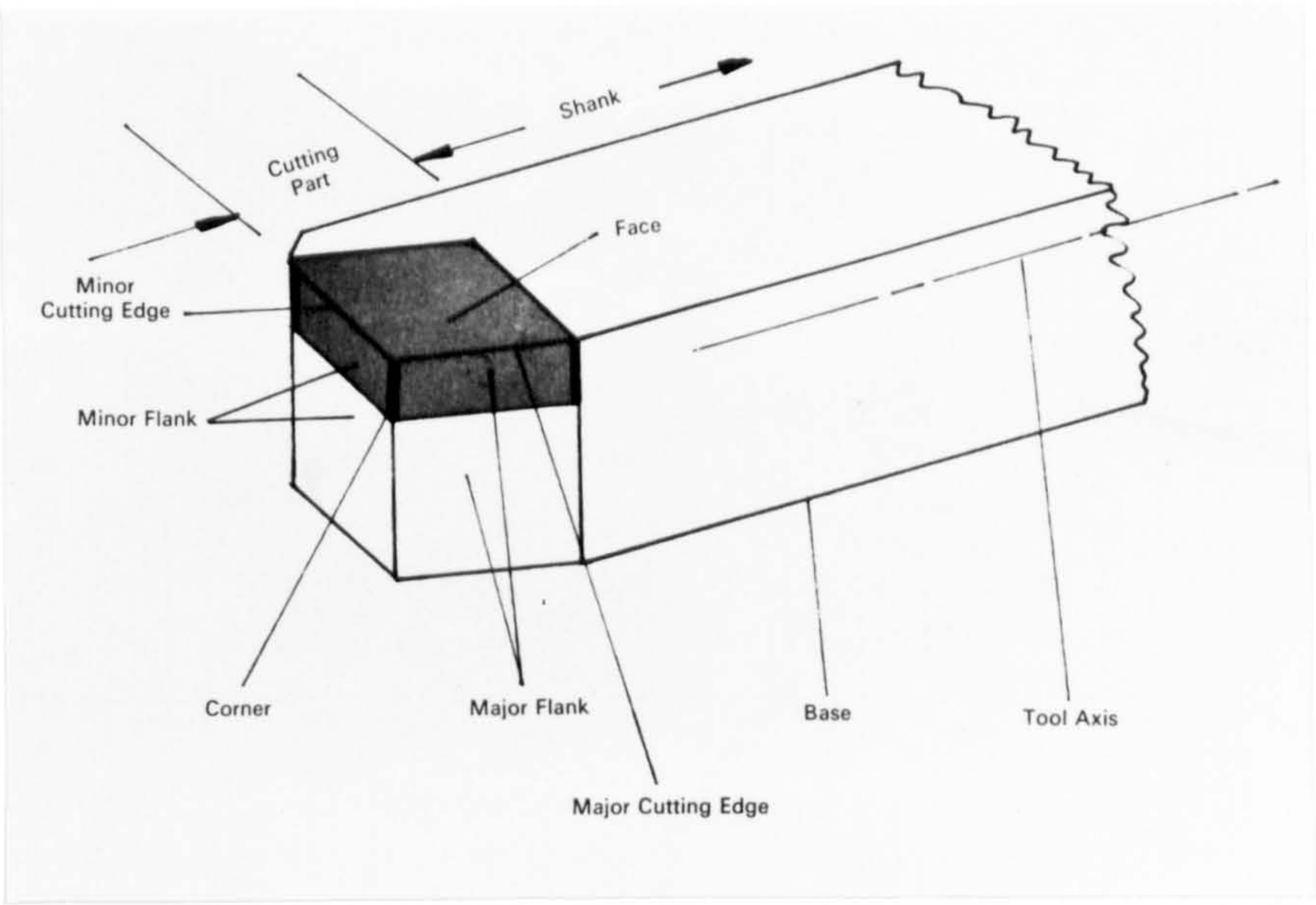

Fig 1. Typical single-point turning tool

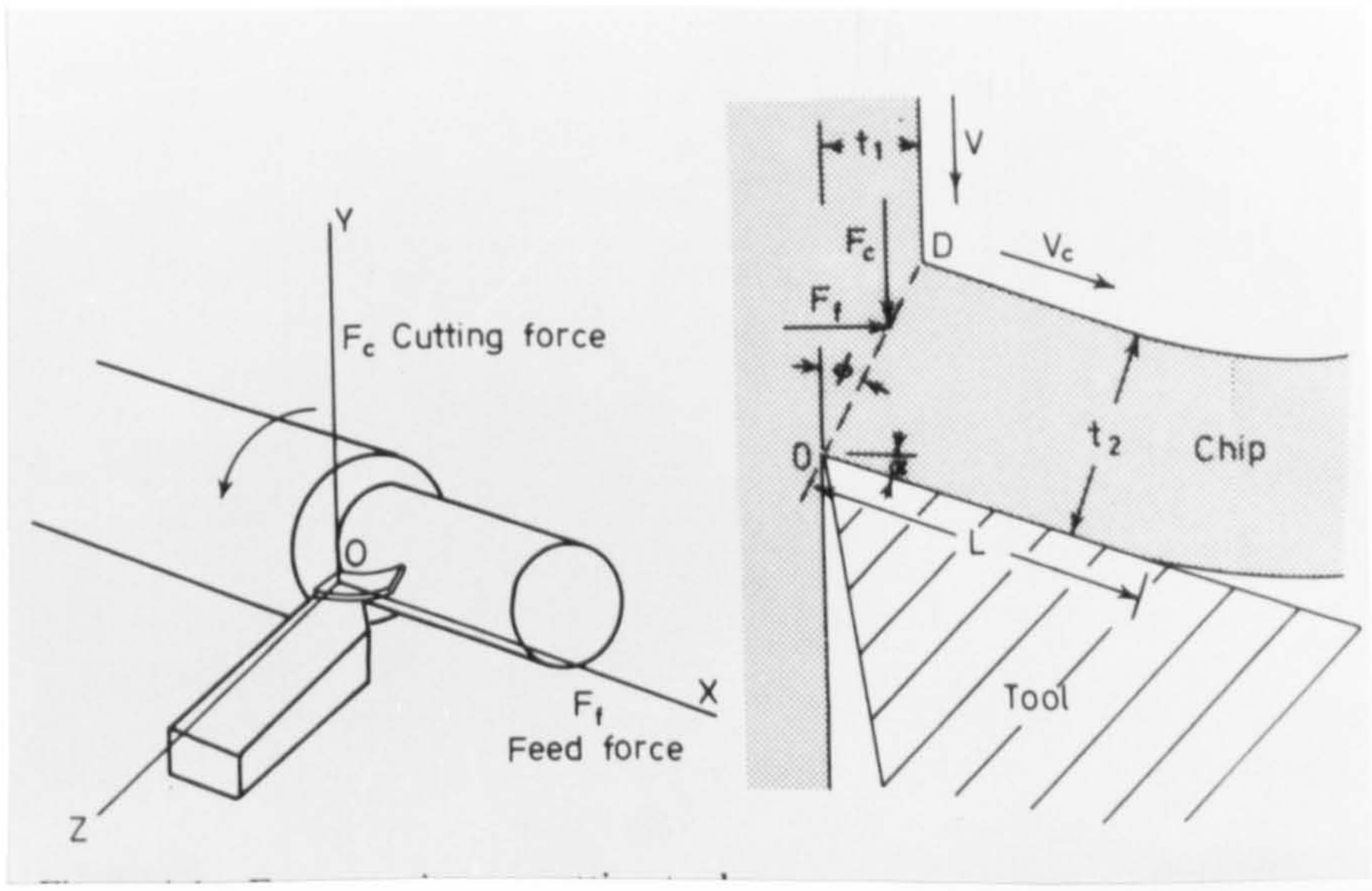

Fig 2. Forces acting on the tool (9)

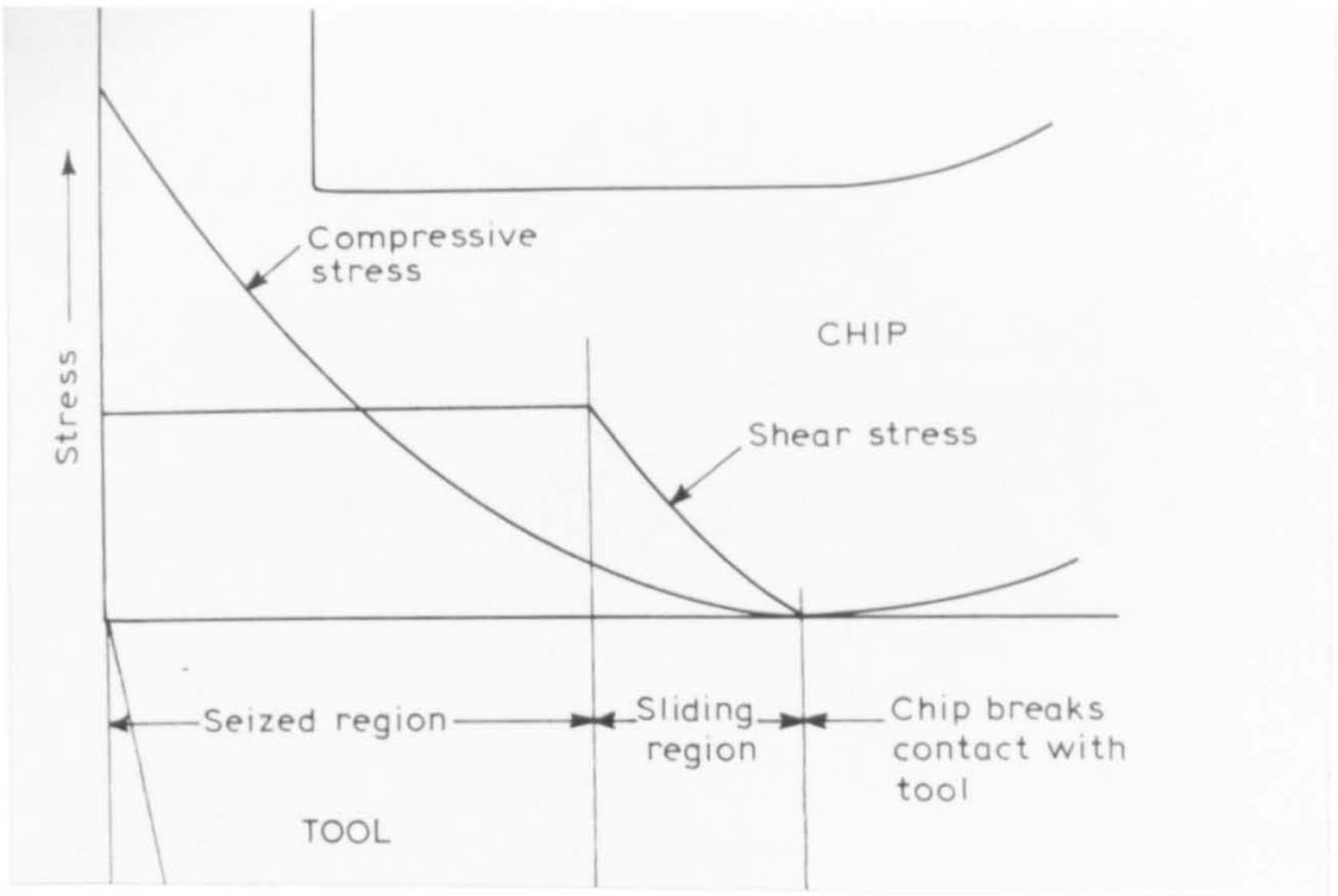

Fig 3. Model of stress-distribution on tool when machining steel (9)

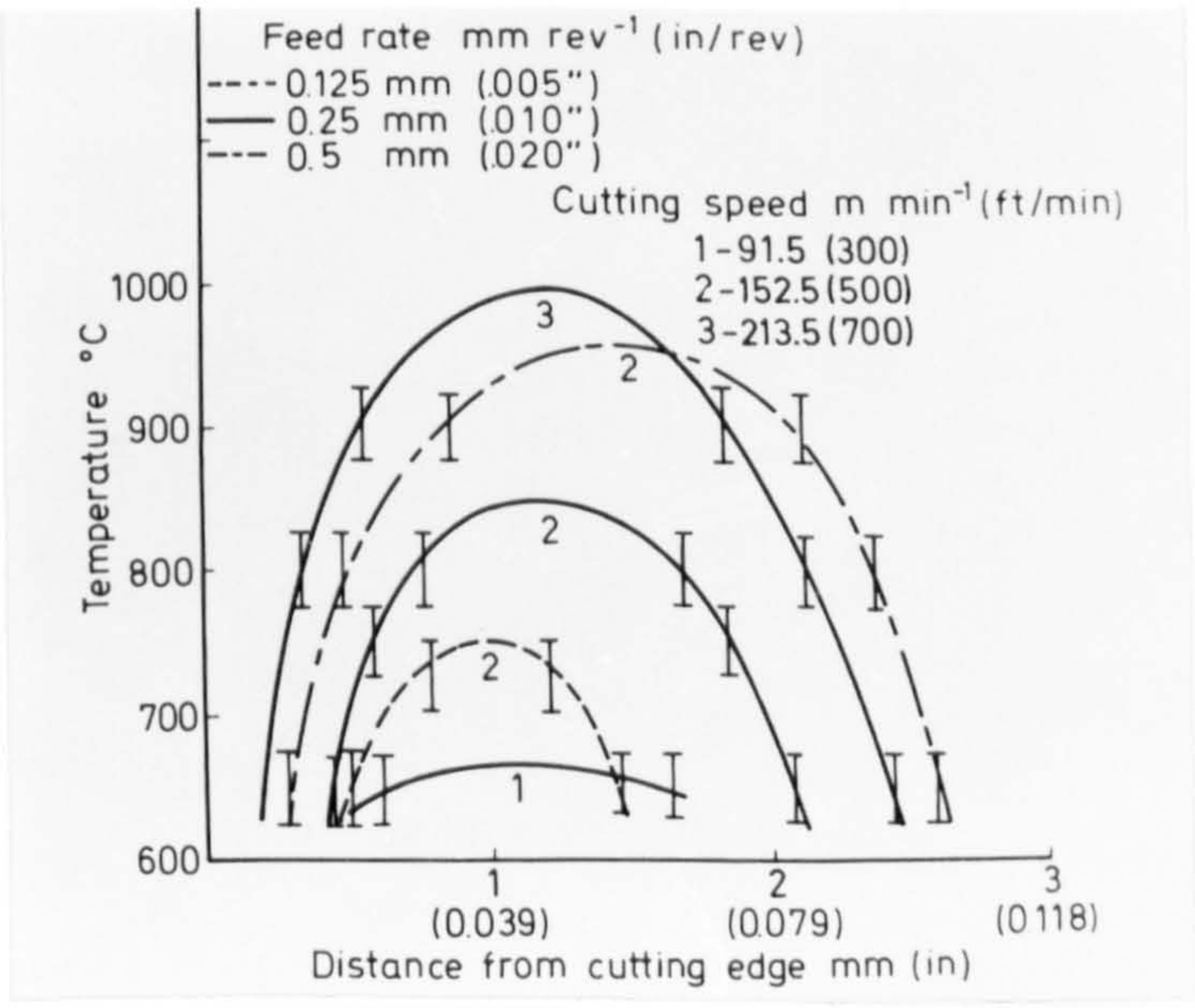

Fig 4. Temperature distribution on rake face when machining low carbon steel at different speeds and feeds (9)

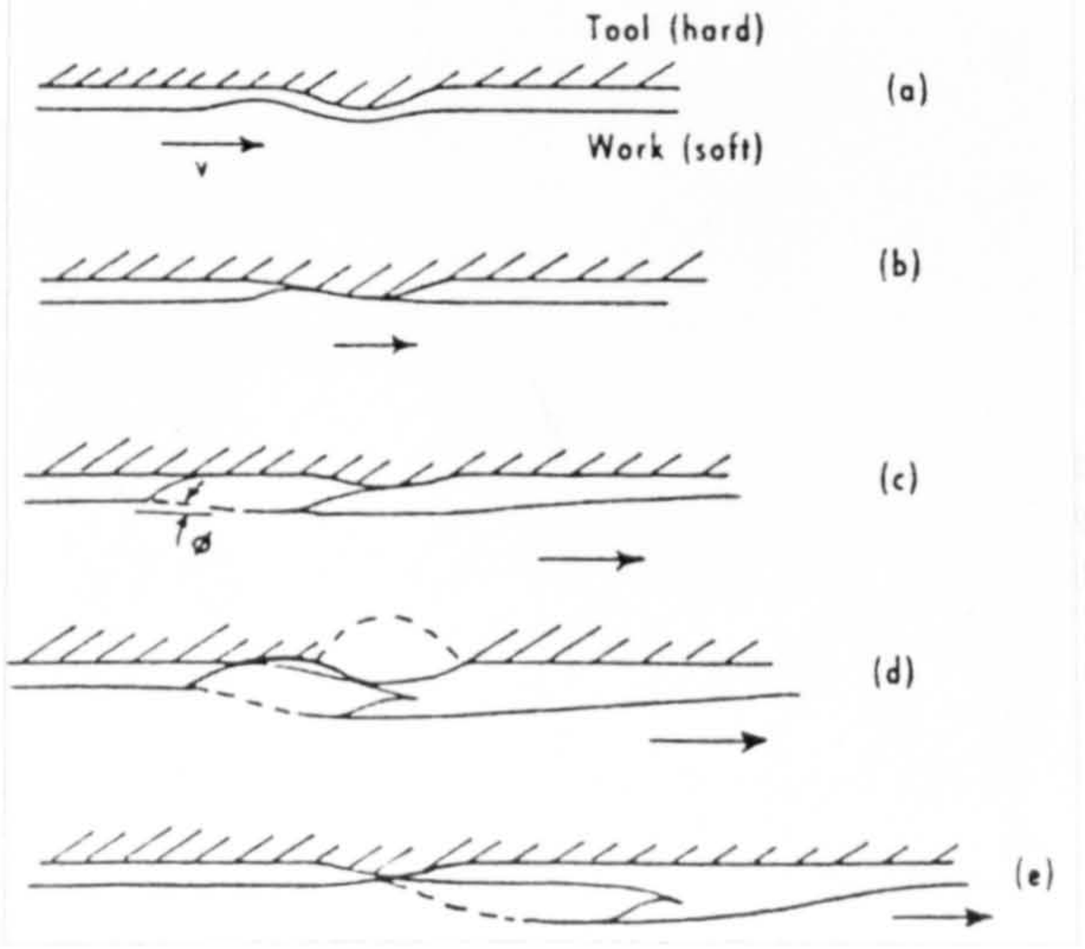

Fig 5. Mechanism of microchip formation on tool flank (46)

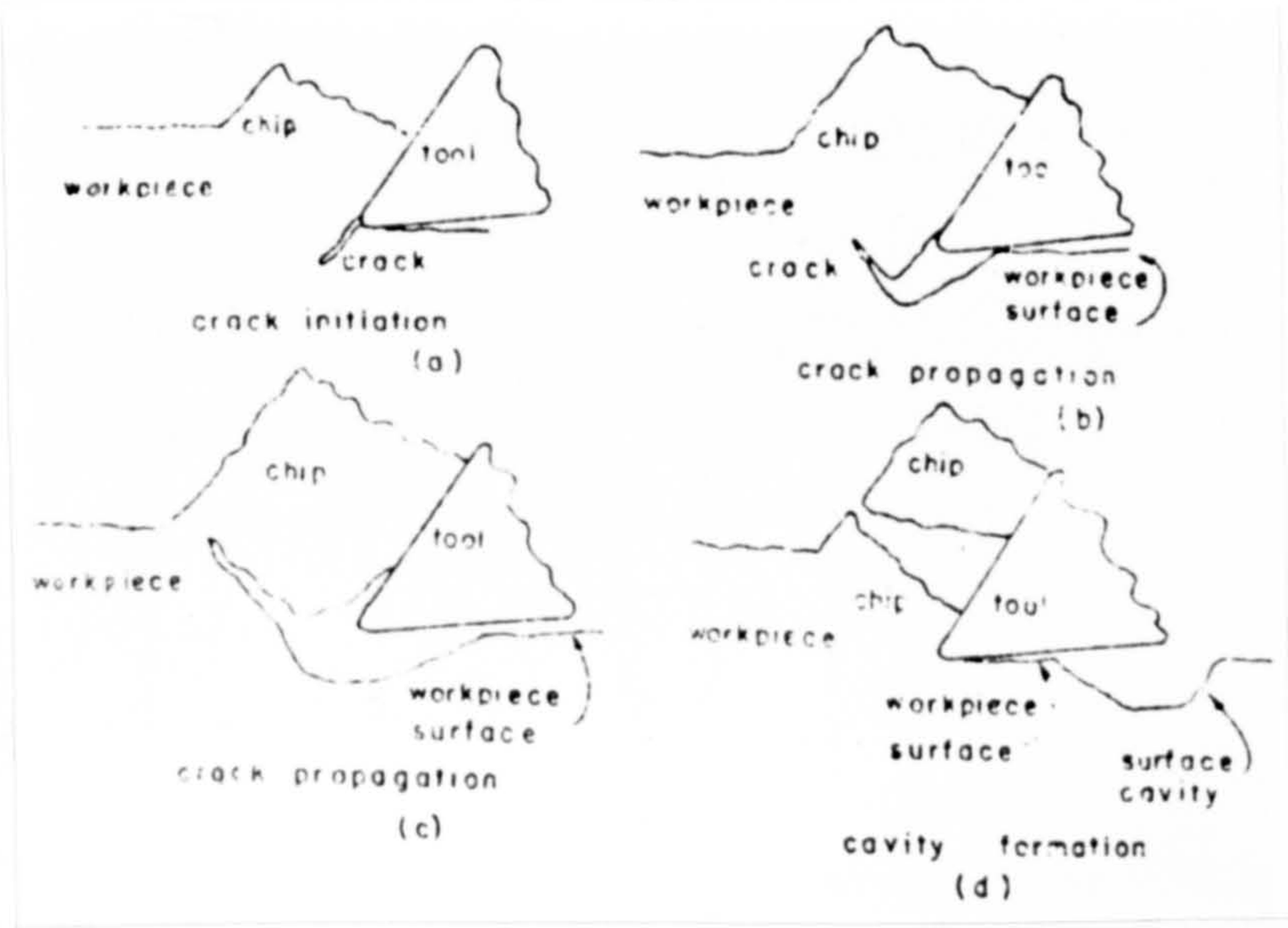

Fig 6. Schematic diagram showing a mechanism of crack propagation (61)

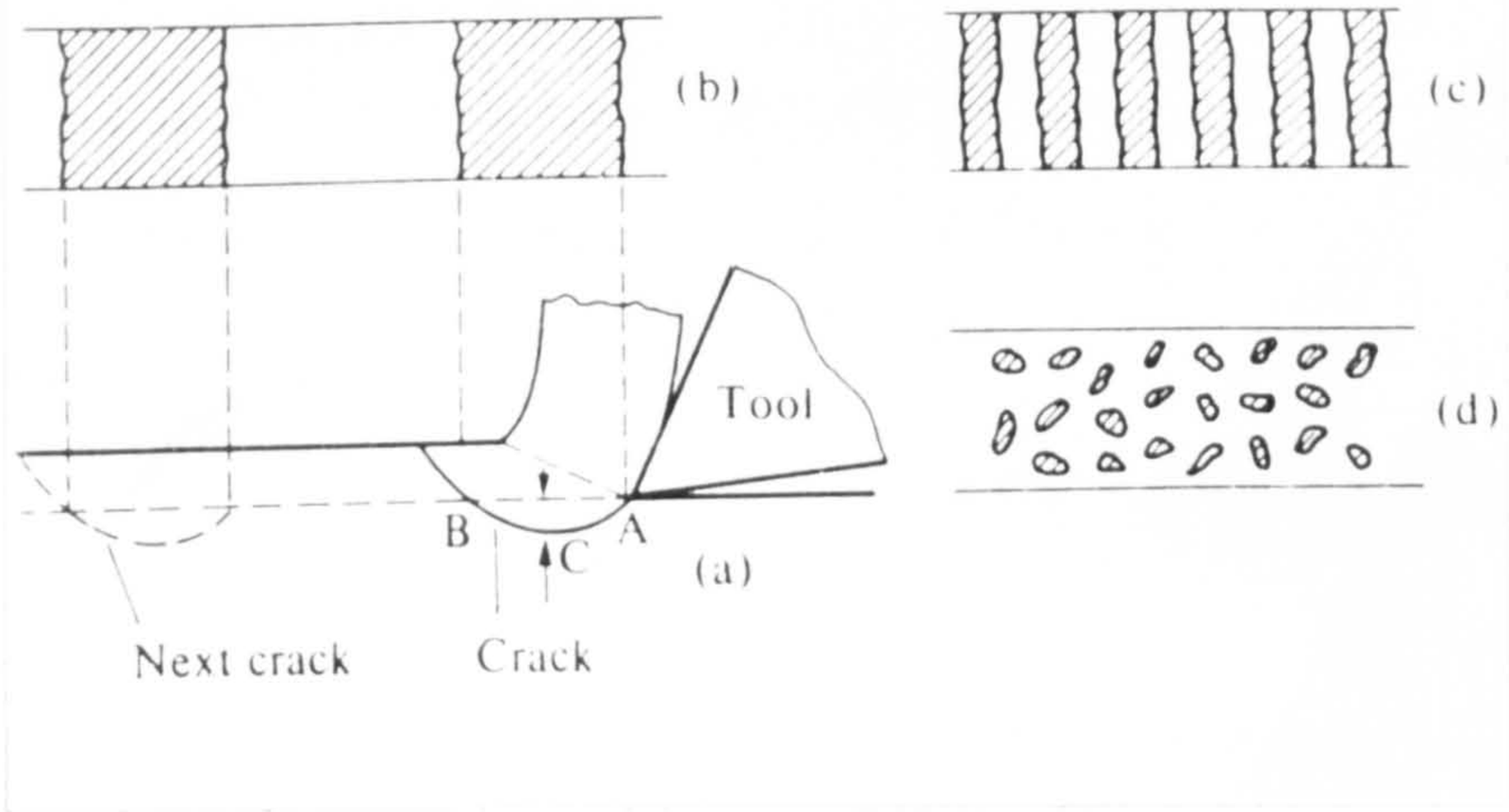

Fig 7. Schematic diagram showing cracks and their influence on surface texture (62)

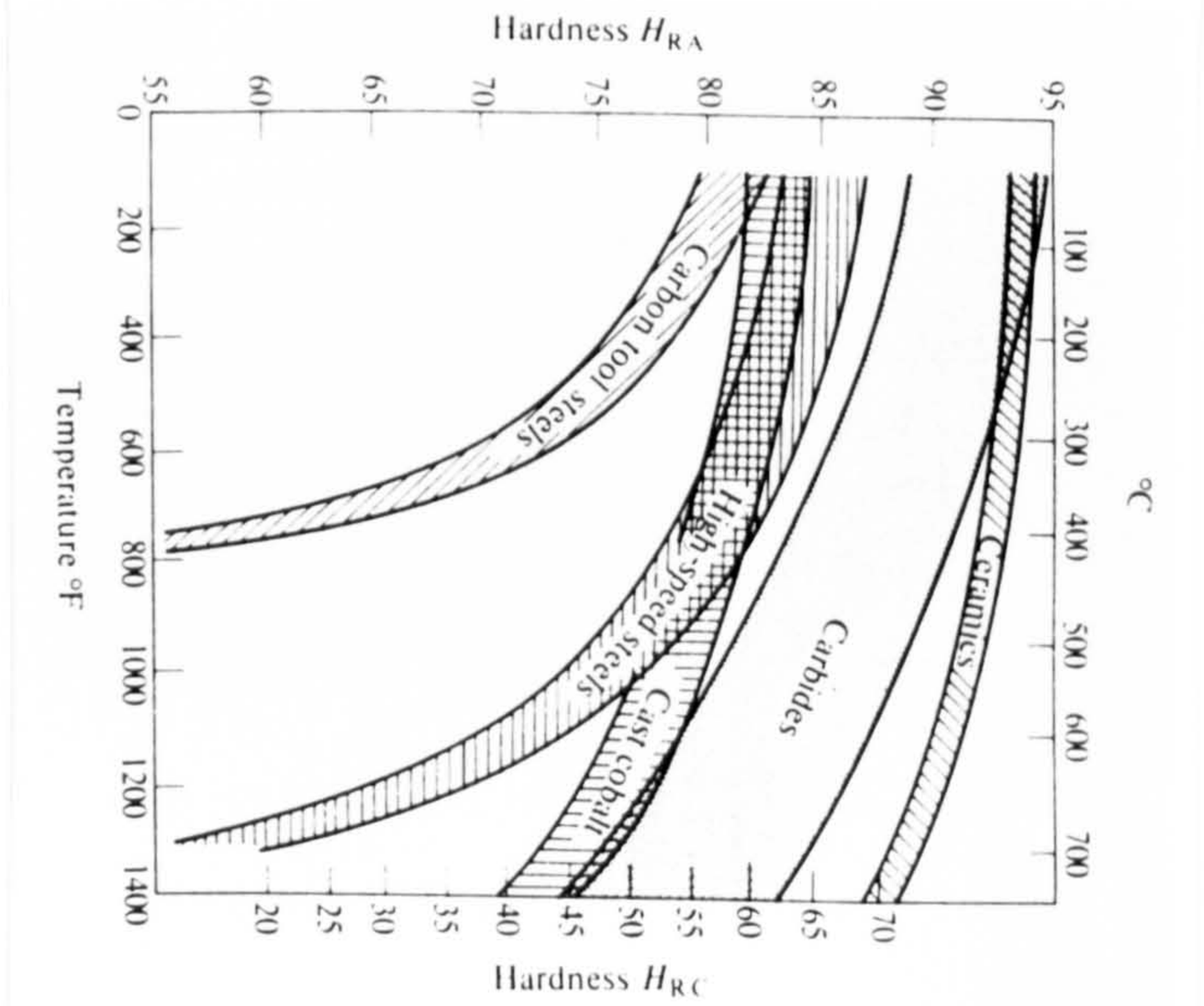

Fig 8. Hot-hardness of several types of tool materials (54)

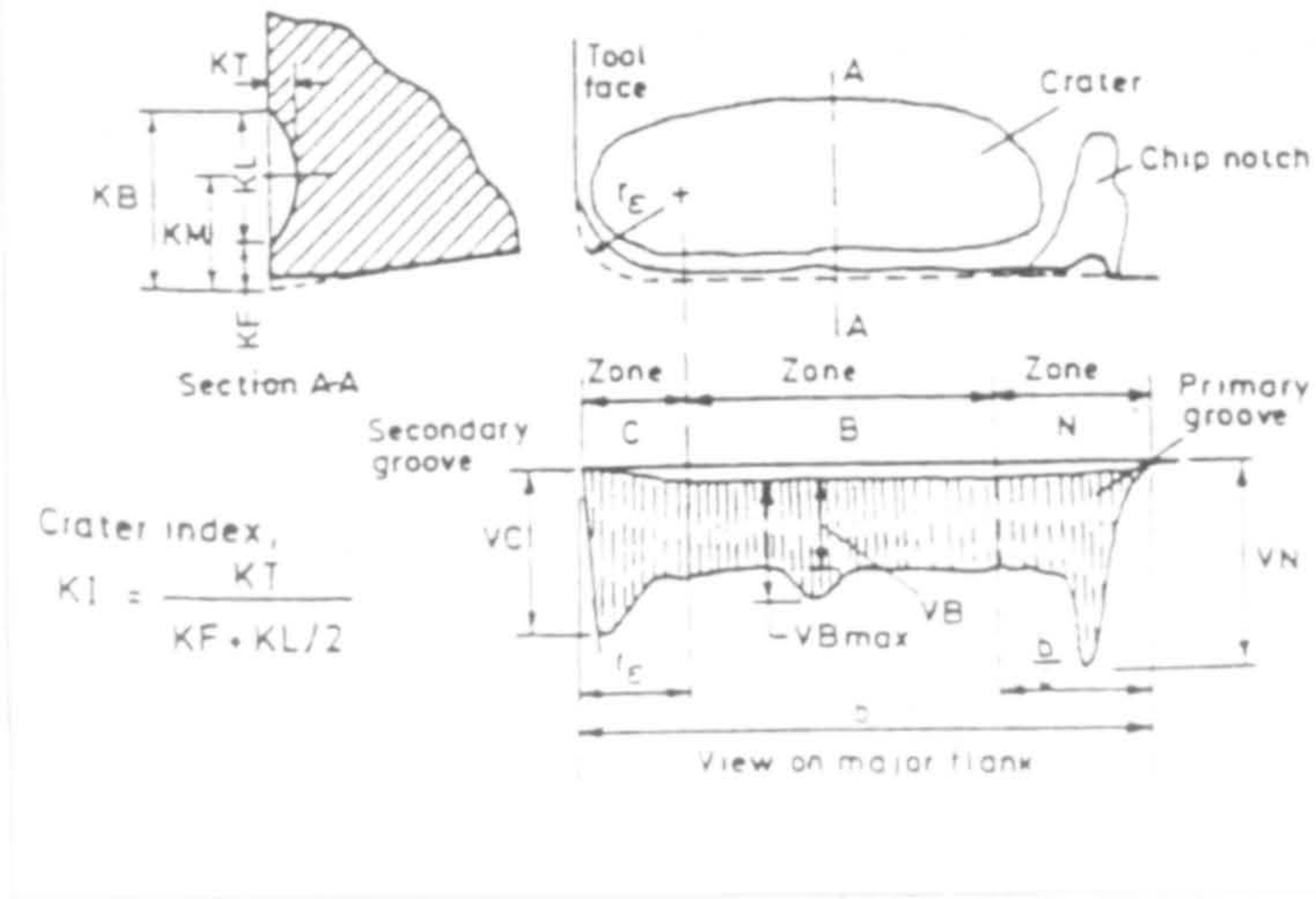

Fig 9. Common features of tool wear (97)

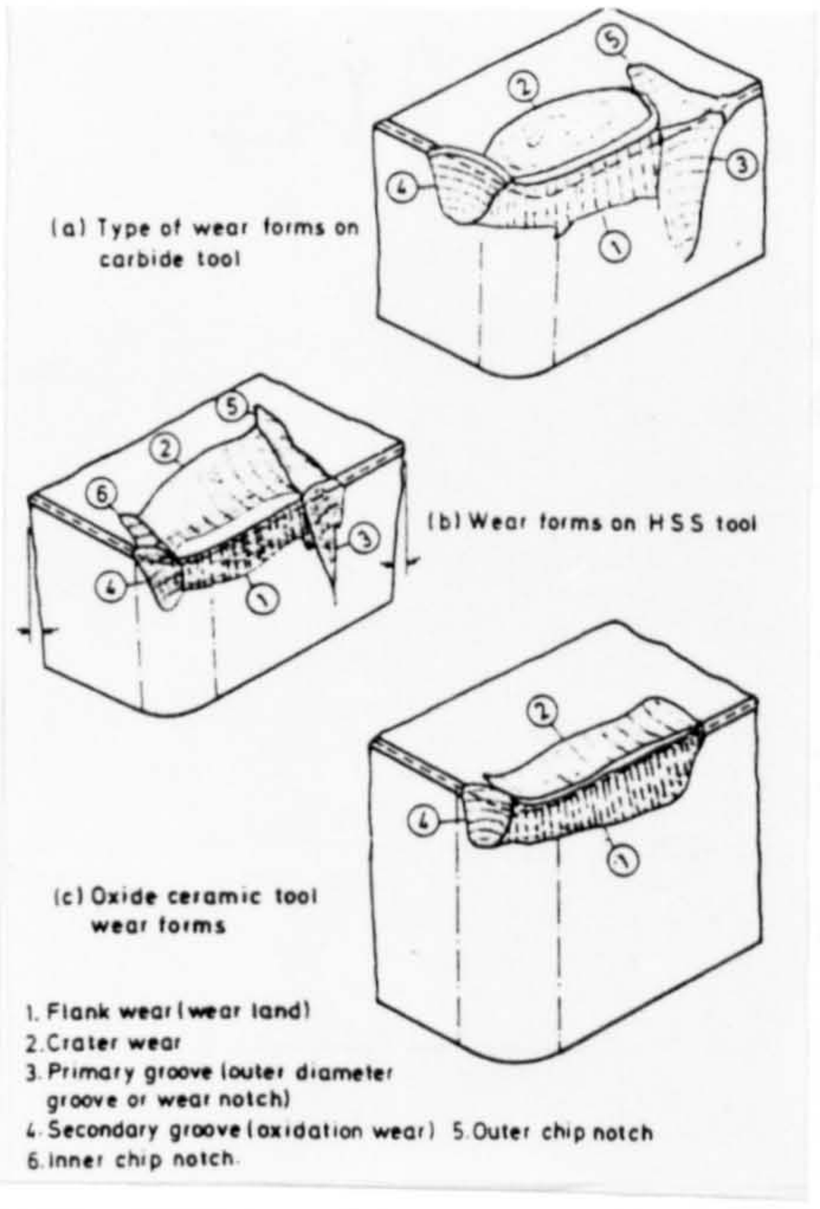

Fig 10. Wear forms of various cutting tools (64)

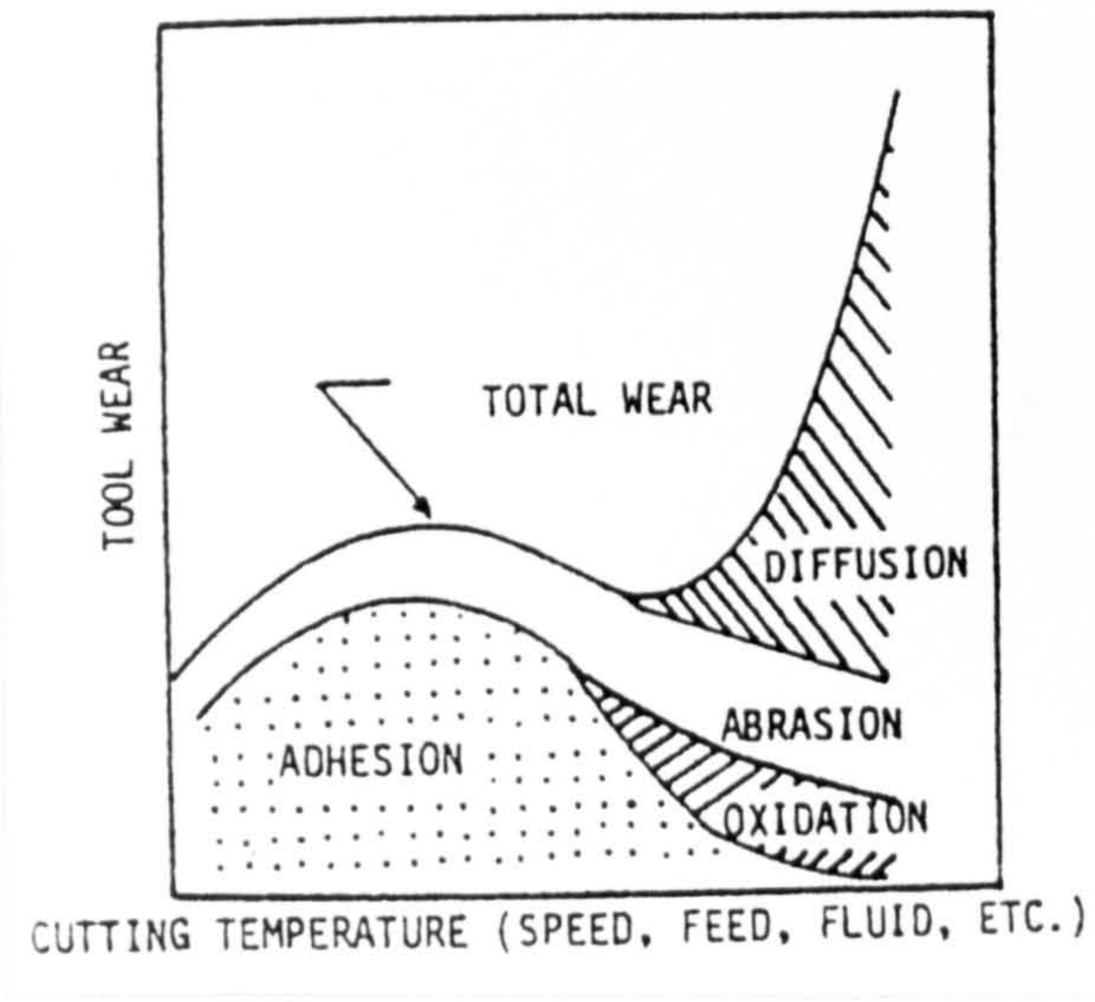

Fig 11. Contributions of various aspects to total tool wear as a function of cutting temperature (66)

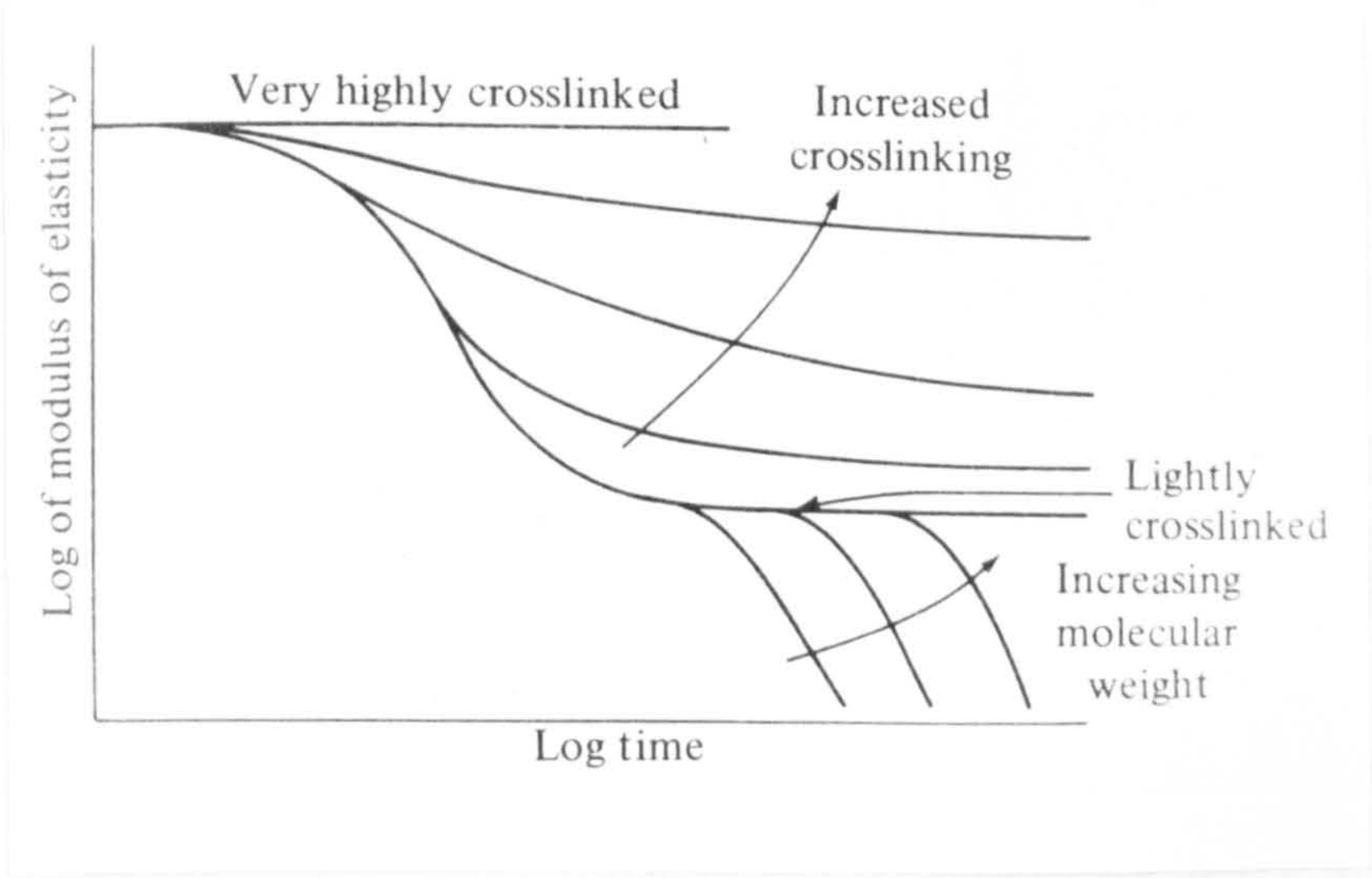

Fig 12. Effect of cross-linking and molecular weight of polymers on the modulus of elasticity (110)

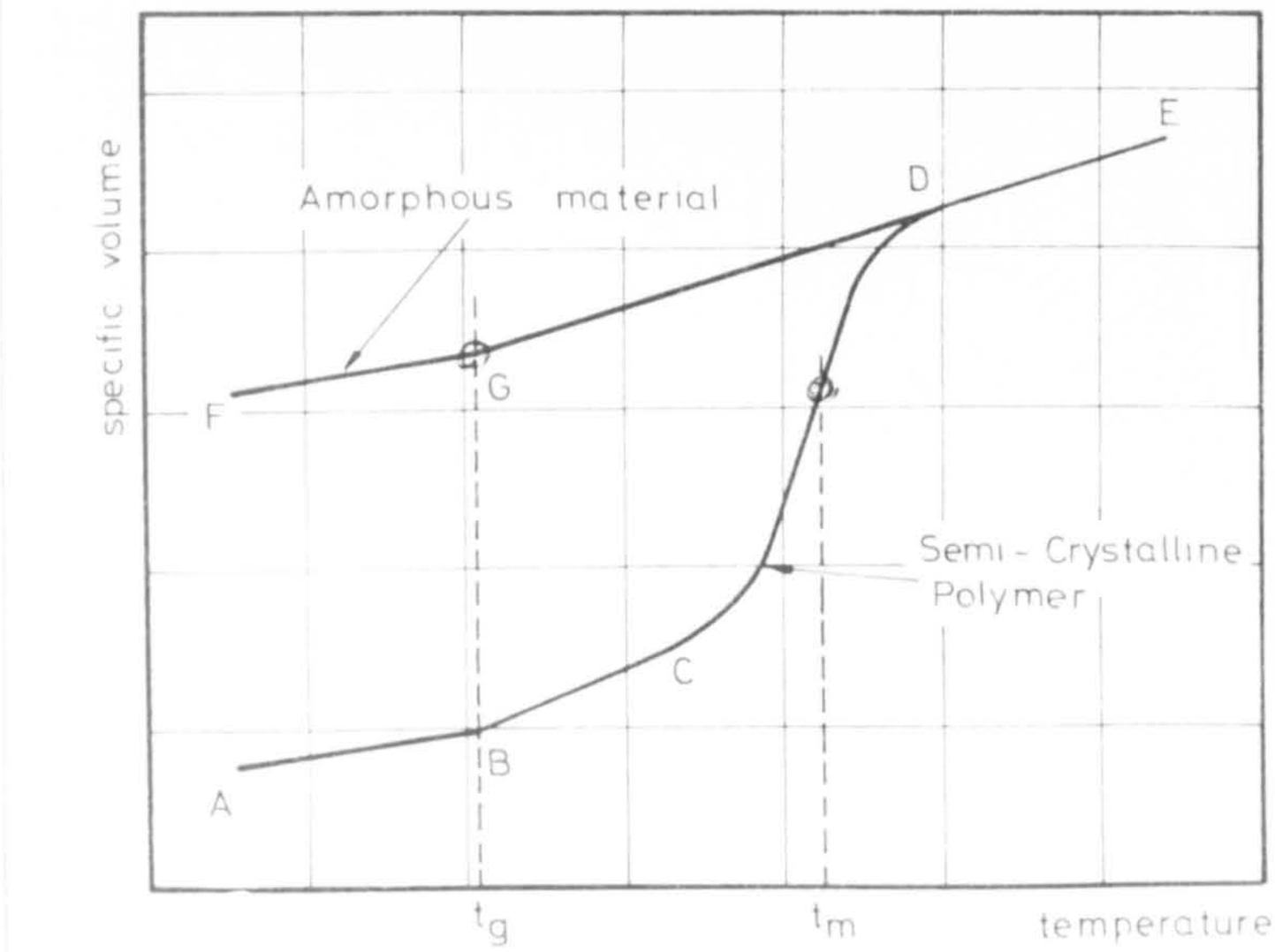

Fig 13. Specific volume-temperature curves for amorphous and semi-crystalline polymers (1)

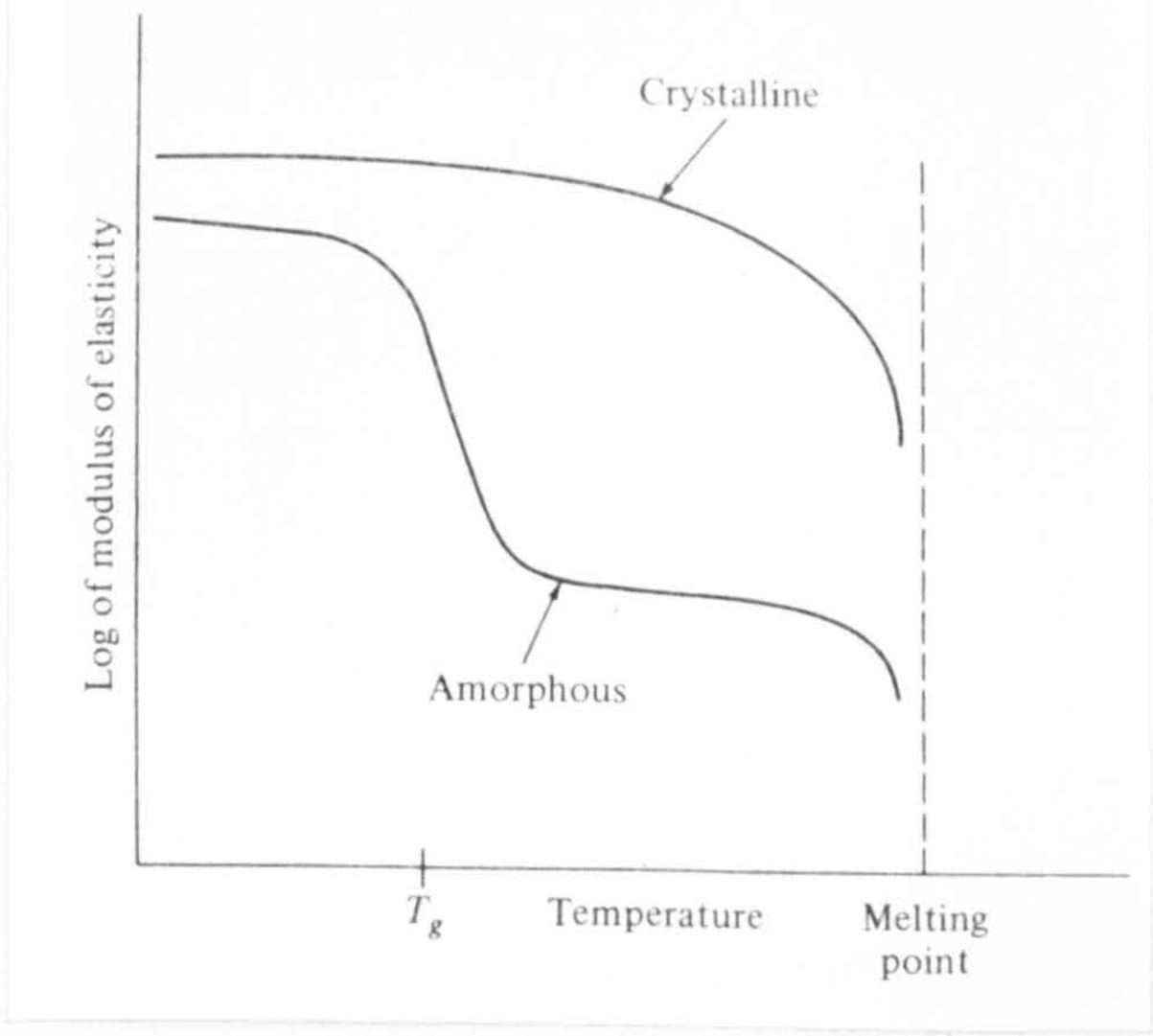

Fig 14. Effect of crystallinity on the modulus of elasticity (110)

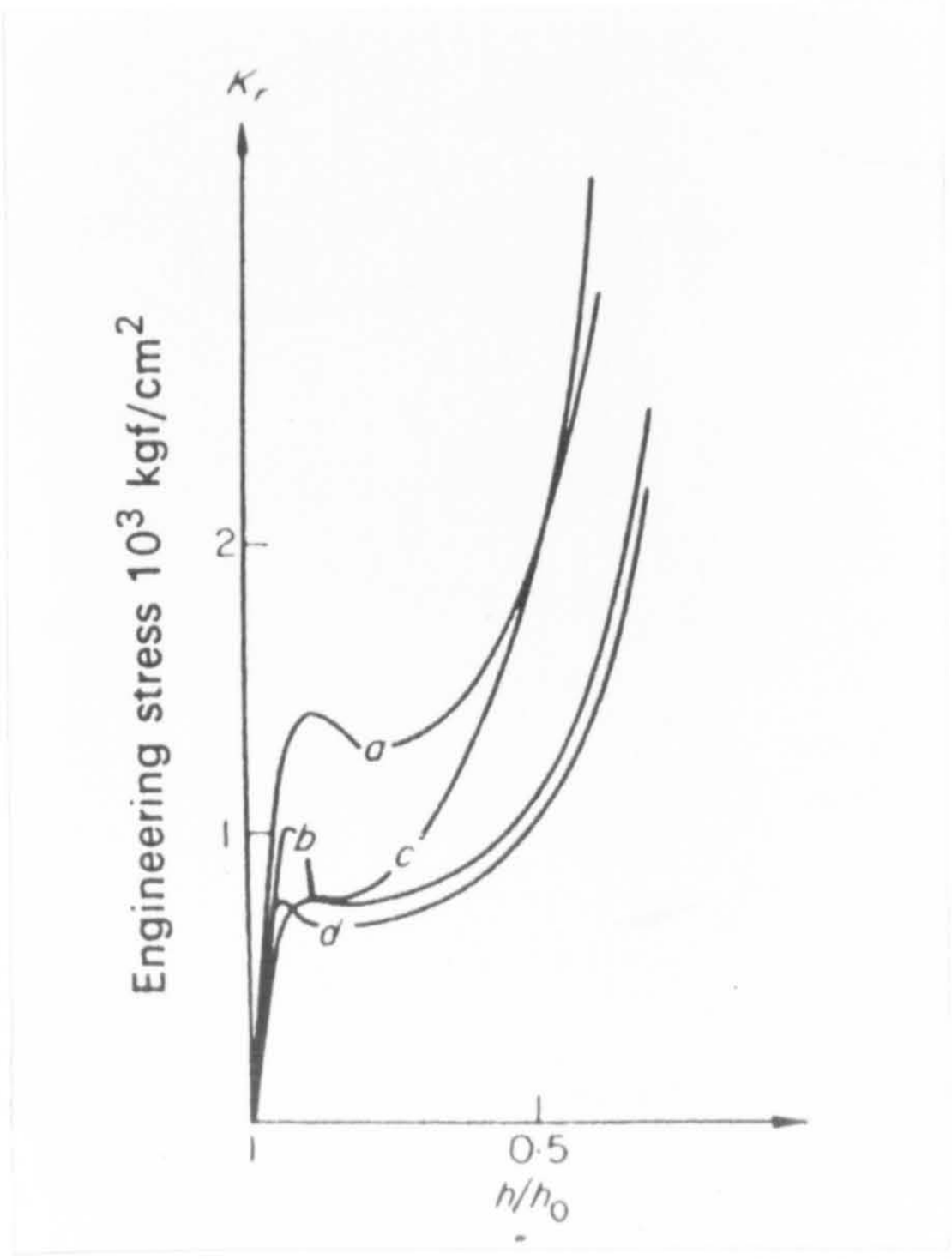

Fig 15. Compression curves for different glassy polymers exhibiting strain-softening (175)

(a) Polymethyl Methacrylate (b) Polystyrene
(c) Polycarbonate (d) Polyvinyl Chloride

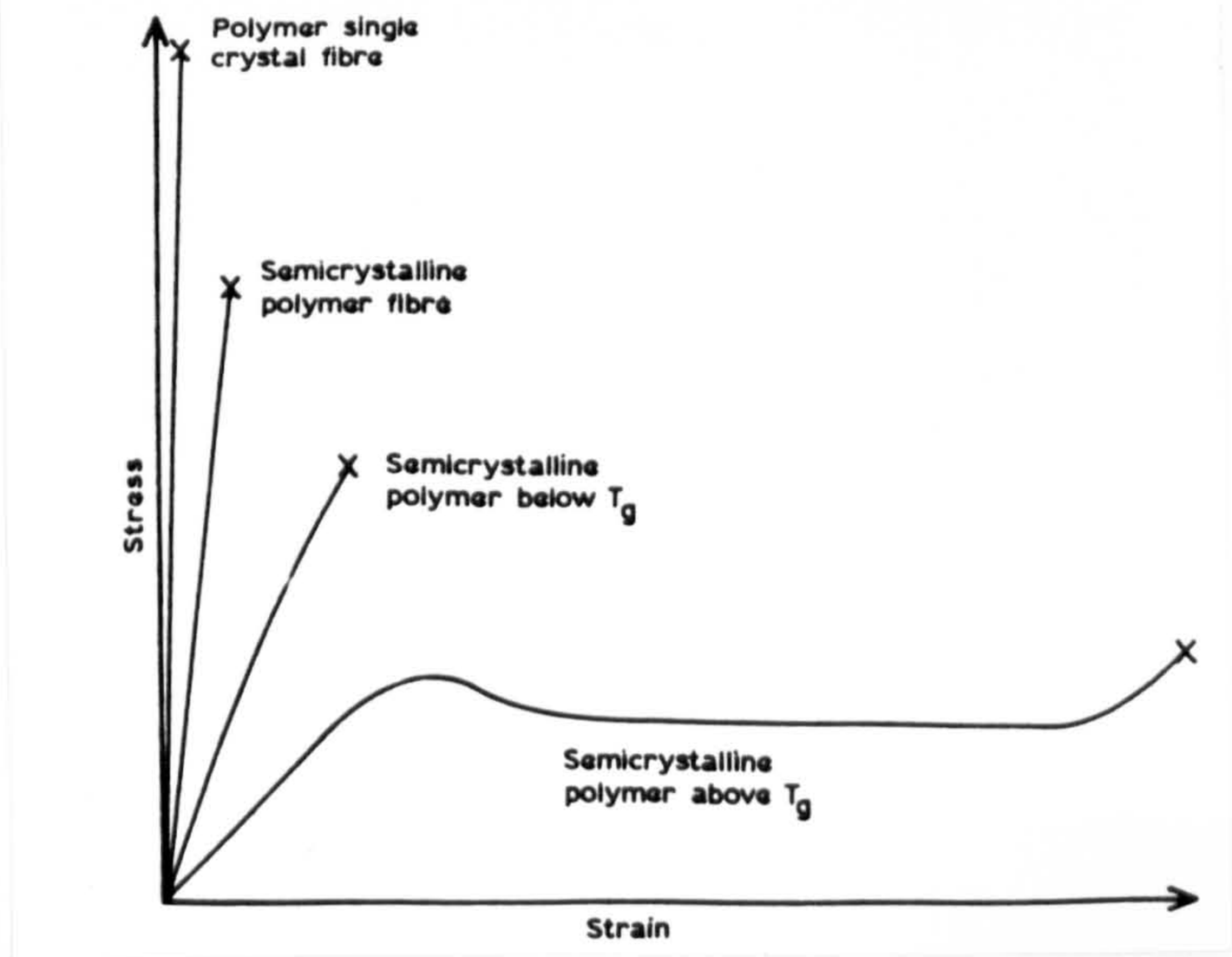

Fig 16. Schematic stress/strain curves for crystalline polymers in different morphological forms (111)

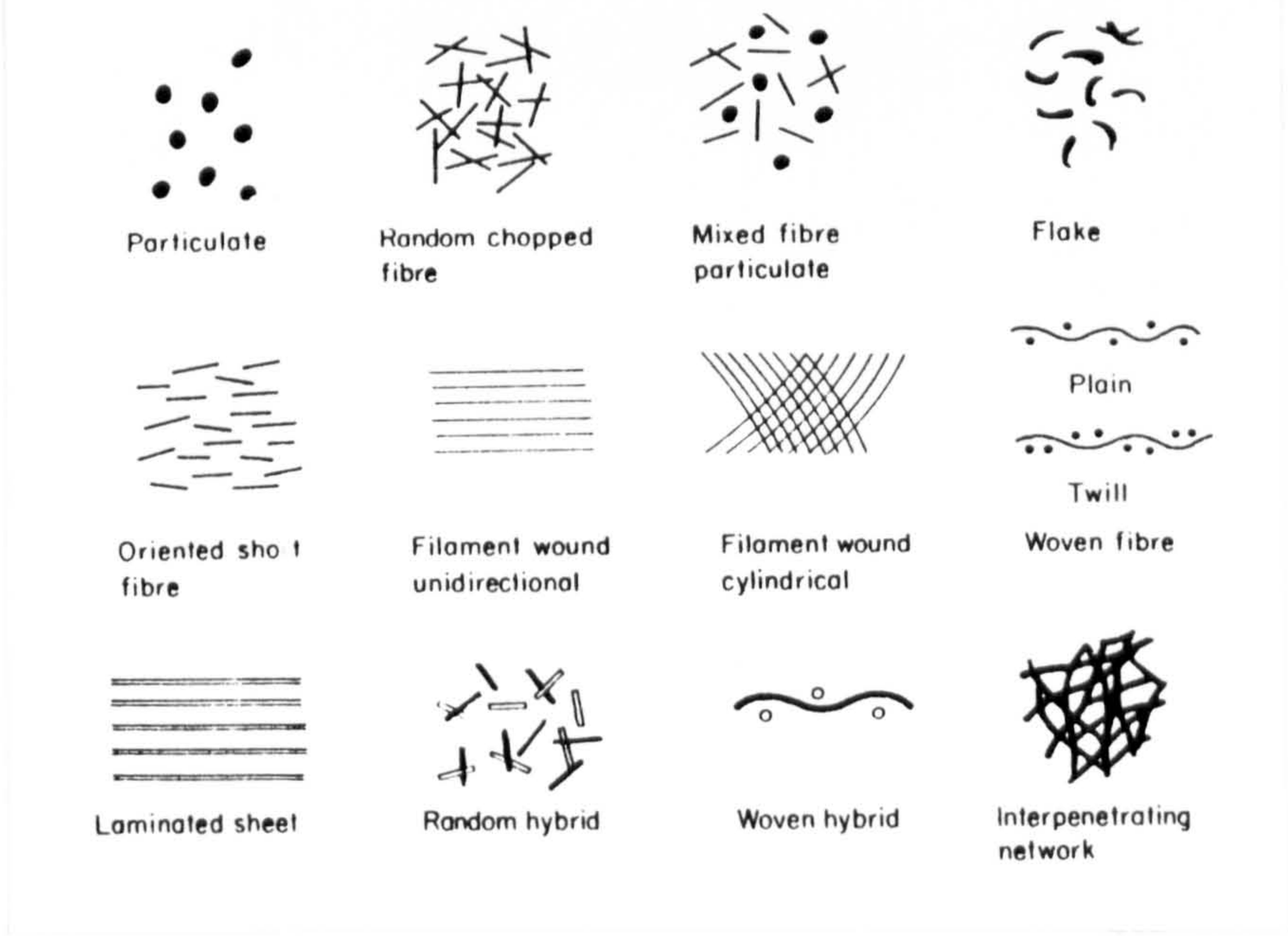

Fig 17. Examples of different composite geometrical arrangement (6)

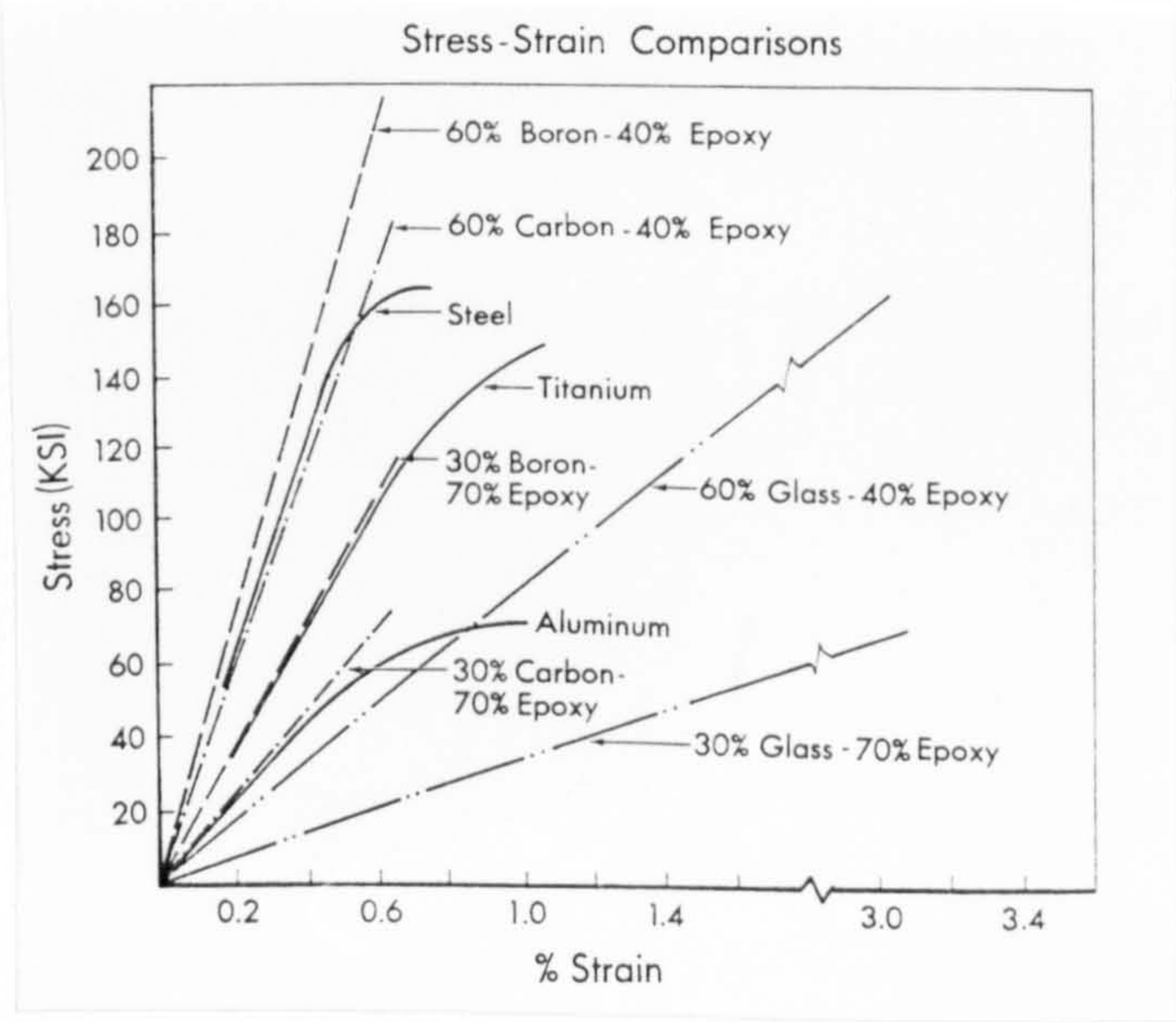

Fig 18. Comparison of the tensile properties of engineering materials at 20°C (136)

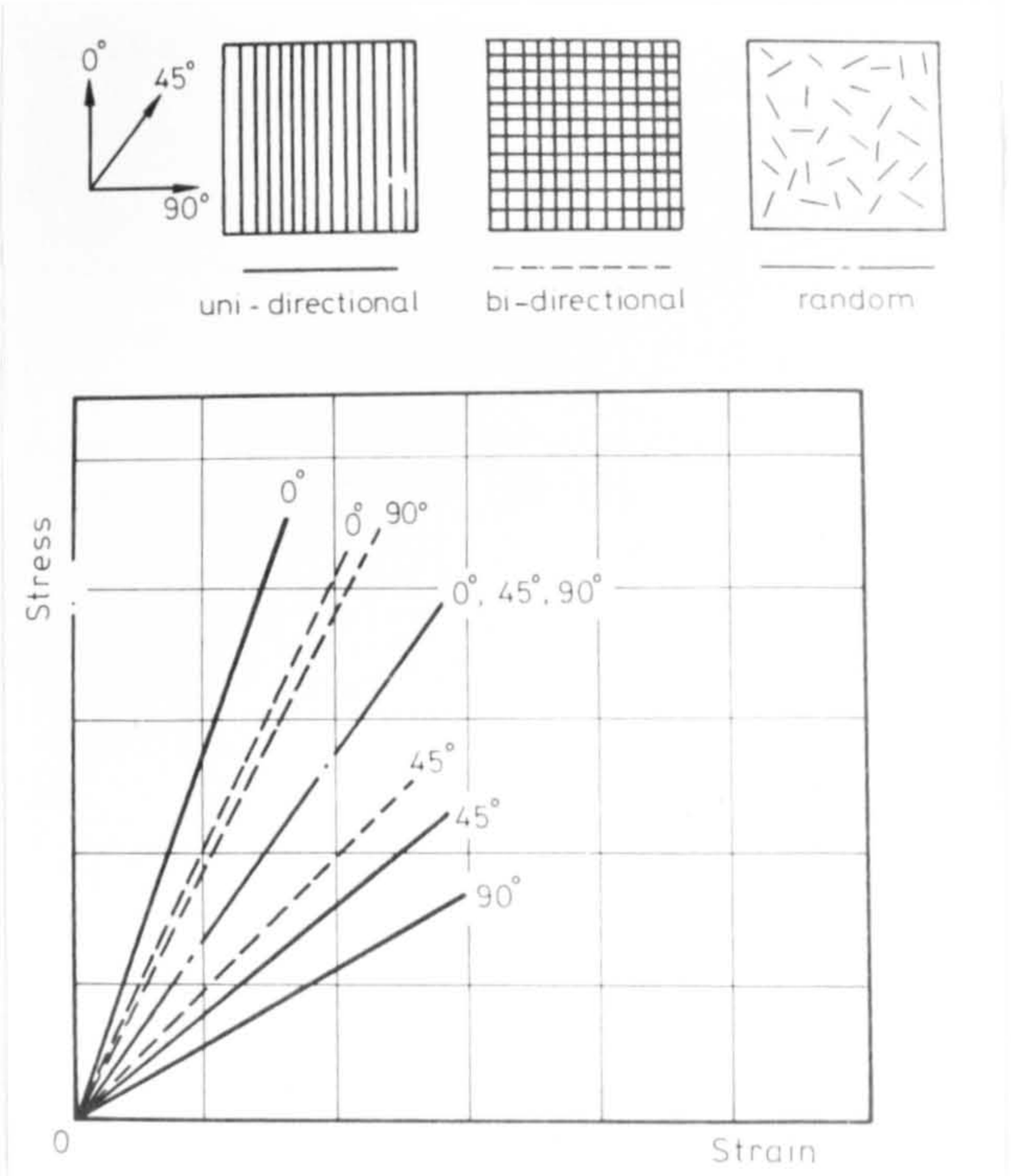

Fig 19. Stress/strain behaviour of several types of fibre reinforcement (1)

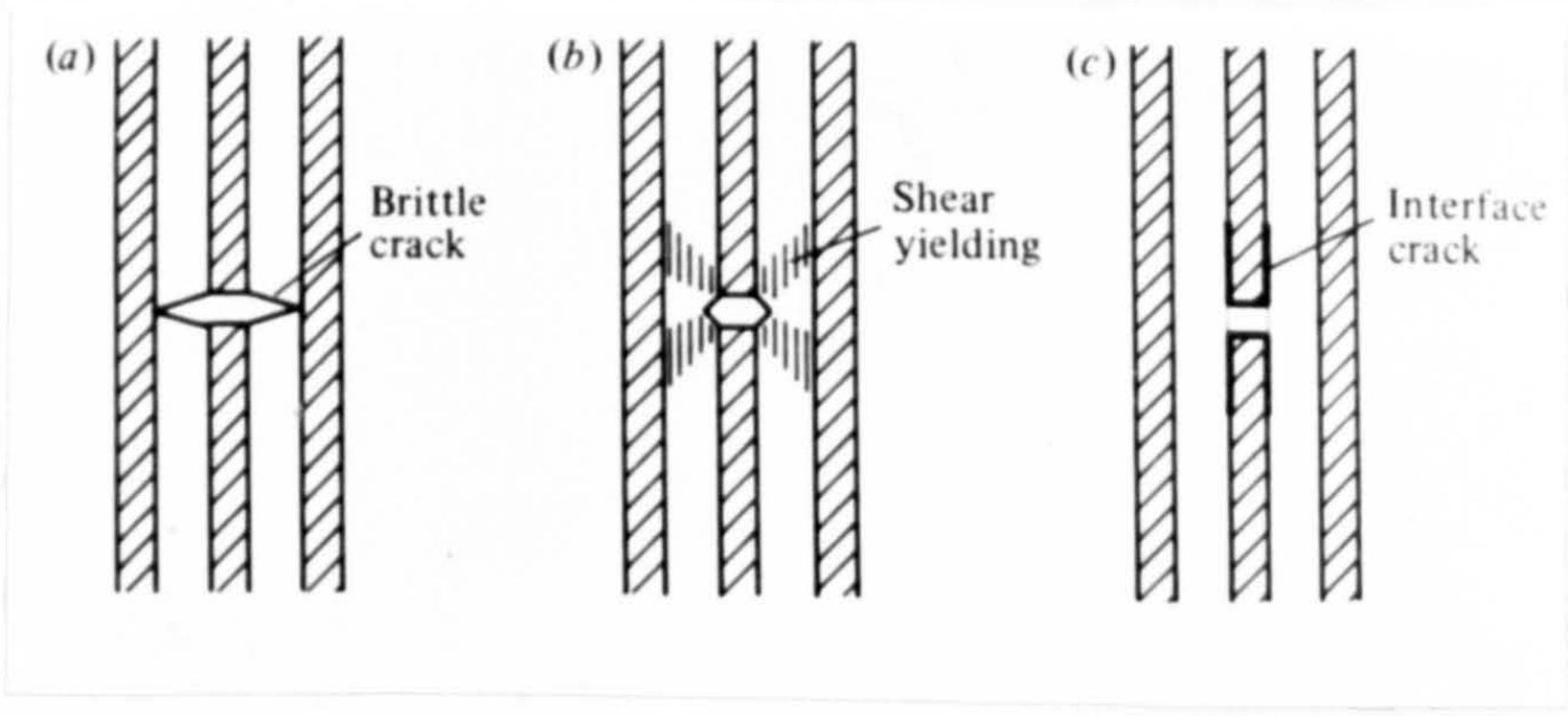

Fig 20. Failure processes around a fibre fracture (134)

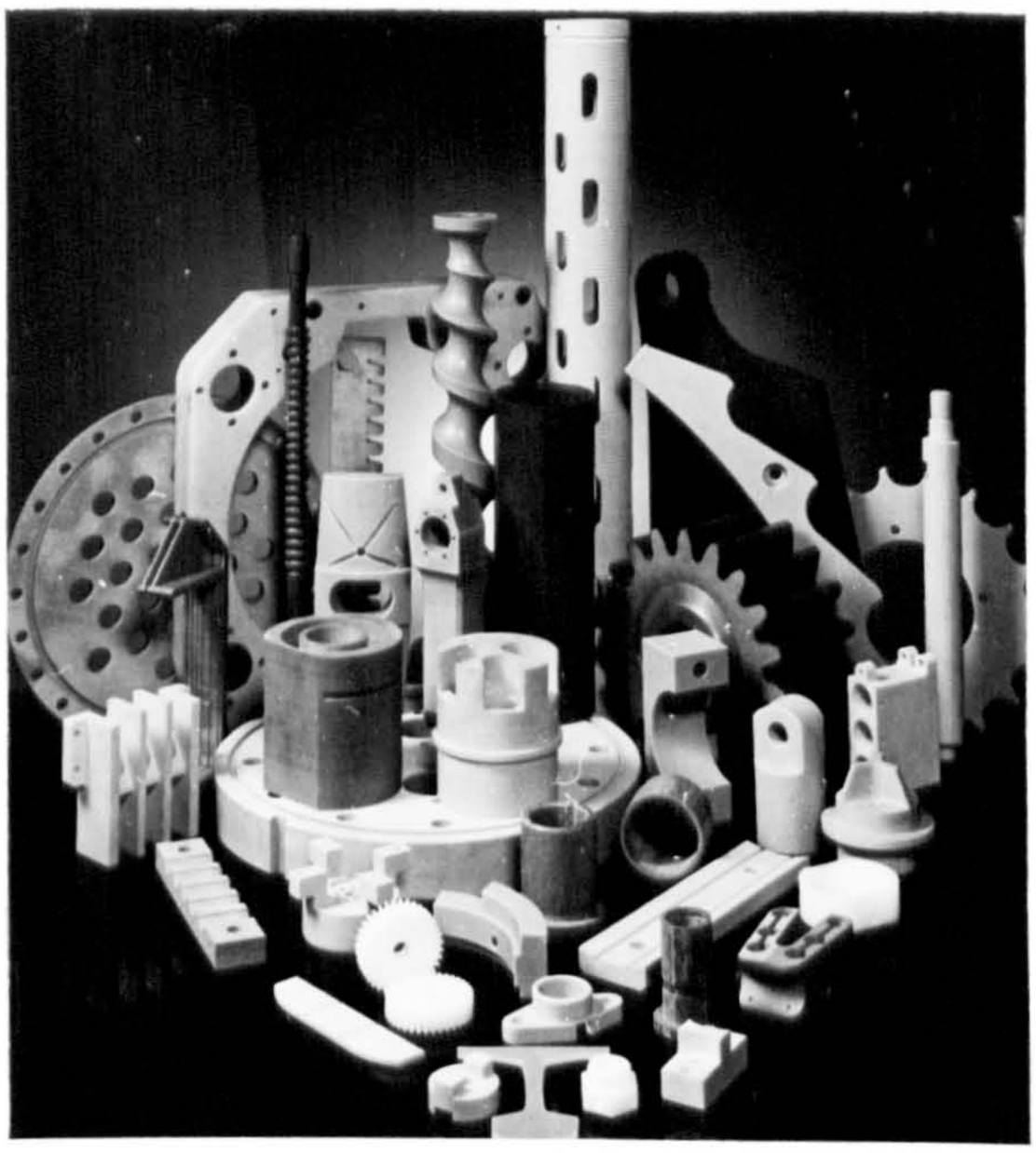

Fig 21. Composite products involving machining operations (from Tufnol Limited)

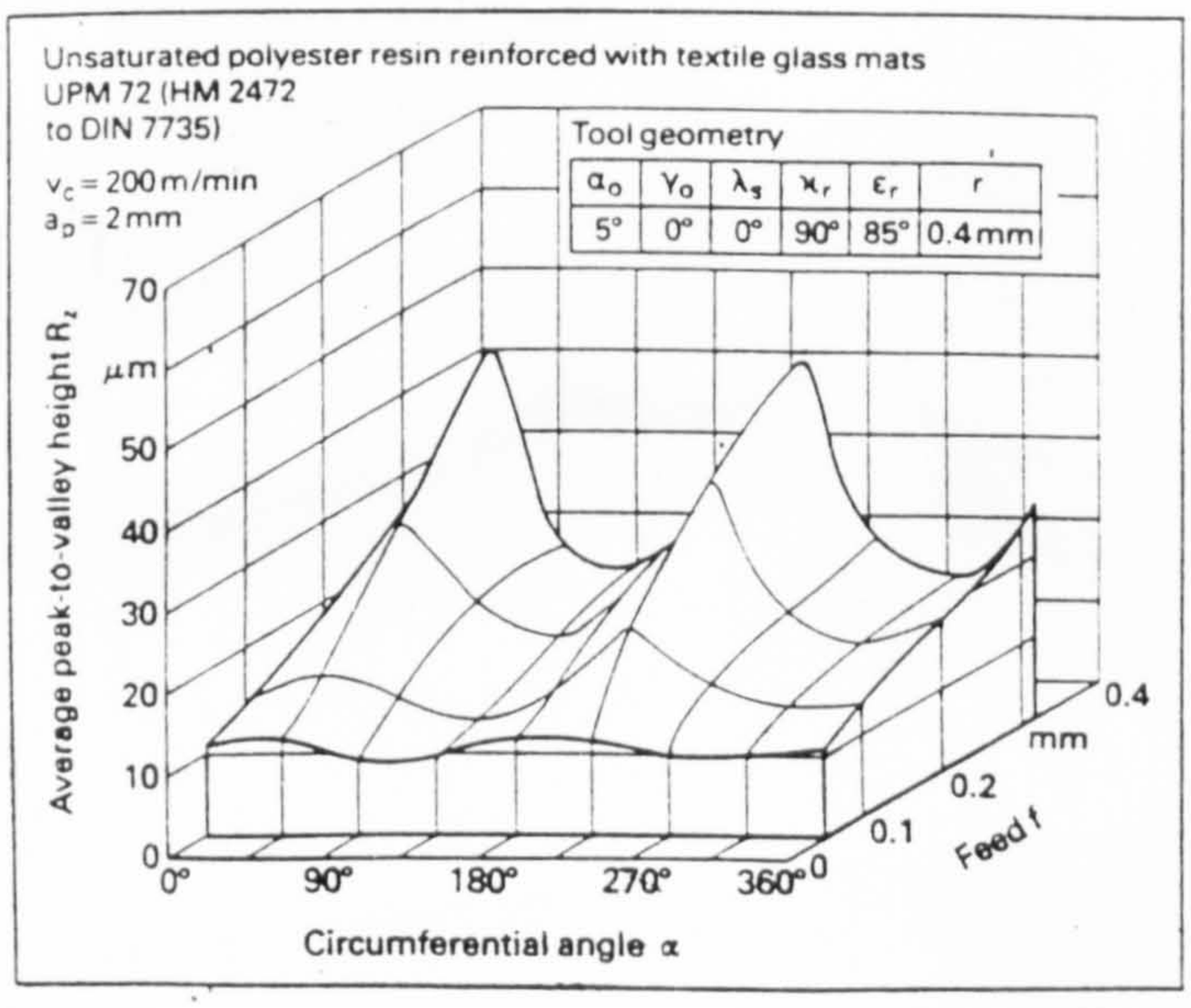

Fig 22. Effects of feed rate and angular position on surface roughness (144)

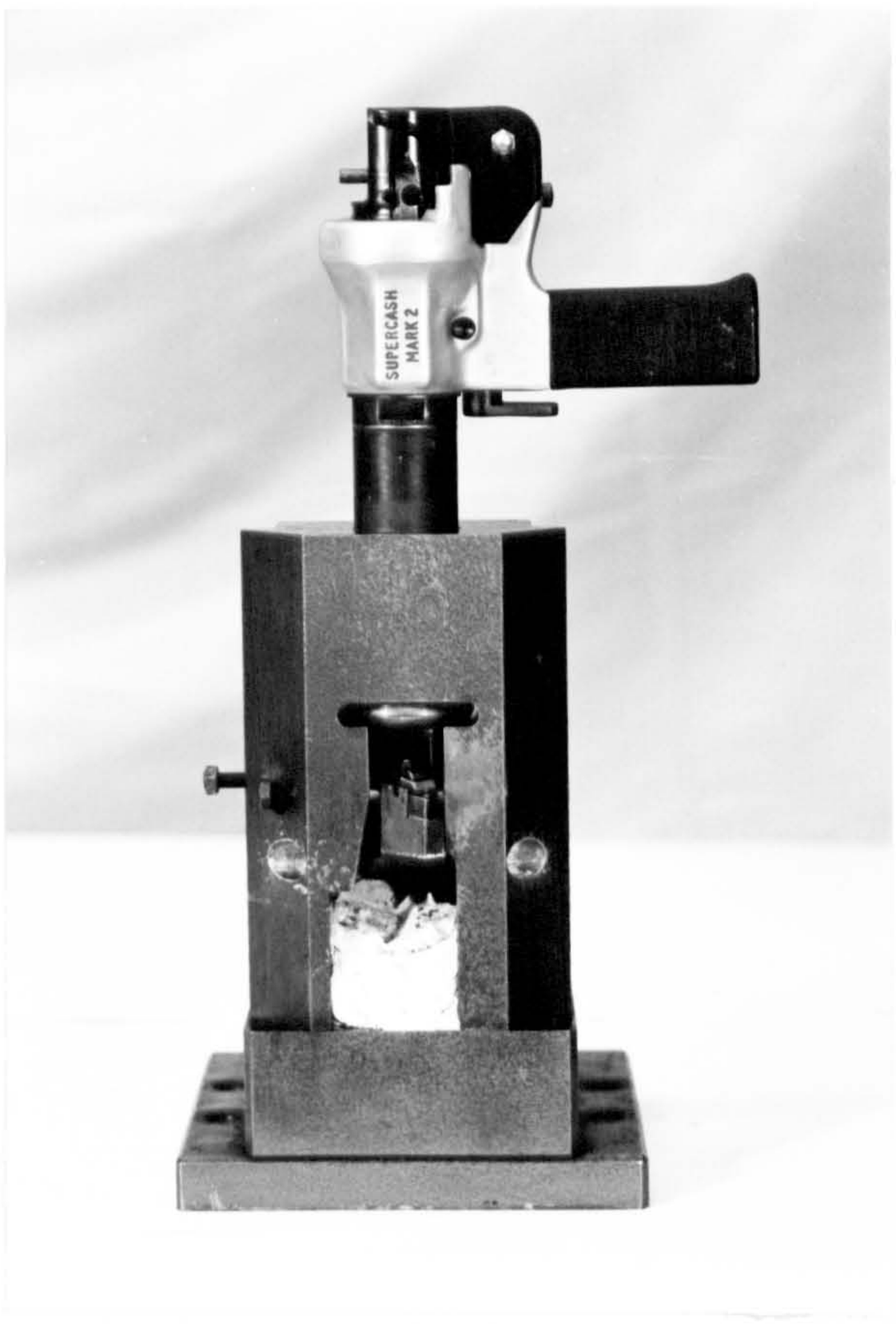

Fig 23. Quick-stop device

Fig 24. Scanning Electron Microscope (SEM)

Fig 25. Types of PVC chips at different rake angle and cutting speed (feed = 0.16 mm/rev, DOC = 1.5mm)

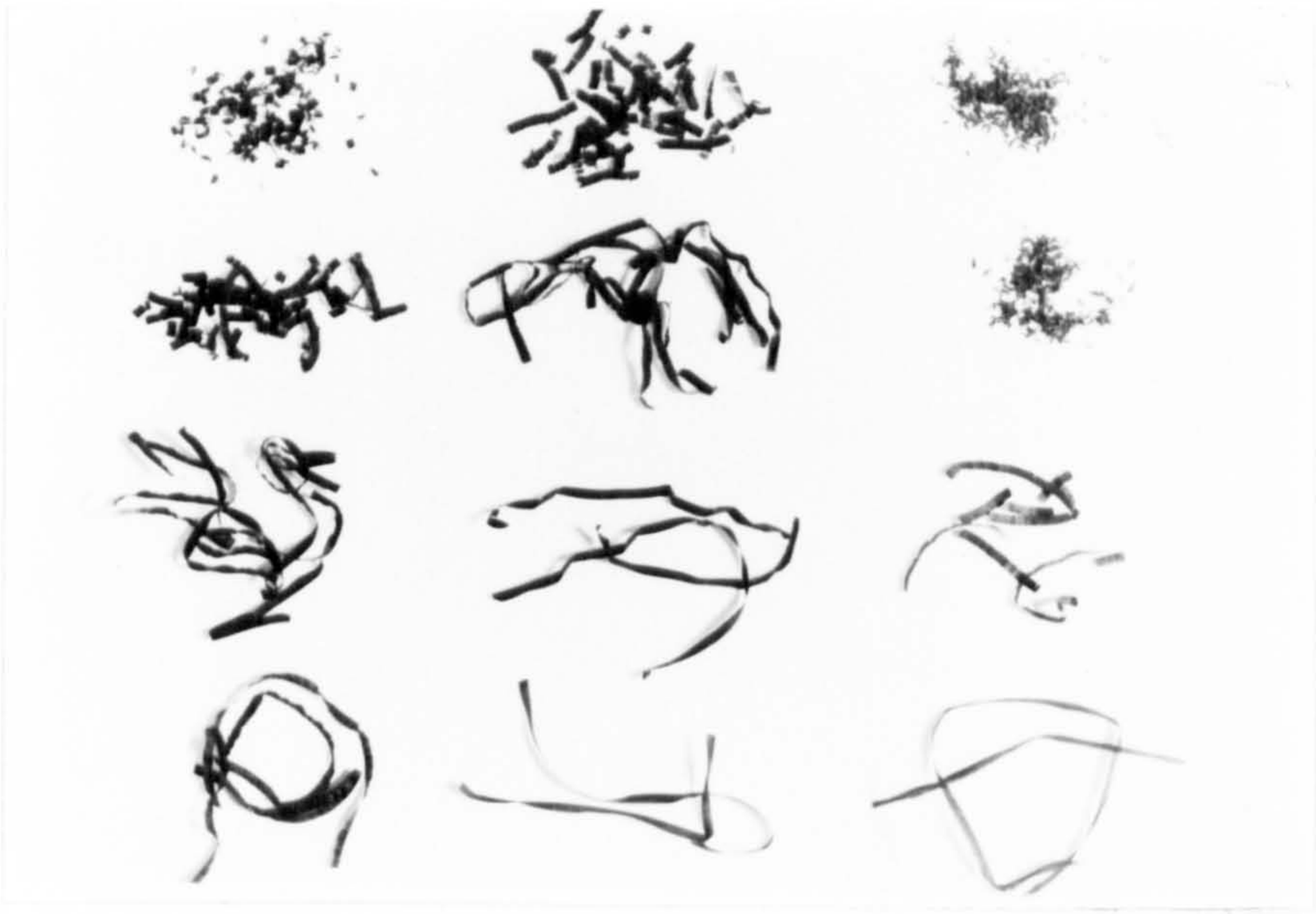

Fig 26. Types of PVC chips at different rake angle and feed rate (speed = 150 m/min, DOC = 1.5mm)

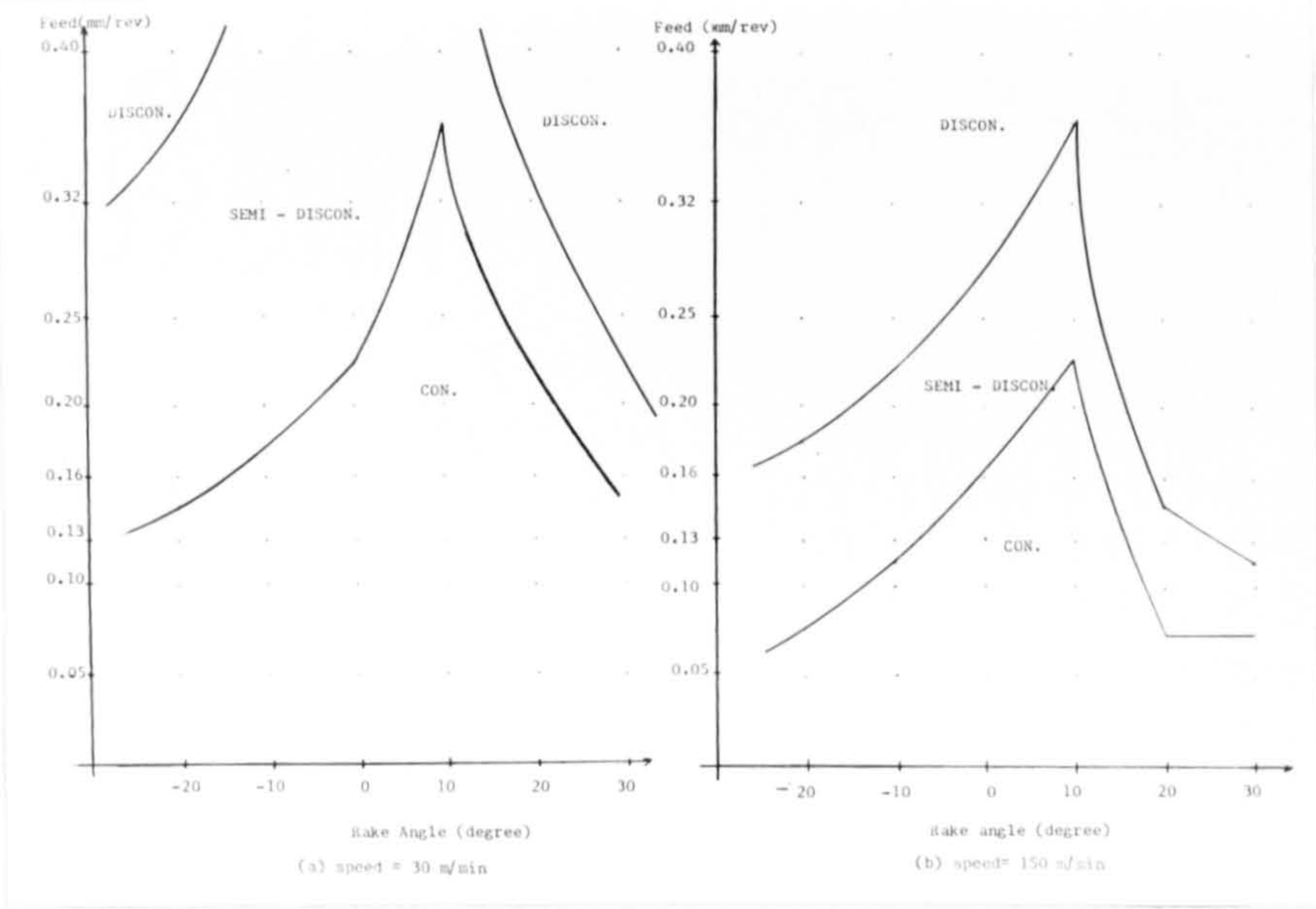

Fig 27. Variation of PVC chip type with rake angle and feed rate (DOC = 1mm)

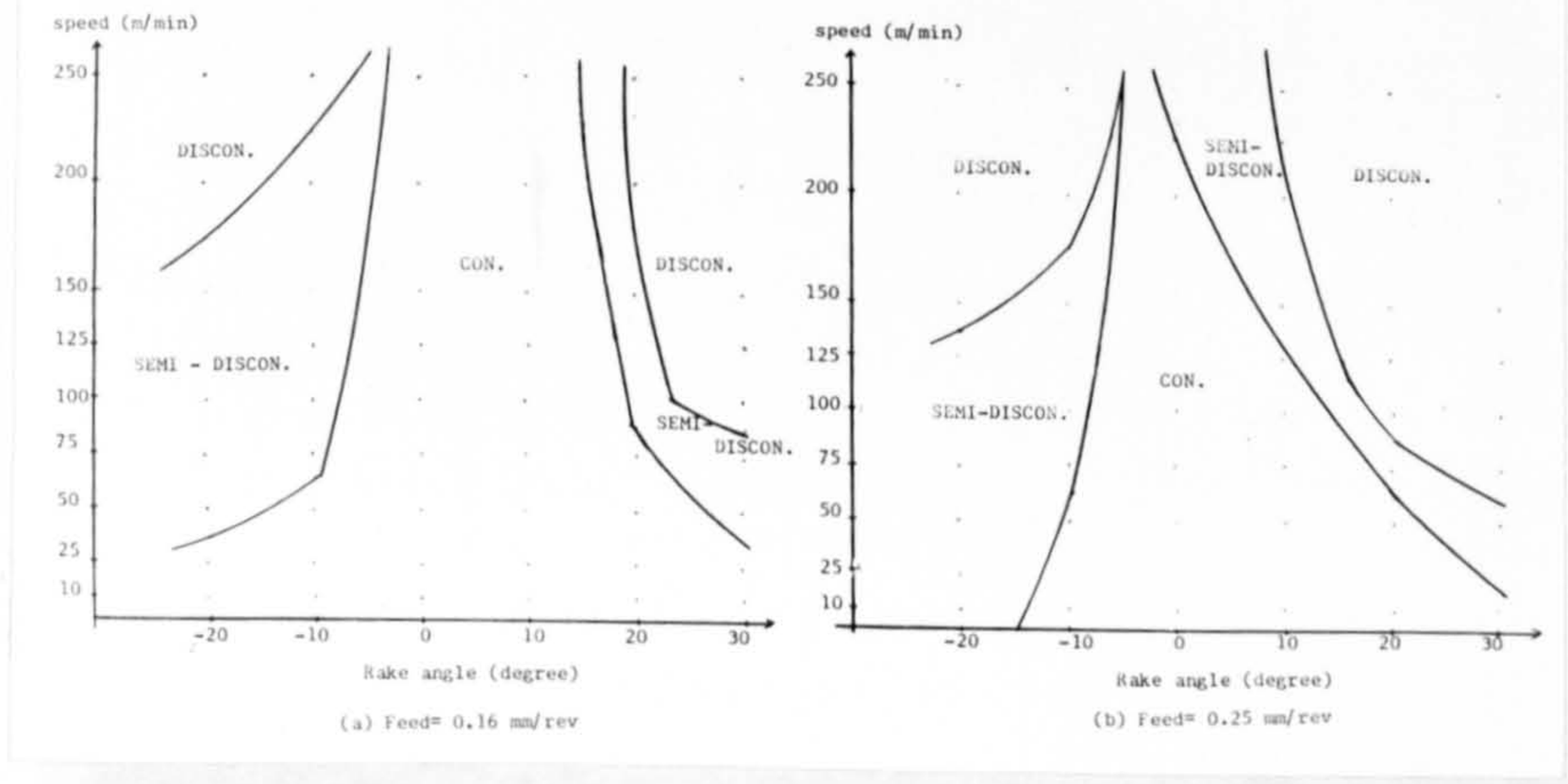

Fig 28. Variation of PVC chip type with rake angle and cutting speed (DOC = 1.5mm)

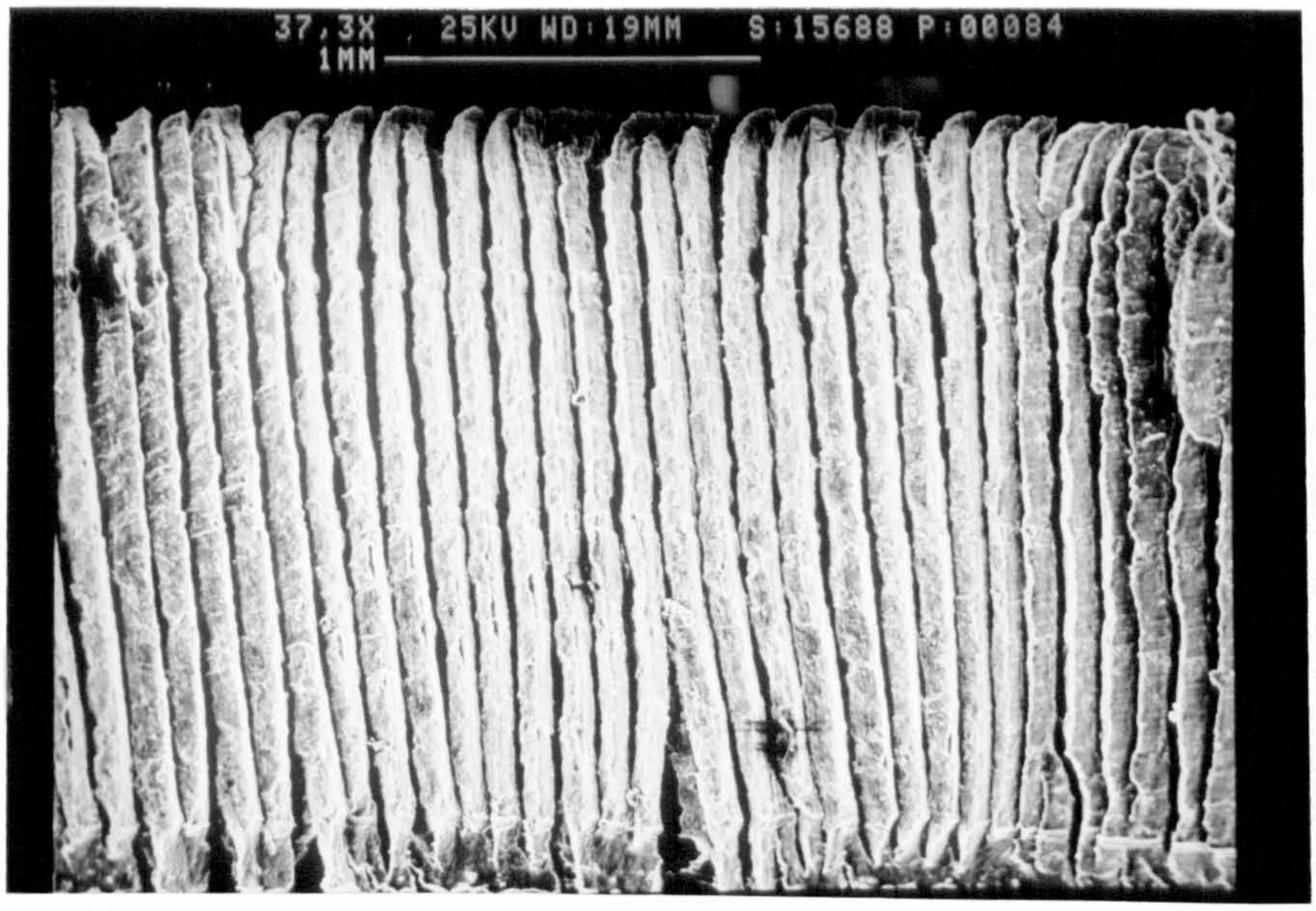

Fig 29. Continuous PVC chip with lamellar structure (Rake angle = 0°, speed = 50 m/min, feed = 0.16 mm/rev)

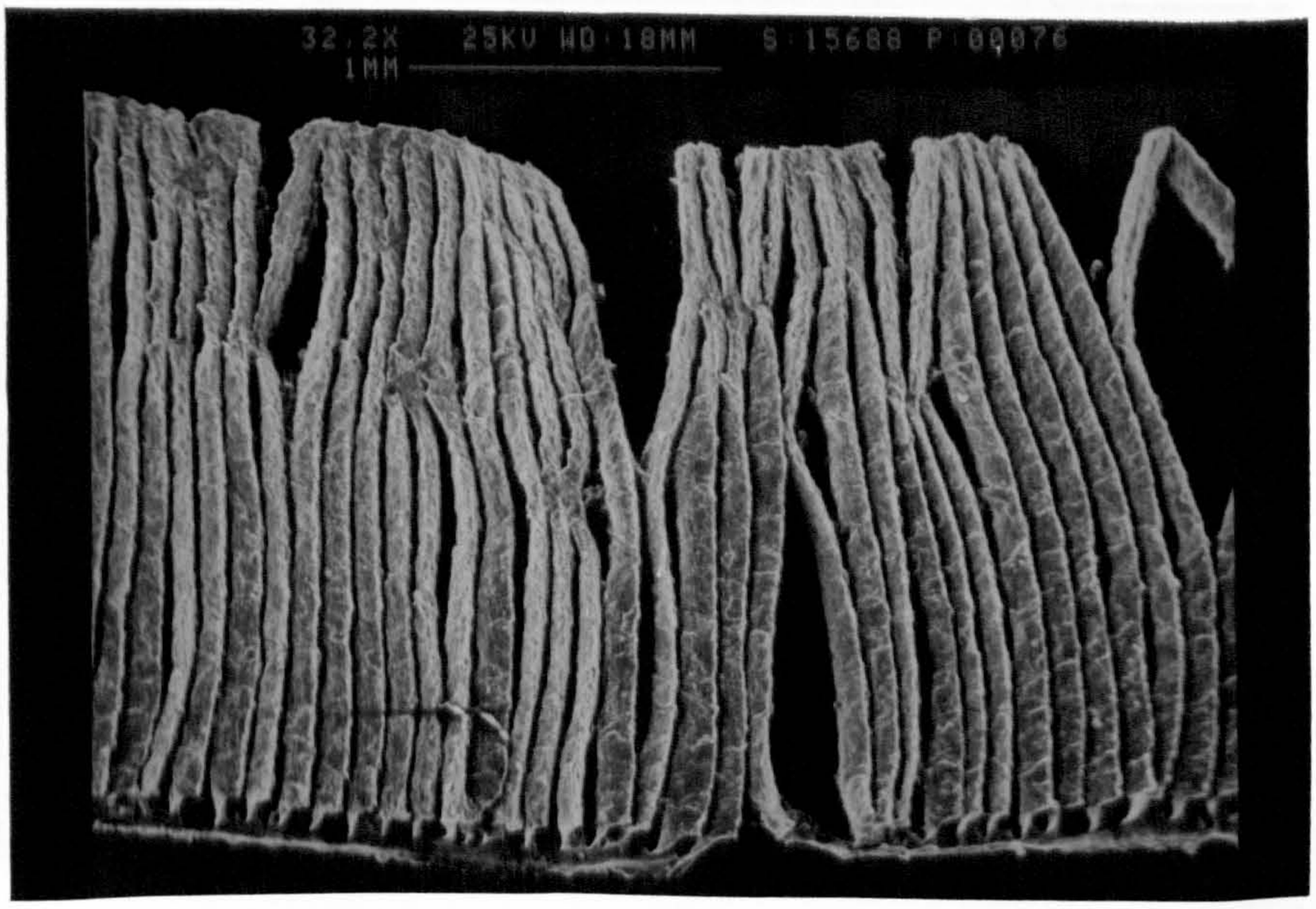

Fig 30. Semi-discontinuous PVC chip showing intermittent separation of lamellae. (Rake angle = 20°, speed = 250 m/min, feed = 0.16 mm/rev)

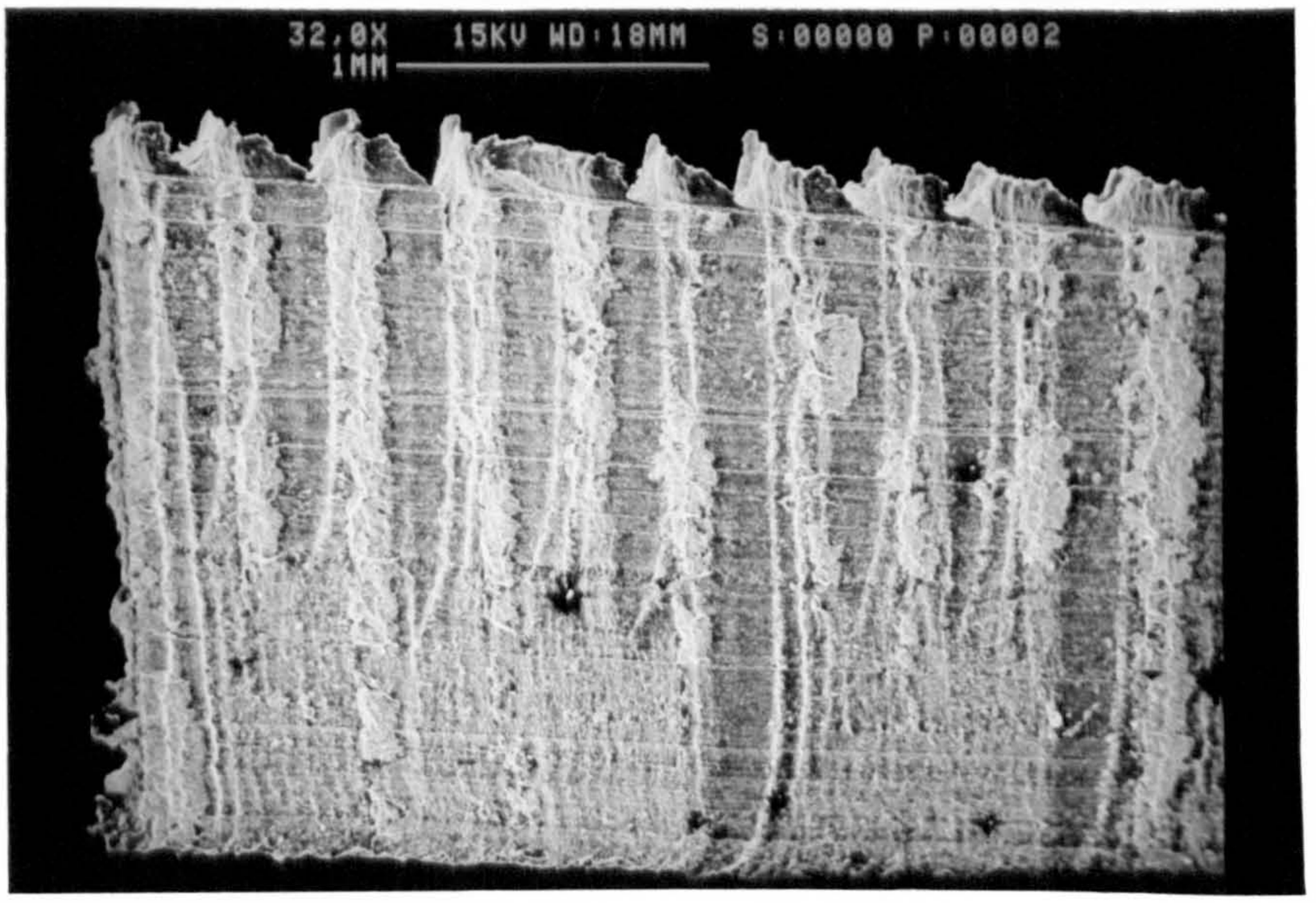

Fig 31. The undersurface of a PVC segmented chip
(Rake angle = 30°, speed = 25 m/min, feed = 0.16 mm/rev)

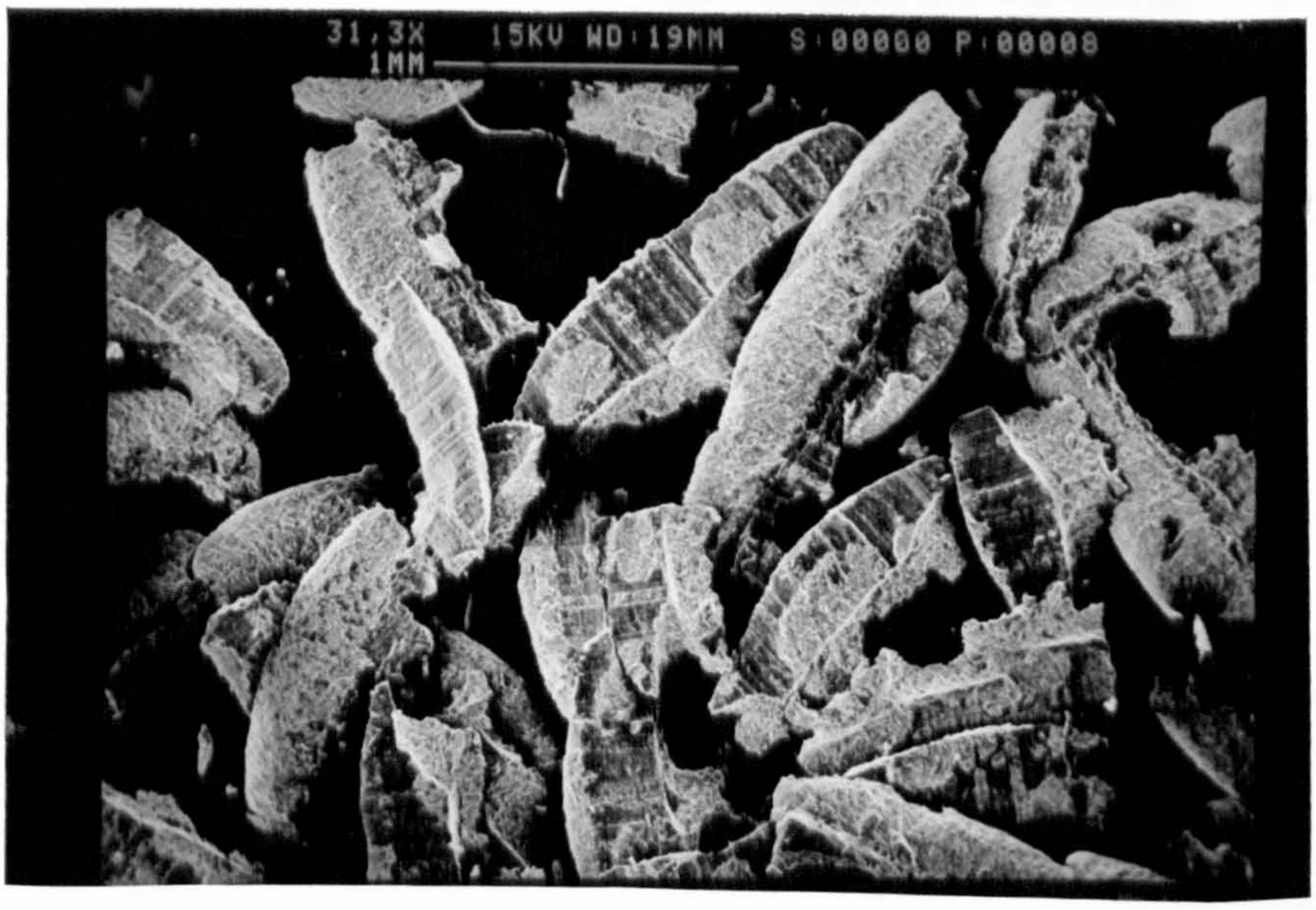

Fig 32. Discontinuous PVC chips showing fractured surfaces
(Rake angle = 30°, speed = 250 m/min, feed = 0.16 mm/rev)

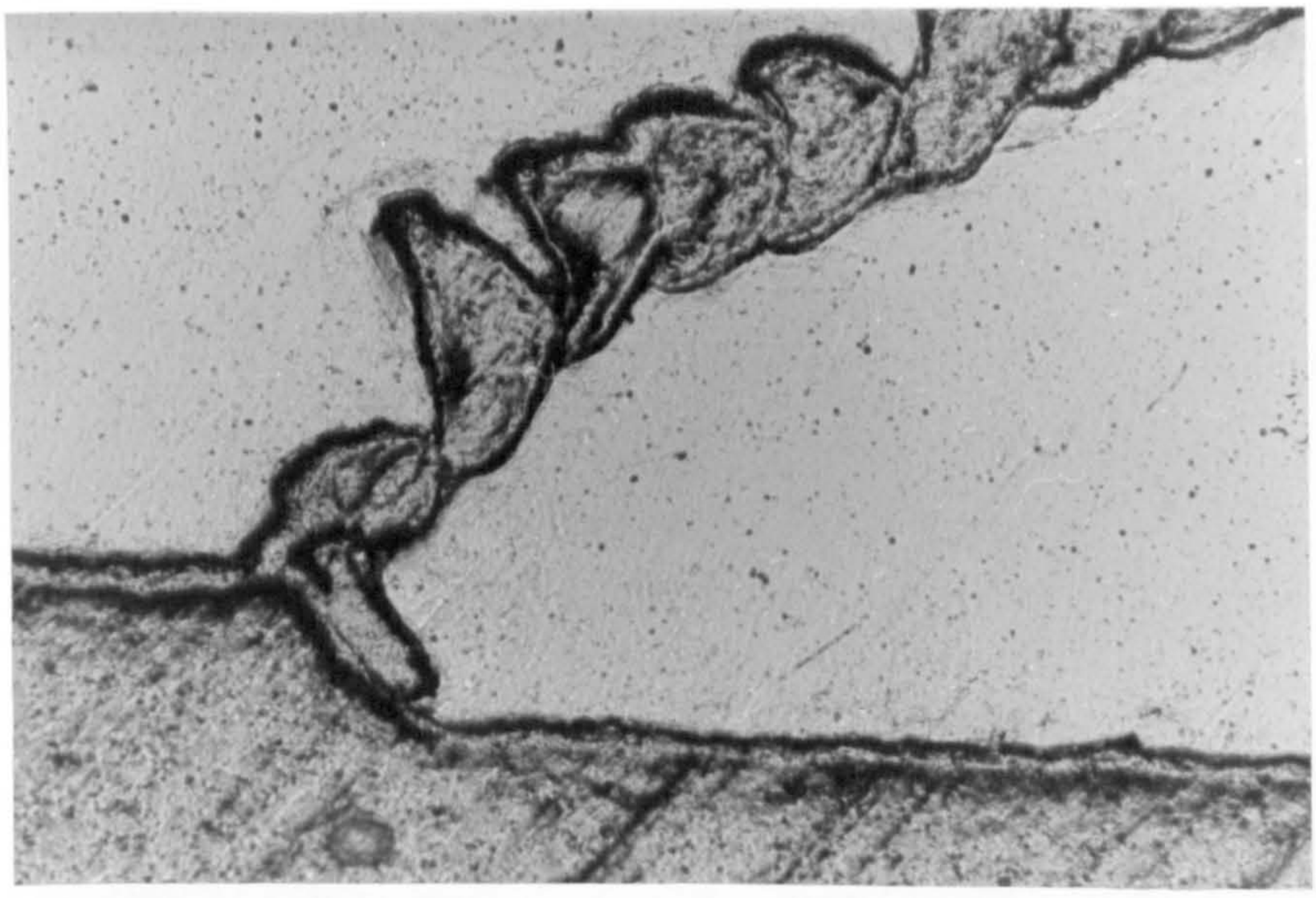

Fig 33. PVC chip root produced at -20º rake angle, showing segmented chip (X70). (Speed = 30 m/min, feed = 0.25 mm/rev)

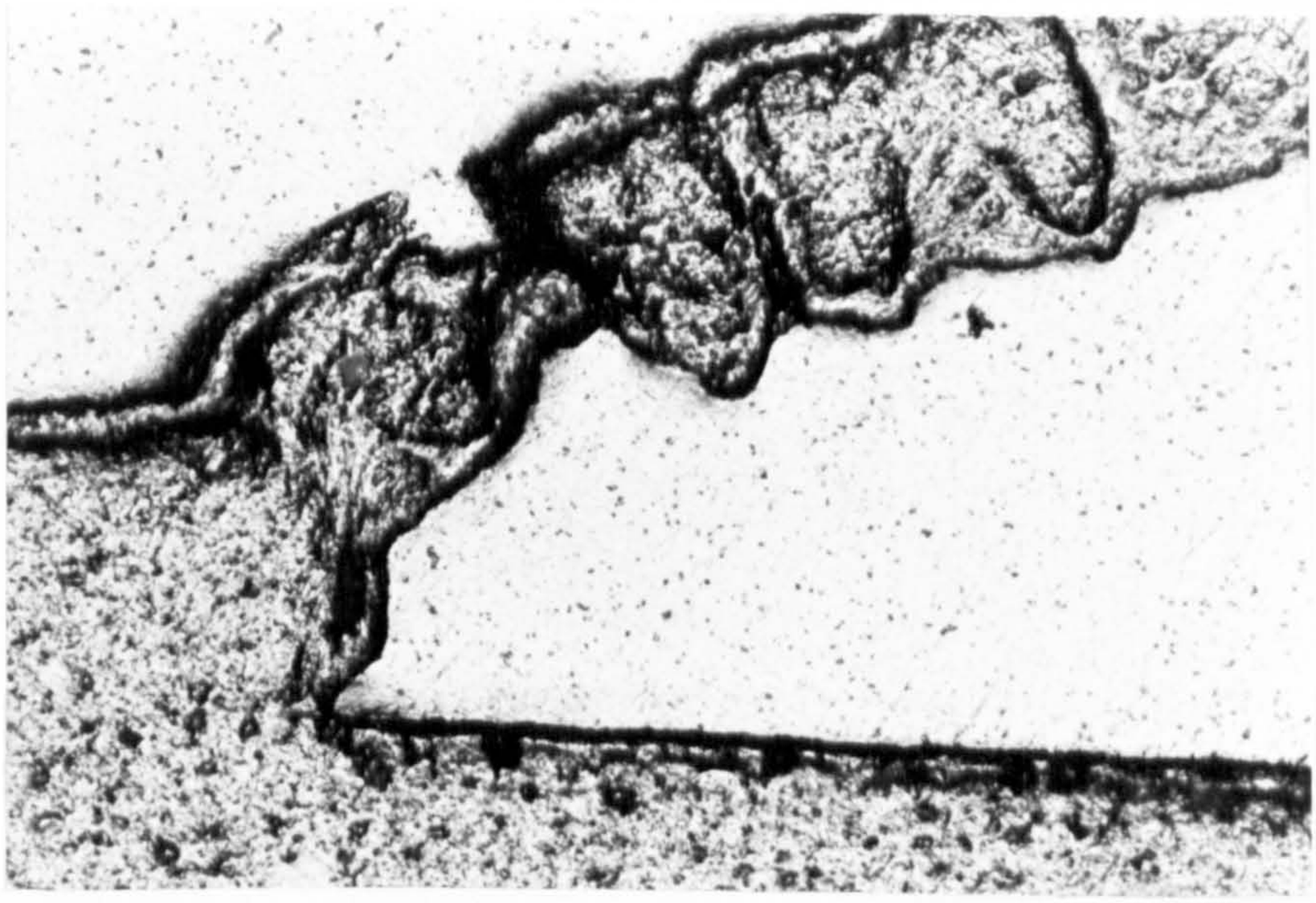

Fig 34. PVC chip root produced at 0º rake angle, showing less segmented chip (X100). (Speed = 30 m/min, feed = 0.25 mm/rev)

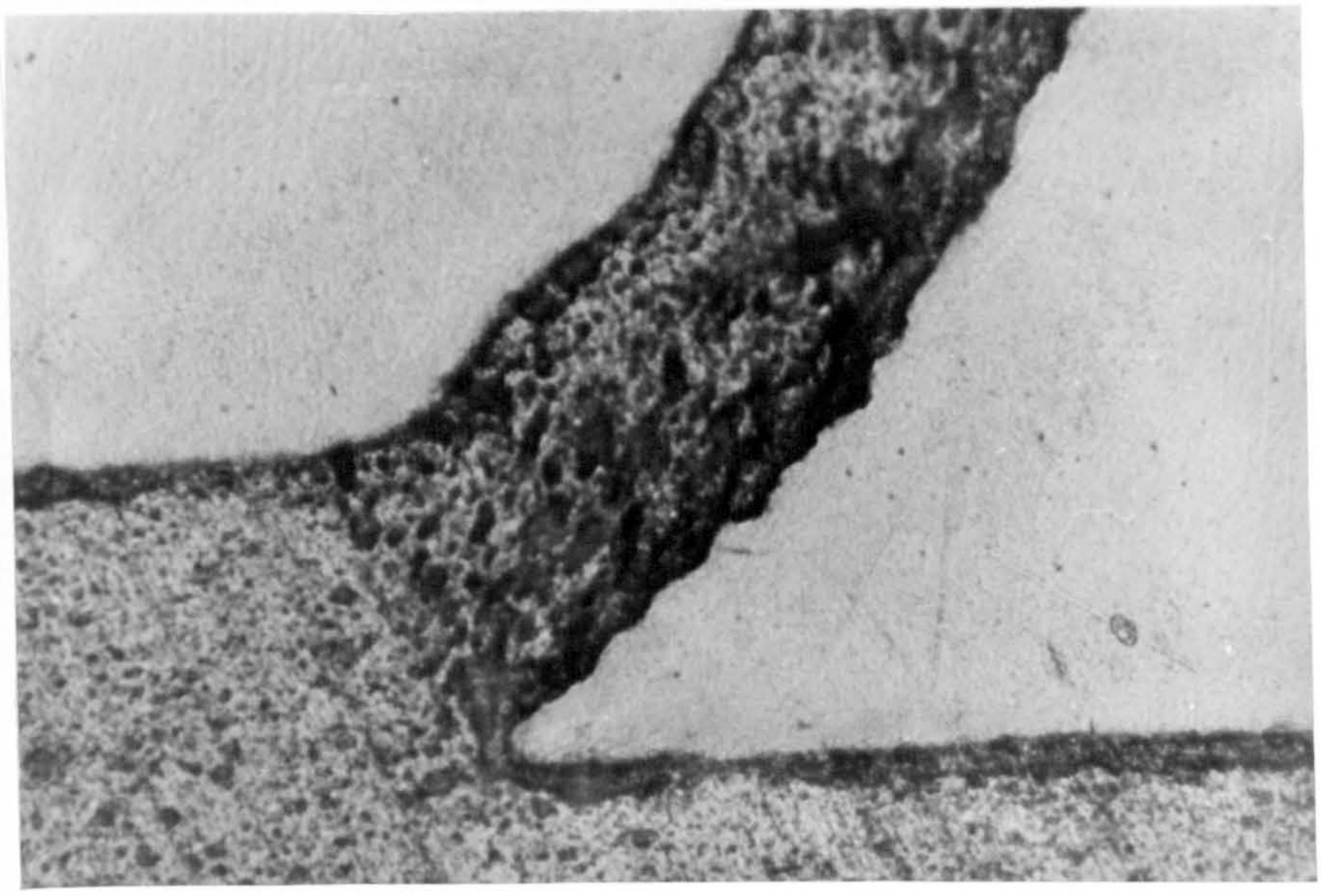

Fig 35. PVC chip root produced at 30° rake angle in discontinuous chip formation (X100). (Speed = 30 m/min, feed = 0.25 mm/rev)

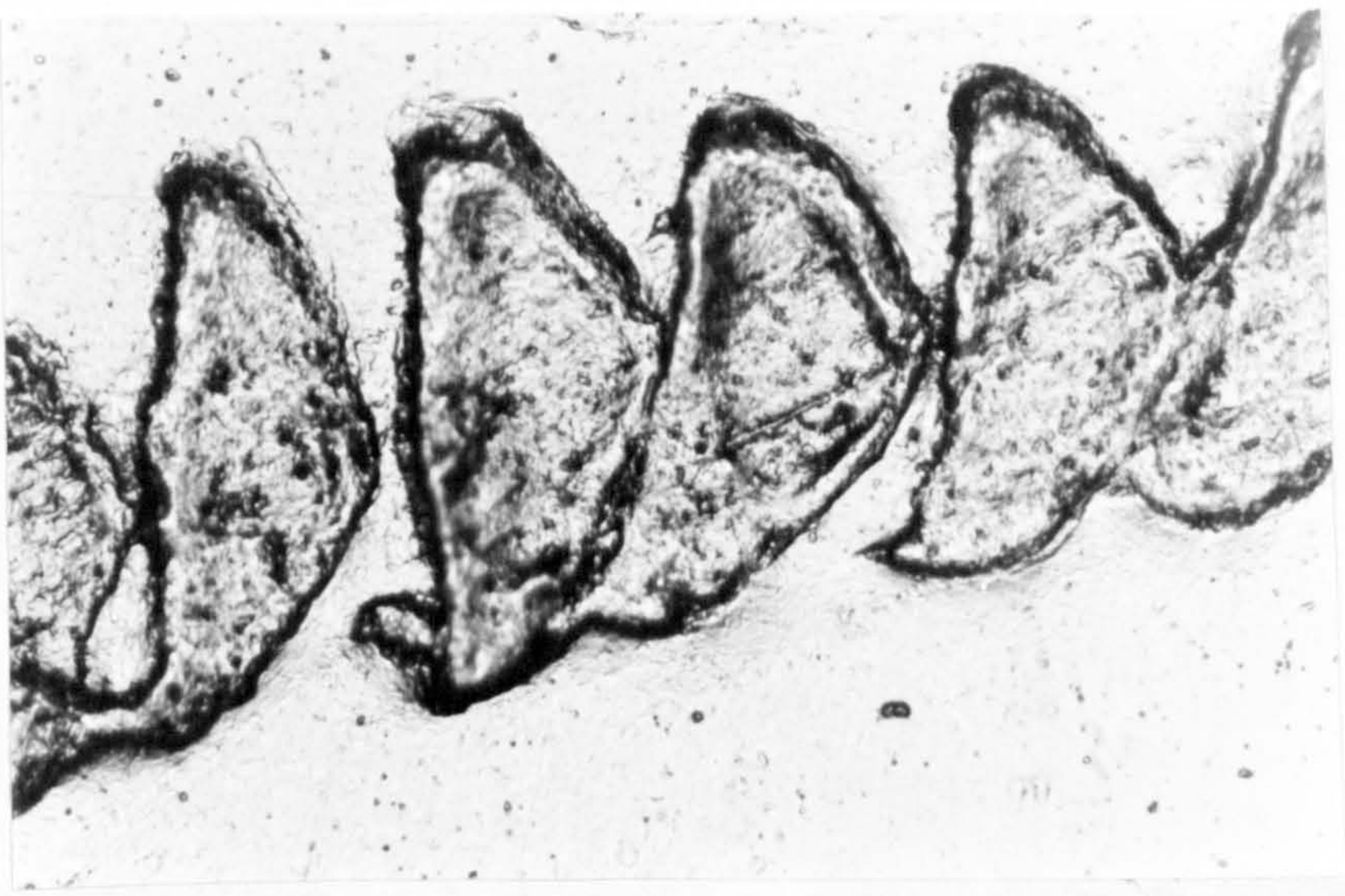

Fig 36. Enlarged view of segmented PVC chip shown in Fig 33 (X140) (Rake angle = -20°, speed = 30 m/min, feed = 0.25 mm/rev)

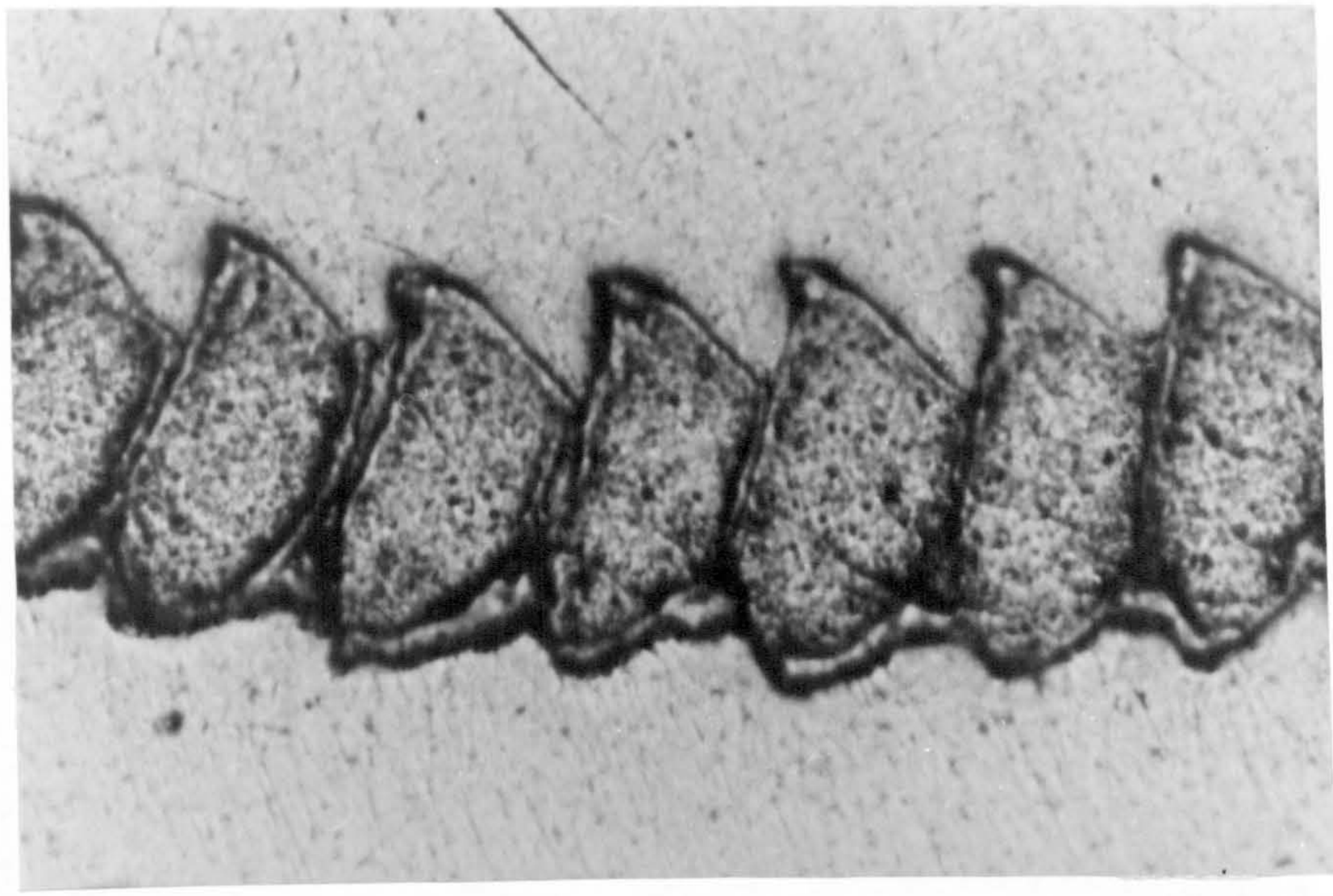

Fig 37. Enlarged view of segmented PVC chip shown in Fig 34 (X140)
(rake angle = 0°, speed = 30 m/min, feed = 0.25 mm/rev)

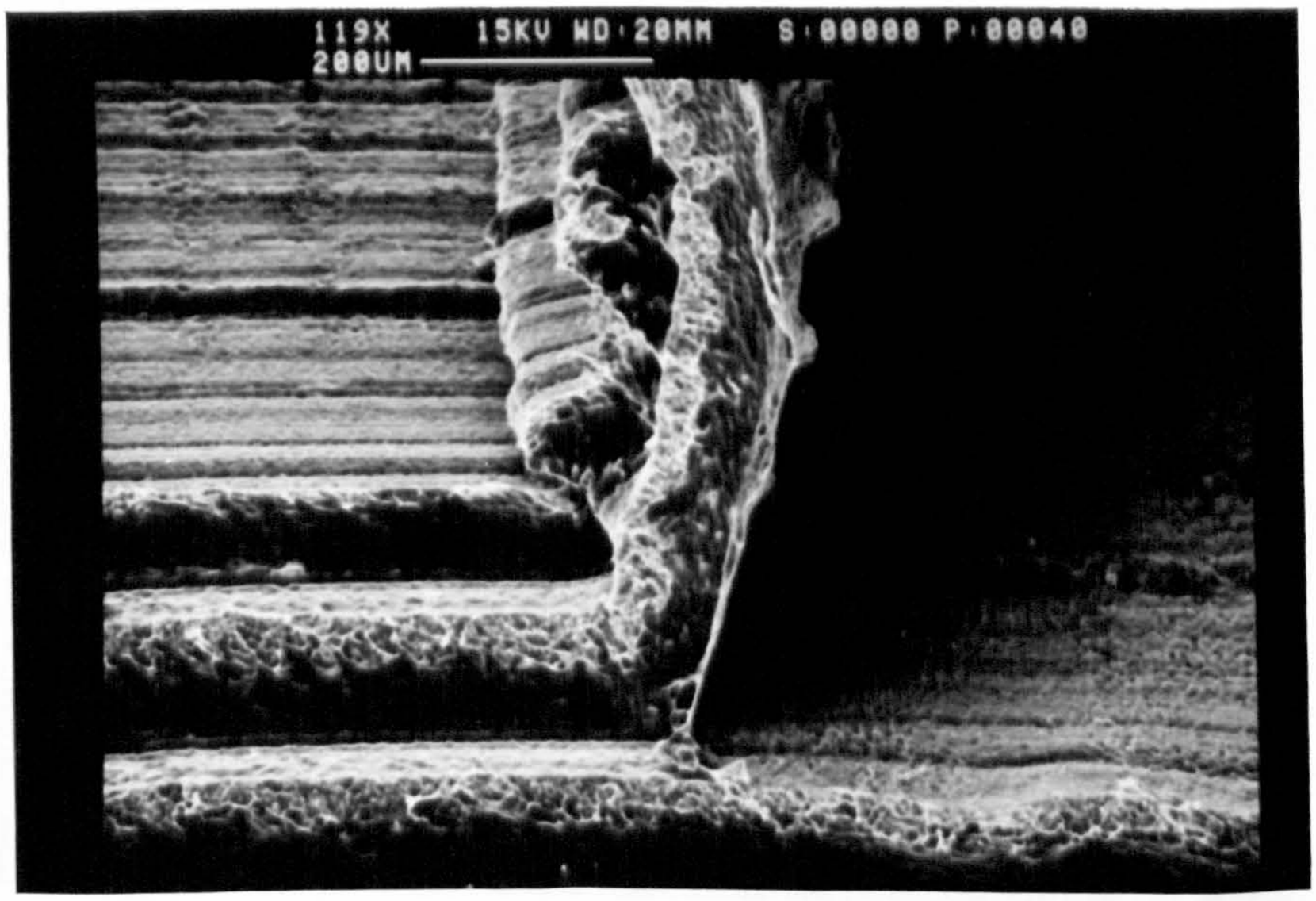

Fig 38. PVC chip root showing the formation of lamella
(rake angle = 0°, speed = 50 m/min, feed = 0.25 mm/rev)

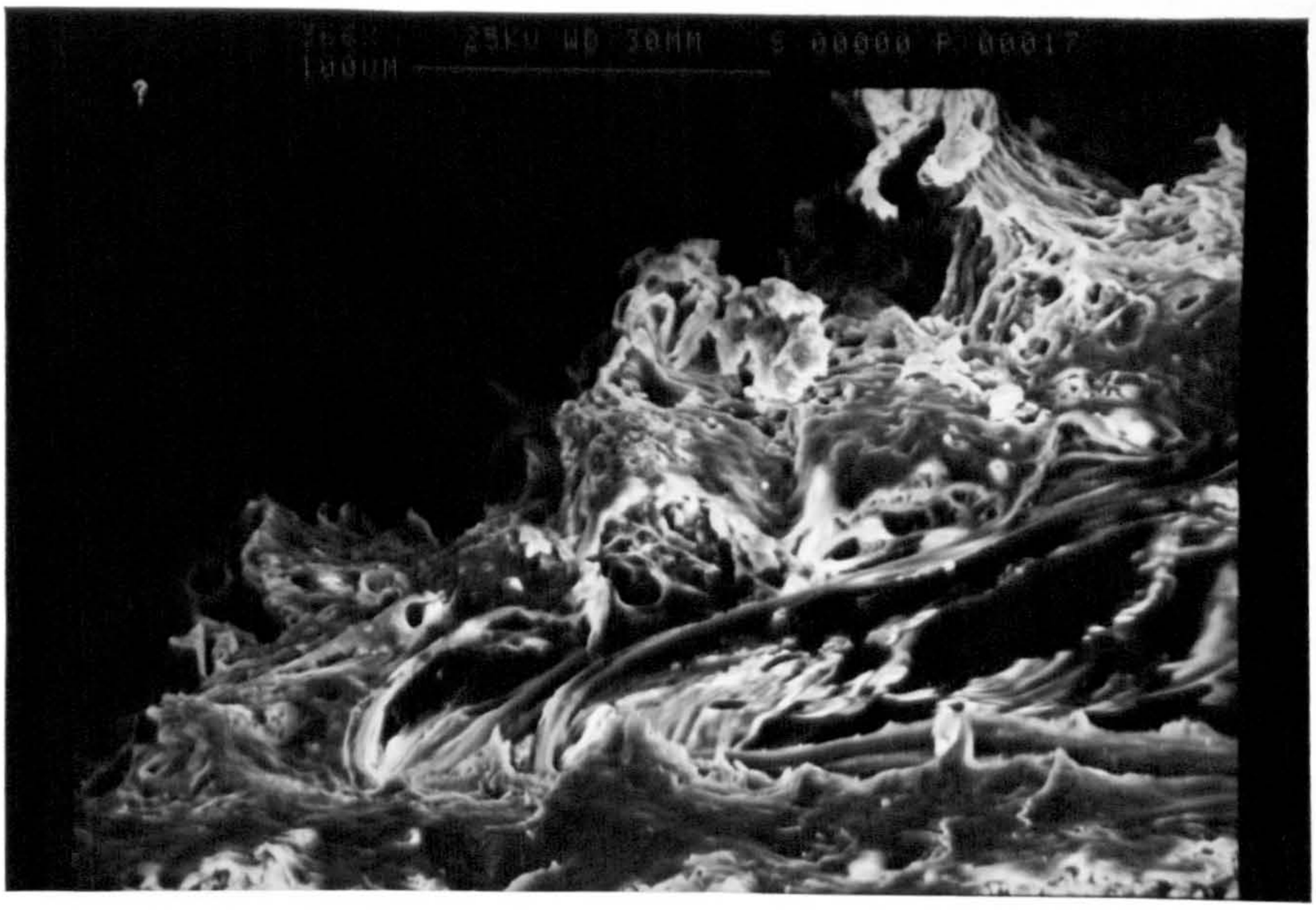

Fig 39. PVC chip root with fibrillar structure in segmented chip formation. (Rake angle = -20°, speed = 30 m/min, feed = 0.25 mm/rev)

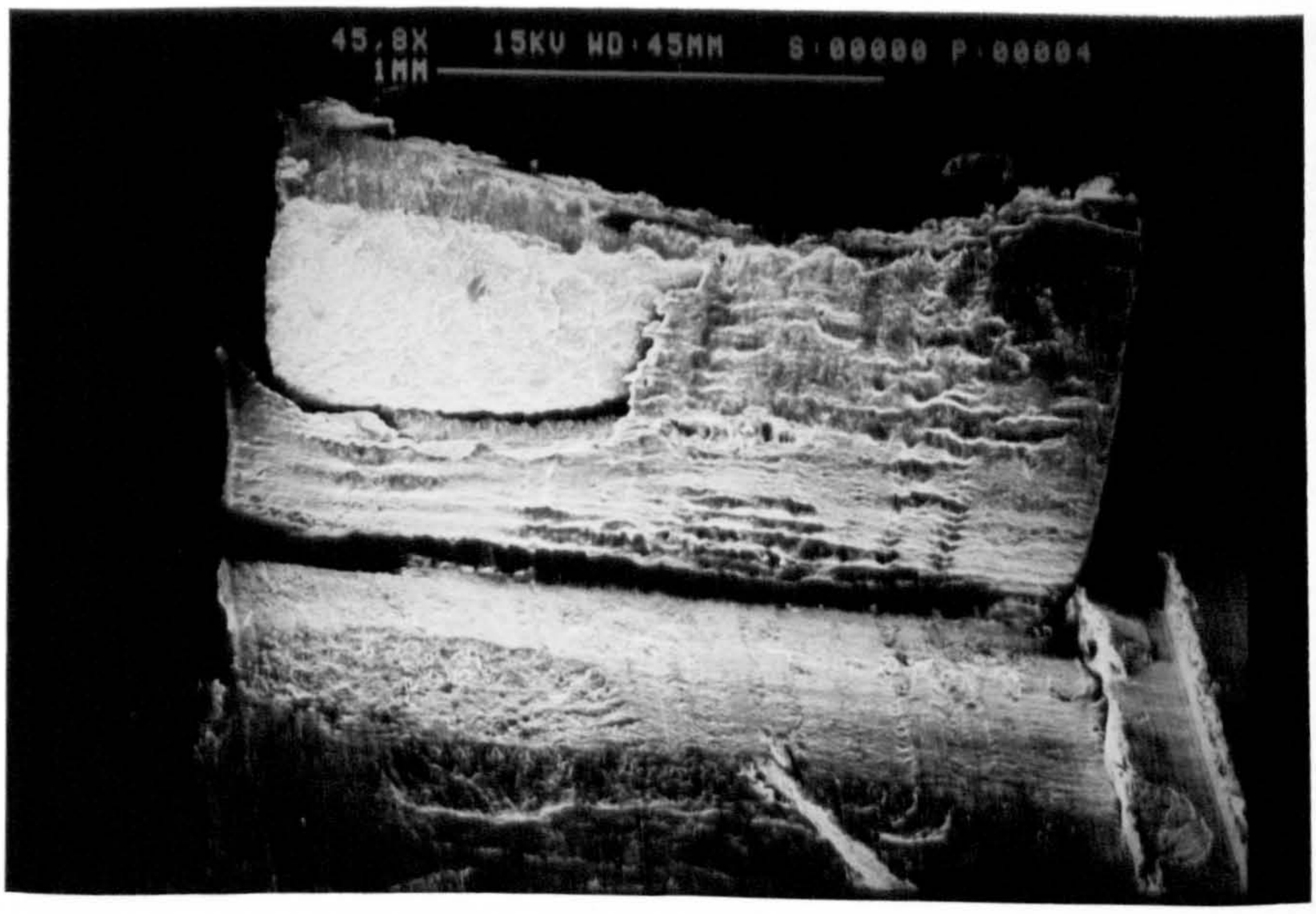

Fig 40. PVC chip root in discontinuous chip formation. (Rake angle = 20°, speed = 30 m/min, feed = 0.25 mm/rev)

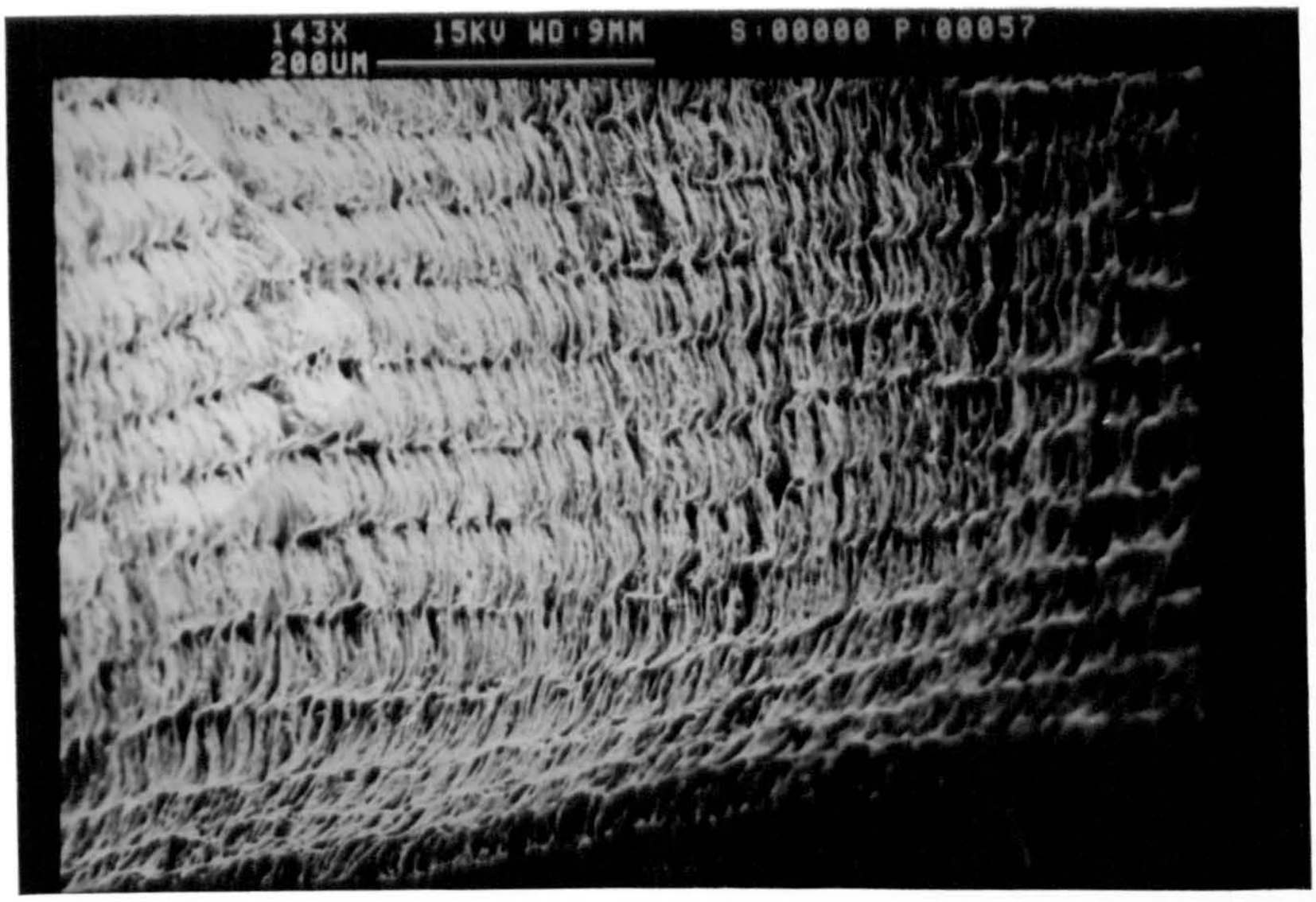

Fig 41. The undersurface of a segmented PVC chip
(Rake angle = -20°, speed = 50 m/min, feed = 0.08 mm/rev)

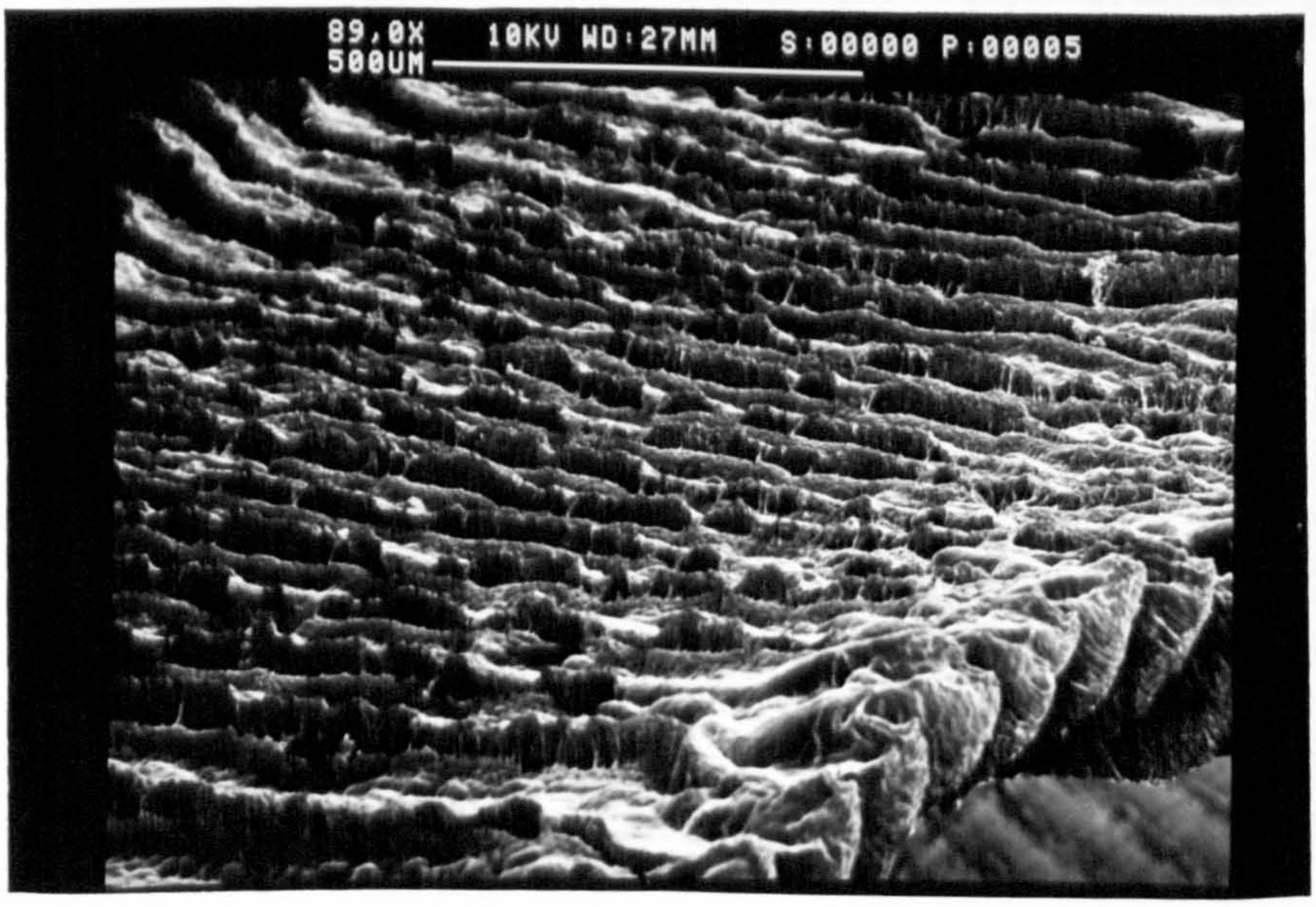

Fig 42. The undersurface of a segmented PVC chip
(Rake angle = 0°, speed = 30 m/min, feed = 0.25 mm/rev)

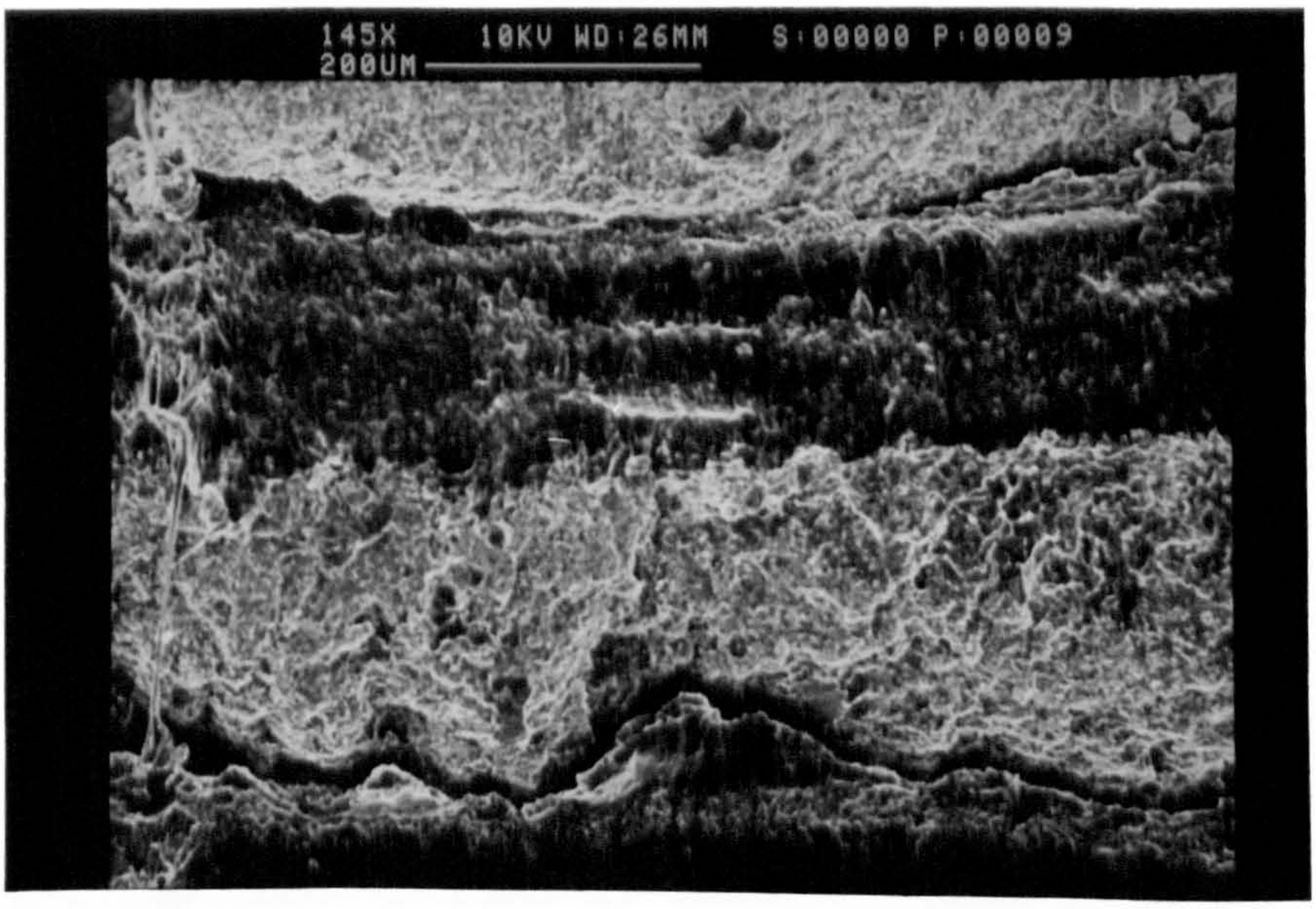

Fig 43. The undersurface of a semi-discontinuous PVC chip (Rake angle = 20°, speed = 30 m/min, feed = 0.16 mm/rev)

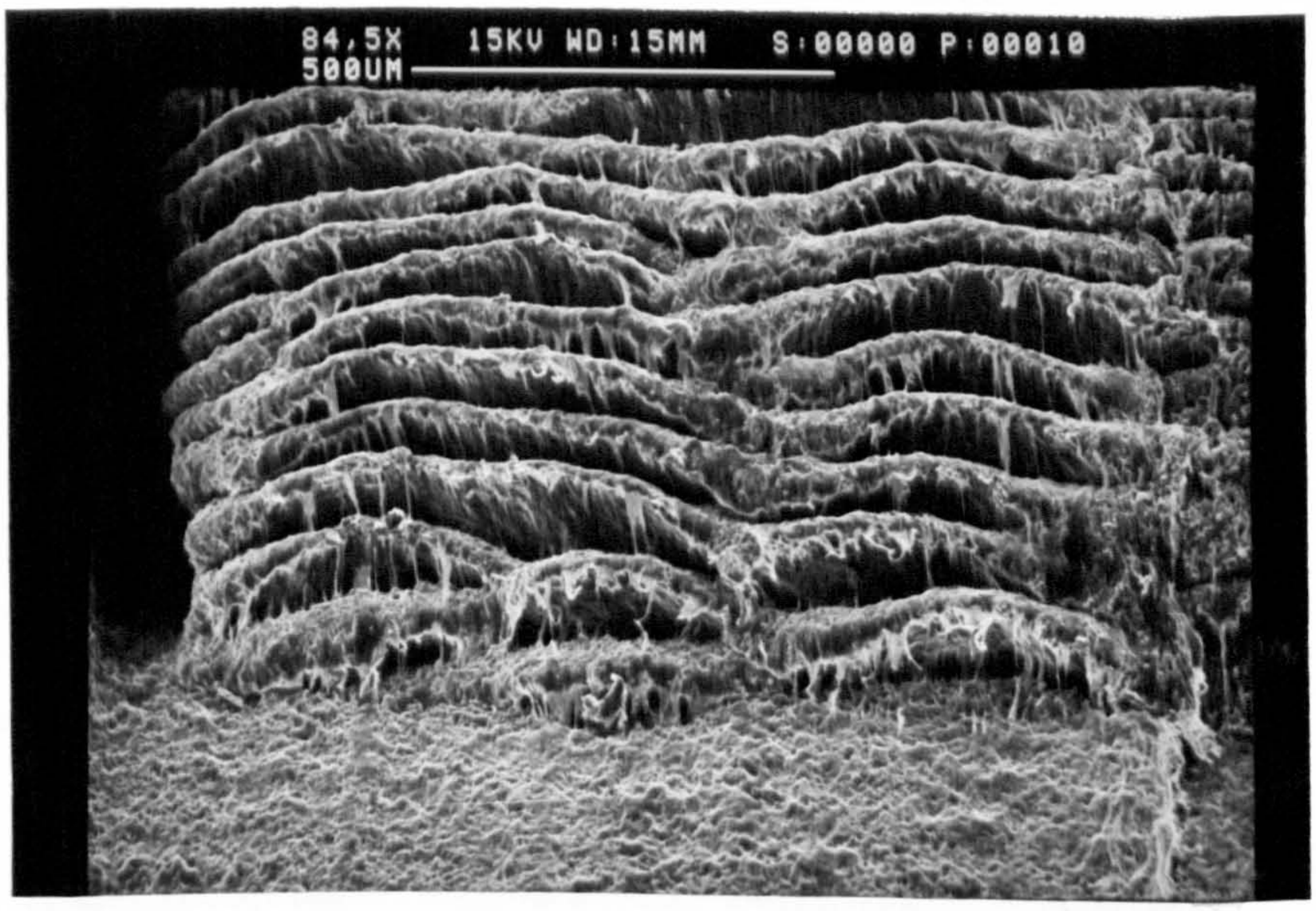

Fig 44. The top surface of PVC chip showing the formation of new lamellae. (Rake angle = -20°, speed = 30 m/min, feed = 0.25 mm/rev)

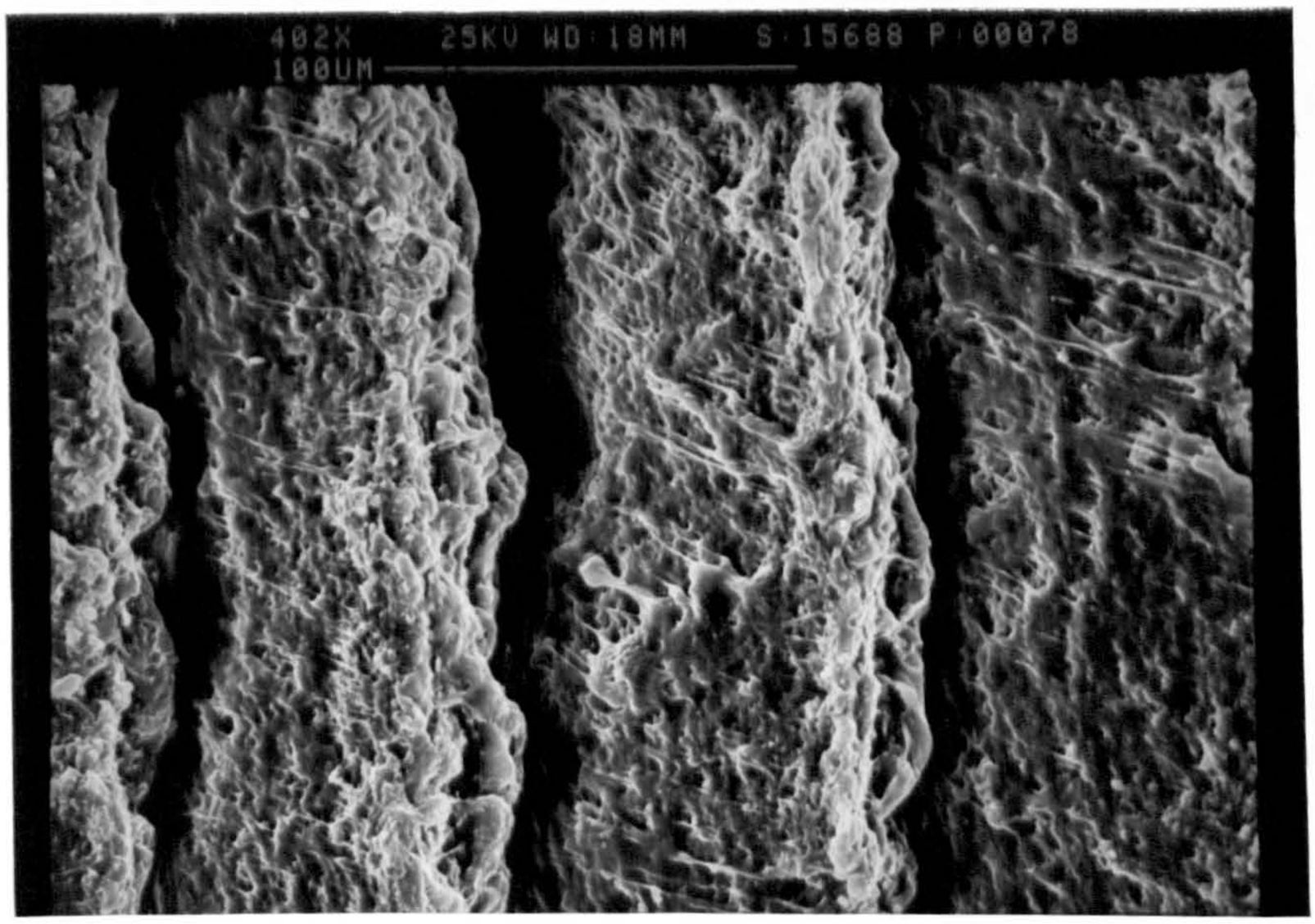

Fig 45. Magnified view of semi-discontinuous PVC chip.
(Rake angle = -20°, speed = 150 m/min, feed = 0.16 mm/rev)

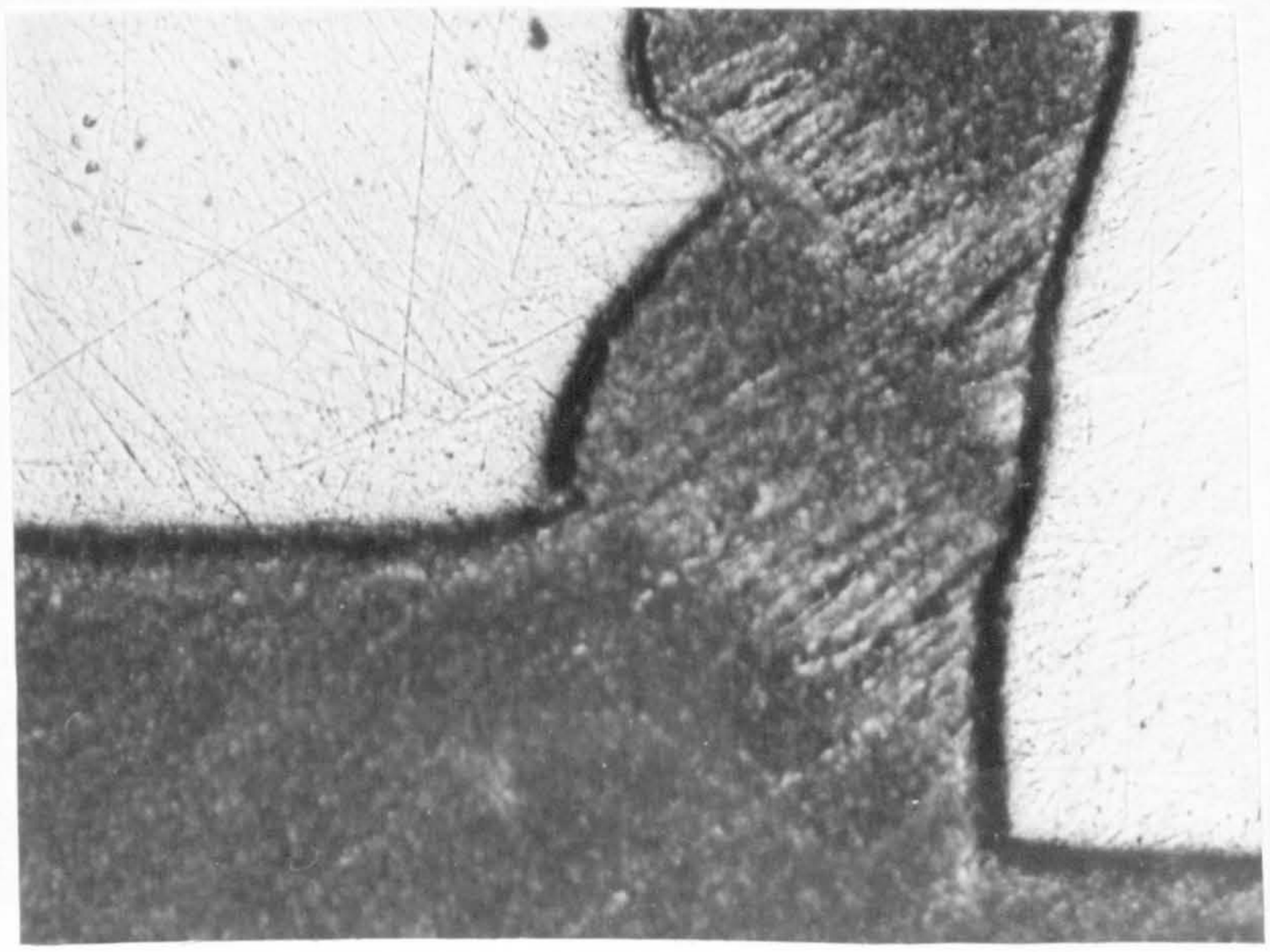

Fig 46. HDPE chip root produced at -20° rake angle, showing irregular chip thickness (X140). (Speed = 30 m/min, feed = 0.25 mm/rev)

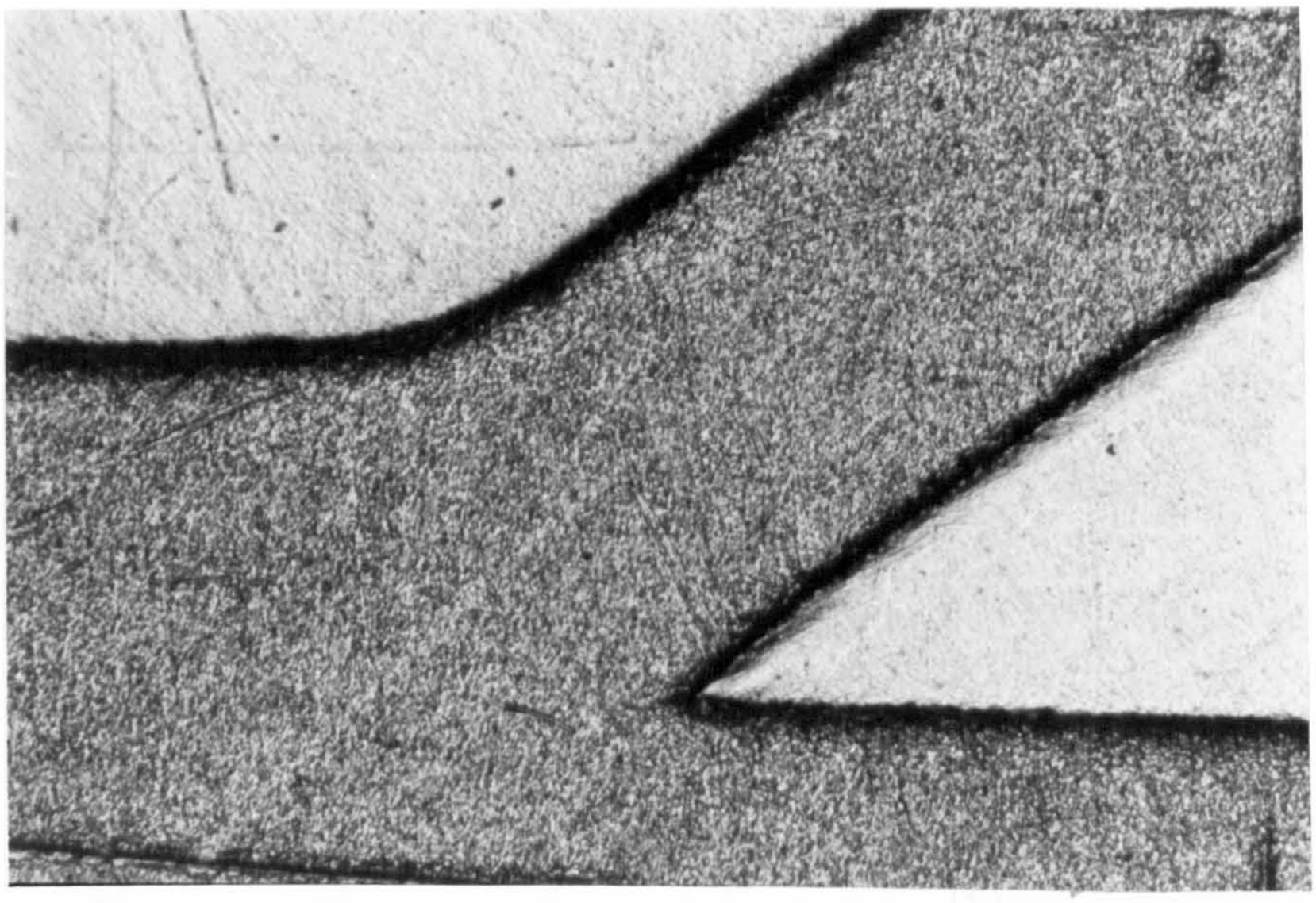

Fig 47. HDPE chip root produced at 0º rake angle, showing continuous chip formation (X140). (Speed = 30 m/min, feed = 0.25 mm/rev)

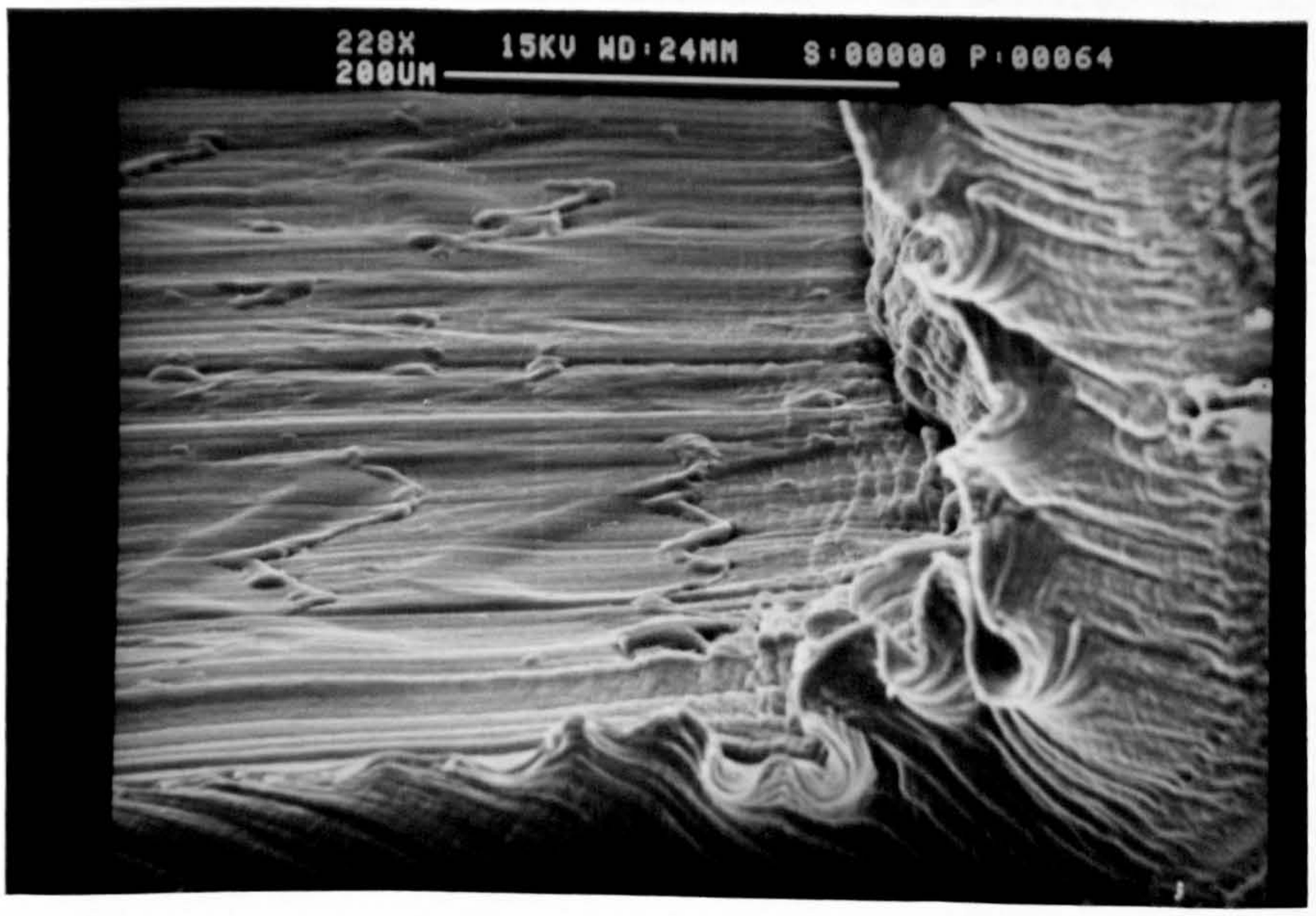

Fig 48. HDPE chip root showing the development of new shear fronts. (Rake angle = -20º, speed = 30 m/min, feed = 0.25 mm/rev)

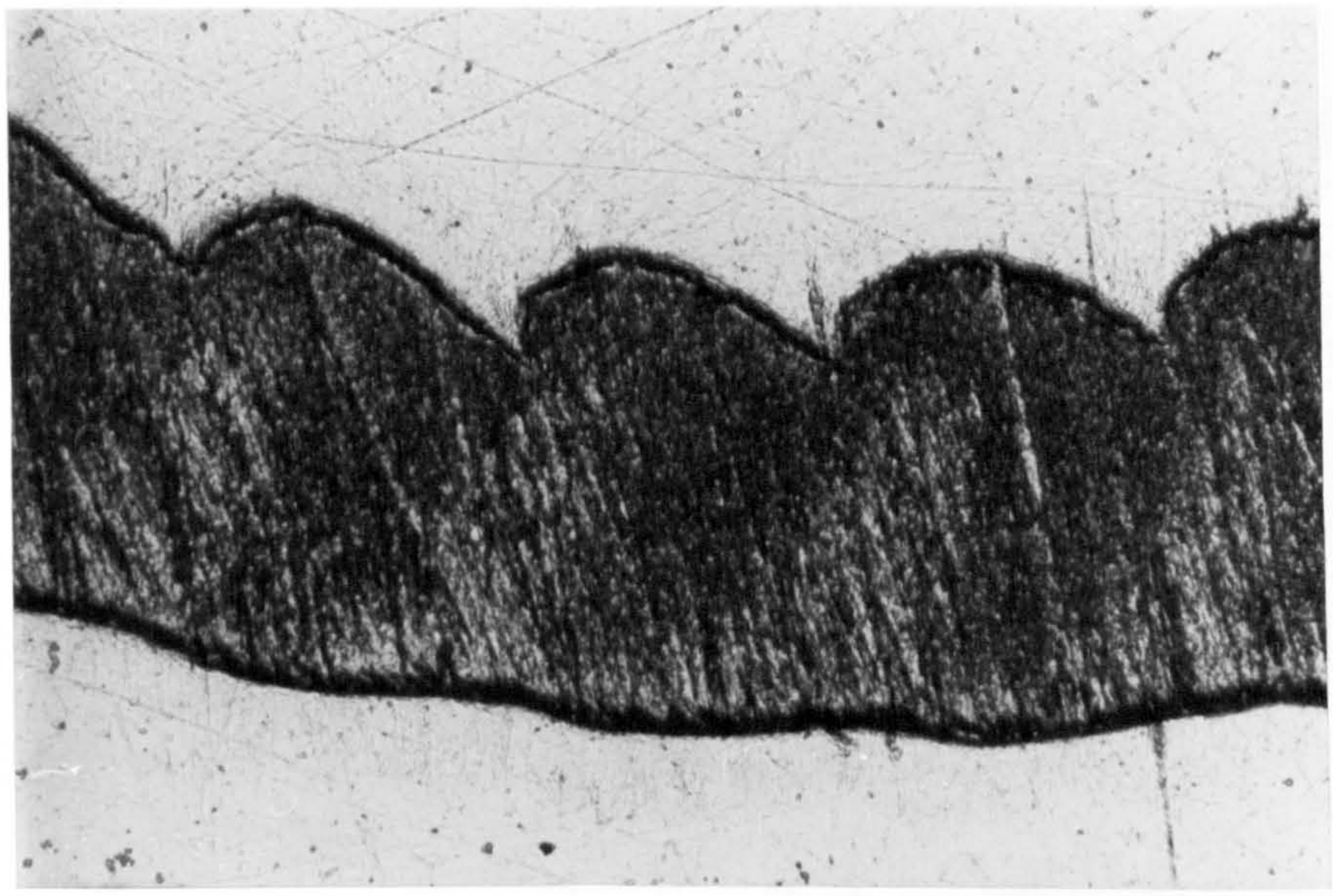

Fig 49. Enlarged view of segmented HDPE chip shown in Fig 46 (X100)

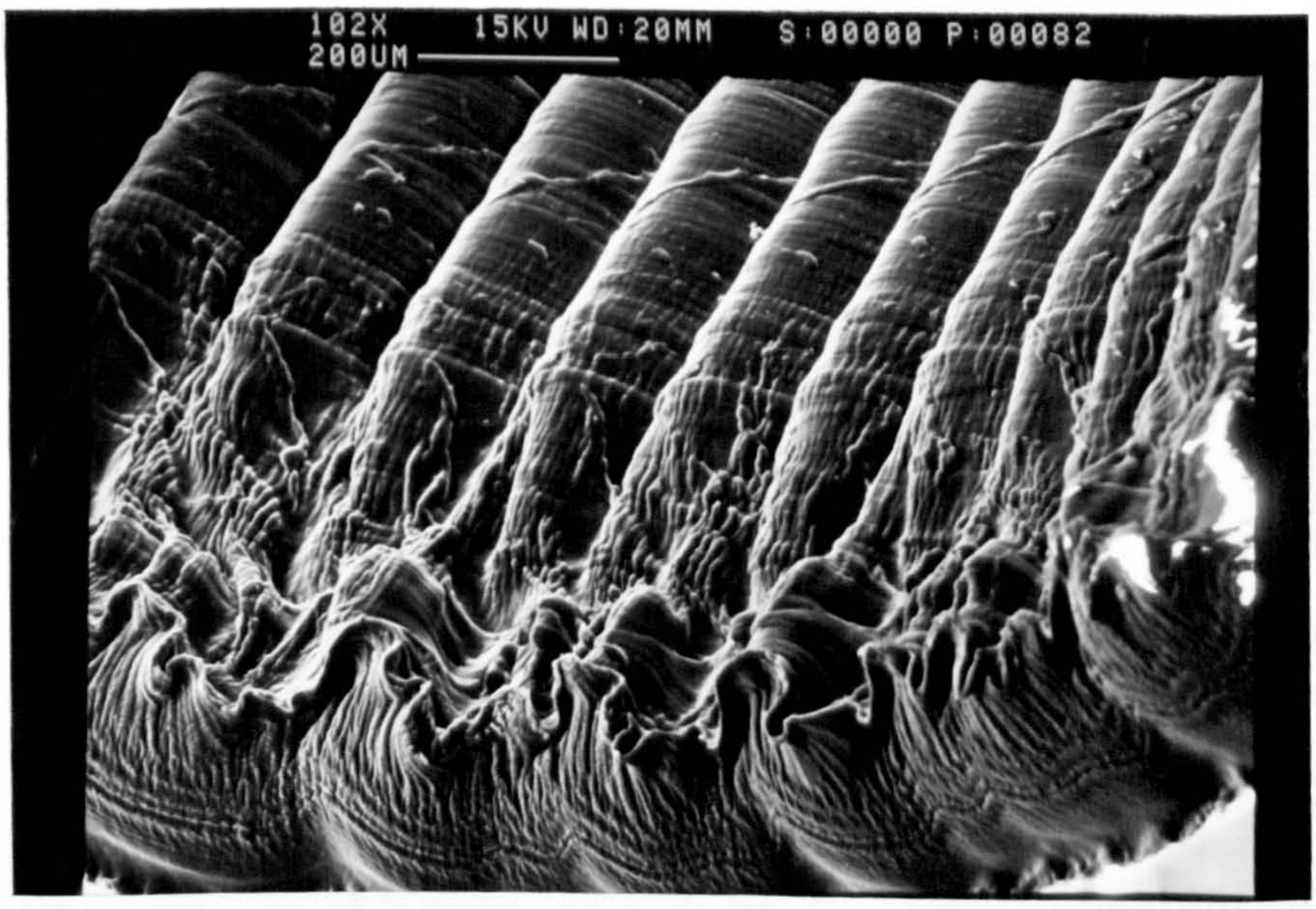

Fig 50. Top and side surfaces of a segmented HDPE chip showing the distortion of the lamellar structure. (Rake angle = -20°, speed = 30 m/min, feed = 0.25 mm/rev)

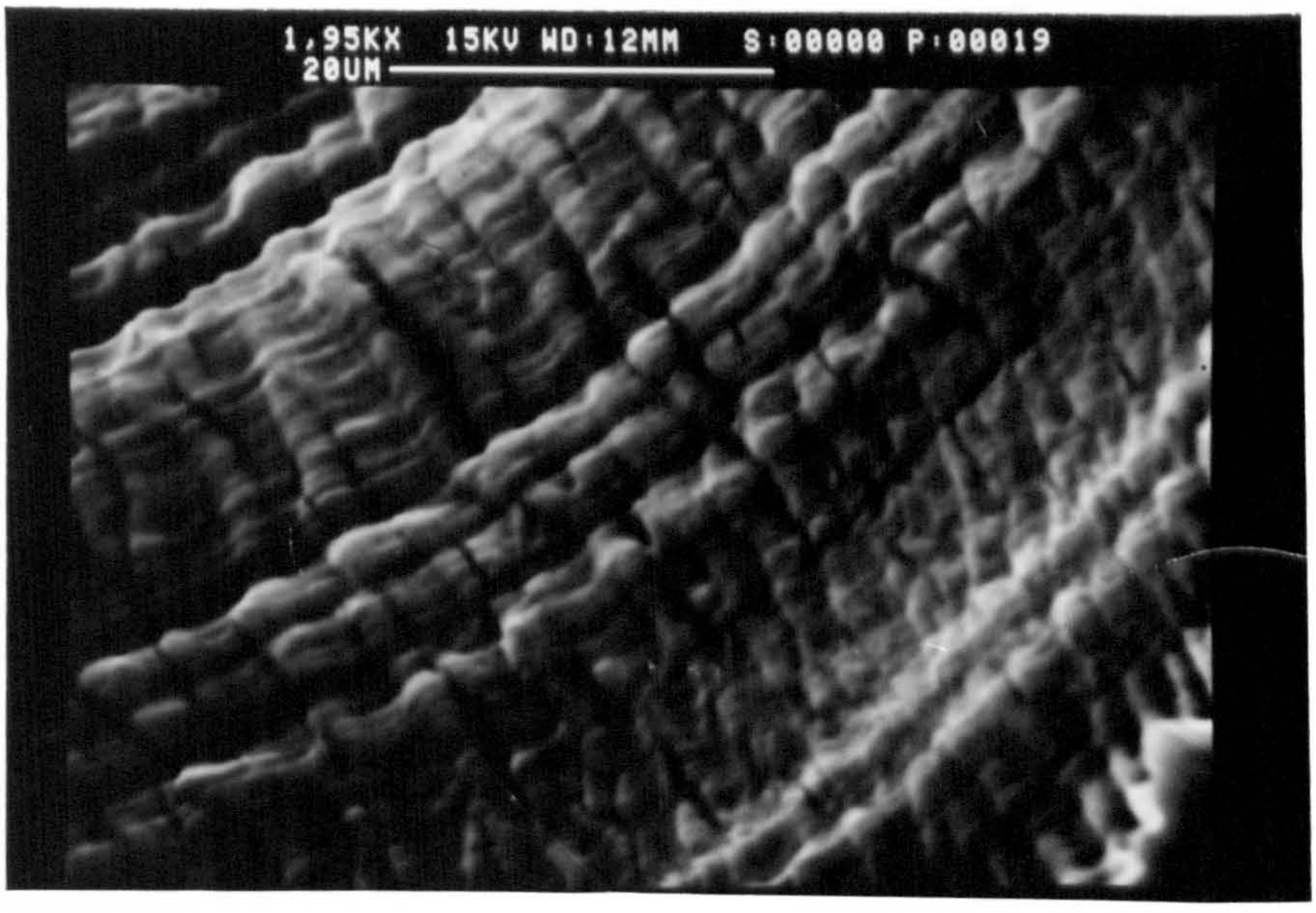

Fig 51. Top surface of a HDPE chip showing lamellar structure (Rake angle = 0°, speed = 150 m/min, feed = 0.25 mm/rev)

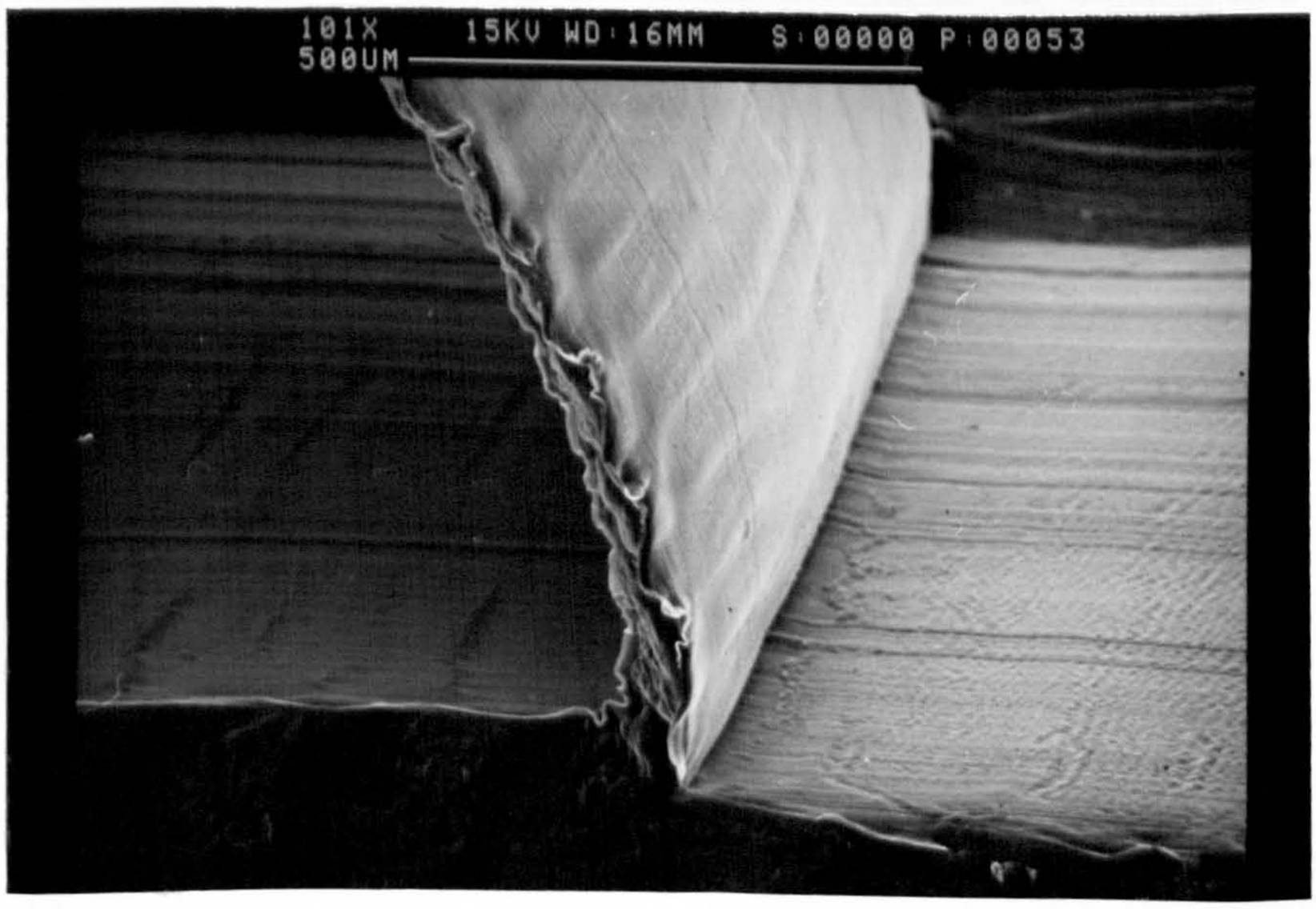

Fig 52. HDPE chip root showing the absence of a lamellar structure on the chip undersurface. (Rake angle = -20°, speed = 50 m/min, feed = 0.08 mm/rev)

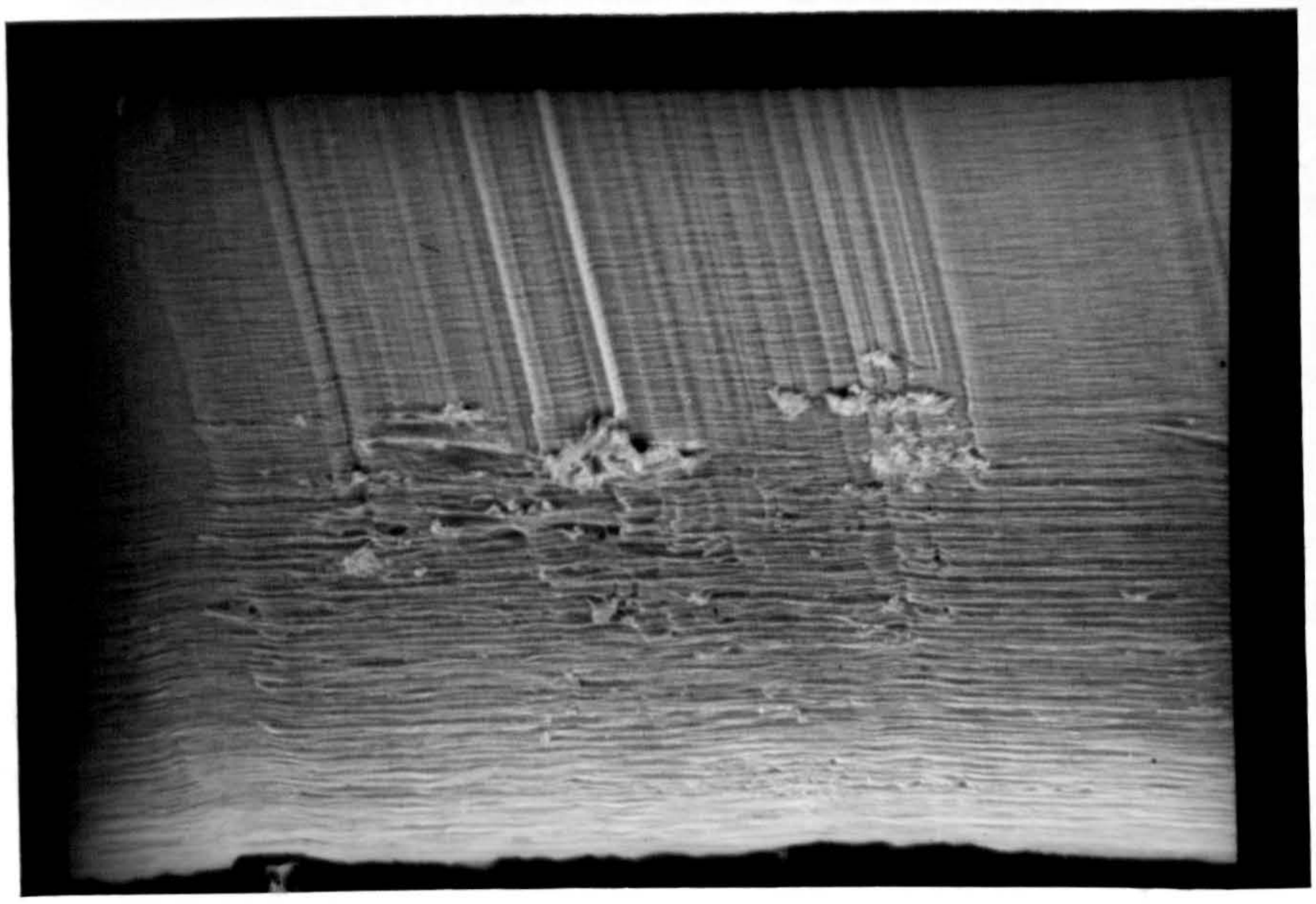

Fig 53. Undersurface of a HDPE chip showing seizure contact
(Rake angle = 0°, speed = 50 m/min, feed = 0.25 mm/rev)

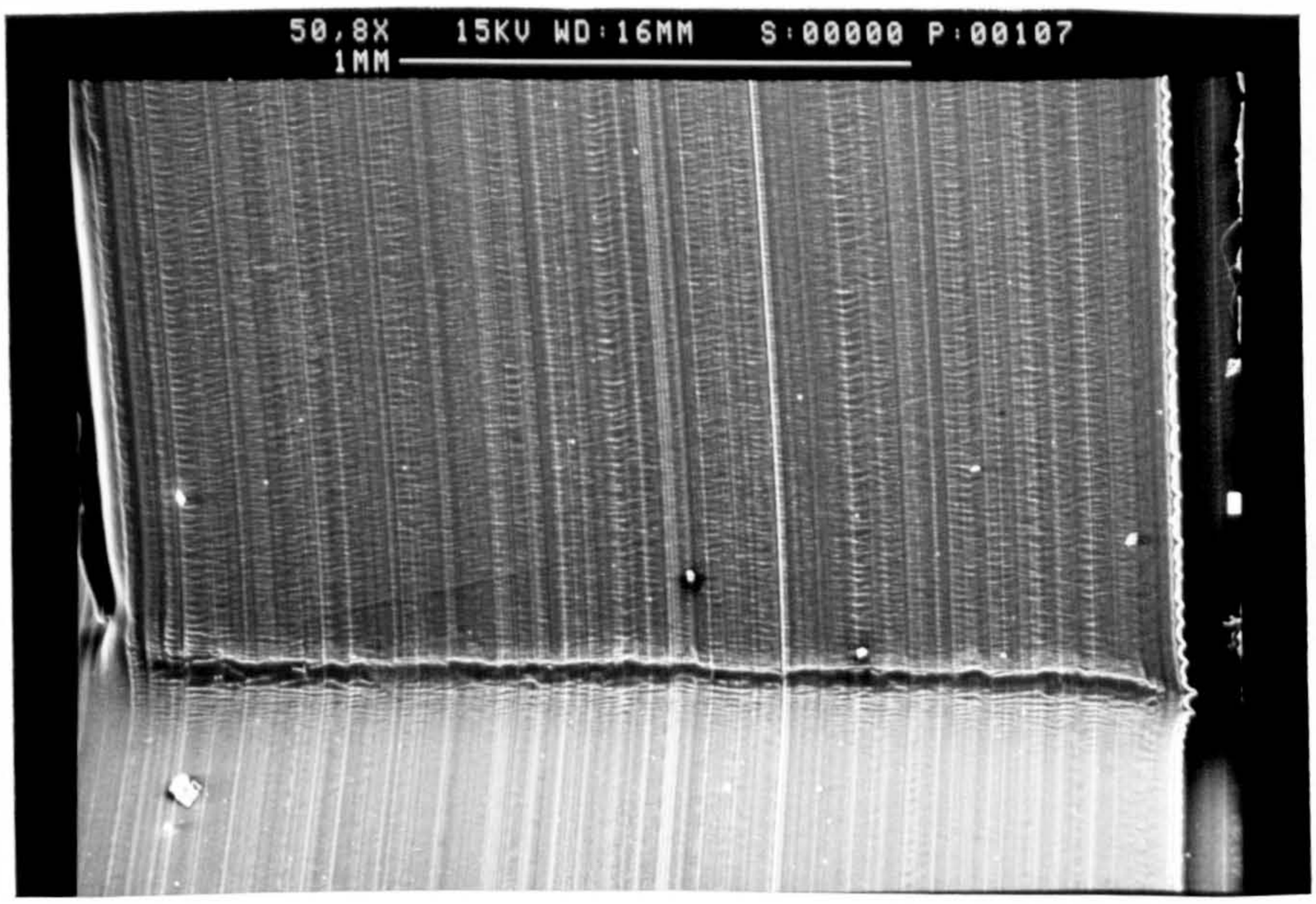

Fig 54. HDPE chip root showing the formation of new shear fronts.
(Rake angle = 30°, speed = 30 m/min, feed = 0.25 mm/rev)

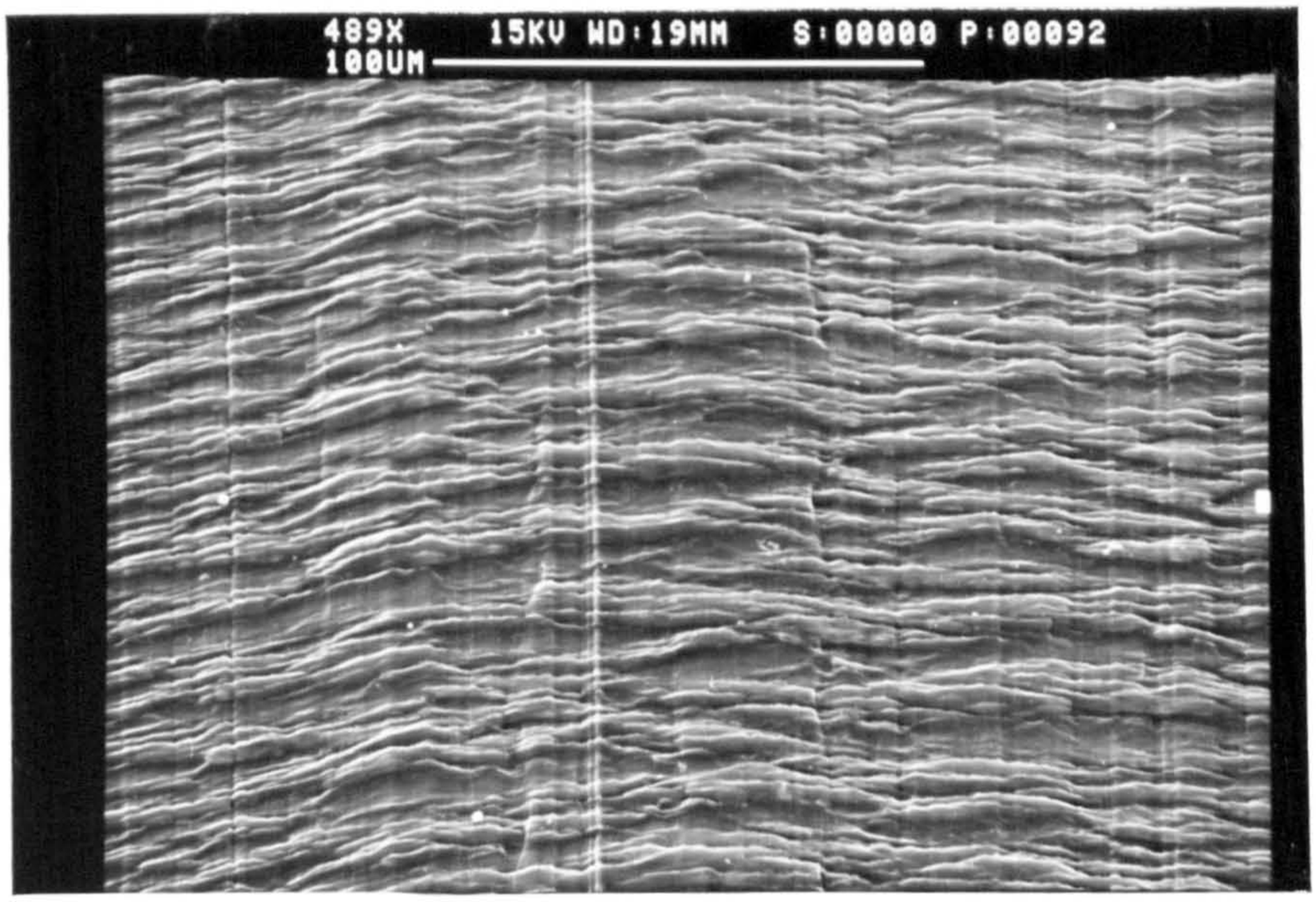

Fig 55. Top surface of a continuous HDPE chip showing inhomogeneous chip formation
(Rake angle = 10°, speed = 30 m/min, feed = 0.25 mm/rev)

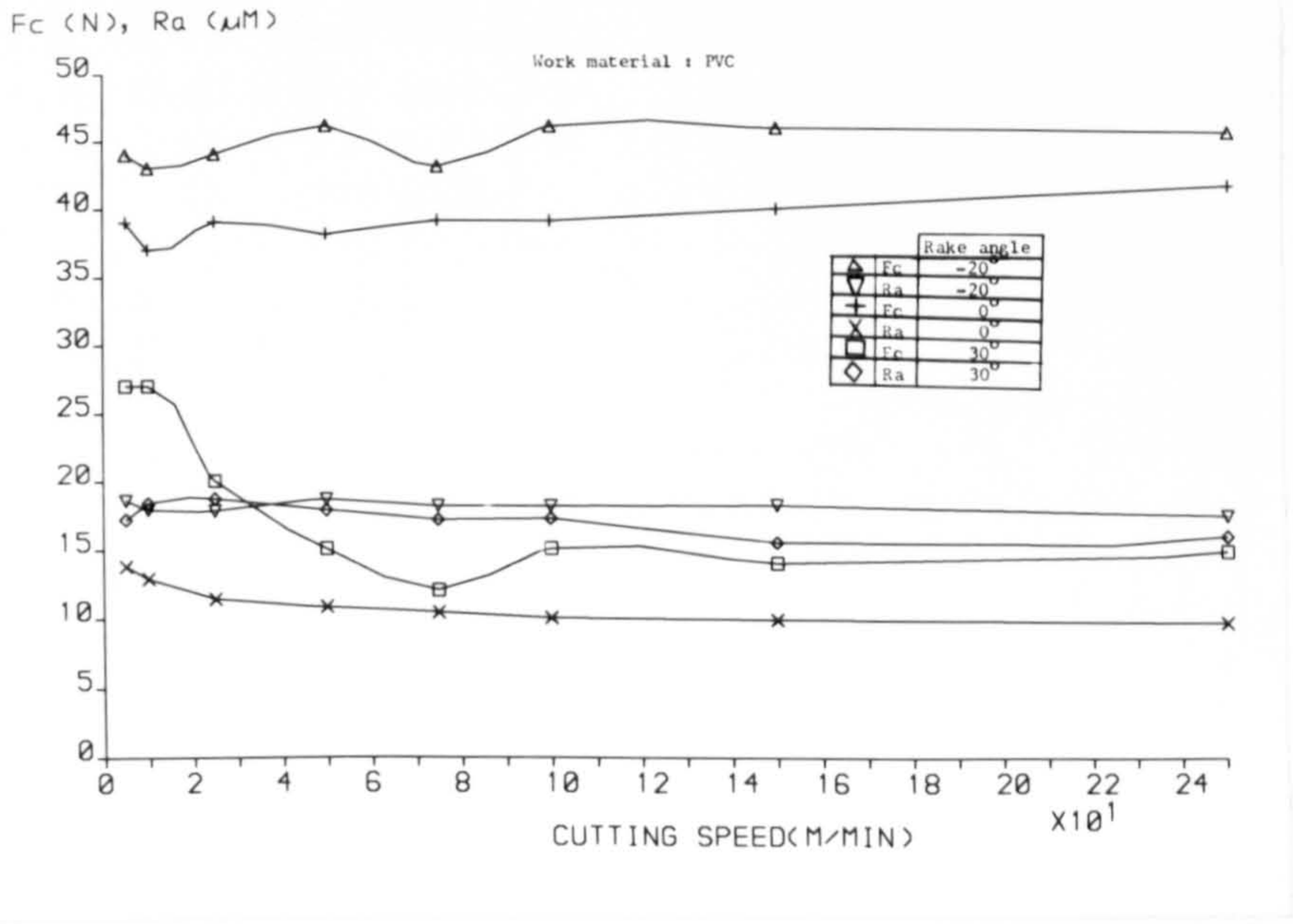

Fig 56. Variation of cutting force and surface roughness with change in cutting speed. (Work-PVC, feed = 0.16 mm/rev, DOC = 1.5mm)

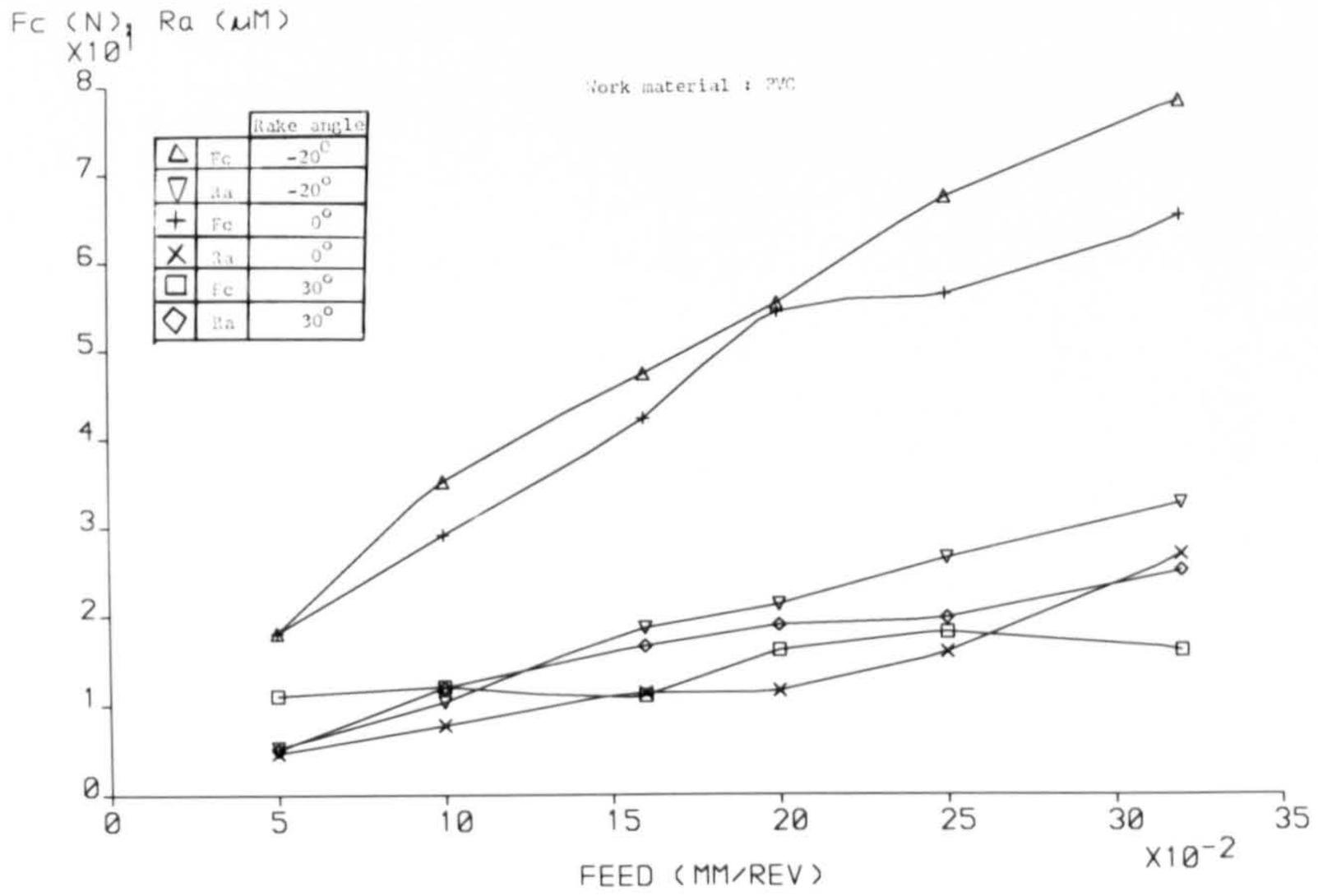

Fig 57. Variation of cutting force and surface roughness against feed rate. (Work-PVC, speed = 150 m/min, DOC = 1.5mm)

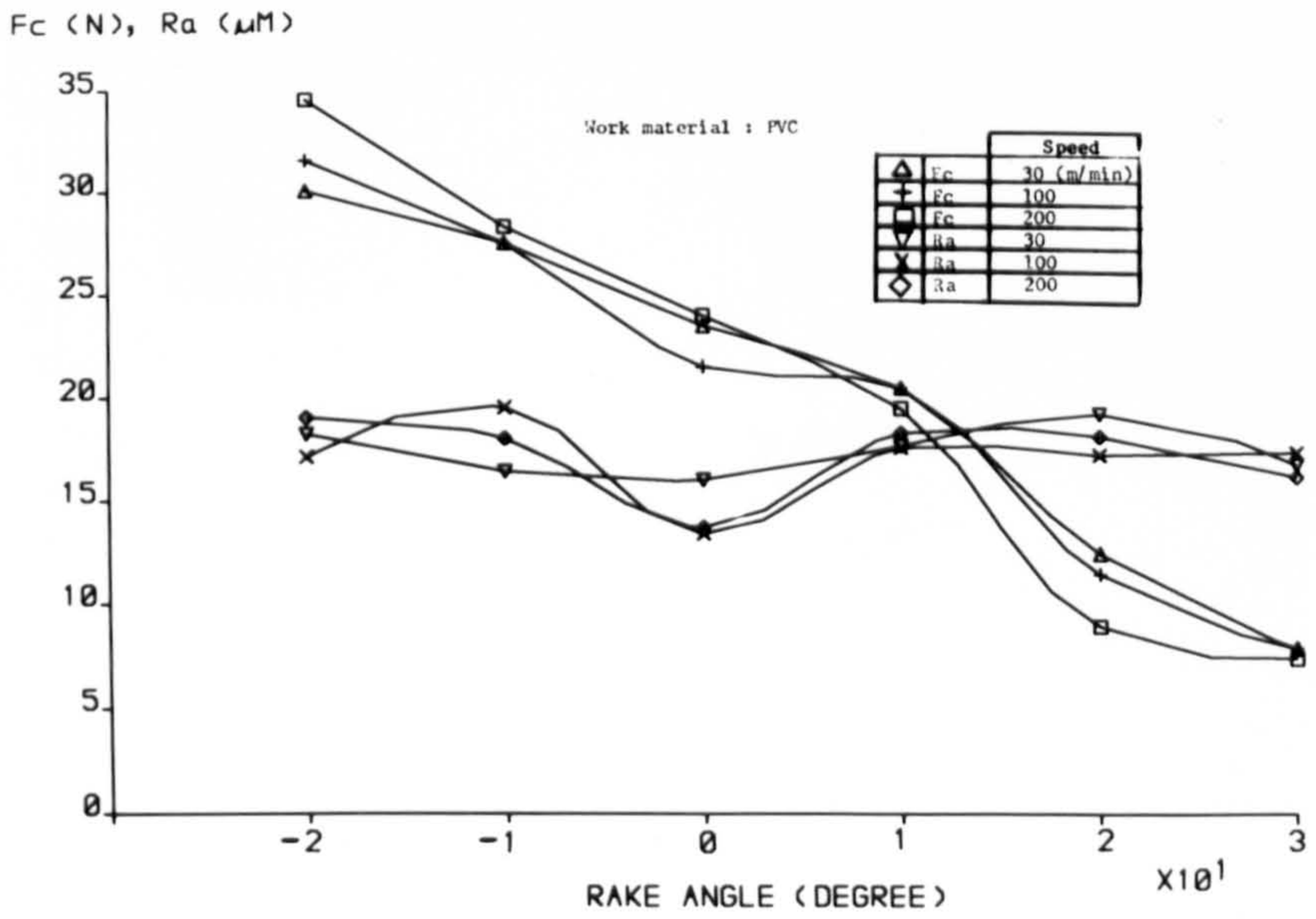

Fig 58. Variation of cutting force and surface roughness against rake angle. (Work-PVC, feed = 0.1 mm/rev, DOC = 1 mm)

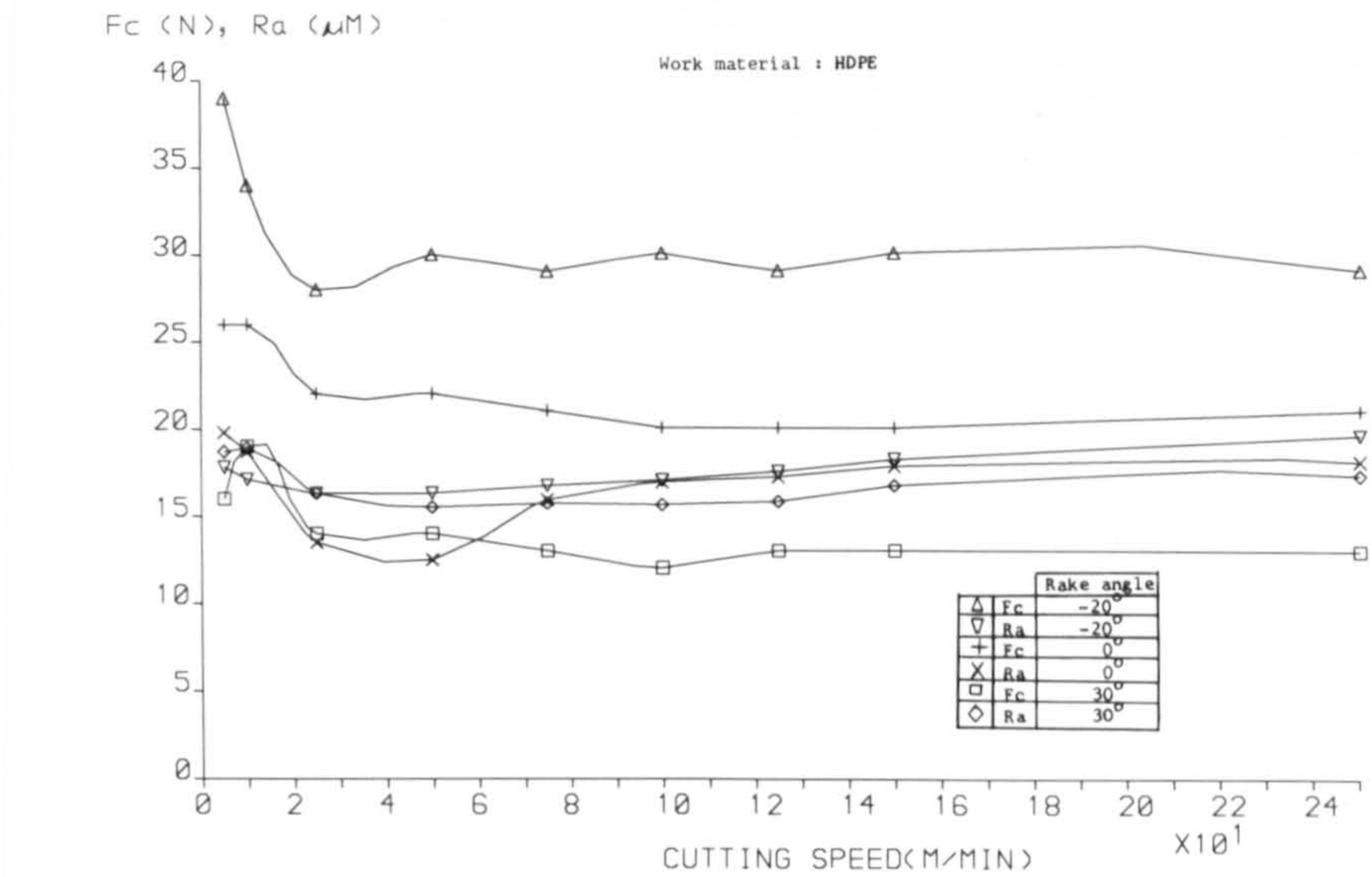

Fig 59. Variation of cutting force and surface roughness with change in cutting speed. (Work-HDPE, feed = 0.16 mm/rev, DOC = 1.5mm)

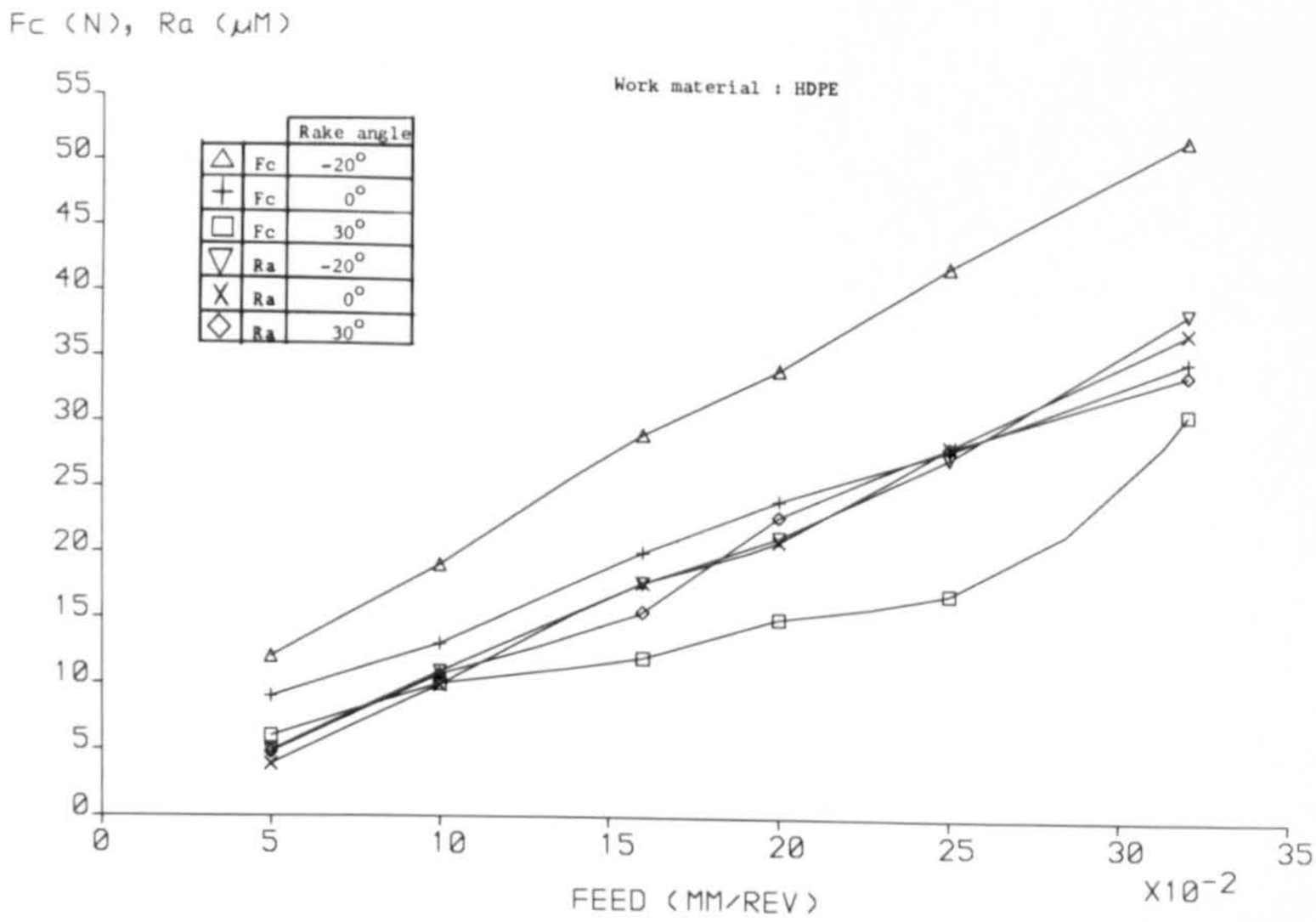

Fig 60. Variation of cutting force and surface roughness against feed rate. (Work-HDPE, speed = 150 m/min, DOC = 1.5mm)

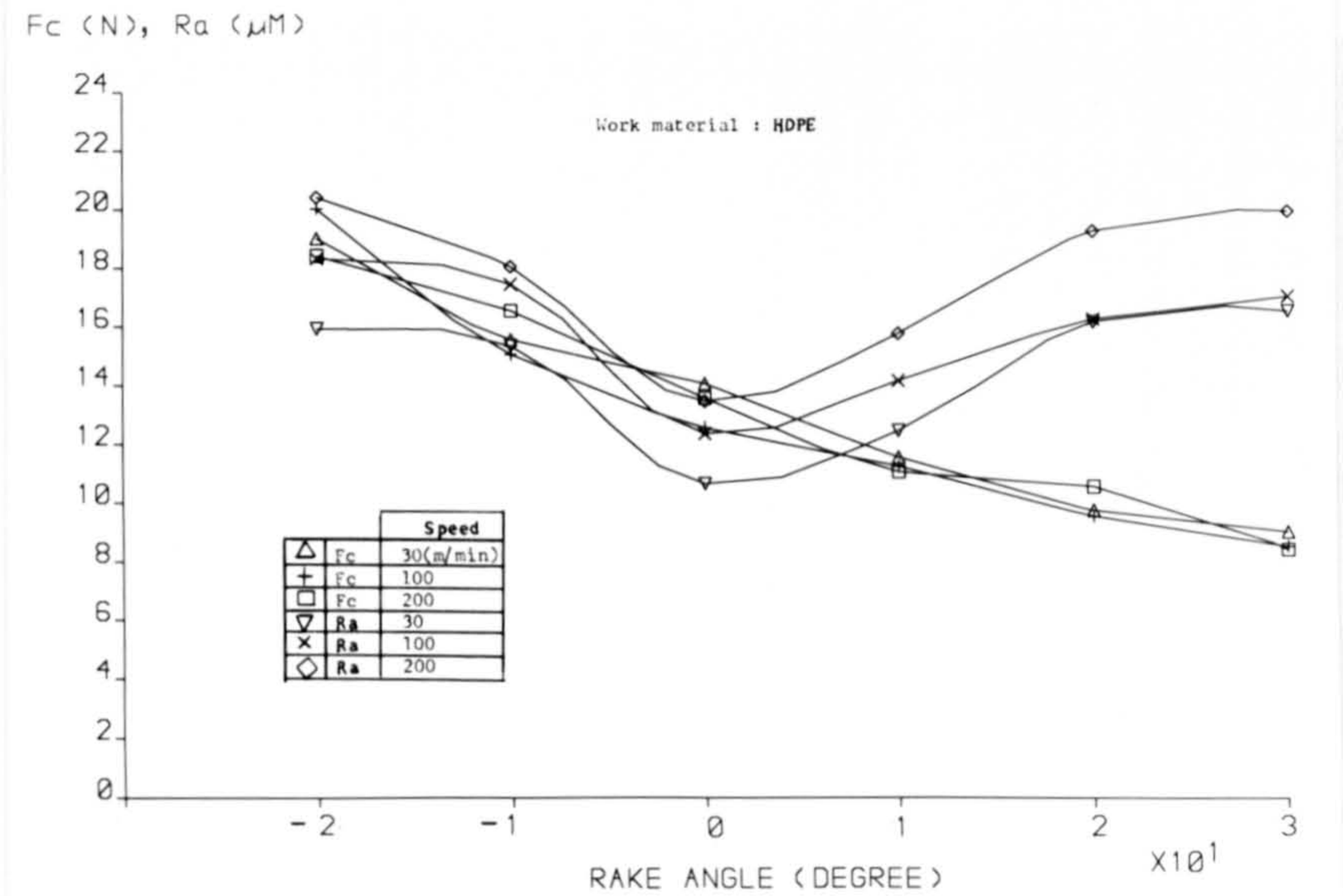

Fig 61. Variation of cutting force and surface roughness against rake angle. (Work-HDPE, feed = 0.16 mm/rev, DOC = 1.5mm)

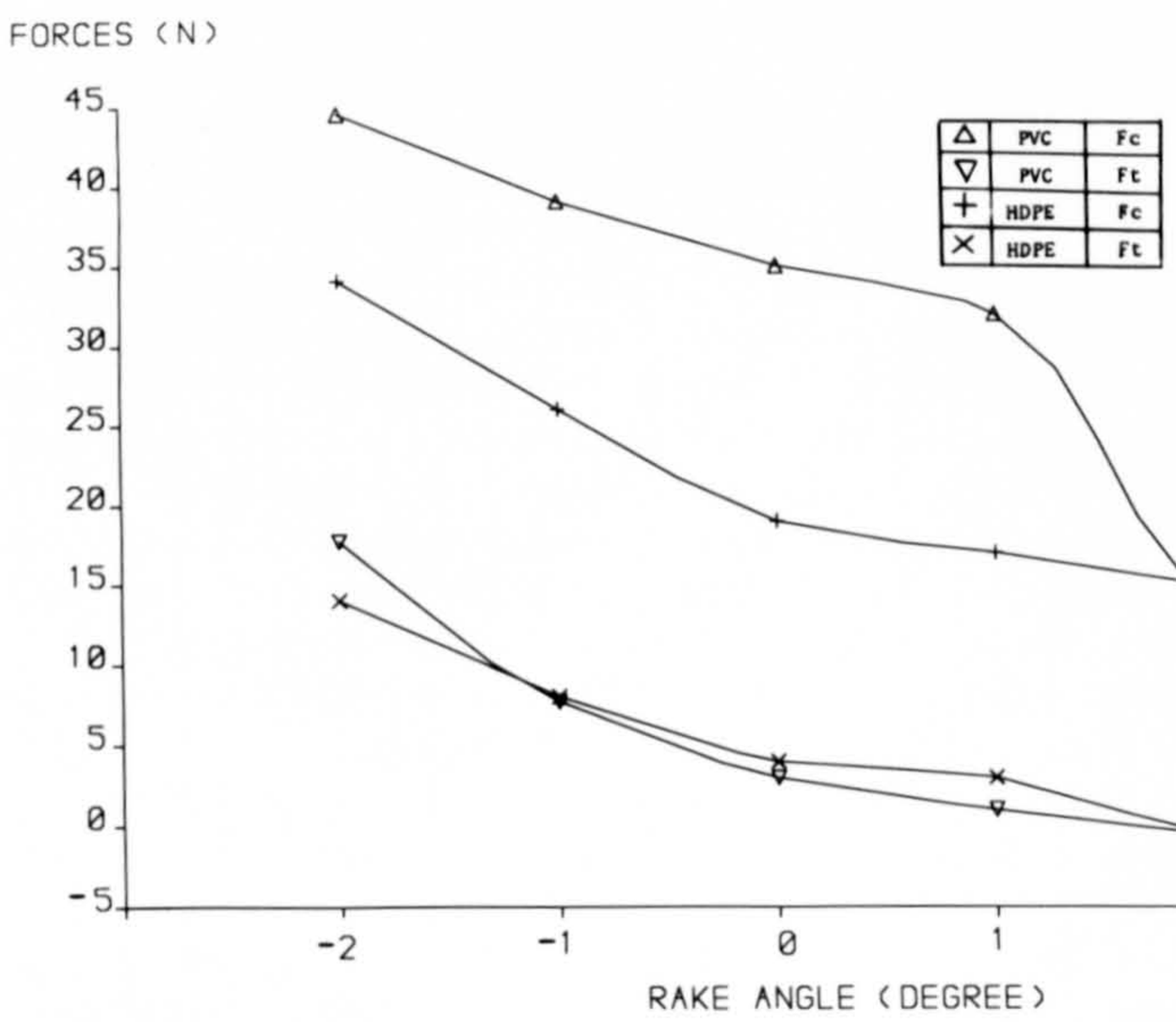

Fig 62. Cutting forces and feed forces at various rake angles. (Speed = 100 m/min, feed = 0.25 mm/rev, DOC = 1mm)

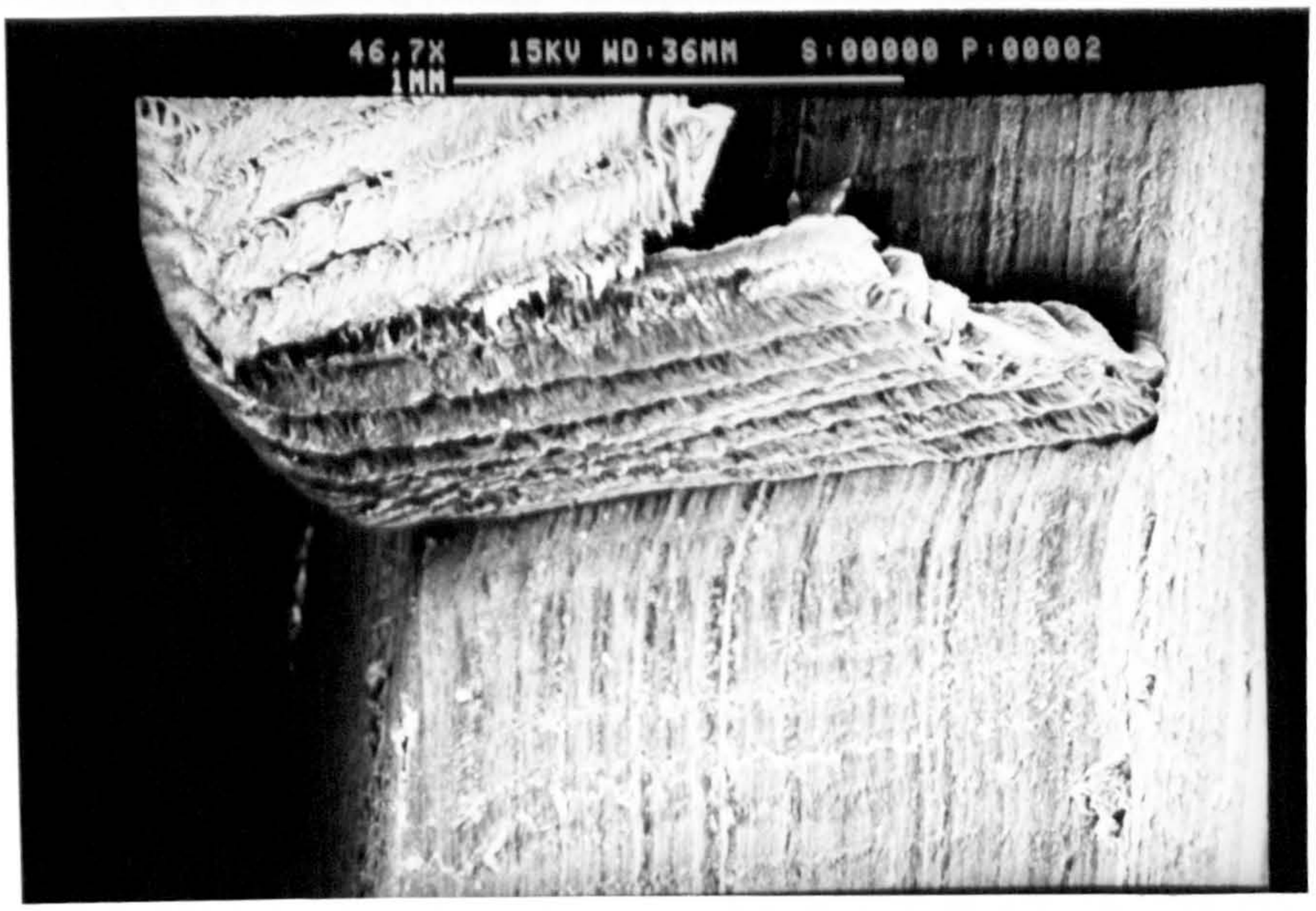

Fig 63. PVC machined surface in continuous chip formation
(Rake angle = -10°, speed = 30 m/min, feed = 0.25 mm/rev)

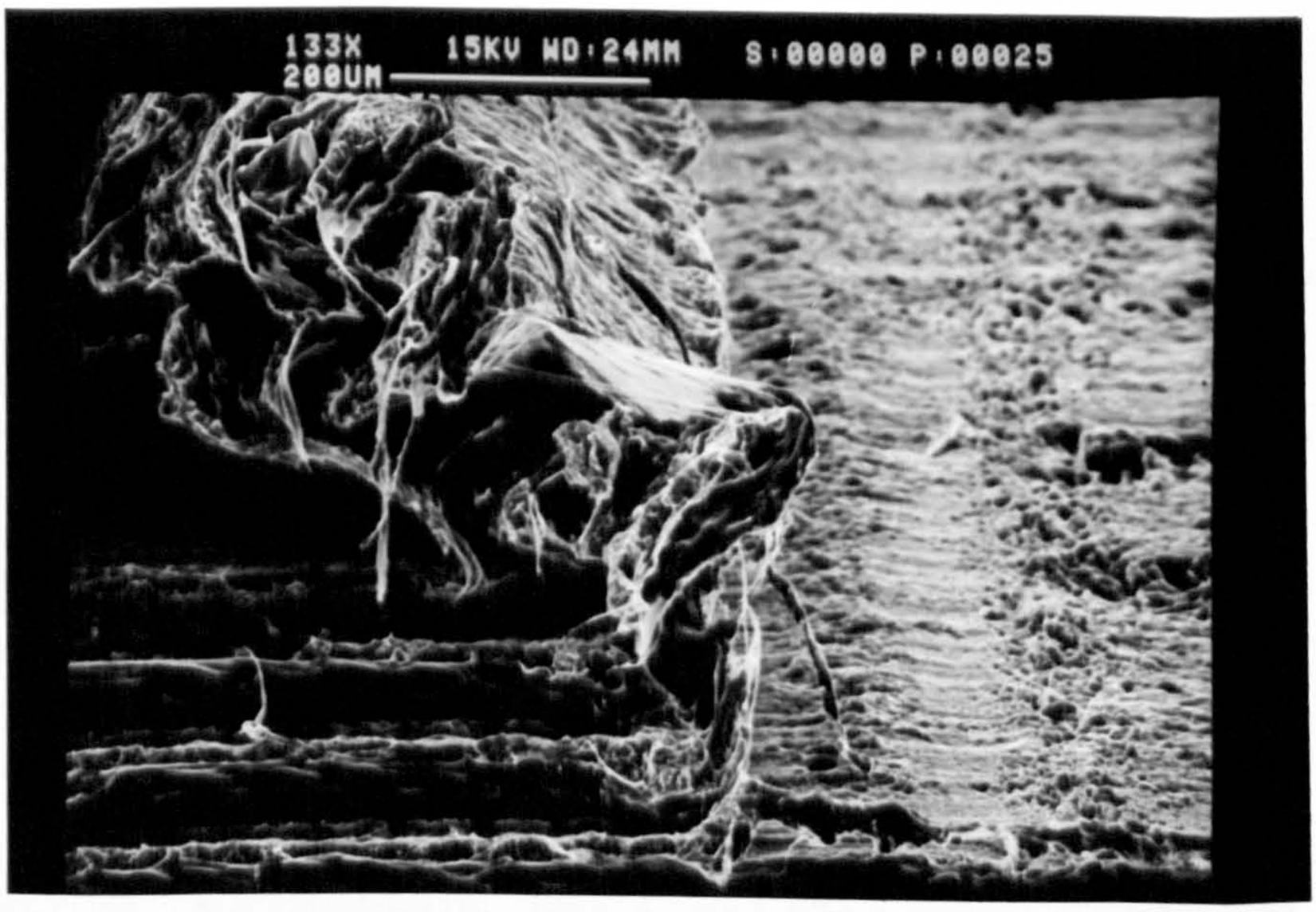

Fig 64. PVC machined surface in segmented chip formation
(Rake angle = -20°, speed = 50 m/min, feed = 0.25 mm/rev)

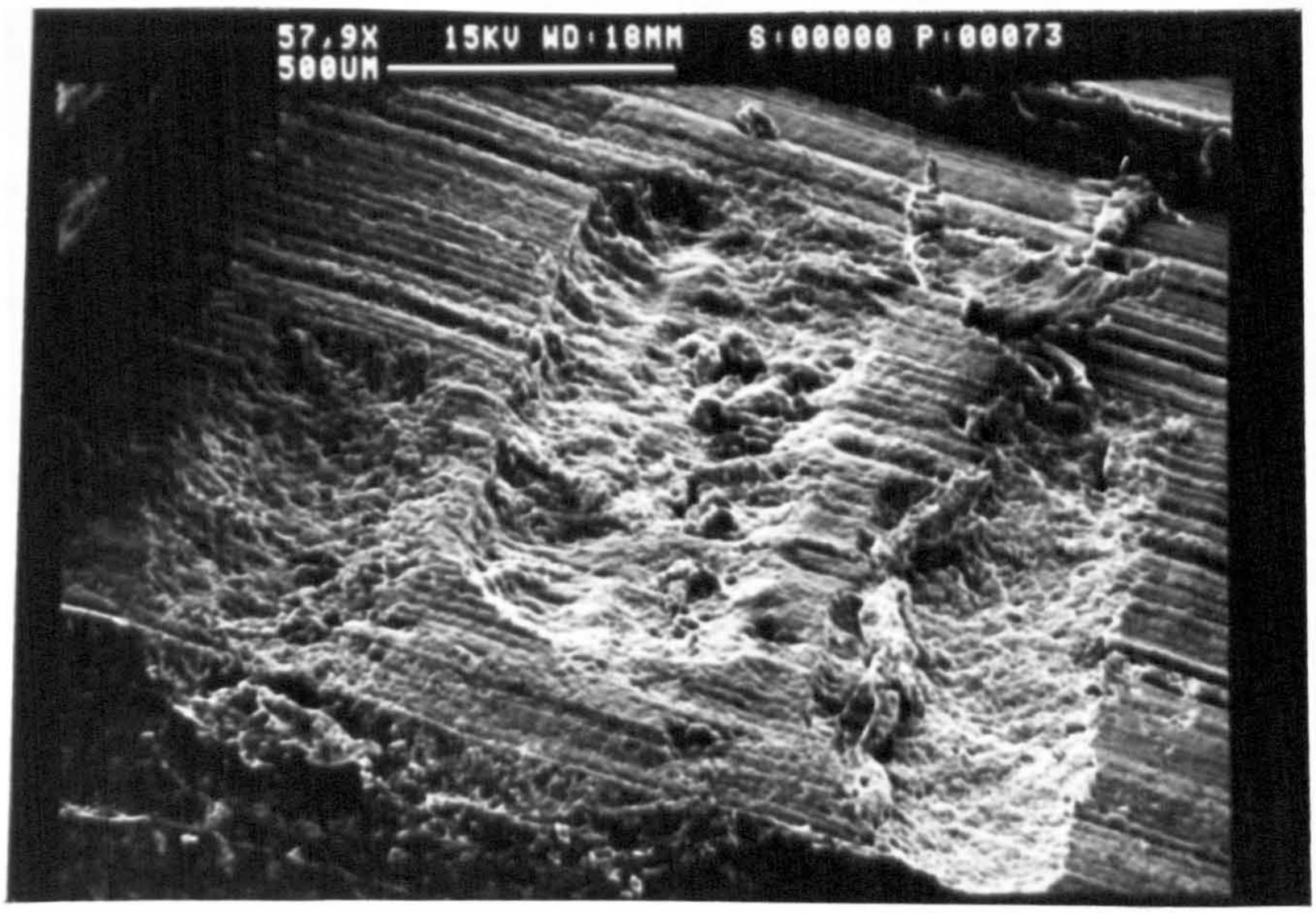

Fig 65. PVC machined surface in discontinuous chip formation (Rake angle = 30°, speed = 50 m/min, feed = 0.25 mm/rev)

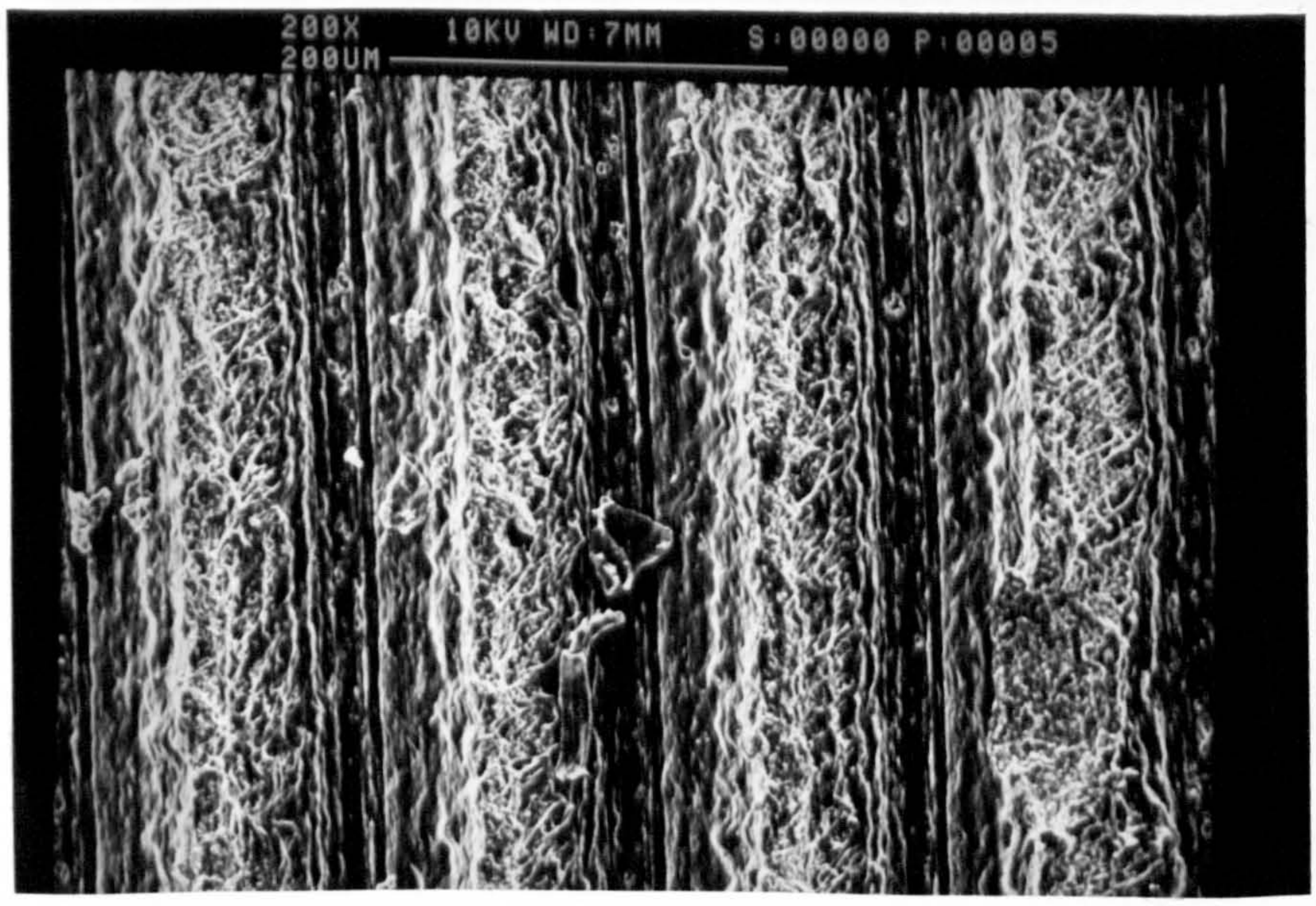

Fig 66. PVC machined surface in continuous chip formation (Rake angle = 20°, speed = 20 m/min, feed = 0.14 mm/rev)

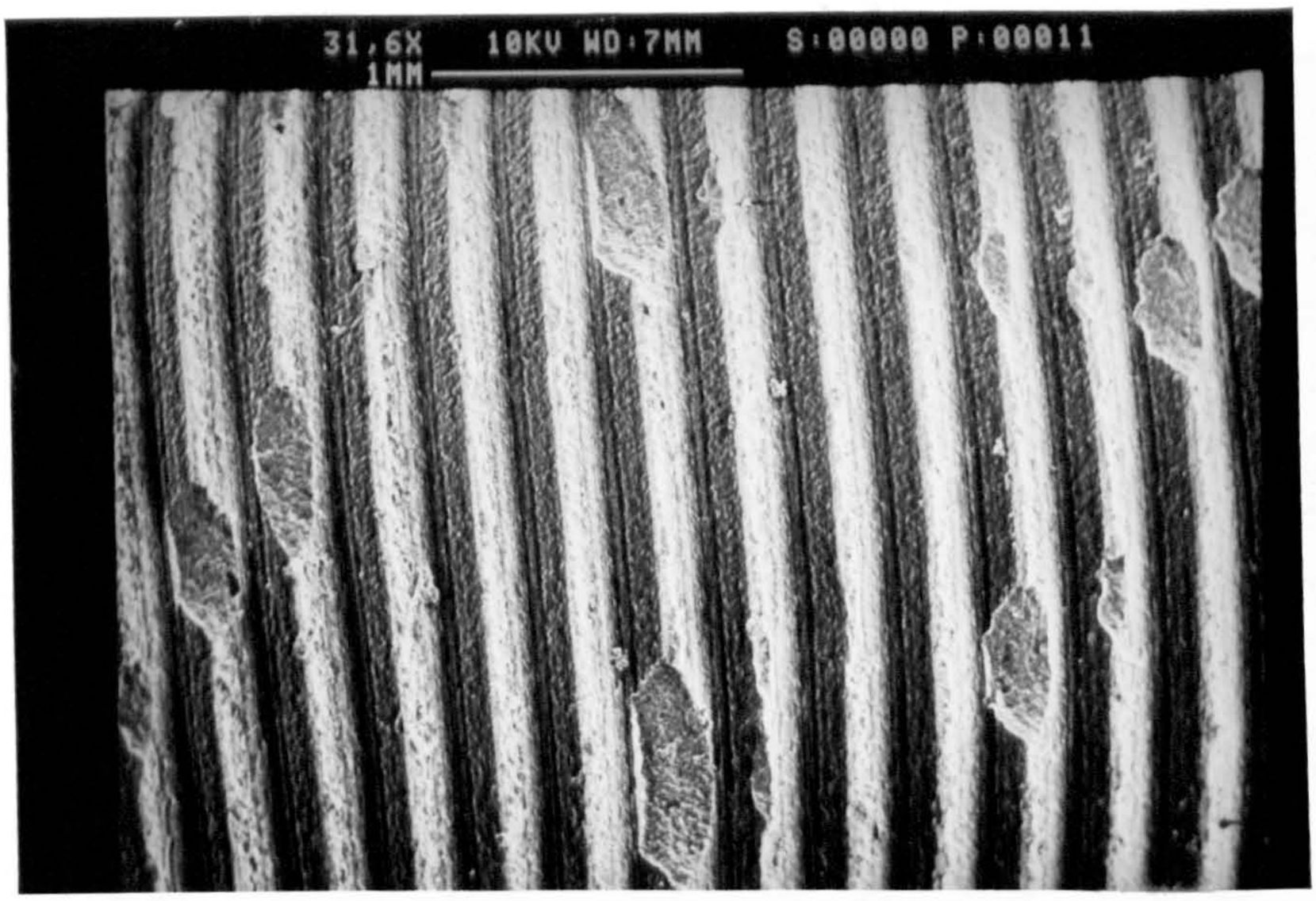

Fig 67. PVC machined surface in semi-discontinuous chip formation (Rake angle = 20°, speed = 100 m/min, feed = 0.28 mm/rev)

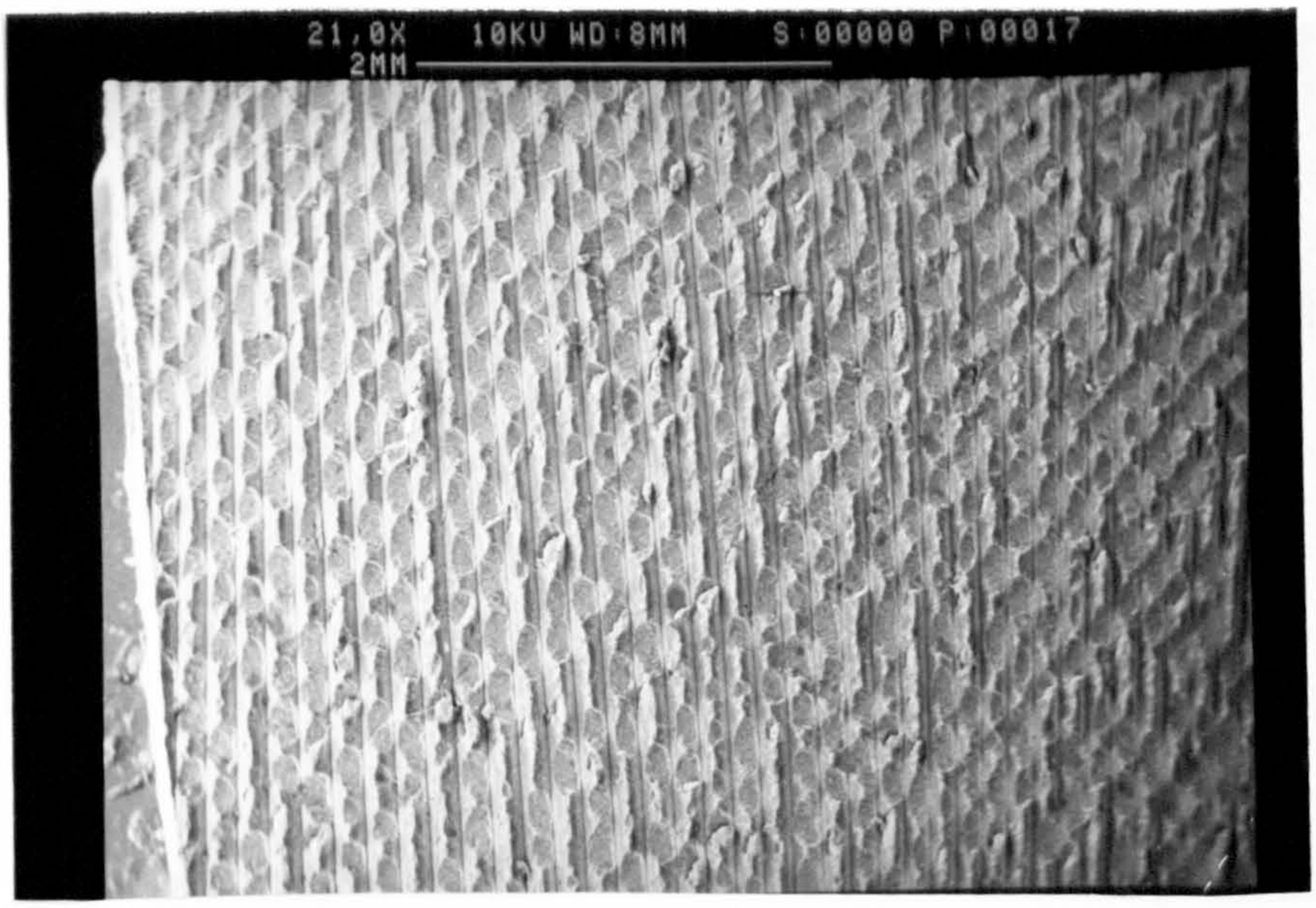

Fig 68. PVC machined surface in discontinuous chip formation (Rake angle = 30°, speed = 100 m/min, feed = 0.14 mm/rev)

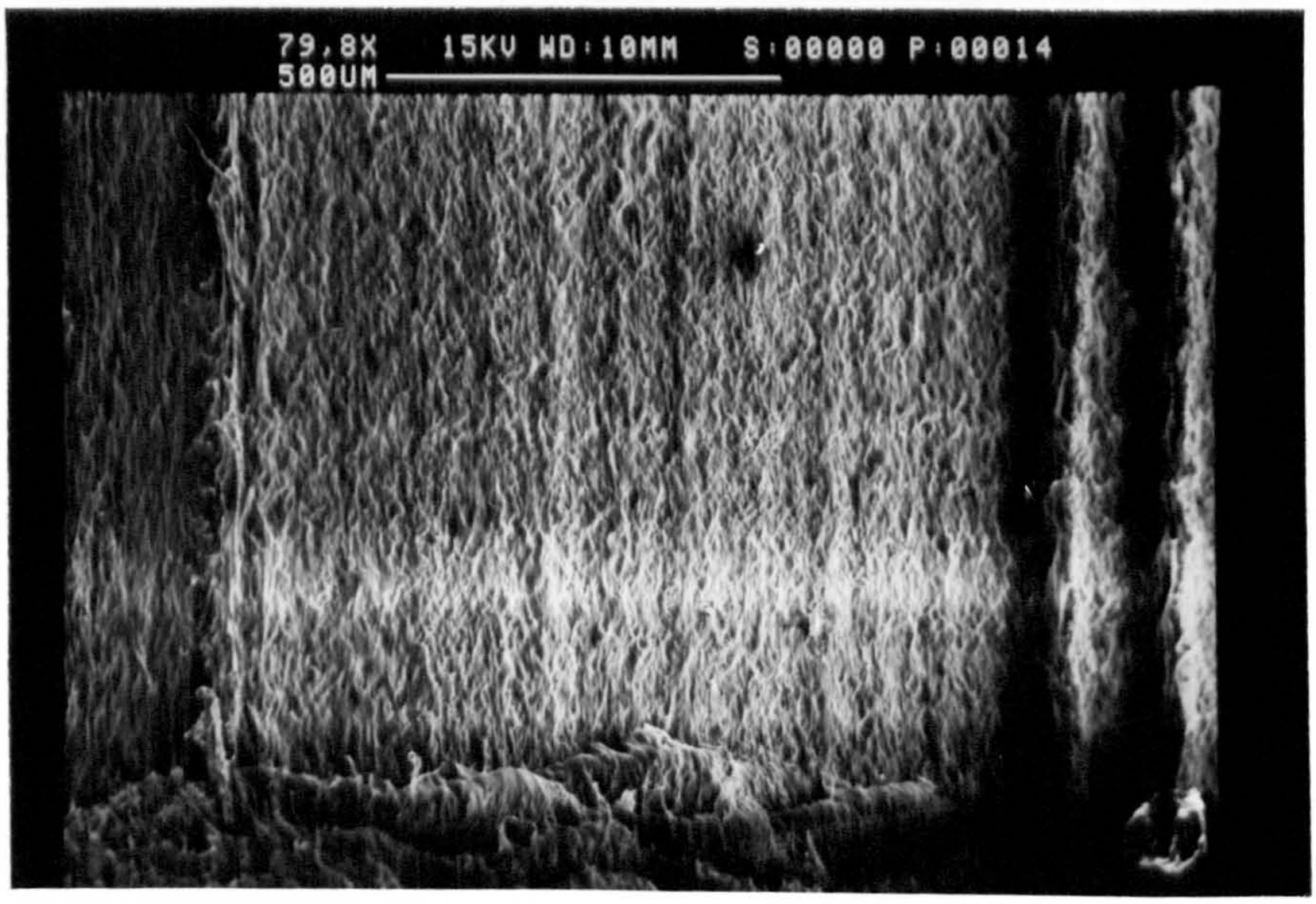

Fig 69. PVC machined surface produced at -20° rake angle showing fibrillar structure. (Speed = 30 m/min, feed = 0.25 mm/rev)

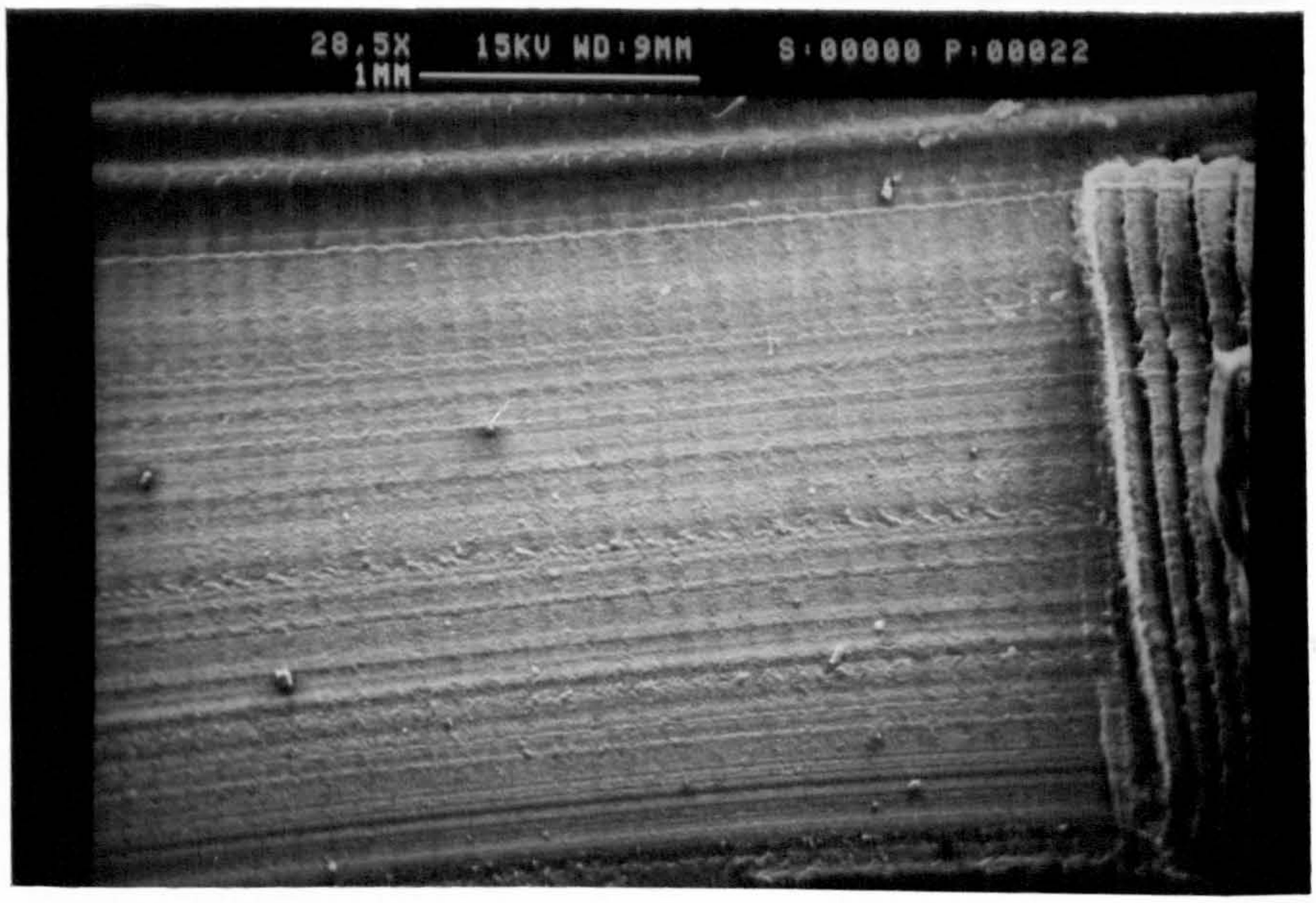

Fig 70. PVC machined surface produced at 0° rake angle showing groove formation. (Speed = 30 m/min, feed = 0.25 mm/rev)

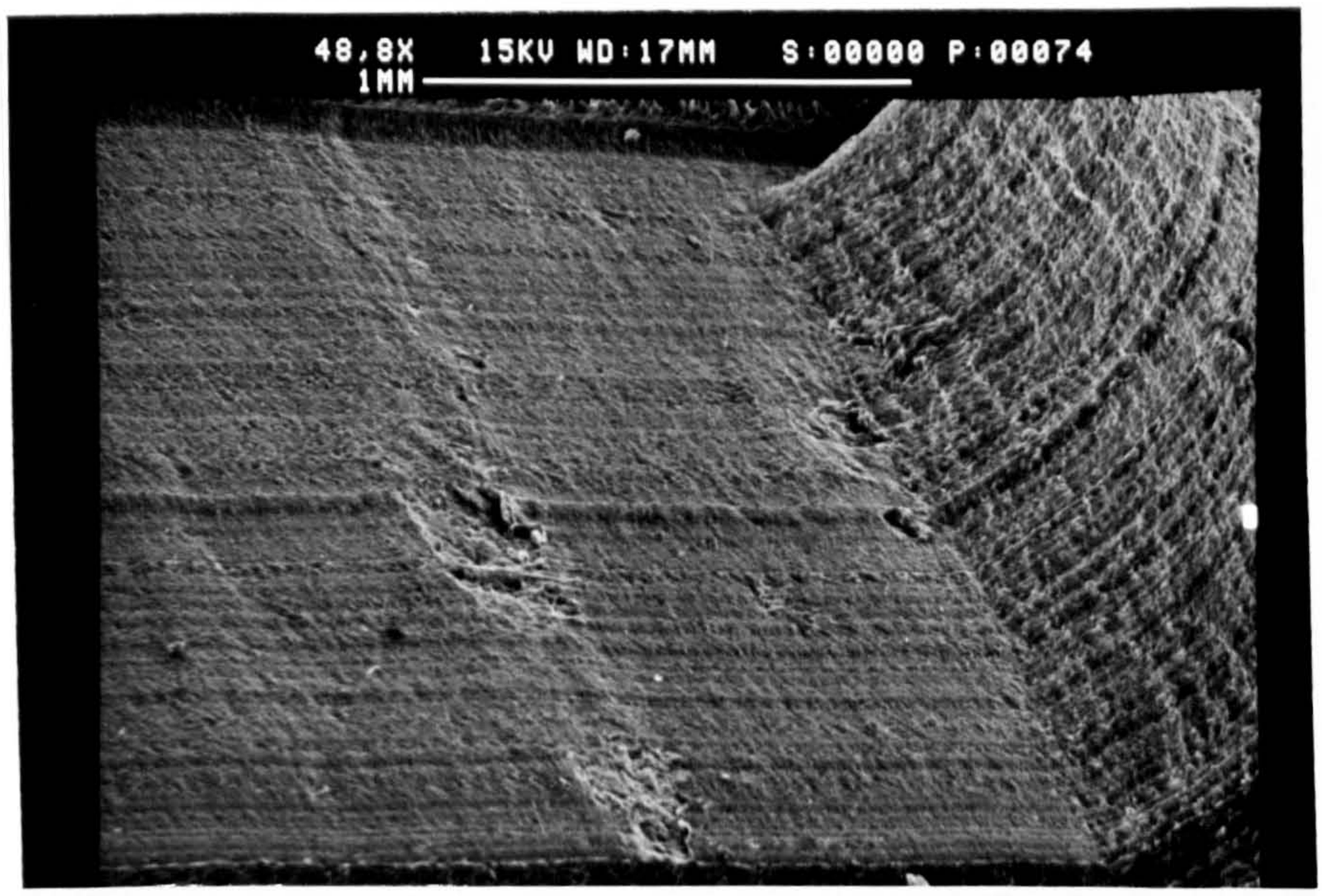

Fig 71. PVC machined surface produced at 30° rake angle showing intermittent fractured areas. (Speed = 30 m/min, feed = 0.25 mm/rev)

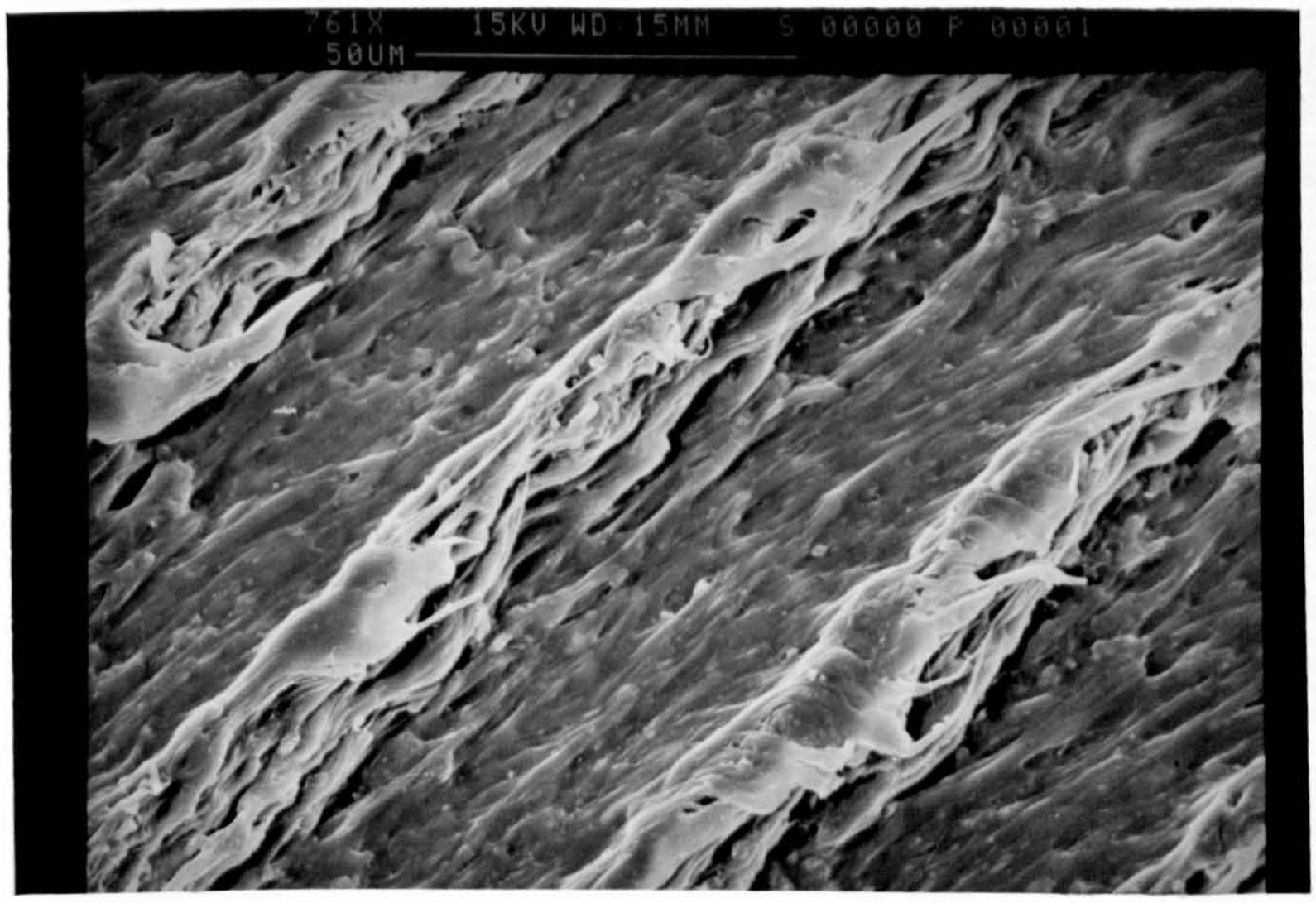

Fig 72. PVC machined surface produced at low cutting speed (25 m/min), showing ductile nature. (Rake angle = 0°, feed = 0.05 mm/rev)

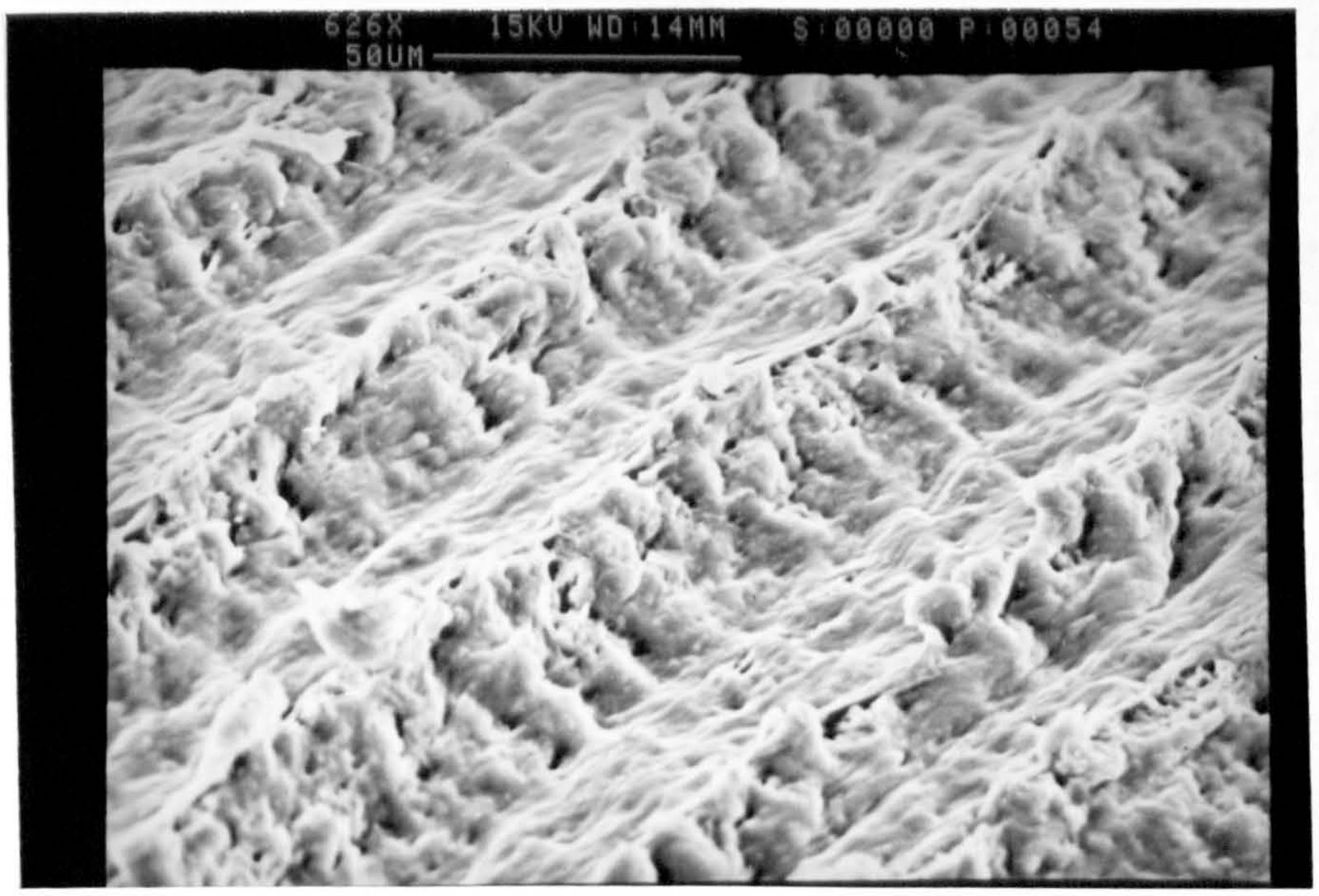

Fig 73. PVC machined surface produced at high cutting speed (250 m/min), showing undulating cut surface.
(Rake angle = 0°, feed = 0.05 mm/rev)

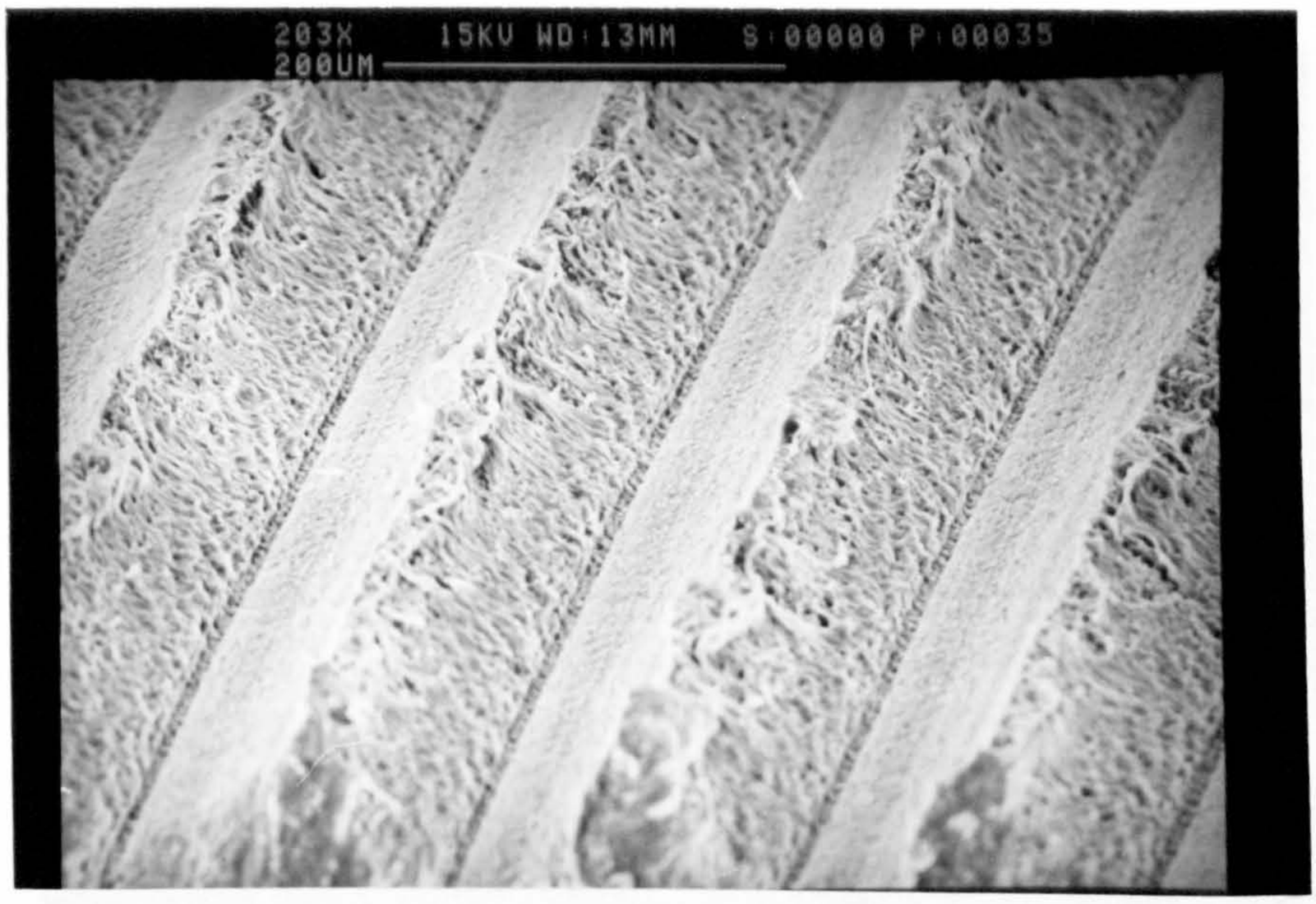

Fig 74. PVC machined surface produced at low cutting speed (25 m/min) suggesting continuous chip formation.
(Rake angle = 30°, feed = 0.16 mm/rev)

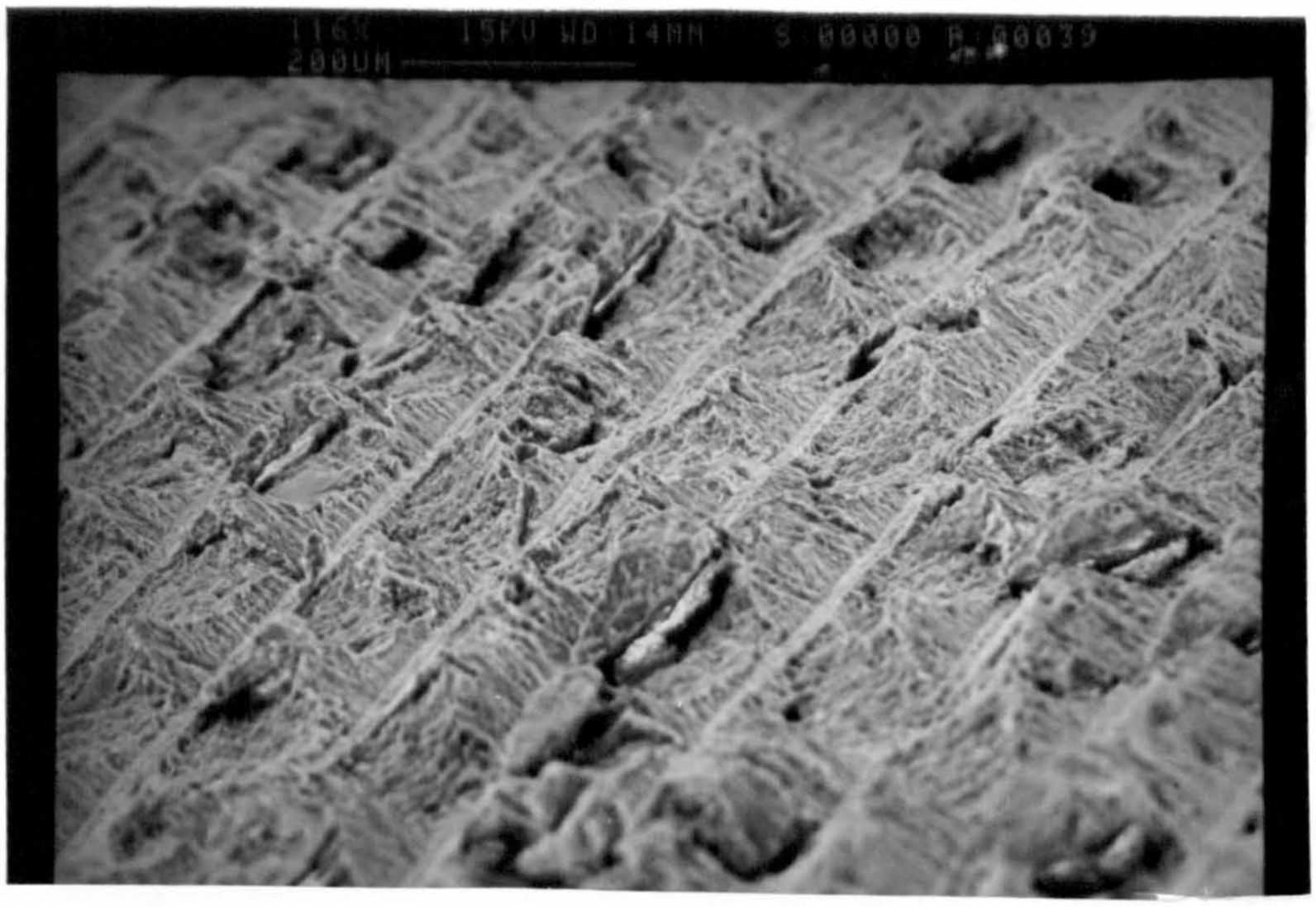

Fig 75. PVC machined surface produced at high cutting speed (250 m/min), suggesting discontinuous chip formation. (Rake angle = 30°, feed = 0.16 mm/rev)

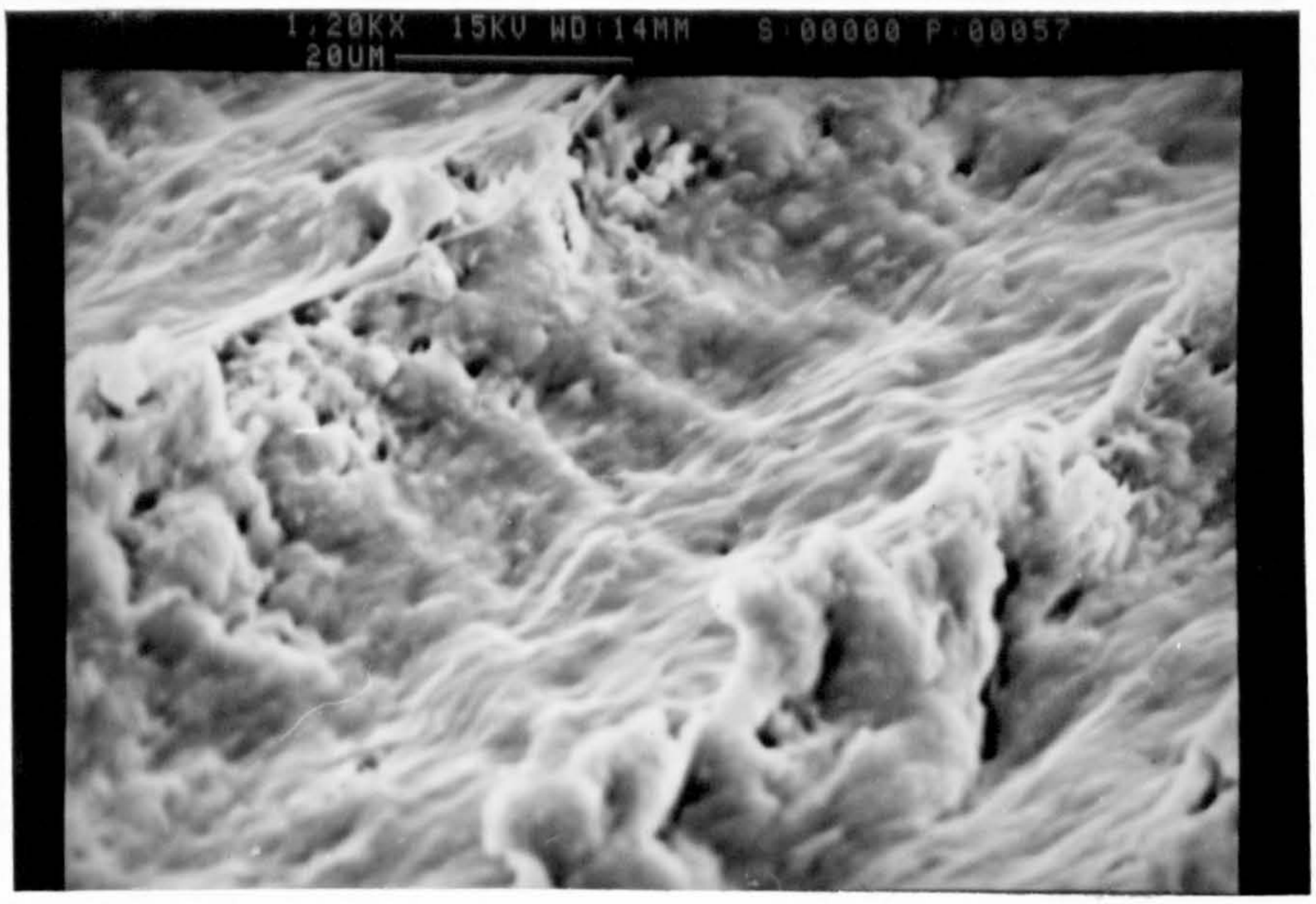

Fig 76. PVC surface machined at low feed rate (0.05 mm/rev) (Rake angle = 0°, speed = 250 m/min)

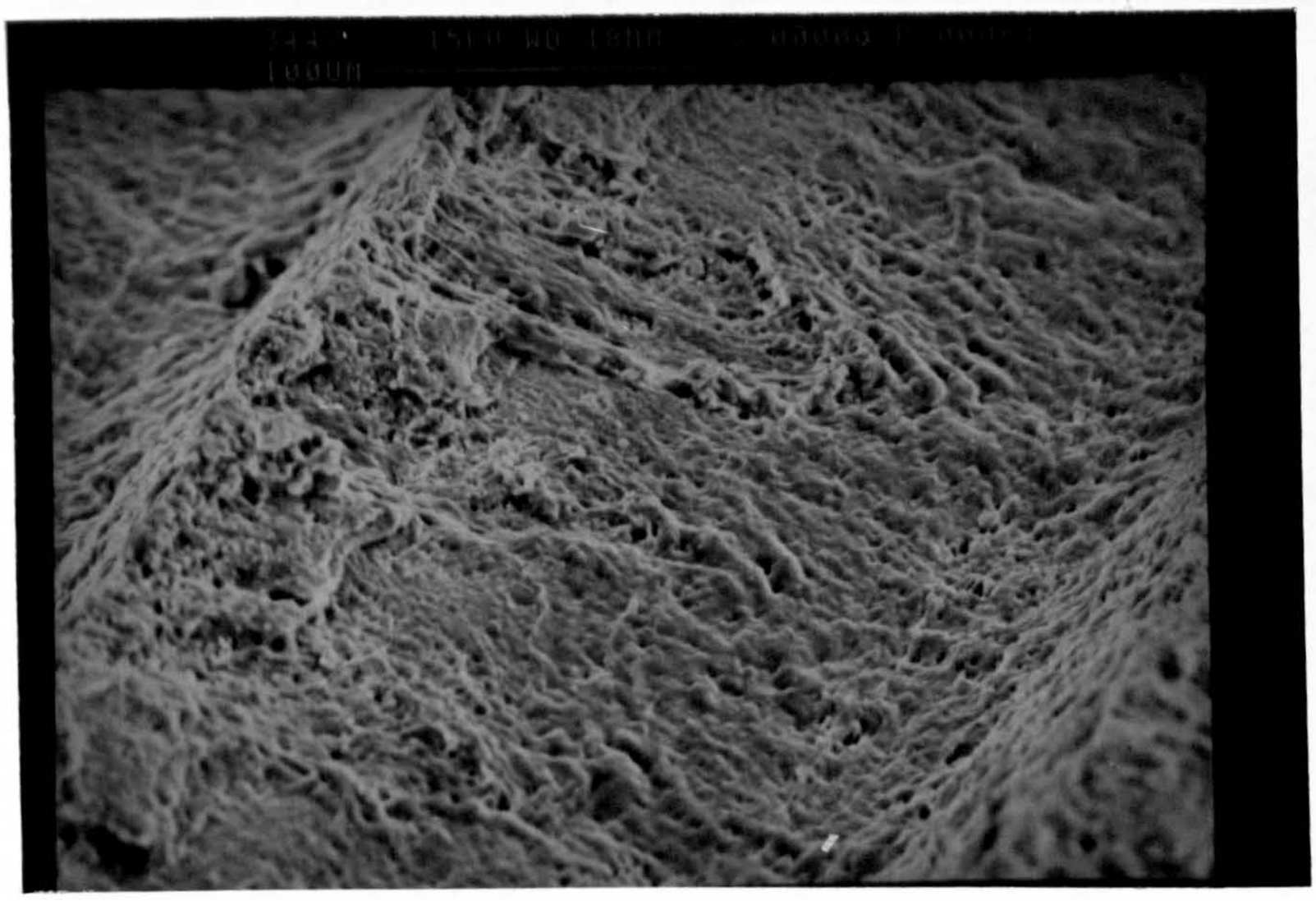

Fig 77. PVC surface machined at high feed rate (0.315 mm/rev) (Rake angle = 0°, speed = 250 m/min)

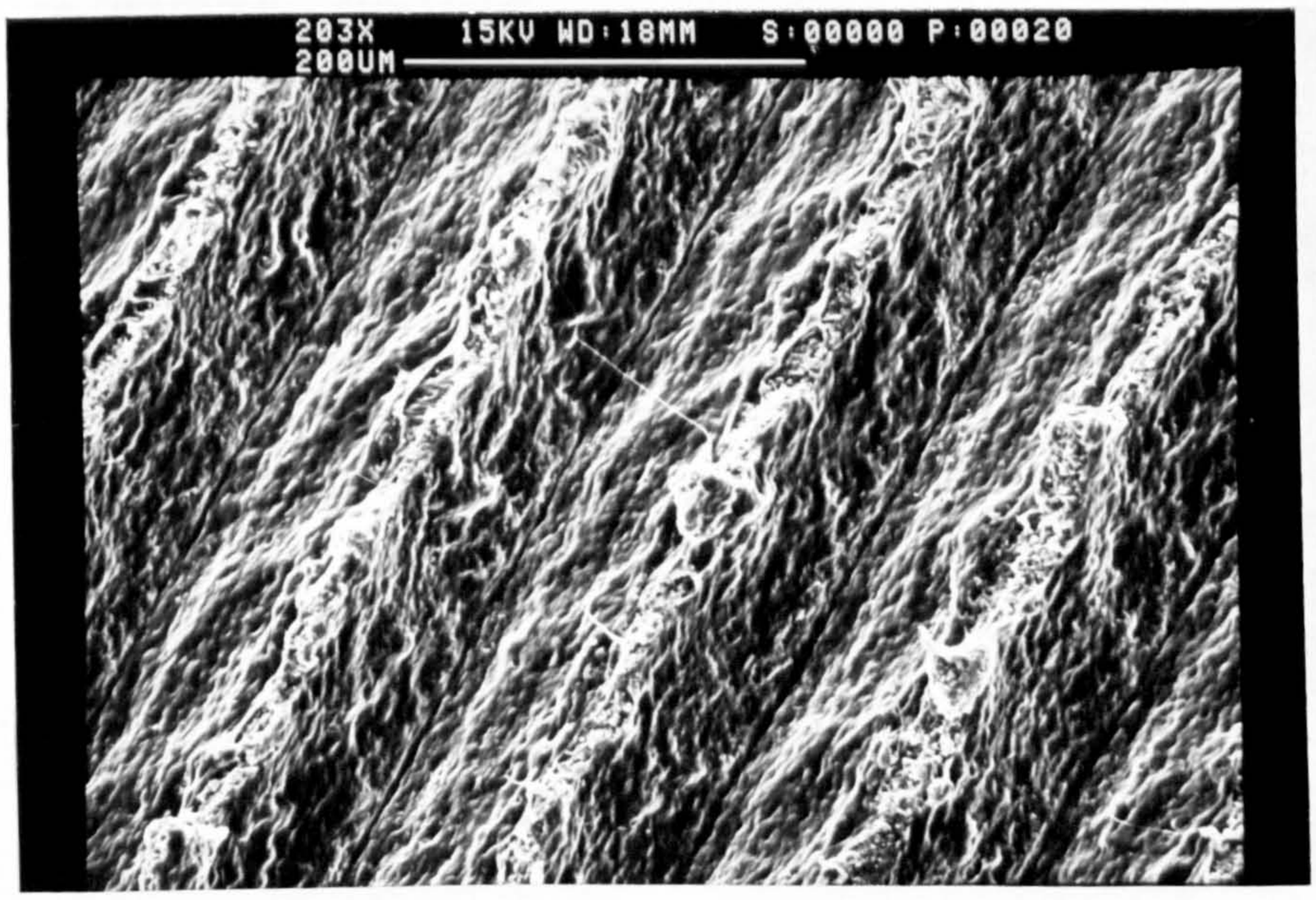

Fig 78. PVC surface machined at -20° rake angle, showing fibrillar structure. (Speed = 150 m/min, feed = 0.14 mm/rev)

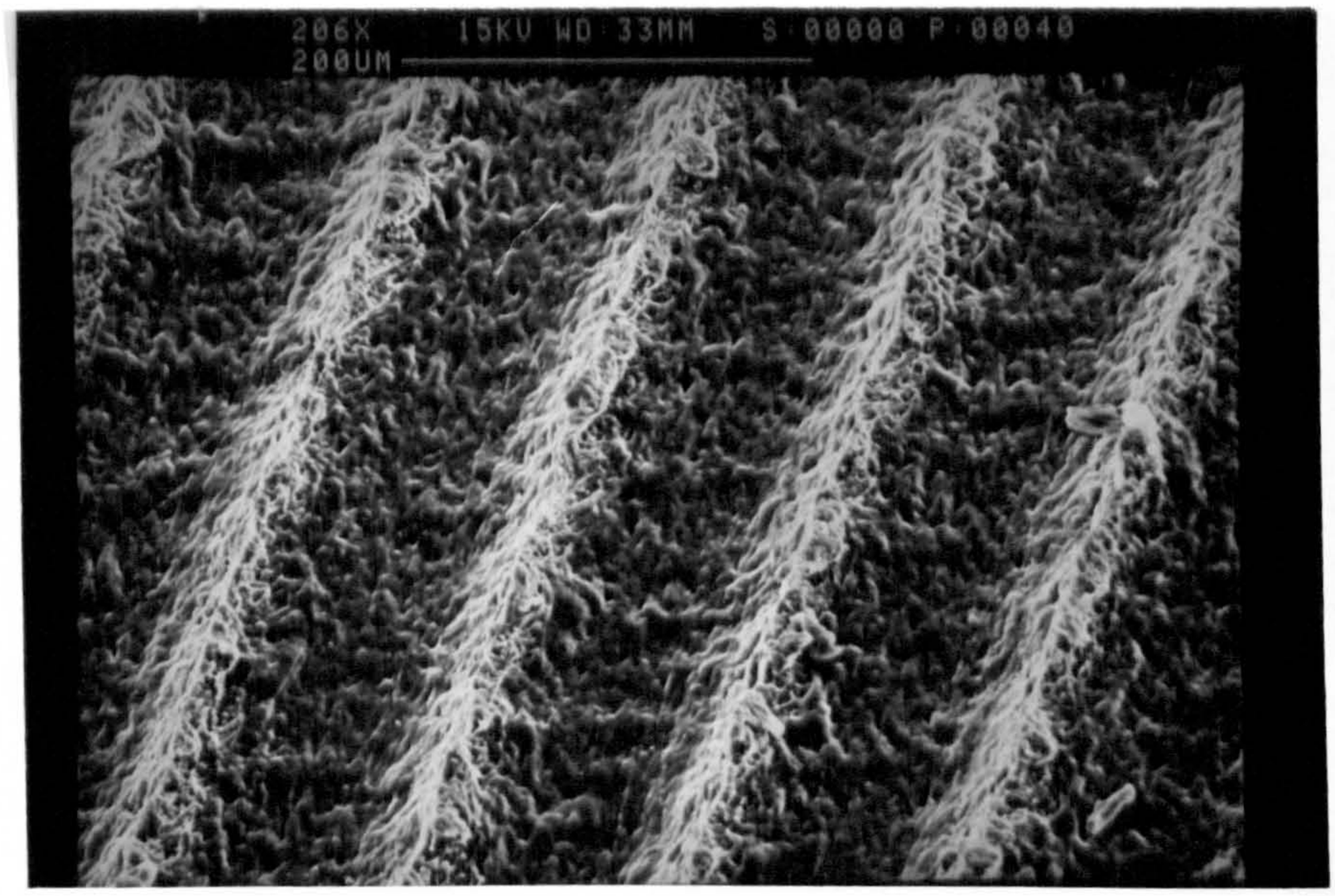

Fig 79. PVC surface machined at 0º rake angle, showing good surface quality. (Speed = 150 m/min, feed = 0.14 mm/rev)

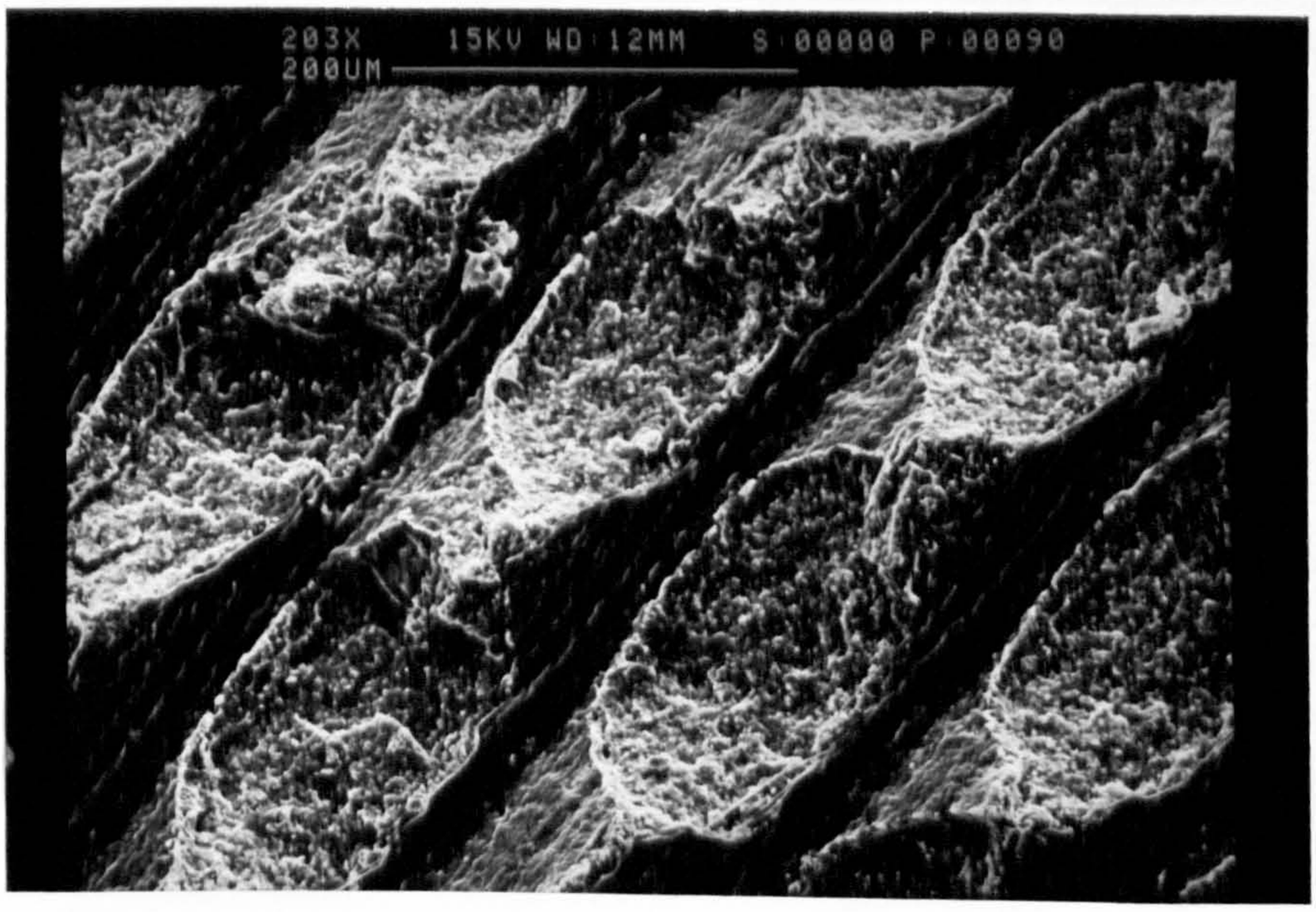

Fig 80. PVC surface machined at 30º rake angle, showing numerous cavities. (Speed = 150 m/min, feed = 0.14 mm/rev)

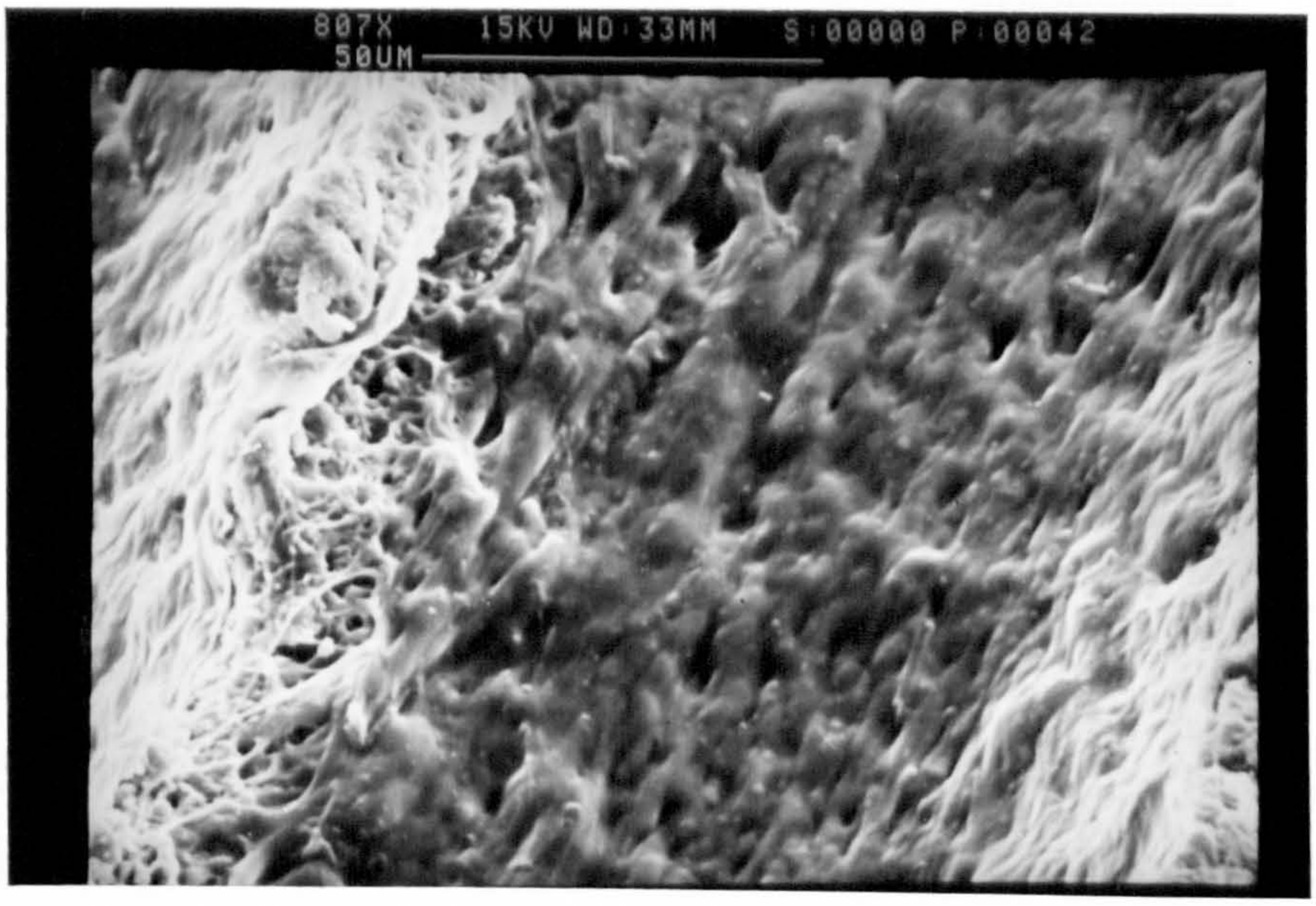

Fig 81. Magnified view of PVC machined surface in continuous chip formation. (Rake angle = 10°, speed = 150 m/min, feed = 0.14 mm/rev)

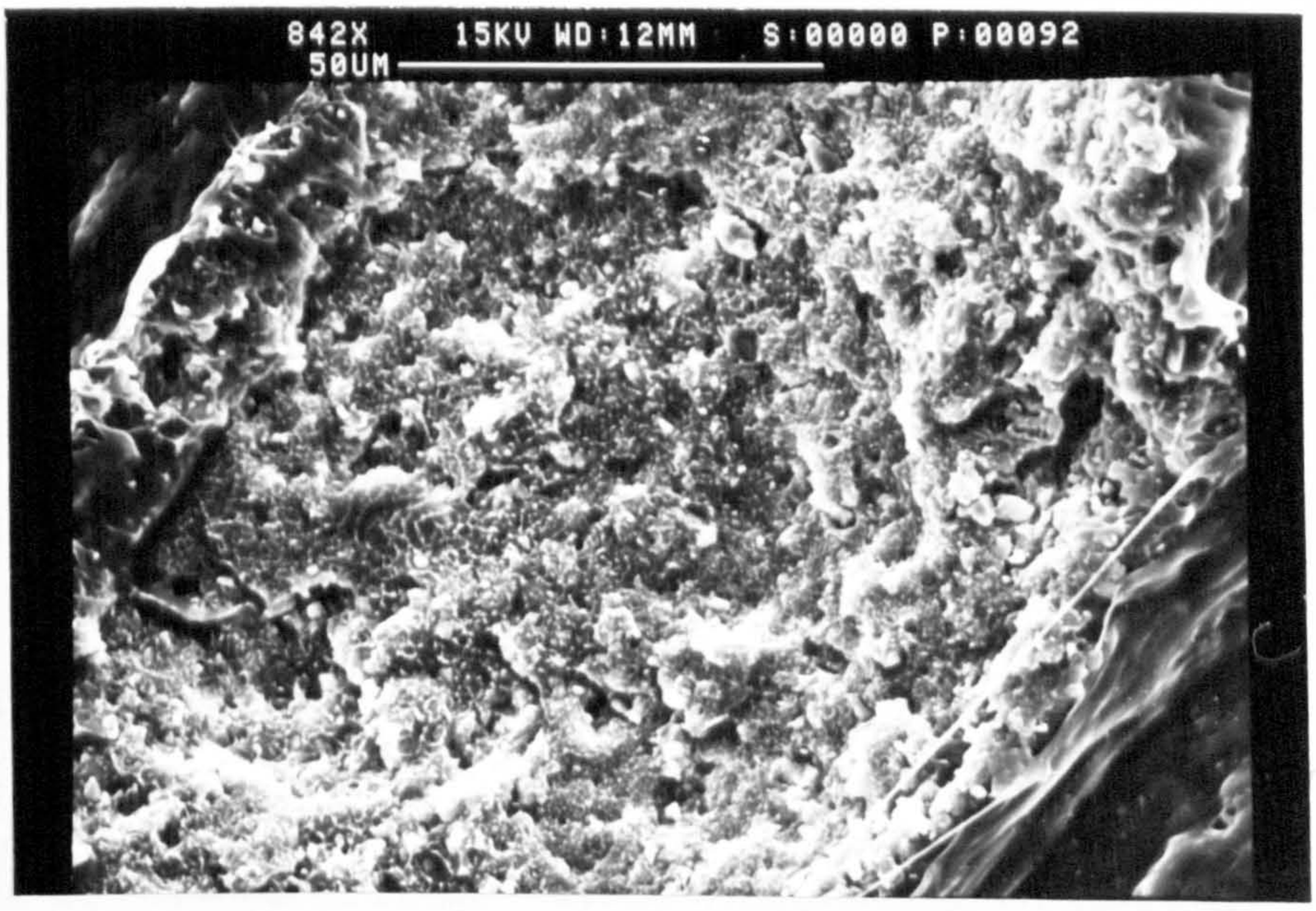

Fig 82. Magnified view of cavities in Fig 80, showing numerous voids and cracks

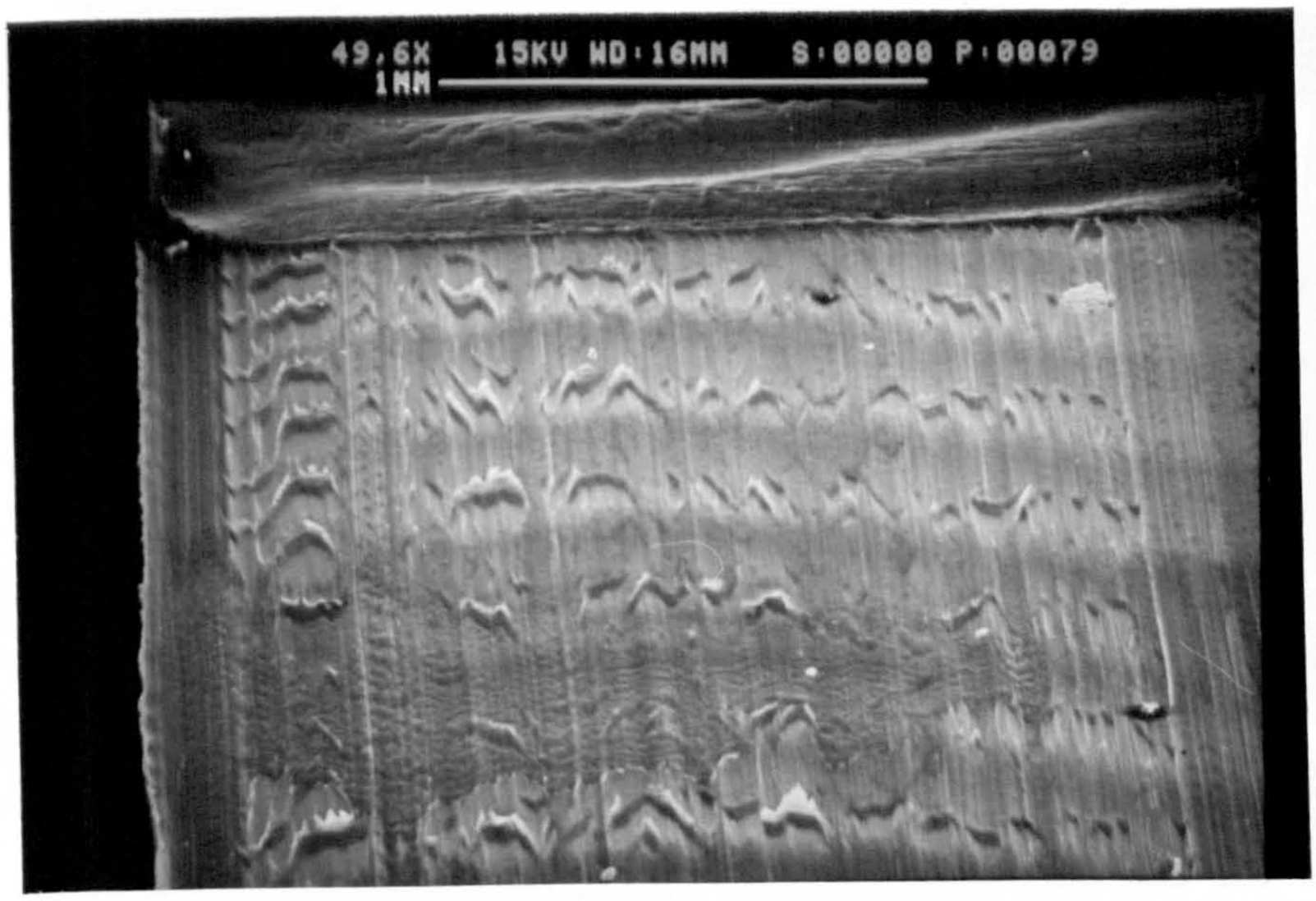

Fig 83. HDPE surface machined at -20° rake angle, showing the micro-chip formation. (Speed = 30 m/min, feed = 0.25 mm/rev)

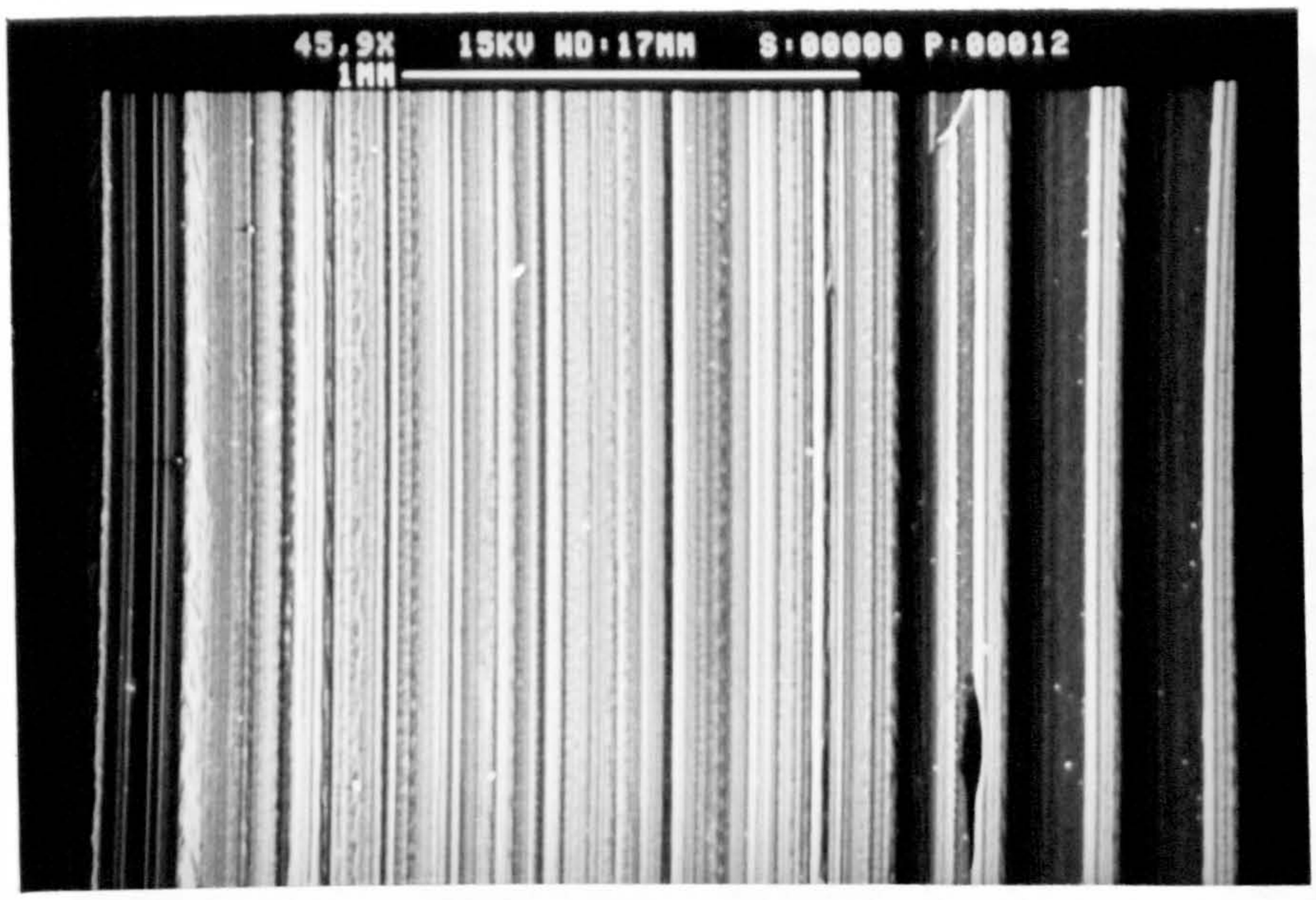

Fig 84. HDPE surface machined at 0° rake angle, showing groove formation. (Speed = 30 m/min, feed = 0.25 mm/rev)

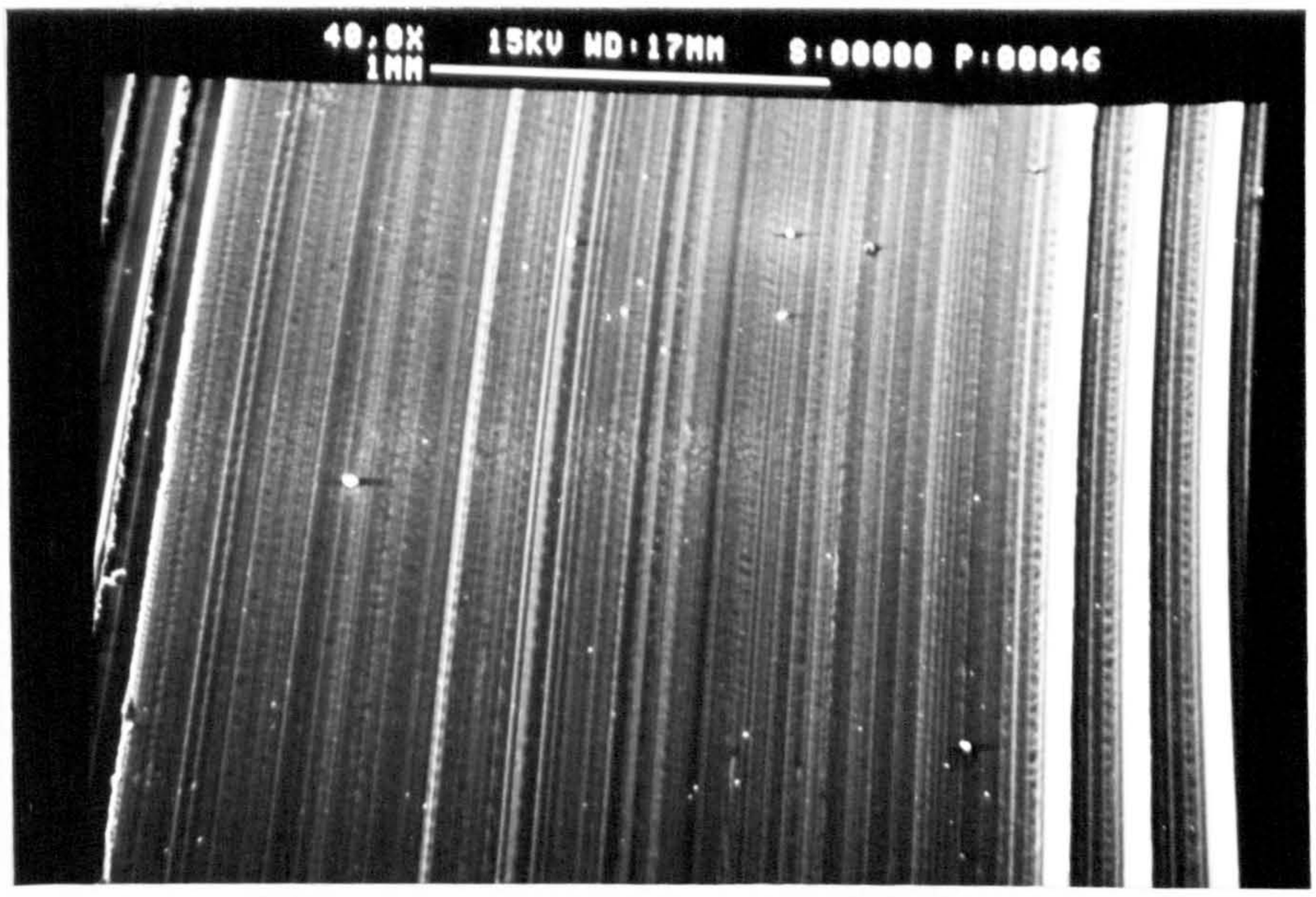

Fig 85. HDPE surface machined at 30° rake angle, showing groove formation. (Speed = 30 m/min, feed = 0.25 mm/rev)

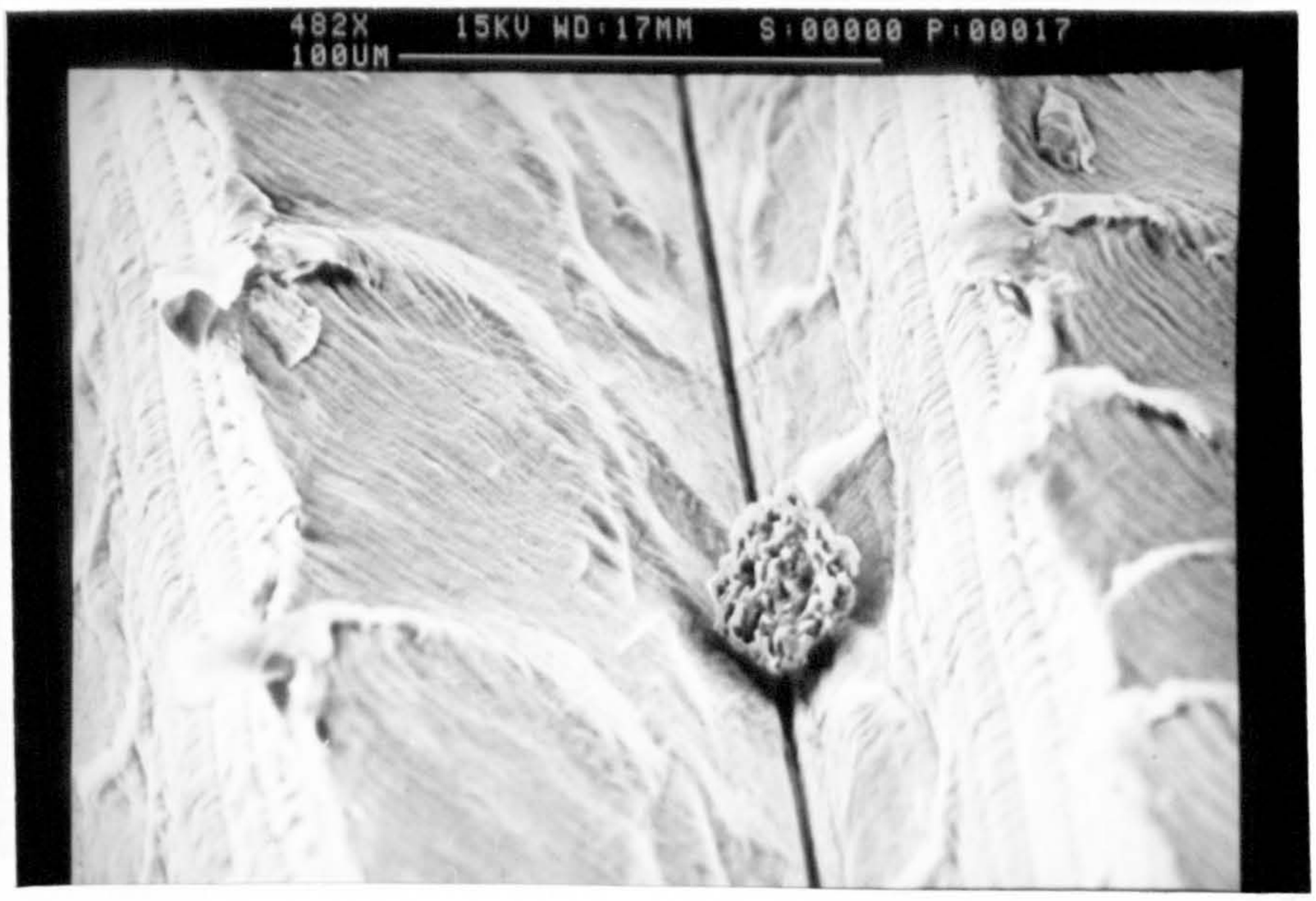

Fig 86. HDPE surface machined at low speed (25 m/min) showing intermittent ridges. (Rake angle = -20°, feed = 0.16 mm/rev)

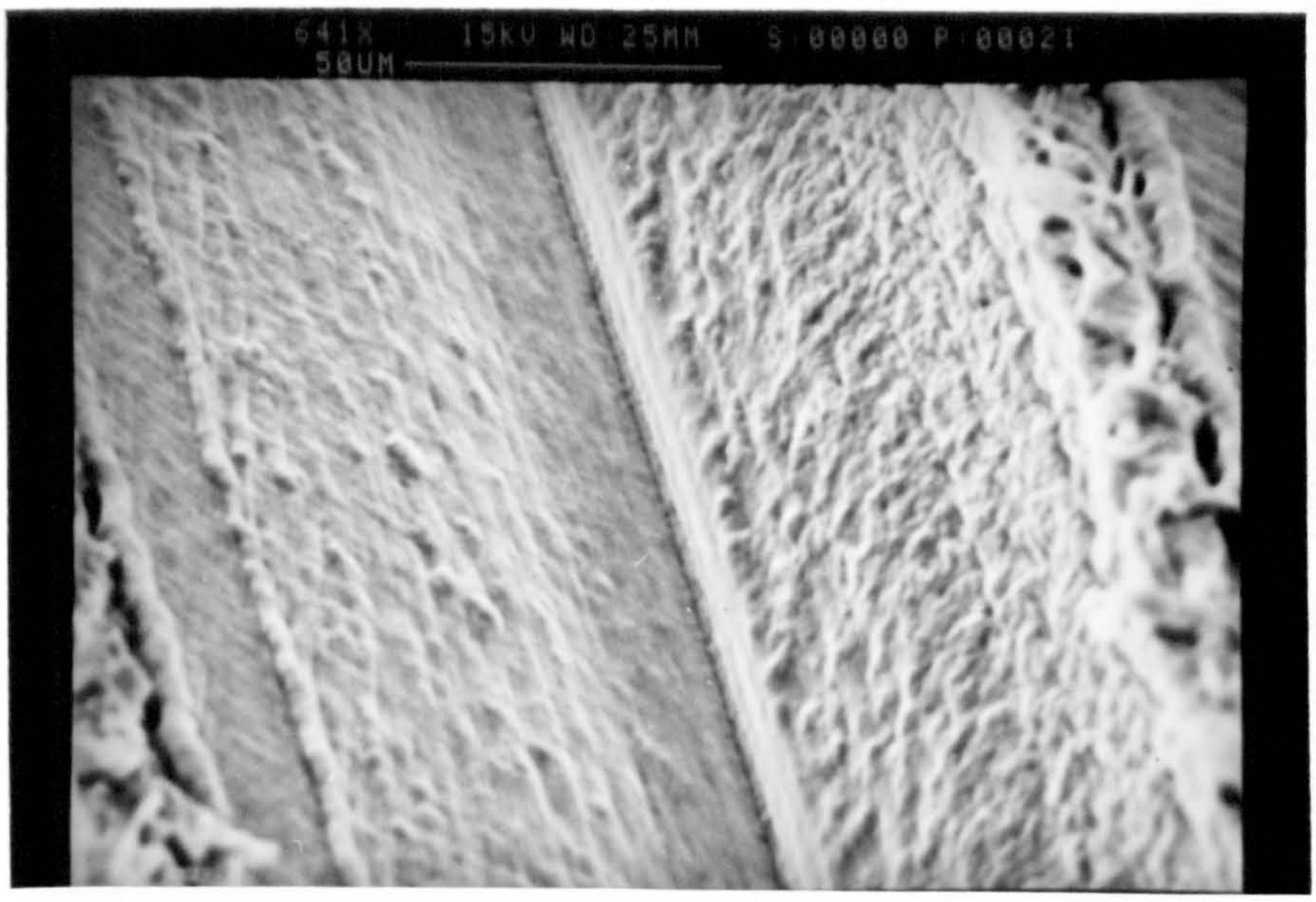

Fig 87. HDPE surface machined at high speed (250 m/min) (Rake angle = -20°, feed = 0.16 mm/rev)

Fig 88. HDPE surface machined at -20° rake angle, showing intermittent ridges. (Speed = 25m/min, feed = 0.16 mm/rev)

Fig 89. HDPE surface machined at 0º rake angle, showing good surface finish. (Speed = 25 m/min, feed = 0.16 mm/rev)

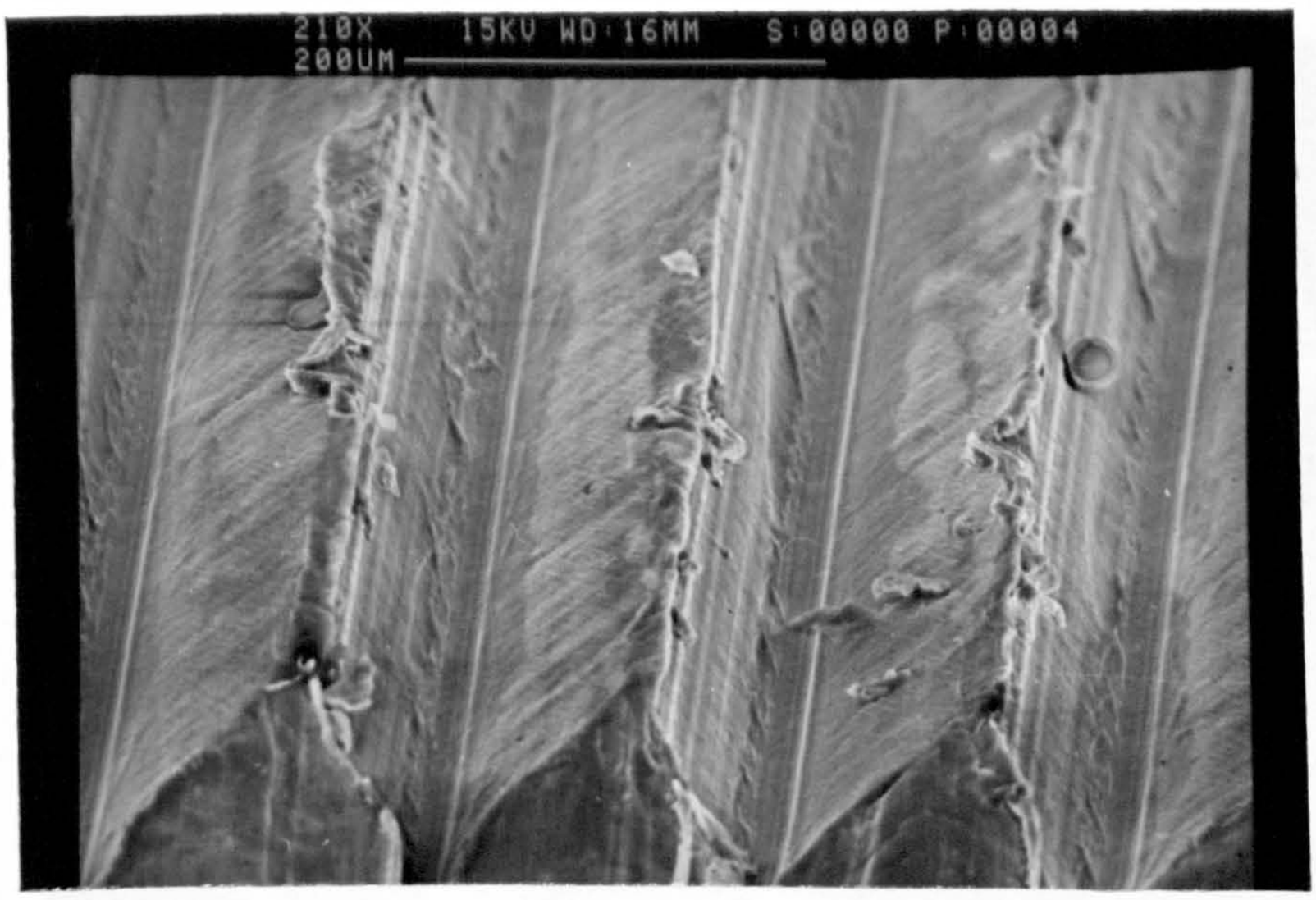

Fig 90. HDPE surface machined at 30º rake angle, showing grooves along the work movement. (Speed = 25 m/min, feed = 0.16 mm/rev)

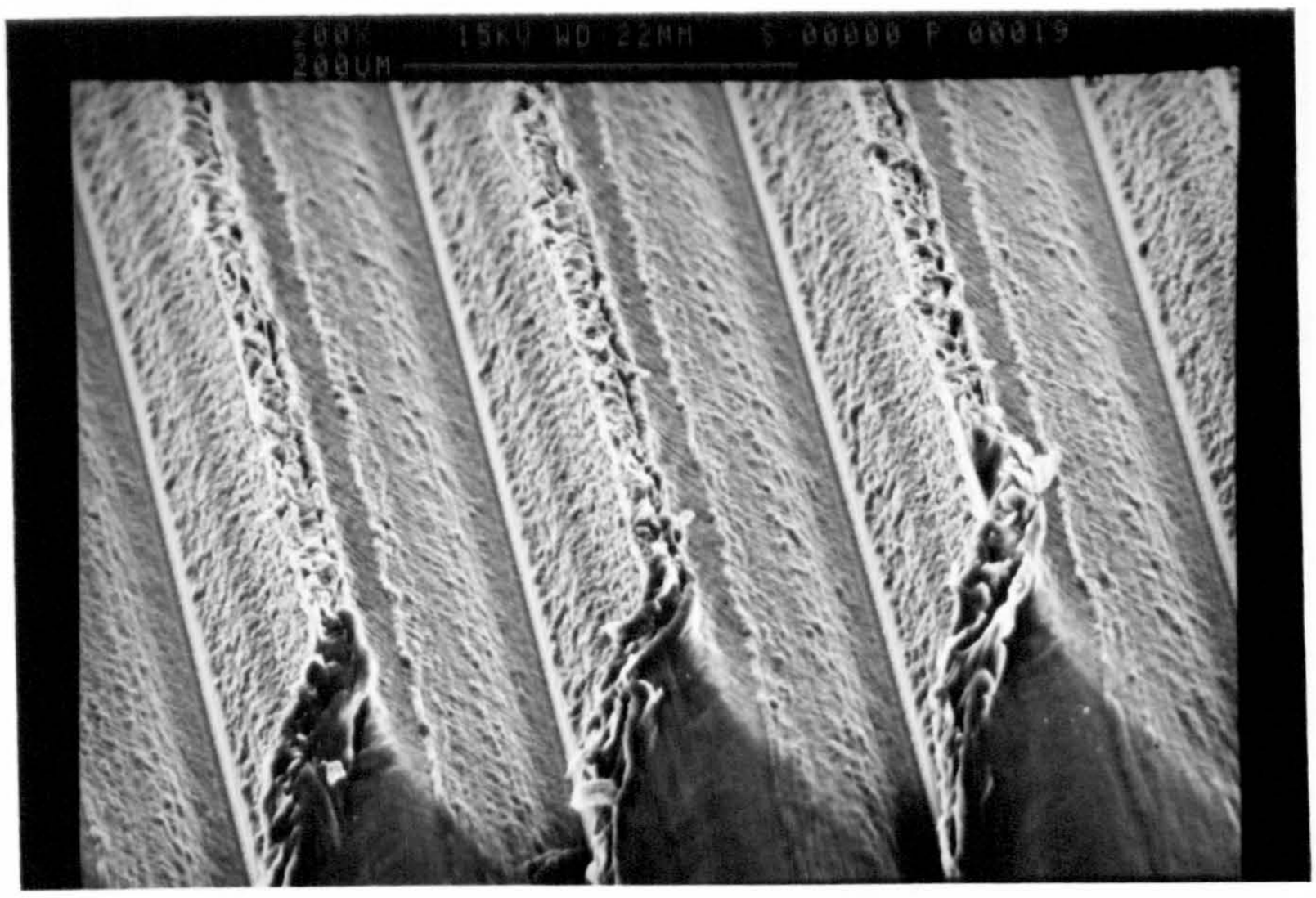

Fig 91. HDPE surface machined at -20° rake angle. (Speed = 250 m/min, feed = 0.16 mm/rev)

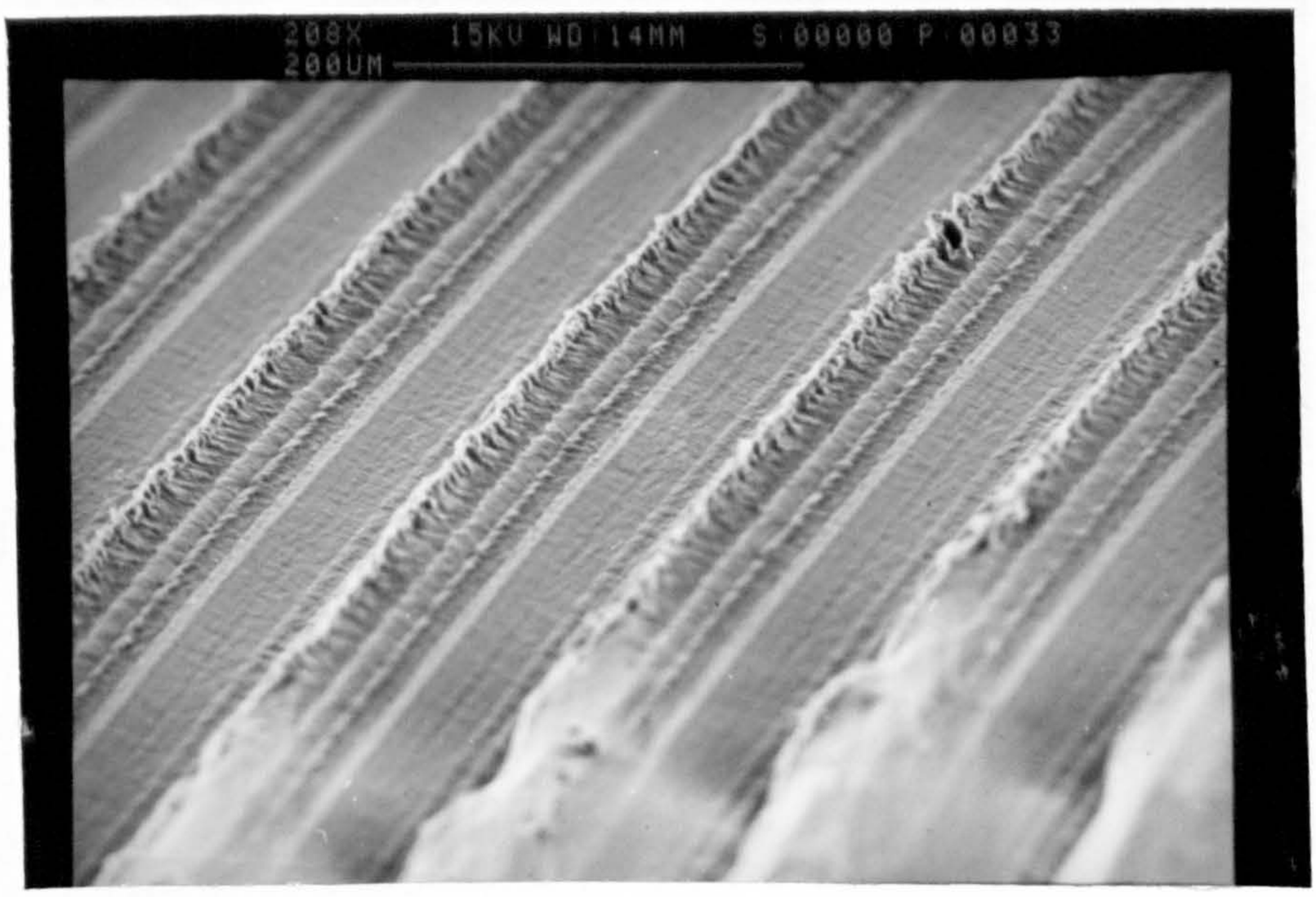

Fig 92. HDPE surface machined at 0° rake angle. (Speed = 250 m/min, feed = 0.16 mm/rev)

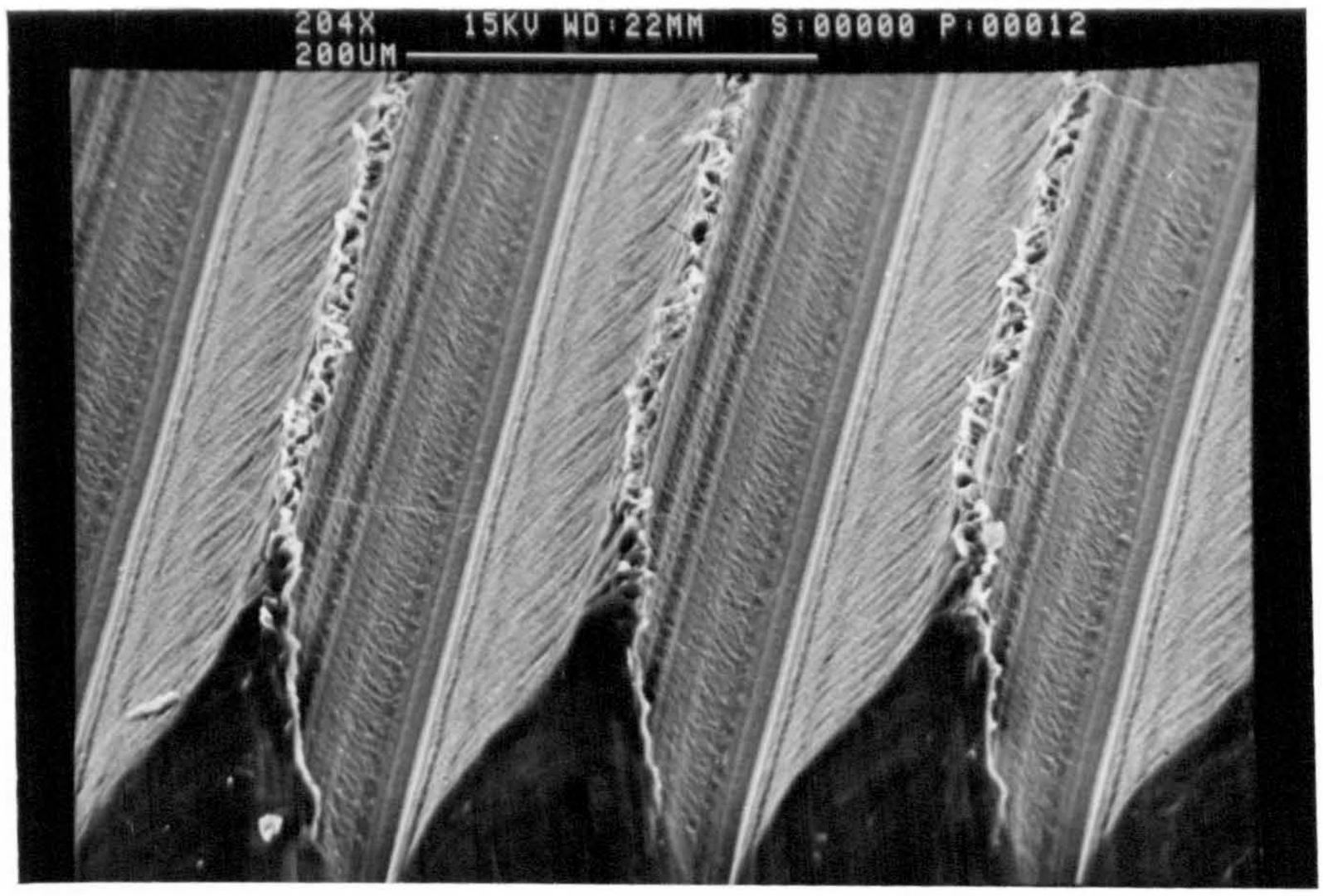

Fig 93. HDPE surface machined at 30° rake angle. (Speed = 250 m/min, feed = 0.16 mm/rev)

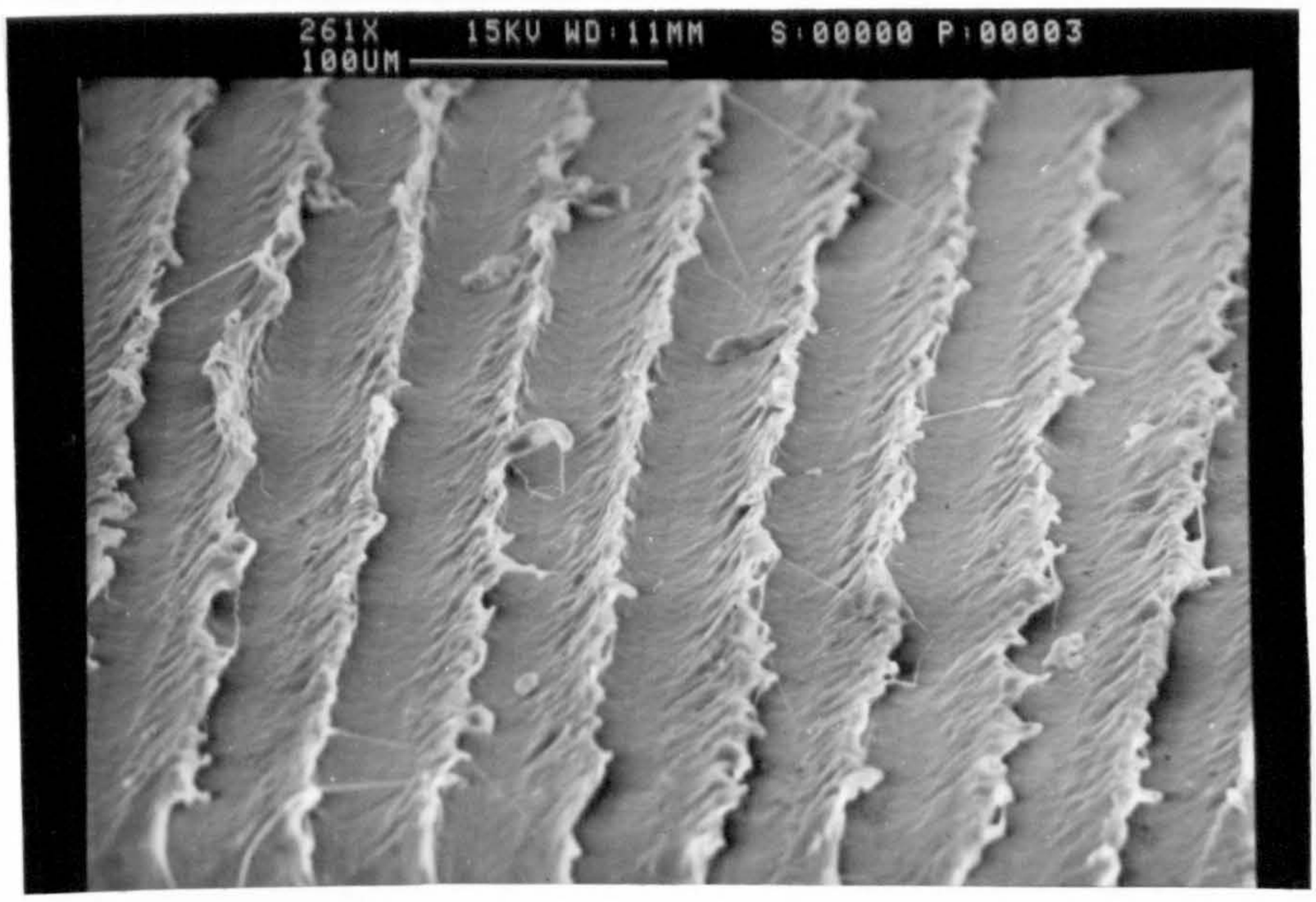

Fig 94. HDPE surface machined at low feed rate (0.05 mm/rev), showing ductile nature. (Rake angle = 10°, speed = 250 m/min)

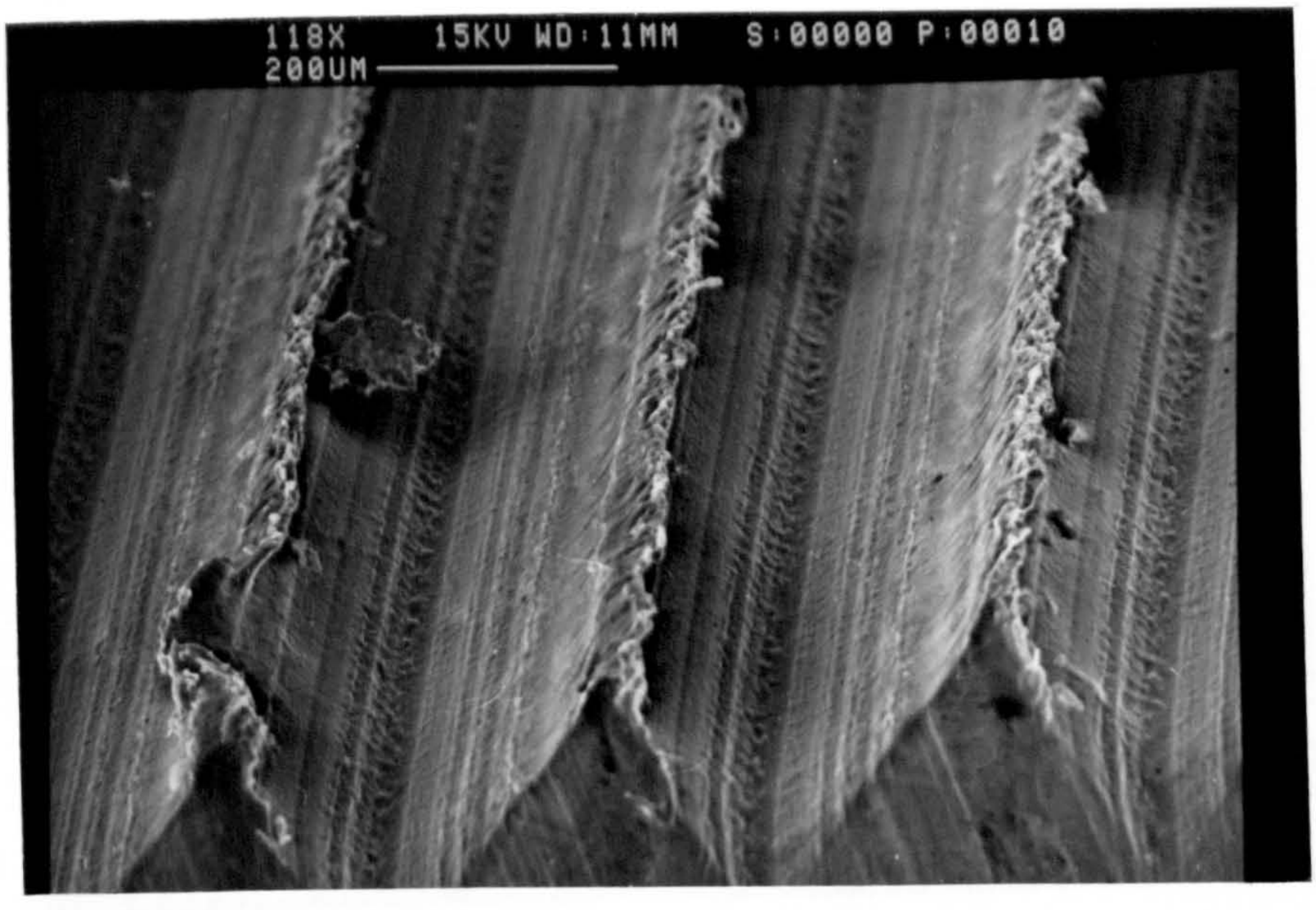

Fig 95. HDPE surface machined at high feed rate (0.315 mm/rev) showing side flow. (Rake angle = 10°, speed = 250 m/min)

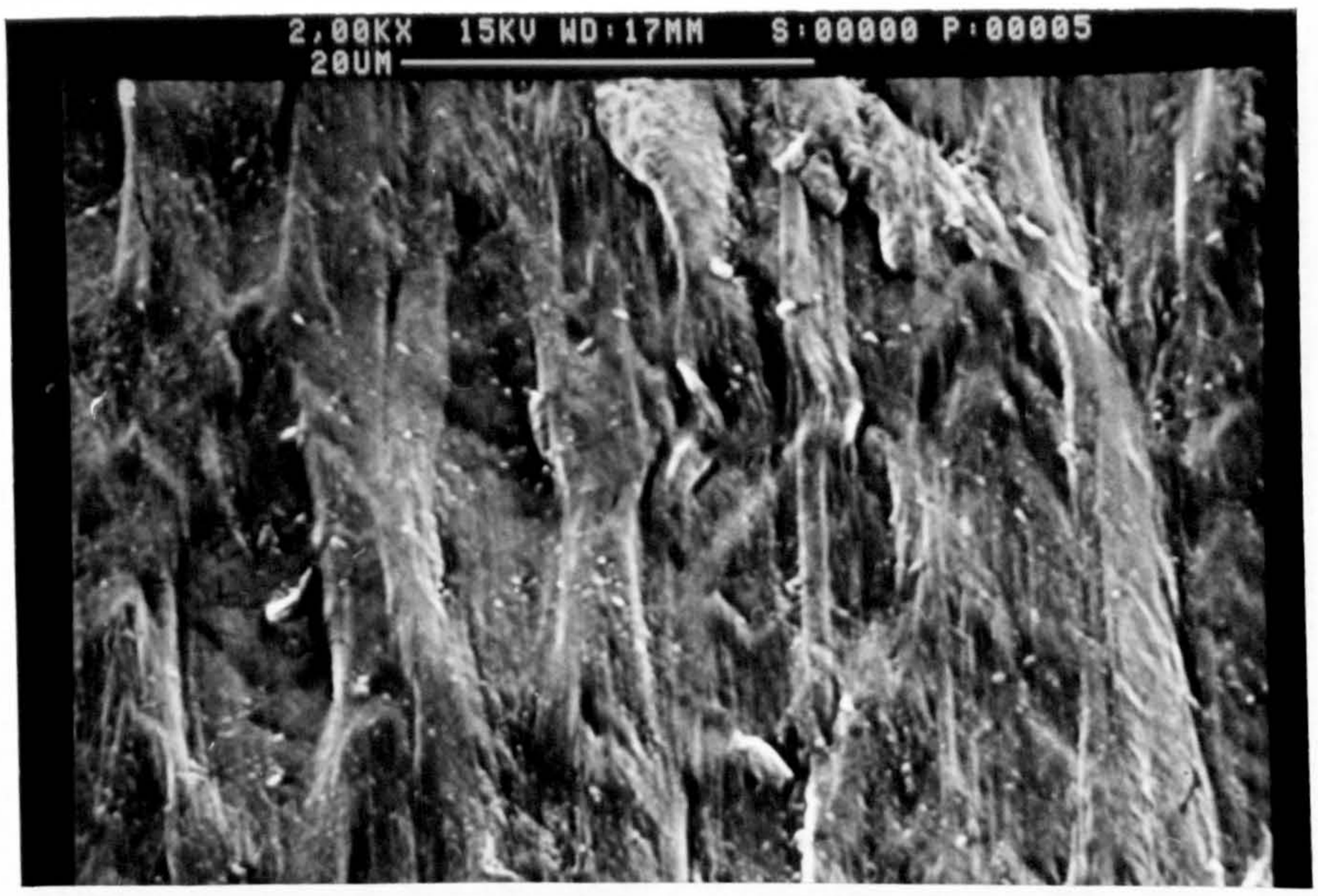

Fig 96. Magnified view of HDPE surface showing elongated cavities (Rake angle = -10°, speed = 30 m/min, feed = 0.14 mm/rev)

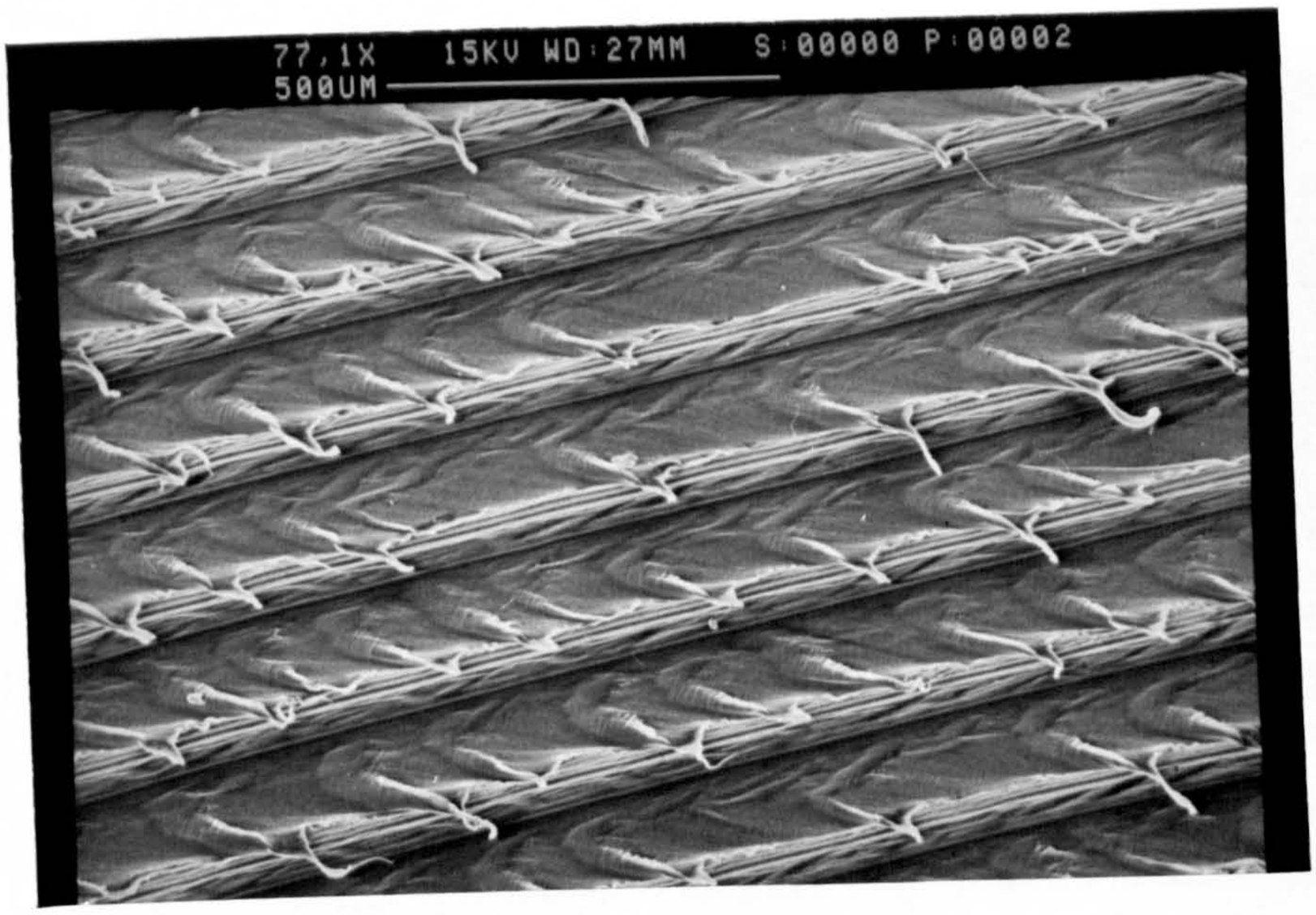

Fig 97. Machined HDPE surface showing the flow of viscous work material. (Rake angle = -20°, speed = 25 m/min, feed = 0.16 mm/rev)

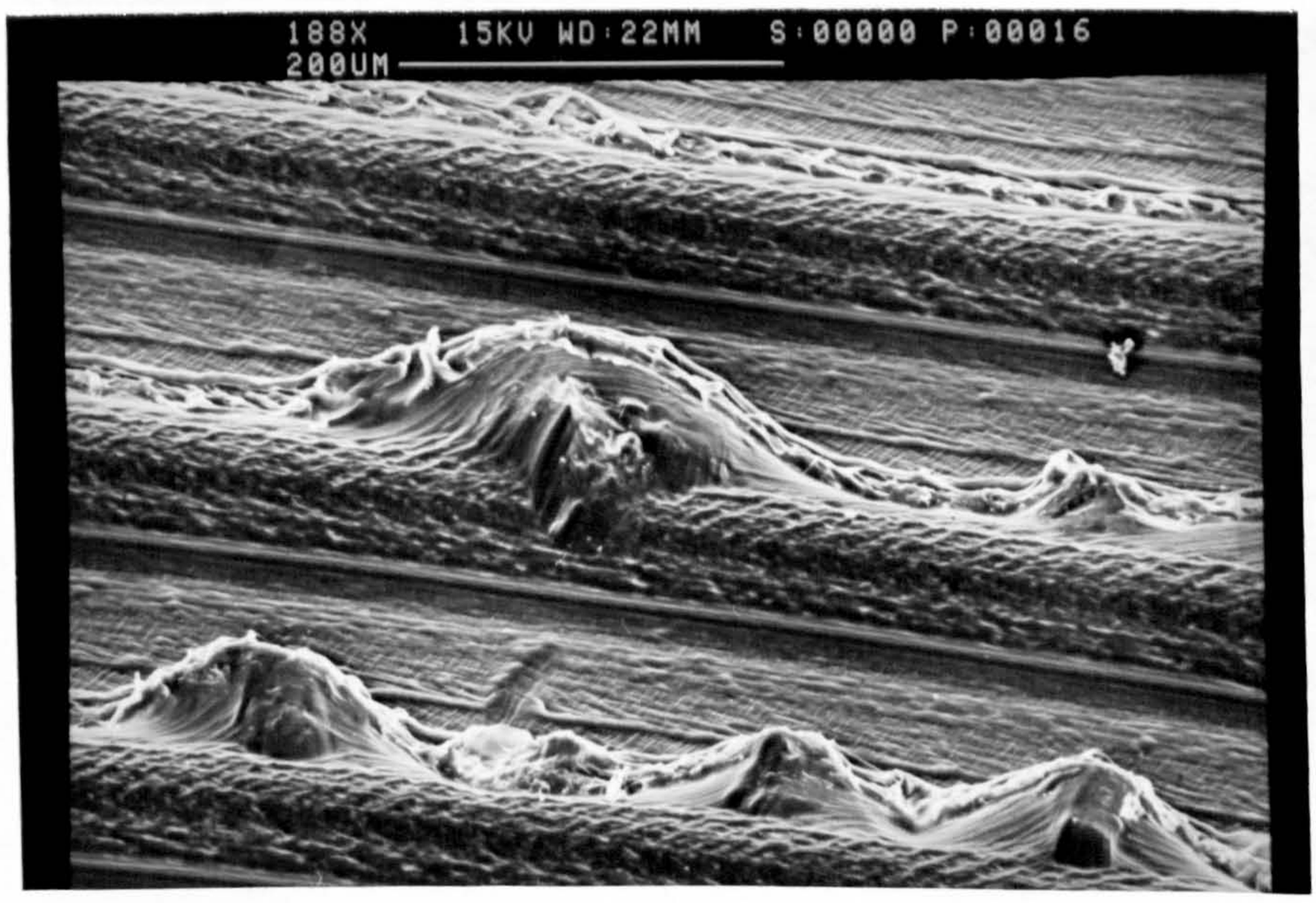

Fig 98. Machined HDPE surface showing the bulging of work material near feed marks. (Rake angle = -20°, speed = 250 m/min, feed = 0.16 mm/rev)

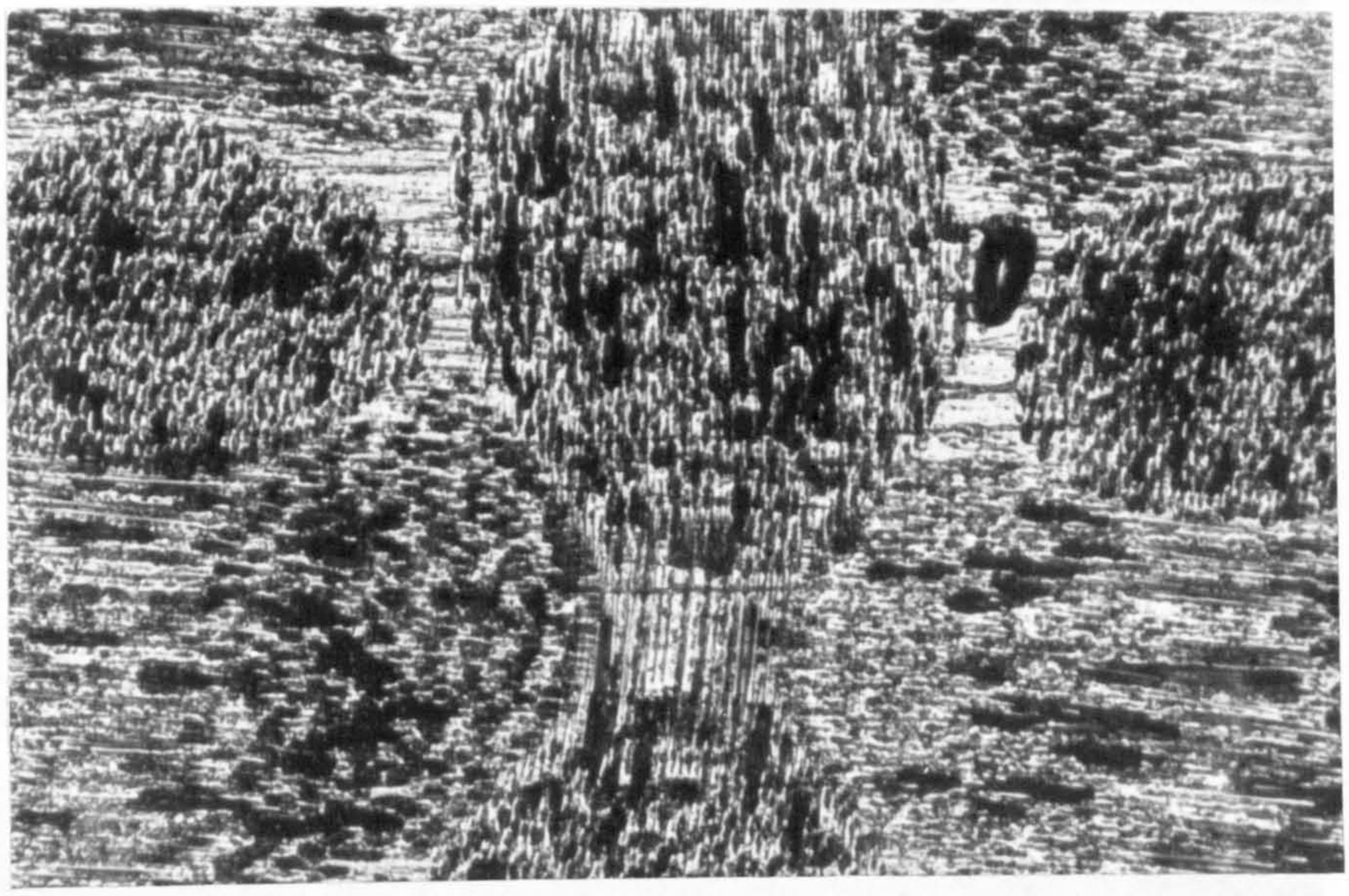

Fig 99. Microstructure of GFRP work surface, showing two directional reinforcements (X83)

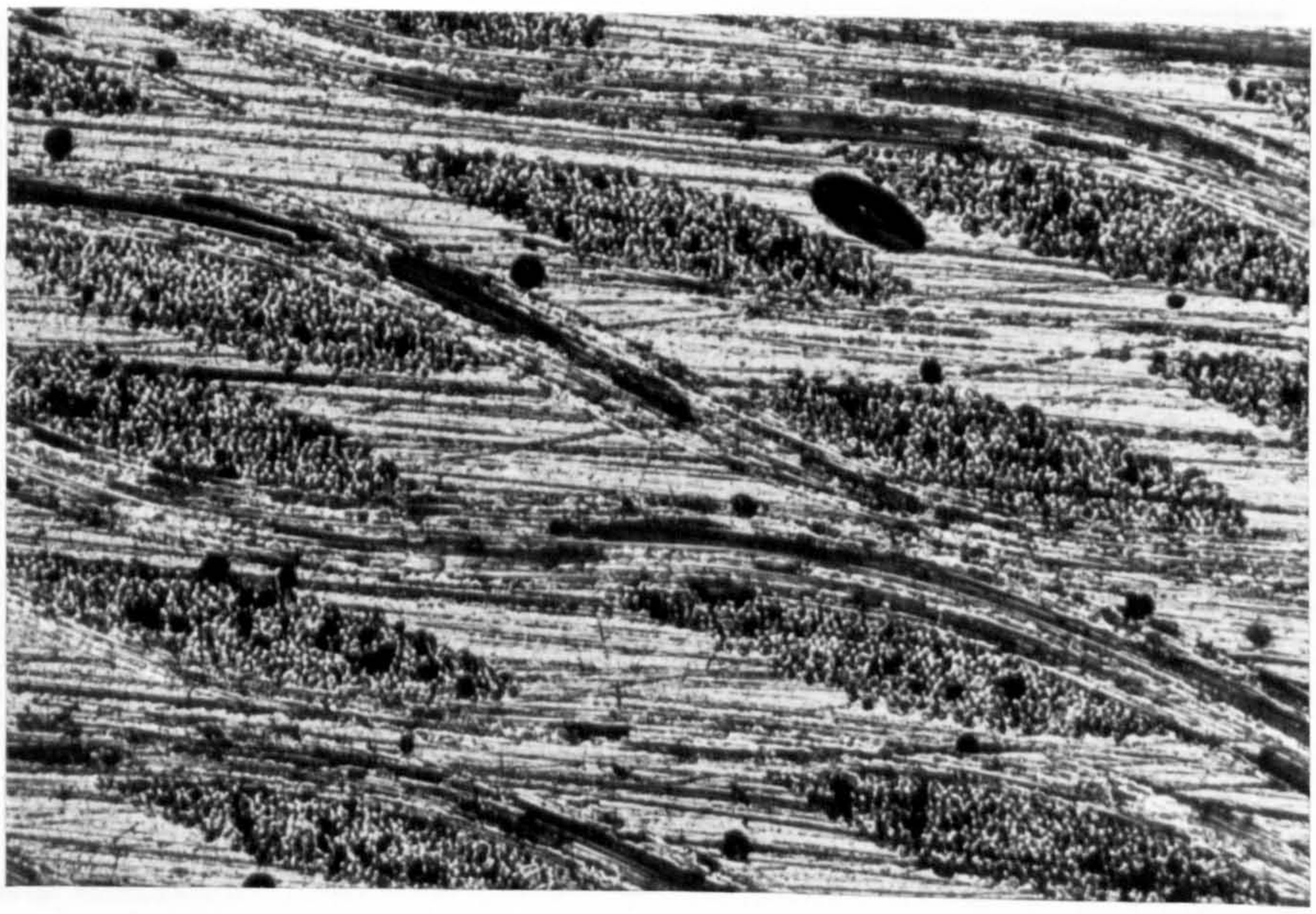

Fig 100. Microstucture of GFRP surface cross section (X83)

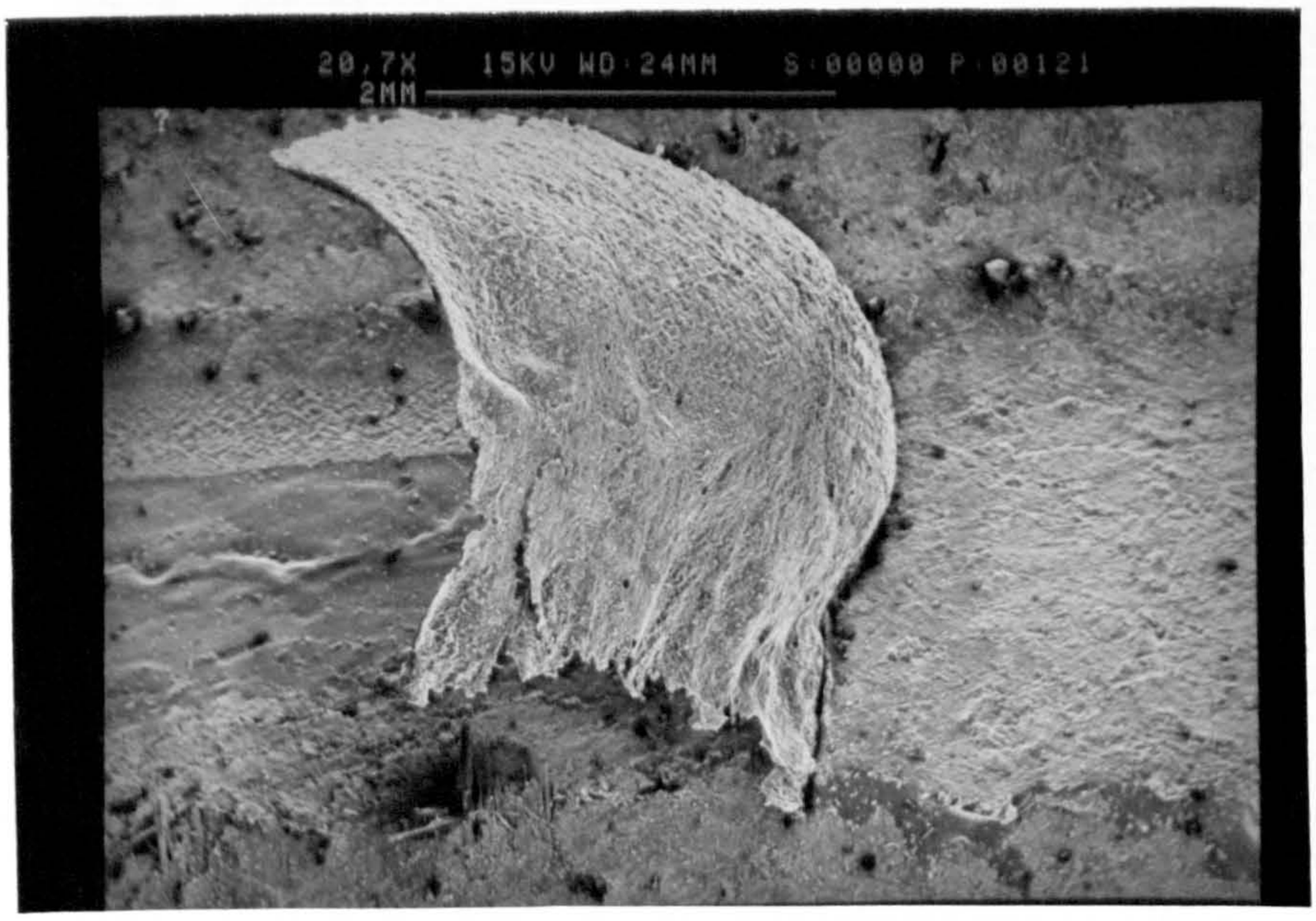

Fig 101. Macrochip root of GFRP after quick-stop test

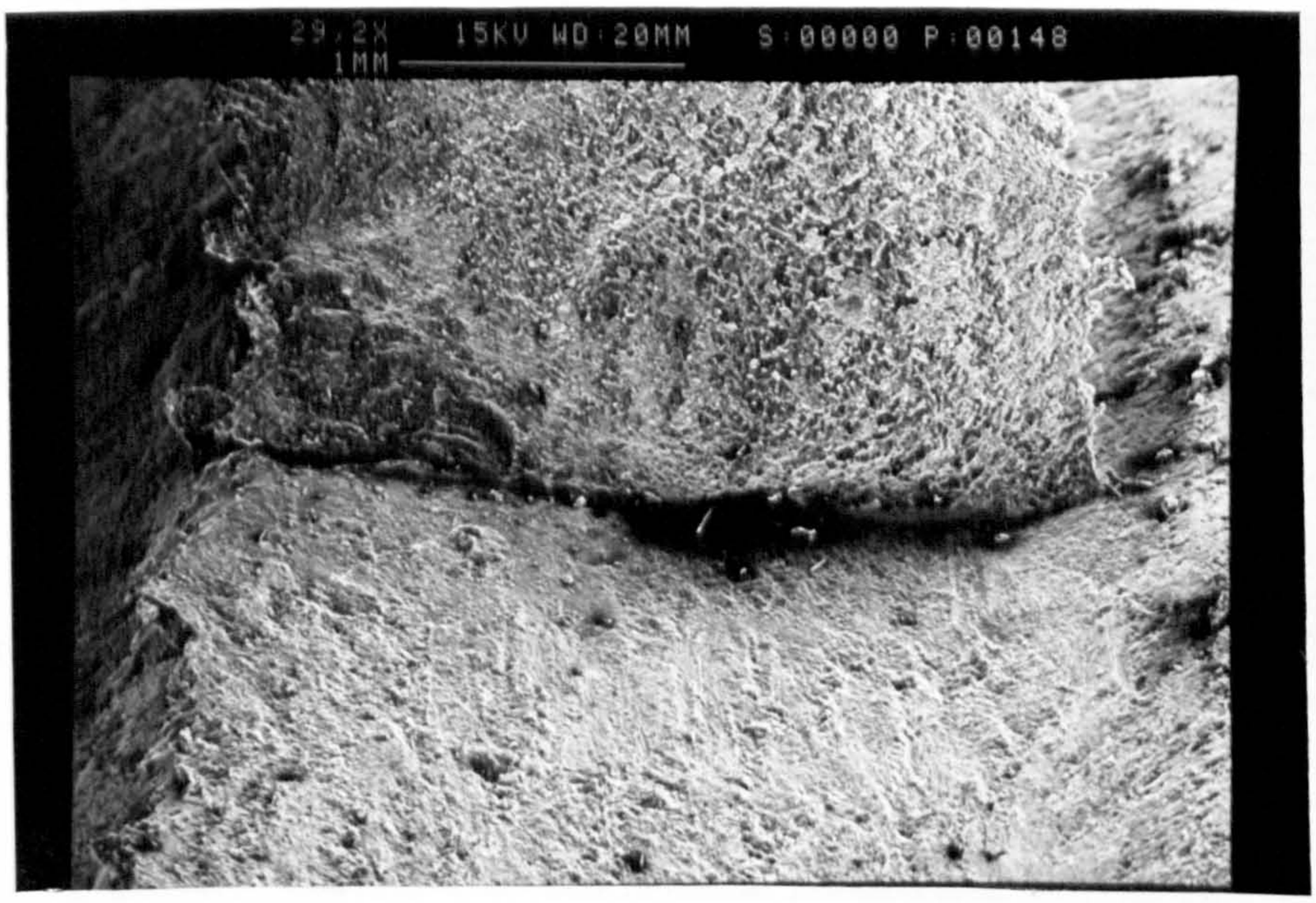

Fig 102. The undersurface of a GFRP chip showing fractured areas.

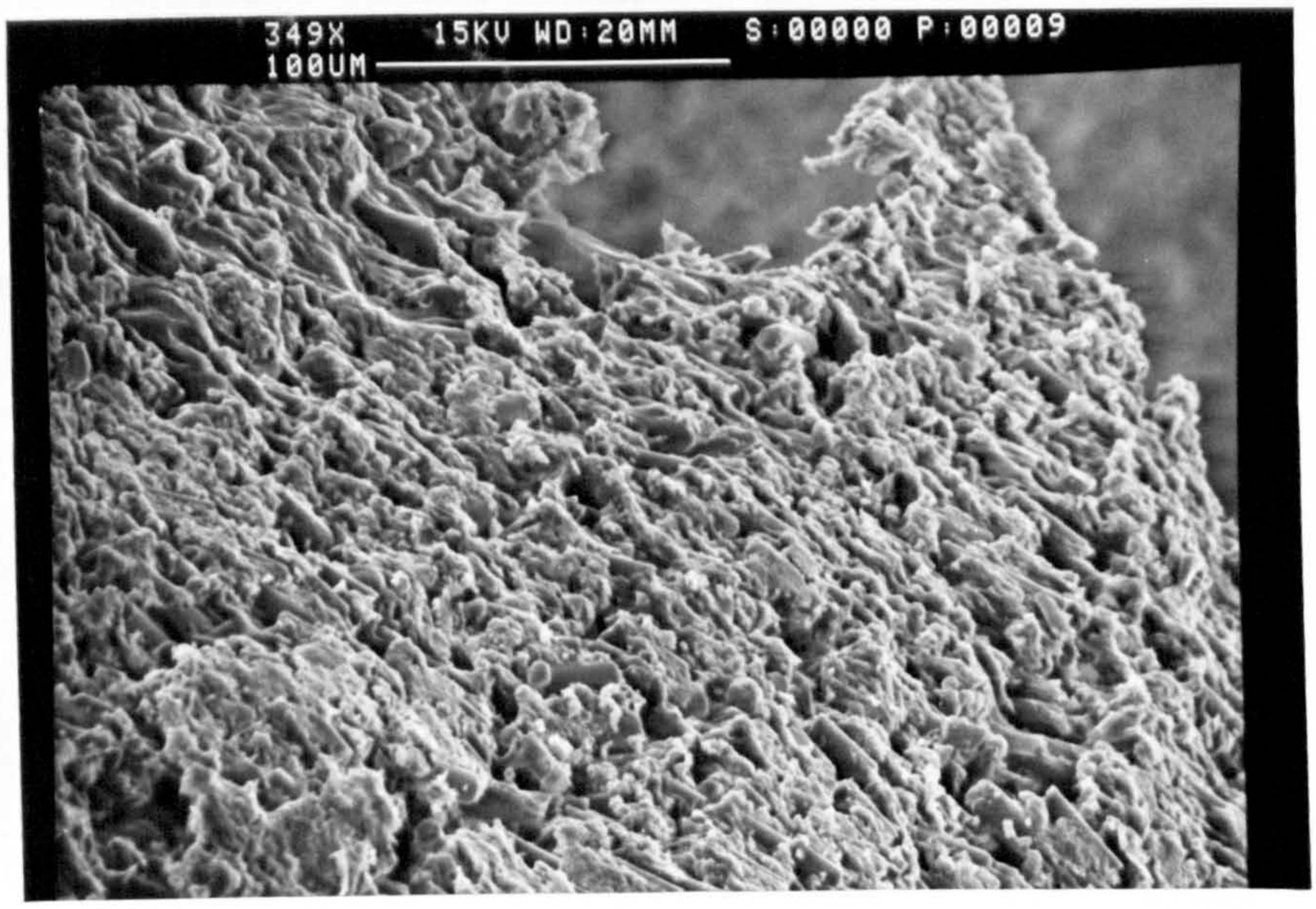

Fig 103. Magnified view of a chip undersurface showing cracked resin and fractured fibres.

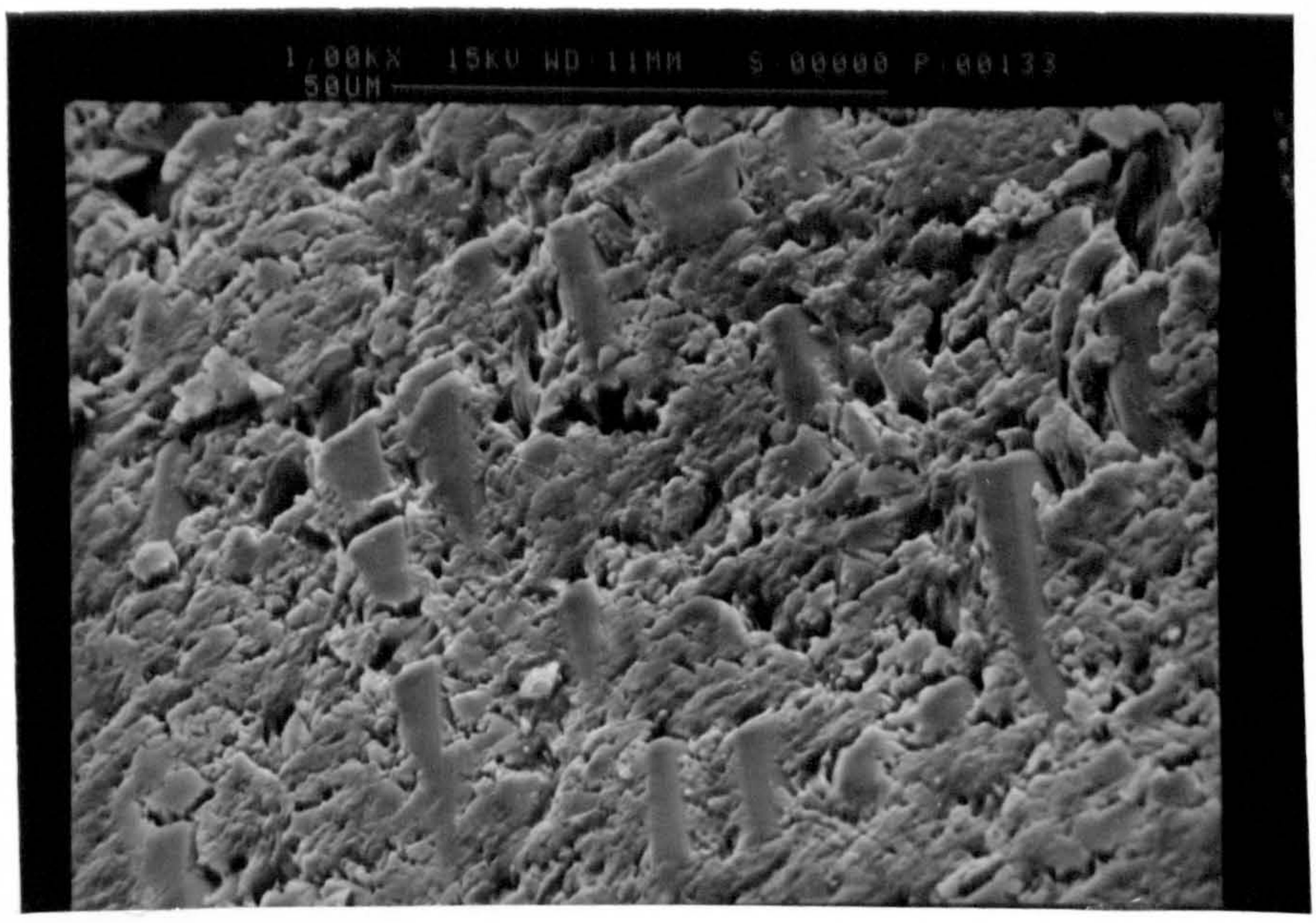

Fig 104. Machined GFRP surface showing embedded fibres and resin cracking

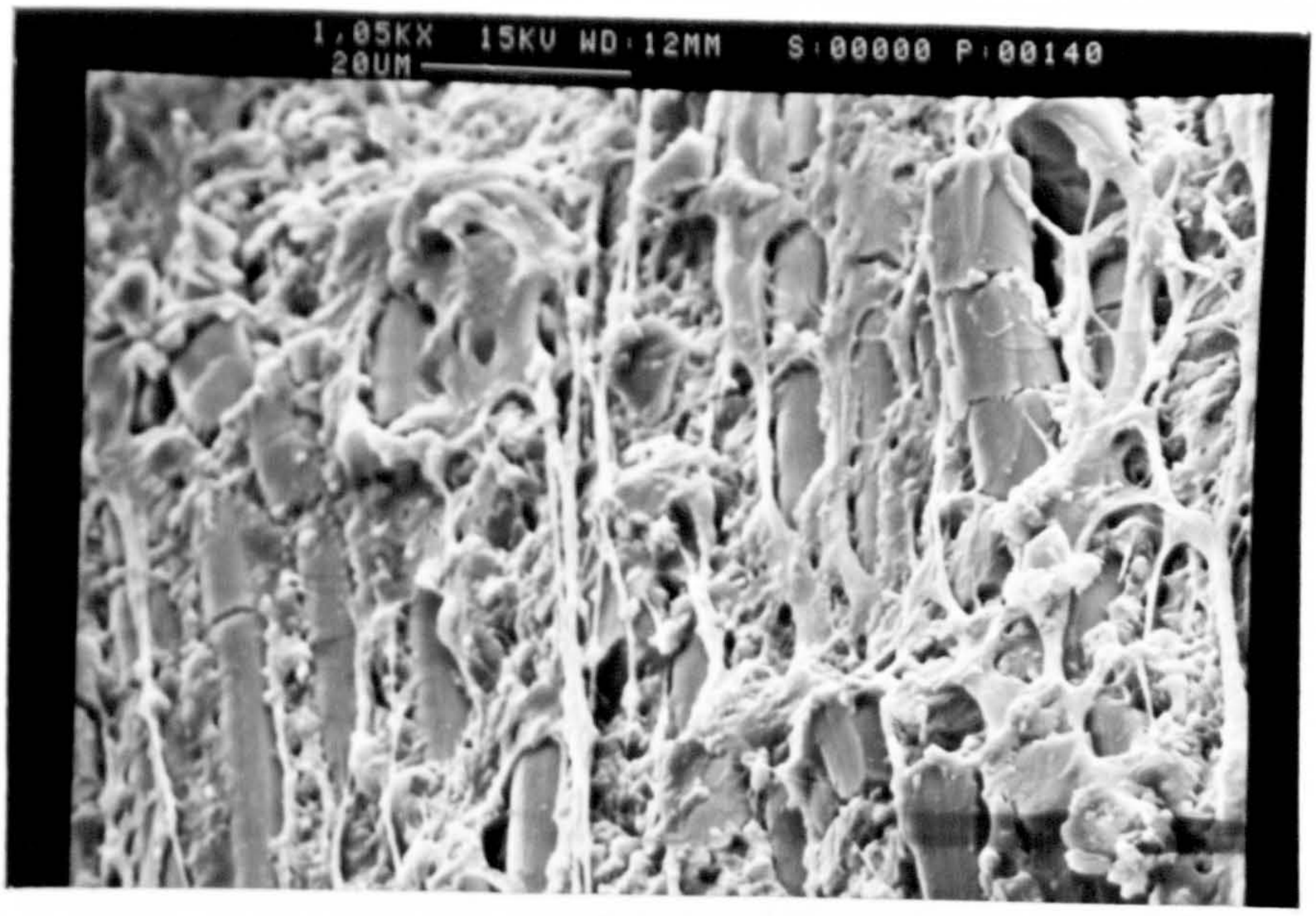

Fig 105. Machined GFRP surface showing debonding and fibre breakage

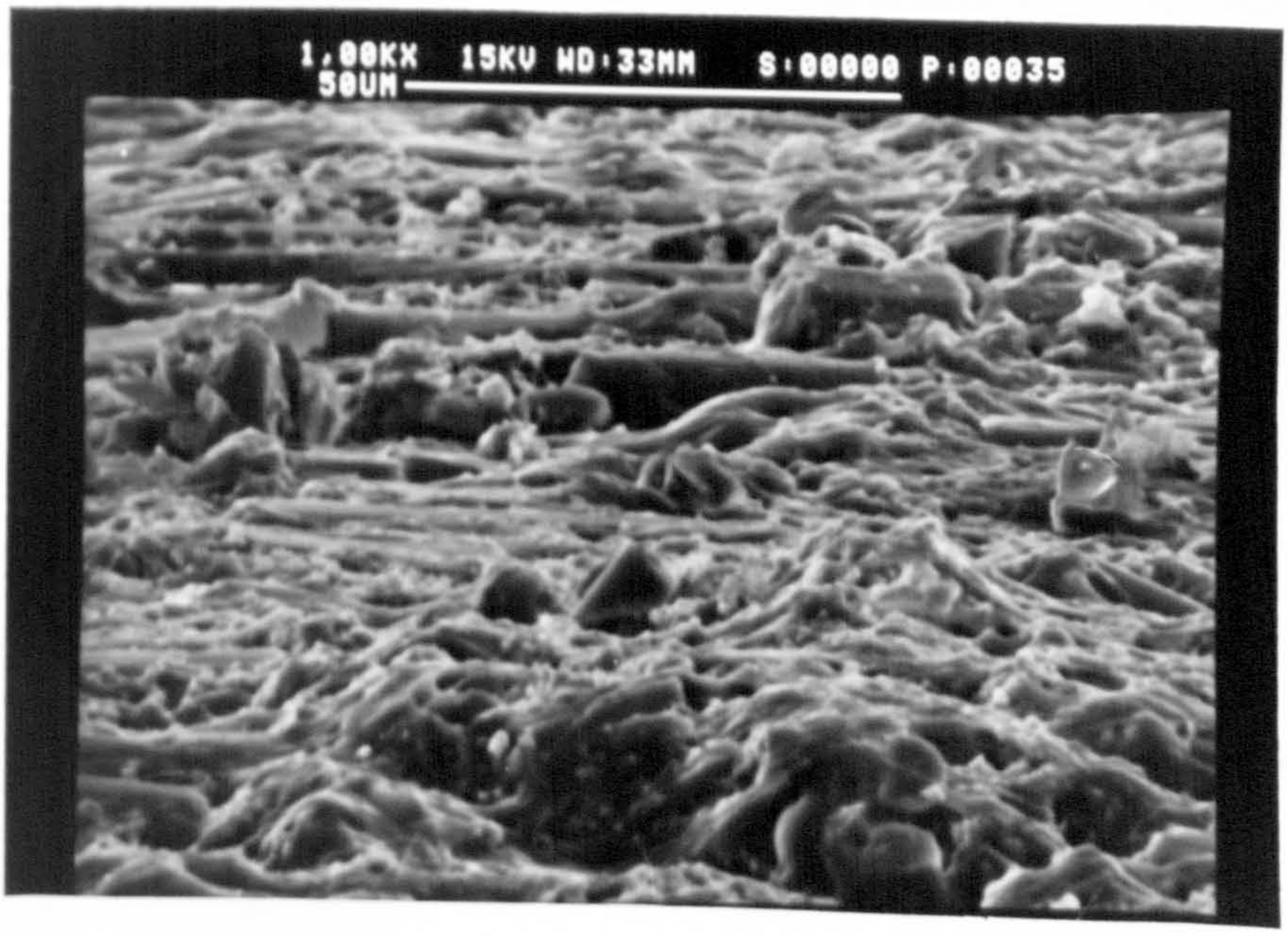

Fig 106. Machined GFRP surface showing the different nature of fibre fracture with fibre orientation

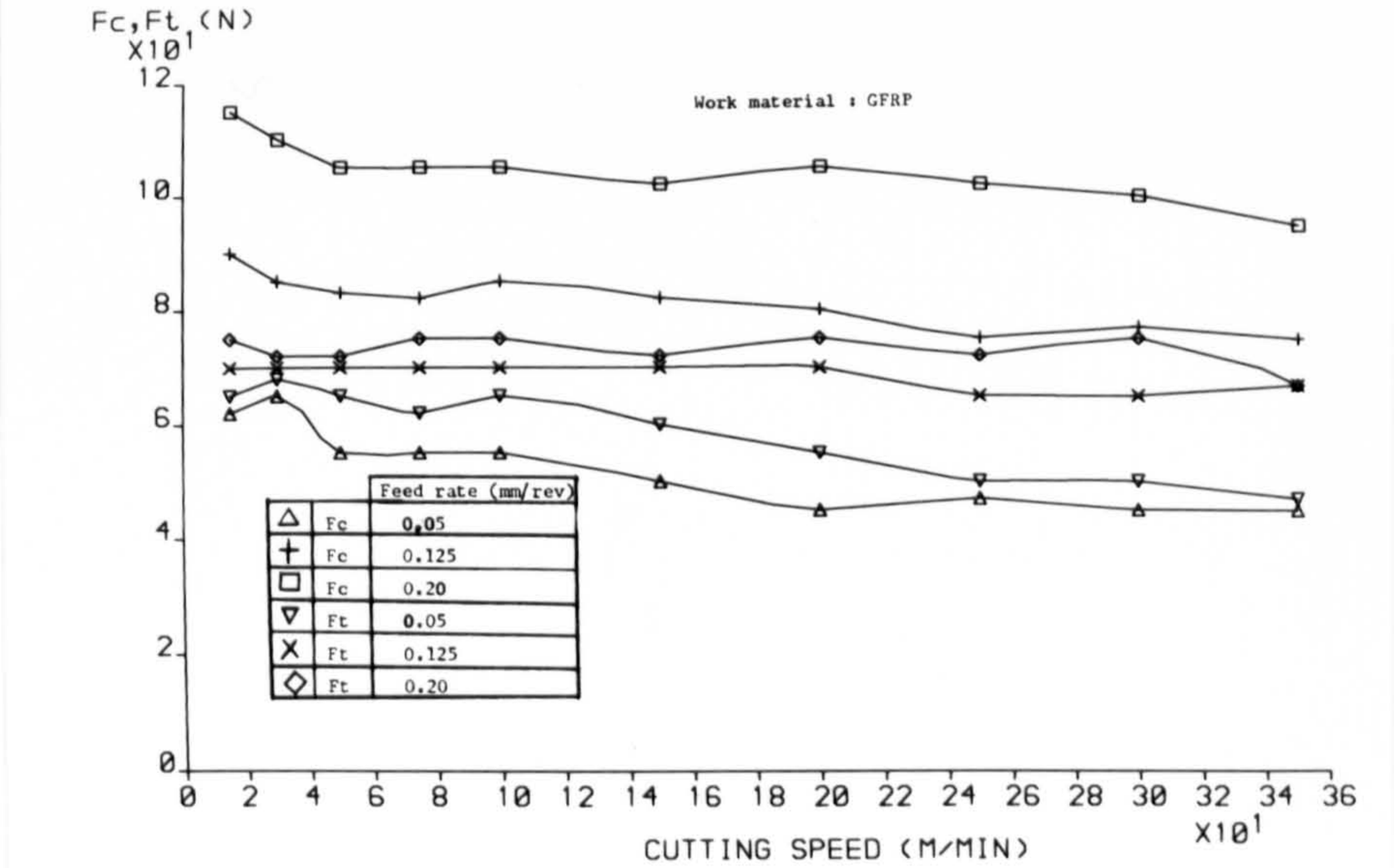

Fig 107. Cutting forces versus cutting speed when machining GFRP (Tool-TiC coated carbide, DOC = 1.5mm)

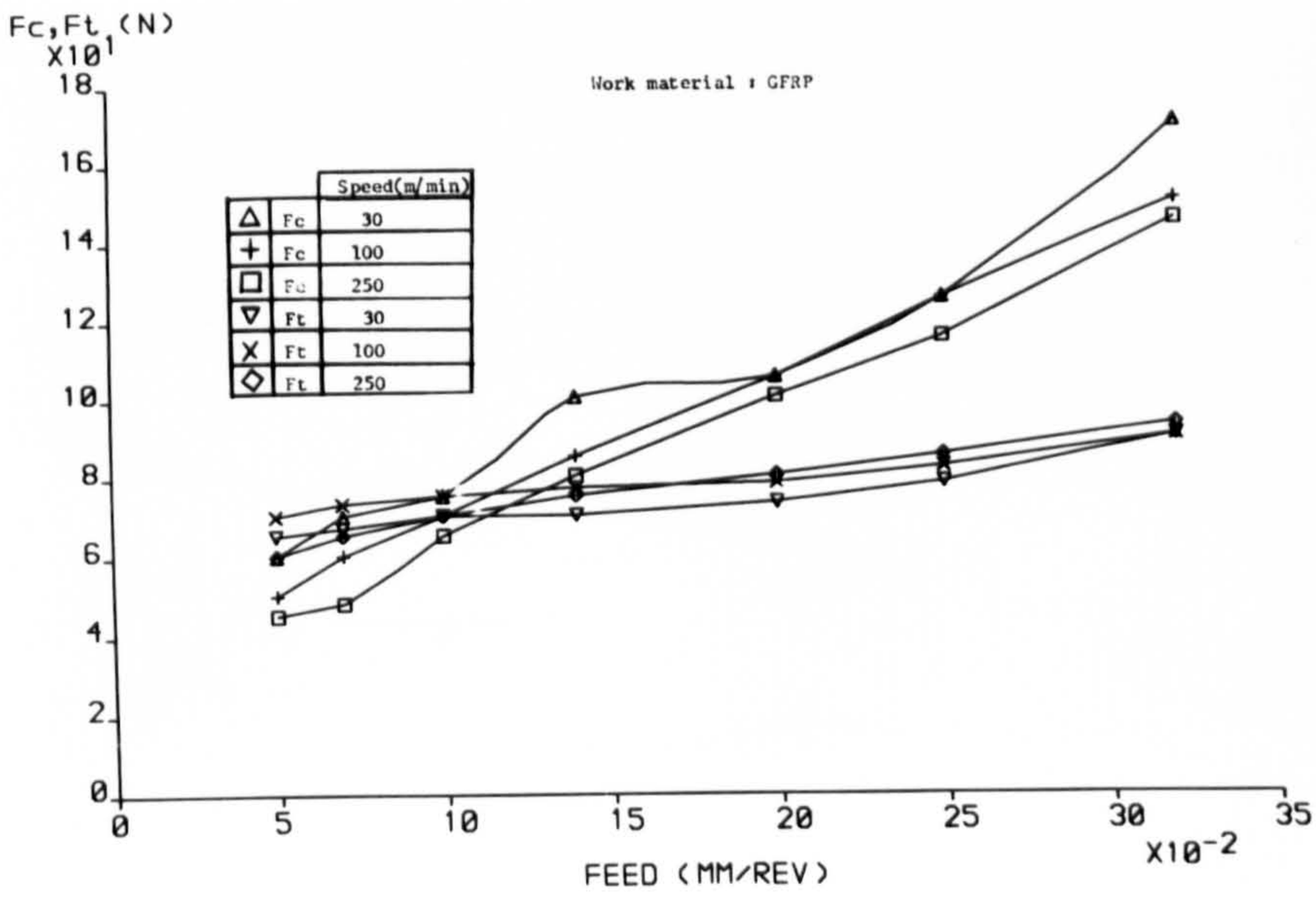

Fig 108. Cutting forces versus feed rate when machining GFRP (Tool-TiC coated carbide, DOC = 1.5mm)

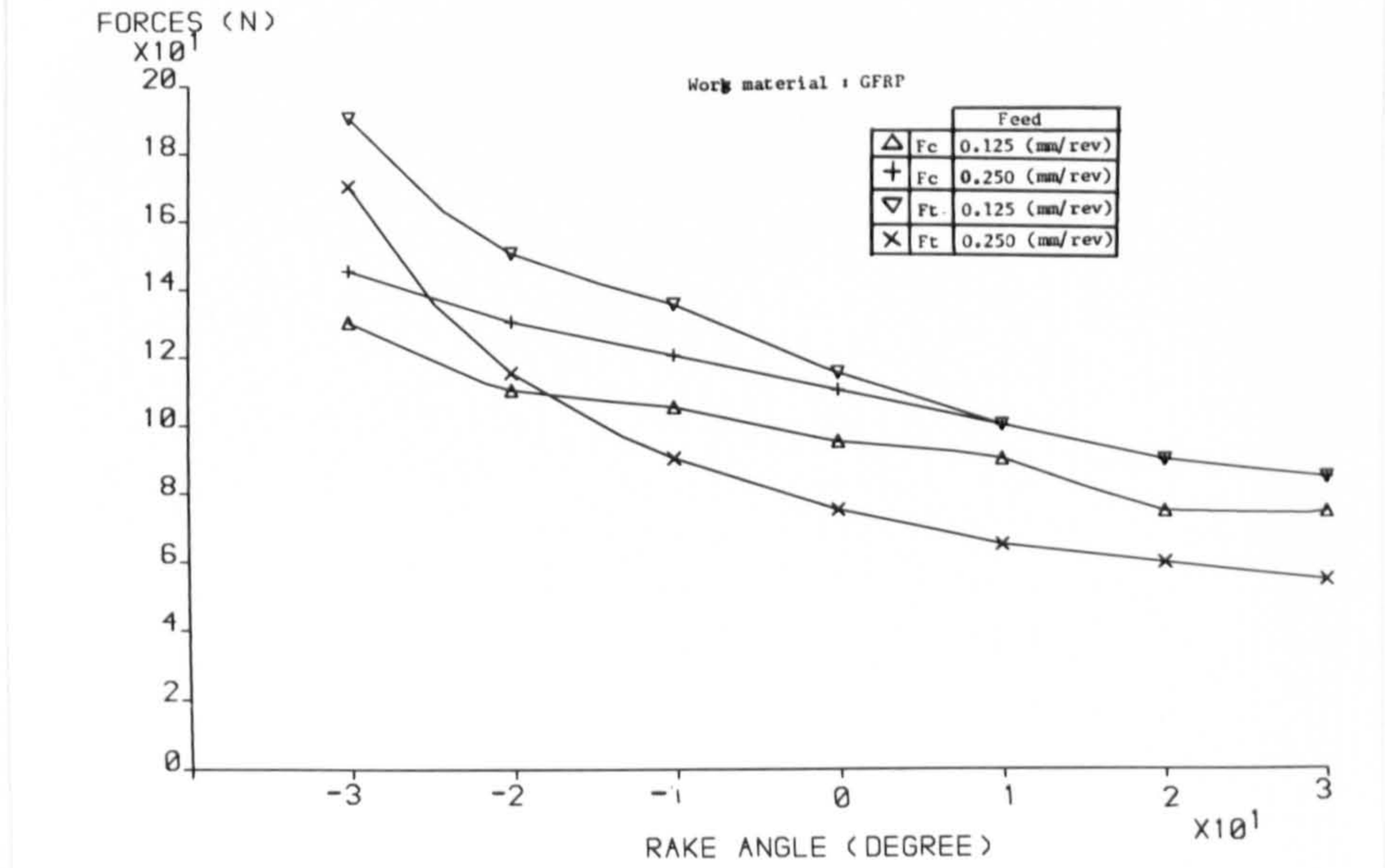

Fig 109. Cutting forces versus rake angle when machining GFRP (Tool-HSS, speed = 30 m/min, DOC = 1.5mm)

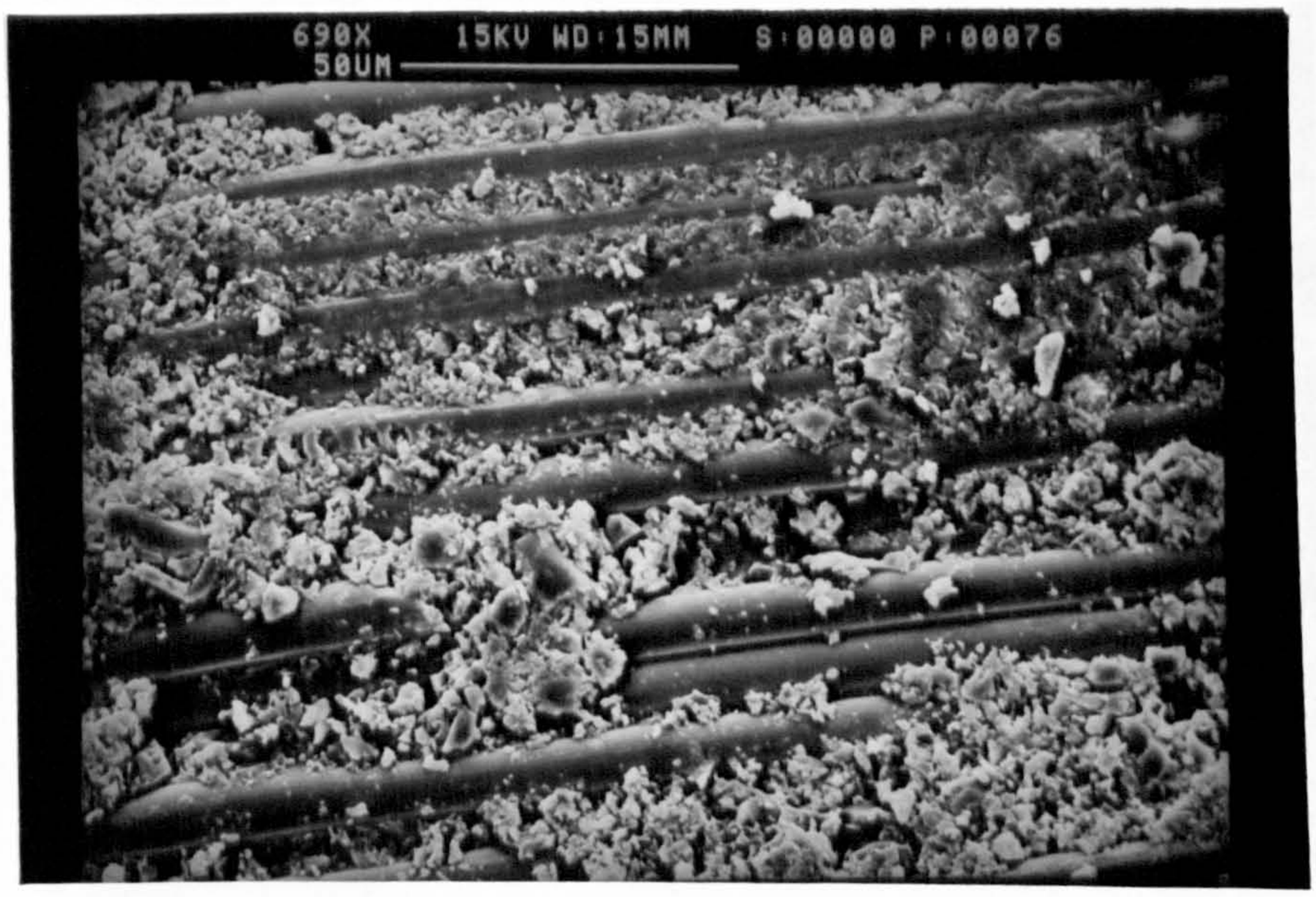

Fig 110. Machined GFRP surface produced at a low feed rate (0.05 mm/rev) showing embedded fibres and cracked resins

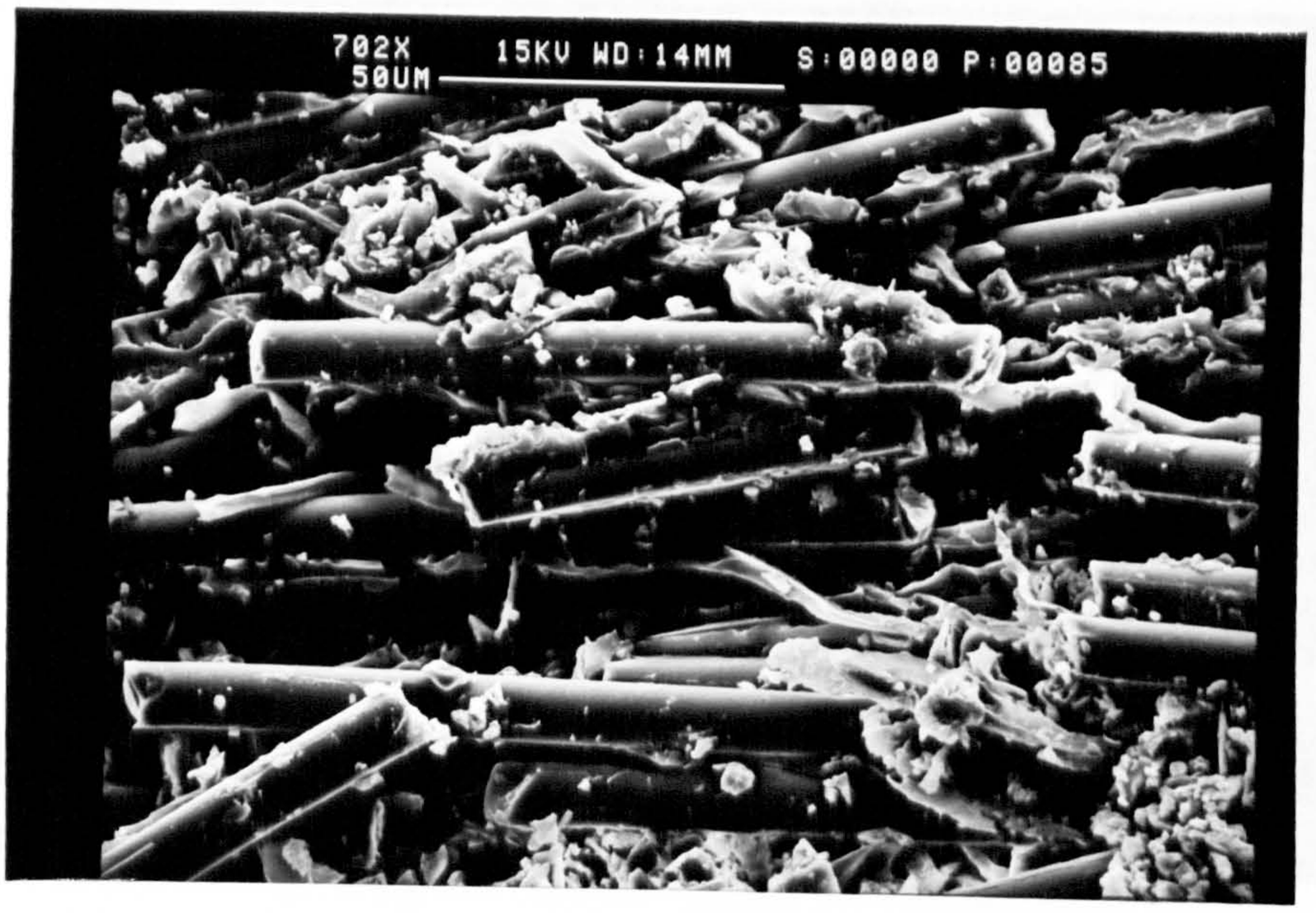

Fig 111. Machined GFRP surface produced at a high feed rate (0.20 mm/rev) showing fractured fibres and removed cracked resins

Fig 112. Machined GFRP surface showing the different nature of fibre fracture according to the fibre orientation

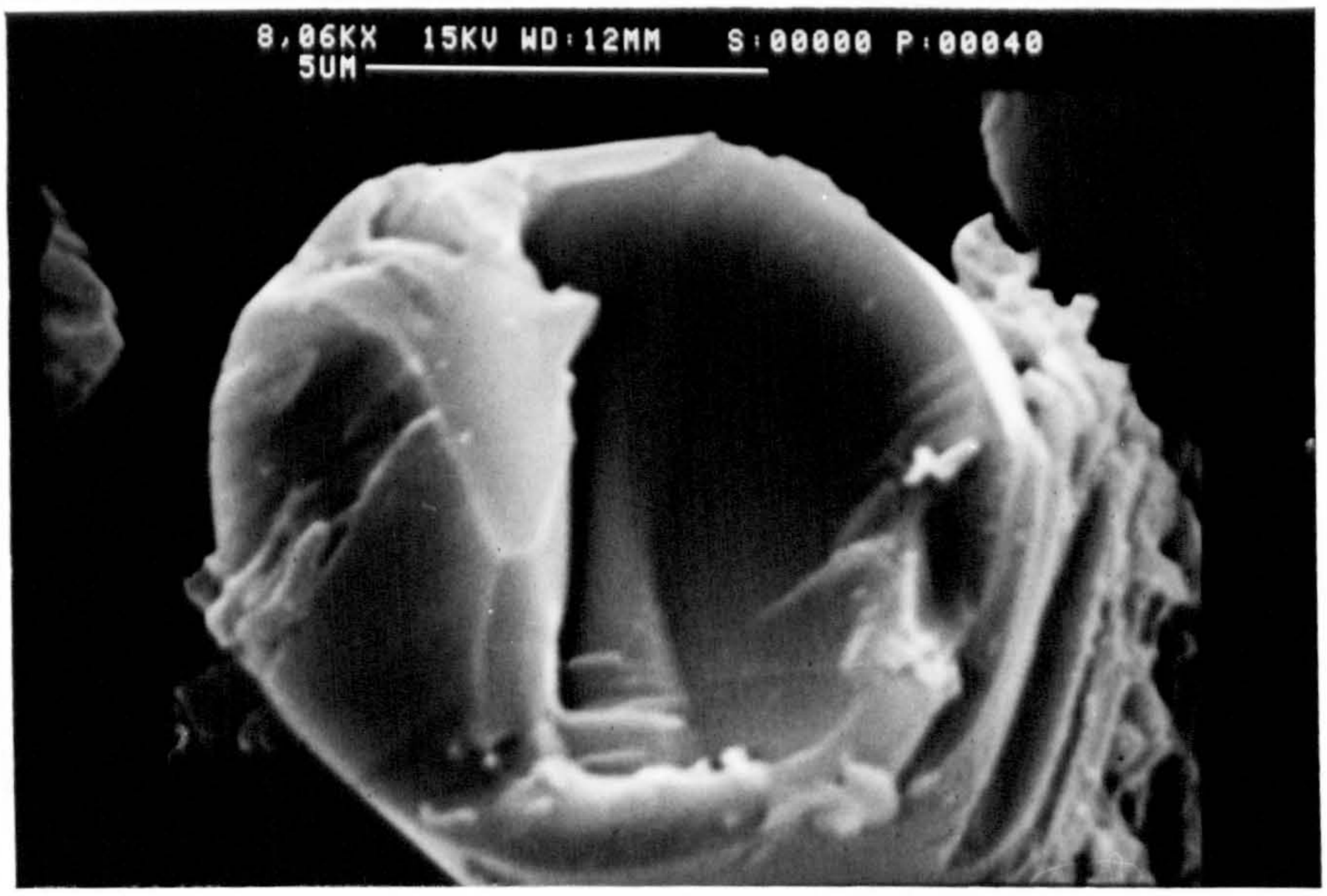

Fig 113. Highly magnified view of the factured surface of a fibre showing its brittle nature

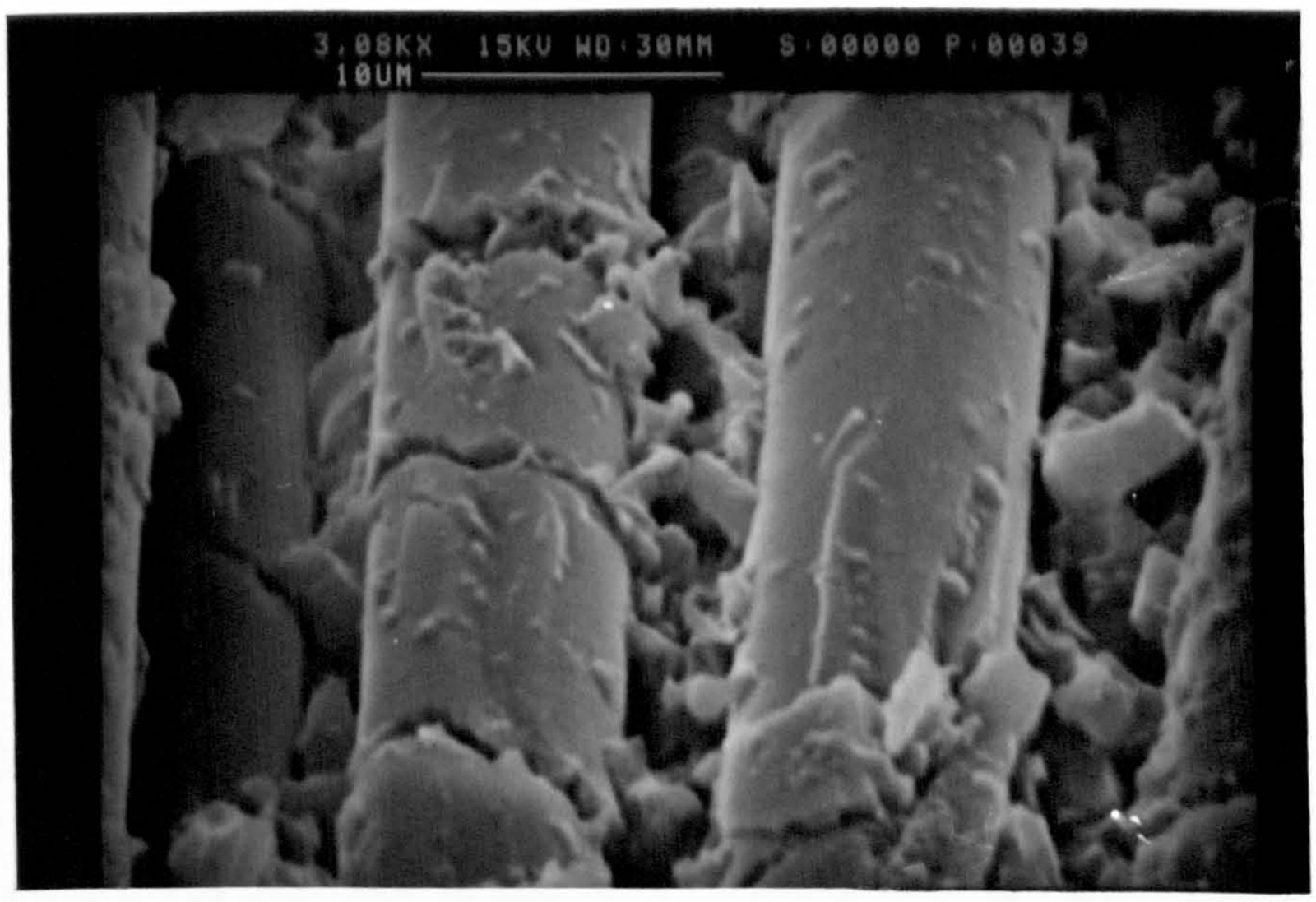

Fig 114. Fracture of glass fibres and pulverised resins

Fig 115. Smooth GFRP surface produced at low speed (30 m/min) showing little evidence of fibre pull-out

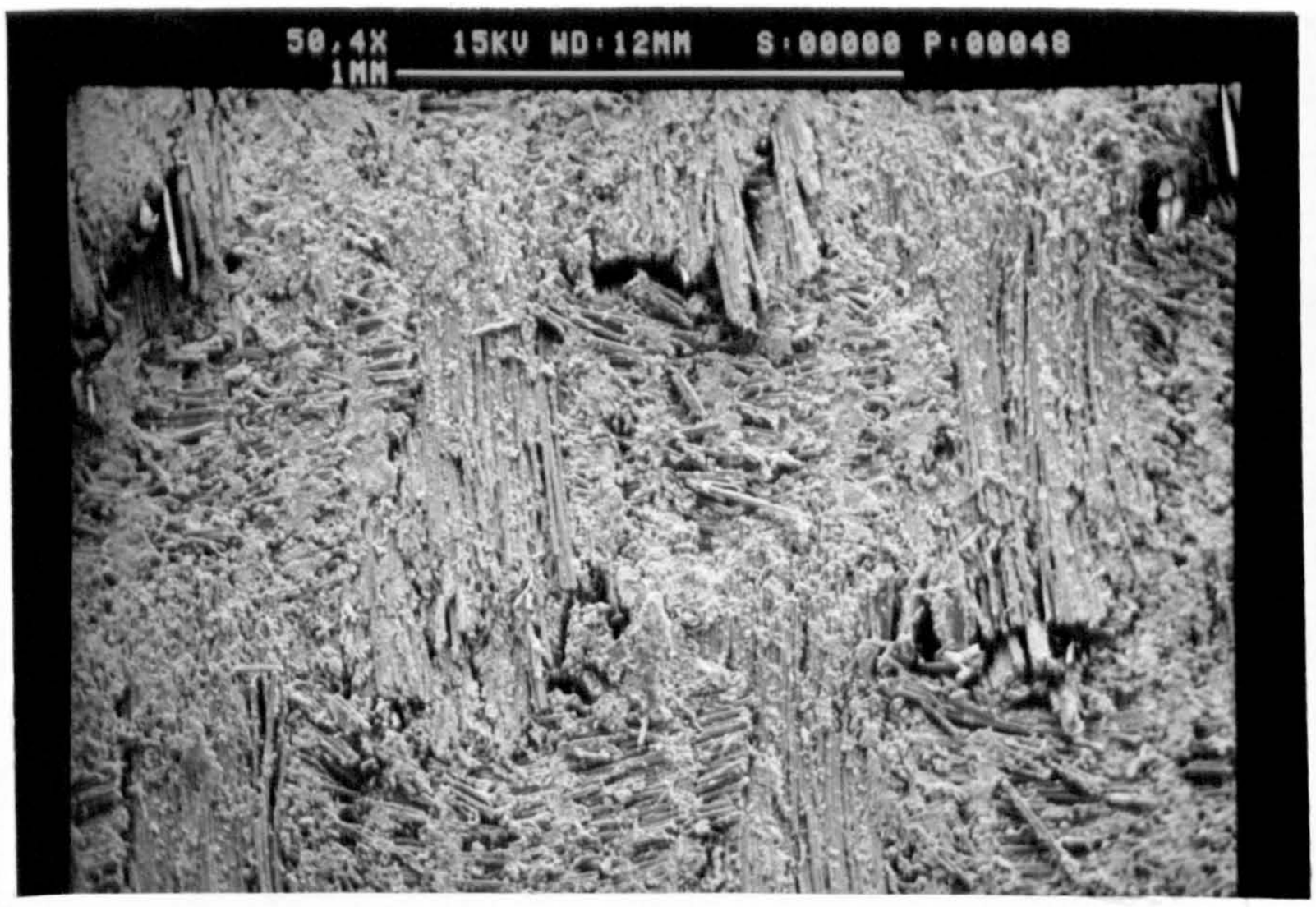

Fig 116. Rough GFRP surface produced at high speed (200 m/min) showing fibre pull-out

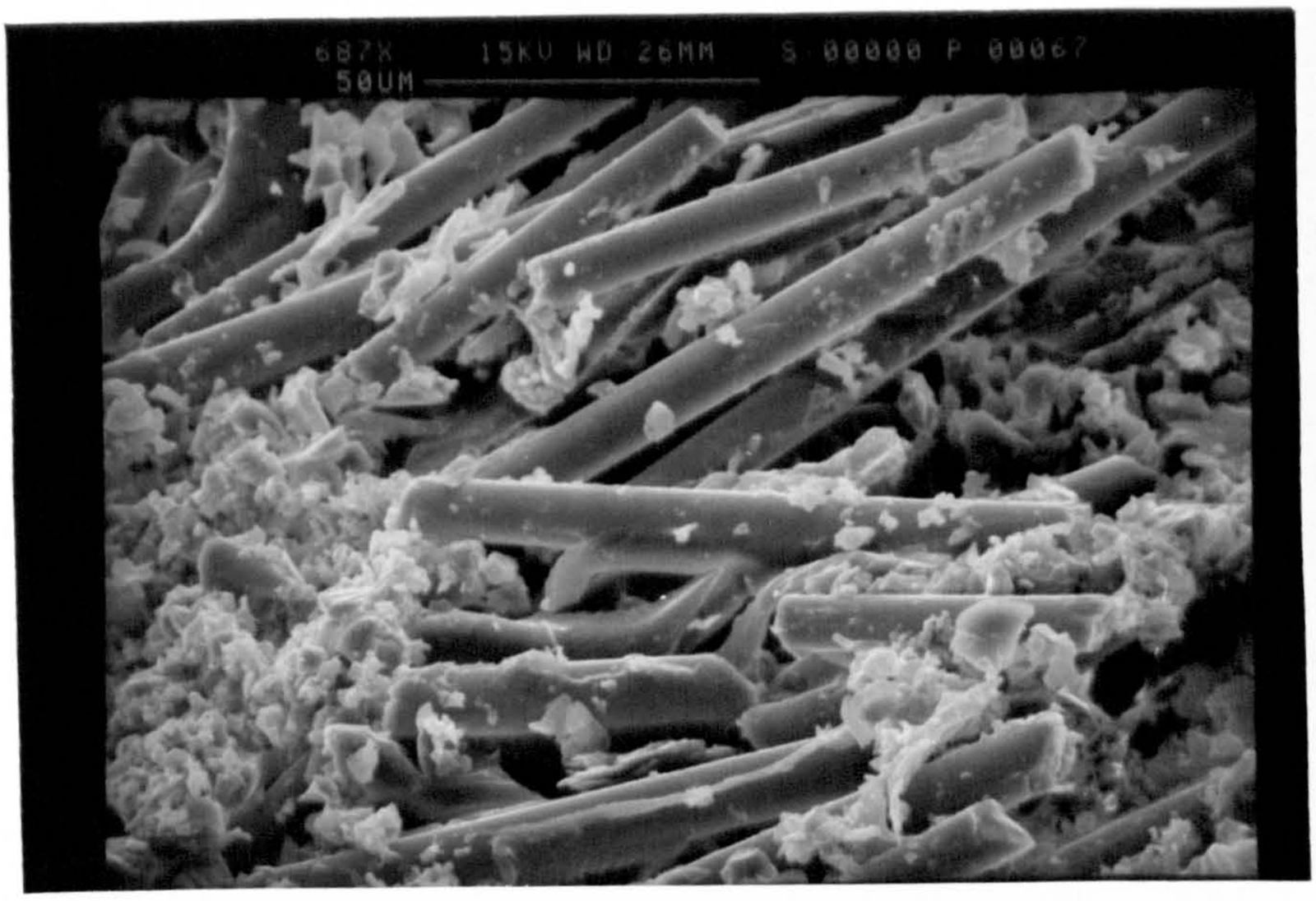

Fig 117. GFRP surface machined with sharp HSS tool showing severe fibre breakage and crumbled resins. (Speed = 100 m/min, feed = 0.125 mm/rev)

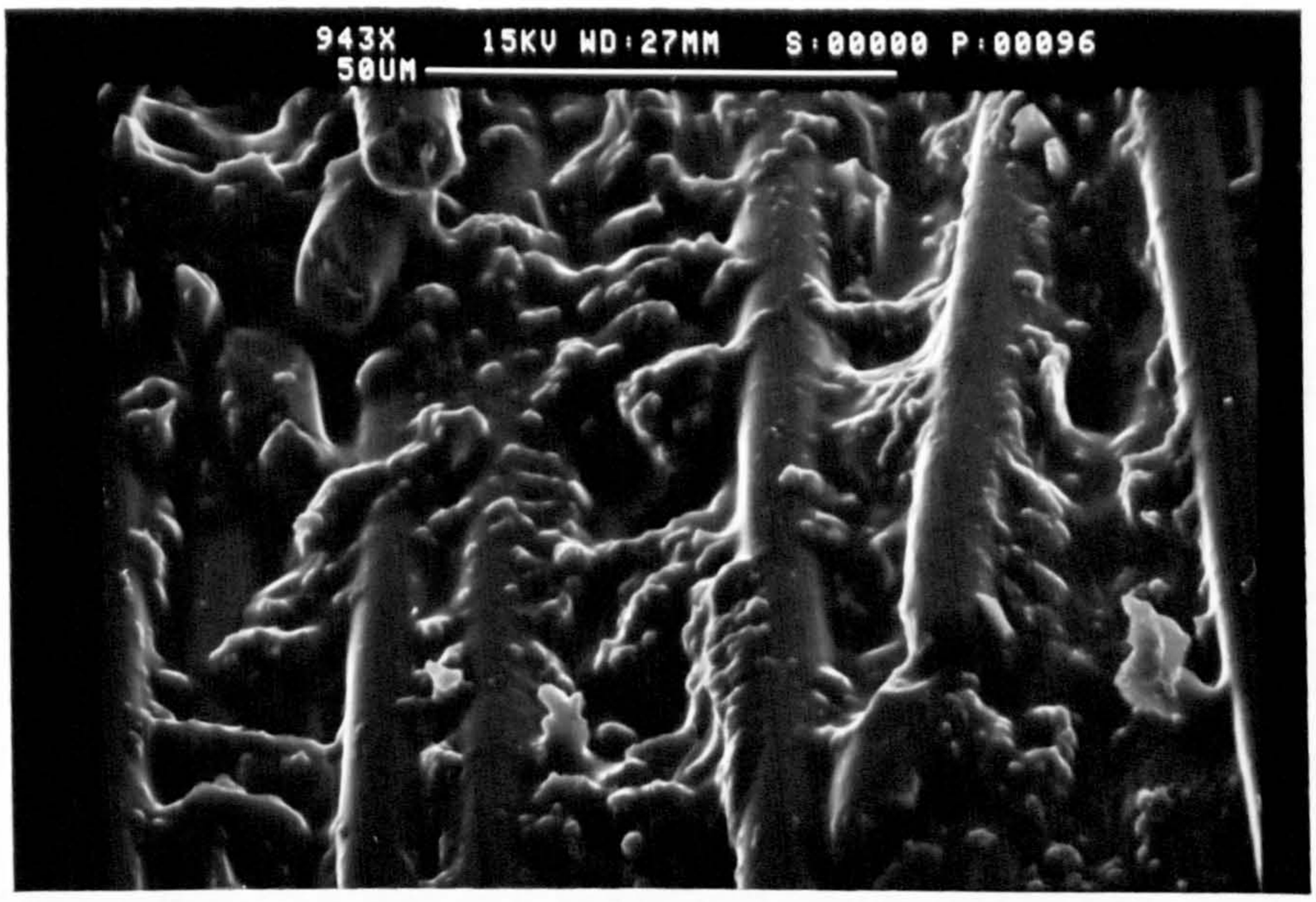

Fig 118. GFRP surface machined with worn HSS tool showing ductile nature of the resin. (Speed = 100 m/min, feed = 0.125 mm/rev)

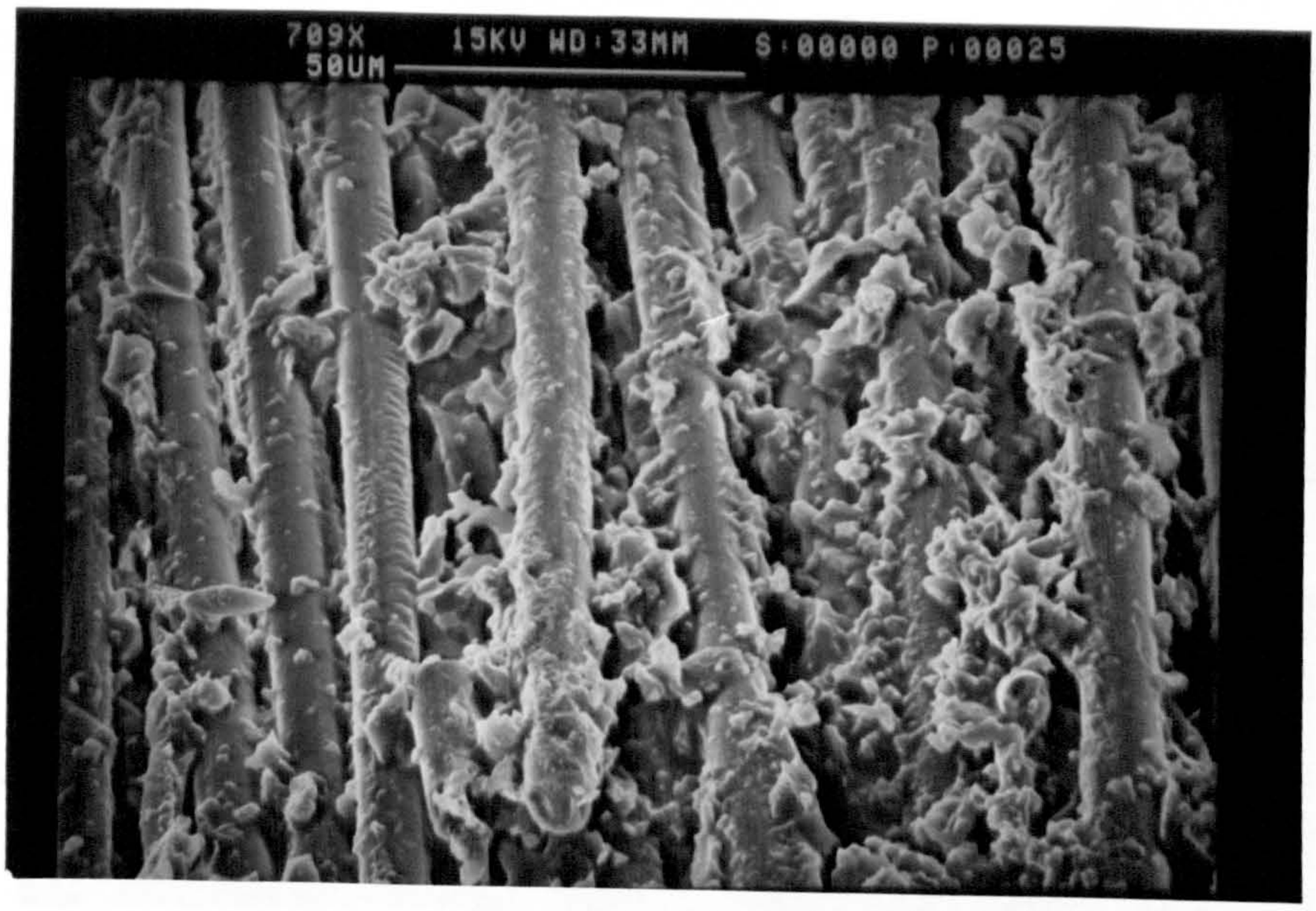

Fig 119. GFRP surface machined by a tool with small nose radius (0.25mm), showing adhering resin on the fibres. (Speed = 200 m/min, feed = 0.125 mm/rev)

Fig 120. GFRP surface machined by zero raked tool showing good finish. (Speed = 30 m/min, feed = 0.125 mm/rev)

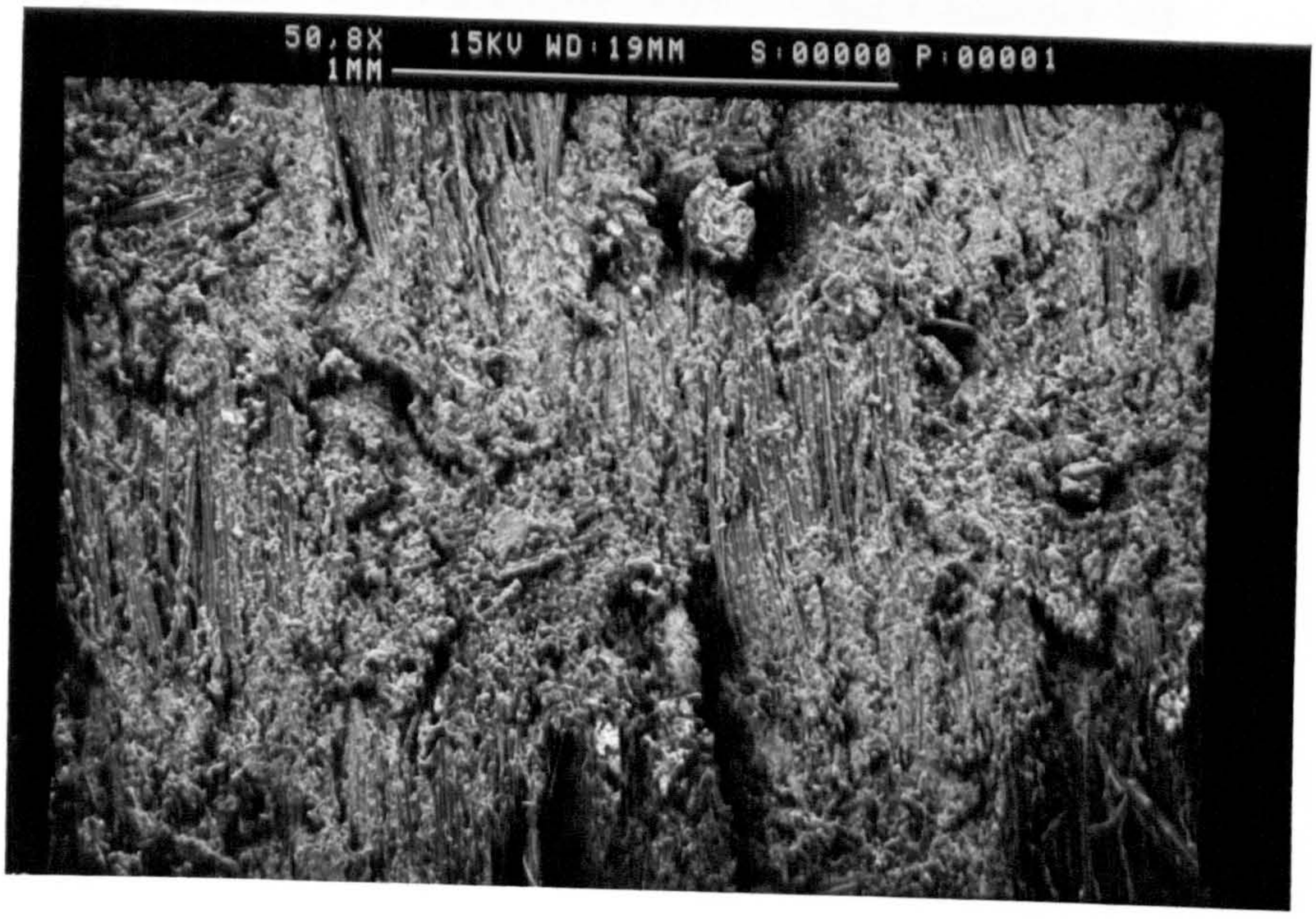

Fig 121. GFRP surface machined by high negative raked (-20°) tool. (Speed = 30 m/min, feed = 0.125 mm/rev)

Fig 122. GFRP surface machined by high positive raked (30°) tool. (Speed = 30 m/min, feed = 0.125 mm/rev)

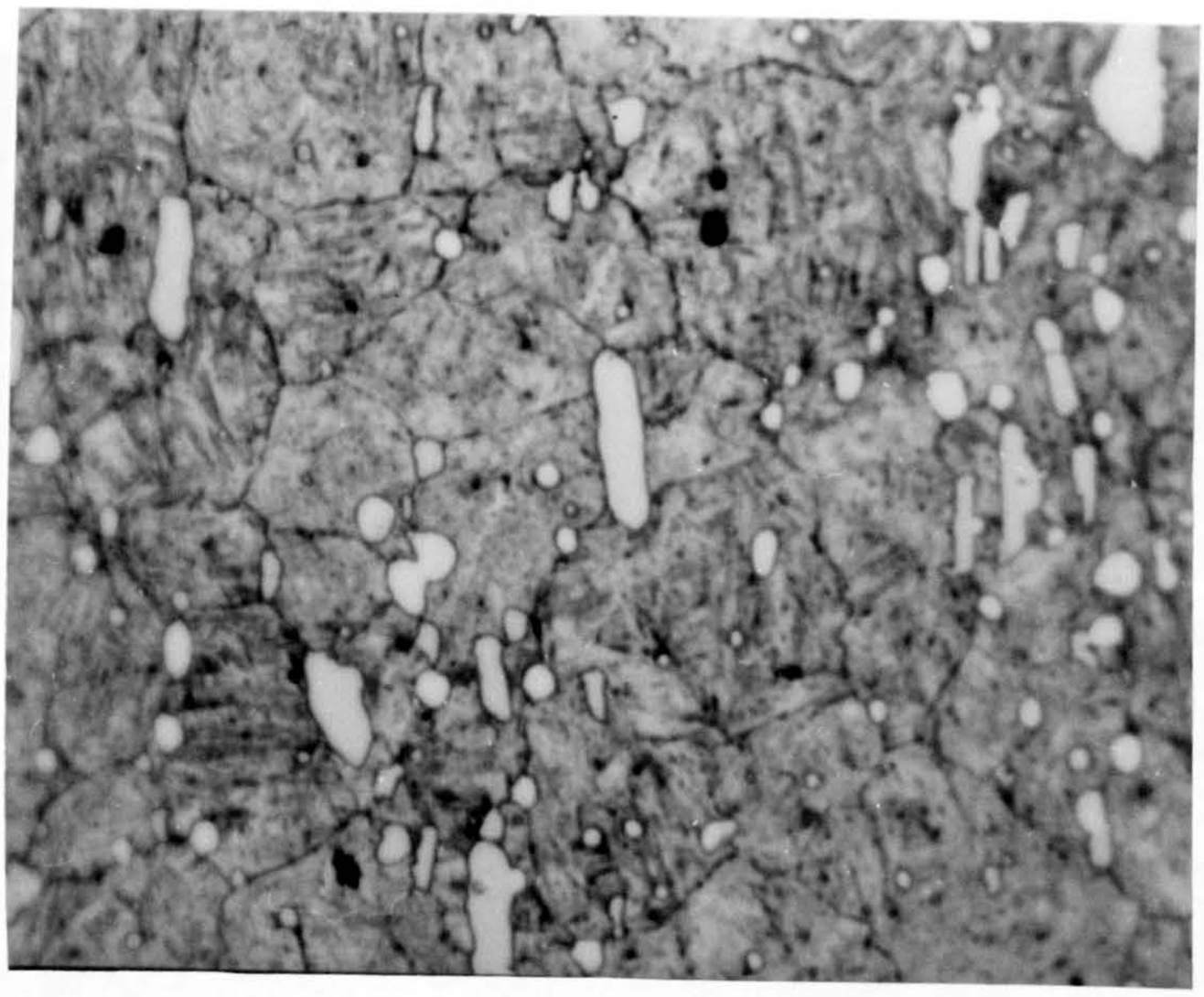

Fig 123. Microstructure of HSS tool (X1650) (etchant - 2% nital solution)

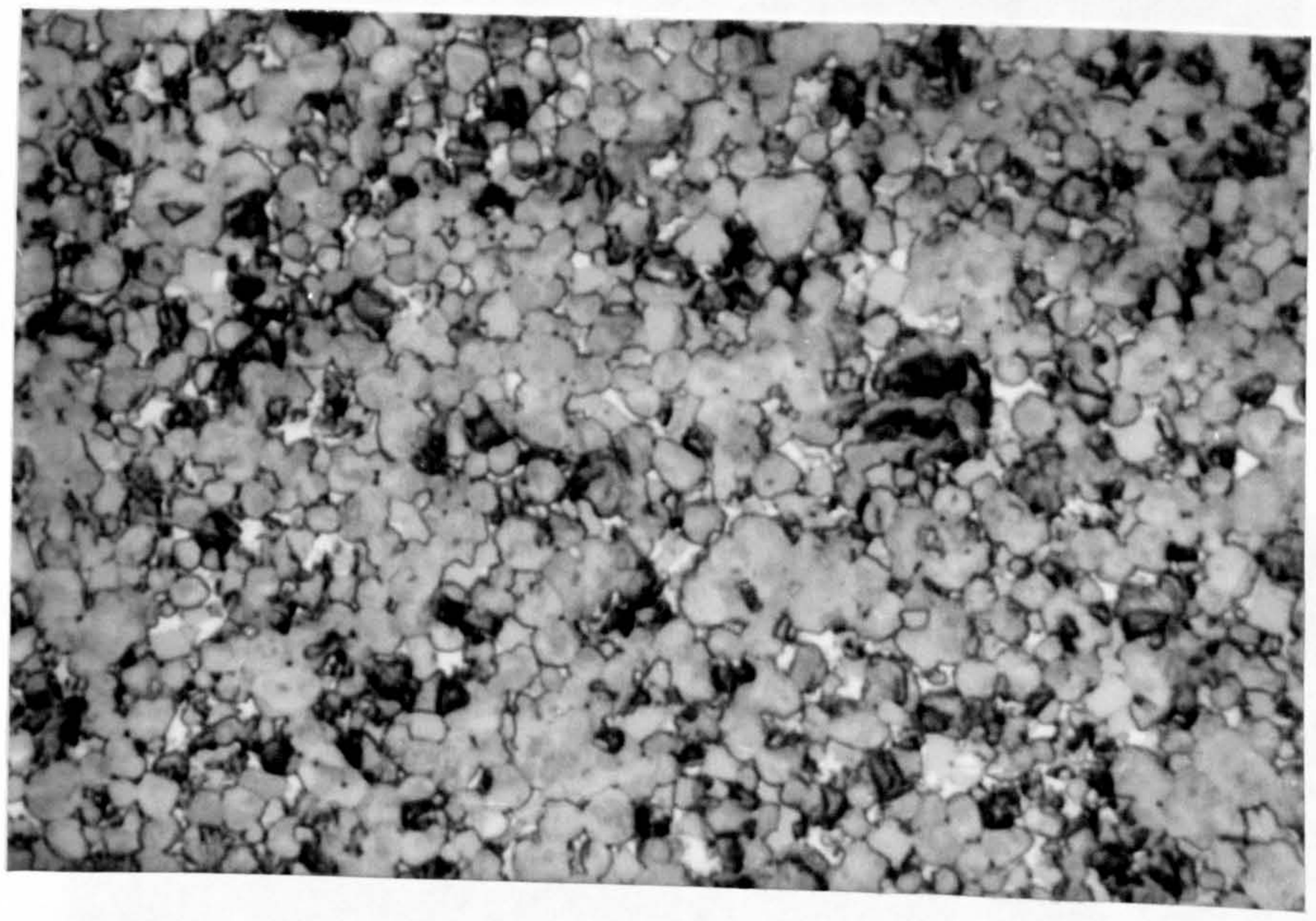

Fig 124. Microstruture of P10 carbide tool (X1650) (etchant - Murakami's solution)

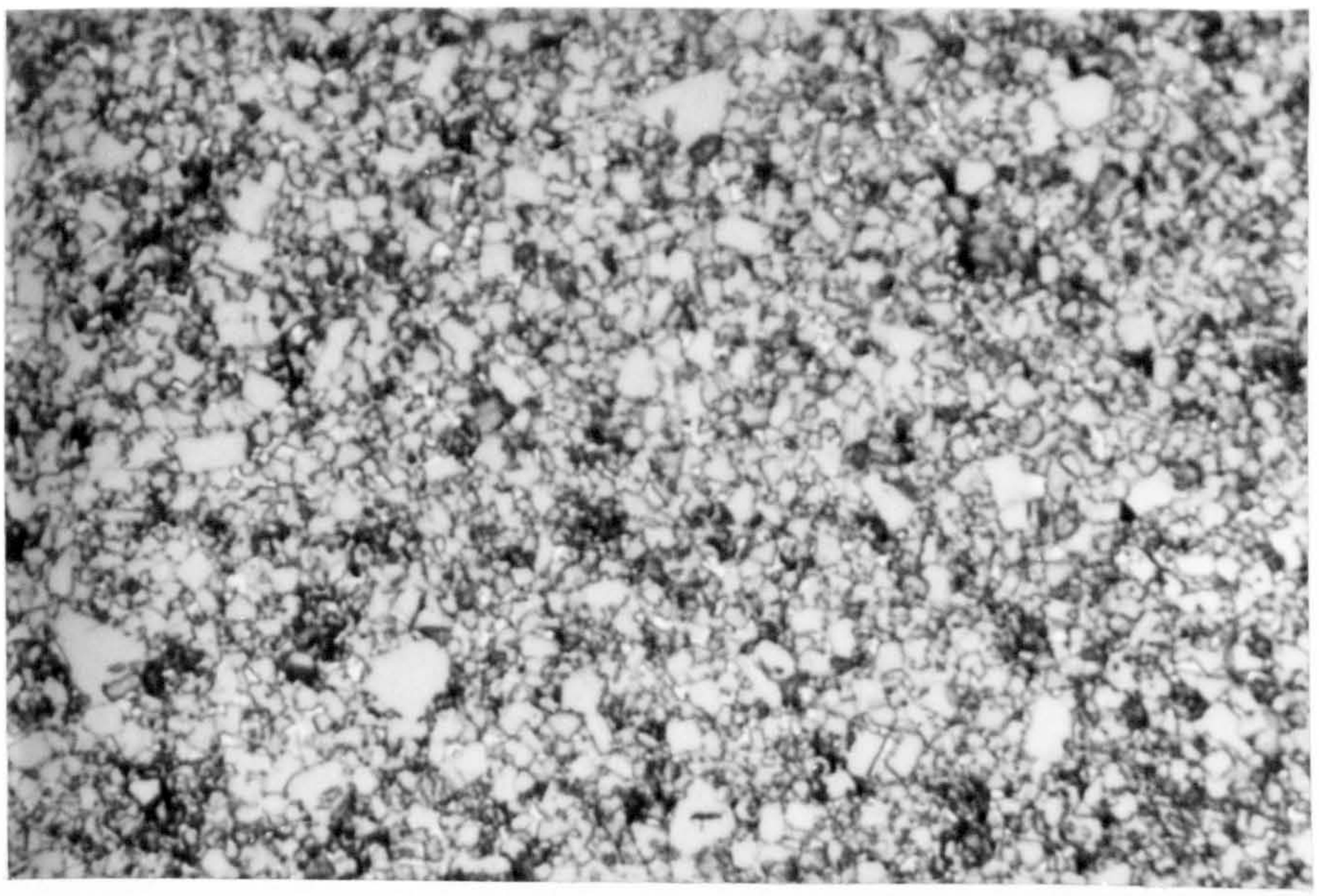

Fig 125. Microstructure of K20 carbide tool (X1650) (etchant - Murakami's solution)

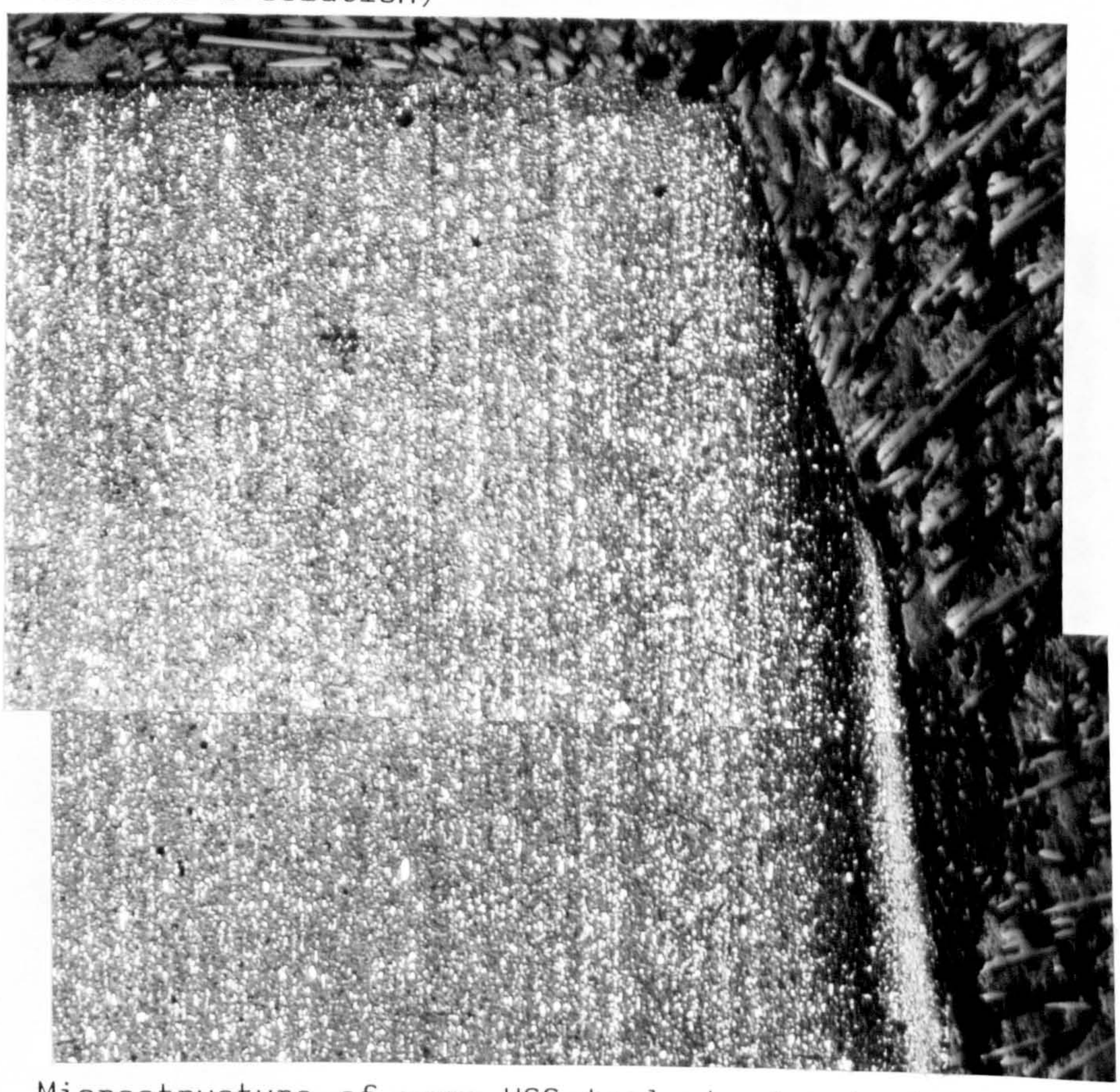

Fig 126. Microstructure of worn HSS tool showing heat affected zone on the flank face (X83)
(Speed = 200 m/min, feed = 0.20 mm/rev, cutting time = 1 min)

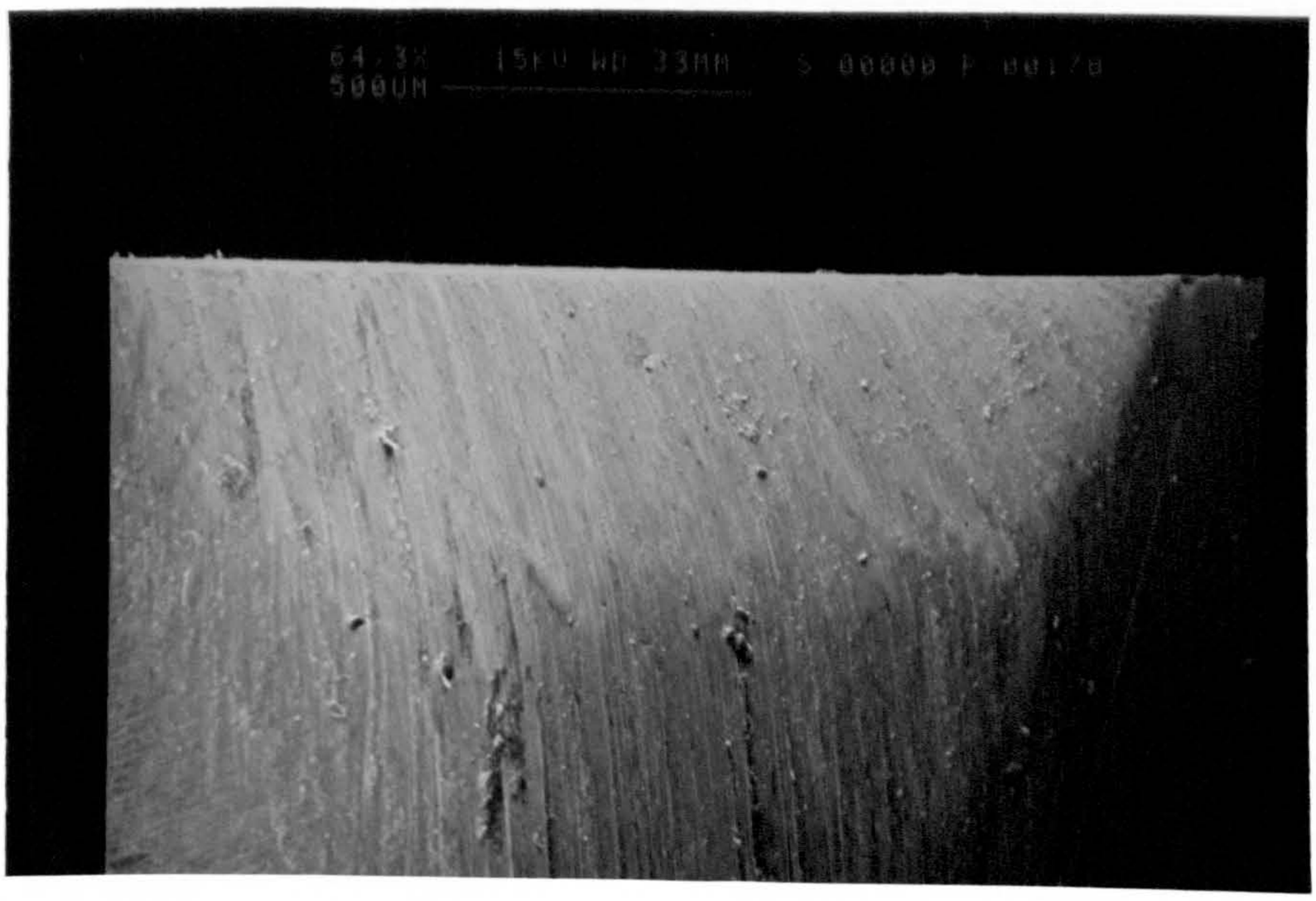

Fig 127. Typical wear pattern of a HSS tool. (Speed = 200 m/min, feed = 0.125 mm/rev, cutting time = $\frac{1}{2}$min)

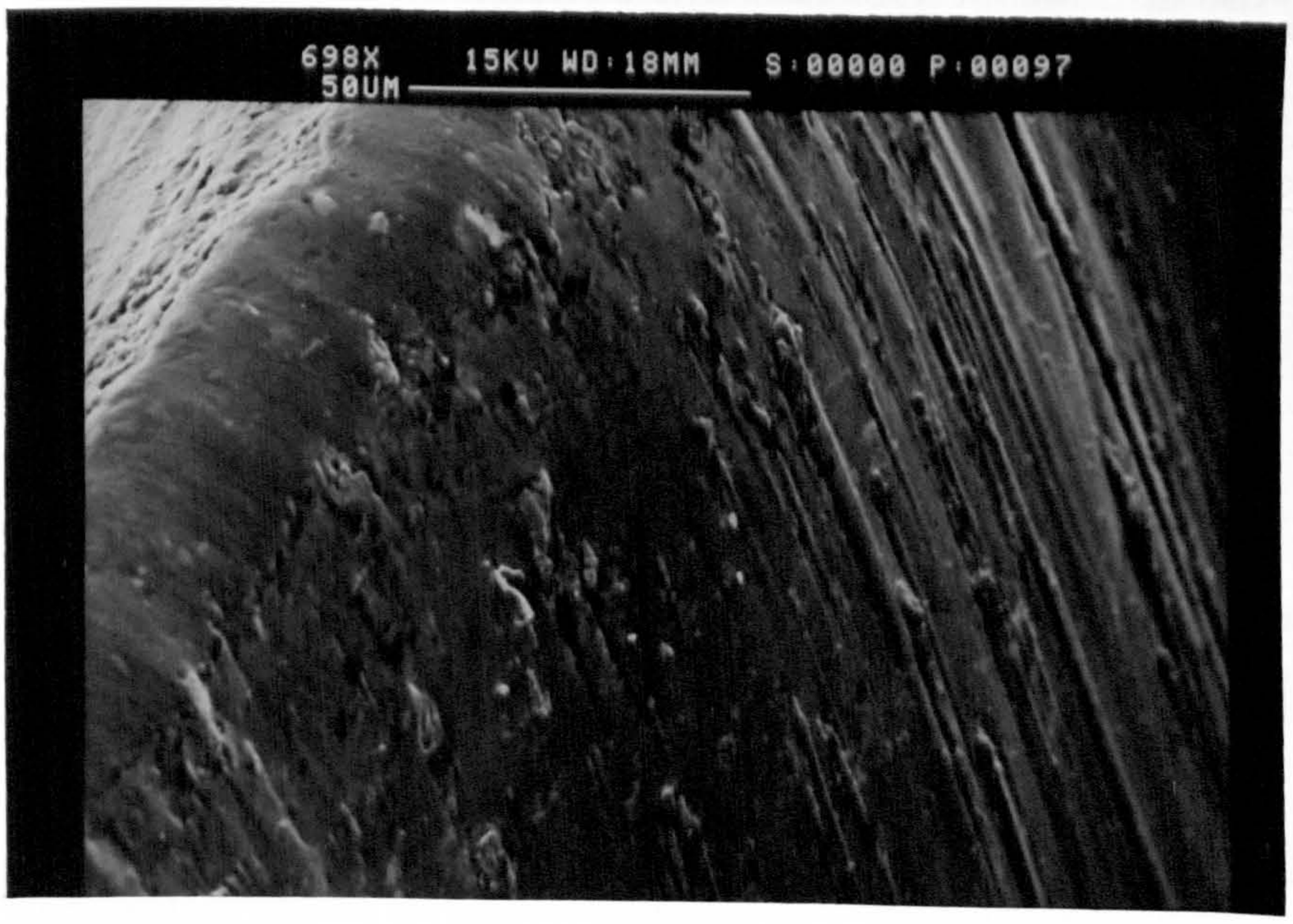

Fig 128. Flank wear land of HSS tool showing ridged structure

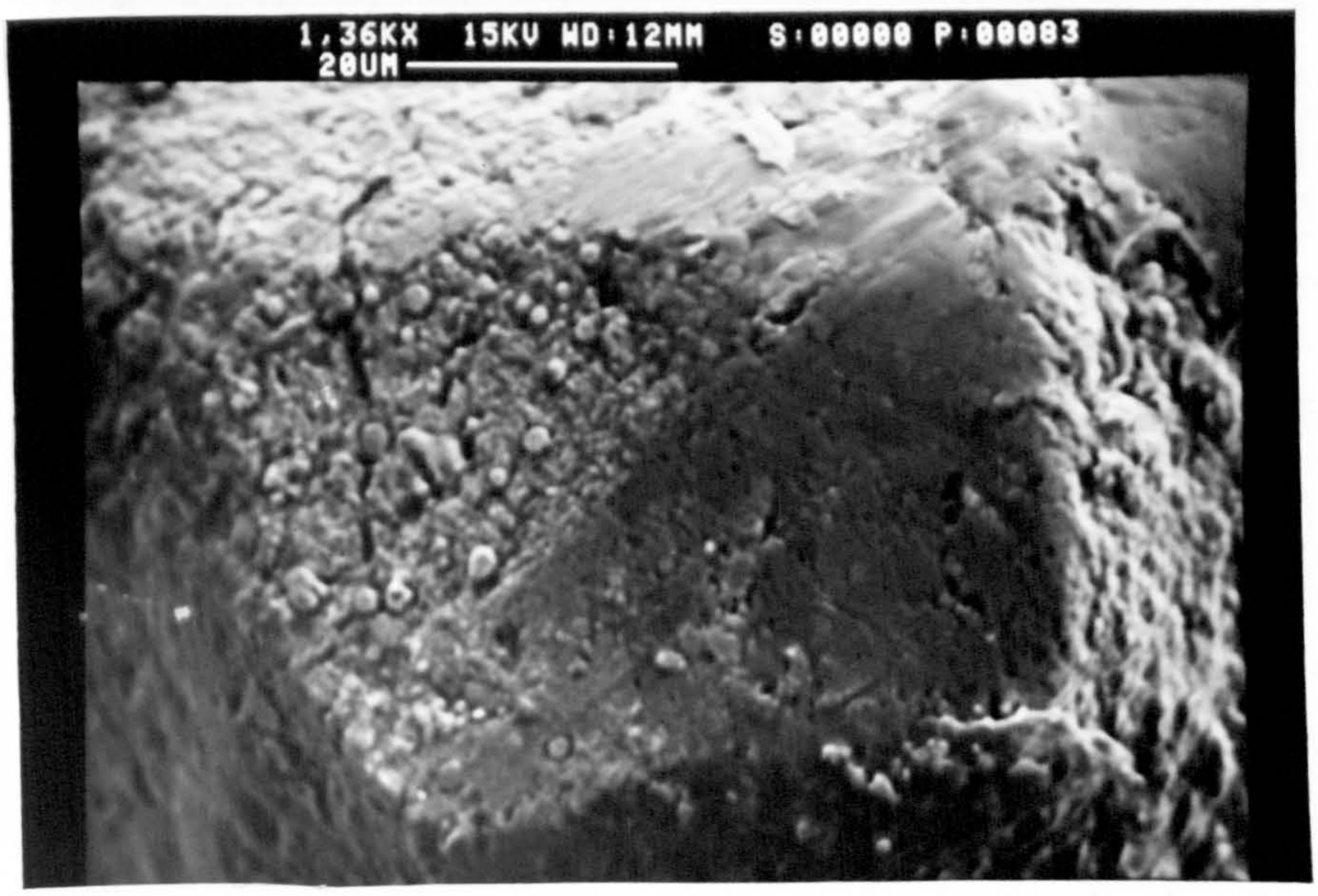

Fig 129. Nose-chipping of HSS tool after cutting at a speed of 200m/min (feed = 0.125 mm/rev, cutting time = $\frac{1}{2}$ min)

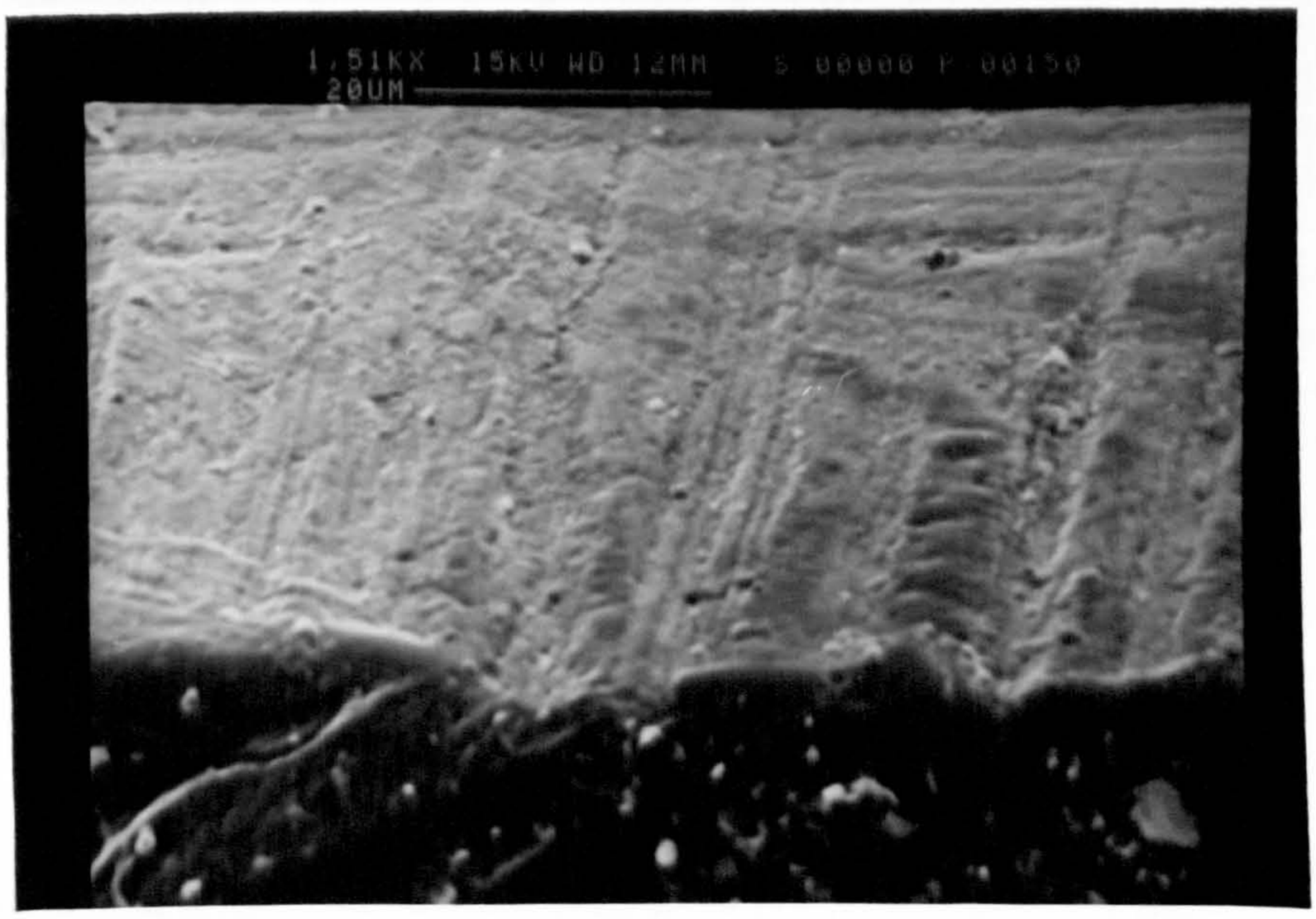

Fig 130. Rake face of worn HSS tool showing intermittent grooves (Speed = 150 m/min, feed = 0.20 mm/rev, cutting time = 1 min)

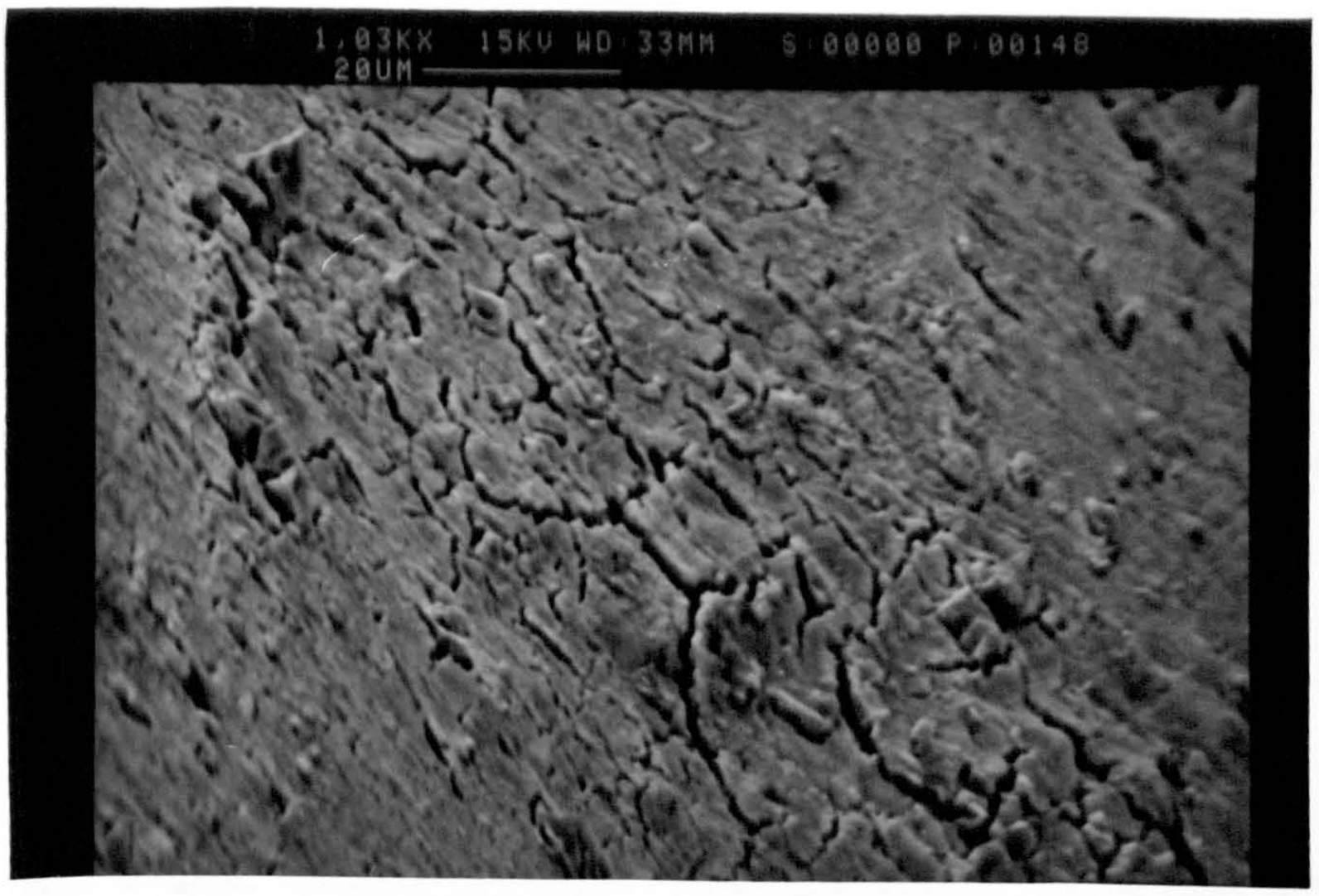

Fig 131. Cracking on the flank wear land of HSS tool.
(Speed = 200 m/min, feed = 0.125 mm/rev, cutting time = $\frac{1}{2}$ min)

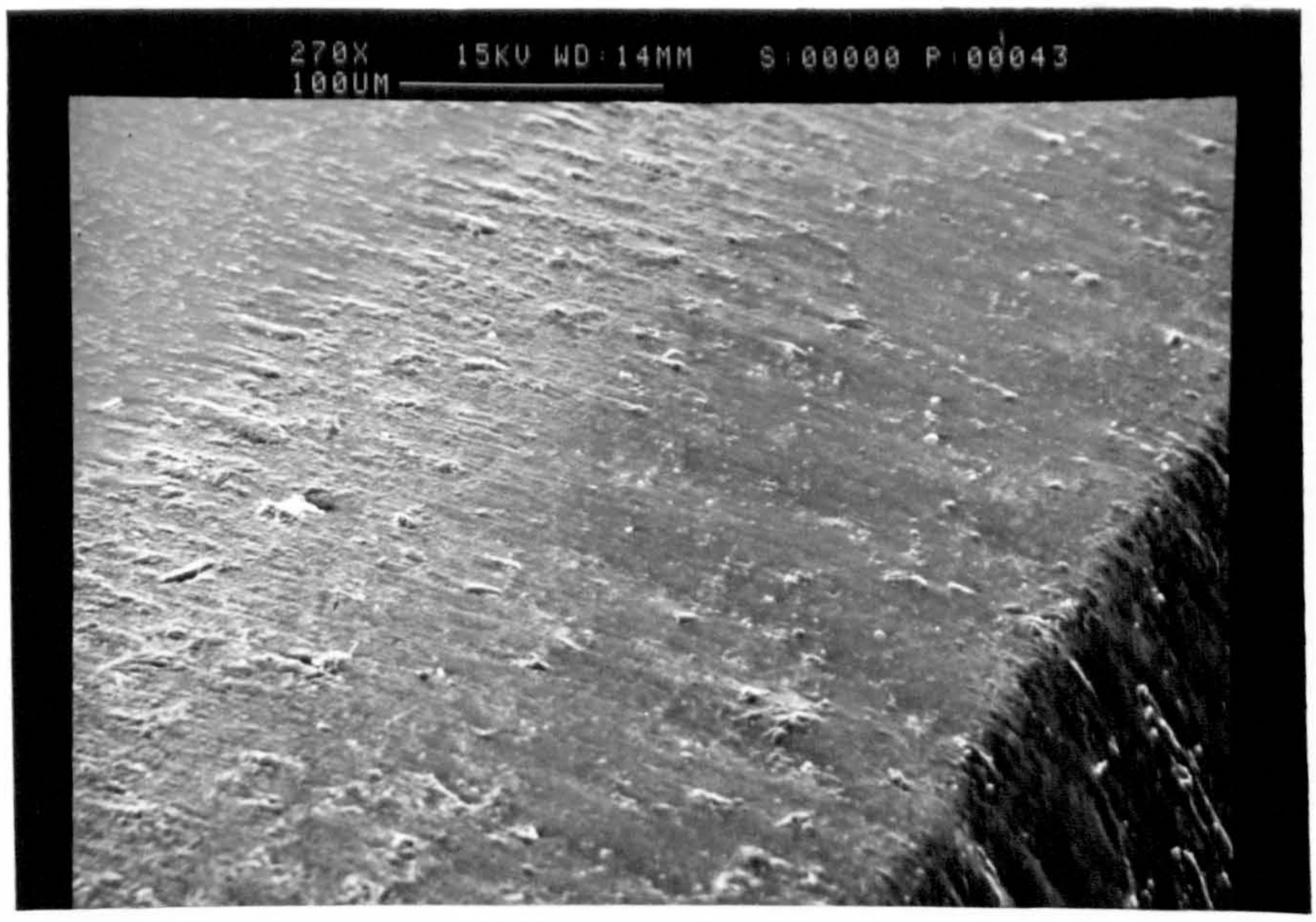

Fig 132. Smooth rake face of worn HSS tool showing no crater formation. (Speed = 100 m/min, feed = 0.20 mm/rev, cutting time = 2 min)

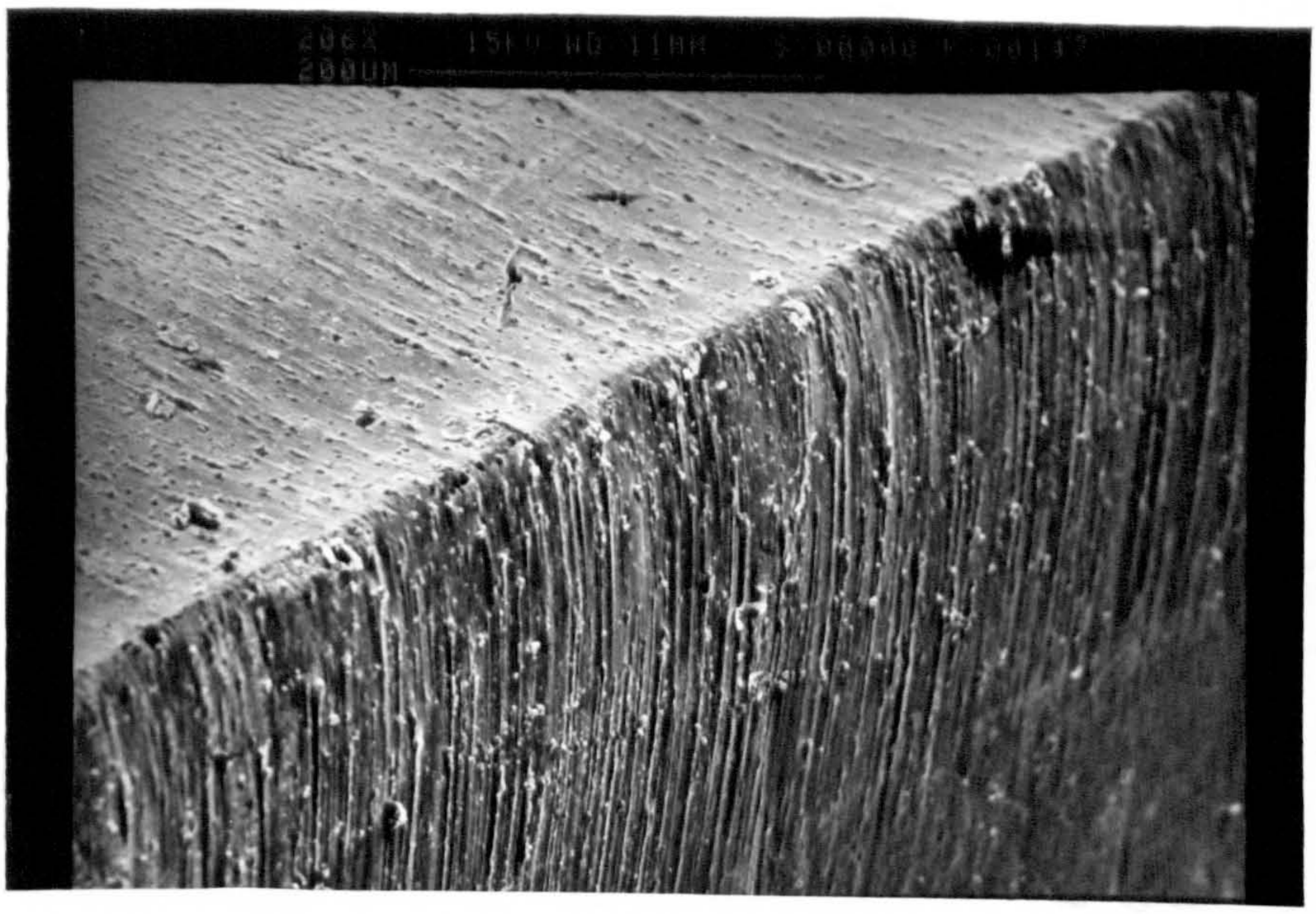

Fig 133. Wear lands of a HSS tool after cutting at a low speed (50 m/min) showing abrasion wear. (Feed = 0.20 mm/rev, cutting time = 1 min)

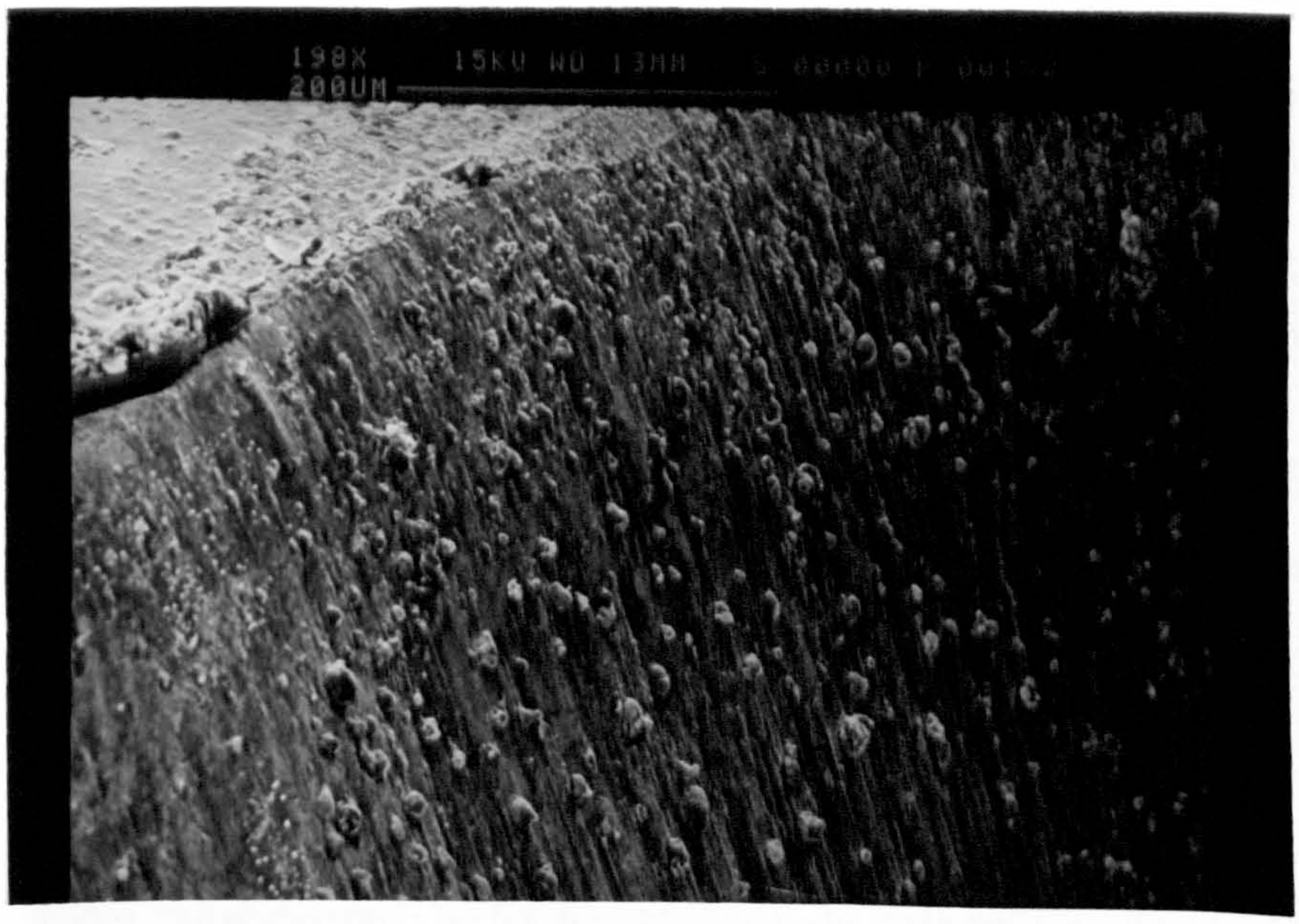

Fig 134. Flank wear land of a HSS tool after cutting at a high speed (200 m/min) showing severe abrasion wear. (Feed = 0.20 mm/rev, cutting time = 1 min)

Fig 135. Nose chipping of a HSS tool after cutting at a low feed rate (0.10 mm/rev) (speed = 150m/min, cutting time = 1 min)

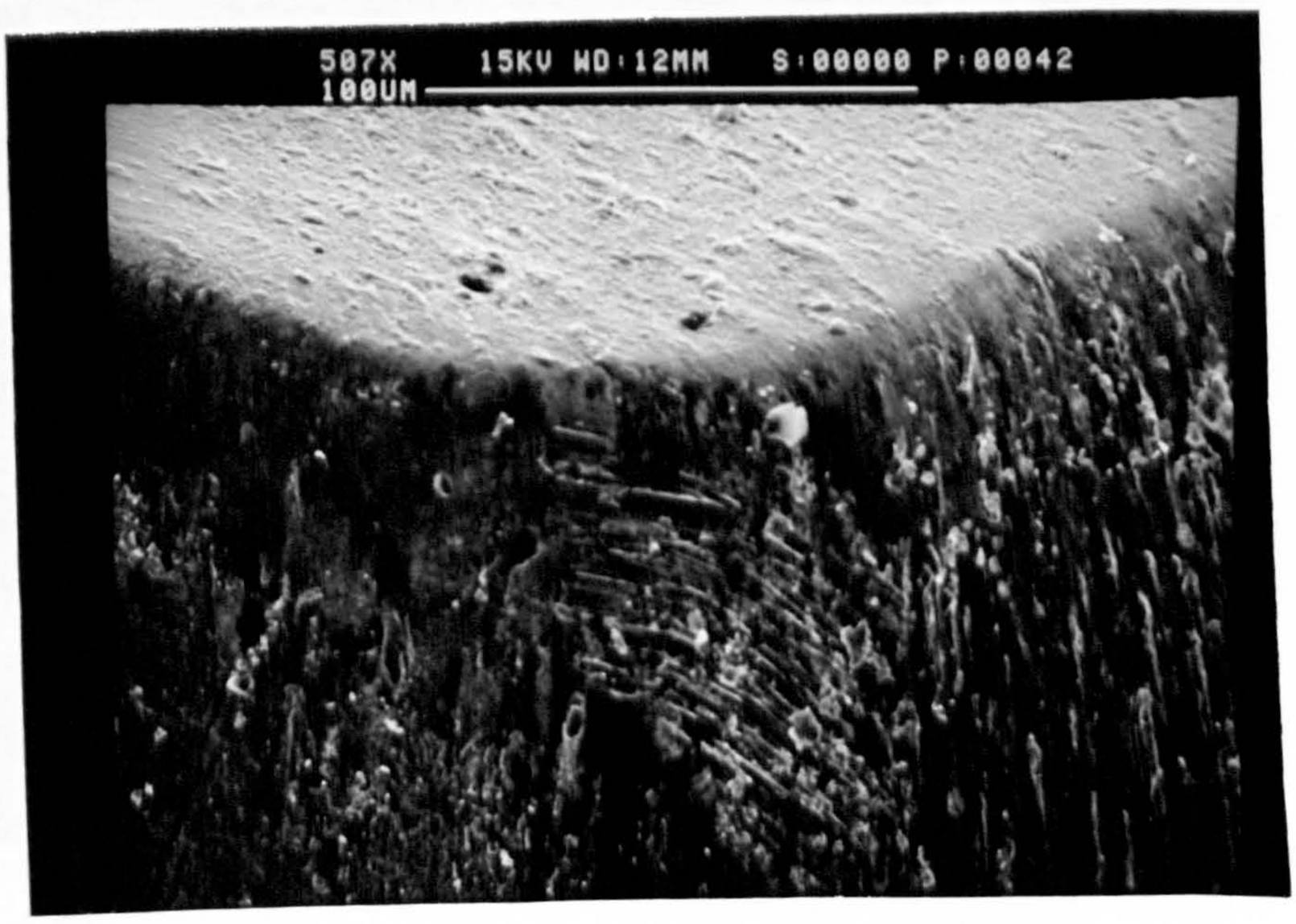

Fig 136. Nose area of a worn HSS tool after cutting at a high feed rate (0.25 mm/rev) (speed = 150 m/min, cutting time = 1 min)

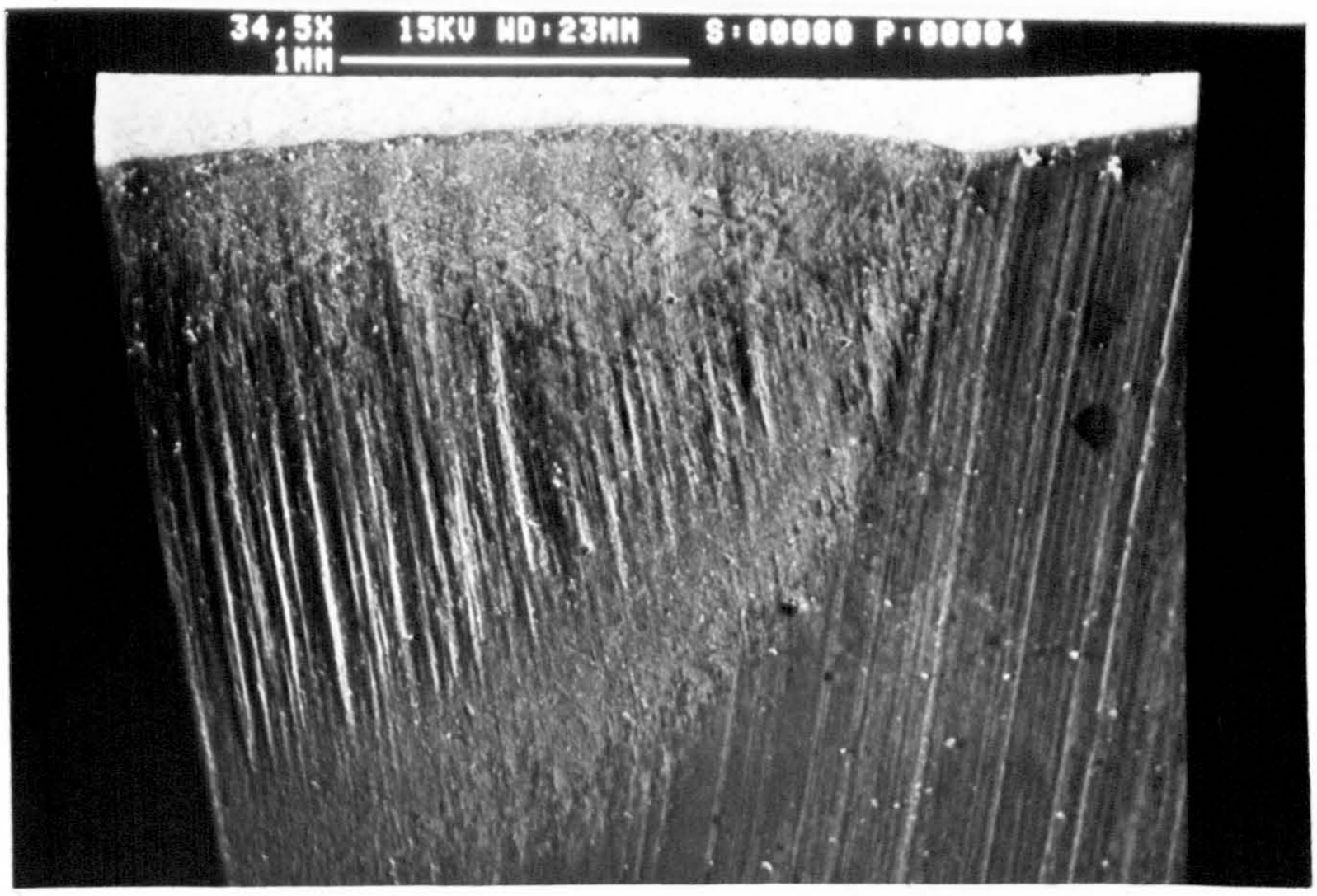

Fig 137. Flank wear land of a HSS tool after cutting at a rake angle of -20° showing smooth surface near the cutting edge

Fig 138. Flank wear land of a HSS tool after cutting at a rake angle of 30° showing ridged structure

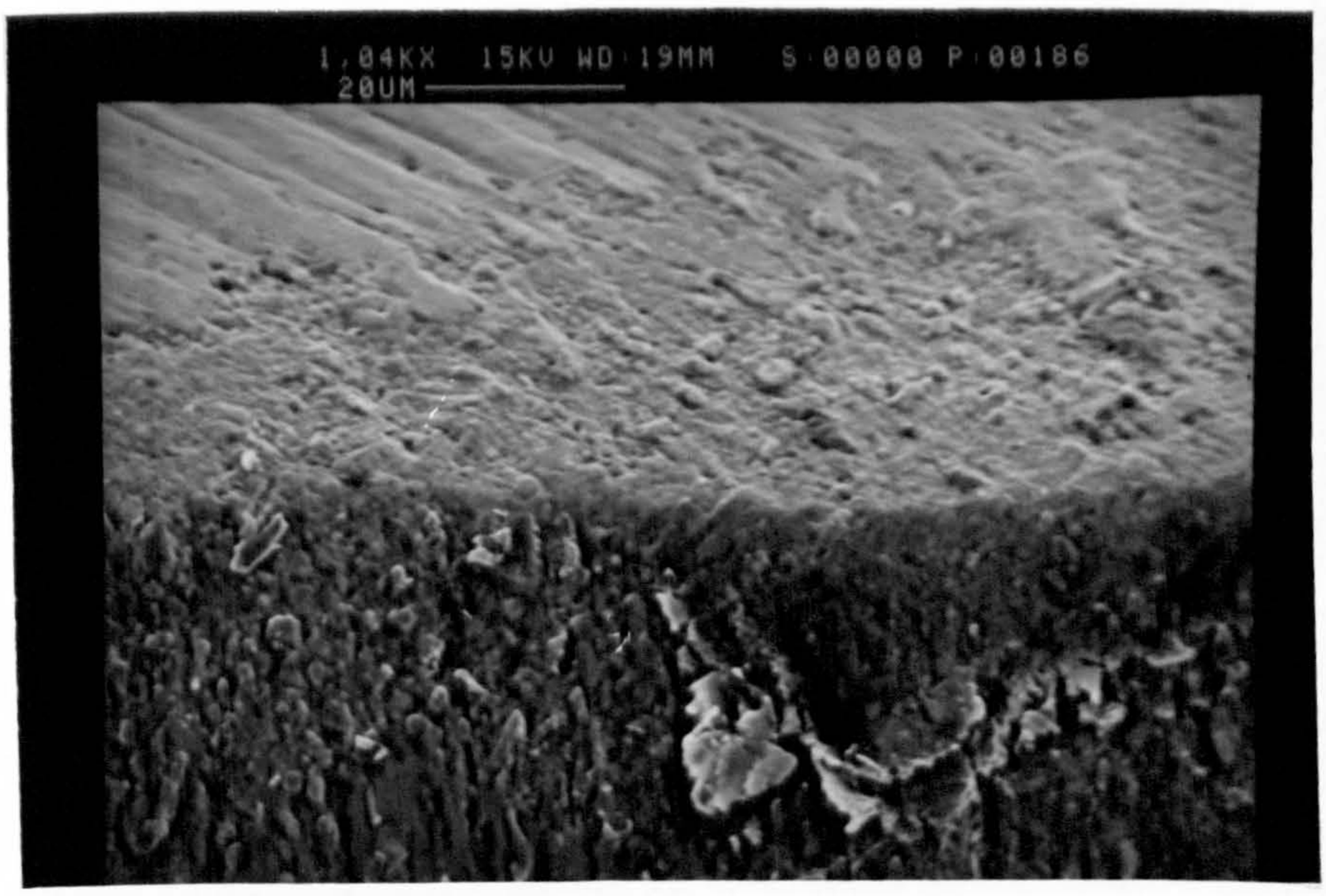

Fig 139. Nose area of a HSS tool with a large nose radius (1.0mm) showing little evidence of nose chipping

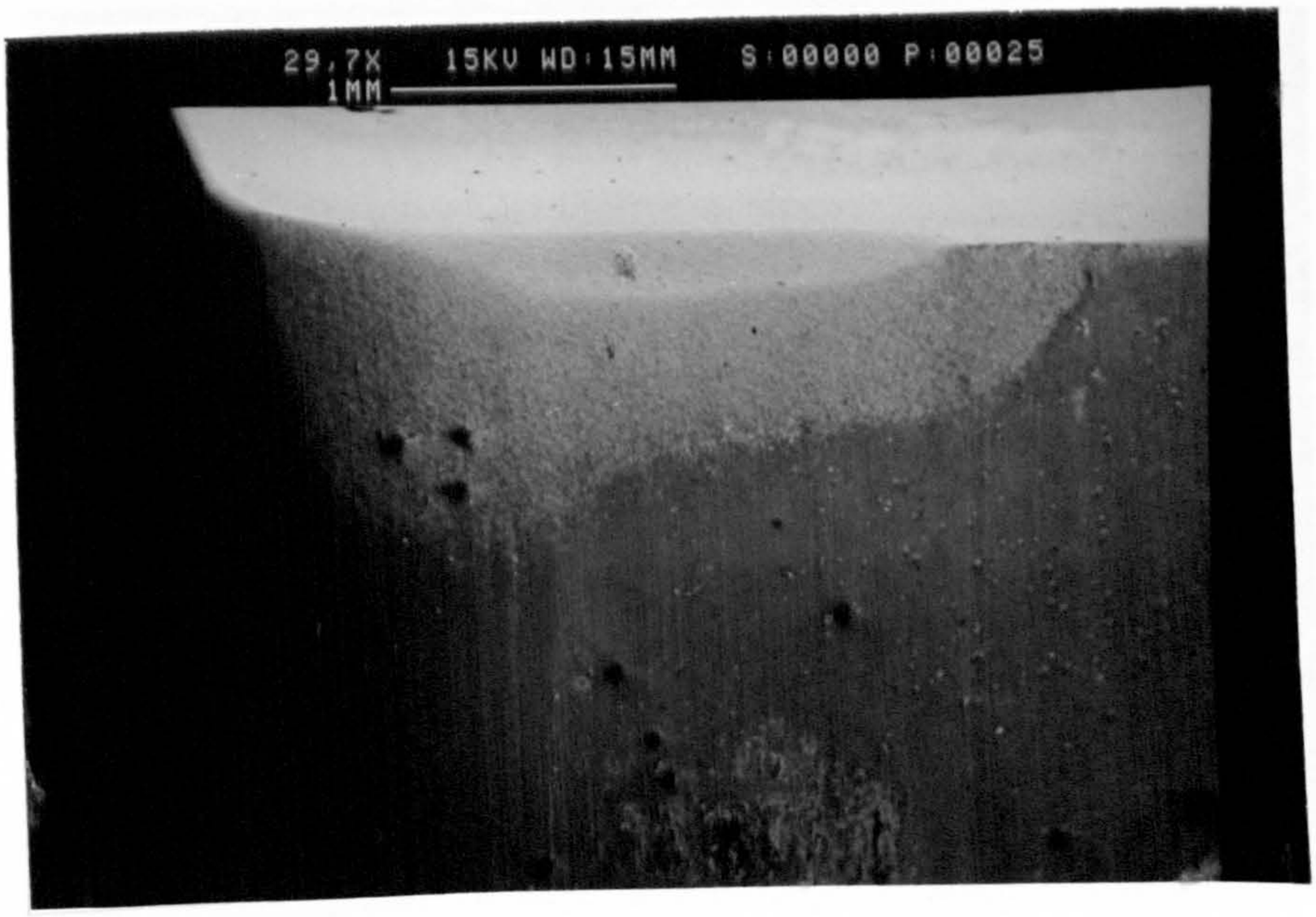

Fig 140. Typical wear pattern of a P10 carbide tool showing severe wear near the cutting edge
(Speed = 200 m/min, feed = 0.20 mm/rev, cutting time = 2 min)

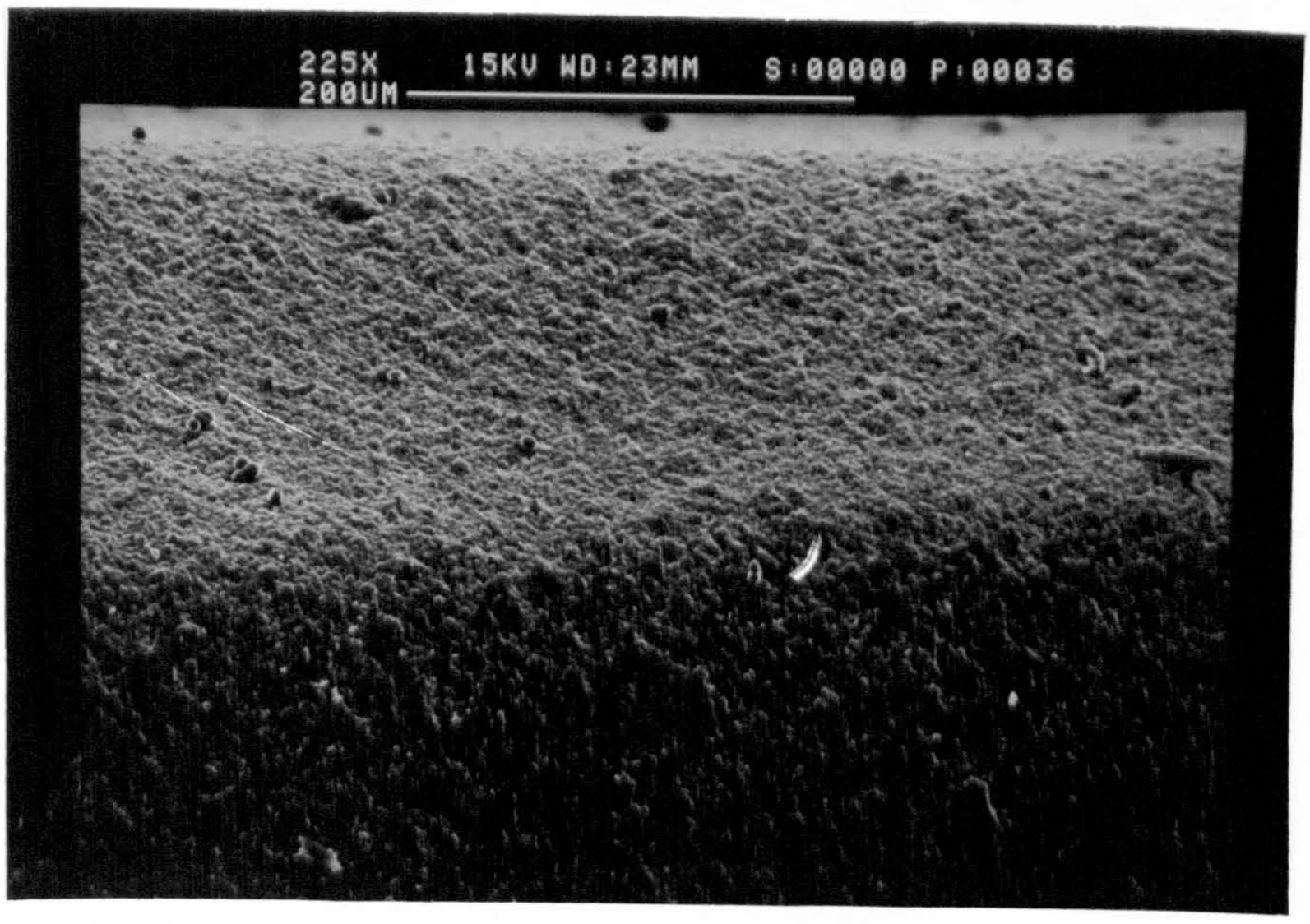

Fig 141. Magnified view of flank wear land near the cutting edge (P10 carbide tool)

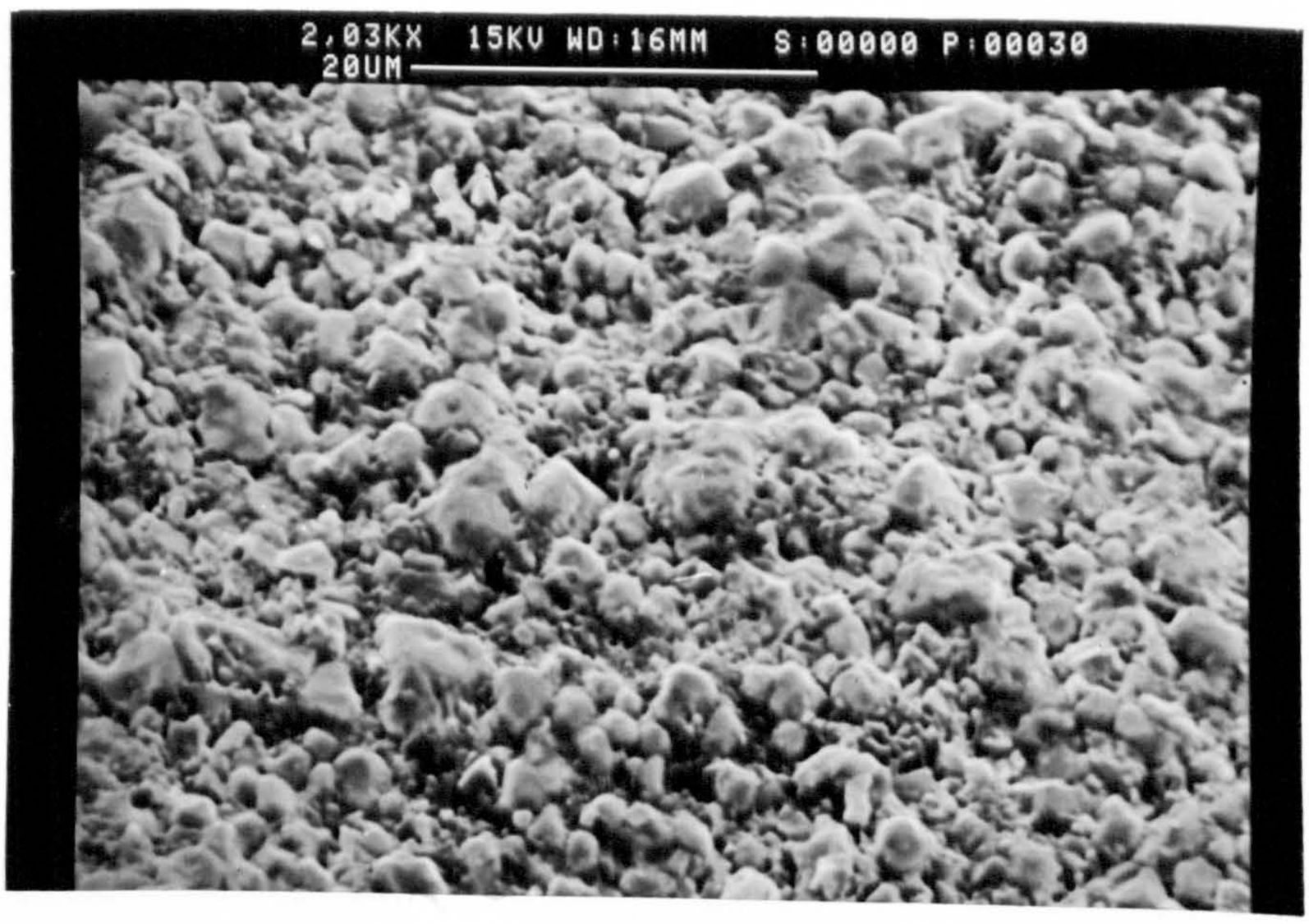

Fig 142. Highly magnified view of flank wear land near the cutting edge (P10 carbide tool)

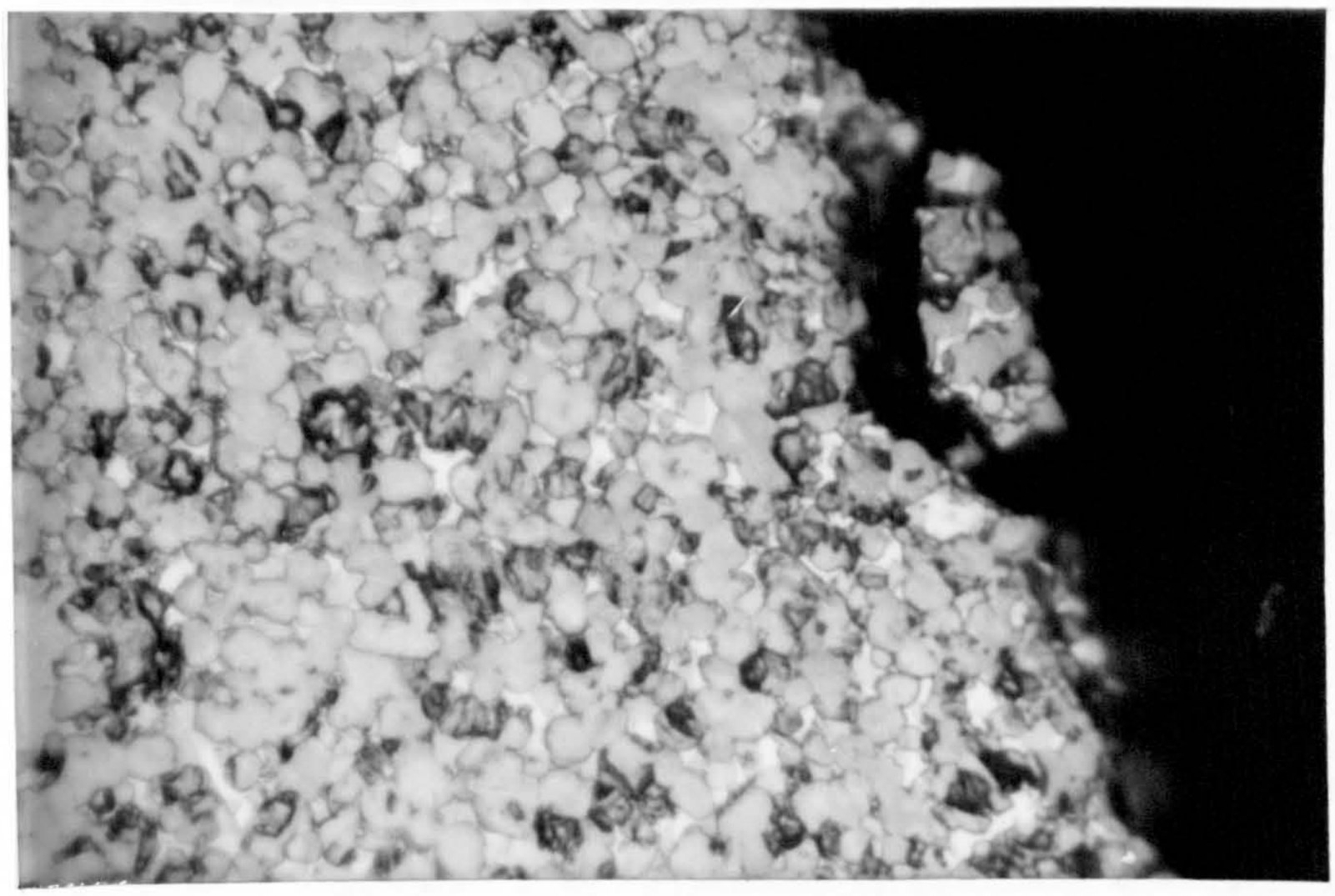

Fig 143. Microstructure of the flank wear land of a P10 carbide tool showing attrition wear (X1650)

Fig 144. Typical wear pattern of a K20 carbide tool. (Speed = 300 m/min, feed = 0.16 mm/rev, cutting time = 2 min)

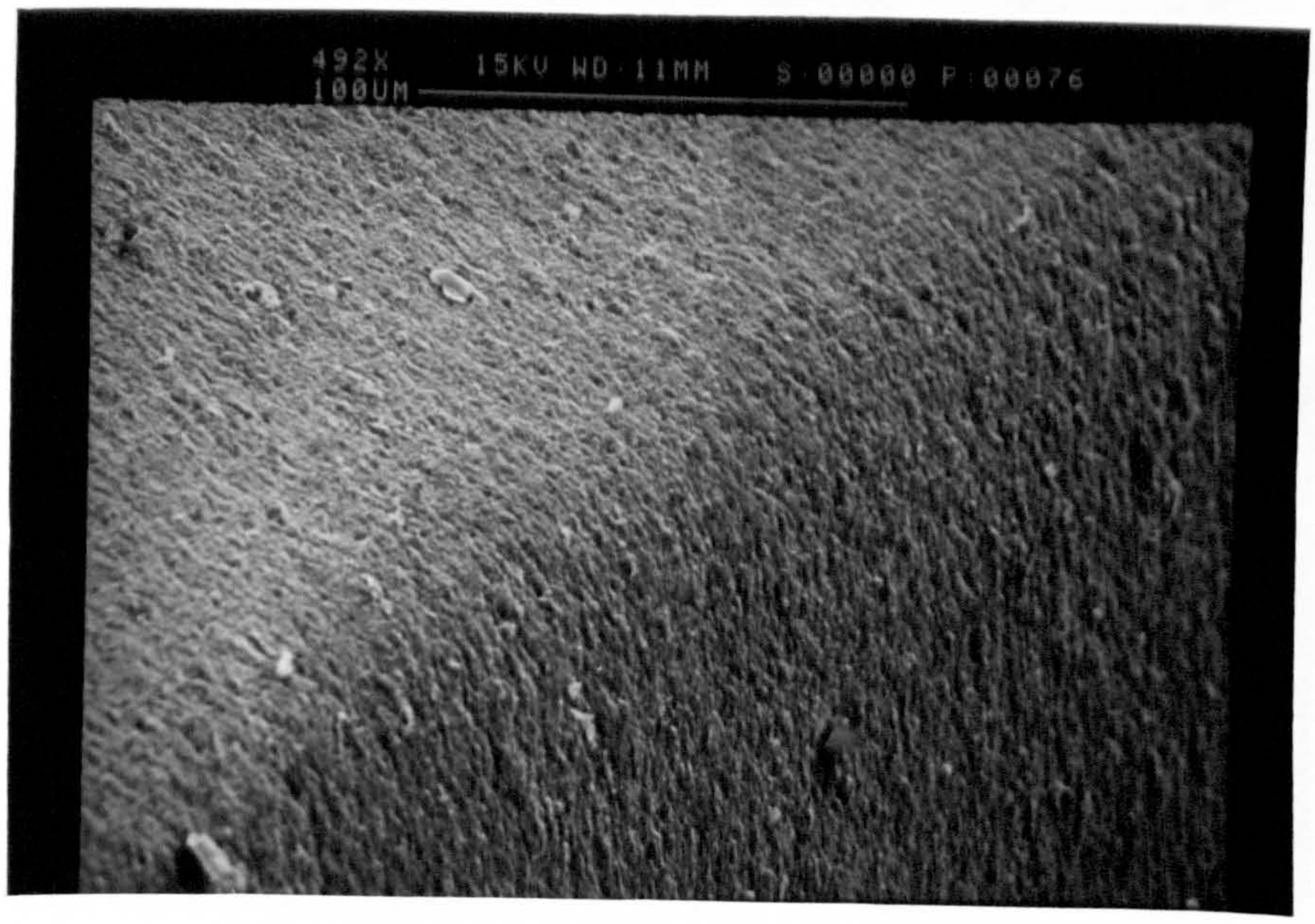

Fig 145. Enlarged view of the cutting edge region showing a rough surface.

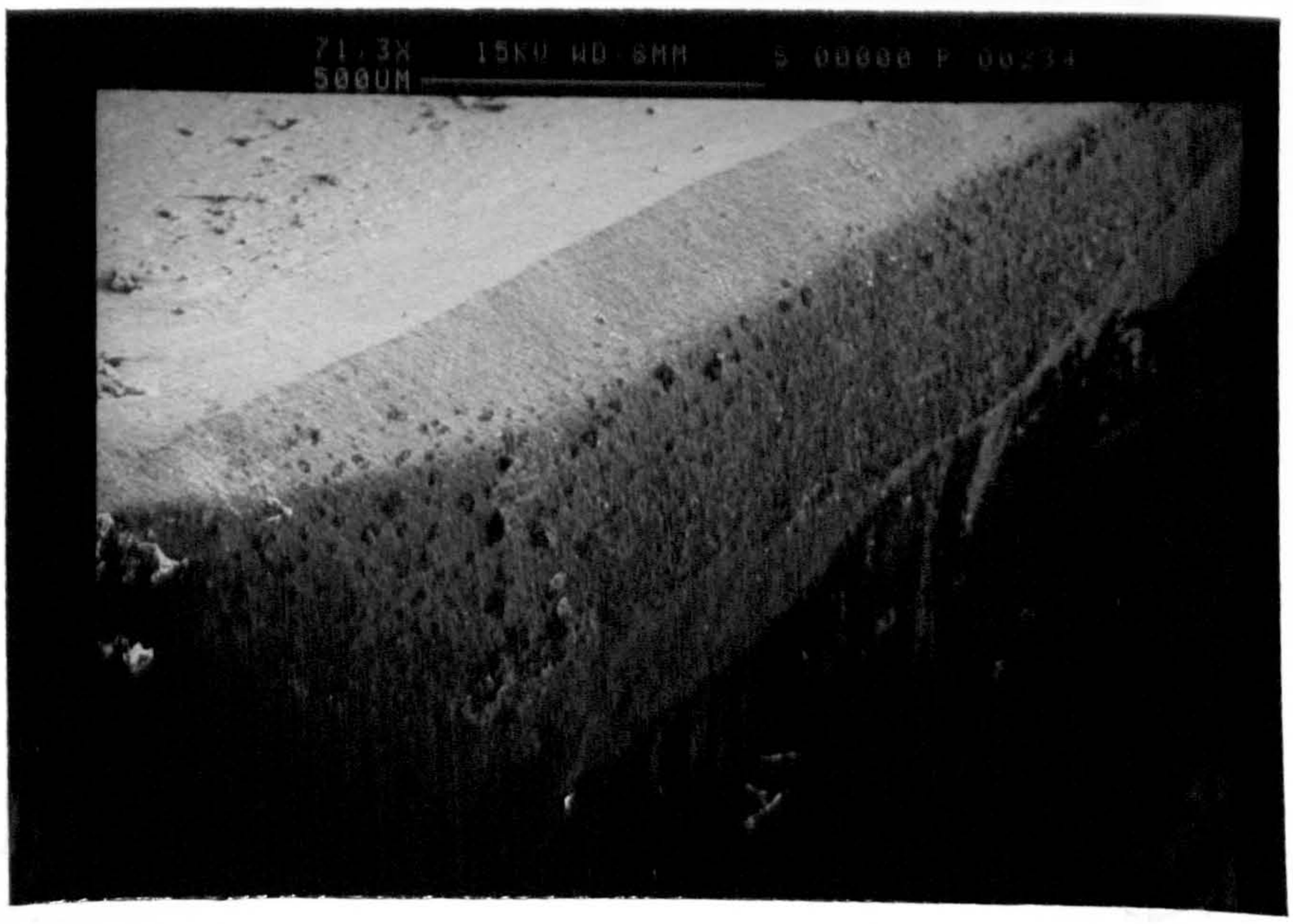

Fig 146. Wear lands of a K20 carbide tool showing plucking near the tool nose. (Speed = 300 m/min, feed = 0.25 mm/rev, cutting time = $3\frac{1}{2}$ min)

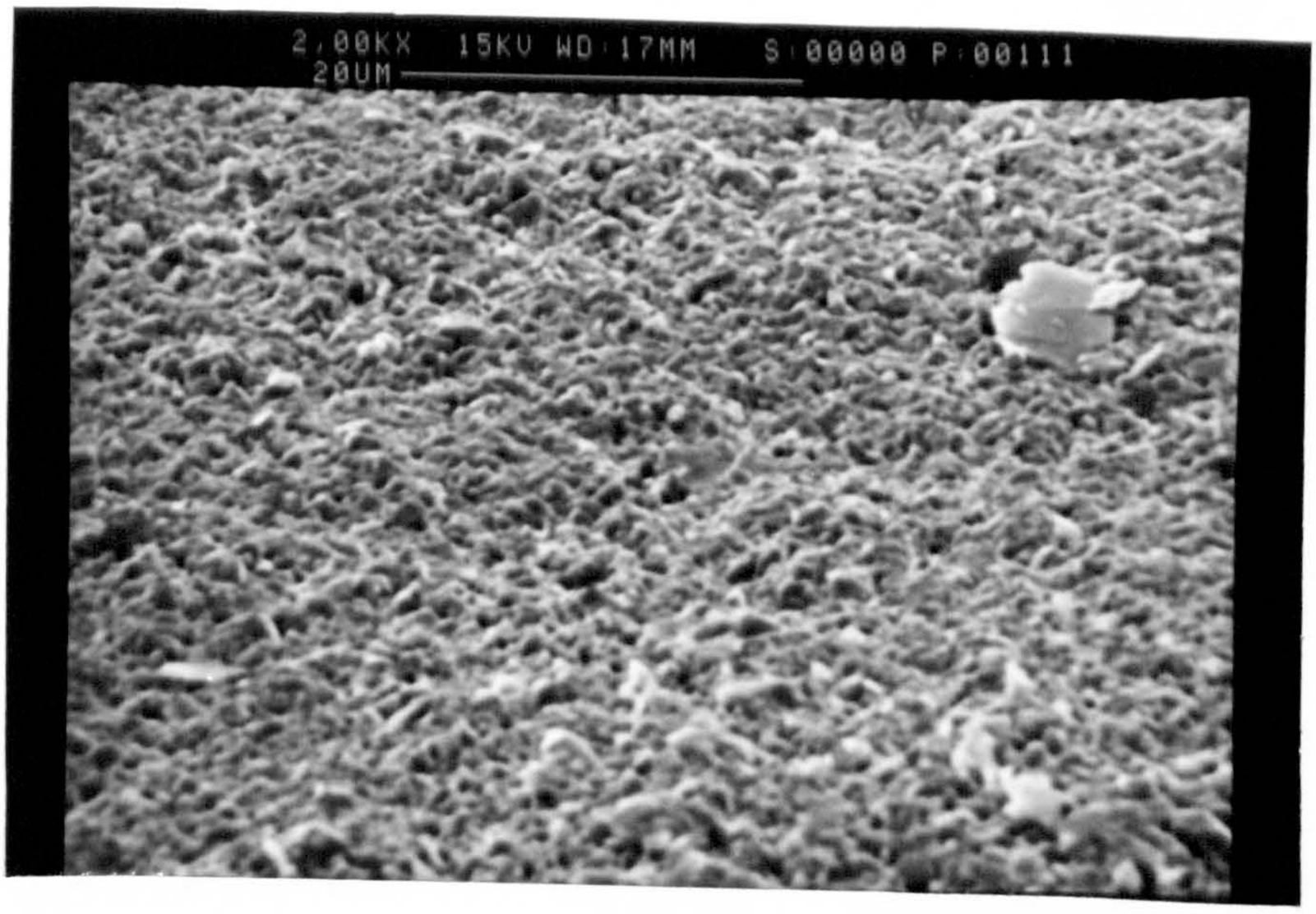

Fig 147. Magnified view of the rake wear land of K20 carbide tool

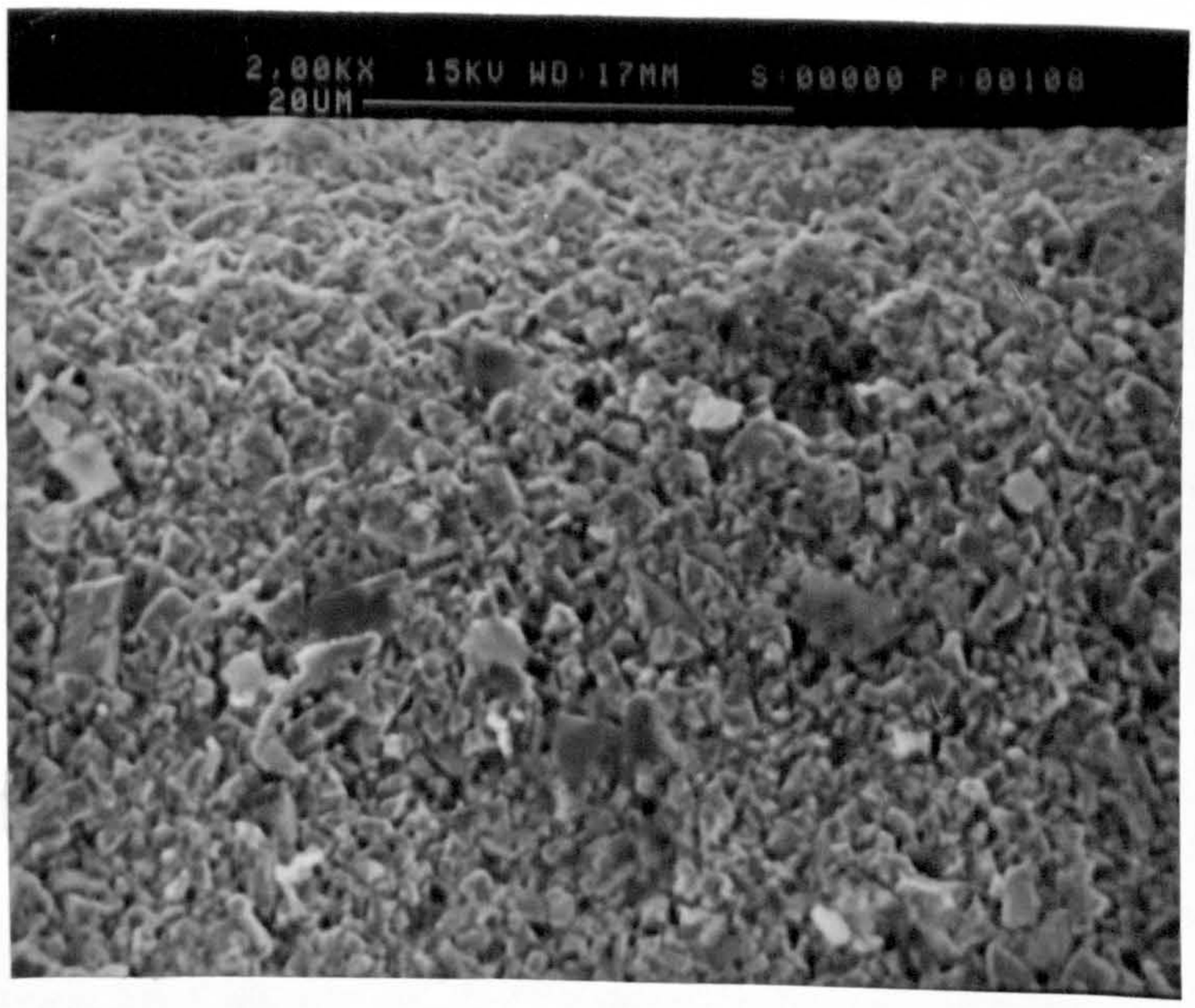

Fig 148. Magnified view of the flank wear land of a K20 carbide tool showing disaggregation of carbides

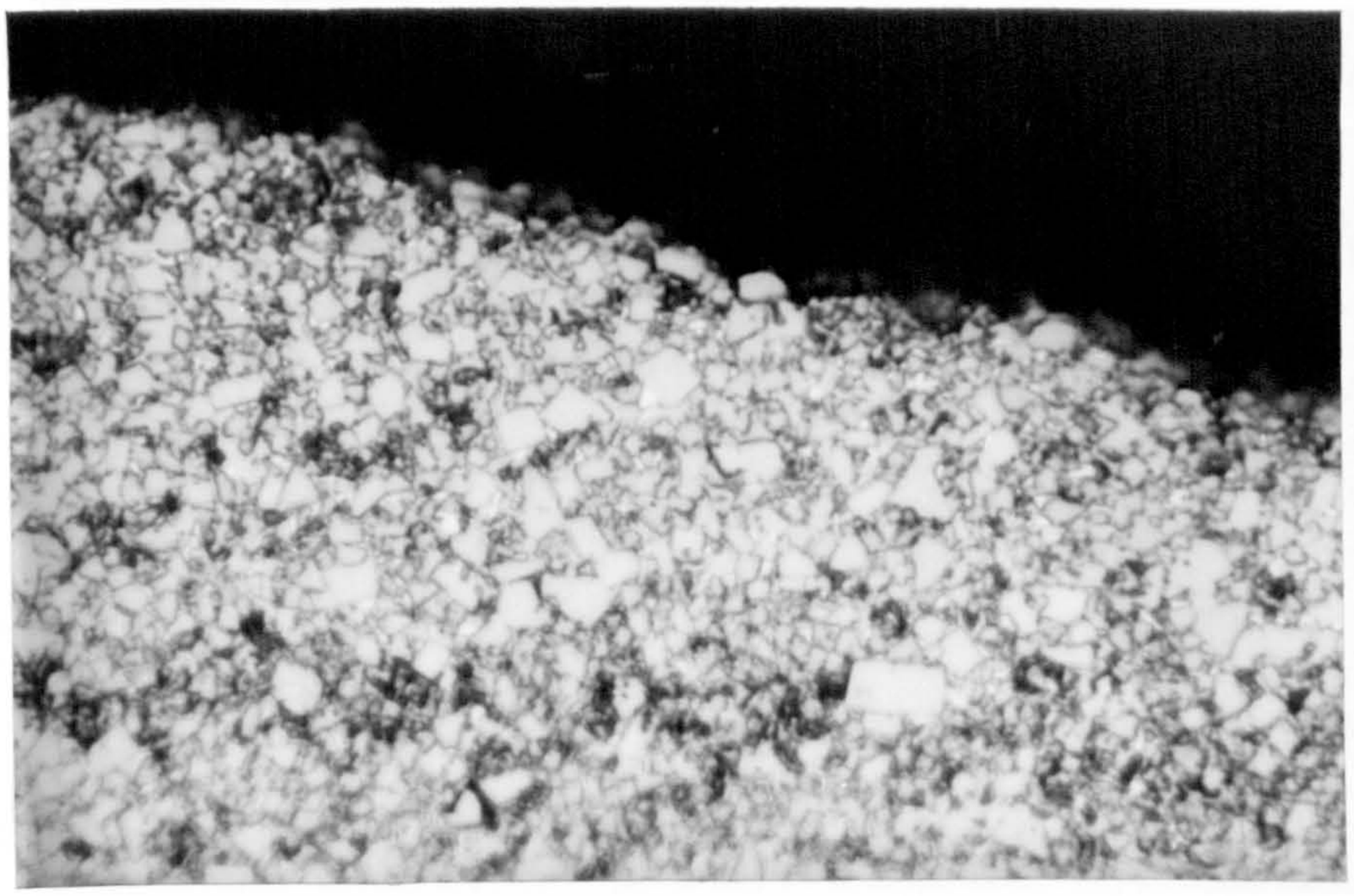

Fig 149. Microstructure of the flank wear land of a K20 carbide showing attrition wear (X1650)

Fig 150. Typical wear pattern of a TiC-coated carbide tool (Speed =150m/min, feed = 0.20 mm/rev, cutting time = 5 min)

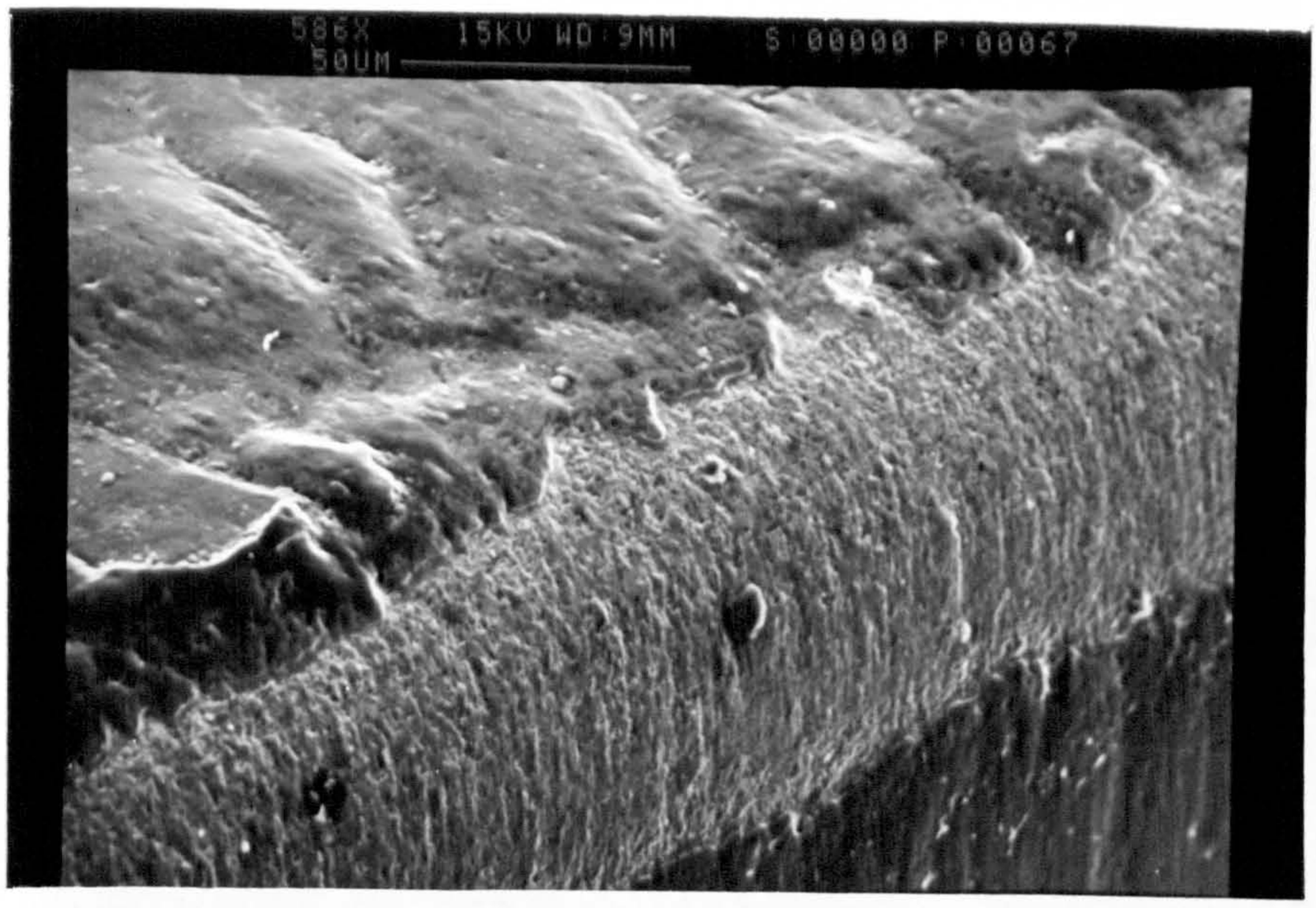

Fig 151. Wear lands of TiC coated carbides after cutting at a low speed (50 m/min) (Feed = 0.20 mm/rev, cutting time = 2 min)

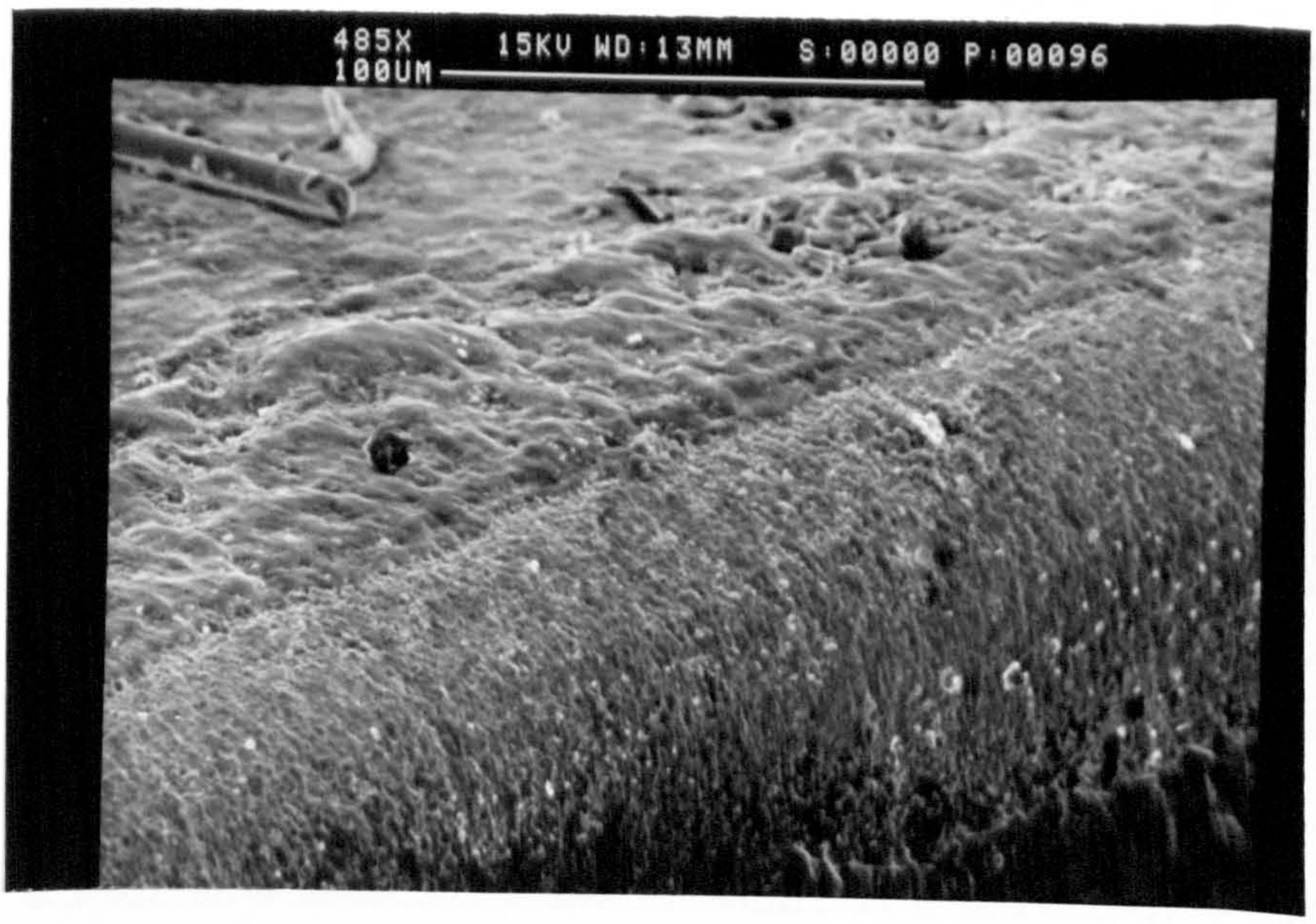

Fig 152. Wear lands on a TiC coated carbide tool after machining at a high speed (250 m/min) (Feed = 0.20 mm/rev, cutting time = 2 min)

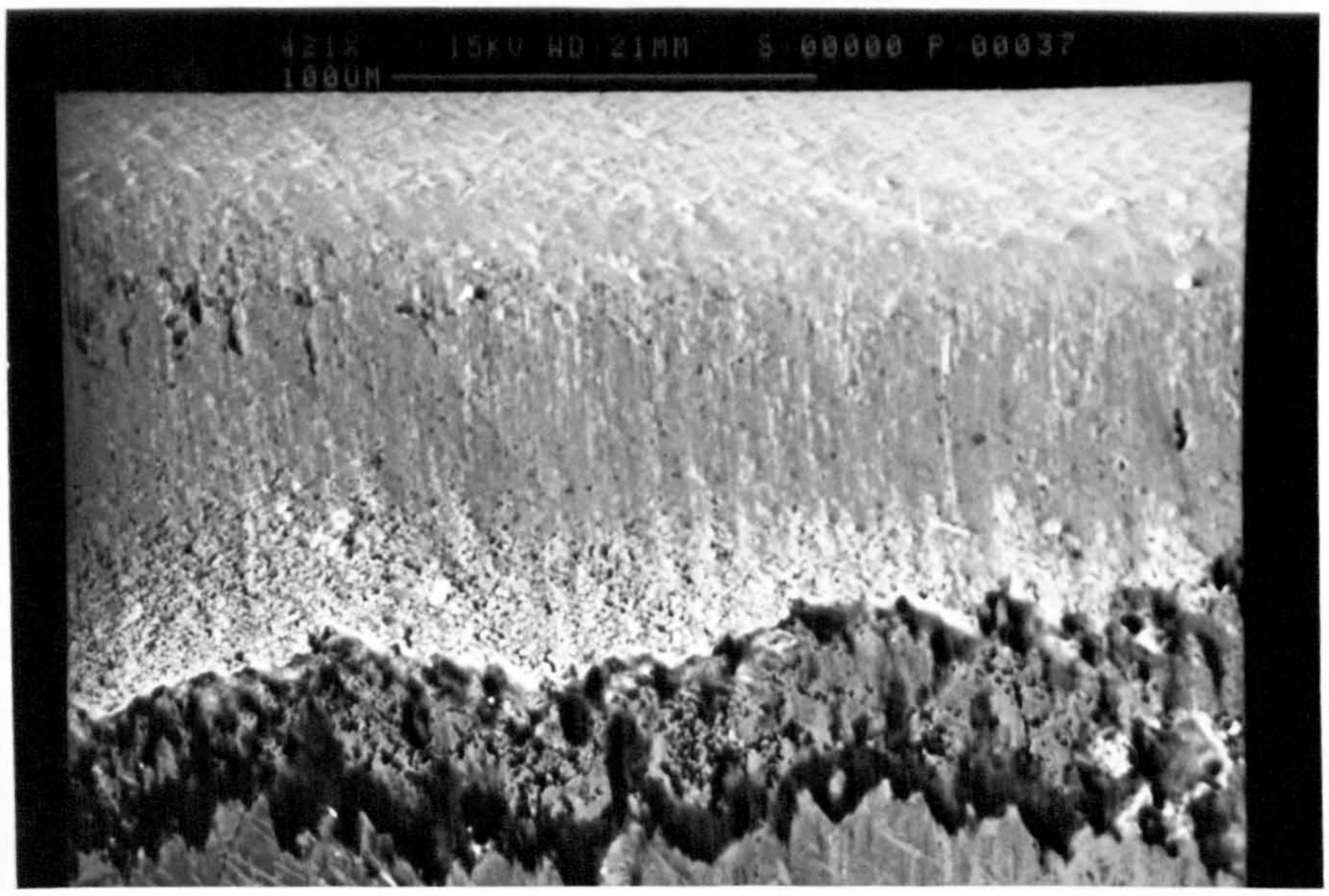

Fig 153. Flank wear land of a TiC coated carbide showing the non-uniform removal of the coating. (Speed =300m/min, feed = 0.20 mm/rev, cutting time = 5 min)

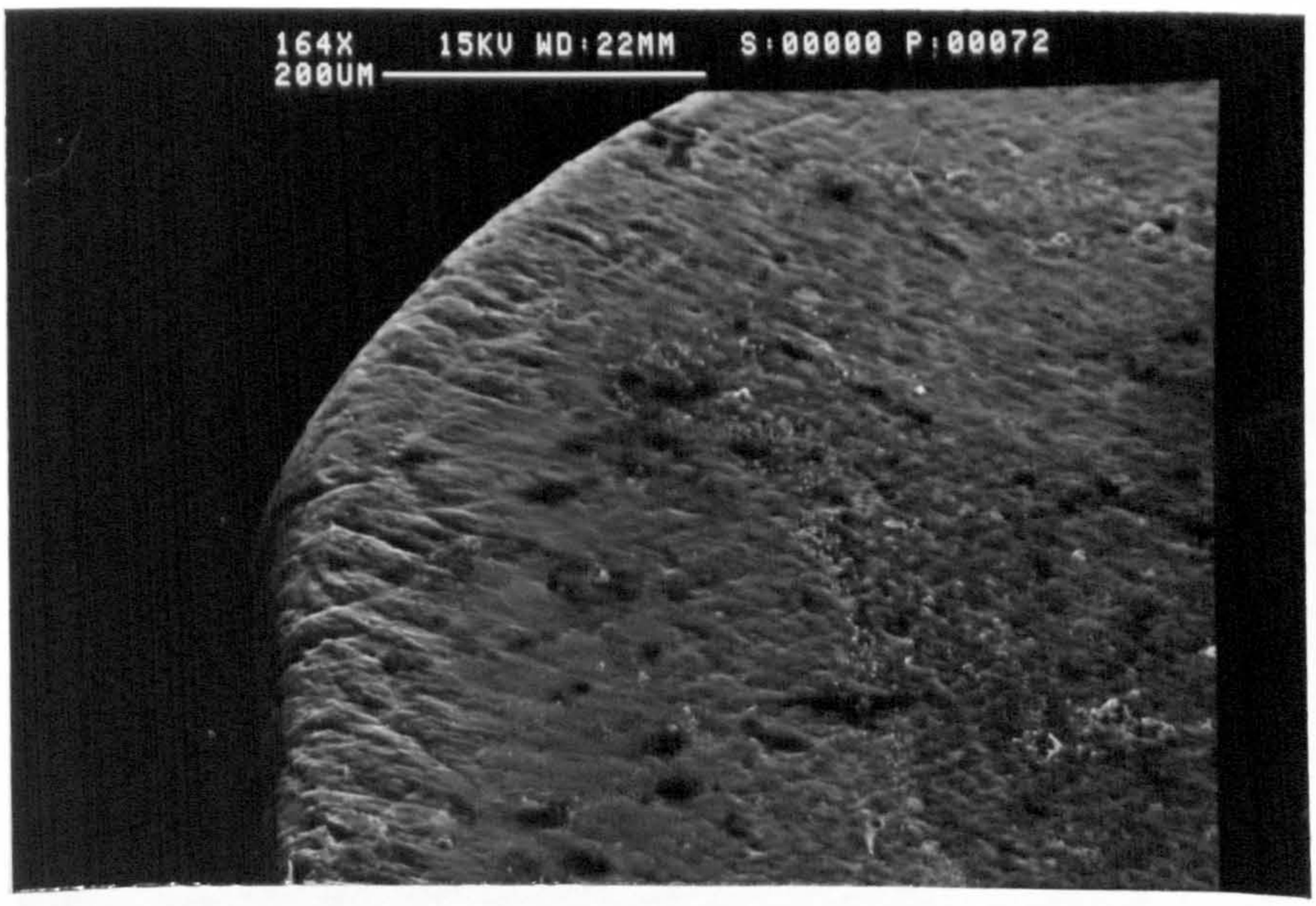

Fig 154. Rake face of a worn TiC coated carbide showing discrete plastic deformation. (Speed = 50 m/min, feed = 0.20 mm/rev, cutting time = 7 min)

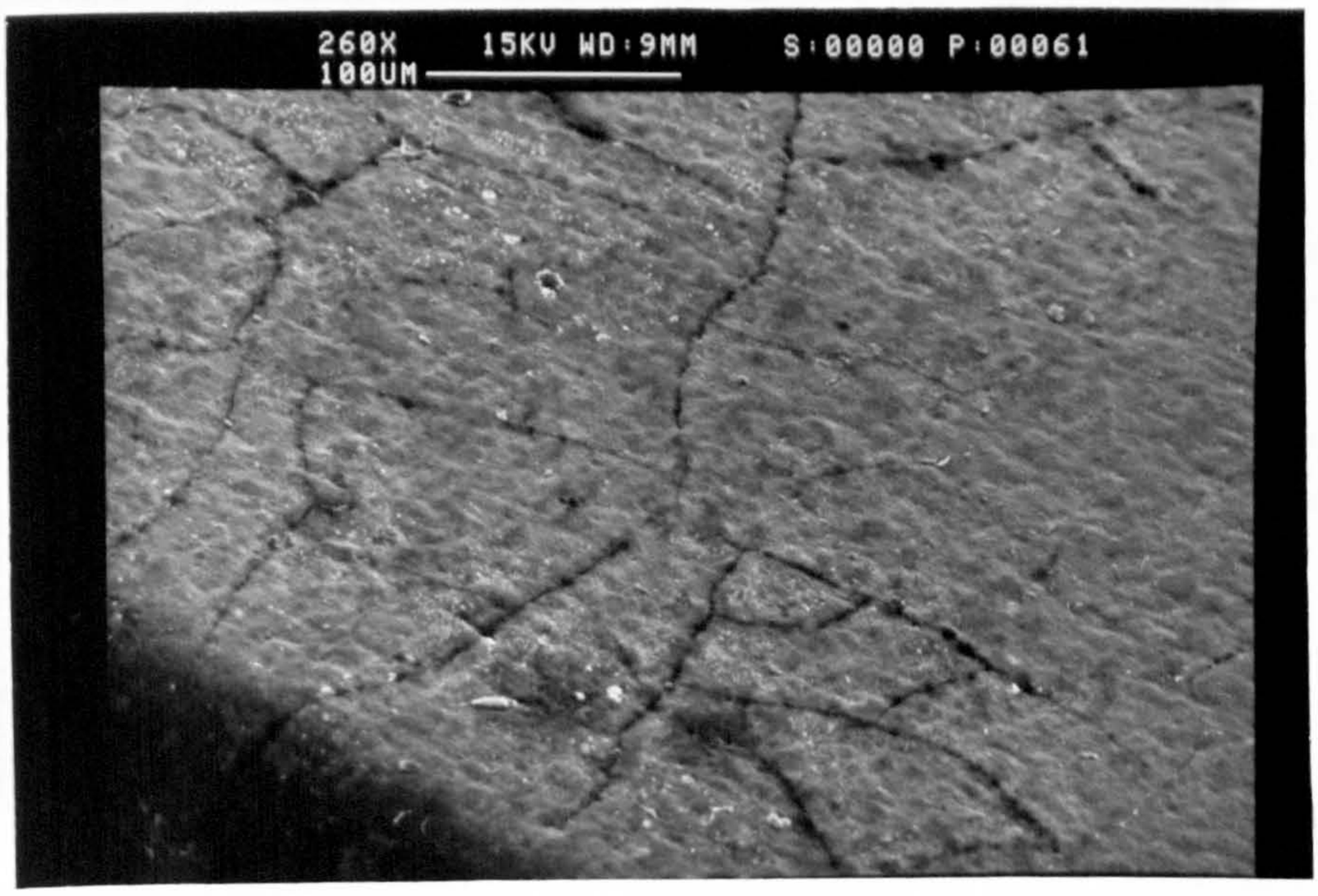

Fig 155. Rake face of a TiC coated carbide near the secondary cutting edge showing crack propagation

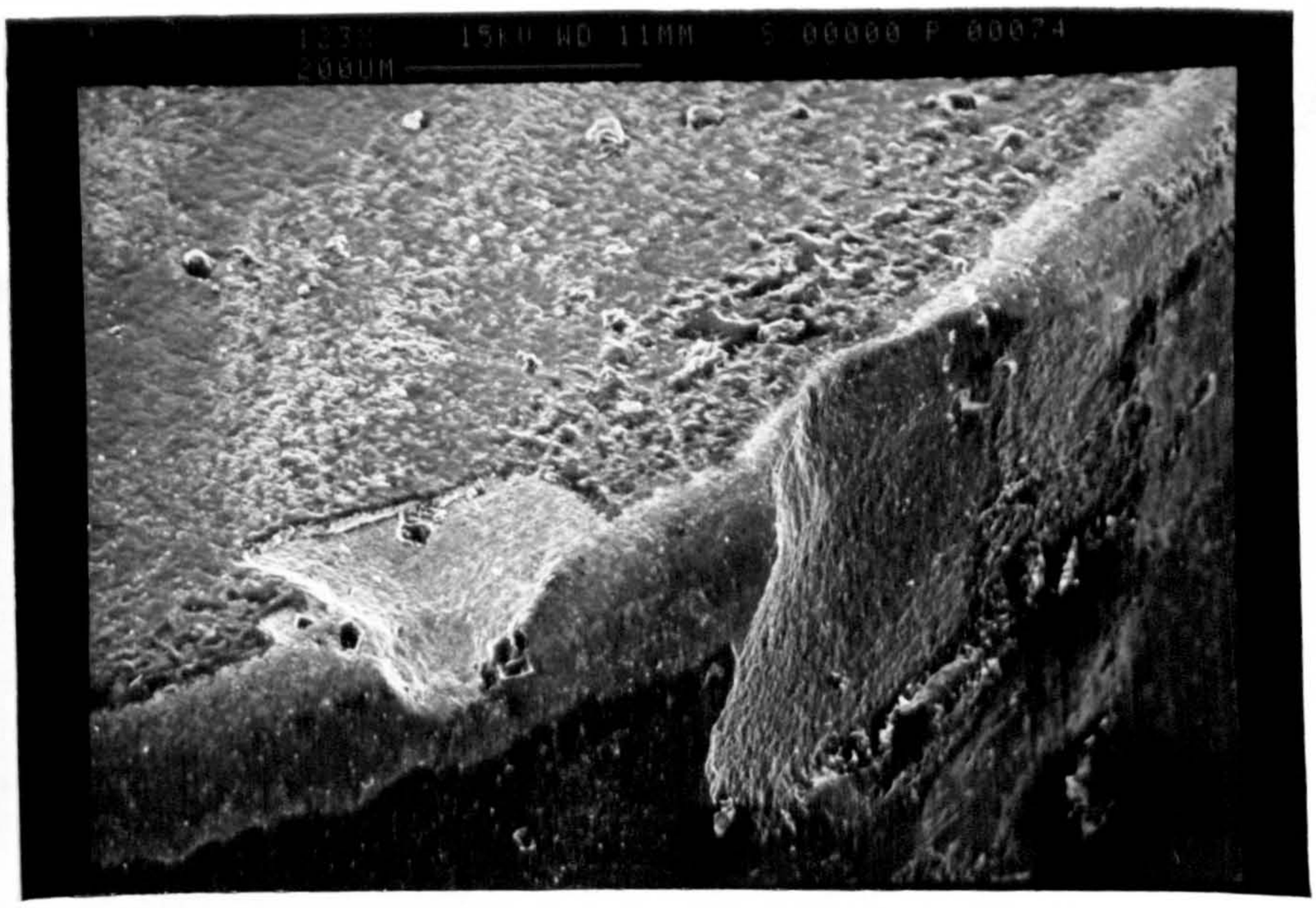

Fig 156. Flaking of the coating near the nose of a TiC-coated carbide tool. (Speed = 250 m/min, feed = 0.10 mm/rev, cutting time = 4 min)

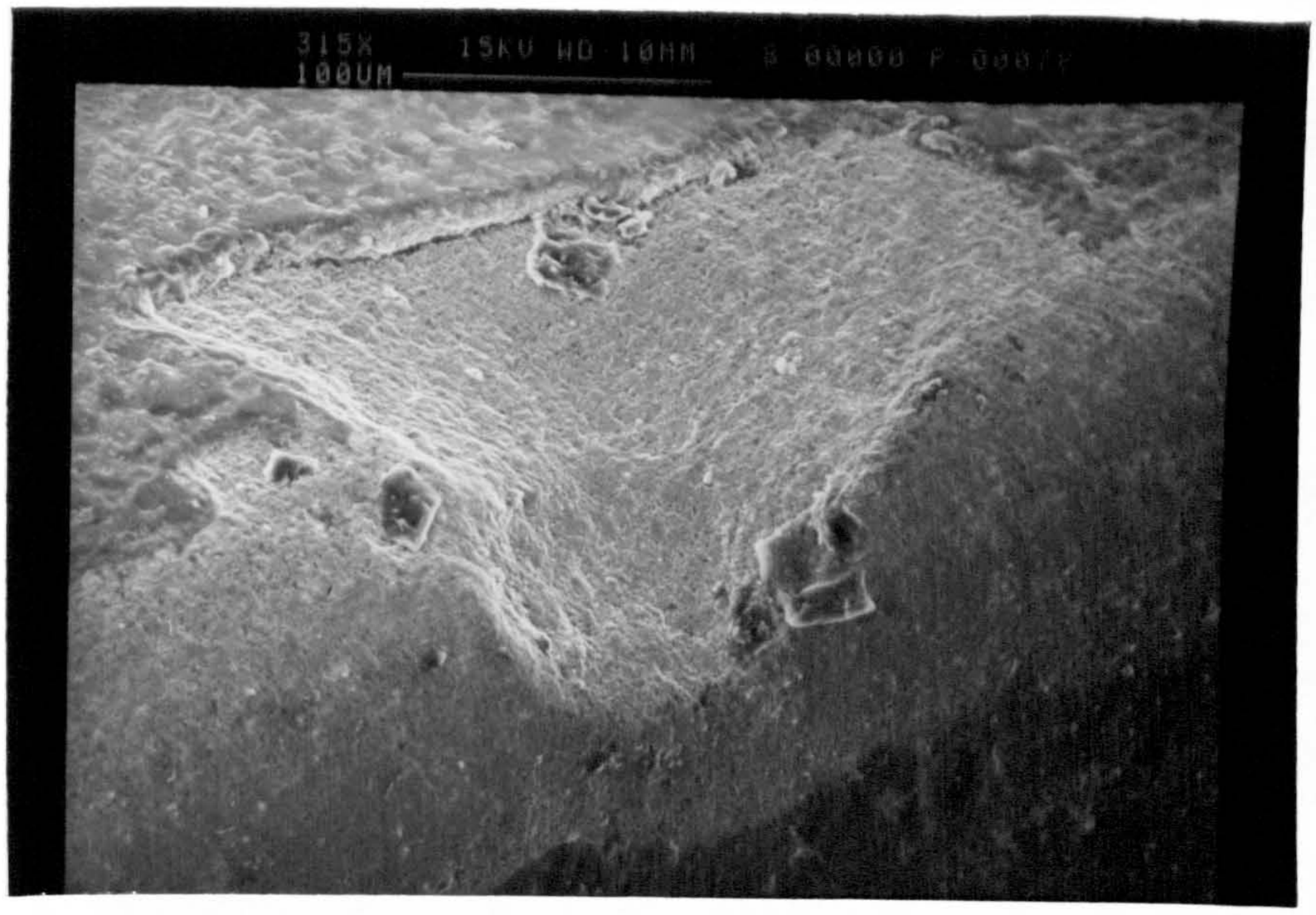

Fig 157. Enlarged view of flaked area shown in Fig 156.

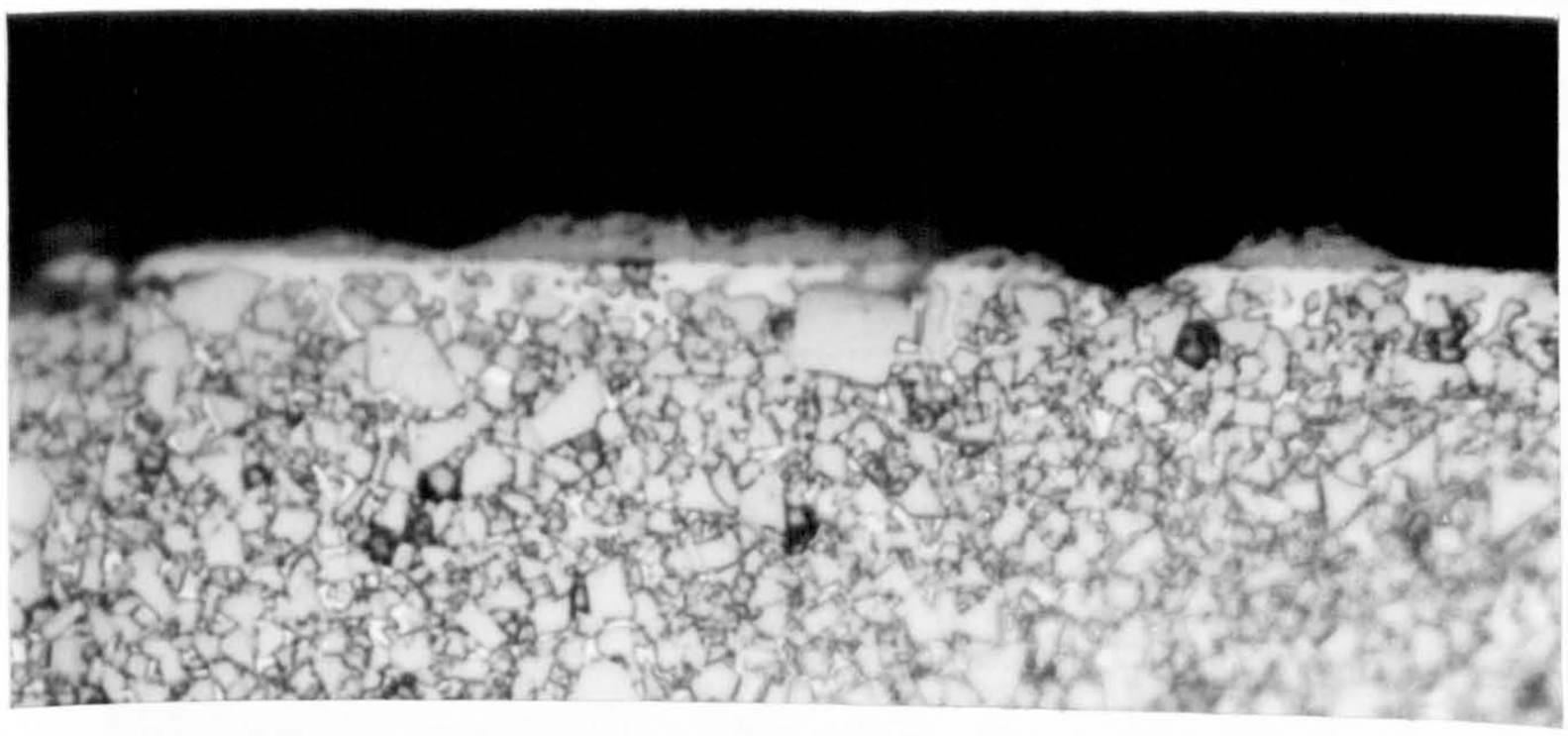

Fig 158. Microstructure of the flank wear land on a TiC-coated carbide tool (X1650)

Fig 159. Typical wear pattern of a triple-coated carbide tool. (Speed = 250 m/min, feed = 0.20 mm/rev, cutting time = 7 min)

Fig 160. Wear concentration on the nose area of a triple-coated carbide tool

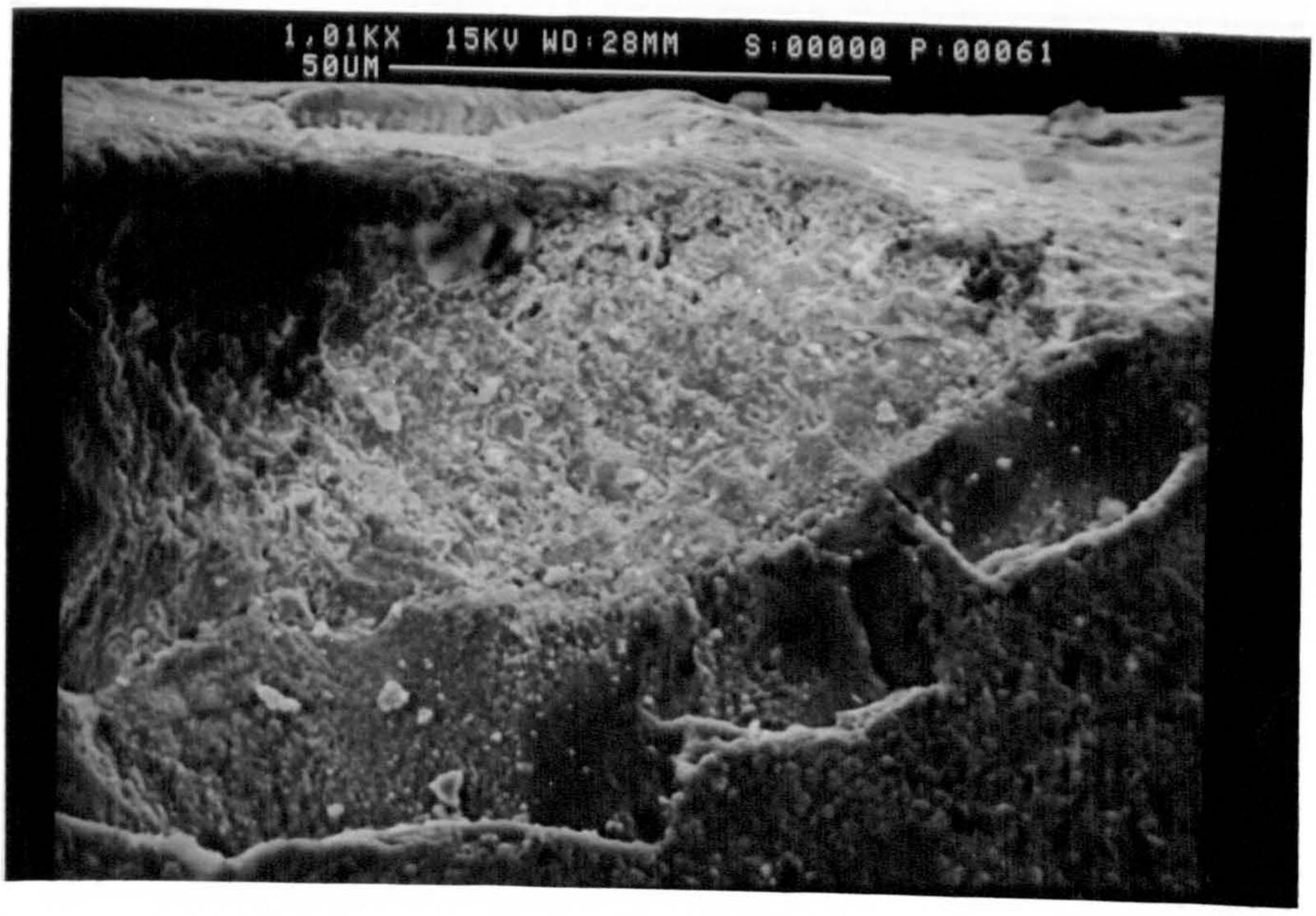

Fig 161. Enlarged view of fractured area near the secondary cutting edge of a triple-coated carbide tool

Fig 162. Nose area of a worn triple-coated carbide tool after machining at a speed of 250 m/min

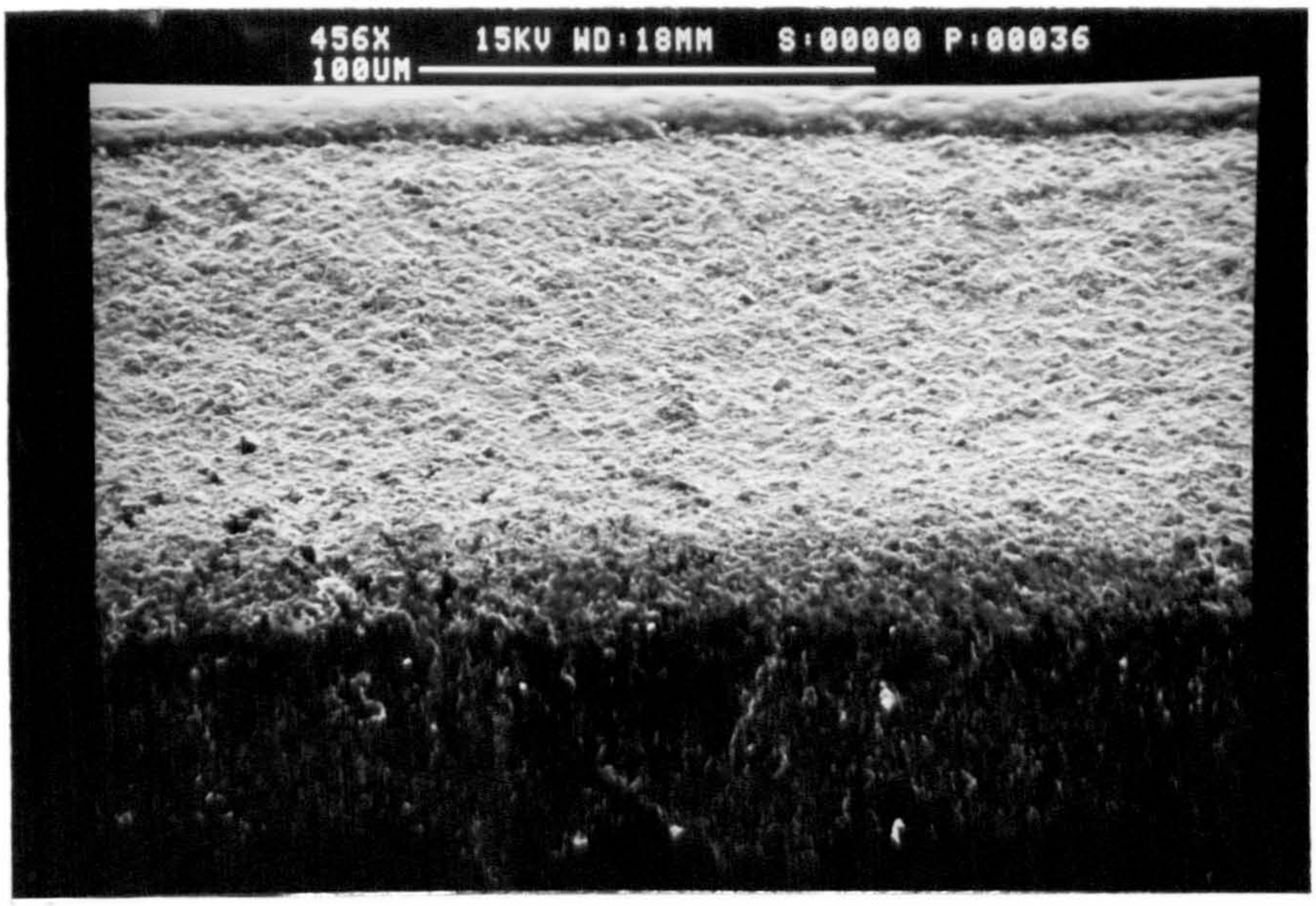

Fig 163. Wear lands of triple-coated carbide tool at the middle of the depth of cut showing rough worn surfaces

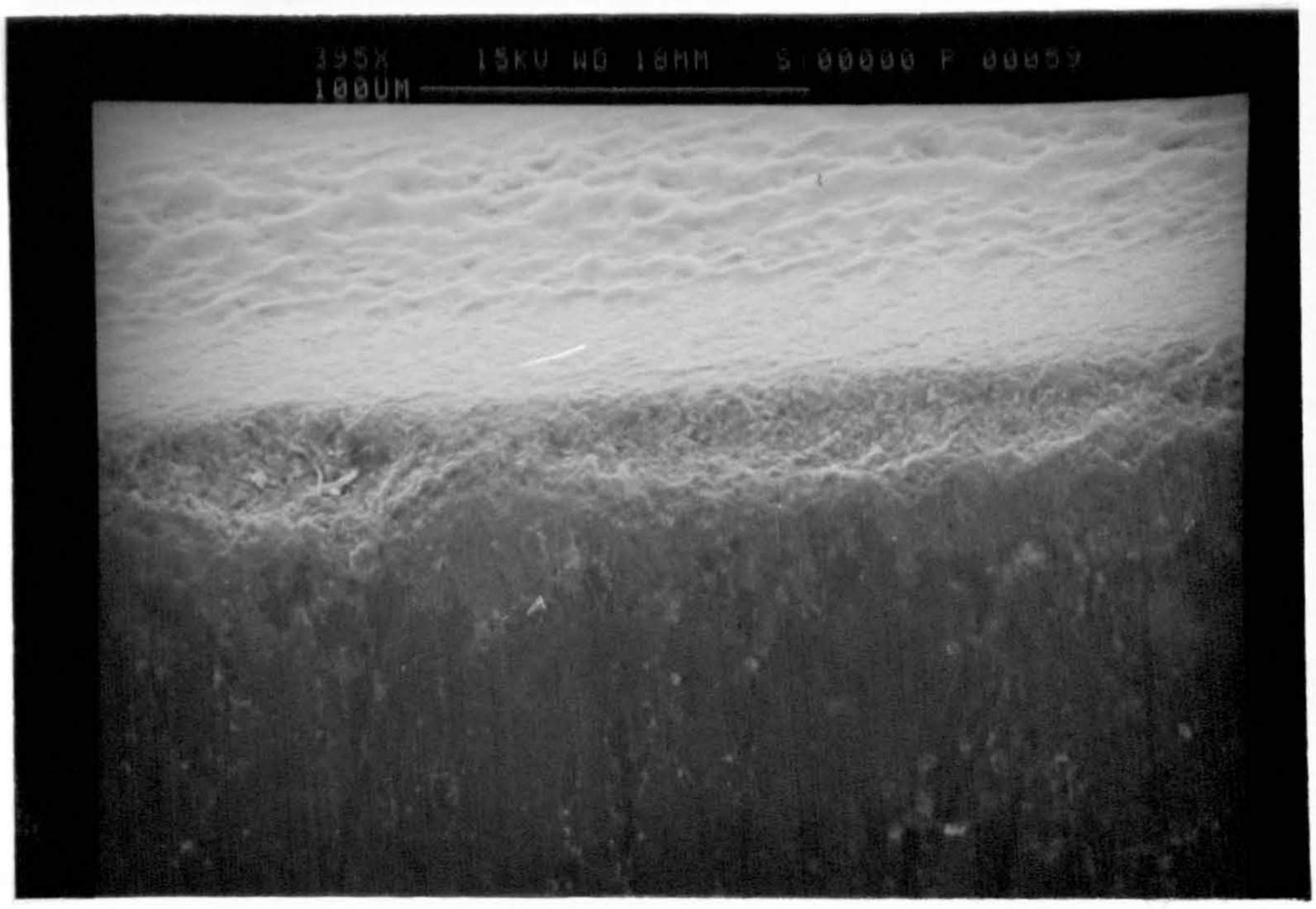

Fig 164. Chipping at the cutting edge of a triple-coated carbide tool

Fig 165. Rake face wear land on a worn triple-coated carbide showing a rough surface

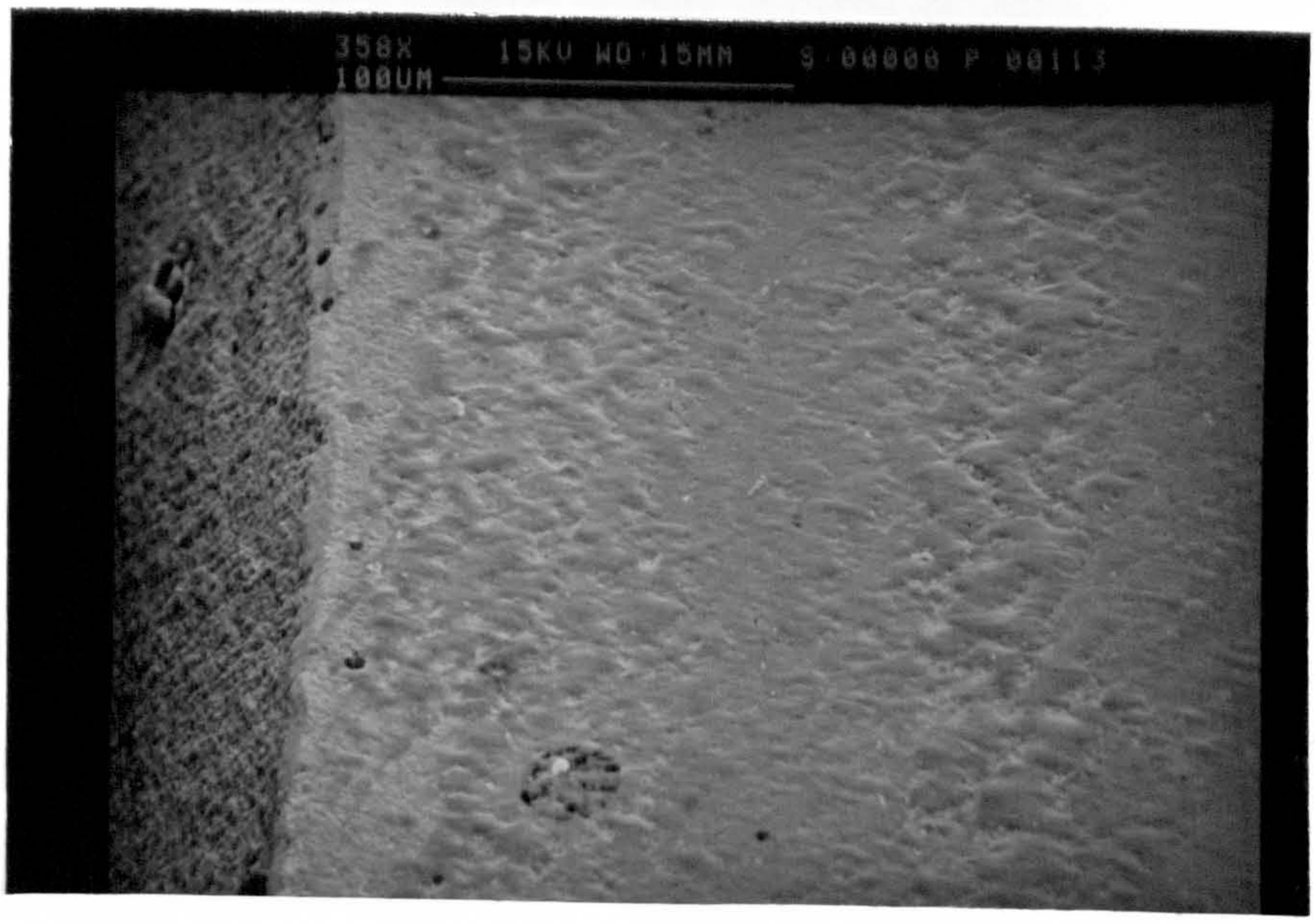

Fig 166. Rake face of a worn triple-coated carbide tool showing the plastically deformed coating. (Speed = 400 m/min, feed = 0.25 mm/rev, cutting time = 5 min)

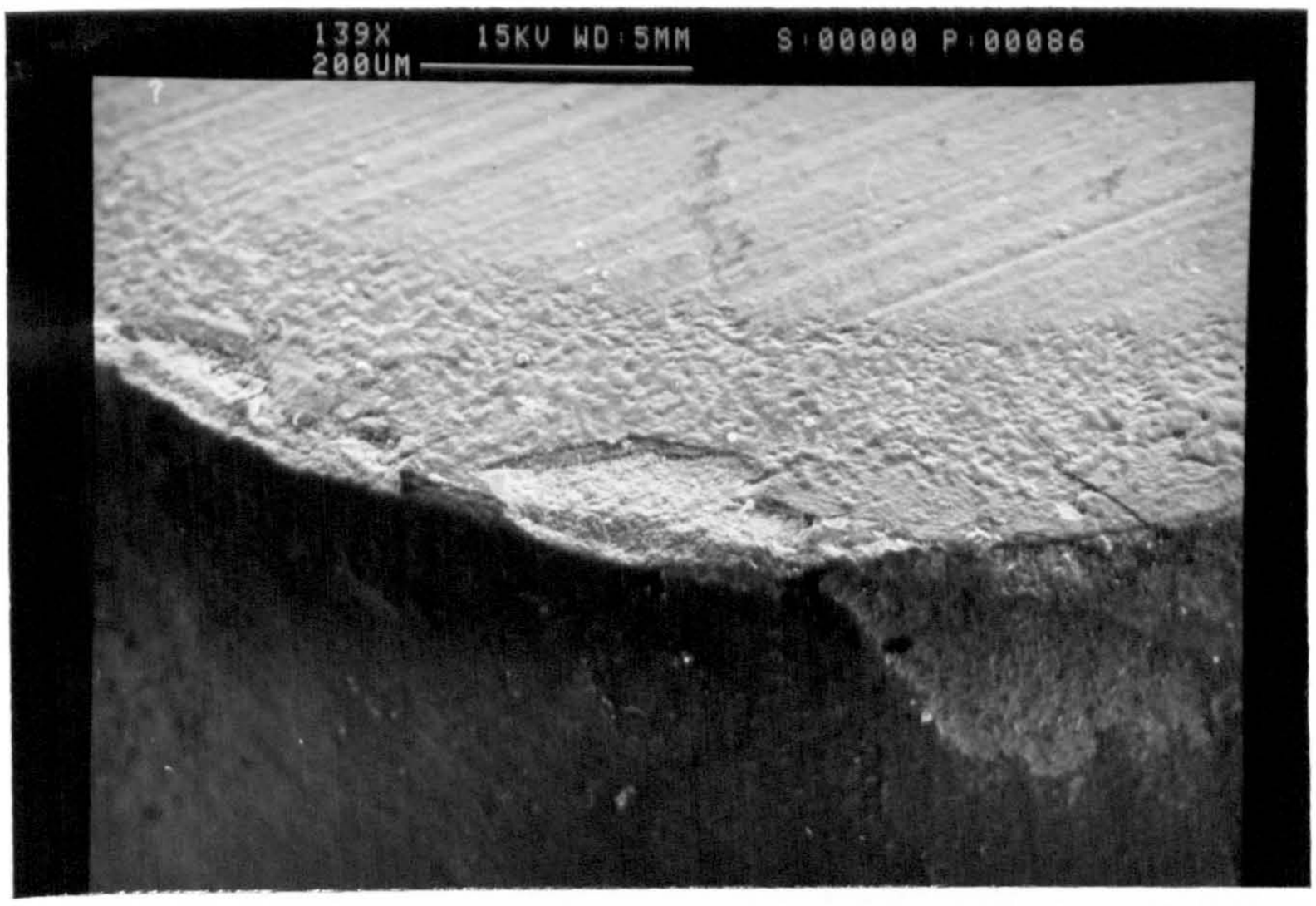

Fig 167. Nose area of a worn triple-coated carbide tool showing the flaking of the coating. (Speed = 400 m/min, feed = 0.25 mm/rev, cutting time = 5 min)

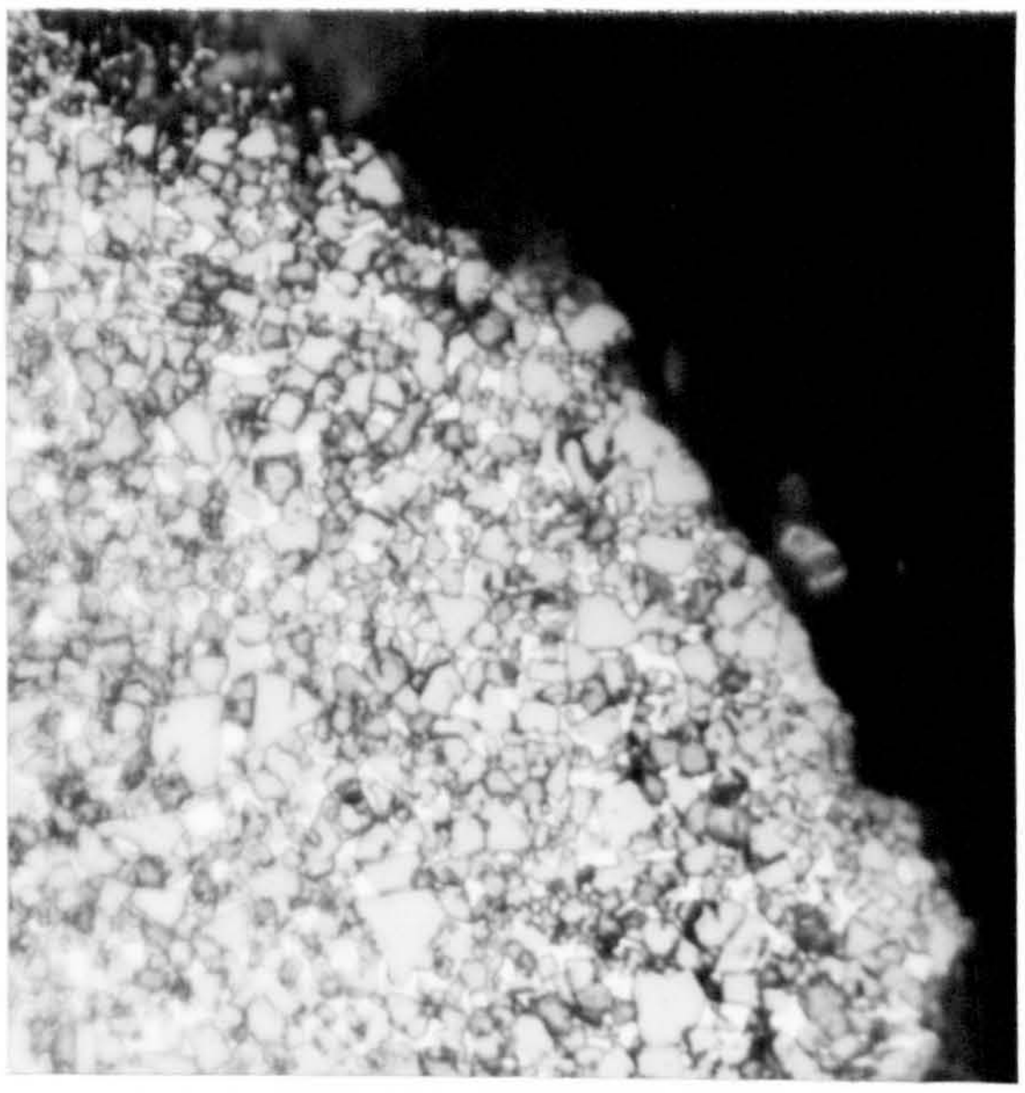

Fig 168. Microstructure of the flank wear land on a triple-coated carbide tool showing attrition wear (X1650)

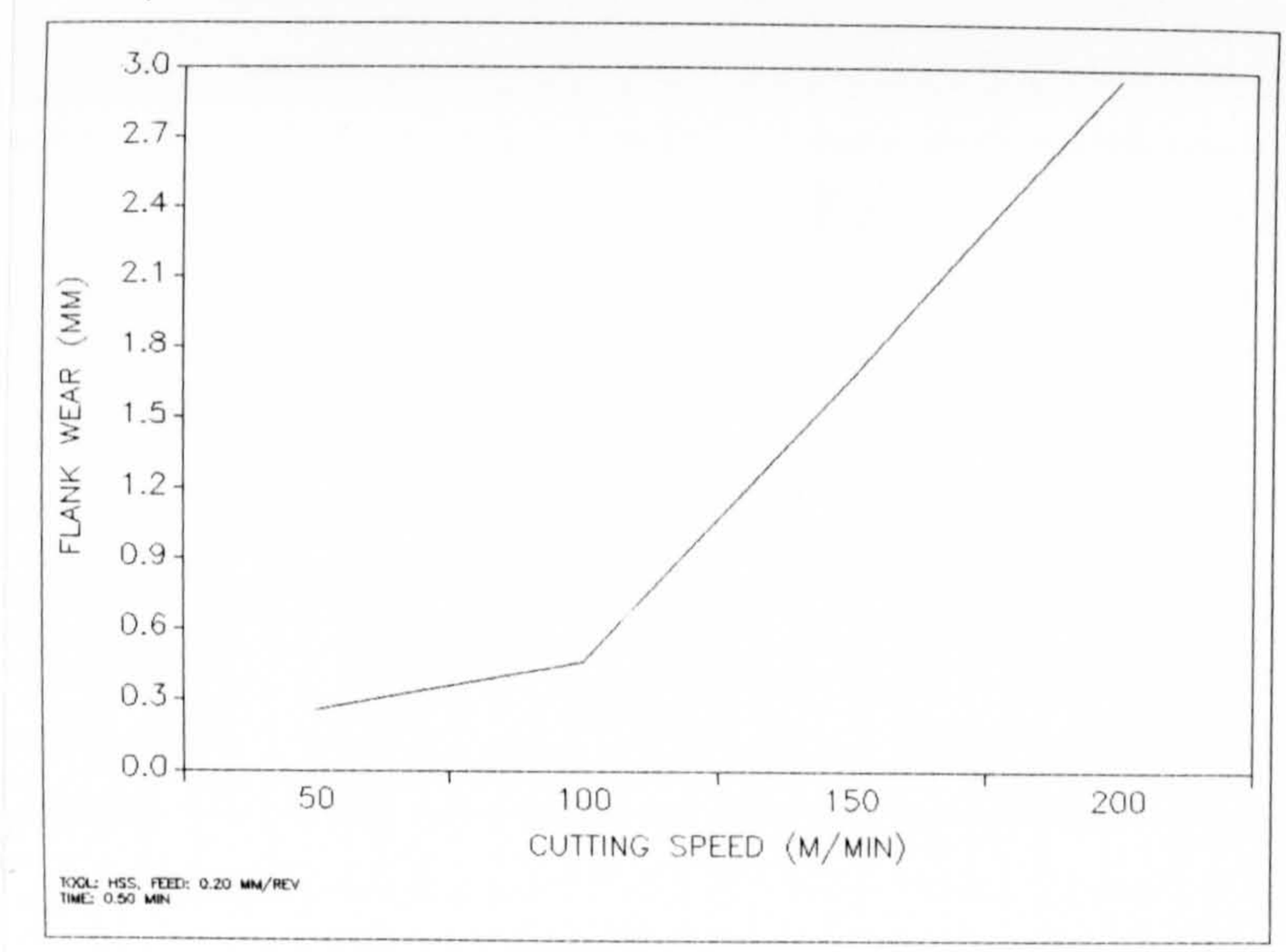

Fig 169. Flank wear versus cutting speed when machining GFRP (HSS tool, feed = 0.20 mm/rev, cutting time = $\frac{1}{2}$ min)

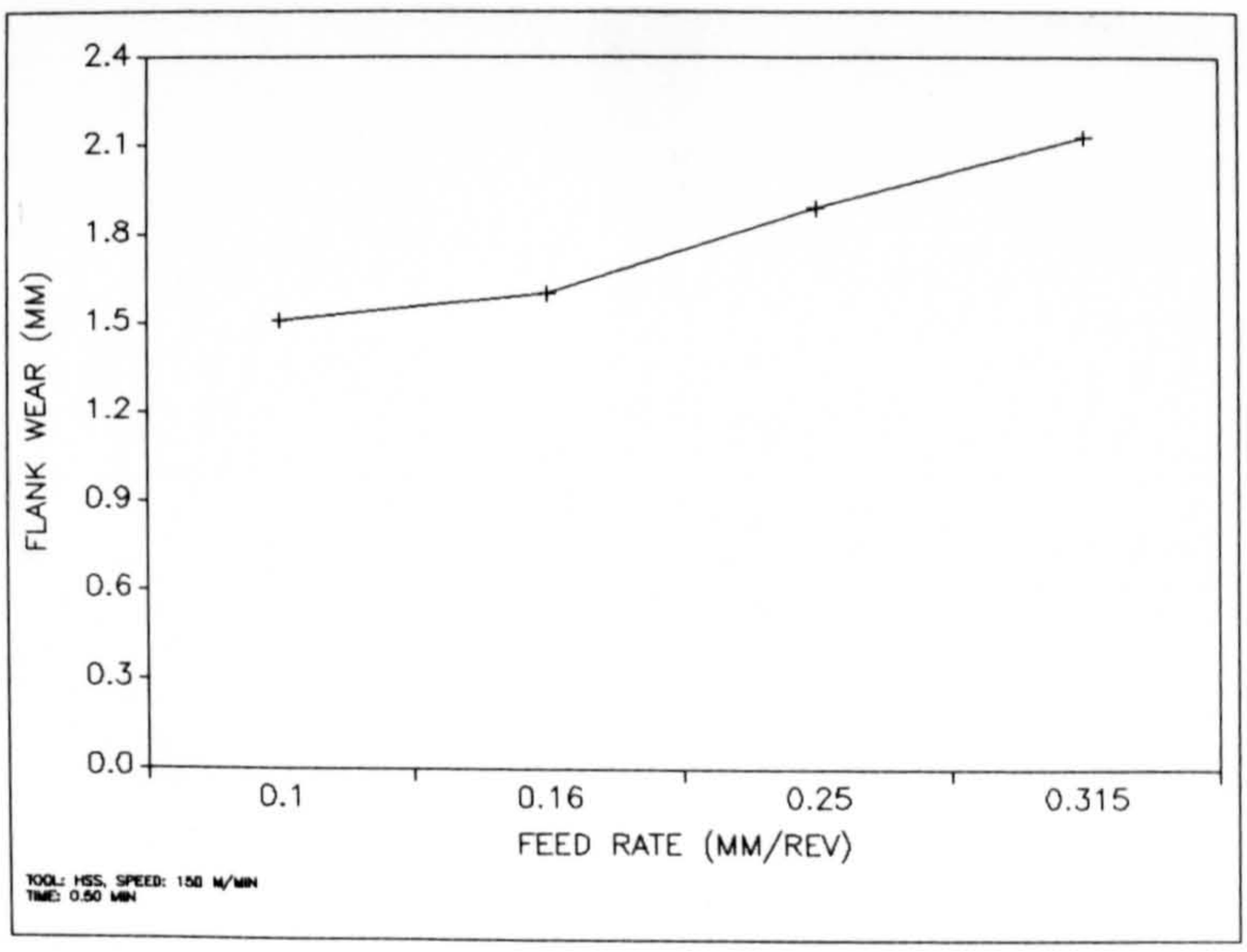

Fig 170. Flank wear versus feed rate when machining GFRP (HSS tool, speed = 150 m/min, cutting time = $\frac{1}{2}$ min)

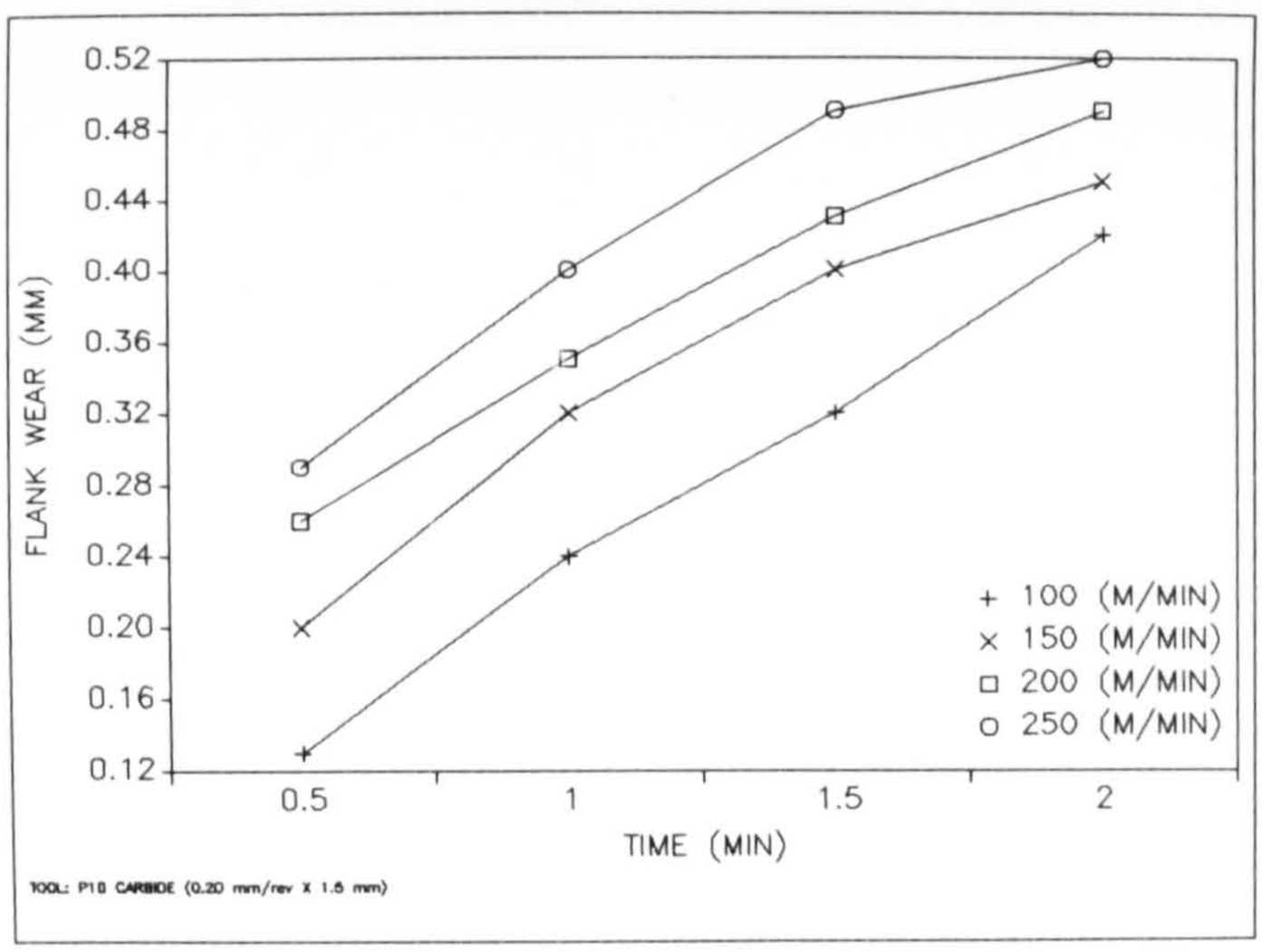

Fig 171. Flank wear versus cutting time when machining GFRP (P10 carbide, feed rate = 0.20 mm/rev)

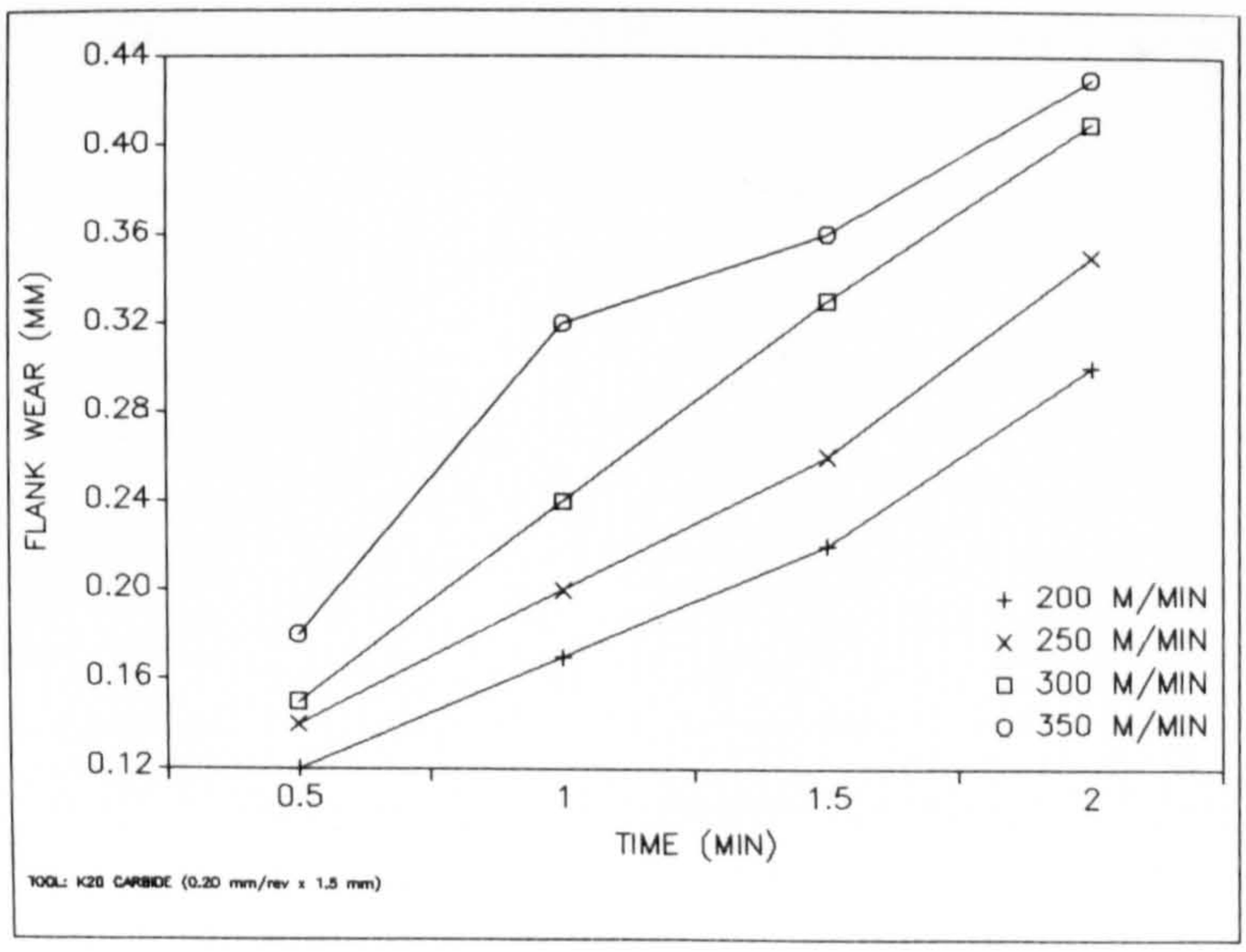

Fig 172. Flank wear versus cutting time when machining GFRP (K20 carbide, feed rate = 0.20 mm/rev)

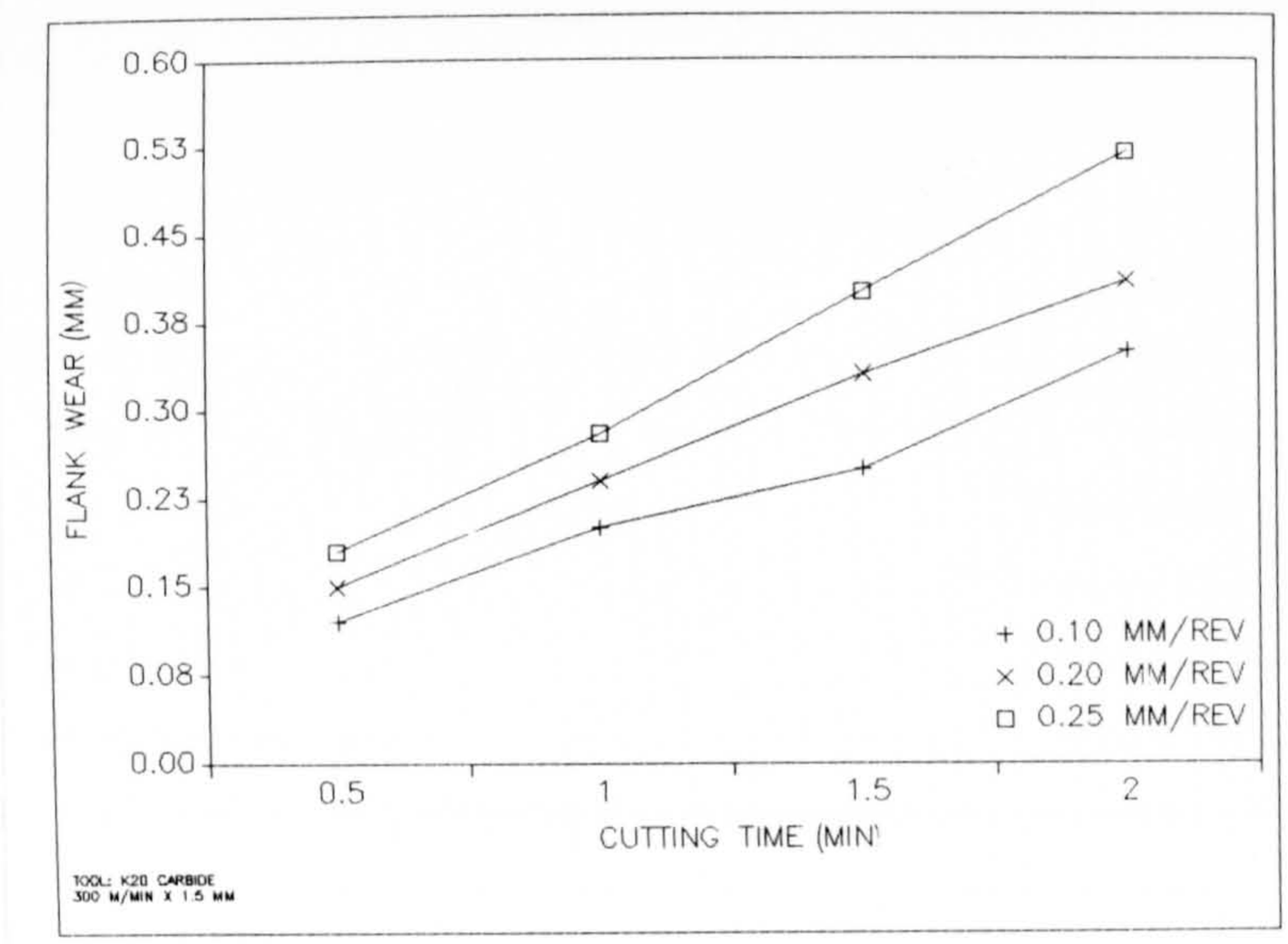

Fig 173. Flank wear versus cutting time when machining GFRP (K20 carbide, speed = 300 m/min)

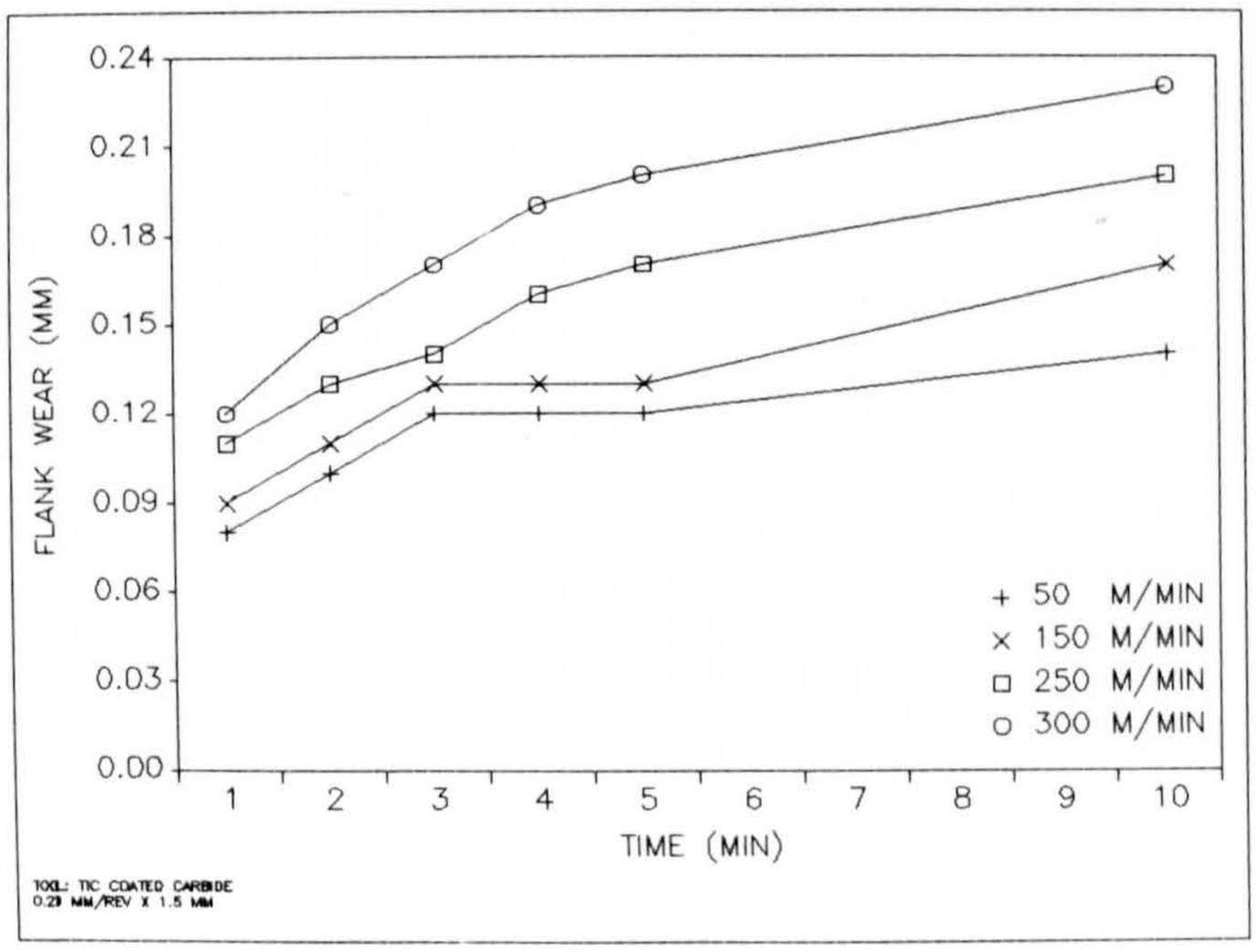

Fig 174. Flank wear versus cutting time when machining GFRP (TiC-coated carbide, feed rate = 0.20 mm/rev)

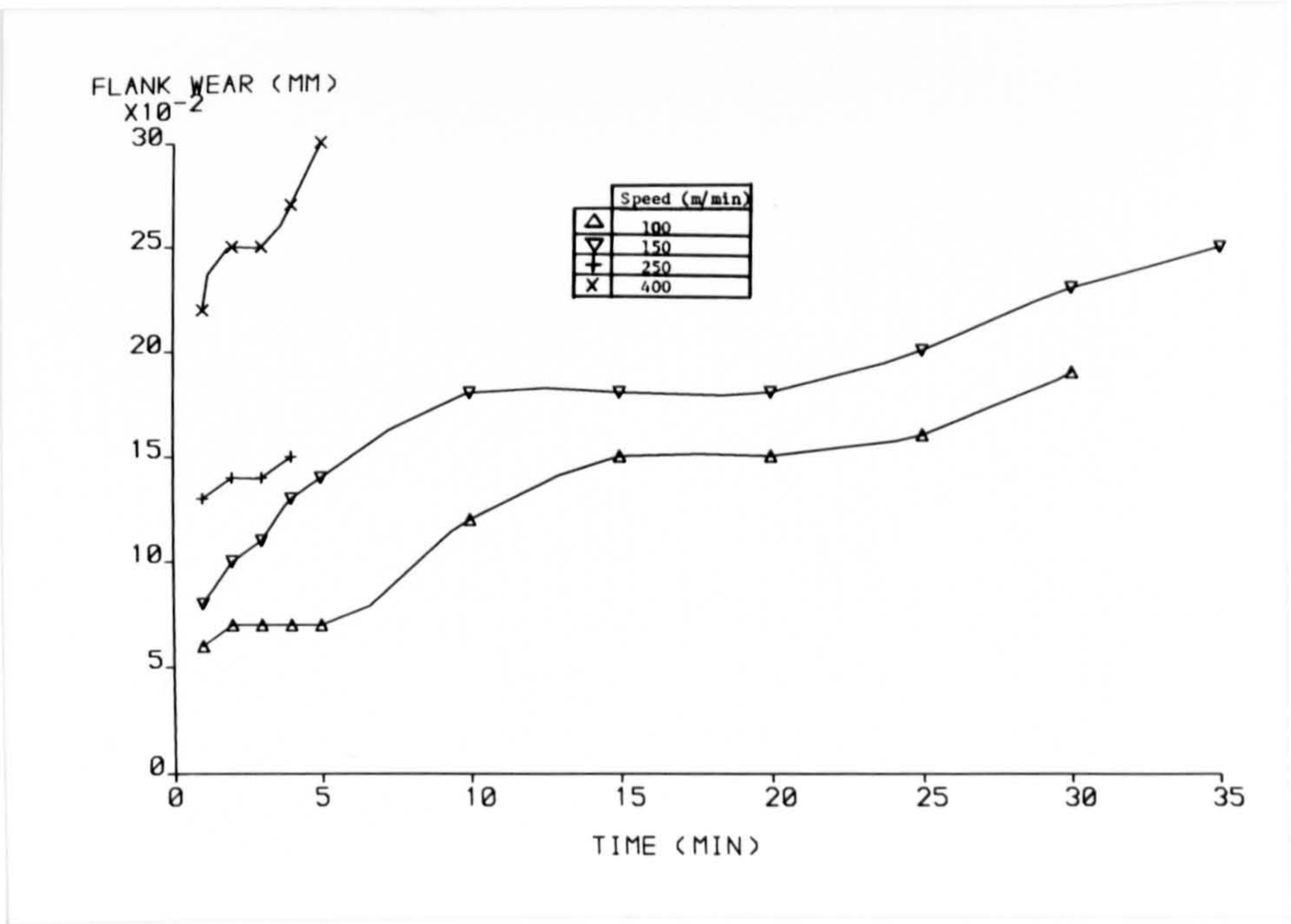

Fig 175. Flank wear versus cutting time when machining GFRP (Triple-coated carbide, feed rate = 0.20 mm/rev)

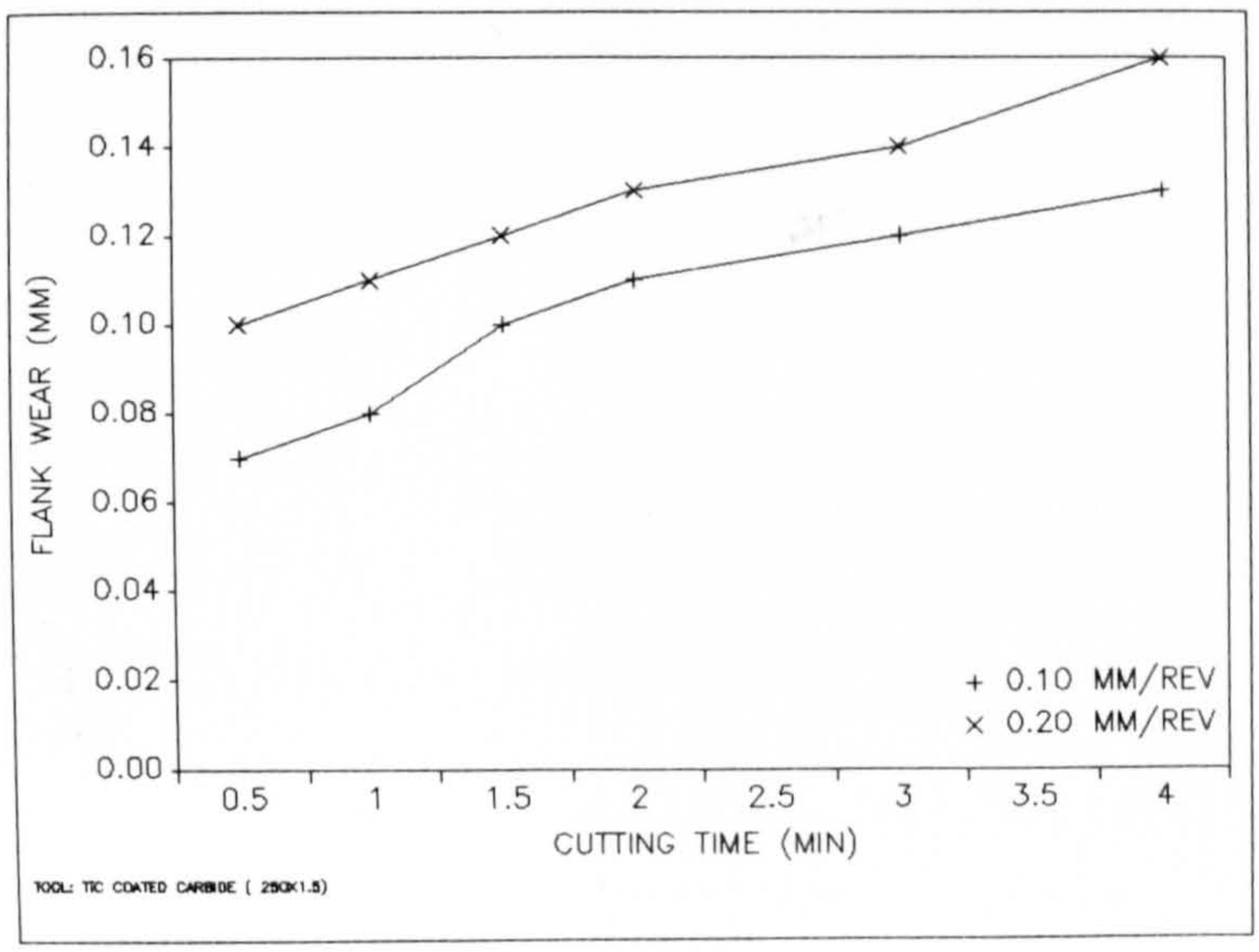

Fig 176. Flank wear versus cutting time when machining GFRP (TiC-coated carbide, speed = 250 m/min)

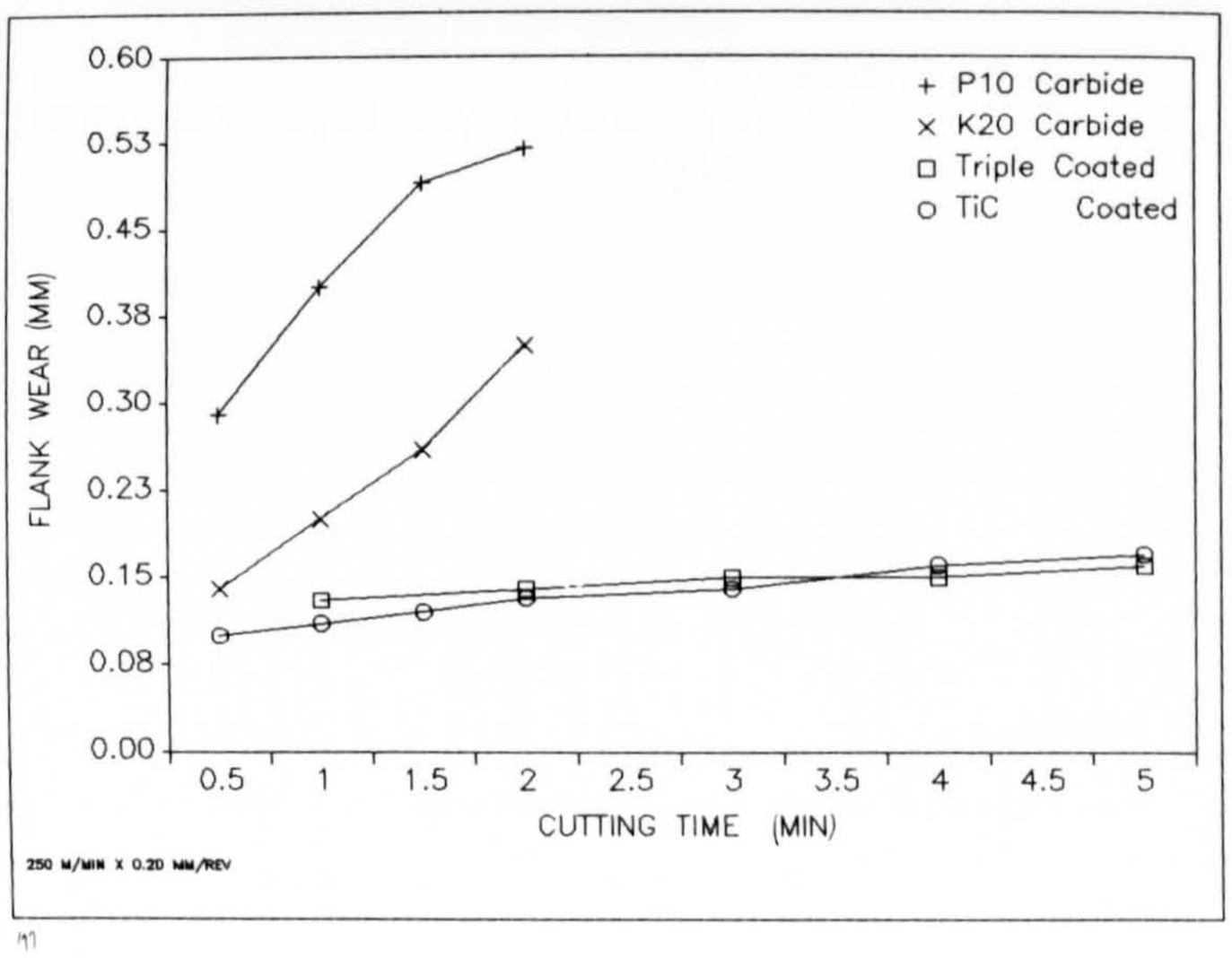

Fig 177. Flank wear versus cutting time when machining GFRP with various tool materials. (Speed = 250 m/min, feed rate = 0.20 mm/rev)

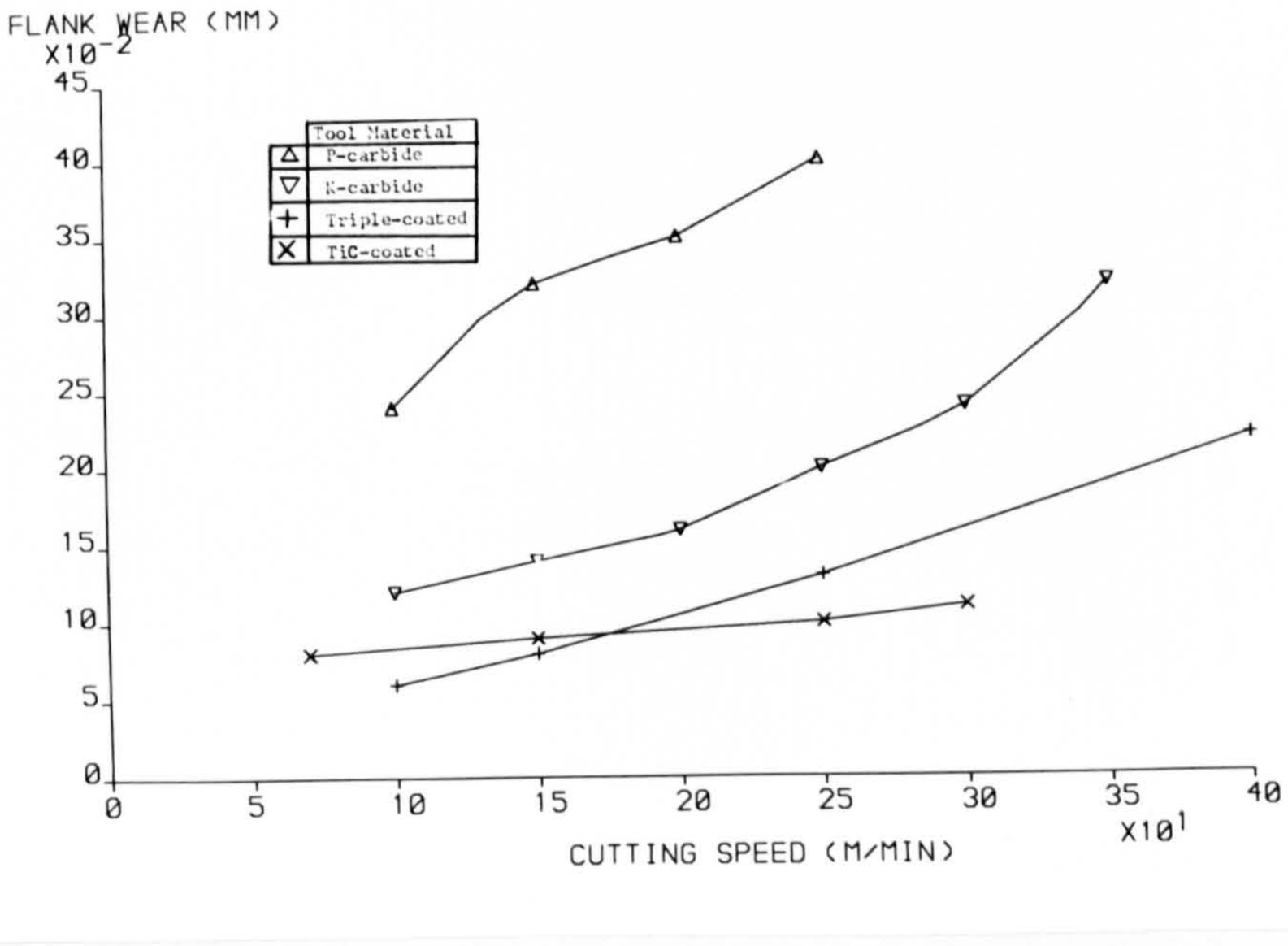

Fig 178. Flank wear versus cutting speed when machining GFRP with various tool materials. (Feed rate = 0.20 mm/rev, cutting time = 1 min)

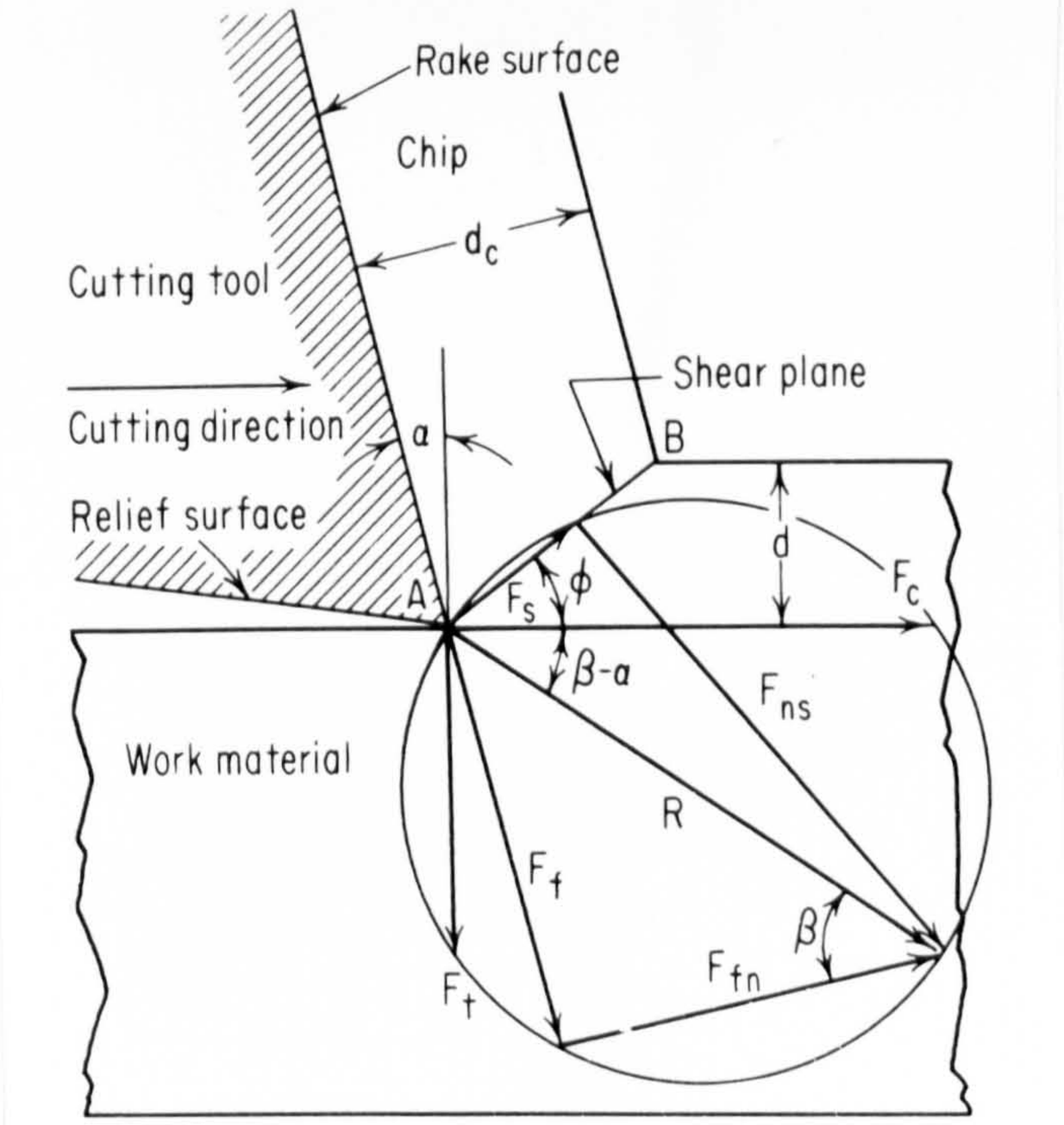

Fig 179. Equilibrium of cutting forces during cutting when a shear plane is formed (118)

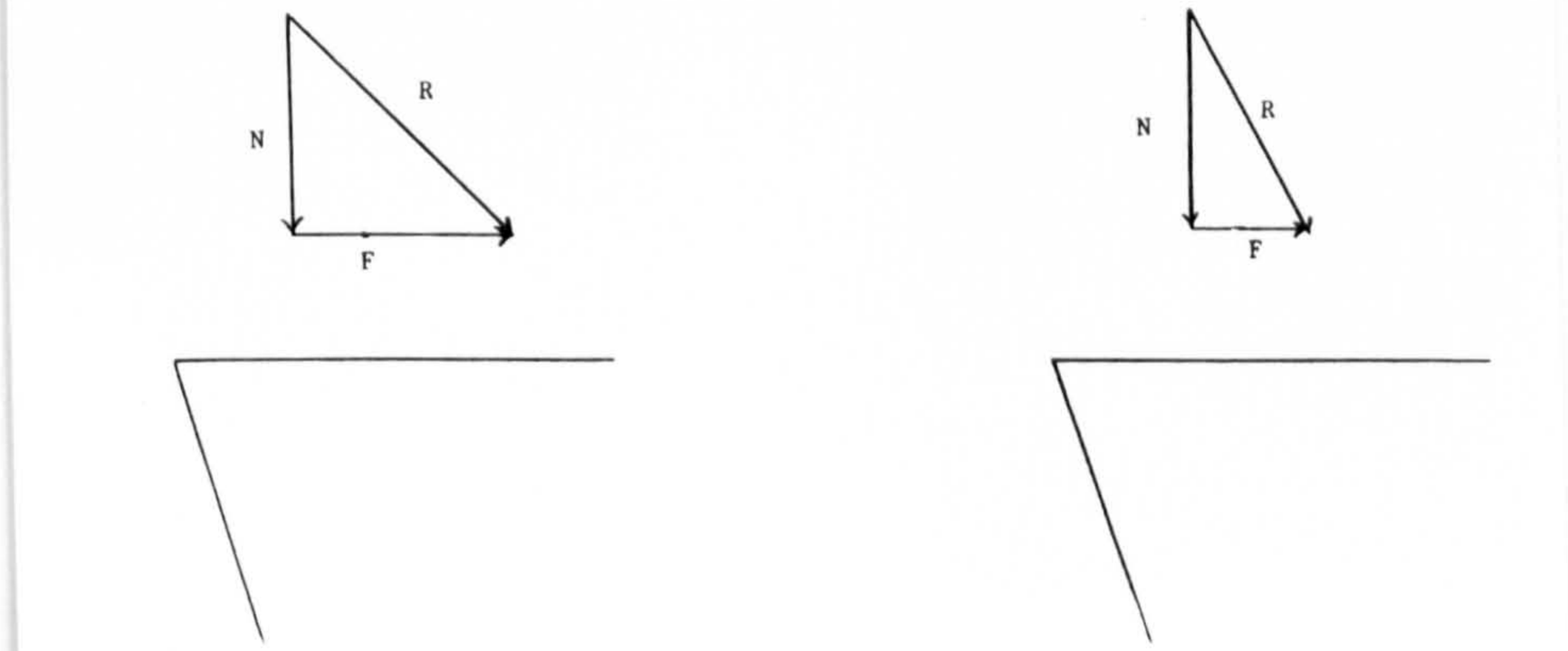

(a) metals (b) plastics

Fig 180. Schematic force diagram on a tool rake face at a rake angle of 0°

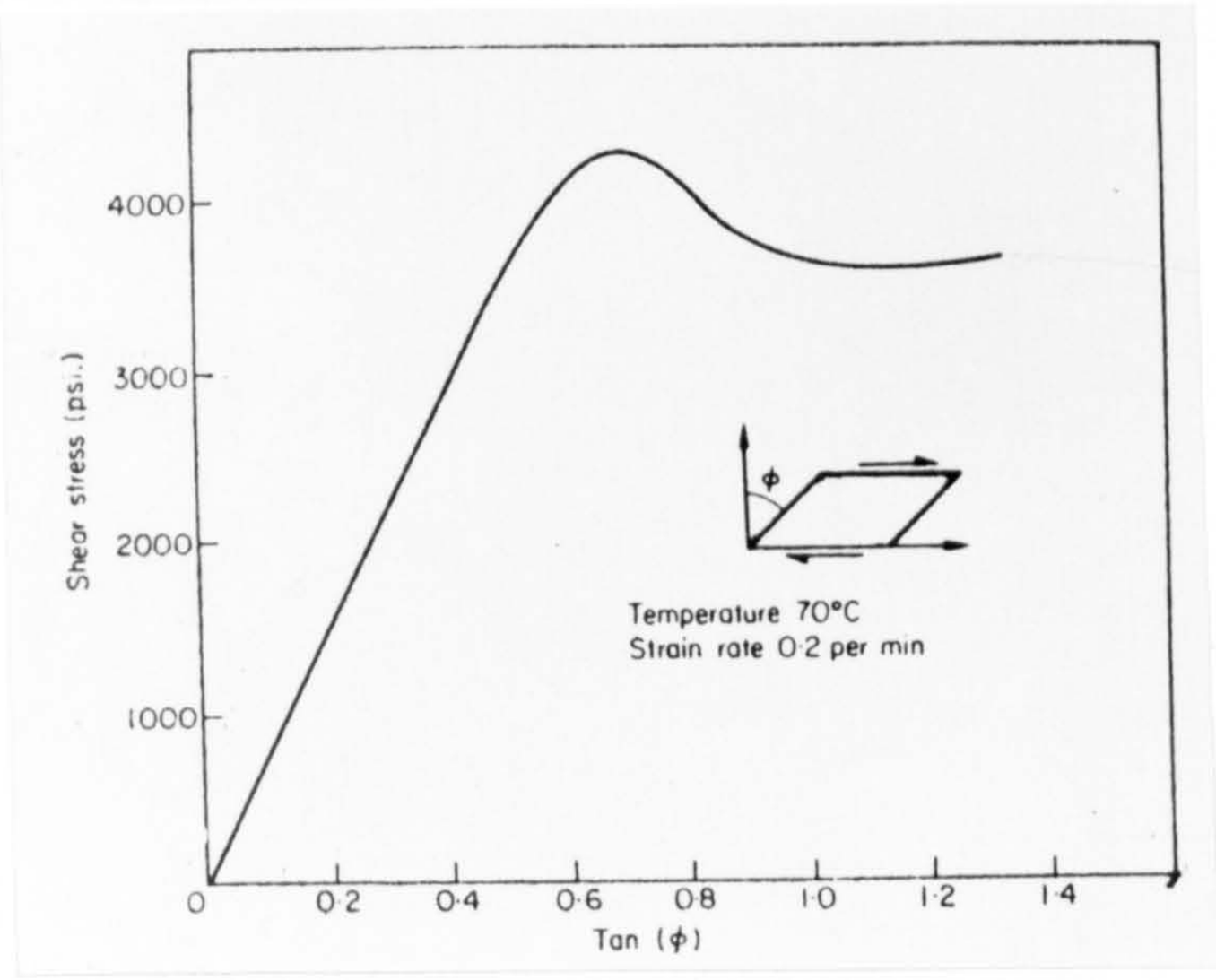

Fig 181. Strain-softening in shear with Polymethylmethacrylate (175)

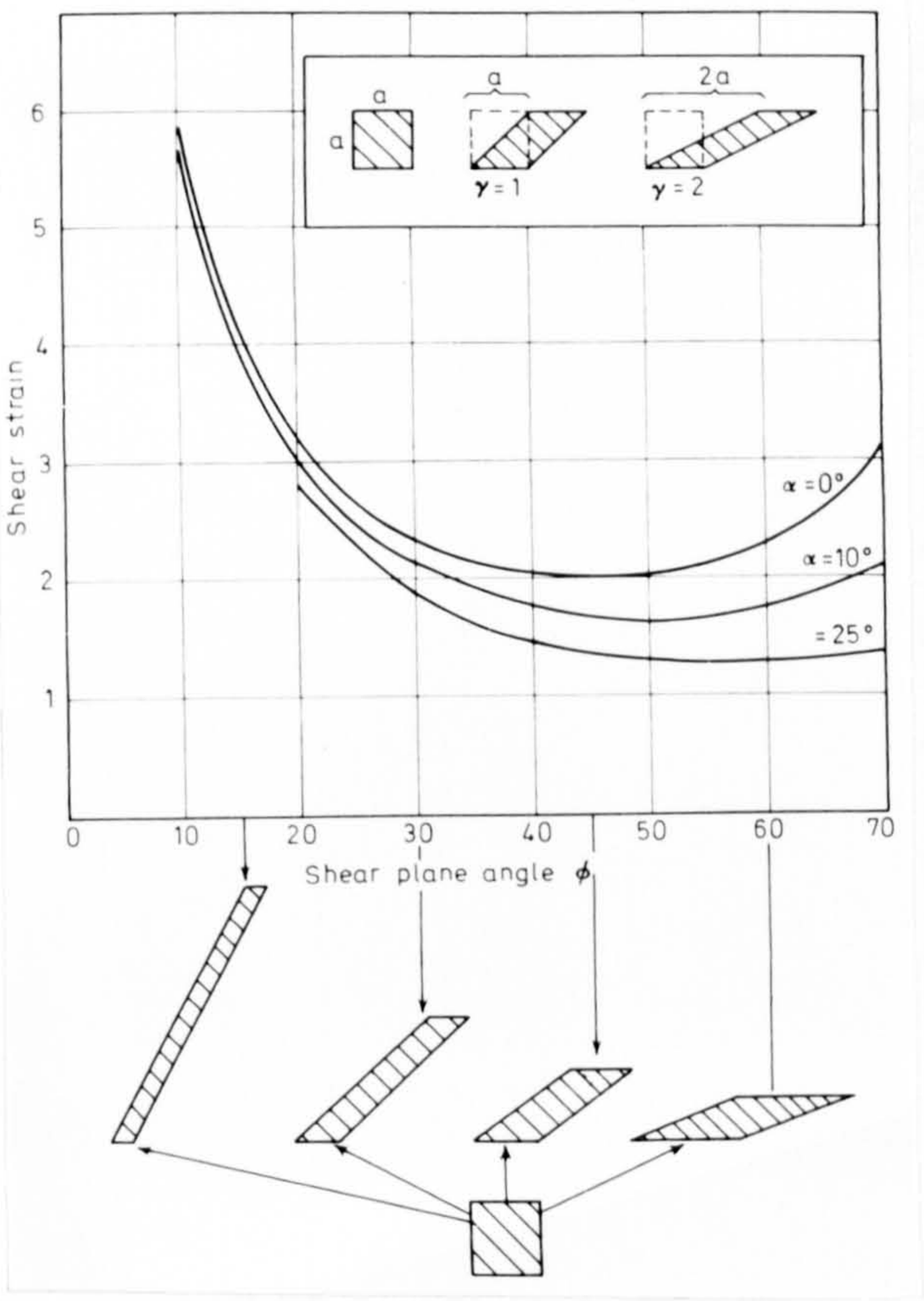

Fig 182. Strain on the shear plane versus shear plane angle for three values of rake angle (9)

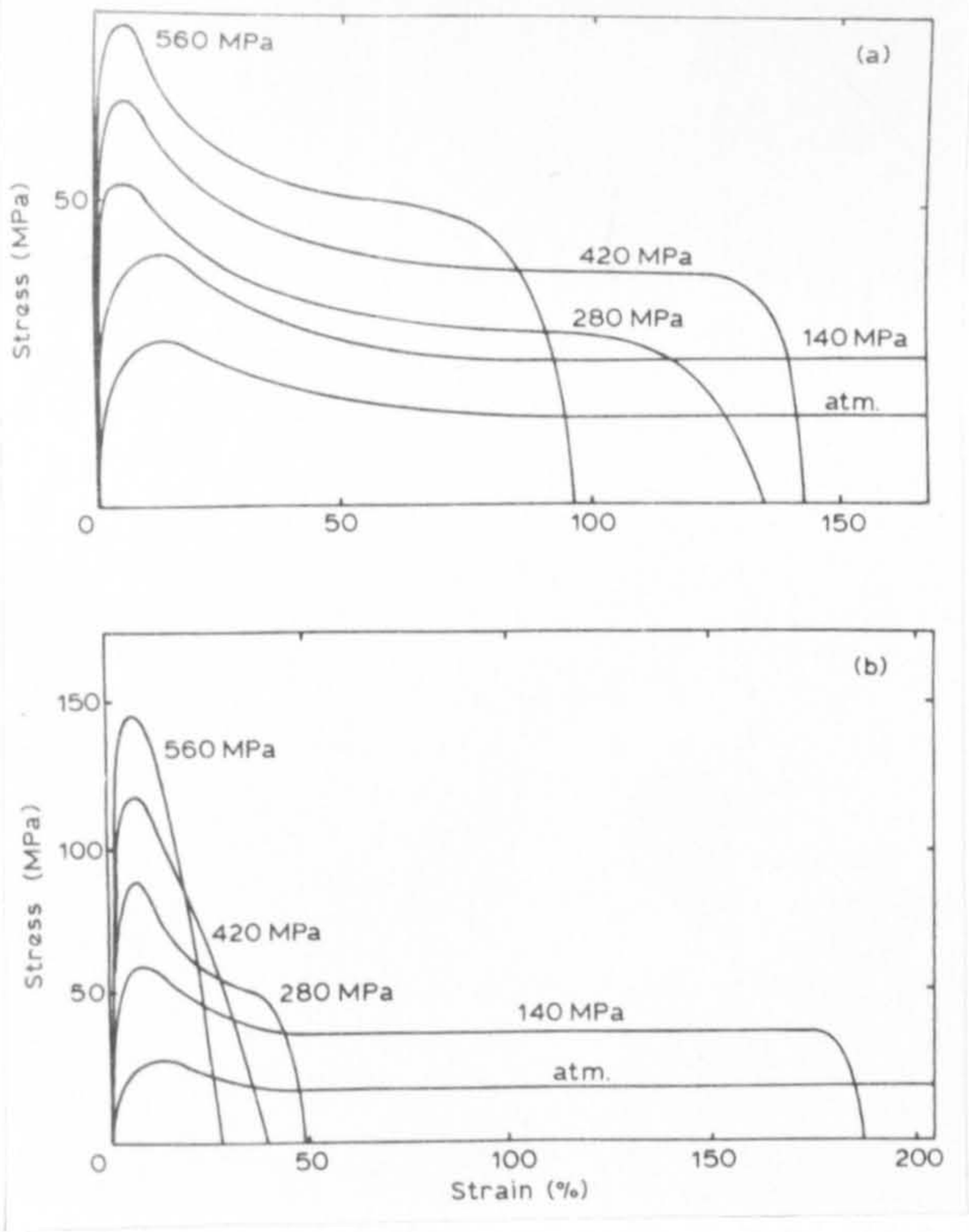

Fig 183. Stress/strain curves for crystalline polymers deformed in tension under the stated superimposed hydrostatic pressures (11)
(a) Medium-density Polyethylene (b) Polypropylene

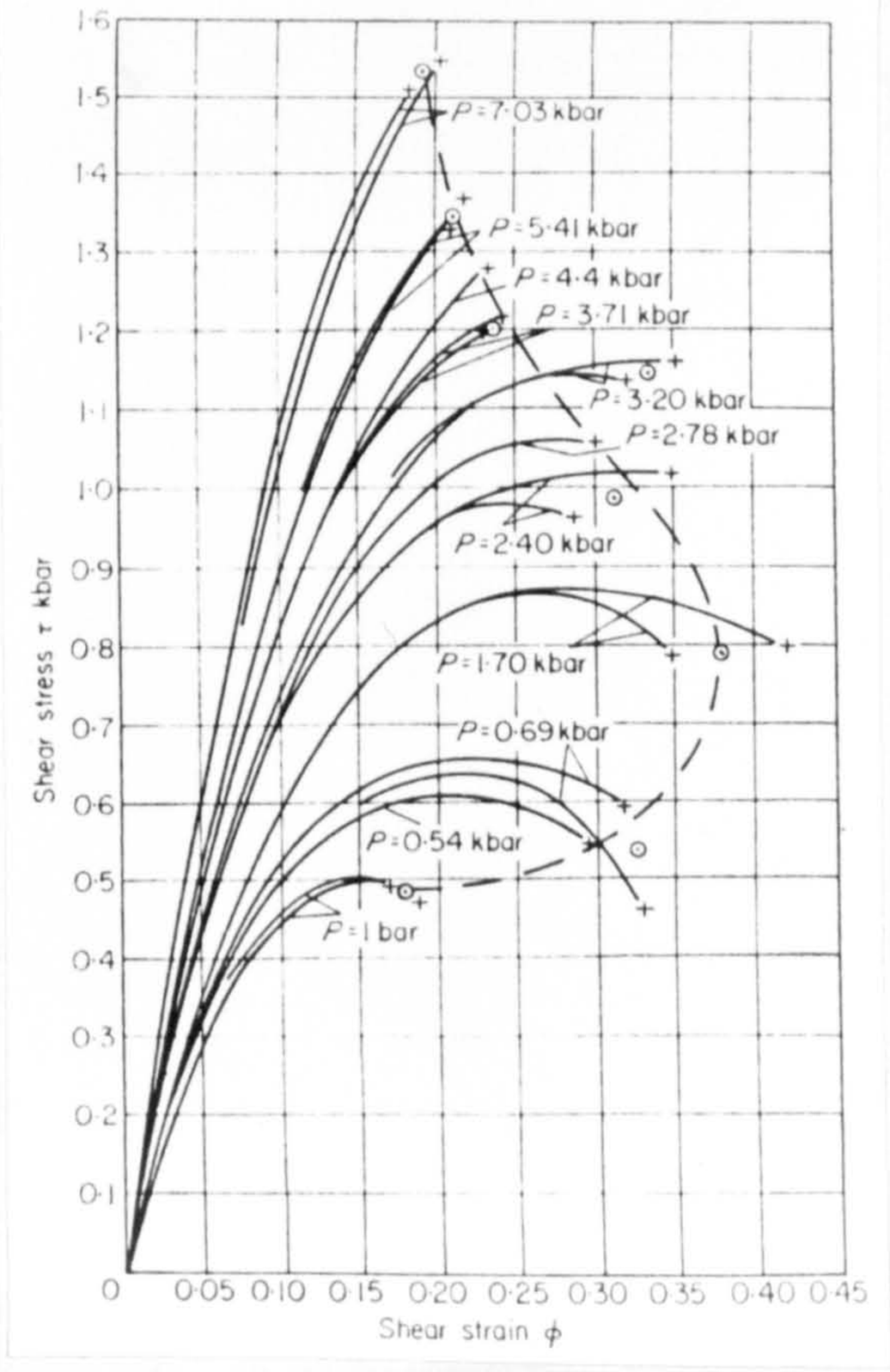

Fig 184. Stress/strain curves for PMMA determined in simple shear under different hydrostatic pressures at 22°C at a strain rate of 4×10^{-4}/sec (175)